ANL/PHY-97/1
ConF-9607156

# Proceedings of the Conference on Nuclear Structure at the Limits

*July 22 - 26, 1996*
*Argonne National Laboratory*
*Argonne, Illinois*

# FOREWORD

These Proceedings constitute a written record of the Conference on Nuclear Structure at the Limits held at Argonne on July 22-26, 1996. The Conference was attended by 197 scientists including 90 from abroad. The program sessions were characterized by very lively and spirited discussions. There was a general feeling among the participants that the nuclear structure field is in a healthy state right now. From the comments received from the attendees we feel that the conference achieved its aim of reviewing the status of nuclear structure physics while stimulating new ideas.

We express our thanks to the members of the advisory committee for their suggestions concerning the program. We also thank the participants for making the conference successful. The assistance of Jeannie Glover and Colleen Tobolic in handling the many secretarial duties before and during the conference is greatly appreciated.

*The Organizing Committee*

# Acknowledgments

The Organizing Committee greatfully acknowledges financial support from the following companies and organizations:

*Bicron/Crismatec BGO Detectors*

*EG&G/Ortec*

*LeCroy*

*Sun Microsystems*

*The University of Chicago*

*Argonne National Laboratory*

TABLE OF CONTENTS

**SESSION I-A (Monday Morning)**
Chairperson: R. M. Diamond



**SESSION I-B (Monday Morning)**
Chairperson: B. Hass



**No Submission*

**SESSION II-A (Monday Afternoon)**
Chairperson: B. Herskind



**SESSION II-B (Monday Afternoon)**
Chairperson: M. A. Deleplanque-Stephens



**No Submission*

**SESSION III-A (Tuesday Morning)**
Chairperson: S. Lunardi



**SESSION III-B (Tuesday Morning)**
Chairperson: L. L. Riedinger



**No Submission*

**SESSION IV-A (Tuesday Afternoon)**
Chairperson: N. Benczer-Koller



**SESSION IV-B (Tuesday Afternoon)**
Chairperson: D. Cline



**SESSION V-A (Wednesday Morning)**
Chairperson: D. G. Sarantites



**No Submission*

**SESSION V-B (Wednesday Morning)**
Chairperson: U. Garg



**SESSION VI-A (Thursday Morning)**
Chairperson: W. Nazarewicz



**SESSION VI-B (Thursday Morning)**
Chairperson: M. Thoennessen



**No Submission*

**SESSION VII-A (Thursday Afternoon)**
Chairperson: A. M. Baxter



**SESSION VII-B (Thursday Afternoon)**
Chairperson: D. Ward



**No Submission*

**SESSION VIII-A (Friday Morning)**
Chairperson: J. A. Cizewski



**SESSION VIII-B (Friday Morning)**
Chairperson: D. B. Fossan



**No Submission*

**SESSION IX (Friday Afternoon)**
Chairperson: J. C. Waddington



**No Submission*

# Discrete–Line Transitions from Superdeformed to Yrast States in $^{194}$Hg and $^{192}$Hg

G. Hackman,[a] T.L. Khoo,[a] D. Ackermann,[a] A. Lopez–Martens,[b] M.P. Carpenter,[a] T. Lauritsen,[a] S. Agarwala,[a] I. Ahmad,[a] H. Amro,[a] D.J. Blumenthal,[a] I. Calderin,[a] T. Døssing,[c] S.M. Fischer,[a] F. Hannachi,[b] R.V.F. Janssens,[a] A. Korichi,[d] I.Y. Lee,[e] A.O. Macchiavelli,[e] E.F. Moore,[f] D. Nisius,[a] and J. Young[a]

[a] *Argonne National Laboratory, 9700 S. Cass Ave., Argonne, IL 60439, U.S.A.*
[b] *C.S.N.S.M., IN2P3–CNRS, bat 104–108, 91405 Orsay, France*
[c] *Niels Bohr Institute, DK-2100 Copenhagen 0, Denmark*
[d] *I.P.N., bat 104, 91405 Orsay, France*
[e] *Lawrence Berkeley National Laboratory, Berkeley, CA 94720, U.S.A.*
[f] *North Carolina State University, Raleigh, NC 27965, U.S.A.*

Discrete–line $\gamma$-ray decay from superdeformed (SD) to yrast states in $^{194,192}$Hg has been studied with the Gammasphere spectrometer. The previously established decay for the yrast SD band of $^{194}$Hg has been characterized further. In addition, one–step decays have been observed for $^{194}$Hg SD band 3, which fixes the excitation energy and spin of the last observed level of this band at $E^* = 7.455$ MeV, $J = 11\hbar$. So far no direct decays from superdeformed to yrast states have been observed in $^{192}$Hg or in $^{194}$Hg band 2, a result which is consistent with fluctuations of the transition strengths.

High–spin superdeformed (SD) bands have been known for some time now [1] , and a considerable effort has been devoted to understanding their many fascinating properties, *e.g.* the exact nature of excited bands and the physical origin of the identical bands phenomenon. Progress on these fronts has in the past been impeded by the fact that the spins and excitation energies of these SD bands could not be measured by traditional discrete–line $\gamma$ spectroscopy, *i.e.* by the straightforward application of coincidence relationships and energy differences (the Ritz principle) to deduce with confidence a level scheme. At the point of decay–out, the lowest members of the SD bands are located at very high excitation energies relative to the yrast line. The coupling to excited "normal–deformed" (ND) states is very weak, but once the wave function picks up a small component of the hot ND states, the decay can proceed via a multitude of paths which are difficult to resolve. The branching ratio for a primary $\gamma$ decay directly from a SD state to a ND yrast or near–yrast level is very small, and until recently, the ever–evolving $\gamma$-ray spectroscopy arrays simply did not have the sensitivity to detect these primary decays. Early attempts to measure the spins and excitation energies of SD bands [2-4] did not or could not use coincidence and Ritz principle information, and therefore were not fully satisfactory.

Recently, a network of primary decays from $^{194}$Hg SD band 1 to yrast states [5] was observed. Shortly thereafter, experiments on $^{194}$Pb [6] revealed a network comprising both "one–step" primary decays from SD to yrast levels and "two–step" decays, that is, primary decays to non–yrast ND states where the deexcitations from these previously unknown ND states to the yrast line were also observed.

Clearly, the third–generation $\gamma$-ray detector arrays have reached one of their most important milestones; they have the sensitivity to measure the spin and excitation energies of SD states directly through traditional discrete–line spectroscopy methods. Two new Gammasphere experiments have been undertaken to search for the one–step decays from SD bands 2 and 3 of $^{194}$Hg, and band 1 of $^{192}$Hg. The main motivation behind these experiments lies in the fascinating, and always controversial, problem of identical bands: one of the excited bands of $^{194}$Hg (band 3) is isospectral with $^{192}$Hg band 1, that is, the in-band $\gamma$ rays have the same energy. Determining the spins and parities

of these two bands would constrain the possible explanations for identical bands, for example, by ascertaining whether or not states emitting $\gamma$ rays of the same energy also have the same spin and parity. Furthermore, measuring the excitation energies of bands 2 and 3 in $^{194}$Hg would lend further insight into the nature of these excitations, namely whether they are two–quasiparticle excitations or whether they pertain to octupole vibrations or some other collective excitation mode. Finally, by better characterizing the one–step decay network for band 1 (including measurements of the transition probabilities), it was hoped to gain insight about the nature of the fluctuations in transition intensity.

At the time of the experiments, Gammasphere comprised 85 high–purity germanium detectors. The reactions employed were $^{150}$Nd($^{48}$Ca,4n)$^{194}$Hg at $E_{\rm beam}$=202 MeV and $^{160}$Gd($^{36}$S,4n)$^{192}$Hg at $E_{\rm beam}$=160 MeV. In both cases, the targets were backed with a $\sim$ 15 mg/cm$^2$ Au layer. The first, highest–spin transitions in the SD cascade were emitted while the recoiling Hg nucleus was in flight. In contrast, the lowest transitions in the band were emitted from a fully stopped nucleus, as were all of the normal deformed lines following the decay–out. This provided a *distinctive signature* for primary decay $\gamma$ rays; they also had to be *fully stopped* and their peaks had to be *sharp*.

The sum of double–gated $\gamma$–$\gamma$–$\gamma$ coincidence spectra of band 1 of $^{194}$Hg and $^{192}$Hg are shown in Figure 1, which demonstrates the quality of the data. Most of the analyses have been done with triple–coincidence events. For the high–energy primary transitions, this yields the best tradeoff between statistics and background, and therefore the best sensitivity.

In the new data on $^{194}$Hg, the previously–reported [5]4485, 4195 and 3489 keV lines associated with the primary decay of SD states, as well as their coincidence relationships with intraband SD and yrast transitions, are spectacularly reproduced. In addition, two more primary transitions have been added to the decay scheme; a 3942 keV "one–step" decay from the $12^+$ SD state to the $13^-$ ND state, and a 3565 keV transition which de–excites the $10^+$ SD state. The level fed by the latter transition should be highly non–yrast, and there is evidence in the coincidence spectrum for a 919 keV decay to the $9^-$ yrast state which completes this "two–step" path.

For three primary transitions, angular distributions have been measured and $A_2/A_0$ coefficients extracted. (See Figure 2.) The new data show with much greater confidence that the $A_2/A_0$ coefficient

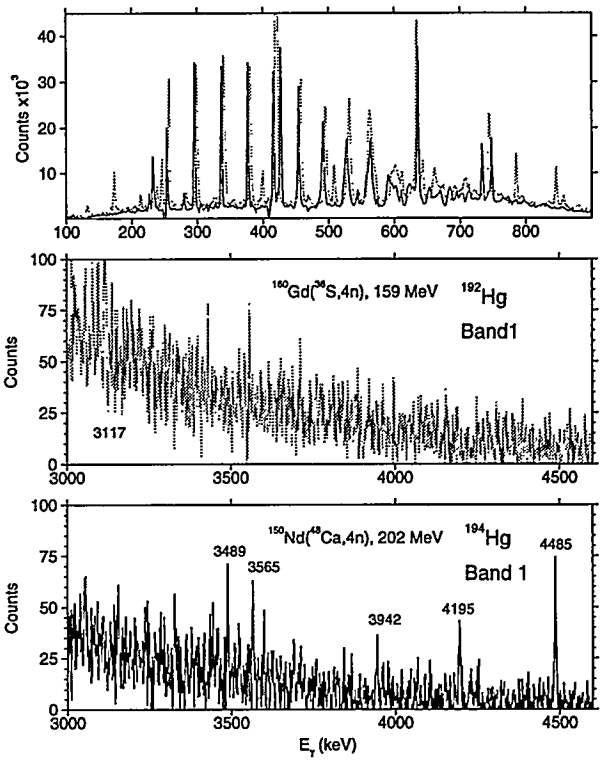


**Figure 1:** Sums of double–gated coincidence spectra on $^{192}$Hg band 1 (gray) and $^{194}$Hg band 1 (black). Top panel: low–energy portion of both spectra, overlaid, showing the SD band members. Note that the higher–energy transitions of the SD band become broadened due to Doppler shift. Middle and bottom panels: High–energy portion of these spectra in the range where one–step decays would be expected.

of the 4485 keV line is negative and consistent with stretched or anti–stretched dipole radiation. The measured $A_2/A_0$ values for the 3489 and 4195 keV transitions also favour the same multipole character. Furthermore, the coefficients all rule out the possibility of stretched quadrupole transitions or dipole transitions with a spin change of 0. All of these results are fully consistent with the spin assigments given previously. Dipole transitions are more likely E1 in nature than M1, since neutron capture data [7] show that the transition rate for the former should be five times that of the latter.

For $^{194}$Hg band 3, which is isospectral to $^{192}$Hg band 1, two $\gamma$ rays with energies of 4980 and 5032 keV have been assigned as one–step primary transitions de–exciting the SD band. Figure 3 shows how these transitions have been placed. In the top–left coincidence spectrum, which is the sum

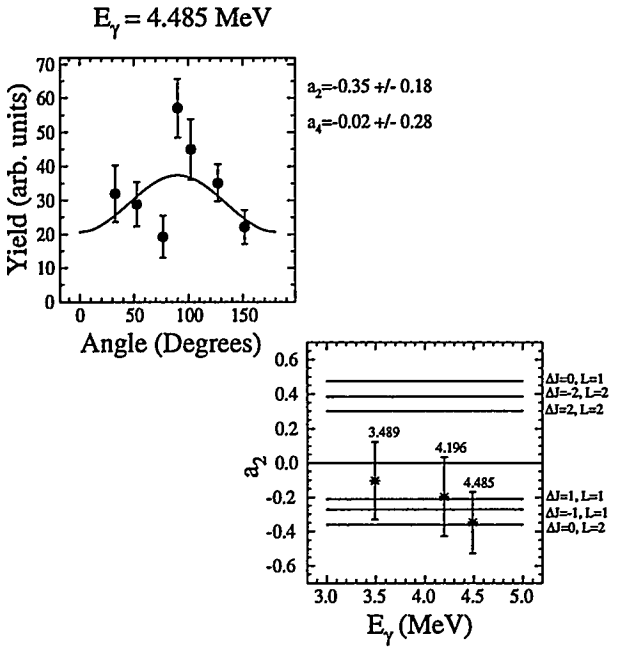


**Figure 2:** Top left panel: angular distribution and best polynomial fit for the 4485 keV primary transition. Bottom right panel: extracted $A_2/A_0$ coefficients for the three strongest primary transitions associated with $^{194}$Hg SD band 1, compared with expected values for indicated multipolarities and spin–changes.

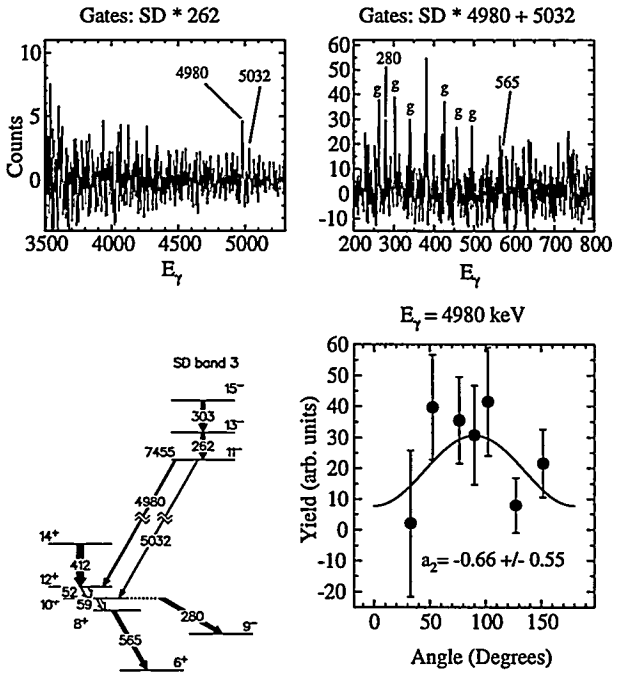


**Figure 3:** Details of the primary transitions of band 3. Top left: spectrum gated once on the 262 keV SD transition and once on the remaining members of the SD band. Top right: spectrum gated once on all SD transitions and once on the primary transitions. Bottom left: proposed level scheme. Bottom right: angular distribution and best polynomial fit for the 4980 keV $\gamma$ ray.

of double–gates where one of the gating transitions was always the last transition observed in the band, both primary lines are present, indicating they must both be emitted from the bottom of the band. In the coincidence spectrum where one gate is part of the SD band and the second gate is either of the primary lines, there is clear evidence for the $\gamma$ rays associated with the positive–parity ground state band. Finally, the difference in measured $\gamma$-ray energies between these two primary lines, 52±2 keV, corresponds to the energy difference betwen the $12^+$ and $10^+$ levels. Based on this evidence the level scheme shown in Figure 3 is proposed, and the last observed state of band 3 is assigned as $J^\pi = 11^-$ at an excitation energy of 7.455 MeV. Here again, the parity is expected on the basis of relative E1/M1 strengths seen in neutron capture. The measured angular distribution of the 4980 keV primary line yields a negative $A_2$ coefficient, consistent with an anti–stretched dipole character.

Knowing the spins and excitation energies of both $^{194}$Hg SD bands 1 and 3, we can calculate the experimental routhians $e'$ in the prescription of Bengston and Frauendorf [8] . The Harris parameters have been adjusted to match the dynamic moment $\mathcal{J}^{(2)}$ of band 1, and the results are shown in Figure 4. If the routhians are extrapolated to zero rotational frequency, their difference is about $\Delta e'_0 = 0.8$ MeV. Any model of the band 3 excitation, whether collective (*e.g.* octupole phonon) or quasiparticle, must account for this energy. For example, it has been proposed [9] that the lowest excitations in the even–Hg SD well are octupole vibrations, and the calculated routhians for the $K = 2$ octupole component yield slopes which compare favourably to the experimental data, although the excitation energy $\Delta e'_0 = 1.1$ MeV is a bit too high. By contrast, if band 3 is interpreted as a two–quasiparticle excitation [10] , then in a simple BCS picture, this places an upper limit of 0.4 MeV on the pairing gap at zero rotational frequency, compared to neutron pairing gaps of typically $\sim 0.8$ MeV adopted for such calculations [11] . (It should be noted that a self–consistent solution to a two–quasiparticle system could yield $\Delta e'_0 < 2\Delta_{\rm BCS}$.) Clearly there is a need for more

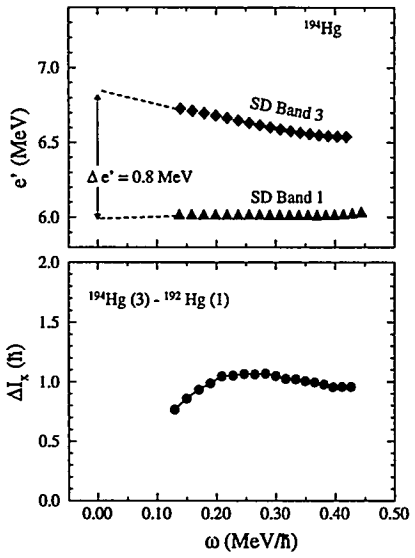


**Figure 4:** Upper panel, routhians for $^{194}$Hg bands 1 and 3. Lower panel, difference in spin projection $I_x$ between $^{194}$Hg band 3 and its isospectral partner $^{192}$Hg band 1.

detailed theoretical predictions (*e.g.* crossover M1 strengths for bands 2 and 3 and intraband E1 strength to band 1) before the exact nature of the excitation leading to band 3 can be determined.

As presented above, band 3 has odd spin and negative parity. Since band 1 of $^{192}$Hg is believed to be the vacuum SD band and, hence, should have even spin and positive parity, one may conclude that states emitting $\gamma$ rays of the same energy do not necessarily have the same spin and parity. Another way of looking at this feature is to project the spins onto the rotation axis and look at the difference between $^{194}$Hg band 3 and $^{192}$Hg band 1. This is presented in Figure 4; it is clear that at high $\omega$, states with the same rotational frequency, and hence emitting $\gamma$ rays with the same energies, have one extra unit of projected spin in $^{194}$Hg band 3 than $^{192}$Hg band 1.

Itis believed that the states in $^{192}$Hg SD band 1 *almost certainly* have even spin and positive parity. Nevertheless, it is essential to confirm this expectation through the detection of the primary decays. Figure 1 shows that data of comparable quality were accumulated for bands 1 in both $^{192}$Hg and $^{194}$Hg. Assuming that the SD bands in these nuclei have roughly the same excitation energy, then all other things being equal, it would seem reasonable to expect to see primary decays from the $^{192}$Hg SD to normal states with the same quality as was seen in $^{194}$Hg. Yet, the high–energy portion of the spectrum, where the $^{192}$Hg one-step transitions are expected, is remarkably free of any salient candidates. In fact, out of all of the peak–like fluctuations in the spectrum, only a line at 3117 keV near the low end of the spectrum has been very tentitatively placed as the first component of a two–step cascade to the yrast line, where one possible candidate for a second step is a 696 keV transition to the $10^+$ ND state. With this information it is not possible to make any statements regarding the spin or parity of this band, but the analysis is on–going. It should be noted that for $^{194}$Hg band 2, which is likely to be a signature partner to band 3 (based on the transition energies of one being midway between those of the other), no respectable candidates for a network of primary decays could be observed, even though the expected energies are known.

Reduced transition probabilities for the observed primary transitions were calculated and tabulated (see Table 1). It was assumed that the transition quadrupole moment of the low–spin members of the SD band is the same as that measured recently by Moore *et al.* [12] at higher spin. These primary transitions are extremely retarded, for example the two transitions from the $12^+$ state of band 1, have values of about $10^{-8}$ of a Weisskopf unit.

There are fluctuations in the strengths of the primary $\gamma$ rays from the SD levels, which can be understood in the following manner. A SD state exists in a sea of highly excited normal states (ND*). These ND* states are complex, much like the compound states populated in neutron capture. The SD band mixes with one or two of the nearest–lying ND* states, *i.e.* its wave function acquires a small admixture of this ND state,

$$|\Psi\rangle = |\mathrm{SD}\rangle + \alpha|\mathrm{ND}^*\rangle.$$

The decay then occurs due to this admixed component, *i.e.*

$$\langle \mathrm{ND}|\mathcal{M}|\Psi\rangle \simeq \alpha\langle \mathrm{ND}|\mathcal{M}|\mathrm{ND}^*\rangle.$$

If the ND* states are indeed compound states, then they should not be charactarized by any quantum numbers apart from spin and parity, and the transition strengths $|\langle\mathcal{M}\rangle|^2$ of primary decays should exhibit the same Porter–Thomas fluctuations as seen in neutron capture. At the current sensitivity levels, this would be manifest in observing the one–step decays only when one is fortunate enough to select a case which samples the high–strength portion of the distribution.

| Band, $Q_0$ (eb) | $E_\gamma$ (keV) | $J_i^\pi \rightarrow J_f^\pi$ | $I_\gamma/I_{SD}$ (%) | $B$(E1) (W.u.) | $B$(M1) (W.u.) |
|---|---|---|---|---|---|
| $^{194}$Hg | 3489 | $12^+ \rightarrow 13^-$ | 1.2(1) | $2.8(3)\times10^{-8}$ | |
| Band 1, | 3565 | $10^+ \rightarrow$ ? | 0.5(1) | $< 8\times10^{-7}$ | $< 9\times10^{-5}$ |
| $18.4 \pm 1.1$ | 3942 | $10^+ \rightarrow 11^-$ | 0.3(1) | $< 8\times10^{-7}$ | |
| | 4195 | $12^+ \rightarrow 11^-$ | 0.8(1) | $1.1(3)\times10^{-8}$ | |
| | 4485 | $10^+ \rightarrow 9^-$ | 1.0(1) | $< 4\times10^{-7}$ | |
| | (3710) | $12^+ \rightarrow 12^-$ | | $< 4\times10^{-9}$ | |
| | (4076) | $10^+ \rightarrow 10^-$ | $< 0.2$ | | |
| | (4205) | $10^+ \rightarrow 10^+$ | | | |
| | (4408) | $12^+ \rightarrow 12^+$ | | | $< 3\times10^{-7}$ |
| $^{194}$Hg | 4980 | $11^{(-)} \rightarrow 12^+$ | 3.7(8) | $< 2\times10^{-7}$ | $< 2\times10^{-5}$ |
| Band 3 | 5032 | $11^{(-)} \rightarrow 10^+$ | 2.0(6) | $< 1\times10^{-7}$ | $< 1\times10^{-5}$ |
| $17.7 \pm 1.4$ | | | | | |

**Table 1:** Reduced transition rates for $^{194}$Hg SD decay–out primary transitions.

In $^{192}$Hg, only one primary transition can be tentatively placed as part of a two–step decay. $^{194}$Hg band 1 exhibits a robust network of strong one–step transitions to the yrast line. In $^{194}$Hg band 2, there are no reputable candidates for primary decays, and band 3 has two one–step decays directly to the yrast line. Clearly the primary decays are governed by some form of transition strength fluctuation, although whether it has a Porter–Thomas distribution is an open question which we hope to answer in the near future.

One interesting observation is that in the decay of $^{194}$Hg band 1, four dipole transitions with $\Delta J = \pm 1\hbar$ are observed. However, there was no evidence for $\Delta J = 0$ transitions to yrast states, with or without a parity change. The non-observation of the $\Delta J = 0$ transitions may hint at the persistence of some quantum number (beyond spin and parity) in the ND* states at excitations of $\sim 4.3$ MeV above yrast. It is interesting to note that the Clebsch–Gordon coefficient $\langle J, 0; 1, 0 | J, 0 \rangle$ is identically 0 for all $J$. One might expect this to be relevant, for example, to $K = 0$ components in the intrinsic frame. SD band 1 is very likely a $K = 0$ band, and one might speculate that if it coupled only to the $K = 0$ components of the hot ND* states, and if in turn the near–yrast states are mostly $K = 0$, then dipole transitions with no spin change might be suppressed.

In conclusion, a new study of the primary decays of the SD states of $^{194}$Hg has shown that the level fed by the 262 keV transition of band 3 is a $J^\pi = 11^-$ state at an excitation energy of 7.455 MeV. This gives band 3 an excitation energy of $\sim 0.8$ MeV relative to band 1 at zero rotational frequency. The spins of the states in band 3 are likely $1\hbar$ higher than those in $^{192}$Hg band 1 that emit $\gamma$ rays of the same energy. The transition rates for the primary transitions are very retarded, typically $10^{-8}$ Weisskopf units.


1. P.J. Twin *et al.*, Phys. Rev. Lett. 57, 811 (1986).
2. A. Ataç *et al.*, Phys. Rev. Lett. 70, 205 (1993).
3. R.G. Henry *et al.*, Phys. Rev. Lett. 73, 777 (1994).
4. M.J. Brinkman *et al.*, Phys. Rev. C 53, R1461 (1996).
5. T.L. Khoo *et al.*, Phys. Rev. Lett. 76, 1583 (1996).
6. A. Lopez–Martens *et al.*, Phys. Lett. B380, 18 (1996); K. Hauschild *et al.*, these proceedings.
7. L.M. Bollinger, Phys. Rev. C 2, 1951 (1970).
8. R. Bengtsson and S. Frauendorf, Nucl. Phys. A327, 139 (1979).
9. T. Nakatsukasa *et al.*, Phys. Rev. C 53, 2213 (1996), and these proceedings.
10. M.A. Riley *et al.*, Nucl. Phys. A512, 178 (1990).
11. R. Wyss, W. Satula, W. Nazarewicz and A. Johnson, Nucl. Phys. A511, 324 (1990).
12. E.F. Moore *et al.*, private communication.

# Observation of the Single Step Links of the Yrast Superdeformed Band in $^{194}$Pb

F. Hannachi[1], A. Lopez-Martens[1], A. Korichi[2], S Leoni[3], C. Schück[1], E. Gueorguieva[1], Ch. Vieu[1], B. Haas[4], R. Lucas[5], A. Astier[6], G. Baldsiefen[7], M. Carpenter[8], G. de France[4], R. Duffait[6], L. Ducroux[6], Y. Le Coz[5], Ch. Finck[4], A. Gorgen[7], H. Hübel[7], T.L. Khoo[8], T. Lauritsen[8], M. Meyer[6], D. Prévost[4], N. Redon[6], C. Rigollet[4], H. Savajols[4], J.F. Sharpey-Schafer[9], O. Stezowski[4], Ch. Theisen[5], U. Van Severen[7], J.P. Vivien[4], A.N. Wilson[10]

[1] *CSNSM, IN2P3-CNRS, bat 104-108, F-91405 Orsay, France*
[2] *IPN, F-91406, Orsay Cedex, France*
[3] *Niels Bohr Institute, 4000 Roskilde, Denmark*
[4] *CRN, IN2P3-CNRS, F-67037 Strasbourg, France*
[5] *DAPNIA SPhN, CEA Saclay, 91191 Gif sur Yvette, France*
[6] *IPN, IN2P3-CNRS and Univ. Lyon-1, F-69622 Villeurbanne Cedex, France*
[7] *ISKP, Universitat Bonn, D-53115 Bonn, Germany*
[8] *ANL, Argonne, Illinois 60439, USA*
[9] *NAC, PO Box 72, Faure, ZA-7131 South Africa*
[10] *Oliver Lodge Laboratory, University of Liverpool, PO Box 147, L69 3BX UK*

**Abstract**

The EUROGAM array has been used to investigate the decay out of the yrast superdeformed (SD) band in $^{194}$Pb. Eigth single step decays from the lowest observed SD states to low-lying states at normal deformation (ND) have been identified. From this observation, the excitation energy (4877 $\pm$ 1.5 keV) and the spin ($6^+$) of the lowest observed SD state in $^{194}$Pb are established.

Superdeformation in lead nuclei was first discovered in 1990 in two independent experiments, using respectively the Osiris array in Berlin and the Hera array at LBL [1, 2]. The yrast SD band in $^{194}$Pb was found as a sequence of 12 transitions with energies ranging between 169 keV and 602 keV and an intensity of 1 % relative to the the $2^+$ - $0^+$ 965 keV transition. The survival of the SD band down to very low rotational frequency (and therefore low spin) and the substantial intensity of the band together with the fact that the level density in the first well of this nucleus is reduced due to the close proton shell Z=82 already indicated that this nucleus should be a good candidate to investigate the decay out of the SD band. Several attempts have been made in order to find the linking transitions between the superdeformed (SD) and the normally deformed (ND) states in this nucleus [3, 4, 5]. On figure 1 are shown the results of a comparative study of the decay-out spectra of the $^{192}$Hg and $^{194}$Pb yrast SD bands, using the fluctuation analysis method [6, 7]. The data were obtained with the Eurogam1 array which consisted of 45 compton suppressed Ge detectors [9, 10]. Excited states in $^{192}$Hg and $^{194}$Pb were populated in the $^{160}$Gd($^{36}$S,4n) and $^{184}$W ($^{16}$O,6n) reactions at beam energies of 159 MeV and 113 MeV respectively. The beam was provided by the 20 MV tandem Van de Graaff accelerator of the Nuclear Structure Facility at Daresbury Laboratory. The targets consisted of 1 mg/cm$^2$ of $^{160}$Gd (enriched to 98.7%) deposited on a 10 mg/cm$^2$ gold backing

in the $^{192}$Hg experiment and of two stacked 325 $\mu$g/cm$^2$ enriched $^{184}$W deposited on 10 $\mu$g/cm$^2$ Carbon backing in the $^{194}$Pb experiment. Two data sets consisting of 660 $\times$ 10$^6$ ($^{192}$Hg) and 860 $\times$ 10$^6$ events ($^{194}$Pb) were recorded on tape with the requirement that at least 5 unsuppressed Ge detectors fired in prompt coincidence. The $\mu_2/\mu_1$ fluctuation spectra obtained for $^{192}$Hg and $^{194}$Pb in the 1 to 3 MeV transition energy region are shown in the bottom of figure 1, in comparison to the intensities of the discrete peaks which we proposed as possible decay out transitions (top part of figure 1). As one can see, strong fluctuations were observed in the case of $^{194}$Pb which were correlated with the measured discrete peak intensities, while in the $^{192}$Hg, not only was the fluctuation spectrum more smooth and closer to the statistical limit, but also the measured peak intensities were weaker, which indicates a higher degree of fragmentation in the statistical decay. This provided strong indications that a search for discrete linking transitions would be more promising in $^{194}$Pb than in $^{192}$Hg.

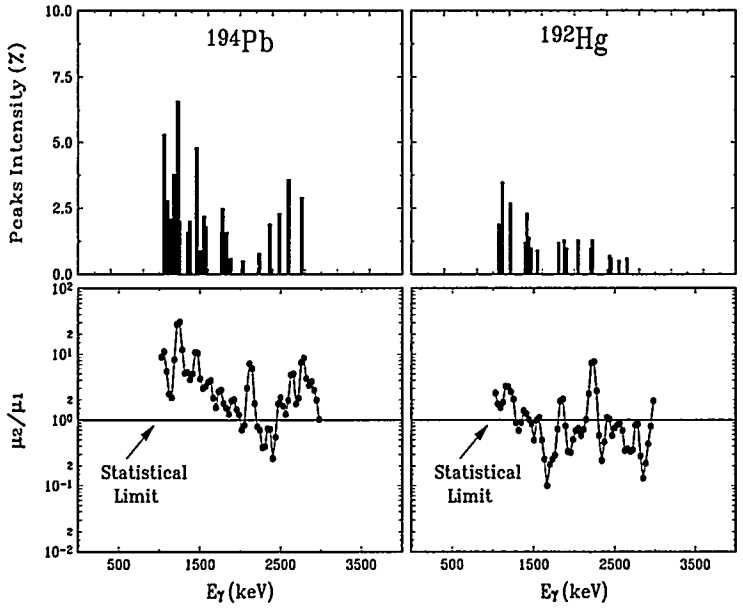


Figure 1: The top part of the figure shows the intensities of the lines proposed as decay out transitions in the 1 to 3 MeV region, normalized to 100% in the SD band plateau region, for both $^{194}$Pb (left part) and $^{192}$Hg (right part). The bottom of the figure shows the $\mu_2/\mu_1$ fluctuation spectra calculated on basis of triple SD gated spectra.

We have recently investigated again the deexcitation of the SD band in $^{194}$Pb using the Eurogam2 array in similar experimental conditions ( same target, beam and beam energy). Eurogam2 consists of 54 Compton-suppressed Ge detectors. Thirty of these are 73 % efficiency coaxial Ge detectors located in the forward and backward hemispheres, and 24 are clover detectors located in two rings near 90 degrees relative to the beam direction [11, 12]. The higher statistics collected in this experiment (10$^9$ triple and higher-fold events ) has allowed the identification of some high energy transitions connecting the SD

states to the ND states of the first well in $^{194}$Pb. These are visible around $E_\gamma = 2.5$ MeV in figure 2.

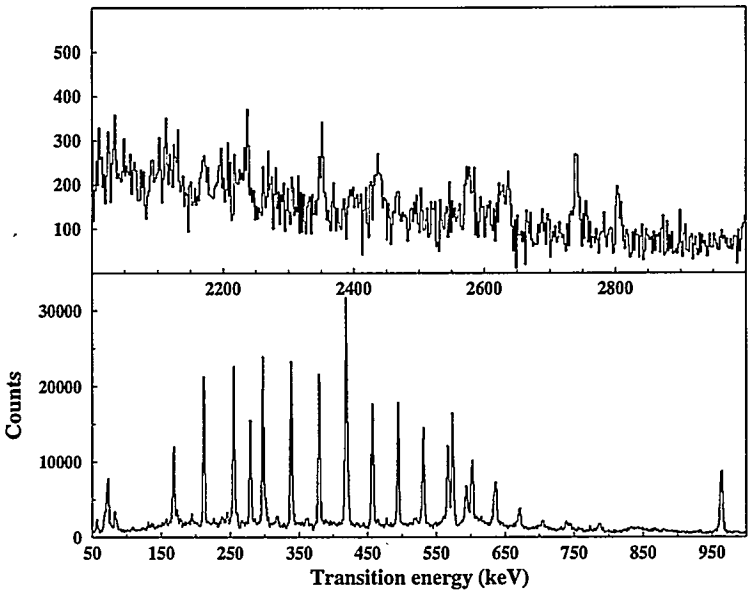


Figure 2: Background subtracted triple SD gated spectrum of the yrast SD band of $^{194}$Pb showing the high energy transitions directly connecting the SD and the ND levels. The background is a fraction of the corresponding double SD gated spectrum.

Their concidence relationships establish the level scheme presented in figure 3 for the deexcitation of the yrast SD band [13].
The excitation energy of the last observed SD state is measured for the first time as 4877 keV $\pm$ 1.5 keV and its spin is uniquely determined to be $6\hbar$. This is in very good agreement with the theoretical predictions [14, 15]. The SD band decay is mainly of a statistical nature [6, 16, 17, 18], that is, it proceeds via a quasi-continuum of transitions and resolved lines (for less than 15% of the SD band intensity) and both positive and negative parity states are populated. The transition strengths have been obtained for the decay transitions under the reasonable assumption of a dipole nature (it was not possible with the available statistics to measure their angular distributions). Assuming a constant quadrupole moment of 20 eb for the SD band [19], the lifetimes of the $8^+$ and $6^+$ SD levels can be obtained. From the branching ratios of the primary transitions, transition strengths ranging from $10^{-8}$ to $5\text{x}10^{-8}$ W.u. and from $1.5\text{x}10^{-6}$ to $5.3\text{x}10^{-6}$ W.u. have been obtained assuming E1 and M1 transitions respectively. These represent highly retarded transitions and indicate very small mixing between ND states and SD states at the point of decay. From the in-band / out-of-band intensity ratios, again assuming a constant quadrupole moment in the SD band and using a standard level density formula together with the GDR strength function of Bartholomew et al [20], it has been possible to deduce the mixing of the decaying SD states with the ND states. The $\alpha^2$ values obtained are respectively 0.0016 and 0.005 for the $8^+$ and $6^+$ SD states.

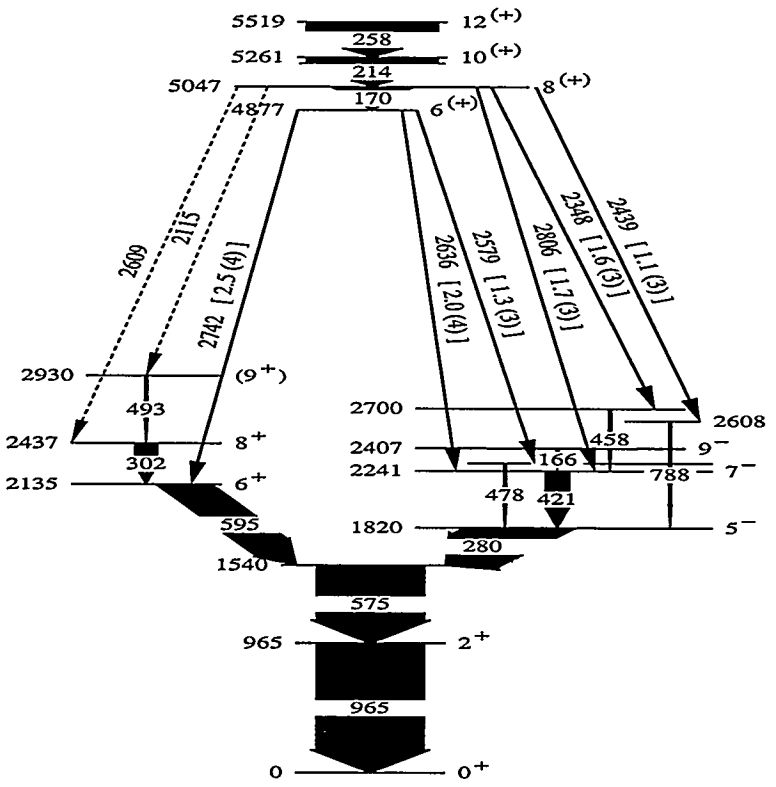


Figure 3: Partial decay scheme of the yrast SD band in $^{194}$Pb. The precision on the new transitions and on the SD states energies is of the order of 1.5 keV. The intensities of the linking transitions are indicated in brackets (in % of the SD band intensity). The dashed arrows indicate tentative emplacements for the transitions.

The factor 3.2 increase of $\alpha^2$ over one transition explains the sudden disappearance of the SD band at low rotational frequency.
In conclusion, by discovering eight high energy $\gamma$-rays directly connecting the SD states to the ND states in $^{194}$Pb, the excitation energy and spins of the SD yrast states have been measured for the first time using the Eurogam2 array. This method, which was successfully used for the first time in the case of $^{194}$Hg [21], allows, 10 years after the discovery of superdeformation at high spin, the precise measurement of some of the most fundamental properties of the SD nuclei.

**Acknowledgements**
The EUROGAM project is funded jointly by the EPSRC (UK) and the IN2P3 (France). We would like to thank all the staff members of the Vivitron, all the EUROGAM collaborators involved in the setting up of the array and R. Darlington from the Daresbury Laboratory for making the targets. One of us (ANW) acknowledges the receipt of an EPSRC postgraduate studentship. Work at Bonn was supported by the BMBF (Germany), under contract 06BN664-I, and at Argonne by the U.S. DOE, Nuclear Physics Division, under contract W-31-109-ENG-38.

# References


[1] K. Theine et al., Z. Phys. A336(1990)113

[2] M. Brinkman et al., Z. Phys. A336(1990)115

[3] F. Hannachi et al., Proc of Int. Conf. on Nucl. Struct. at high angular momentum, Ottawa May 18-21 1992 and Nucl. Phys. A557 (1993)75c-82c

[4] W. Korten et al., Z. Phys. A344 (1993)475

[5] M. Brinkman et al, Phys Rev C53 (1996)R1461

[6] A. Lopez-Martens et al., Phys. Rev. Letts 26(1996)1707, and contribution to this conference

[7] T. Dossing *et al.,* to be published in Physics Reports

[8] B. Herskind and S. Leoni, Nucl. Phys. **A520** , (1990) 539c-554c

[9] P.J. Nolan, Nucl. Phys. A520 (1990) 657

[10] F. A. Beck, Prog. Part. Nucl. Phys. 28 (1992) 443

[11] G. Duchêne et al., Proc of Int. Conf. on Nucl. Struct. at high angular momentum, Ottawa May 18-21 1992 and Nucl. Phys. A557 (1993)359-375

[12] P.M. Jones et al., NIM A362 (1995) 556

[13] A. Lopez-Martens et al., Phys. Lett. B380(1996)18

[14] S.J. Krieger et al., Nucl. Phys. A542(1992)43

[15] M. Girod et al., cont. to the Int. conference on nuclear structure around the turn of the century, Crete, Greece, July 1996

[16] E. Vigezzi et al., Phys. Lett. B249(1990)163

[17] R.G. Henry et al., Phys. Rev. Lett. 73 (1994) 777

[18] T. Lauritsen et al., contribution to this conference

[19] P. Willsau et al., Z. Phys. A344(1992)351 and R. Krucken et al., Phys. Rev. Letts 73(1994)3359

[20] Bartholomew et al., Adv. Nucl. Phys. 7(1973)229

[21] T. L. Khoo et al., Phys. Rev. Lett. 76(1996)1583

# *Primary transitions between the Yrast Superdeformed Band and Low–lying Normal deformed states in $^{194}Pb$*

K. Hauschild, L.A. Bernstein, J.A. Becker, D.E. Archer, R.W. Bauer
*Lawrence Livermore National Laboratory, Livermore, California 94550*

D.P. McNabb, J.A. Cizewski, K.-Y. Ding, W. Younes
*Rutgers University, New Brunswick, New Jersey 08903*

R. Krücken, G.J. Schmid, R.M. Clark, P. Fallon, I.-Y. Lee, A.O. Macchiavelli, R. MacLeod, R.M. Diamond, M.A. Deleplanque, F.S. Stephens
*Nuclear Science Division, Lawrence Berkeley Laboratory Berkeley, California 94720*

W.H. Kelly
*Iowa State University, Ames, Iowa 50011*

The observation of one–step "primary" gamma–ray transitions directly linking the superdeformed (SD) states to the normal deformed (ND) low–lying states of known excitation energies ($E_x$), spins and parities ($J^\pi$) is crucial to determining the $E_x$ and $J^\pi$ of the SD states. With this knowledge one can begin to address some of the outstanding problems associated with SD nuclei, such as the identical band issue, and one can also place more stringent restrictions on theoretical calculations which predict SD states and their properties. This information may also lead to a more detailed understanding of the SD de–excitation process itself.

The resolving power of the new generation of $4\pi$ $\gamma$–ray spectrometers allows the prospect realizing this goal. Brinkman, *et al.*, used the early implementation of the GAMMASPHERE spectrometer array (32 detectors) and proposed a single, candidate $\gamma$ ray linking the $^{194}$Pb yrast SD band to the low–lying ND states in $^{194}$Pb [1]. Using 55 detectors in the GAMMASPHERE array Khoo, *et al.*, observed multiple links between the yrast SD band in $^{194}$Hg and the low–lying level scheme and conclusively determined $E_x$ and $J$ of the yrast SD states [2]. Here we report on an experiment in which Gammasphere with 88 detectors were used and the $E_x$ and $J^\pi$ values of the yrast SD states in $^{194}$Pb were uniquely determined. Twelve one–step linking transitions between the yrast SD band and low–lying states in $^{194}$Pb have been identified, including the transition proposed by Brinkman. These transitions have been placed in the level scheme of $^{194}$Pb using coincidence relationships and agreements between the energies of the primary transitions and the energy differences in level spacings. Furthermore, measurements of angular asymmetries have yielded the multipolarities of the primaries which have allowed $J^\pi$ assignments of the $^{194}$Pb SD states to be unambiguously determined for the first time without *a priori* assumptions about the character of SD bands. A study performed in parallel to our work using the EUROGAM–II array reports similar, but somewhat less extensive, results [3].

The experiment was performed at the Lawrence Berkeley Laboratory 88–Inch Cyclotron facility. High–spin states in $^{194}$Pb were populated following the $^{174}$Yb($^{25}$Mg,5n) reaction at E($^{25}$Mg) = 130 MeV. Coincident $\gamma$ rays emitted during the decay of these high–spin states were detected using the GAMMASPHERE array [4]. The isotopically enriched (>98%) $^{174}$Yb target was 1.21-mg/cm$^2$ thick, and was evaporated directly onto a 6.13-mg/cm$^2$ Au backing. The signal–to–noise ratio of the SD primary $\gamma$ rays is enhanced when a thick backing is used. (The lower–lying SD states have lifetimes that are longer than the characteristic stopping times of the evaporation residuals in the Au foil. Therefore, the linking transitions do not exhibit angle–dependent Doppler shifts, or broadening, and the intrinsic detector lineshape is expected.) Approximately $7 \times 10^9$ events were recorded with suppressed Ge fold $\geq 4$.

The search for linking transitions was performed using a RadWare cube [5], gated by at least one $\gamma$ ray with an energy that corresponded to a $^{194}$Pb yrast SD transition energy [7-11]. The SD–gate list excluded the 419.9-keV $\gamma$ ray of the SD cascade due to its proximity to the 421.1-keV $7^- \rightarrow 5^-$ low–lying transition. In addition, the $\gamma$ rays were required to be in prompt coincidence with respect to the beam pulse. Events were sorted with the Beausang correction, which ensured that the increments to the cube were not weighted by fold or gating conditions [6]. Energy and efficiency calibrations over the range 0.100 – 3.548 MeV were obtained from the standard $^{56}$Co, $^{152}$Eu and $^{182}$Ta sources. Figure 1 illustrates two energy regions of a triple–gated, background subtracted spectrum for the yrast SD band in $^{194}$Pb projected from this cube. All possible combinations of double gates on the SD lines between 170 – 532 keV, inclusive, were summed to produce this spectrum. Relative in–band intensities are given in Table 1; 56(4), 34(6) and 10(7)% of the SD band decay out occurs from the three lowest observed SD states, respectively. Figure 1(a) illustrates that a

number of $\gamma$–ray transitions from the low–lying ND states in $^{194}$Pb [12], labeled by the corresponding $J_i^\pi \rightarrow J_f^\pi$, are in coincidence with the SD cascade. Twelve candidates for the discrete single–step transitions feeding into these low–lying ND states can be seen in the higher energy portion of the triple SD–gated spectrum, Figure 1(b). These transitions have energies in the range corresponding to those expected for the primary linking $\gamma$ rays [13].

Coincidence relationships between these candidate primaries, the low–lying $\gamma$ rays, and the yrast SD transitions in $^{194}$Pb were used to verify which, indeed, are linking transitions, and to place them in the $^{194}$Pb level scheme. We give two examples: (1) coincidence relationships for the 2743-keV primary transition were deduced from the background–subtracted spectra shown in Figure 2. Figure 2(a) was obtained by summing all double–gate combinations between the 2743-keV transition and the yrast SD band in $^{194}$Pb. From this spectrum we determined that the 2743-keV $\gamma$ ray depopulates the band below the 170-keV intra–band SD transition since the 170-keV line is observed. Another important feature is the enhancement of the 595-keV $6^+ \rightarrow 4^+$ low–lying yrast transition in comparison with Figure 1(a). Therefore, the 2743-keV transition decays into, or above, the state from which the 595-keV line depopulates. (2) Figures 2(b) and 2(c) present partial spectra obtained by a summation of double gates on the 595-keV and in–band SD transitions. It is apparent from these Figures that the 595-keV $\gamma$ ray is in coincidence with the SD band, the 303-keV $8^+ \rightarrow 6^+$ transition and the 2116-, 2610- and 2743-keV primary transitions.

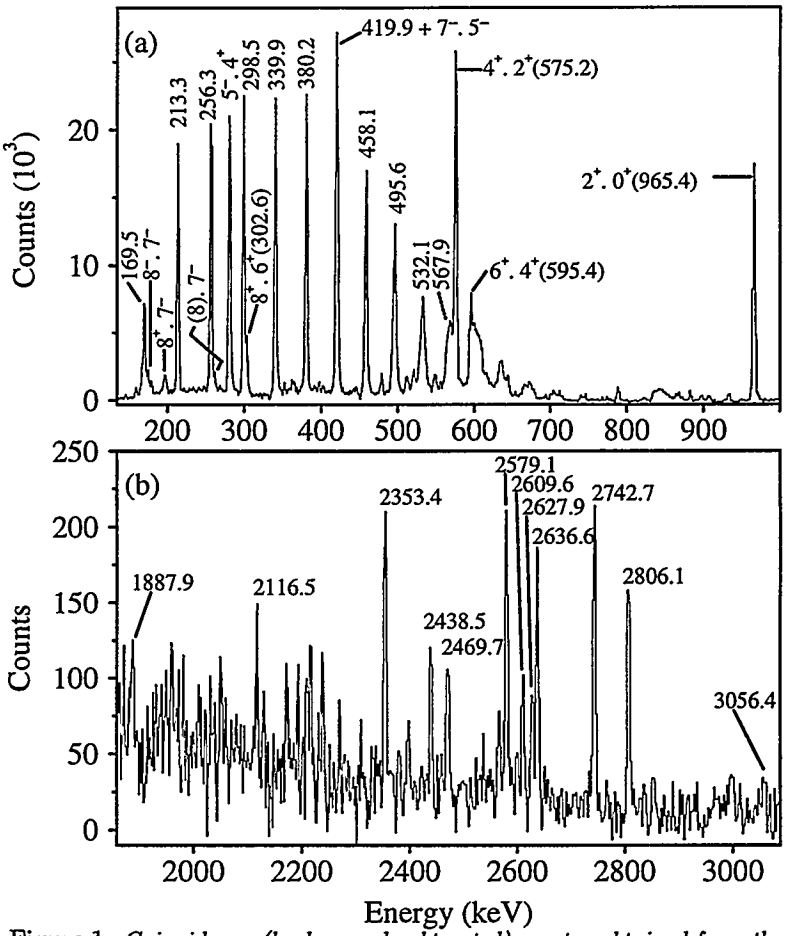


Figure 1: *Coincidence (background subtracted) spectra obtained from the singly–gated cube by summing all possible pairwise gate combinations of the 170 – 532 keV $^{194}$Pb yrast SD transitions. (Exclusion of the 419.9-keV SD-line in the gate list used to create the cube results in it's apparent increased intensity.) The low–energy portion, panel (a), displays the yrast SD band and transitions arising from de–excitation of the low–lying ND states, while (b) presents the one–step transitions (primaries) directly linking the SD and ND states. Transition energies are labeled in keV. Yrast transitions in (a) are labeled by $J_i^\pi \rightarrow J_f^\pi$.*

Table 1: *The in–band SD transitions: $\gamma$–ray energies $E_\gamma$, relative intensities $I_\gamma$[a], intensity decaying out of the band $I_{out}$, asymmetry ratio $R_{asym}$, spin and parity information $J^\pi$, and multipolarities $\sigma L$.*

| $E_\gamma$ (keV) | $I_\gamma$ (%) | $I_{out}$ (%) | $R_{asym}$ | $\sigma L$ | favored $\sigma L$ | $J_i^\pi \rightarrow J_f^\pi$ |
|---|---|---|---|---|---|---|
| 380.20(5) | 91(4) | - | 1.42(5) | $\Delta L$=1,$\Delta J$=0 or $\Delta L$=2,$\Delta J$=2 | E2 | $18^+ \rightarrow 16^+$ |
| 339.90(5) | 92(4) | - | 1.40(5) | $\Delta L$=1,$\Delta J$=0 or $\Delta L$=2,$\Delta J$=2 | E2 | $16^+ \rightarrow 14^+$ |
| 298.49(3) | 94(4) | - | 1.47(5) | $\Delta L$=1,$\Delta J$=0 or $\Delta L$=2,$\Delta J$=2 | E2 | $14^+ \rightarrow 12^+$ |
| 256.32(3) | 100(5) | - | 1.40(5) | $\Delta L$=1,$\Delta J$=0 or $\Delta L$=2,$\Delta J$=2 | E2 | $12^+ \rightarrow 10^+$ |
| 213.26(3) | 90(5) | 10(7) | 1.45(4) | $\Delta L$=1,$\Delta J$=0 or $\Delta L$=2,$\Delta J$=2 | E2 | $10^+ \rightarrow 8^+$ |
| 169.52(4) | 56(4) | 34(6) | 1.48(8) | $\Delta L$=1,$\Delta J$=0 or $\Delta L$=2,$\Delta J$=2 | E2 | $8^+ \rightarrow 6^+$ |
| - | - | 56(4) | - | - | - | - |

[a]Corrected for detector efficiency and electron internal conversion, and normalized to the intensity of the 256.3 keV transition.

Only 7 of the 12 candidate linking transitions could be placed with the adopted level scheme of $^{194}$Pb compiled by Browne and Singh [12]. A 0.67 keV/channel RadWare cube was therefore sorted to build a more complete low–lying level scheme. The resulting decay scheme (see Figure 3) is essentially that of Refs. [14] and [15] with the addition of the 664- and 672-keV transitions observed in Ref. [16]. These two transitions depopulate states with $E_x = 2800$ and 2914 keV, respectively. Also, the 283-, 479-, 722- and 788-keV transitions observed in Ref. [16] were placed at $E_x = 2525$, 2299, 2609 and 3522 keV, respectively. Additional states were added at 3471 and 3374 keV. Eleven of the twelve candidate primaries were placed with the aid of the new decay scheme of $^{194}$Pb; the placement of the 2470-keV line is tentative.

Multipolarities of the SD lines and the linking transitions were deduced from an empirical asymmetry ratio $R_{asym}$. Matrices were constructed which contained $\gamma-\gamma$ coincidences between any detector with: (1) detectors located at the three most "forward" (for) and "backward" (back) angles ($\Theta$=17.3°, 31.7°, 37.4°, and 142.6°, 148.3° and 162.7° with respect to the beam line) and, (2) detectors at $\overline{90}^\circ$ ($\Theta$=69.8°, 79.2°, 80.7°, 90.0°, 99.3°, 100.3° and 110.2° with respect to the beam line). The asymmetry ratio $R_{asym} = I_\gamma(\text{for} + \text{back})/I_\gamma(\overline{90}^\circ)$, multiplied for convenience by the ratio of the number of detectors at $\overline{90}^\circ$ to the number at forward and backward angles, was deduced for relevant $\gamma$ rays in these matrices. Mean $R_{asym}$ values of known low–lying stretched $L$=2 and $L$=1 transitions are 1.35(3) and 0.71(2), respectively. $R_{asym}$ values obtained for the SD and linking transitions are given in Tables 1 and 2, respectively. One should note that with these $R_{asym}$ ratios it is not possible to distinguish between (1) $\Delta L$=1, $\Delta J$=1 and $\Delta L$=2, $\Delta J$=0 and (2) $\Delta L$=1, $\Delta J$=0 and $\Delta L$=2, $\Delta J$=2 transitions. Nevertheless, these measurements can be used to place *restrictions* on the primary multipolarities and, since $J_f^\pi$ is known, limits on $J_i^\pi$ (see Table 2: cols. 3-6). On comparing the possible $J_i^\pi$ values deduced for each SD level from the measured linking transition anisotropies (see Table 2: col. 6), one finds that the two lowest SD can only be assigned $J^\pi = 6^+$ and $J^\pi = 8^+$, respectively. These assignments have been made without any assumptions about the SD band spin parity values. In addition, a mean value of $R_{asym} = 1.43(2)$ was measured for the intra–band SD transitions, consistent with the above $J^\pi$ assignments, confirming their $E2$ character (see Table 1).

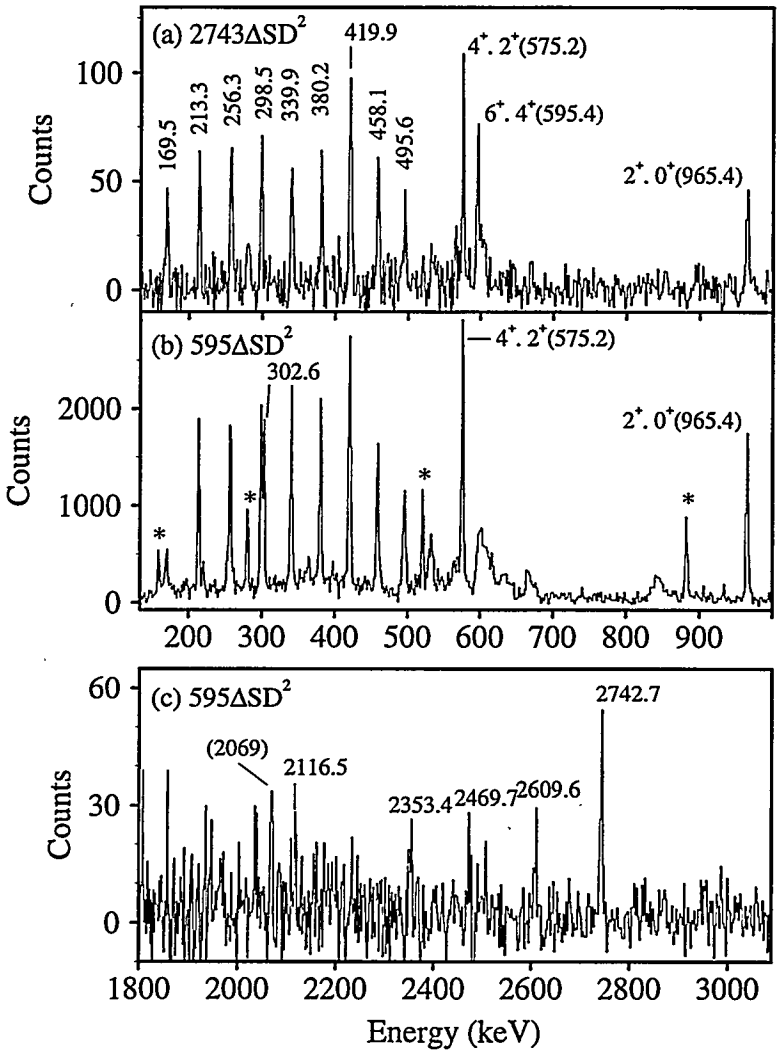


Figure 2: *Coincidence spectra projected from an SD-gated cube obtained from the summation of pairwise gates between the yrast SD band and (a) the 2743-keV transition and, (b,c) the 595-keV yrast* $6^+ \rightarrow 4^+$ *transition. An asterisk denotes a contaminant from* $^{193}$*Pb brought in by the 213⊗595 keV gate. Transition energies are labeled in keV. Yrast transitions in (a) and (b) are labeled by* $J_i^\pi \rightarrow J_f^\pi$.

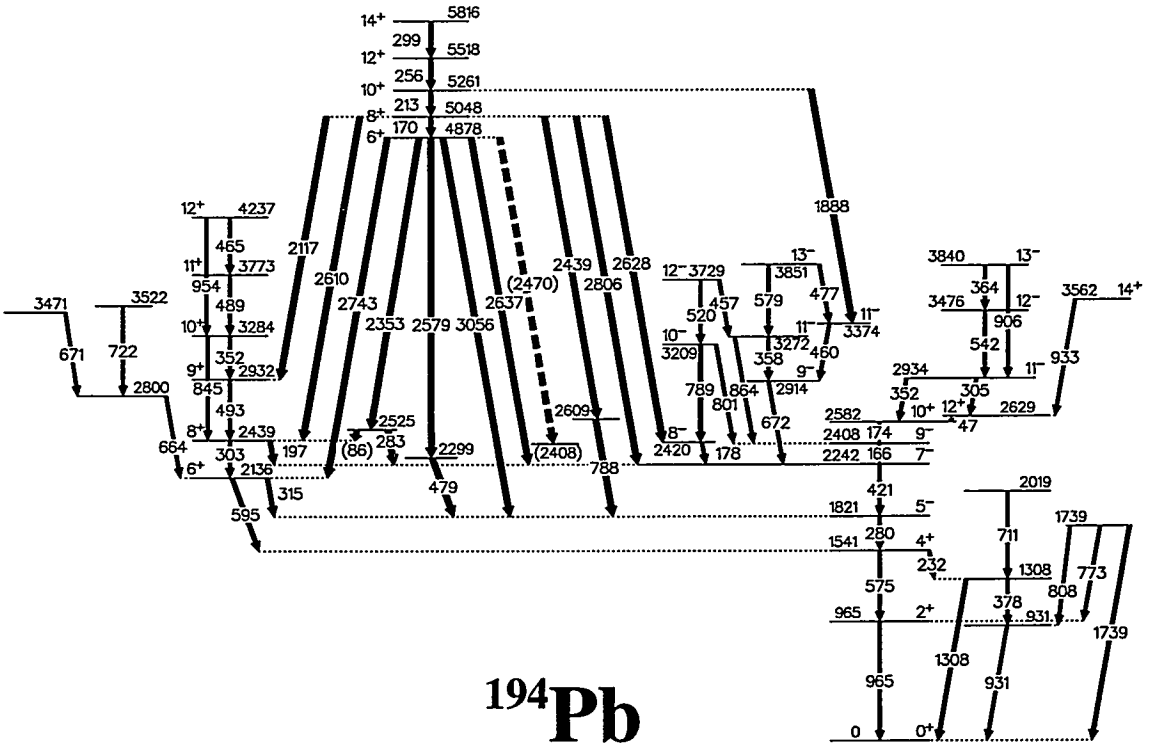


Figure 3: *Decay paths out of the $^{194}Pb$ yrast SD band. Levels are labeled by $E_x$ in keV and $J^\pi$. Transition energies are labeled in keV. For clarity, only states in the immediate $E_x$ and $J^\pi$ region of the lowest observed SD levels are shown.*

Table 2: *The primary decay data: $E_\gamma$, $I_\gamma$, data $R_{asym}$, $J^\pi$, $\sigma L$ and reduced transition probabilities $B(\sigma L)$. $I_\gamma$ is given as a percentage of the SD band population*[a].

| $E_\gamma$ (keV) | $I_\gamma$ (%) | $R_{asym}$ | $\sigma L$ | $J_f^\pi$ | $J_i^\pi$ | favored $\sigma L$ | $B(\sigma L)$ (W.U) |
|---|---|---|---|---|---|---|---|
| | | | Decays out of the third lowest SD level ($J_i^\pi = 10^+$) | | | | |
| 1887.9(3) | 1.0(4) | 0.9(1) | $\Delta L=1, \Delta J=1$ or $\Delta L=2, \Delta J=0$ | $11^-$ | $10^+, 11^-, 12^+$ | (E1) | $5(2).10^{-8}$ |
| | | | Decays out of the second lowest SD level: $J_i^\pi = 8^+$ | | | | |
| 2116.5(4) | 0.9(5) | 0.3(1) | mixed M1/E2 | $9^+$ | $8^+, 9^+, 10^+$ | M1/E2 | - |
| 2438.5(4) | 0.9(4) | 1.0(2) | mixed M1/E2 | - | - | - | - |
| 2609.6(4) | 1.7(6) | 1.4(3) | $\Delta L=1, \Delta J=0$ or $\Delta L=2, \Delta J=2$ | $8^+$ | $6^+, 8^\pm, 10^+$ | M1 | $2.3(9).10^{-6}$ |
| 2627.9(4) | 1.3(6) | 1.4(3) | $\Delta L=1, \Delta J=0$ or $\Delta L=2, \Delta J=2$ | $8^-$ | $6^-, 8^\pm, 10^-$ | E1 | $1.6(7).10^{-8}$ |
| 2806.1(3) | 1.7(5) | 0.7(1) | $\Delta L=1, \Delta J=1$ or $\Delta L=2, \Delta J=0$ | $7^-$ | $6^\pm, 7^-, 8^\pm$ | E1 | $1.7(6).10^{-8}$ |
| | | | Decays out of the lowest SD level: $J_i^\pi = 6^+$ | | | | |
| 2353.4(3) | 2.8(6) | 0.8(1) | $\Delta L=1, \Delta J=1$ or $\Delta L=2, \Delta J=0$ | - | - | - | - |
| 2469.7(4) | 1.5(6) | 1.4(3) | $\Delta L=1, \Delta J=0$ or $\Delta L=2, \Delta J=2$ | - | - | - | - |
| 2579.1(2) | 3.0(6) | 0.7(1) | $\Delta L=1, \Delta J=1$ or $\Delta L=2, \Delta J=0$ | - | - | - | - |
| 2636.6(2) | 1.8(6) | 0.8(2) | $\Delta L=1, \Delta J=1$ or $\Delta L=2, \Delta J=0$ | $7^-$ | $6^\pm, 7^-, 8^\pm$ | E1 | $\geq 12(4).10^{-8}$ |
| 2742.5(2) | 3.3(6) | 1.1(2) | mixed M1/E2 | $6^+$ | $5^+, 6^+, 7^+$ | M1 | $\geq 2.2(5).10^{-5}$ |
| 3056(1) | 0.8(5) | - | - | $5^-$ | - | E1 | $\geq 4(2).10^{-8}$ |
| TOTAL $I_\gamma = 21(2)\%$ of SD band intensity accounted for by primaries | | | | | | | |

[a]Corrected for detector efficiency and normalized to the intensity of the 256.3 keV SD line.

These results have allowed the excitation energy of the yrast $6^+$ SD state in $^{194}$Pb to be unambiguously determined; we find $E_x(6^+)_{SD} = 4878.4(3)$ keV, in agreement with [3]. Assuming a smooth extrapolation to $J = 0$ [17], the bandhead of the SD band is estimated to have $E_x \simeq 4640.7(4)$ keV. This is in very good agreement with the Hartree–Fock–Bogoliubov calculations of Krieger, *et al.* [13], which predict $E_x(0^+_{SD}) =$ 4.86 MeV. For comparison, $E_x(0^+_{SD})$ is estimated to be 6.017 MeV in $^{194}$Hg [2]. (The only other example in the $A \sim 190$ region of an SD cascade to have been unambiguously linked into the low–lying level scheme via primary transitions.) In this case, the same calculations predict the bandhead to lie at 5.00 MeV, approximately one MeV too low. Although the calculations are expected to predict the bulk properties of these nuclei very well it is not clear whether this is a significant discrepancy.

Reduced transition probabilities $B(\sigma L)$ for the primary decays have been calculated by relating the branching ratio of each primary to the in–band $B(E2)$ value assuming a constant in–band transition quadrupole moment $Q_t = 20.6(13)$ eb, derived from both Doppler Shift Attenuation [18] and Recoil Distance measurements [19]. $B(\sigma L)$ values are given in Table 2. Obtaining $B(\sigma L)$'s for the primaries depopulating the $6^+$ SD state required the following additional assumptions about the unobserved $6^+ \rightarrow 4^+$ intra–band transition. Firstly, the energy (124.6 keV) was calculated from a smooth extrapolation of known transition energies. Secondly, the intensity of this transition is estimated to be *leq*4%. The resulting transition strengths indicate that the decay out of the SD states is highly retarded – typical values were found to be $B(E1) \sim 10^{-8}$ W.u. and $B(M1) \sim 10^{-6} - 10^{-5}$W.u. Similar results were obtained for the primary decays from SD states in $^{194}$Hg as summarized in Table 3.

However, there are a number of striking differences between the character of the linking transitions observed in these two cases. From a comparison of Tables 2 and 3 it is apparent that many more primaries are observed in $^{194}$Pb – 12 compared to 4 in $^{194}$Hg. Also, in contrast to $^{194}$Hg in which only E1's have been observed, the linking transitions in $^{194}$Pb are of E1, M1 and mixed M1/E2 multipolarities. A surprisingly large proportion of the $^{194}$Pb band intensity, 21(2)%, is accounted for by the direct one–step decays. Current calculations treating the decay from SD states as a statistical process estimate the branching ratio of single–step primaries to be ~5% compared to the unresolved statistical decays [20]. Indeed, recent results in $^{194}$Hg indicate that only ~ 5% of the yrast SD band intensity is attributed to the primary decays [2]. The root cause of these differences reflects the greater phase space for decay available in $^{194}$Hg compared to $^{194}$Pb. The factors that contribute to this are: (1) The excitation energies of the SD bandheads in $^{194}$Pb and $^{194}$Hg are estimated to be 4.640 and 6.017 MeV, respectively. (2) The spin of the SD states at de–excitation is higher in $^{194}$Hg. (3) The $E_x$ of the ND states into which the primaries decay is ~2.4 and ~ 2.8 MeV for $^{194}$Pb and $^{194}$Hg , respectively. (4) ND $^{194}$Pb is singly magic, and coexisting oblate and prolate minima at low excitation energy further increases the density of ND states in $^{194}$Hg compared to $^{194}$Pb. Therefore, the greater number of final states in $^{194}$Hg leads to a more highly fragmented decay. One should also note that the decays of the shape isomers in $^{236}$U [21] and $^{238}$U [22] are also very different; the predominant $\gamma$–branches are $E1$ and $E2$, respectively. Evidently each case is different and any generalizations about the nature of the primary decays based on a singly case must be viewed cautiously.

In summary, eleven discrete one–step "primary" $\gamma$–ray transitions have been observed linking three members of the $^{194}$Pb yrast SD band to low–lying ND levels. Anisotropy measurements have determined that the primary decays include both E1 and mixed M1/E2 transitions. $J^\pi = 6^+$ $E_x = 4878.4(3)$ keV and $J^\pi = 8^+$ $E_x = 5047.8(3)$ keV have been unambiguously assigned to the two lowest lying observed superdeformed states without making assumptions about the properties of SD bands. These results represent the first self–consistent $J^\pi$ assignments to an SD band. Unique determination of the $J^\pi$ and $E_x$ values of SD bands

Table 3: *The primary decay data for* $^{194}$*Hg.* $E_\gamma$, $I_\gamma$, *and* $\sigma L$ *taken from* [2].

| $E_\gamma$ (keV) | $I_\gamma$ (%) | $\sigma L$ | $B(\sigma L)$ W.U.[a] |
|---|---|---|---|
| 3489.3 | 1.4 | E1 | $2.6(6)\times10^{-8}$ |
| 3709.6 | 0.7 | E1 | $1.1(3)\times10^{-8}$ |
| 4195.2 | 1.2 | E1 | $1.3(3)\times10^{-8}$ |
| 4485.3 | 1.5 | E1 | $1.1(3)\times10^{-7}$[b] |

[a] Assumes constant in–band $Q_t = 17.2(20)$ eb [23].

[b] Assumes $E^{SD}_\gamma(10^+ \rightarrow 8^+) = 211.7$ keV and $I^{SD}_\gamma(10^+ \rightarrow 8^+) = 3\%$ [24].

are needed to place more stringent restrictions upon theoretical calculations which predict the SD states and their properties, and in particular, to address the phenomena of "identical" bands. The yrast SD bands in $^{194}$Pb and $^{192}$Hg, and $^{194}$Hg SD(3) are examples of "identical" bands. Although unambiguous assignments to the $^{194}$Pb yrast SD band have been possible, this has unfortunately not been the case for $^{194}$Hg SD(3) [25] and $^{192}$Hg [26]. However, with the resolving power of the "complete" GAMMASPHERE and EUROBALL arrays, greater understanding of these properties is anticipated.

We would like to thank Torben Lauritsen for help with data acquisition and David Radford for RADWARE. Joanne Heagney of MicroMatter fabricated the targets. The 88–Inch Cyclotron crew is thanked for faultless operation. This work has been funded in part by the U.S. Department of Energy, under Contracts No. W-7405-ENG-48 (LLNL) and AC03-76SF00098 (LBNL), and the National Science Foundation (Rutgers and Iowa State).

# References

[1] M. J. Brinkman, *Proceedings of the Conference on Physics from Large $\gamma$–Ray Detector Arrays*, Berkeley, California, p. 242, August 1994; Phys. Rev. C **53**, R1461 (1996).

[2] T. L. Khoo *et al., Phys. Rev. Letts.* **76**, 1583 (1996).

[3] A. Lopez–Martens *et al., Phys. Lett. B* **380**, 18 (1996); *Proceedings of the Conference on Nuclear Structure at the Limits, Argonne National Laboratory, 1996 (unpublished).*

[4] I. Y. Lee, *Nucl. Phys.* **A520**, 641c (1990).

[5] D. C. Radford, *Nucl. Instr. and Methods* **A361**, 306 (1995).

[6] C. W. Beausang, D. Prevost, M. H. Bergstrom, G. deFrance, B. Haas, J. C. Lisle, Ch. Theisen, J. Timàr, P. J. Twin, and J. N. Wilson, *Nucl. Instr. and Meth.* **A364**, 560 (1995).

[7] K. Theine *et al., Z. Phys.* **A336**, 113 (1990).

[8] M. J. Brinkman *et al., Z. Phys.* **A336**, 115 (1990).

[9] H. Hübel *et al., Nucl. Phys.* **A520**, 125c (1990).

[10] W. Korten *et al., Z. Phys.* **A334**, 475 (1993).

[11] B. J. P. Gall *et al., Phys. Lett.* **B345**, 124 (1995).

[12] E. Browne and B. Singh, *submitted to Nucl. Data Sheets* (1996).

[13] S. J. Krieger, P. Bonche, M. S. Weiss, J. Meyer, H. Flocard, and P. H. Heenen, *Nucl. Phys.* **A542**, 43 (1992).

[14] D. Metha *et al., Z. Phys.* **A345**, 169 (1993).

[15] M. G. Porquet *et al., J. Phys.* **G20**, 765 (1994).

[16] P. Van Duppen, E. Coenen, K. Deneffe, M. Huyse and J. L. Wood, *Phys. Rev.* **C35**, 1861 (1987).

[17] J. A. Becker *et al., Nucl. Phys.* **A520**, 187 (1990).

[18] P. Willsau *et al., Z. Phys.* **A344** 351 (1993).

[19] R. Krücken *et al., Phys. Rev. Lett.* **73**, 3359 (1994).

[20] T. Døssing *et al., Phys. Rev. Letts.* **75**, 1276 (1995).

[21] J. Schirmer, J. Gerl, D. Habs, and D. Schwalm, *Phys. Rev. Letts.* **63**, 2196 (1989).

[22] J. Kantele, W. Stöffl, L. E. Ussery, D. J. Decman, E. A. Henry, R. J. Estep, R. W. Hoff, and L. G. Mann, *Phys. Rev.* **C29**, 1693 (1984).

[23] J. R. Hughes *et al., Phys. Rev. Lett.* **72**, 3150 (1994).

[24] M. P. Carpenter *et al., Proceedings of the Workshop on* GAMMASPHERE *Physics, Berkeley, California, 1995.*

[25] G. Hackman *et al., Proceedings of the Conference on Nuclear Structure at the Limits, Argonne National Laboratory, 1996 (unpublished).*

[26] D. Ackermann *et al., Proceedings of the Conference on Nuclear Structure at the Limits, Argonne National Laboratory, 1996 (unpublished).*

# Decay Out of the Yrast and Excited Highly-Deformed Bands in the Even-Even Nucleus $^{134}$Nd

C.M. Petrache[1], D. Bazzacco[1], S. Lunardi[1], C. Rossi Alvarez[1], R. Venturelli[1], P. Pavan[1], N.H. Medina[1], M.N. Rao[1], R. Burch[2], G. de Angelis[2], A. Gadea[2], G. Maron[2], D.R. Napoli[2], L.H. Zhu[2], R. Wyss[3]

[1] *Dipartimento di Fisica and INFN, Sezione di Padova, Padova, Italy*
[2] *INFN, Laboratori Nazionali di Legnaro, Legnaro, Italy*
[3] *Royal Institute of Technology, Physics Department Frescati, Stockholm, Sweden*

The resolving power achieved by the new generation of $\gamma$-ray detector arrays allows now to observe transitions with intensities of the order of $\sim 10^{-3}$ of the population of the final residual nucleus, making therefore feasible the study of the very weakly populated excited bands built on the superdeformed (SD) minimum or of the decay out of the SD bands. As a matter of fact, numerous excited SD bands have been observed in the different regions of superdeformation, which led to a deeper understanding of the single-particle excitation in the second minimum [1]. However, the lack of experimentally determined excitation energies, spins and parities for the SD bands prohibited to infer definitive conclusions. The first experimental breakthrough in the study of the decay out process has been achieved in the odd-even $^{133,135}$Nd nuclei of the A=130 mass region [2,3,4]. There, the observation of the discrete linking transitions has been favored by the relatively higher intensity of the highly-deformed bands ($\sim$10%), as well as by the small excitation energy with respect to the yrast line in the decay-out region ($\sim$ 1 MeV). We call highly deformed (HD) the bands built on the second well in the A=130 mass region; they have elipsoidal shapes with major to minor axis ratios of 3:2 and a smaller deformation ($\beta \sim 0.3 - 0.4$) than that of the SD bands of the A=80, 150, 190 regions ($\beta \sim 0.5 - 0.6$). Unlike the A=150, 190 nuclei, which have nearly spherical shapes in the first minimum, the A=130 nuclei are prolate ($\beta \sim 0.2$) at normal deformation (ND). The transition from low to high deformation in these nuclei requires only one or two level crossings, and therefore induces much less fragmentation of the decay-out flux than in the other regions of superdeformation [5]. Very recently, Khoo et al. [6] discovered a few linking transitions in $^{194}$Hg, which account for $\sim$ 5% of the decay-out strength. Following this first result in the A=190 region, other one step linking transitions have been observed in nuclei of the same region, which are reported in this conference. No discrete linking transitions have been so far observed in the A=80, 150 mass regions.

The HD bands in the even-even Nd nuclei are much weaker than in the odd-even ones, being of the order of 1% of the total population of the nucleus. The task to identify the discrete linking transitions is as difficult as that in the other regions of superdeformation. As a matter of fact, no linking transition have been so far observed in the even-even $^{134,136}$Nd nuclei, where HD bands have been identified [7,8,9]. The configuration assigned to these bands are based on the behavior of the dynamical moments of inertia and therefore are only tentative. The identification of discrete linking transitions, which would establish the excitation energies, spins and eventually parity of the band levels, was highly requested, in order

to discriminate between the different theoretical scenarios proposed for the configurations of the HD bands. On the other hand, the study of the decay out mechanism in an even-even Nd nucleus was expected to help, through the comparison with the odd-even ones, the understanding of the interplay between the pairing correlations and mixing between the ND and SD states in the decay-out process [10,11].

With the goal of answering to the above questions, we have undertaken a study of the decay out in the even-even nucleus $^{134}$Nd. The reaction used for populating the high spin states in $^{134}$Nd was $^{28}$Si+$^{110}$Pd at 130 MeV. The target consisted of two self-supporting foils of $^{110}$Pd with a total thickness of 1.36 mg/cm$^2$. The GASP array with 40 Compton-suppressed Ge detectors and the 80-element BGO ball has been used for a coincidence measurement. Events were accepted when at least three suppressed Ge detectors and three detectors of the BGO ball fired in coincidence. A total of $1.9\times10^9$ events have been collected.

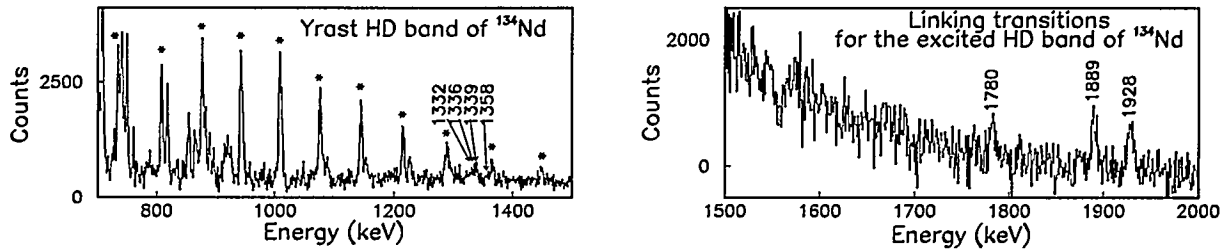


Figure 1: Left panel: doubly-gated spectrum of the yrast HD band in which the $\gamma$-rays of the HD band are indicated by asterisks. Right panel: high-energy part of the single-gated spectrum of the excited HD band.

The excited HD band has been extended at lower spins by two transitions (765.1 and 726.4 keV) and the two lowest $\gamma$-rays in the yrast HD band have been determined with higher precision (733.3 and 667.9 keV). Furthermore, transitions linking both HD bands to the ND states have been identified. Examples of spectra proving the coincidence relationships of the identified linking transitions with transitions in the HD bands and in the low-spin part of the level scheme are given in Figs. 1 and 2. A partial level scheme of $^{134}$Nd relevant for the decay-out process is given in Fig. 3.

The spectra obtained by double-gating on decay-out transitions and on transitions in the HD yrast band, shown in the left panel of Fig. 2, clearly indicate the position of the linking transitions in the decay scheme. The gate on the 1332 keV $\gamma$-ray proves that it is in coincidence with the HD band and with the 740 keV $\gamma$-ray, whereas the gates on the 1336 keV and 1339 keV $\gamma$-rays prove that they are in coincidence with the 736 keV and 733 keV $\gamma$-rays, respectively. The sum of all these three couples of transitions gives 2072 keV, firmly establishing the energy difference between the third low-lying state of the HD band and the $18^+$ state of band 3. Spectra obtained by double-gating on the decay-out transitions or on transitions of the excited HD band are shown in the right panel of Fig. 2. The gate on 726 keV $\gamma$-ray shows in coincidence only the 1889 keV high-energy transition, whereas the 765 keV $\gamma$-ray is in coincidence with all three high-energy linking transitions. The gate on the 1889 keV linking transition shows both the HD and the ND transitions. The spins of the HD states have been determined from the analysis of the DCO ratios using the procedure described e.g. in Ref. [12].

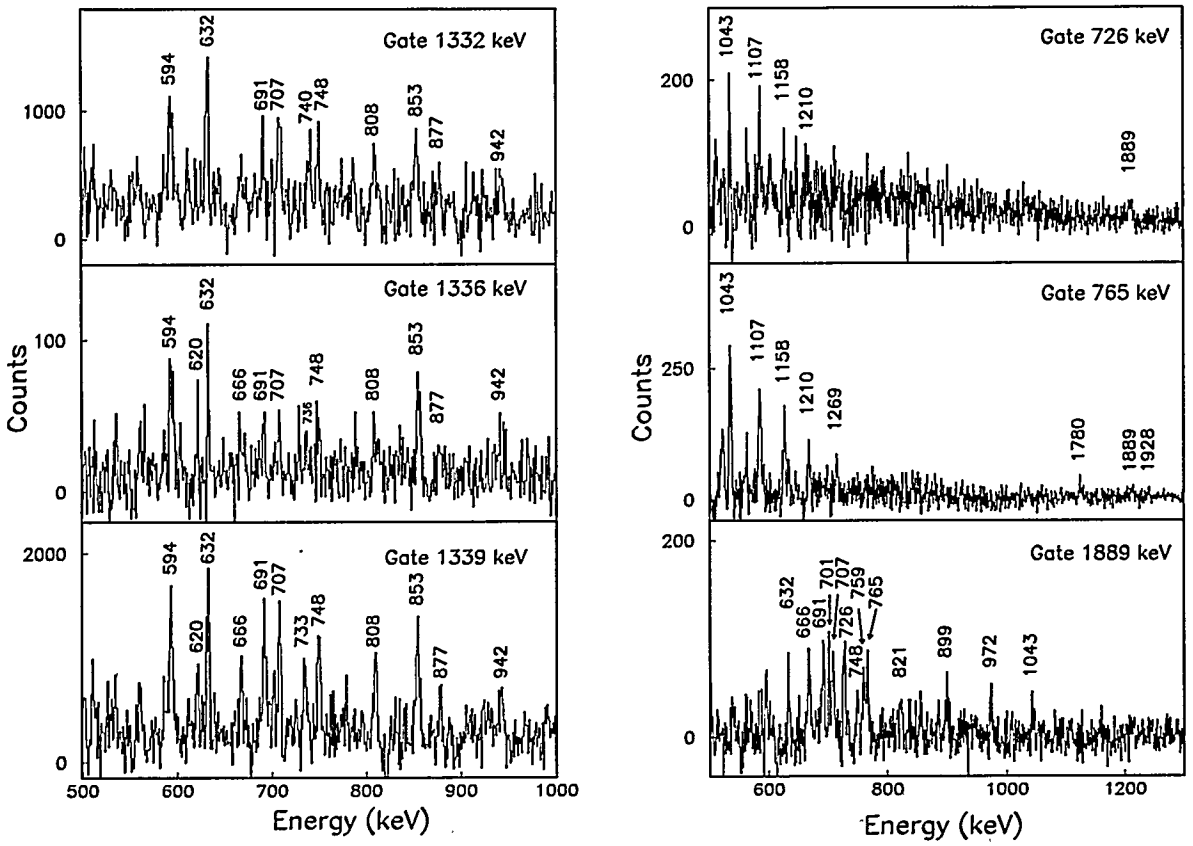


Figure 2: Left panel: doubly-gated spectra with gates on the transitions of the yrast HD band and on the 1332, 1336 and 1339 keV linking transitions. Right panel: doubly-gated spectra with gates on the transitions of the excited HD band and on the 726 and 765 keV in-band transitions and on the 1889 linking transition.

Because of the very weak intensity of the high-energy linking transitions, definite values of their DCO ratio could not be obtained. However, the linking transitions of the yrast HD band show strong 90°-34° anisotropy when gating on all in-band E2 transitions and therefore their dipole character is established. For the 736 and 740 keV $\gamma$-rays which are strongly contaminated, no DCO ratios could be obtained. They are assumed to have $\Delta$I=2, E2 character. The negative parity indicated in parenthesis for the yrast HD band accounts for the theoretically assigned configuration (see discussion below). The linking transitions of the excited HD band do not show significant anisotropy between 90° and 34°; this is consistent with a $\Delta$I=2, E2 character and leads to even spins and positive parity. The present measured energies and spins of the HD band-head levels determine their excitation energy relative to the yrast ND line in the decay-out region, which is ~1100 keV for the yrast HD band and ~1200 keV for the excited HD band.

Two different types of decay-out pathways are observed experimentally: that of the excited HD band, which most likely consists of stretched E2 transitions, and that of the yrast HD band, where the decay out proceeds via E2 and E1 transitions. For the 1780 and 1928 keV linking transitions of the excited HD band we estimated the B(E2)-strengths from the ratio between the decay-out and the in-band (726 keV) transition intensities by a simple energy scaling of the transition operators. Assuming an in-band B(E2)-strength of 400 W.u., similar to that measured for the HD band in the neighboring $^{133}$Nd nucleus [13], B(E2)-strengths

of the order of 1 W.u. are obtained for the linking transitions. Such sizable out-of-band strengths clearly indicate a spread of the ND states into the HD minimum, which leads to a significant mixing between the HD and ND states. The final 1889 keV decay-out transition de-exciting the lowest observed HD state has somewhat stronger intensity than the other linking transitions. Since the energy of the in-band transitions is decreasing in contrast to that of the out-of-band ones, the enhanced decay-out strength is indeed expected. Examining the decay out of the yrast HD band one observes that the $21^-$ state decays into three $19^-$ levels, that are within 6 keV of excitation energy. It is difficult to give an exact assignment for the additional two states. However, knowing the limited number of HD configurations and the high level density at that excitation energy, we can rather firmly conclude that their origin involves states with ND shapes. The presence of even a very small interaction will lead to a sizable mixing of the corresponding wavefunctions, a fact which is indicated by the similar de-excitation pattern of the three $19^{(-)}$ states. The analysis of the out-of-band strengths of both HD bands in $^{134}$Nd, together with the ~50% intensity of the observed discrete transitions, suggests that the decay-out mechanism in $^{134}$Nd is only partially due to the stochastic mixing between the ND and HD states as proposed by Vigezzi et al. for the A=150, 190 regions [10]. In other words, it indicates that the quantum structure of the ND bands in the region where the HD bands decay is still of importance.

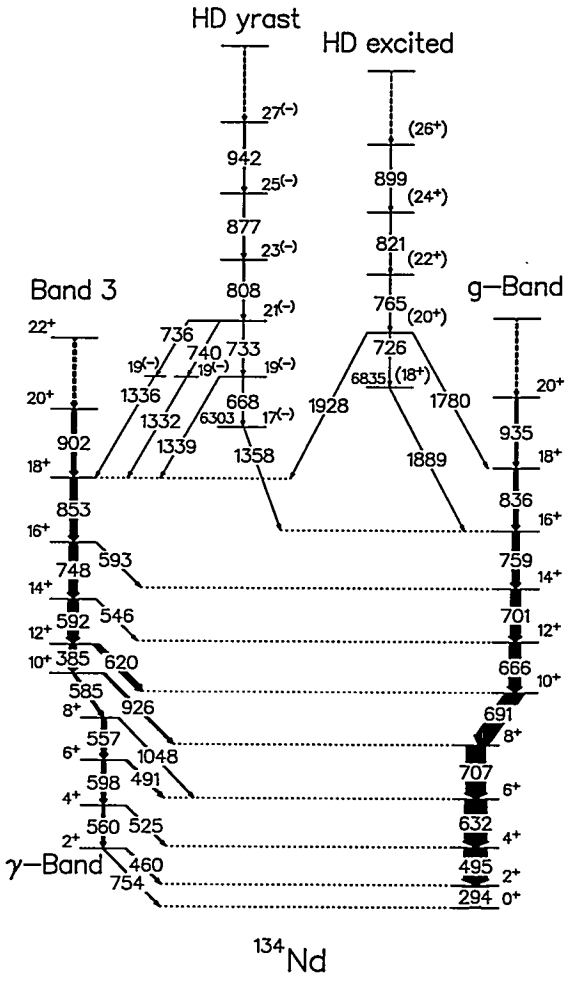


Figure 3: The level scheme of $^{134}$Nd relevant for the decay out process.

The identification of one more state in the yrast HD band below the $19^-$ level, allows to extract a value of $0.11\times10^{-6}$ $(fm^{-2})$ for the B(E1)/B(E2) ratio between the 668 keV (E2) and 1339 (E1) transitions. Assuming again a B(E2) value of 400 W.u., we get a B(E1)-strength of $\sim10^{-3}$ W.u., comparable to those observed in the heavy Ba-Sm region, for which stable octupole deformations have been predicted. Since the neutron Fermi-surface at high deformation is almost between the $f_{7/2}$ and $i_{13/2}$ orbitals and the HD yrast band of $^{134}$Nd is assumed to involve the $\nu i_{13/2}-h_{9/2}/f_{7/2}$ configuration [7], one can indeed expect octupole couplings to be present. Apparently, the enhanced deformation has a similar effect as an increase of the neutron number.

Possible configurations of the HD bands of $^{134}$Nd were already discussed in Ref. [7] in terms of occupation of the available Nilsson orbitals at high deformation. In order to interpret the present more detailed informations, we have performed new calculations for $^{134}$Nd within the cranked Strutinsky approach based on a Woods-

Saxon potential including pairing interaction [14,15]. Each configuration is treated diabatically, thus avoiding unphysical level crossings between different structures.

As established previously [7], a proton gap is present at Z=60 for deformations ranging from $\beta_2 \approx 0.20$ to 0.37, which cover the quadrupole deformations of the ND and HD states. The occupied proton orbitals do not encounter therefore any level crossing in the collective path from high to low deformation. The situation is different for neutrons, in that a pair of particles is moved from the up-sloping $[404]7/2^+$ Nilsson orbit into the down-sloping $[541]1/2^-$ one when the deformation is changing from ND to HD (see also the Fig. 3 in Ref. [7]). In addition, at least one neutron is moved from the $[402]5/2^+$ Nilsson state into the $[660]1/2^+$ ($i_{13/2}$) one. In our assignment, the excited HD band involves the $\nu i_{13/2} - [402]5/2^+$ configuration that is crossed at higher frequencies by the $\nu(i_{13/2})^2$ one, whereas the yrast HD band involves the $\nu i_{13/2} - \nu h_{9/2}/f_{7/2}$ configuration. The spins and parities indicated for the HD bands in Fig. 2 are in accord with these assignments. A more detailed discussion about the configurations of the different bands involving the neutron $i_{13/2}$ orbital can be found in Ref. [16].

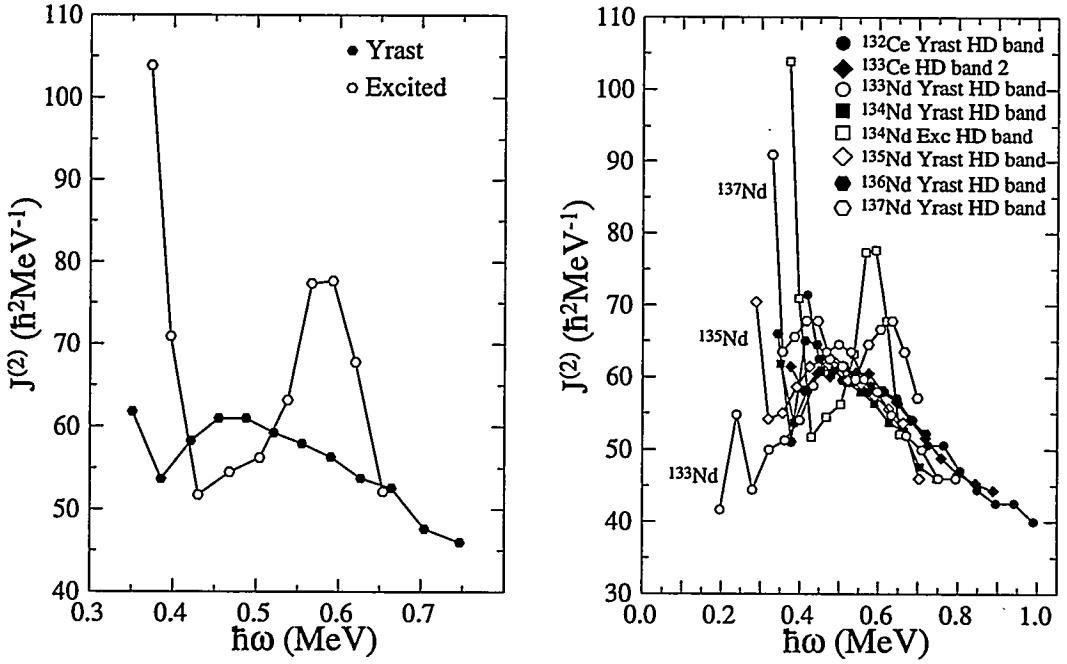


Figure 3: Left panel: dynamical moments of inertia of the yrast and excited HD bands of $^{134}$Nd. Right panel: dynamical moments of inertia of HD bands in several nuclei of the A=130 mass region.

In the decay-out region, the dynamical moments of inertia of both HD bands show an irregularity which is also observed in all HD bands of the other Nd nuclei [2,3,4,9,12] and appears at rotational frequencies which decrease with decreasing neutron number. From the present calculations, but also from an inspection of the single-particle diagram (see e.g. Fig. 3 of Ref. [7]), one can easily see that the $\nu i_{13/2}$ intruder crosses the $\nu[402]5/2^+$ ($d_{5/2}$) Nilsson orbital in the frequency region where the increase in $\mathcal{J}^{(2)}$ is observed in the HD bands of Nd nuclei. As the variation of $\mathcal{J}^{(2)}$ is always associated with a change in structure of the corresponding rotational band, we associate the observed irregularity to the crossing between the $\nu i_{13/2}$ and $\nu d_{5/2}$ orbitals. The rise in $\mathcal{J}^{(2)}$ thus corresponds to a partial de-occupation

of the strongly deformation driving $\nu i_{13/2}$ intruder orbital. When no pairing is present, the transition between the states at different deformations (which form orthogonal sets) are severely hindered, since the related operators act only on a single particle. The presence of pairing correlations, on the other hand, helps the nucleus to tunnel between the minima.

A further insight into the role played by the pairing correlations in the decay-out process can be obtained from a comparison of the decay-out pattern in the even-even nucleus $^{134}$Nd with the known decay out in the odd isotope $^{133}$Nd. There, the crossing between the N=4 and N=6 ($i_{13/2}$) neutron orbitals is actually observed, but the HD band is traced to lower spin values. The reason for this difference can be related to the lower excitation energy of the $\nu i_{13/2}$ band in $^{133}$Nd: in fact, the crossing here occurs when the HD band is rather cold and this explains why it continues at lower spins. In the case of $^{134}$Nd the HD structures involve two-quasiparticle (qp) excitations that lie higher in energy with respect to the ground state, because of the pair gap. Moreover, the pairing correlations are smaller in the two-qp HD bands of $^{134}$Nd than in the one-qp HD band of $^{133}$Nd. As the decay out occurs at similar excitation energies above yrast in both HD nuclei, we can conclude that the mixing with the ND states plays a more important role than the sliding via the pairing interaction. In all cases however, static pair gaps are calculated to exist and pairing is believed to be essential for the decay towards the ND states.

In conclusion, the present results suggest that the decay out of the HD bands in $^{134}$Nd is triggered by the crossing with the N=4 $[402]5/2^+$ Nilsson orbital, that has a smaller deformation than the corresponding N=6 intruder configuration. The crossing favours the mixing with the ND rotational bands strongly enhancing the decay-out process and weakening the in-band transition strength. The HD band becomes fragmented and looses part of its character. The intensity of the decay-out transitions increases when the spin of the HD state decreases, indicating enhanced ND amplitude in the wavefunction when going down the band. Lifetime measurements of the HD bands are crucial to further elucidate the decay-out process.

**References**


[1] W. Nazarewicz, R. Wyss and A. Johnsson, Nucl. Phys. **A503**, 285 (1989).
[2] E.M. Beck et al., Phys. Rev. Lett. **58**, 2182 (1987).
[3] M.A. Deleplanque et al., Phys. Rev. **C52**, R2302 (1995).
[4] D. Bazzacco et al., Phys. Lett. **B309**, 235 (1993).
[5] J. Dudek et al., Phys. Rev. **C38**, 940 (1988).
[6] T.L. Khoo et al., Phys. Rev. Lett. **76**, 1583 (1996).
[7] C.M. Petrache et al., Phys. Lett. **B335**, 307 (1994).
[8] R.M. Clark et al., Phys. Lett. **B343**, 59 (1995).
[9] C.M. Petrache et al., Phys. Lett. **B373**, 275 (1996).
[10] E. Vigezzi, R.A. Broglia and T. Døssing, Phys. Lett. **B249**, 163 (1990).
[11] T. Døssing et al., Phys. Rev. Lett. **75**, 1276 (1995).
[12] S. Lunardi et al., Phys. Rev. **C52**, R6 (1995).
[13] S.A. Forbes et al., Z. Phys. **A352**, 15 (1995).
[14] R. Wyss et al., Phys. Lett. **B215**, 211 (1988).
[15] W. Satuła and R. Wyss, Phys. Scr. **T56**, 159 (1995).
[16] C.M. Petrache et al., Phys. Lett. **B**, in press.

# Search for Linking Transitions in $^{143}$Eu

F. Lerma, D.R. LaFosse, M. Devlin, D.G. Sarantites
Chemistry Department, Washington University, Saint Louis, MO 63130

S. Asztalos, R.M. Clark, P. Fallon, I.Y. Lee, A.O. Macchiavelli, R.W. Macleod
Lawrence Berkeley National Laboratory, Berkeley, CA 94720

C. Baktash, M.J. Brinkman, D. Rudolph
Oak Ridge National Laboratory, Oak Ridge, TN 37831

August 23, 1996

**Abstract**

Six SD bands were populated in $^{143}$Eu and $^{144}$Eu, two of which had not been previously observed. Sum spectra were generated to search for two step links from the yrast SD band in $^{143}$Eu. However, no two step links were found. A single link from the SD band in $^{143}$Eu was found at 3364 keV. The level where it feeds into has not been identified. Alpha-particle energy ($E_\alpha$) spectra leading to the SD band and to normal states in $^{143}$Eu were measured and a correlation was found between $E_\alpha$ and the level spin of the residual nucleus.

## 1 Experimental

An experiment was performed at the 88-inch Cyclotron at Lawrence Berkeley National Laboratory. A 230-MeV beam of $^{51}$V and a $^{100}$Mo 328$\mu$g/cm$^2$ self-supporting target were used to induce the $^{100}$Mo($^{51}$V,$\alpha xn$) reaction, populating high-spin states in $^{143}$Eu and $^{144}$Eu. The Gammasphere array, which consisted of 57 Compton-suppressed high purity Ge detectors, was used to detect the gamma-rays emitted by the residual nuclei. The charged particles emitted by the compound nuclei were detected by the Microball, a $4\pi$ array consisting of 95 CsI(Tl) scintillators. The Microball allowed for good identification of the $\alpha$ particles as well as determination of $\alpha$–particle energies. A total of $4.3\times10^8$ $\alpha$–gated events were selected, 67% of which were 4-fold Ge-coincidences, the remaining events being 5-fold and higher Ge-coincidences. Partial recoil momentum correction was applied using the measured $\alpha$–particle energies. This led to a more accurate Doppler shift correction which improved the $\gamma$–ray energy resolution.

## 2 Six SD Bands Identified

Six superdeformed (SD) bands were identified in the data. Three of them have been previously identified and assigned to $^{144}$Eu [1]. Another SD band in the data is the known yrast SD band in $^{143}$Eu [2]. The other two SD bands had not been observed before; one of these was assigned to $^{143}$Eu, the other to $^{144}$Eu. The new SD band in $^{144}$Eu has identical transitions to those in the known SD band [2] in $^{143}$Eu above 1 MeV $\gamma$–ray energies (see Fig. 1).

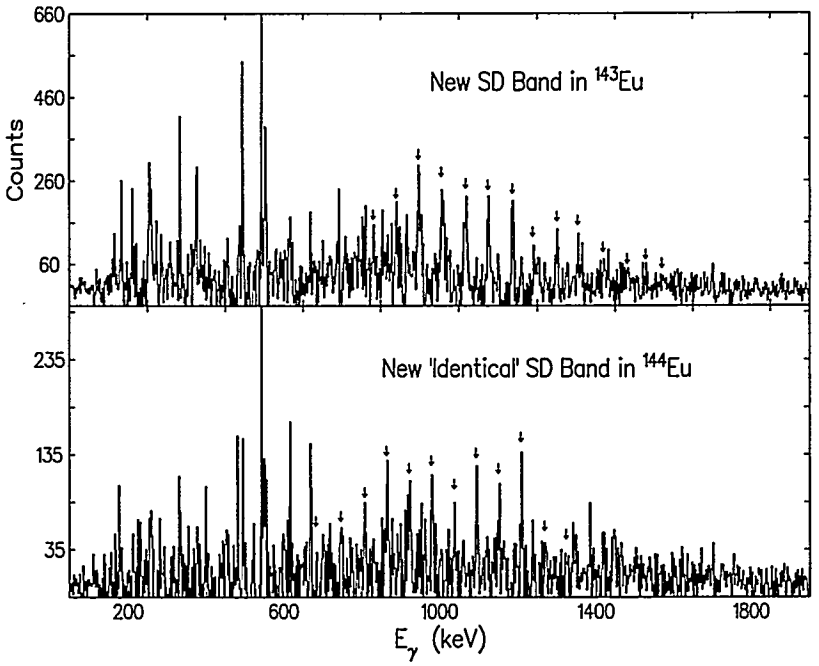


Figure 1: Double gated coincidence spectra of the two new SD bands in $^{143}$Eu and $^{144}$Eu. The arrows point to the transitions in the SD bands.

## 3 Linking Transitions

An attempt was made to link the yrast SD band in $^{143}$Eu to the normal deformed (ND) states in the $^{143}$Eu decay scheme by one-transition and two-transition links (see Ref. [2] for level scheme). A nucleus which decays out from an SD state to an ND state by a cascade of two discrete transitions may have many intermediate levels due to the high level density available, but the sums of the energies involved in a two step link must be sharply defined. The sums of pairs of $\gamma$−ray energies in coincidence with the SD band were generated in order to identify such links, and confirm previously reported [2] two step links in $^{143}$Eu.

The sum spectra were created using two different methods. First, the events were gated from a list of SD transition energies; when a $\gamma$ ray was found to be inside one of the gates, the remaining $\gamma$ rays in the event were added pair-wise, and the sums incremented into a sum spectrum. This analysis was performed in a spike-free manner, as described in Ref. [3]. Not all of the available pairs of $E_\gamma$ were incremented into sum spectra. $E_\gamma$ pairs were incremented if the difference in $E_\gamma$ was less than 1 MeV, and if both $E_\gamma$ were greater than 300 keV. These criteria were employed in single, double, and triple gating of the data. The spectra produced in this first method were not background subtracted. Background subtracted n-fold-gated sum spectra were obtained by subtracting a portion of the (n-1)-fold-gated sum spectrum from the n-fold-gated sum spectrum. A portion of a sum spectrum of the ungated data became the zero-fold-gated sum spectrum subtracted from the singly-gated sum spectrum.

In the second approach, the data were single, double, and triple gated with a list of SD transitions into spike-free [3] $E_\gamma$−$E_\gamma$ matrices. The matrices were background subtracted via the Palameta-Waddington method [4]. Individual ($E_i$, $E_j$) pairs were extracted from the background subtracted matrices and their sums were incremented into sum spectra, yielding single, double,

and triple gated background subtracted sum spectra. This method of background subtraction was successful in the 2-fold, and 3-fold gating, however, the single gated sum spectrum displayed an under-subtracted background. The background in the single gated matrix was therefore subtracted

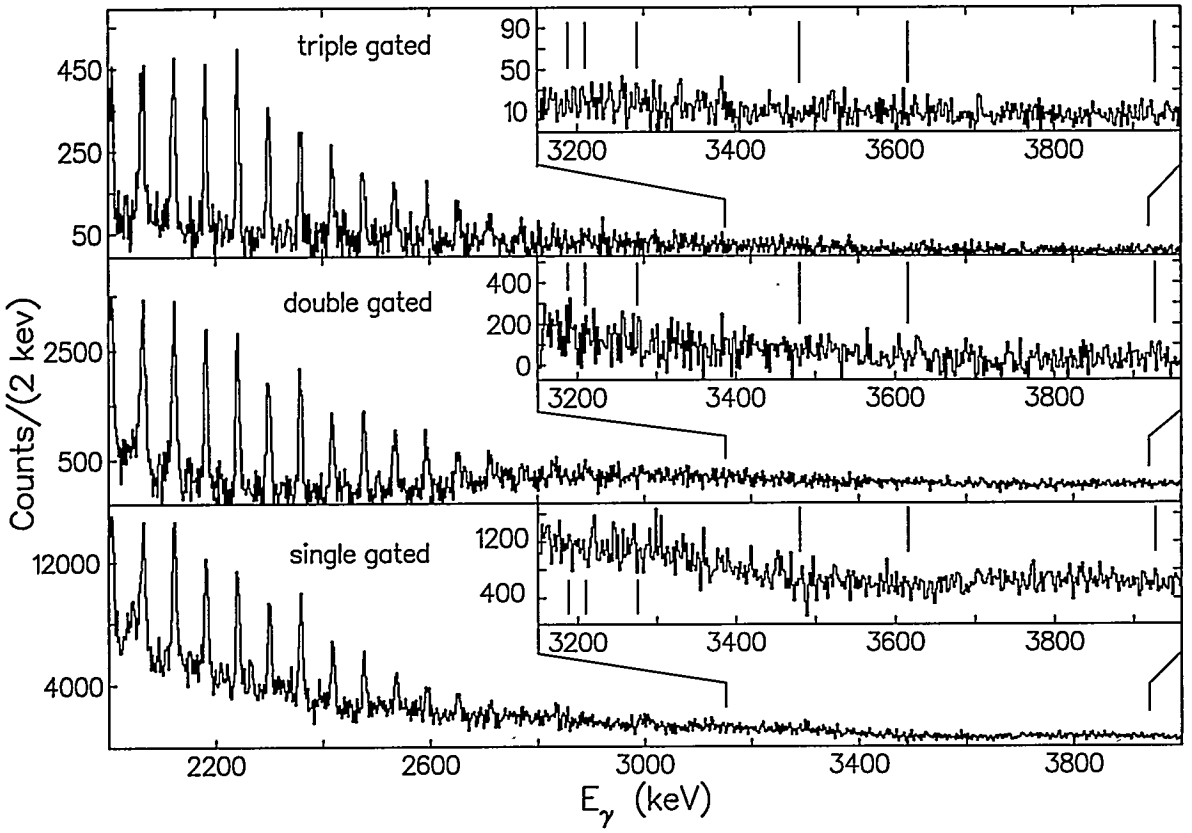


Figure 2: Spectra of the sums of individual ($E_i$,$E_j$) pairs from the backgound subtracted single, double, and triple gated matrices. The gates used were transitions in the yrast SD band in $^{143}$Eu. Vertical lines in the expanded inserts show the energies of previously reported sum peaks.

by another method [5]. A background $E_\gamma$–$E_\gamma$ matrix was sorted by single gating the data on $E_\gamma$ which did not include SD band transition energies or any strong $^{143}$Eu transitions. This background $E_\gamma$–$E_\gamma$ matrix was subtracted from an SD single gated matrix. The resultant matrix was further background subtracted according to Ref. [4]. The single gated sum spectrum was extracted from this final matrix.

All sum spectra displayed large peaks corresponding to the sums of transitions in the SD band (see Fig. 2). A description of the pairing and summing details explains why these large peaks arise. If an event has met the gating conditions, it is more likely that the remaining $\gamma$ rays in the event will also correspond to members of the SD band. The transitions in the SD band are evenly spaced at intervals of 59 keV to 61 keV, so that several combinations of pairs of transitions in the SD band will sum to the same peak in the sum spectrum, enhancing the intensity of the sums of transitions in the SD band.

The sum spectra generated by either method do not display the previously reported peaks [2]. There are some peak-like features in other regions of the spectra above 3 MeV which are not sums of transitions in the SD band, nor sums of transitions in the ND level scheme, and do not correspond to the previously reported sum links. The origin of these features in the sum spectra is not clear.

These features may be statistical fluctuations in the spectra. If these features were real sum links then they should appear at the same energies in all the fold spectra, yet most of them do not appear in more than one of the sum spectra, and no sum spectrum contained all of these peaks. As a result, the sum spectra do not seem to contain well-defined sum links. This does not imply that a significant fraction of the SD band does not decay out in two step links. The evidence suggests, however, that there are not strong two step links in $^{143}$Eu, and if a significant fraction of the SD band does feed out by two step links then it may feed out through many weak, two step links which are unobservable in a sum spectrum at the available level of sensitivity.

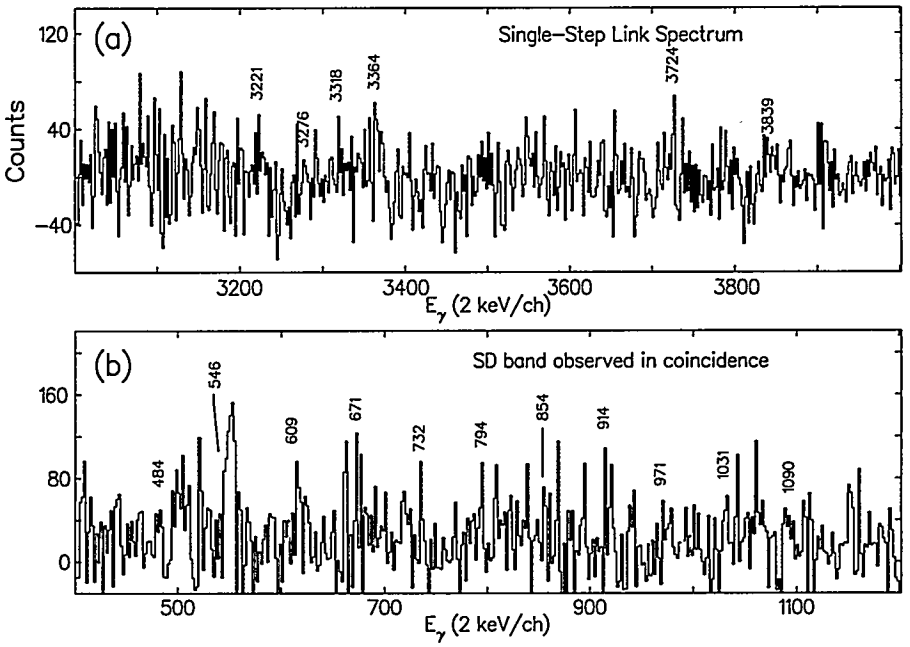


Figure 3: A sum of double gates on transitions in the yrast SD band produces the single-step transition link in panel (a). Transitions in the SD band are observed in the spectrum in panel (b) when the single gated matrix is gated on the 3364 keV single-step link.

The same $E_\gamma - E_\gamma$ matrices, and $E_\gamma - E_\gamma - E_\gamma$ cubes were employed to investigate the transitions in the decay schemes of $^{143}$Eu and $^{144}$Eu. Several SD bands were identified, and the feeding-out of the yrast SD band in $^{143}$Eu was studied. One single step linking transition was conclusively identified in $^{143}$Eu. The linking transition was observed when a single gated matrix was gated on members of the SD band [see Fig. 3(a)]. The energy of the linking transition was found to be 3364±2 keV. This same transition could be observed in spectra generated by gating on the double and triple gated matrices, and double gating the cube. There were three other potential links around 3.5 MeV which could be in coincidence with the SD band. The coincidence of the 3364 keV peak with the SD band was confirmed when a gate at 3364 keV was paired with a list of SD transition gates into double gates, and the double gates were added, producing a spectrum which contained transitions in the SD band [see Fig. 3(b)]. Similar spectra were generated using the other three transitions in place of the 3364 keV gate, but the SD band did not appear in the spectra. So far, double gating directly on the 3364 keV transition in combination with the SD band has produced spectra with too few counts to help in determining the level into which the 3364 keV transition feeds.

# 4 Alpha-Particle Energy Spectra

In order to shed some light on the entry state regions responsible for the population of the SD states one can use $\alpha$–particle spectra as a probe. If the SD states preferentially originate from high (E*,I) entry states, then downward shifts in the $E_\alpha$ spectra are expected due to reduced available phase space.

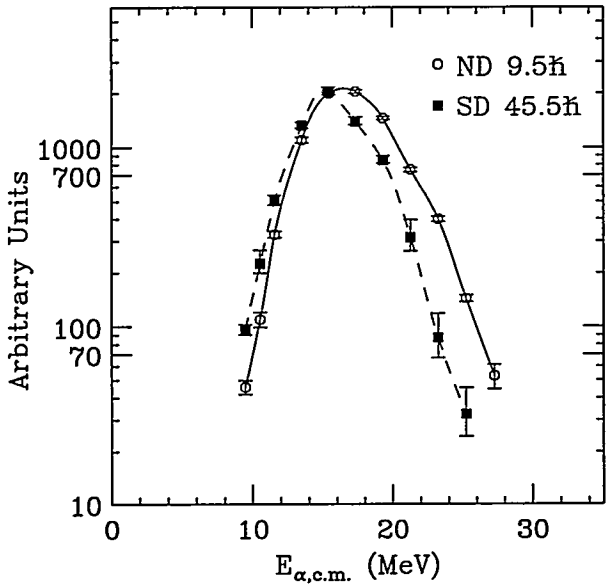


Figure 4: Alpha-particle energy spectra by doubly gating on transitions in the decay of $^{143}$Eu. The spins corresponding to the depopulated levels by the measured $\gamma$ transitions are indicated.

Alpha-particle energy spectra in coincidence with several ND transitions and SD transitions of $^{143}$Eu were produced. The data were gated on $E_\alpha$, in 2 MeV bins. A separate $E_\gamma$–$E_\gamma$–$E_\gamma$ cube was then sorted from each $E_\alpha$ bin. Each cube was doubly gated on a list of transitions in the yrast SD band in $^{143}$Eu to produce an $E_\alpha$–$E_\gamma$–$E_\gamma$–gated $\gamma$ spectrum. Additional spectra in coincidence with ND transitions were also produced by gating on ND transitions in $^{143}$Eu. Background was subtracted from these spectra using standard methods [6]. The intensities of non-gated SD transitions were measured in the spectra gated on the SD band. Similarly, the intensities of non-gated ND transitions were measured in the spectra gated on ND transitions. This procedure was performed for all of the $E_\alpha$–gated cubes, resulting in spectra representing the intensity of the transitions as a function of $E_\alpha$. In all cases the second gating transitions were lower in the level scheme than the measured transition. Two such spectra coincident with the 443-keV (19/2 level) and 1266-keV (91/2 level) transitions from the ND and SD cascades, respectively, are shown in Fig. 4. A large downward shift in the $\alpha$ spectrum is indeed observed when the SD band is fed. A similar shift was seen in the $\alpha$ spectra for the SD band in $^{150}$Tb [7].

In addition, the average $\alpha$–particle energy showed a clear decrease in $< E_\alpha >$ with increasing spin of the populated level. This trend includes both ND ans SD levels and it is shown in Fig. 5.

Furthermore, the present data allowed a measurement of the relative population of the SD band as a function of $E_\alpha$. It was found that the relative intensity of the SD band at $E_\alpha$ = 9.5 MeV was approximately 10 times higher than the relative population at $E_\alpha$ =25.5 MeV. The top 3 transitions in the SD band were identifiable only in the lower $E_\alpha$–gated $\gamma$ spectra, and were not observed in coincidence with higher energy $\alpha$ particles.

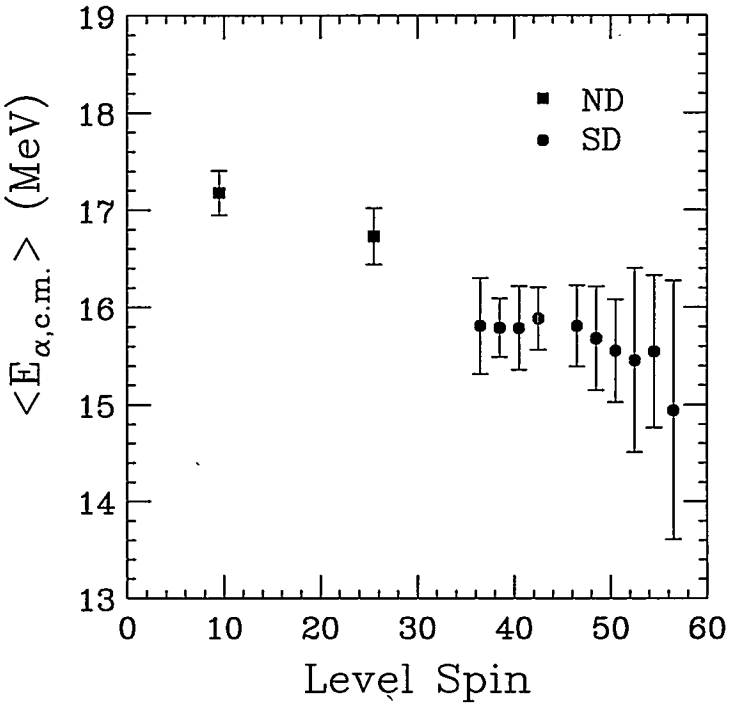


Figure 5: Average $\alpha$−particle energy as a function of spin of the level ( ND shown by full squares and SD by full circles) populated in $^{143}$Eu.

## 5 Conclusion

An experiment was performed to study high-spin states in $^{143,144}$Eu. Six SD bands were identified in the data, two of which had not been previously observed. A search for linking transitions revealed that there is a single link from the yrast SD band in $^{143}$Eu to the ND states. However, this transition could not be placed definitively in the level scheme. In addition an analysis of sum spectra was performed. Previously reported sum-links were not observed in our data. There was also no evidence for other sum-links. A correlation has been observed between evaporated particle energies and the population of high spin states of $^{143}$Eu in the $^{100}$Mo($^{51}$V, $\alpha$4n) reaction. It was also found that the SD band was populated at the highest relative intensity and highest spin when the data were gated on the lower $\alpha$−particle energies.

Work supported in part by the U.S. Department of Energy under grant number DE FG05-88ER40406.

## References

[1] S.M.Mullins *et al.*, to be published.
[2] A. Ataç *et al.*, Phys. Rev. Lett., **70**, 1069, (1993).
[3] C.W. Beausang *et al.*, Nucl. Instrum. Meth. Phys. Res., **A 364**, 560 (1995).
[4] G. Palameta and J.C.Waddington, Nucl. Instrum. Meth. Phys. Res.**A 234**, 476 (1985).
[5] J.C.Waddington, private communication (1996).
[6] D.C.Radford, Nucl. Instrum. Meth. Phys. Res., **A 361,** 297 (1995).
[7] G.Viesti *et al.*, Phys. Lett. **B 382,** 24 (1996).

# Single-Step Linking Transition from Superdeformed to Spherical States in $^{143}$Eu

**A. Ataç[1], A. Axelsson[1], I. Bearden[2], M. Bergström[2], B. Herskind[2], J. Nyberg[3], M. Palacz[4,5], J. Persson[1], M. Piiparinen[6], C. Fahlander[3], G. Hagemann[2],S. Leoni[2], M. Lipoglavšek[1,7], P. Nolan[8], E. Paul[8], N. Redon[9], L. Roos[1], G. Sletten[2], K. Tuček[3]**

[1] Department of Radiation Sciences, Uppsala University, Uppsala, Sweden
[2] The Niels Bohr Institute, University of Copenhagen, Copenhagen, Denmark
[3] The Svedberg Laboratory, Uppsala University, Uppsala, Sweden
[4] Soltan Institute for Nuclear Studies, Swierk, Poland
[5] Physics Department, Royal Institute of Technology, Stockholm, Sweden
[6] Department of Physics, University of Jyväskylä, Jyväskylä, Finland
[7] J. Stefan Institute, Ljubljana, Slovenia
[8] Oliver Lodge Laboratory, University of Liverpool, Liverpool, U.K.
[9] Institut de Physique Nucléaire, IN2P3-CNRS and Université Lyon-1, France

**Abstract:** A discrete $\gamma$-ray transition which connects the second lowest SD state with a normally deformed one in $^{143}$Eu has been discovered. It has an energy of 3360.6 keV and carries 3.2 % of the full intensity of the SD band. It feeds into a nearly spherical state which is above the I = $35/2^+$, $E_x$=4947 keV level. The exact placement of the single-step link could, however, not be established due to the especially complicated level scheme in the region of interest. The angular correlation study favours a stretched dipole character for the 3360.6 keV transition. The single-step link agrees well with the previously determined two-step links, both with respect to energy and spin.

The linking transitions between the SD bands and the normally deformed (ND) states have been one of the greatest challenges in the study of superdeformation. Identification of the linking transitions not only gives the spins, excitation energies and parities of the SD bands but also provides valuable information on the decay mechanism itself and the structure of the nucleus in the transition region. From a theoretical point of view [1], the deexcitation of an SD band occurs due to small admixtures with the ND states. The SD state is embedded in a sea of hot ND states and it decays statistically by $\gamma$-ray emission. In the mass 150 and 190 regions the SD bands lie at high energies and the deexcitation pattern is expected to be governed by multi-step transitions, although it has now been proven in the mass 190 region [2,3,4] and in $^{143}$Eu [5] that single-step transitions do occur.

Recently, with modern Ge arrays it has been possible to identify single-step linking transitions and to localize the SD bands in a few nuclei in the mass 130 [6] and 190 regions. The situation is, however, more complicated for the $^{143}$Eu nucleus. The lowest SD states in this nucleus lie higher in energy above the yrast line as compared to the mass 130 region and they have a higher spin as compared to the mass 190 region.

One possible way of studying the linking transitions is to assume that a significant fraction of the decay goes via cascades of two $\gamma$-ray transitions (two-step link) and to search for the corresponding discrete sums of the two $\gamma$-ray energies. In an earlier paper [7] several discrete sum energies were identified in $^{143}$Eu and the lowest SD state was proposed to be at I=35/2, $E_x$=8582 keV.

The present experiment was carried out in Strasbourg using the EUROGAM II array [8]. Excited

states in $^{143}$Eu were populated in the reaction $^{110}$Pd($^{37}$Cl,4n)$^{143}$Eu with a beam energy of 160 MeV. The $^{110}$Pd target was enriched to 98.9% and consisted of three thin foils with a total thickness of 1.1 mg/cm$^2$. With a trigger requirement of seven or more $\gamma$ rays in prompt coincidence (before Compton suppression) a total of $1.8\times10^9$ Compton-suppressed events with an average fold of 4.4 were collected. A much compressed version of the data set was stored on magnetic hard disks for fast access and sorting. A short experiment by using a 1.1 mg/cm$^2$ layer of $^{110}$Pd sputtered onto a 10 mg/cm$^2$ Au backing was also carried out at the end of the main experiment. With a trigger requirement of six or more $\gamma$ rays in prompt coincidence a total of $2.2\times10^8$ Compton-suppressed events were collected. The aim of the backed target experiment was to improve the ND level scheme.

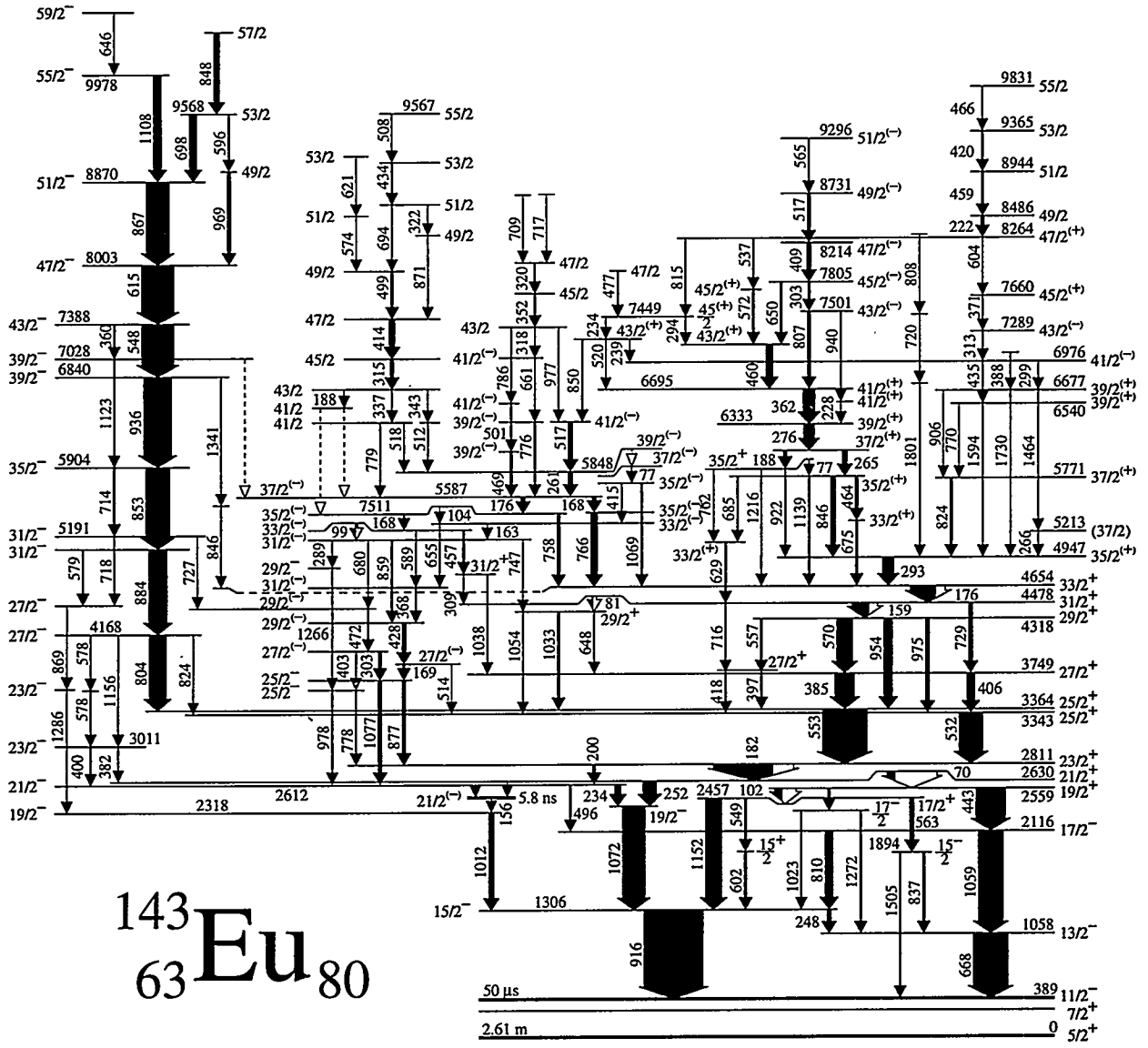


Fig. 1 : Level scheme of $^{143}$Eu basically taken from ref. [9] and slightly modified. The widths of the arrows are proportional to the intensities observed in the $^{110}$Pd($^{37}$Cl,4n)$^{143}$Eu reaction at 160 MeV.

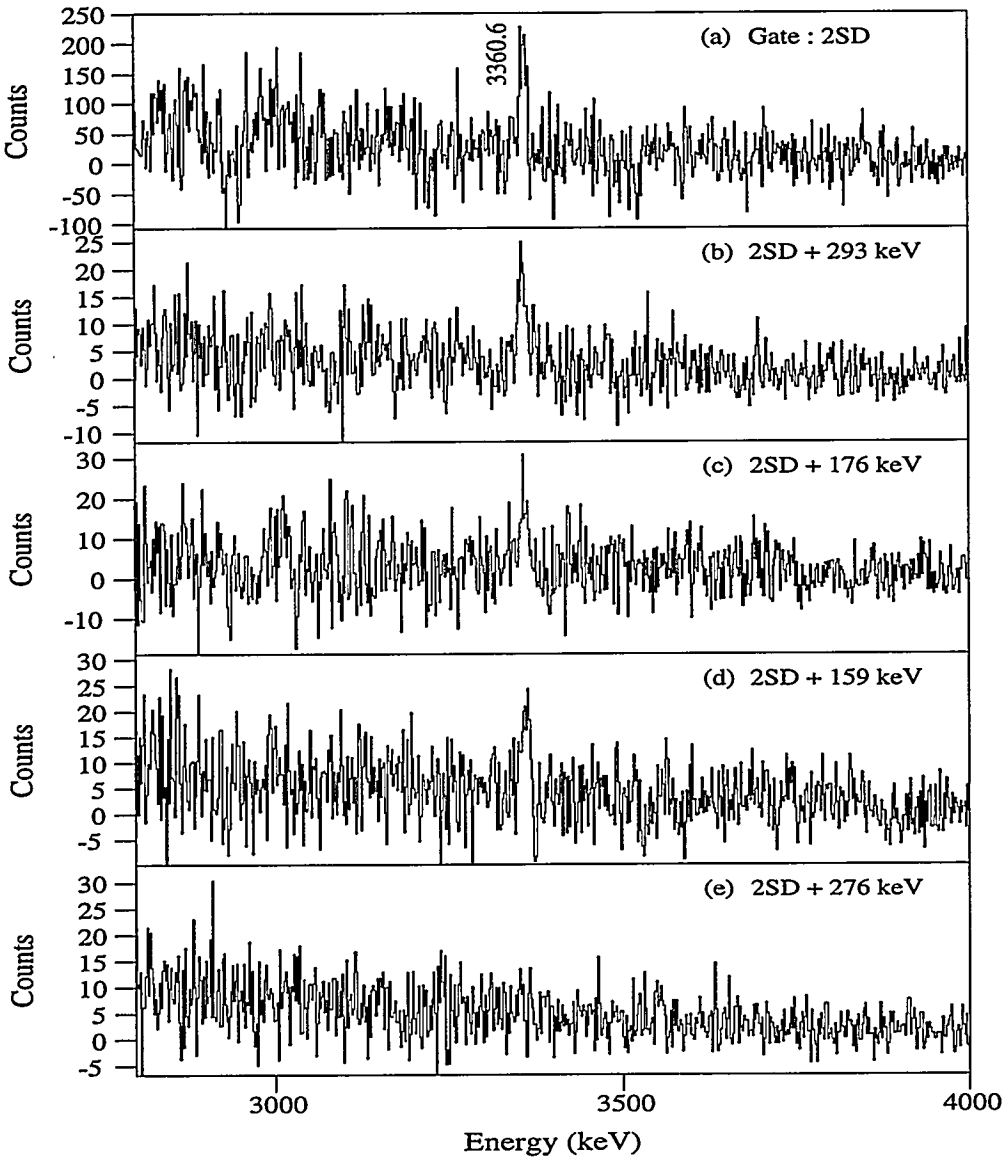


Fig. 2 : The high energy part of a $\gamma$-ray spectrum (a) coincident with three SD band members. All 22 SD transitions were used to gate on in order to increase the statistics and a portion of the total projection was subtracted as the background. The transition observed at 3360.6 $\pm$ 0.7 keV with a FWHM of 10.1 keV is proposed to be a single-step linking transition. The lower spectra have two gates on the cleanest SD transitions and a gate on the 159 keV (b), 176 keV (c), 293 keV (d) and 276 keV (e) lines in the ND level scheme.

Fig. 1 shows the level scheme of $^{143}$Eu. It is basically taken from ref. [9] and modified using the current data set. The irregular and very complex structure of the level scheme at low spins is typical of a nearly spherical, slightly oblate nucleus. A sequence of collective states starting from I = 27/2, $E_x$ = 4.2 MeV and forming a triaxially deformed band is also observed coexisting with the spherical states. A study of the triple or quadruple gated spectra shows that the SD yrast band feeds into the spherical near-yrast states bypassing the triaxial states which lie about 1 MeV above the yrast states in the feeding region. This result is also confirmed by a recent study [10] of the

quasicontinuum of the SD transitions in this nucleus.

Fig. 2a shows the high energy part of a $\gamma$-ray spectrum. It is double gated on the 22 transitions [7] of the SD band in $^{143}$Eu. The peak at 3360.6(7) keV is observed at a 5.5 $\sigma$ level and is identified as a one-step link to a ND state since it is in coincidence with the SD band and some of the ND states. The 3360.6 keV line represents 3.2 % of the total intensity in the SD band.

Once a single-step linking transition is observed, it is a big challenge to localize it by determining the SD state it comes from and the ND level it feeds into. The SD state from which the 3360.6 keV transition deexcites was investigated in double gated spectra where one gate was set on one of the three lowest transitions in the SD band, namely the 483, 547 or 609 keV transitions and the second gate was set on one of the few clean, higher lying transitions in the band (fig.3). The two spectra with gates at 483 and 609 keV are relatively clean. There is, however, a strong 548 keV transition lower in the ND level scheme (triaxial band) making the 547 gate specially difficult. Therefore it is important to select carefully the cleanest gate combinations especially for this case. The result is that the 3360.6 keV transition is seen in the spectra gated by the 609 and 547 keV transitions whereas it disappears in the spectrum gated by the 483 keV transition. Therefore we propose that the 3360.6 keV linking transition depopulates the SD state just below the 547 keV transition, i.e. the second lowest state of the SD band.

Fig. 4 shows the low energy part of a triple gated spectrum. It has two gates on the cleanest transitions in the SD band and a gate on the 3360.6 keV high energy line. The 159, 176 and 293 keV transitions are in a cascade in the ND level scheme and the 293 keV transition lies highest in excitation energy. The 3360.6 keV line is also clearly seen in the spectra gated on these lines (see fig. 2 b, c, d). The 182 keV transition deexcites a $23/2^+$, 2813 keV state and it collects nearly all the intensity coming from above. The intensities of the strongest peaks of fig. 4 were determined and corrected for internal conversion. Normalizing to the strength of the 182 keV transition, the 159 and 176 keV transitions carry 93 % and 92 % of the intensity, respectively, while the intensity of the 293 keV transition is only 38 %. Thus, we conclude that the 3360.6 keV transition does not directly populate the $35/2^{(+)}$, 4947 keV state from which the 293 keV transition decays. It rather populates a higher energy level which partially decays into the 4947 keV level and partially down to the $33/2^+$, 4654 keV level from which the 176 keV transition decays.

Fig. 2e shows that the 3360.6 keV transition is not in coincidence with the 276 keV transition indicating that it either feeds into a level which has a lower energy than the $39/2^+$, 6333 keV state or it selects a parallel branch feeding into the $35/2^{(+)}$, 4947 keV level. Above $E_x$=4947 keV, the level scheme of $^{143}$Eu is particularly complicated and the decay paths feeding into this state are fragmented making it difficult to locate the linking transition. An identification of a few other single-step links would be of great help for reaching more conclusive results.

An angular correlation study of the 3360.6 keV line gives a value of R = 1.0(2) where R is the ratio between $\gamma$ rays detected by the tapered and clover detectors located at an average angle of 38.4° and 75.5° respectively, relative to the beam axis. This ratio is 0.85(2) for the known E1 transition at 252 keV [9] and 1.59(7) for the 1443 keV E2 transition in the SD band. Thus, the 3360.6 keV transition is either a stretched dipole transition or it can be a mixed E2/M1 transition with $\Delta I$ = 0 or 1. A pure statistical decay would, however, favour an E1 transition.

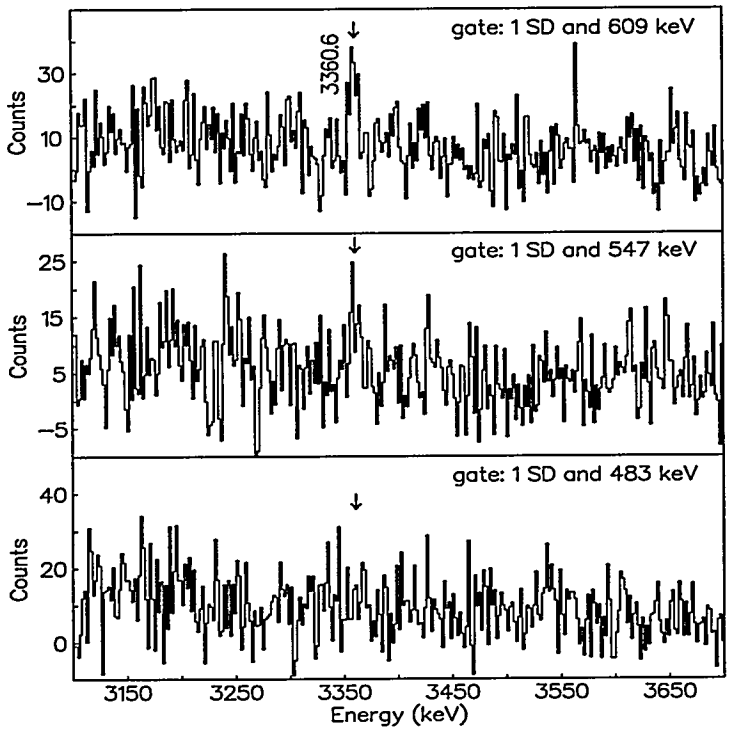


Fig. 3 : Double gated $\gamma$-ray spectrum where one gate is set on one of the three lowest SD transitions (a) 483 keV, (b) 547 keV and (c) 609 keV and the second gate is set on one of the few clean, higher lying transitions in the band.

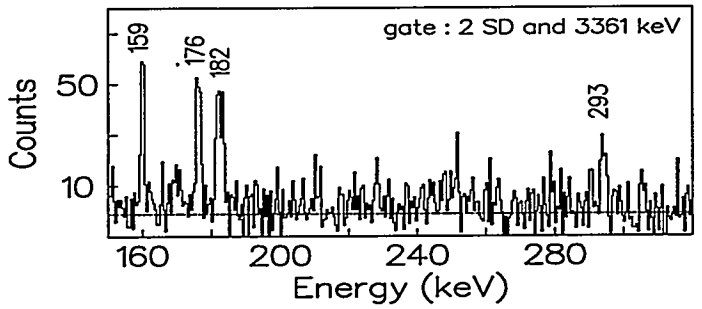


Fig. 4 : The low energy part of a triple gated spectrum which has two gates on the cleanest transitions between the SD states and a gate on the 3360.6 keV high energy line. A portion of the total projection is subtracted as background and the spectrum is corrected for the relative detector efficiencies.

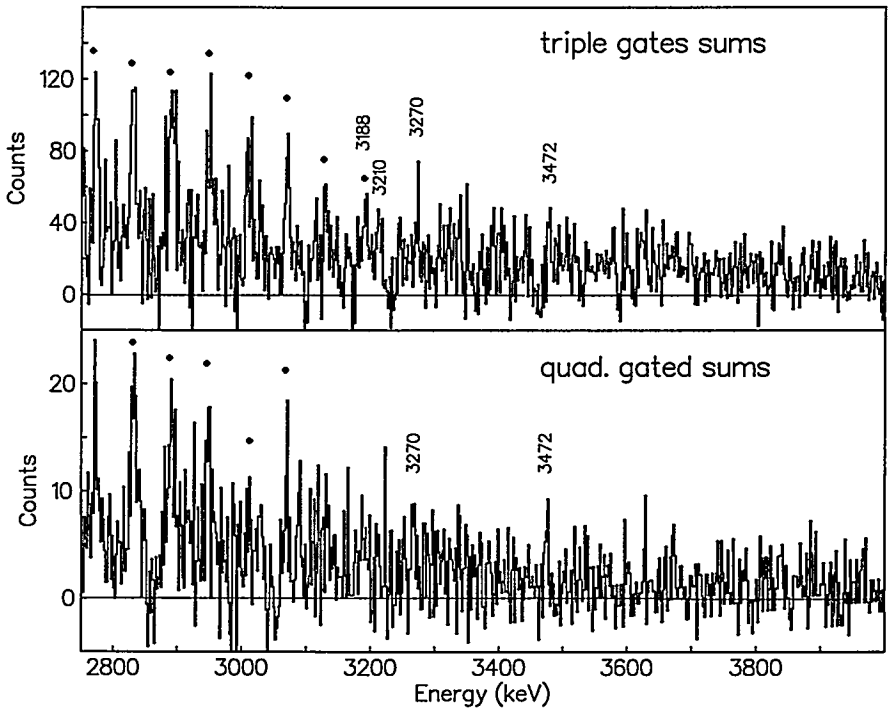


Fig. 5 : The energy sum of two $\gamma$-ray transitions which are in coincidence with the SD band members. It is obtained by adding 15 clean gates and is background subtracted. The sums of two transitions which are in the SD band are shown by (•)'s.

The single-step link has an energy which agrees very well with the sum energies identified as two-step links in the previous work [7], where energies between 3187-3925 keV were reported. It also feeds into the same region of the ND level scheme as the two-step links. Furthermore, four out of six sum peaks reported earlier, namely the 3188, 3210, 3270 and 3472 keV transitions, are observed in this experiment at a 2-4 $\sigma$ level, see fig. 5. Their energies agree with the earlier results within the error limits of 4-5 keV.

**References:**

1) E. Vigezzi et al., *Phys. Lett. B*249 (1990) 163.
2) T. L. Khoo et al., *Phys. Rev. Lett.* 76 (1996) 1583.
3) A. Lopez-Martens et al., *Phys. Lett. B* 380 (1996) 18.
4) M.J. Brinkman et al., *Phys. Rev. C*53 (1996) R1461.
5) A. Ataç et al., *Z. Phys.*, in press.
6) S. Lunardi et al., *Phys. Rev. C*52 (1995) R1 and M. Deleplanque et al., *Phys. Rev. C*52 (1995) R2302.
7) A. Ataç et al., *Phys. Rev. Lett.* 70 (1993) 1069.
8) P.J. Nolan et al., *Annu. Rev. Nucl. Part. Sci.* 45 (1994) 561.
9) M. Piiparinen et al., *Nucl. Phys. A*605 (1996) 191.
10) S. Leoni et al., *Phys. Rev. Lett.* 76 (1996) 3281.

# The Quasi-Continuum of Gamma Rays Following the Decay of Superdeformed Bands in the Hg Region

T. Lauritsen[a], A. Lopez-Martens[b], T.L. Khoo[a], R.V.F. Janssens[a], M.P. Carpenter[a], G. Hackman[a], D. Ackermann[a], I. Ahmad[a], H. Amro[a,c], D.J. Blumenthal[a], S.M. Fischer[a], F. Hannachi[b], A. Korichi[b], E.F. Moore[c] and D.T. Nisius[a].

[a] *Argonne National Laboratory, Argonne, Illinois 60439, USA.* [b] *Centre de Spectrométrie Nucléaire et de Spectrométrie de masse, IN2P3-CNRS, bat 104-108, F-91405 Orsay, France and Institut de Physique Nucléaire, F-91406, Orsay Cedex, France.* [c] *North Carolina state University, Raleigh, North Carolina 27695, USA*

The quasi-continuum part of the spectrum associated with the decay-out of the yrast superdeformed band in $^{194}$Hg has been extracted. It has for the first time been possible to compare the spin and excitation energy determined from the analysis of the quasi-continuum $\gamma$ rays to the exact result obtained from the one-step linking transitions.

## INTRODUCTION

About 175 superdeformed (SD) bands have by now been found in the A=80,150 and 190 mass regions; yet only a few of these have been firmly linked to the normal deformed (ND) states they decay into. Thus, fundamental quantities such as *spin, parity* and *excitation energy* have not been experimentally determined for the vast majority of the SD bands. In order to address issues of great recent interest such as: [i] the presence of identical SD bands, [ii] the magnitude of shell corrections at large deformation, [iii] the mechanisms responsible for the sudden decay-out of the SD bands, [iv] the description of pairing and level densities in the SD well, some or all of those quantities must be determined for as many SD bands as possible.

Recently, one-step decays out of the yrast SD bands in $^{194}$Hg and $^{194}$Pb have been reported [1,2]. One-step decays allow for an unambiguous determination of the spin, parity and excitation energy of the states in a SD band. However, the intensity of these special decay branches is only a fraction of that of the SD band itself, and most of the decay proceeds through a quasi-continuum (QC) of $\gamma$ rays. Moreover, the strength of one-step decays varies considerably from nucleus to nucleus and may be subject to Porter-Thomas fluctuations. Therefore, it may not always be possible to observe one or two-step decays – even when data of very good statistics are available. In such cases, the analysis of the QC provides an alternative way to determine the spin and energy of the SD bands, provided that the analysis methods are proven to be reliable.

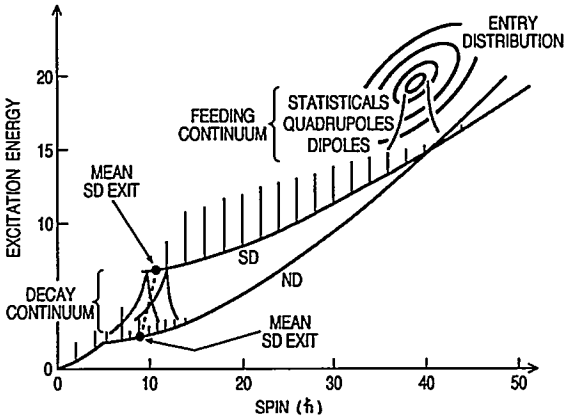


FIG. 1. Schematic diagram of the feeding and decay of SD bands. Gamma emission starts from the entry distribution. After emission of statistical, quadrupole and M1/E2 dipole QC $\gamma$ rays, the deexcitation cascades are trapped either in the ND or SD wells, where discrete gamma rays are emitted. If a $\gamma$ cascade is trapped in the SD well, QC $\gamma$ rays are also emitted when the SD band decays into the ND states.

A schematic diagram of the feeding and decay of a SD band in figure 1 shows that there are two components to the QC: [i] one associated with the feeding of the SD states and [ii] the other originating from the decay towards the yrast states [3]. A simple way to assess where the decay QC $\gamma$ rays are located is to compare coincidence spectra gated on ND and SD transitions. Only the spectra gated on SD $\gamma$ rays should have the 'extra' QC component from the decay-out to ND states at or near the yrast line. Such a comparison for $^{194}$Hg is given in figure 2 (with the discrete peaks left in the spectrum). It is clearly seen in the figure that extra strength is present in the SD gated spectrum above 1 MeV - exactly where the $\gamma$ rays from a statistical decay of the levels at the bottom of the SD band are expected [4]. The spectrum has close similarities with that reported earlier for $^{192}$Hg [3]. In particular, as in the latter nucleus, the excess strength above 1 MeV is ascribed to the decay out of the SD band.

Differences below 1 MeV are also seen in figure 2, but those have to do with the different paths the nucleus takes in the feeding of the ND and SD bands.

In the feeding of the yrast SD band, about six $\gamma$ rays of stretched E2 character are emitted while the nucleus decays through excited, damped SD bands [5]. A pronounced 'E2-bump' is therefore seen in the SD gated spectrum (and it should result in ridges in coincidence matrices). On the other hand, the cascades feeding the ND bands involve less collective states and, as a result, the E2-bump associated with this decay mode is much smaller.

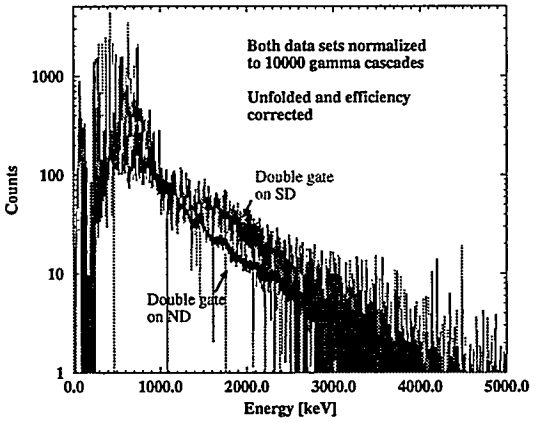


FIG. 2. Comparison of ND and SD gated coincidence spectra in $^{194}$Hg. The spectrum gated on the the SD band shows additional strength above 1 MeV from the QC $\gamma$ rays associated with the decay of the SD band to ND states.

By extracting the QC $\gamma$ rays in coincidence with the SD band, it is possible to deduce both the spin and energy of the SD band at the point of decay. When the QC intensity is normalized to the number of $\gamma$ cascades, the area of the spectrum determines the average multiplicity, i.e., the number of $\gamma$ rays involved in the decay. Similarly, the mean energy of the decay-out QC determines the average energy removed by these $\gamma$ rays. Thus, by simple multiplication of these two quantities, the mean energy removed by the QC is established. It is likewise possible to determine the average amount of spin removed by the $\gamma$ rays.

From the intensities, spins and energies of the ND transitions in coincidence with the SD band, the average spin and energy corresponding to the entry into the ND states can be derived (see figure 1). By vectorially adding the spin and energy removed by the QC to the mean ND entry-point, the *mean SD exit-point* can be found. From this information the spins and energies of the SD band levels can be deduced, once the branching ratios between in-band and out-of-band decay are taken into account for the lower SD states.

## THE EXPERIMENT

The SD band in $^{194}$Hg was populated using the reaction $^{150}$Nd($^{48}$Ca,4n). The beam, delivered by the 88" cyclotron at LBNL, had an energy of 202 MeV. A total of $1.9\times10^9$ quadruple or higher fold coincidence events was collected with GAMMASPHERE, which at the time comprised 85 detectors. The target consisted of a 1.2 mg/cm$^2$ $^{150}$Nd layer evaporated on a thick Au backing, which ensured that all $\gamma$ rays associated with the decay-out of the SD band would not be subject to any Doppler shift.

## THE EXTRACTION OF THE QC

In order to extract the QC $\gamma$ rays from the total spectrum, the data must be processed carefully in a number of steps. Double coincidence gates were placed on SD transitions in order to obtain SD spectra almost free of contaminant coincidences, yet with sufficient statistics for an angle sort. Only 9 of 36 possible double gate combinations were deemed clean enough for use in this analysis. (Triple gating would have provided even cleaner spectra; but the statistics in the angle sort would have been marginal.) Correct background subtraction of the double–gated spectra is vital. The FUL method [6] developed at ANL was used to subtract background-background and peak-background contributions. The data was also sorted according to the prescription in [7] in order to avoid 'spikes' in the gated spectra. In addition, any lines left in the spectra as a result of contaminant coincidences (despite careful selection of gates) were identified, characterized and subtracted.

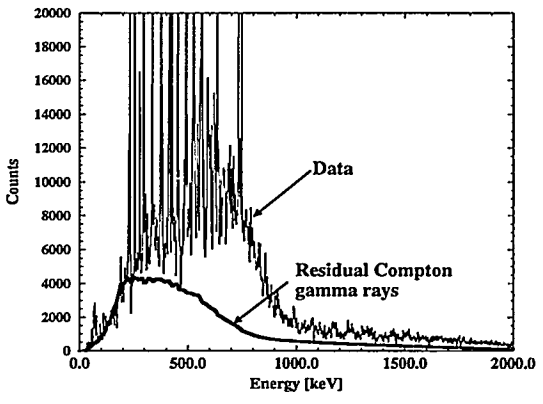


FIG. 3. Residual Compton events in a typical spectrum. The figure shows a gated spectrum before unfolding and the lower solid curve shows the residual Compton events subtracted by the procedure described in [7], using a measured response function for GAMMASPHERE.

The angle sorted spectra were corrected for the response of the GAMMASPHERE array in successive steps described below. First the contributions due to true coincidence summing was removed following a prescription by Radford [8]. The $\gamma$ rays generated from neutron interactions in the Ge detectors (mostly in the forward direction) were subtracted next. This contribution is small (2-3%) and has very little impact in the energy region of the decay-out $\gamma$ rays. A more significant correction is the removal of the Compton events in the spectra . Even with efficient BGO shields, about 1/2 of all Compton events is not suppressed and to extract the true QC, it is necessary to subtract these unwanted $\gamma$ rays.

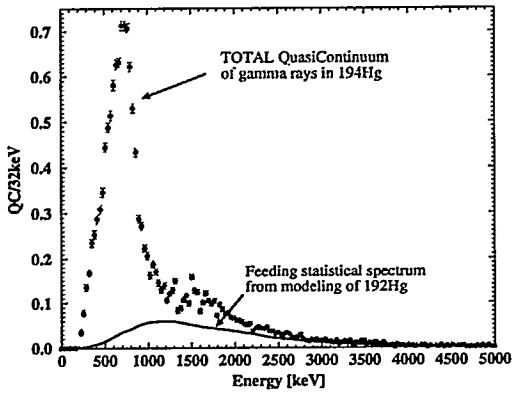


FIG. 4. The total QC after discrete peaks have been removed and the spectra contracted to 32 keV/ch. Also shown is the calculated statistical spectrum from $^{192}$Hg.

By measuring the spectra from single-line and two-line coincidence sources placed at the target position, the response function of GAMMASPHERE was carefully measured. Using the unfolding procedure described in [8], which interpolates between the response-measurement at discrete energies, the residual Compton $\gamma$ rays for the entire spectrum were deduced and subtracted. Figure 3 shows a typical spectrum before the unfolding, together with the residual events left in the spectrum despite Compton suppression (lower curve). It is clearly seen that the procedure by Radford works well, even in the low energy region where it is most difficult to unfold.

Next, the spectra were corrected for detector efficiency, the discrete $\gamma$ rays were removed and the spectra were contracted to 32keV/ch. The remaining QC $\gamma$ rays consist of the three feeding QC components, i.e., [i]statistical, [ii]quadrupole and [iii]dipole transitions from the last step in the feeding [3]. The fourth QC component is the sought-after decay-out spectrum which will be extracted by subtracting the feeding statistical and quadrupole components.

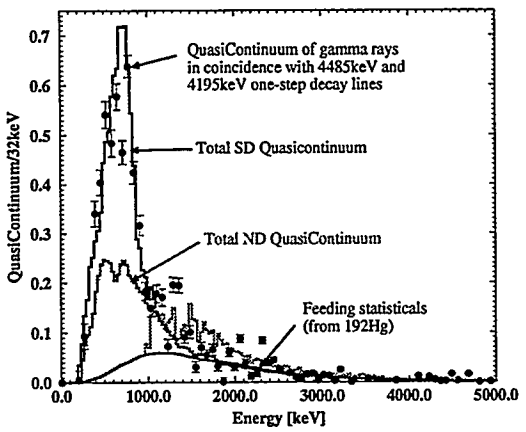


FIG. 5. The QC $\gamma$ rays obtained from double gates placed on the one-step decay-out lines and SD lines in $^{194}$Hg (data with error bars). Also shown are the total SD and ND QC spectra and the calculated statistical spectrum from $^{192}$Hg.

Finally, the QC spectra are normalized so that the area of the $2^+ \longrightarrow 0^+$ ground-state transition in the spectrum is unity, after corrections for internal conversion, angular distribution and changes to the intensity due to isomers have been taken into account. After this normalization, it follows that any area is equal to multiplicity, since the spectrum represents an average $\gamma$ cascade. Figure 4 shows the total QC spectrum corrected for angular distribution effects ('A0' spectrum).

## THE STATISTICAL FEEDING COMPONENT

In reference [5], the statistical spectrum feeding the SD band in $^{192}$Hg was calculated using as input the experimentally measured entry states distribution. This statistical spectrum is also expected to be applicable in the case of $^{194}$Hg. Because the one-step decay lines have been observed in this nucleus [1], it is possible to confirm experimentally this hypothesis by extracting the QC in coincidence with the one-step decay-out lines. This spectrum should *not* contain the decay QC and thus, at higher energies, it should follow the calculated statistical spectrum rather than the total QC.

The sum of coincidence spectra, with double coincidence gates placed on the one-step decay-out $\gamma$ rays and the SD lines, has been corrected for the response of GAMMASPHERE. It is presented in figure 5 overlaid with the total QC spectrum and the calculated statistical spectrum. Despite low statistics, the agreement between this spectrum and that obtained with double gates on SD lines is very good over the 'E2-bump' region, although there appears

to be some contaminant lines just above 1 MeV. At higher energies, the data are seen to follow the statistical spectrum, thus justifying our hypothesis. It should be noticed that the QC spectrum gated on ND transitions also follows the calculated statistical spectrum at higher energies, again suggesting that the calculated statistical spectrum from $^{192}$Hg can be used in $^{194}$Hg. The calculated statistical spectrum is subtracted from the total QC spectrum shown in figure 4, thus eliminating one of the four QC components.

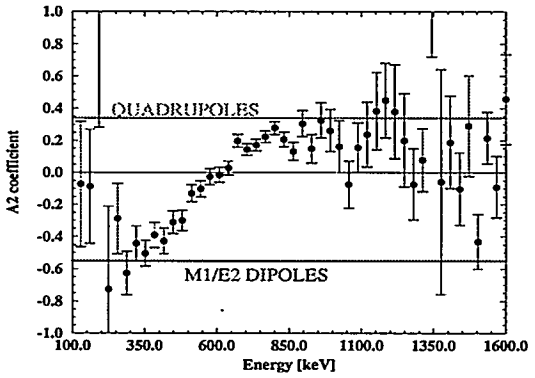


FIG. 6. Angular distribution coefficients, channel by channel, for the QC after the statistical $\gamma$ rays have been subtracted.

## THE QUADRUPOLE FEEDING COMPONENT

After the statistical spectrum has been subtracted, the A2 angular distribution coefficient of the remainder of the spectrum can be found channel by channel: the result is shown in figure 6. If the coefficient is close to the calculated E2 limit of $\approx +0.34$, the QC content of the channel is assumed to be of pure E2 character. Conversely, if the coefficient is close to the large negative value of the M1/E2 dipole transitions, $\approx$ -0.55 , the channel content is taken to be of pure M1/E2 dipole character. (In the analysis, it is assumed that there is no remaining E1 strength in the spectrum up to $\approx$1MeV following the subtraction of the statistical spectrum). For A2 coefficients with values between those extremes, the counts in the channels are split proportionally between the two contributions. In this way, the E2 QC-component was extracted. The QC quadrupole $\gamma$ rays are emitted early in the $\gamma$ cascade, while the nucleus is is still in flight, with a velocity close to the maximum recoil velocity. Hence, the A2 angular distribution analysis is performed on spectra transformed into the center of mass system, and the E2 QC component is subtracted from the spectra of each detector ring after corrections for Doppler shift, angular distribution and relativistic aberration.

## SPIN AND ENERGY OF THE SD BAND

After both the statistical and quadrupole components from the feeding have been subtracted, the remaining spectrum still consists of the M1/E2 feeding $\gamma$ rays and the sought after QC decay-out $\gamma$ rays. There are clear indications of two components in fig. 7. The low energy component has large negative A2 coefficients (indicating M1/E2 nature) and the upper component resembles the 'extra' strength shown earlier in the SD-ND gate comparison in figures 2. Thus, the upper component ($\approx$1MeV and higher) is assigned to the decay out process as it was in reference [3] for the case of $^{192}$Hg.

The mean energy of this decay-out component is 1.8(1) MeV and its area, equal to multiplicity, is 2.3(2). Therefore, it immediately follows that this QC of $\gamma$ rays removes 4.1(4) MeV of energy. From Monte Carlo simulations [5] of a statistical decay at the proper spin and energy it is found that, on the average, 0.5(2)$\hbar$ of spin is removed by these $\gamma$ rays. Thus, 1.1(4)$\hbar$ of spin is removed by the decay $\gamma$ rays in this QC component.

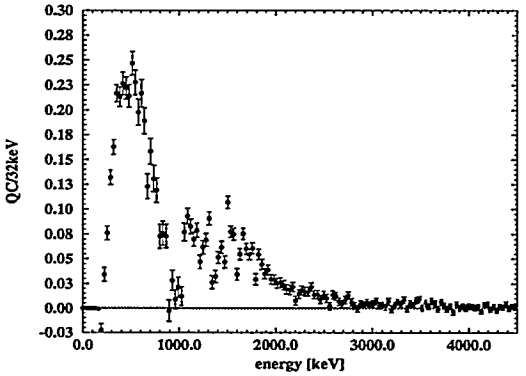


FIG. 7. The QC $\gamma$ rays in $^{194}$Hg after both the feeding statisticals and quadrupoles have been subtracted. The spectrum shows the dipole component of the feeding at low energies and the decay-out QC component at higher energies.

Some SD decay paths will feed into states located above the yrast line, which are either not populated or populated weakly when ND bands are feed. The $\gamma$ rays from the decay of these states can be found by close inspection of all the discrete $\gamma$ rays that were removed in the early stages of the analysis; but have not been assigned in the ND level scheme. (By placing coincidence gates on those candidate transi-

tions, it was checked that the lines are not the result of contaminant coincidences). In [3] it was estimated that, on the average, half (multiplicity 0.5(2)) of the $\gamma$ cascades deexciting the SD band goes through such states and gives rise to discrete lines in a region up to 1 MeV. These $\gamma$ rays need to be taken into account when the spin and energy of the SD band are calculated. In total, these $\gamma$ rays remove $0.8(3)\hbar$ and 0.3(1) MeV which must be vectorially added to the 'regular' QC spin and energy vector in order to find the mean SD exit-point (see figure 1).

From the intensities, spin and energies of the known ND lines in coincidence with the SD band, it is found that the entry point of the SD band into the known ND states is located at a spin of $9.3(5)\hbar$ and an energy of 2.4(1) MeV. The errors quoted here are due [i] to difficulties in assigning intensities to some low energy lines which are not observed well with GAMMASPHERE, and [ii] to the presence of two low spin isomers in the yrast level structure, which complicate the determination of $\gamma$-ray intensities for transitions involved in their deexcitation.

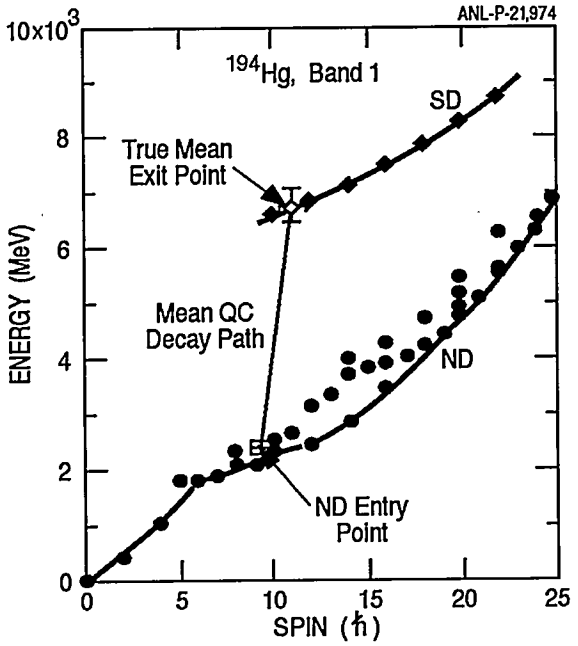


FIG. 8. The mean SD exit-point found by adding the spin and energy removed by known ND lines, new unassigned ND lines and the decay-out QC $\gamma$ rays.

By adding all the contributions; i.e., the known ND lines, the new weak ND lines just discussed and the decay-out QC $\gamma$ rays, the *mean SD exit-point* is determined. The result is displayed in figure 8. In the figure, a vector characterizing the mean QC decay path obtained as described above links the entry point into the ND levels and the SD exit point. It is this SD exit-point located at $11.1(7)\hbar$ and 6.8(3) MeV that can be compared directly to the result from the one-step decays [1]. According to the analysis in [1], 48% of the decay of the SD band occurs from the 6.88 MeV $12^+$ state and 52% from the 6.63 MeV $10^+$ state, establishing the true mean SD exit-point as: ($11.0\hbar$, 6.8 MeV).

The main conclusion of the present analysis is as follows: *the mean exit-point measured from the QC is in remarkably good agreement with the exact result established from the one-step decay $\gamma$ rays.* Another way to present this result is to calculate the spin and energy the QC method would assign to the '$10^+$' state: i.e.,

$$I = 10.1(7)\hbar \quad \text{[true: } 10\hbar\text{]}$$
$$E = 6.7(3) \text{ MeV[true: 6.6 MeV]}$$

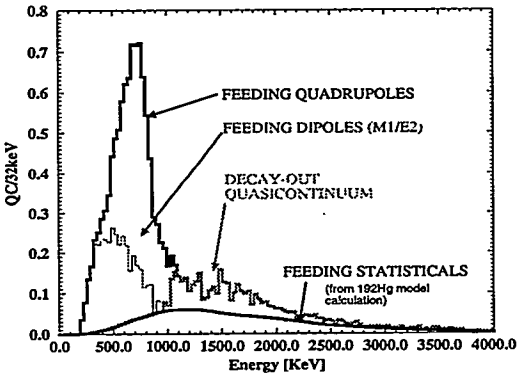


FIG. 9. All the QC components in the feeding and decay of the yrast SD band in $^{194}$Hg.

## THE DECAY MECHANISM

As the nucleus removes spin and energy by emitting stretched E2 $\gamma$ rays along the SD yrast line, the SD states become hotter and hotter with respect to the ND yrast line (see figure 1). Thus, the ratio of ND to SD level densities increases as the nucleus decays in the SD well. Moreover, the in-band transition rates diminish because of the rapidly decreasing transition energies. In addition, there is also evidence that the barrier height is reduced at lower spin. A SD band decays to the ND states when the states in the SD band acquire a sufficient component of the wave-function of the hot ND states located on the other side of the barrier separating the two wells [3,5,9]. Because of the exponential dependence of the mixing as a function of spin, the decay happens suddenly, over a few SD states.

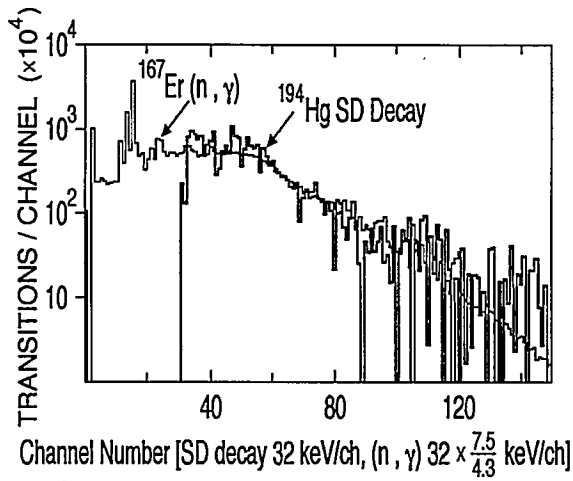


FIG. 10. The QC $\gamma$ rays from the decay of the yrast SD band in $^{194}$Hg overlaid with the gain adjusted QC $\gamma$ rays following neutron capture in $^{167}$Er.

It follows from the above picture of the decay of a SD band that the spectrum of the $\gamma$ rays emitted in the decay process is governed by the levels in the ND well. The end-point of the QC spectrum is determined by the excitation energy of the SD states. Thus, a decay from a fission isomer or from a state populated in neutron capture is expected to be characterized by a decay spectrum of the same form as the one seen in this work. This follows since all these processes are governed by statistical emission of $\gamma$ rays from 'sharp' states, i.e. states with a well defined energy.

The QC $\gamma$ rays following neutron capture in $^{167}$Er have been measured using Tessa-3 at Brookhaven [10]. The spectrum after unfolding, efficiency correction and removal of the discrete peaks below 600 keV is presented in figure 10, where it is overlaid with the SD decay-out QC discussed in this paper. Since the sharp states populated by neutron capture are located at higher energy than the SD levels (7.7 MeV vs. 4.3 MeV), the neutron capture spectrum was gain-adjusted so that its end-point matched that of the SD decay spectrum. The similarity (in shape and magnitude) of the two spectra is striking and suggests that, in both cases the decay is governed by the same mechanism, statistical decay from hot 'compound' states.

## CONCLUSIONS

It has been shown that the *spin* and *excitation energy* of the yrast SD band in $^{194}$Hg which are extracted from the analysis of the QC $\gamma$ rays from the decay-out process are in excellent agreement with the exact result obtained from one-step decay transitions. Thus, spins and excitation energies can be determined with this method in cases where Porter-Thomas fluctuations or other conditions prevent the observation of direct one-step or two-step decays from SD bands.

| component | $\overline{m}$ | $\overline{\epsilon}$ |
|---|---|---|
| Statisticals | 3.2 | 1.68 MeV |
| Quadrupoles | 6.0(1) | 0.73(1) MeV |
| M1/E2 dipoles | 3.37(6) | 0.54(1) MeV |
| Decay-out QC | 2.28(6) | 1.77(6) MeV |
| new ND lines | 0.5(2) | 0.6(2) MeV |

TABLE I. The mean multiplicities and mean energies of the QC components in $^{194}$Hg. Only statistical errors are given. Also listed are the current results of the cataloging of the new ND states (where the error bars are dominated by systematics).

Figure 9 shows all the components of the QC: [i]the statistical, [ii]quadrupole and [iii]dipole $\gamma$ rays associated with the feeding and [iv]the QC $\gamma$ rays from the decay-out of the SD band. Table I shows the mean multiplicities and mean energies of all these components.

Work is still in progress to improve on the errors associated with various contributions by [i]gathering more statistics, [ii]removing contaminant coincidences in the spectra and [iii] doing a more thorough cataloging of the new, unplaced ND lines. The latter process has already yielded more two-step decays which have been added to the decay level scheme in reference [1].

This work was supported in part by the U.S. Dept. of Energy, under Contract No. W-31-109-ENG-38.

[1] T.L. Khoo *et al.*, Phys. Rev. Lett. **76**(1996)1583 and G. Hackman, this conference
[2] A. Lopez-Martens *et al.*, Phys. Lett. **B380**(1996)18, Hannachi *et al.*, this conference
[3] R.G. Henry *et al.*, Phys. Rev. Lett. **73**(1994)777
[4] T. Døssing *et al.*, Phys. Rev. Lett. **75**(1995)1276
[5] T. Lauritsen *et al.*, Phys. Rev. Lett. **69**(1992)2479
[6] B. Crowell *et al.*, Nucl. Instr. & Methods **A235**(1995)575
[7] C.W. Beausang *et al.*, Nucl. Instr. & Methods **A364**(1995)560
[8] D.C Radford *et al.*, Nucl. Instr. & Methods **A258**(1987)111
[9] E. Vigezzi *et al.*, Nucl. Phys. **A520**(1990)179c and E. Vigezzi *et al.*, Phys. Lett. **B249**(1990)163
[10] F. Soramel *et al.* to be published

# First Measurement of the Degree of Fragmentation of the Decay Out Cascade from the Superdeformed Yrast Band in $^{192}$Hg

A Lopez-Martens[1], F Hannachi[1], C Schück[1], R Collatz[1], E Gueorguieva[1], Ch Vieu[1] T Dossing[2], S Leoni[2], B Herskind[2] I Ahmad[3], D Blumenthal[3], M Carpenter[3], D Gassmann[3], R V F Janssens [3], T L Khoo[3], T Lauritsen[3], D Nisius[3] A Korichi[4], C Bourgeois[4] A Astier[5], L Ducroux[5], Y Le Coz[5], M Meyer[5], N Redon[5] J F Sharpey-Schafer[6,*], A N Wilson[6] W Korten[7] A Bracco[8] R Lucas[9]

[1]C.S.N.S.M, IN2P3-CNRS, bat 104-108, Orsay Campus, France
[2]Niels Bohr Institute, 4000 Roskilde, Denmark
[3]Argonne National Laboratory, Argonne, IL 60439, US
[4]I.P.N, bat 104, Orsay Campus, France
[5]I.P.N, Université Lyon-1, Villeurbanne, France
[6]Oliver Lodge Laboratory, University of Liverpool, PO Box 147, L69 3BX UK
[7]Institut fur Strahlen und Kernphysik, Universitat Bonn, Germany
[8]University of Milano, Institute of Physics, I-20133 Milano, Italy
[9]DAPNIA SPHN, CEA Saclay, 91191 Gif sur Yvette, France
*present address: National Accelerator Center, PO Box 72, Faure, ZA-7131 South Africa

**Abstract**

The decay spectrum of the yrast superdeformed band in $^{192}$Hg comprises a quasicontinuum with discrete lines ranging from 1 to 3.2 MeV . The intensity fluctuations of this quasicontinuum give information on the degree of fragmentation of the decay cascades and on the effect of pairing correlations on the level density $\rho$(U) in the normal deformed well ($0 < U < U_{SD}$).

As was explained in the previous talk by Torben Lauritsen, if we compare superdeformed (SD) and normal-deformed (ND) gated spectra in Hg and Pb isotopes, the SD-gated spectrum lies above the ND-gated spectrum for a broad range of transition energies when both spectra are normalised to the same number of $\gamma$ cascades. This excess intensity has been indentified in previous work [1] to be the spectrum of $\gamma$ rays connecting the SD to ND states. It is a quasicontinuum with intermediate-width structures. From a quasicontinuum analysis, the excitation energy of the decaying SD state in $^{192}$Hg was found to be U=4.3±0.9 MeV above the yrast line [1]. If we zoom in on the decay spectrum, we see that it also contains sharp lines which account for only a few percent of the total decay flux. In $^{192}$Hg, for example, 51 resolved lines have been identified [2]. However, no single-step decays could be observed. So far, these have been reported only in 2 nuclei of the mass 190 region: $^{194}$Hg and $^{194}$Pb [3,4,5].

A quasicontinuum as well as primary and secondary lines are also observed in the $\gamma$ spectrum following thermal neutron capture. This is further evidence for the stochastic coupling of the localised SD state with highly excited ND states across the potential barrier [6]. So, effectively, it is the statistical decay from the hot ND states which is observed.

What spectrum does one expect in such a decay ?

T. Dossing et al have calculated the spectra corresponding to the statistical decay

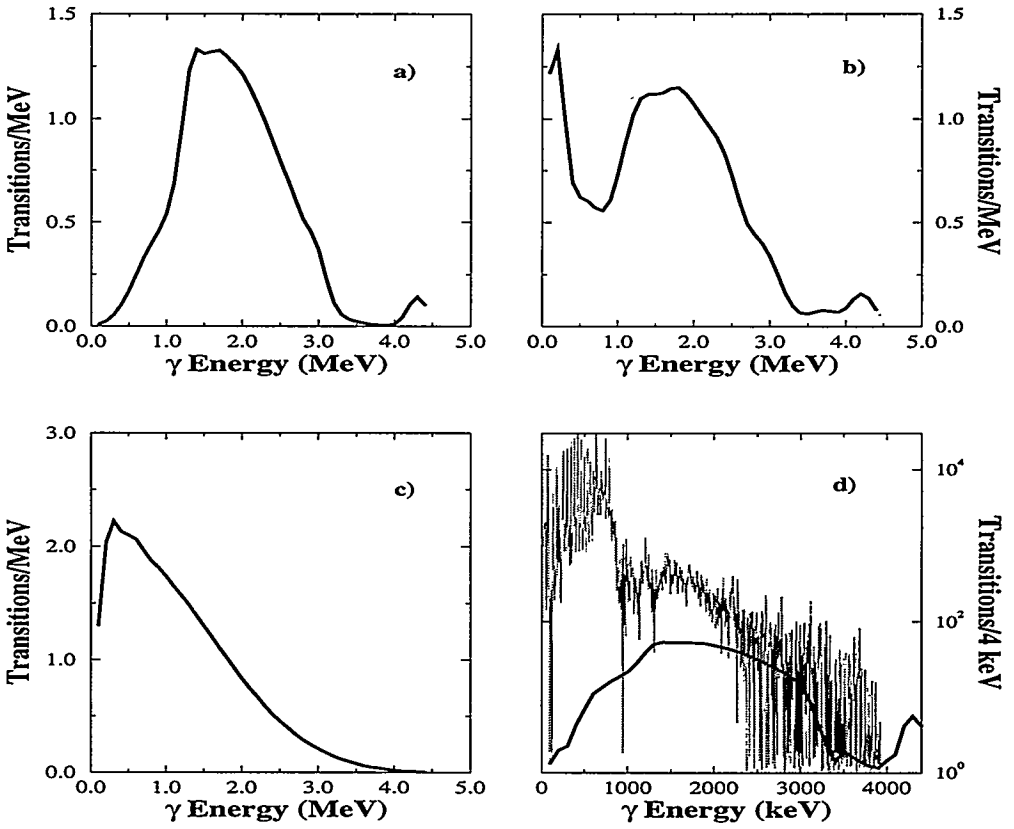


Figure 1: Statistical decay spectra from an initial state at U=4.3 MeV calculated with (a) the paired even-even level density, (b) the paired odd-even level density and (c) the unpaired even-even level density. (d) Efficiency-corrected experimental decay spectrum and calculated decay spectrum from (a)

from a ND state at 4.3 MeV in three different cases [7]. The level densities are obtained by counting quasiparticle energies starting from equidistant single-particle levels, with pairing treated using the BCS method, followed by particle-number projection and diagonalisation. The decay spectra for an even-even and odd-even paired nucleus and for an even-even nucleus without pairing are shown in fig 1a-c. In the unpaired case, the monotonic increase of the level density with excitation energy gives rise to a smooth decay spectrum. In the even-even paired case, there is a depleted yield below 1.2 MeV and between 3.2 and 4 MeV. Both these features are due to the pair gap below the energy for 2 quasiparticle excitations. The compression of the spectrum, together with the last step transitions across the pair gap, give rise to a broad bump centered around 1.6 MeV. For the odd-even case, the filling of the pair gap gives an appreciable yield at low energy. Above 1 MeV transition energy, the best experimental approximation of the spectrum of $\gamma$ rays feeding the SD band is the ND-gated spectrum stripped of all strong high-energy lines. The difference between the SD-gated spectrum and this smoothed ND-gated spectrum is then the decay spectrum. In fig 1d, the efficiency-corrected decay spectrum is shown together

with the calculated spectrum obtained with the even-even paired level density. The qualitative agreement is very good since the calculations reproduce the general shape of the decay spectrum. The model also predicts up to 5% yield at high energy which corresponds to the expected intensity for single-step decays. The fact that this yield varies so much from one nucleus to the other may be due to the chaoticity of the excited decaying ND state, in which case, we would expect the fluctuations in the strengths of the primary $\gamma$ rays to follow a Porter-Thomas distribution [8].

What can we learn from the decay spectrum ?

If it contains strong sharp lines, we can directly deduce the excitation energy, spin and parity of the SD state. If these lines are too weak, we can carry out a quasicontinuum analysis [9] to extract the average excitation energy and spin of the SD state. With the Fluctuation Analysis Method (FAM), we can extract the effective number of transitions sampled by the nucleus in the decay; in other words, we can measure *the degree of fragmentation of the decay.* As it turns out, this method goes even further and can be used as a new probe of the ND level density up to high excitation energy.

How does it work ?

The aim of the FAM [10,11,12] is to determine the effective number of transitions sampled by the nucleus without knowing the details of the transition energies or transitions strengths involved. This number can be directly extracted from the first (mean) and second (variance) moments ($\mu_1$ and $\mu_2$) of the intensity distribution of the decay spectrum. The method relies on the fact that, below the excitation energy of the SD state at the point of decay, the level density in the $1^{st}$ well, although large, is finite. If the number of recorded events ($N_{evt}$) is larger than the number of available transitions ($N_t$), this will lead to an enhancement of the intensity fluctuations in the decay spectrum above those generated by pure counting statistics. Correction factors have to be added to account for finite detector resolution ($p$), probable Porter-Thomas fluctuations (2), background subtraction and the separation of true coincidences into 2 components, such as into the SD decay spectrum and the underlying continuous statistical feeding spectrum in the 1 to 3 MeV region of the SD-gated spectrum. One then obtains the following equation for the effective number of transitions:

$$N_t = 2 \times p \times f^2 \times \frac{N_{evt}(A) \times \mu_1(A)}{\mu_2(A) - \mu_1(C) - g^2\mu_1(B)} \qquad (1)$$

Spectrum A = C - gB, where C is the raw spectrum of all the events in coincidence with the SD band and B the appropriate background spectrum scaled by a factor g. Spectrum A needs to be corrected for the detector response [13]. $f$ is the fraction of events belonging to the decay in spectrum A. Fig 2a shows the effective number of sampled transitions as a function of transition energy obtained for the SD decay and feeding cascades in $^{192}$Hg studied with the Eurogam 2 array [14]. Above 2 MeV, fewer transitions are sampled by the nucleus in its decay from the SD band. This can be explained by the fact that these transitions are primary $\gamma$ rays starting off from a few initial states and taking the nucleus down to regions of low level density. Thus, for the decay cascade, the number of transitions is expected to decrease at high transition energy in proportion to the final state level density $\rho(U_{final})$. On the other hand, the feeding cascade starts from a multitude of initial states populated by the neutron decay; in this case, the number of transitions reflects the product of the final and initial state level densities $\rho(U_{initial})\rho(U_{final})$. The low-energy transitions of the

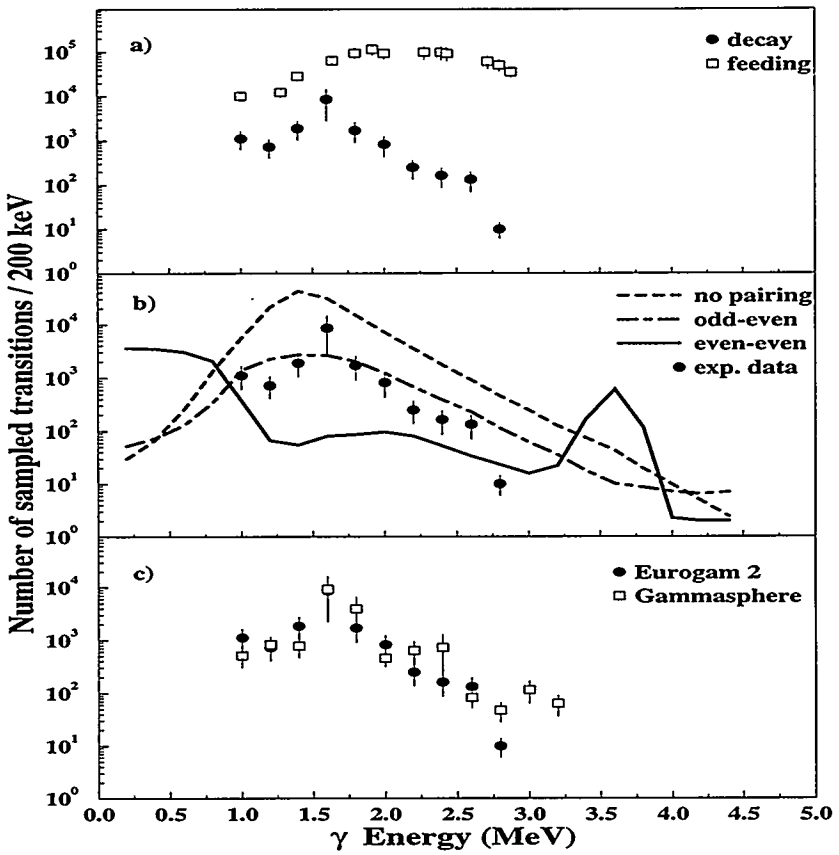


Figure 2: (a) Experimental effective number of transition sampled in the decay and feeding cascades in $^{192}$Hg. (b) Calculated and experimental effective number of transitions sampled in the decay cascade. (c) Comparison between the experimental effective number of transitions in the decay cascade obtained with Eurogam 2 and Gammasphere data

decay cascade tend to come from the last decay steps. They connect states in a region of low level density. This explains the initial increase in the number of transitions as a function of transition energy. A total of ~9000 transitions are sampled in the decay out of the SD band in $^{192}$Hg. By examining figure 2a above 2 MeV where the first decay steps dominate the fluctuations, one can see that ~1000 transitions are available in the initial stage of the decay [2]. This tells us that the decay is indeed highly fragmented, as expected in a statistical decay. In figure 2b, the experimental effective number of transitions is compared to calculations based on the schematic model described earlier on. The comparison between the experimental data and the calculations is satisfactory and is a stringent test for calculations of the decay and of $\rho(U)$ up to high excitation energy. The fact that the experimental values are in better agreement with the odd-even calculated values may be due to factors that have not been included in the model: first of all, angular momentum which causes the pairing correlations in the even-even nucleus to weaken and hence lowers the ground state

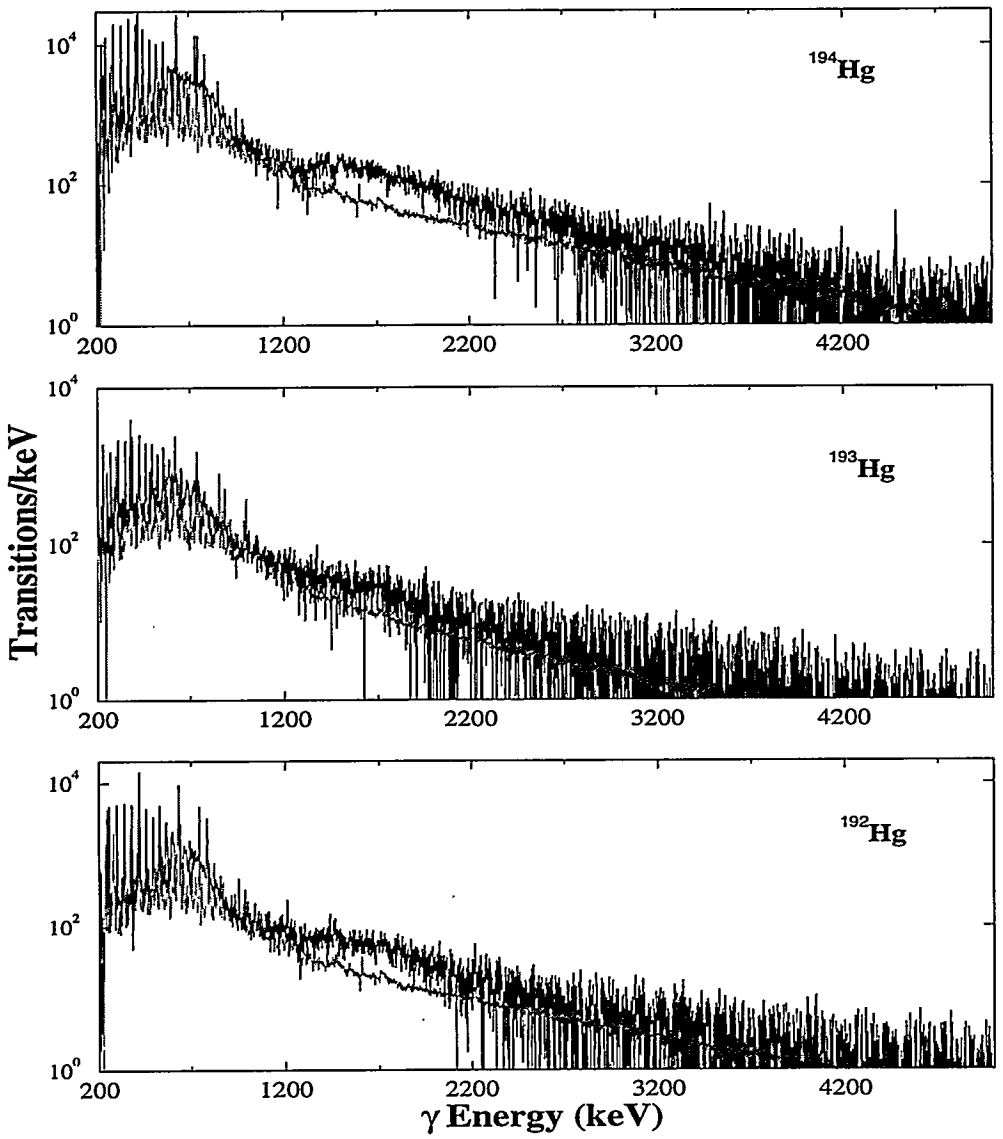


Figure 3: SD and ND-gated spectra obtained in $^{192,193,194}$Hg

pairing gap, secondly, symmetries in the nuclear potential and shell effects which may slightly displace both calculated curves. It is essential to carry out a similar analysis on other nuclei and especially an odd-even nucleus of the same mass region. In fig 3 are shown the SD and ND-gated spectra for 3 Hg isotopes studied at Gammasphere [15]. We can immediately see that both even-even nuclei present a more pronounced bump than the odd-even nucleus. A careful inspection of the $^{193}$Hg spectra reveals an excess intensity at low energy, as predicted by T. Dossing's calculations. A preliminary Fluctuation Analysis on the $^{192}$Hg decay spectrum gives practically an identical distribution of effective number of transitions as the Eurogam $^{192}$Hg data. The comparison is shown in fig 2c. The analysis of the $^{193}$Hg and $^{194}$Hg decay spectra is still in progress.

In conclusion, we have shown that the decay from the SD band in $^{192}$Hg starts off from

a few initial states and is highly fragmented. We have measured of the order of 1000 different first step transitions. The decay has been shown to be of statistical nature but it remains to be proven that Porter-Thomas fluctuations govern the distribution of the SD intensity among the different decay paths. This can be done by measuring the intensity distribution of the discrete transitions lying above 2 MeV which stem directly from the hot ND states. This analysis could then provide a direct measure of the onset of chaos in excited nuclear states. By studying the various components of the decay spectrum, we are able to extract the fundamental spectroscopic quantities for the SD band, such as excitation energy, spin and parity. These quantities can help us check the assignments of yrast and excited SD bands and measure the mixing of the SD and ND states. We can also study the statistical feeding via the single-step decays. Finally, we have direct access to the ND level density and the quenching of pairing with excitation energy and spin via the Fluctuation Analysis Method. The decay spectrum is thus a very good laboratory for the study of fundamental properties of SD and ND nuclei and the study of the SD-to-ND shape transition.

[1] R. G. Henry *et al.,* Phys. Rev. Lett **73**, 777 (1994)
[2] A. Lopez-Martens *et al.,* Phys. Rev. Lett **26**, 1707 (1996)
[3] T. L. Khoo *et al.,* Phys. Rev. Lett. **76**, 1583 (1996)
[4] A. Lopez-Martens *et al.,* Phys. Lett. **B380**, 18 (1996)
[5] K. Hauschild *et al.,* proceedings of this conference
[6] E. Vigezzi *et al.,* Phys. Rev. Lett. **B249**, 163 (1990)
[7] T. Dossing *et al.,* Phys. Rev. Lett. **75**, 1276 (1995)
[8] C. E. Porter and R. G. Thomas, Phys. Rev. **104**, 483 (1956)
[9] T. Lauritsen *et al.,* proceedings of this conference
[10] B. Herskind and S. Leoni, Nucl. Phys. **A520**, (1990) 539c-554c
[11] S. Leoni, thesis work
[12] T. Dossing *et al.,* Phys. Rep. **268**, 1 (1996)
[13] D. C. Radford *et al.,* Nucl. Instrum. Methods Phys. Res., Sect. A **258**, 111 (1987)
[14] P. J. Nolan *et al.,* Nucl. Phys. **A520**, (1990) 657c
[15] I. Y. Lee *et al.,* Nucl. Phys. **A520**, (1990) 641c

# Superdeformation

F. S. Stephens
*Nuclear Science Division, Lawrence Berkeley National Laboratory, Berkeley, CA 94720, USA*

Recent progress in the study of superdeformed nuclei is reviewed. Topics covered include: the onset of superdeformation in the mass 130-150 region; collective octupole bands; identical bands; and ΔI=2 staggering. Some comments about the futureof studies on superdeformed nuclei are included.

## 1. Introduction

This talk will consist of three parts: an introduction to the current situation regarding superdeformed bands; some recent highlights; and a quick look at the future. Due mainly to the large gamma-ray detectors coming into use, there is a lot going on in this area and I will not try include it all here. Rather, after a few general observations I will select several highlights and try to discuss those in some depth. Finally I will give my thoughts as to the future of studying superdeformed nuclei.

My definition of superdeformation is rather broad and generally includes nuclei where the long axis is 1.5-2 times longer than the short axis. Typically this is a second minimum in the potential energy surface; the first having smaller (perhaps "normal") deformation. With this definition there are now five regions of superdeformation known in the heavier elements, having masses centered around 80, 130, 150, 190 and 240, the last of these being the fission isomers discovered more than 30 years ago. Altogether there are around 200 bands presently known in these five regions. The newest region is that around mass 80, where already some 20 bands are known in 10 nuclei. These bands show all the familiar properties seen in the heavier regions: assigned configurations, band crossings, identical bands, etc. It is an exciting area and Cyrus Baktash is going to talk about it tomorrow morning, so I will not discuss it further here.

There are some special properties in the mass 130-150 region that are interesting and perhaps unique. The other three superdeformed regions mentioned above are well isolated from each other and transitions into or out of these regions involve changes in the occupation of several orbitals which do not occur easily. In fact, this morning we heard that in the mass 190 region the decay out of the superdeformed bands is a statistical process that occurs through a small mixing of normal states into the superdeformed ones. Only in the mass 130-150 regions can we observe the onset of superdeformation orbit by orbit.

In the mass 130 region it is the N=6 neutrons that trigger the onset of superdeformation, and this transition can be observed to occur in individual bands in $^{134}$Nd. Fig. 1, taken from a contribution by Petrache et al., shows several band energies in $^{134}$Nd (minus a rotational contribution). The normal deformation bands in this figure are sharply rising; whereas, the superdeformed bands are horizontal or slightly down sloping. Both bands 2 and 3 start out as normal bands and then undergo rearrangements, presumably involving the filling of two N=6 neutrons, that induce the superdeformation. Another way to view this change is as a crossing of the normal and superdeformed bands with a reasonably large interaction so that the lower energy pieces of the two bands looks like a single band with a deformation change. In either picture the differences between the bands cannot be large - probably only the change of this pair of neutrons.

As we move up in N and Z, the deformation increases in superdeformed bands, but not always smoothly. First the N=6 protons are filled and then, above N=80, the N=7 neutrons fill. In both cases there is evidence that the key changes can occur within individual bands. Later today Zhu will talk about lifetimes in $^{144}$Gd, where a backbend at frequency about 0.45 MeV is

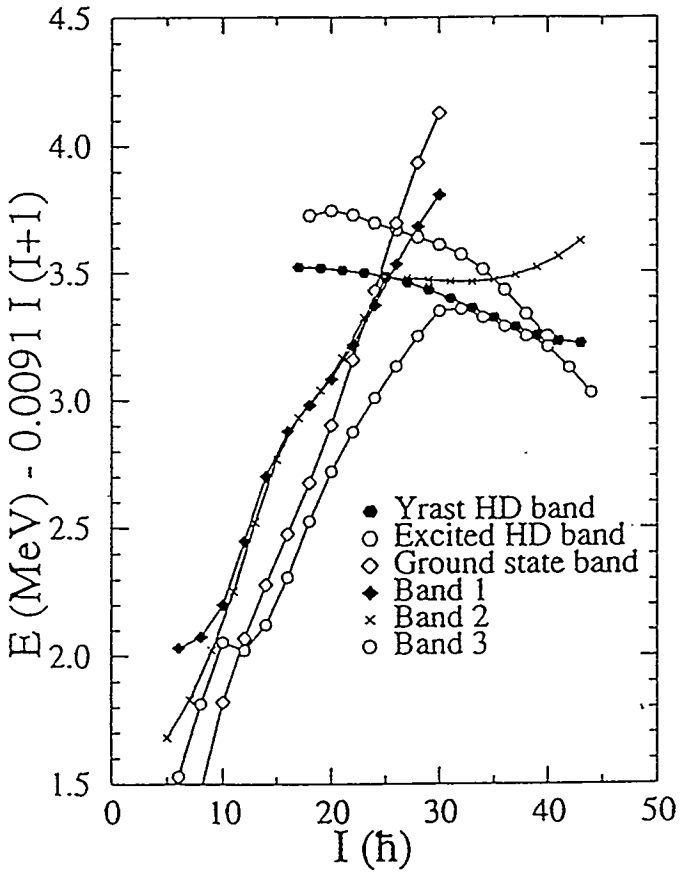


Fig. 1 Rotational bands in $^{134}$Nd from the contribution of Petrache et al. Bands 2 and 3 appear to change character form normal deformed to highly ( super- ) deformed.

shown to be associated with a change in deformation from $\varepsilon = 0.45$ to 0.51. Again a large shift in deformation occurs with apparently a small configuration change that is associated with a pair of N=6 protons. Similarly, in $^{148}$Gd de France et al., [1] have proposed that a backbend in one of the bands may be due to the occupation of the first N=7 neutrons. There is additional work in this region on Pm and Sm nuclei in abstracts to this Conference by Pfohl et al., and Jin et al.

This is a fascinating region where we can follow the evolution of deformation step by step from the normal deformed mass 130 region to the strongly superdeformed nuclei of the N=150 region. One can observe the effect of filling each of the key sets of intruder orbitals. This region offers an opportunity to learn about the microscopic origins of deformation effects.

## 2. Some Highlights

There are a lot of recent superdeformation highlights, one of which on links we heard about this morning and another on the mass 80 region we will hear about tomorrow. I will discuss three others: evidence for octupole effects; the news about identical bands; and the situation on $\Delta I=2$ staggering. One other point I would like to mention here is the progress in identifying configurations in superdeformed bands. Mottelson [2] emphasized here in Argonne eight years ago how important this is for understanding superdeformation. Not only does this place these nuclei in the TRS calculations (or vice versa), but it also gives the microscopic background for all the new and unusual effects we may hope to see. Fortunately there has been real progress in this area, and most bands in most nuclei have been assigned configurations.

***Octupole Bands.*** Earlier this morning Dirk Schwalm presented some evidence for excited collective bands in the superdeformed fission isomers, and such bands have been predicted in other regions. Collective octupole excitations should be especially important in superdeformed

nuclei due to the proximity of orbitals with both parities, as was also pointed out by Mottelson [2] here in Argonne eight years ago. He emphasized particularly the $Y_{31}$ "banana" shapes.

The first evidence for an octupole band in superdeformed nuclei came from Crowell et al.,[3] for a band in $^{190}$Hg that decayed to the lowest superdeformed band rather than to normally deformed states. The connecting transitions were shown to be stretched dipole, rather than quadrupole and, if E1, were about $10^{-3}$ Wu, which is typical for collective octupole states in normal nuclei. Recently Nakatsukasa [4] has calculated the octupole effects in $^{190,192,194}$Hg and he will discuss these calculations tomorrow morning. He has found impressive agreement with these $^{190}$Hg experimental results. In addition he predicts band crossings in $^{192}$Hg and there is evidence to support this, although the situation is not yet clear.

Nakatsukasa also predicts a small octupole-type signature splitting (odd spins lower) in $^{194}$Hg which inverts at higher frequencies due to non-collective quasi-particle admixtures. This is a very characteristic signature inversion for which we have found experimental evidence. Fig. 2 shows the situation. The plot is the signature splitting ($\alpha$=0 Routhian minus $\alpha$=1 Routhian) *vs.* the rotational frequency, so that positive values indicate octupole-type splitting. There are two calculated lines: the upper for a constant pairing strength as a function of frequency; and the lower for pairing that decreases at the higher frequencies. The data points are connected by a line and fall rather convincingly between the two pairing limits of the calculations. The initial octupole-type splitting and the later downturn (toward signature inversion) in both data and calculations are clear. The sensitivity to the pairing is surprising and it seems likely that a good fit to the data could be achieved by an intermediate value for the pairing. We take this agreement to be rather strong support for octupole effects in these excited bands of $^{194}$Hg.

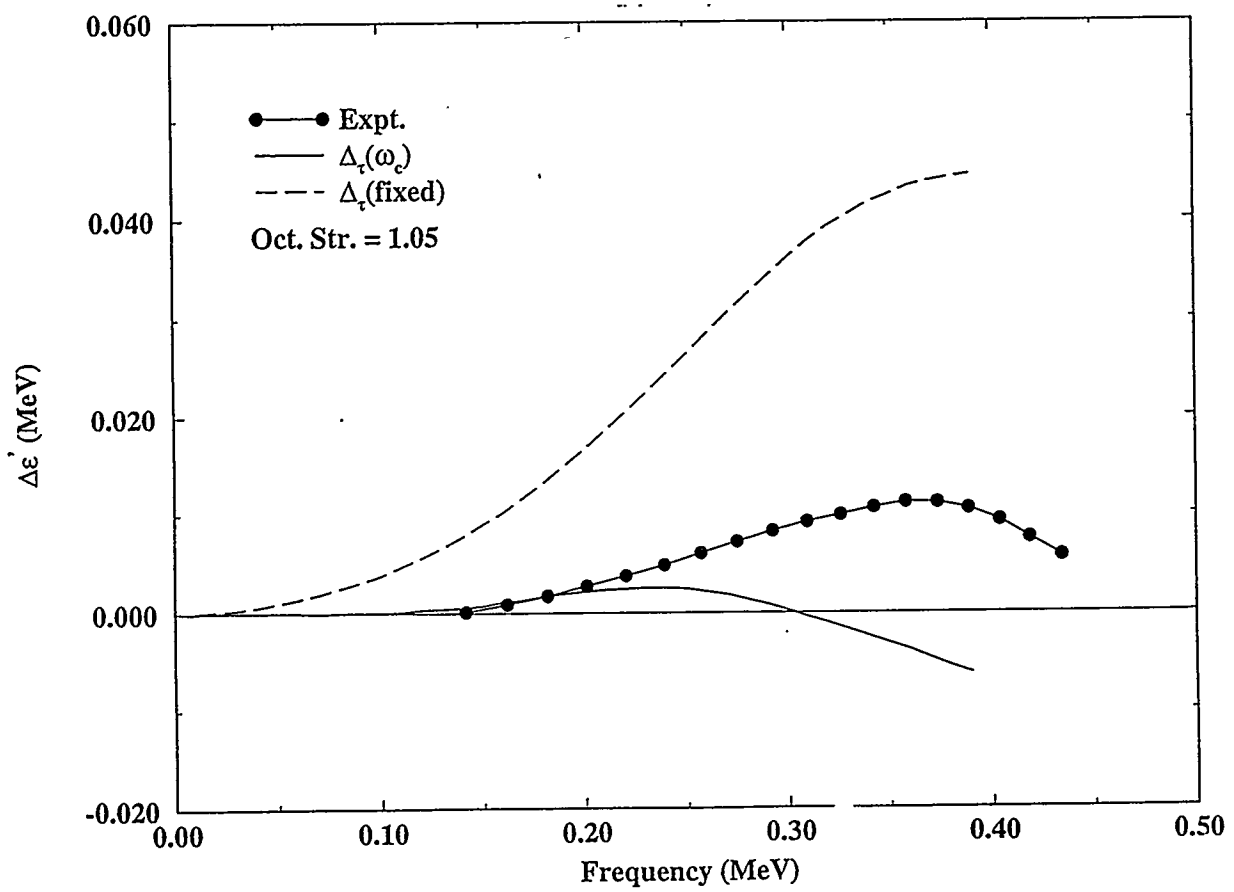


Fig. 2 Signature splitting in $^{194}$Hg compared with calculations of Nakatsukasa.

In summary, there are two pieces of evidence for octupole effects in these superdeformed Hg nuclei: the connecting transitions in $^{190}$Hg and the signature splitting in $^{194}$Hg. Work is underway to see if $^{192}$Hg fits this pattern and it looks promising at present. Tomorrow, Azaiez will also report some new evidence for octupole bands in $^{196}$Pb. This has become a "hot" topic now as we try to establish the types and strength of the octupole effects in superdeformed nuclei.

***Identical Bands.*** The identical bands are a rather long-standing puzzle in nuclear structure physics and significant progress has been made recently. There are two aspects of these bands that are necessary in our definition of "identical". First, the moments of inertia, $dI/d\omega$, have to be equal (and some people already call such bands "identical") and second, there must be a relationship between the gamma-ray transition energies in the two bands. Either these energies must be equal or they must fall at the one-quarter, half, or three-quarter point of the interval between transition energies in the other band. These points arise because they are the allowed points on a single I *vs.* $\omega$ line due to the quantization of spin (where the interval between transitions in each band is $2\hbar$). Thus, if confined to this single line, a band in an even-mass nucleus (having integer spin) would always fall at the zero or half points of the interval (assuming an even-even reference nucleus); whereas one in an odd-mass nucleus would fall at the quarter or three-quarter point. Since we generally do not know the spins in superdeformed bands, the above "identical" relationship only implies that the bands lie on parallel lines that are the same (as assumed above) or are shifted in spin by integer or half-integer values. Half-integer shifts invert the even- and odd-mass relationships given above. These shifts in spin at a given frequency are called "alignments" and identical bands, in our definition, imply quantized alignments (in integer or half-integer values).

The first important question about identical bands is: do they occur more often than expected if alignments are random. The answer from an analysis of superdeformed bands in the mass-190 region [5] seems to be that they do. The next important question is; what are the alignments, and to answer this question one must know the spins. This is an area where important progress has recently been made with the discovery of linking transitions. The spins of superdeformed bands in the mass-190 region were first proposed from model-dependent analyses of the rotational energies [6]. These indicated that a number of bands identical to $^{192}$Hg had alignments very close to one. The recent discovery [7] of links between two superdeformed bands in $^{194}$Hg and the known states near the ground state have been extended by Hackman this morning, establishing the partial level scheme shown in Fig. 3 which determines the spins of this superdeformed band as indicated. These agree with those from the rotational-energy analyses and show that this band, which is identical to the yrast SD band in $^{192}$Hg, has a relative alignment of one. This is not so easy to understand, because either "no change" or "several small compensating changes" would result in an alignment close to zero. It may involve some new physics, as has been discussed [8].

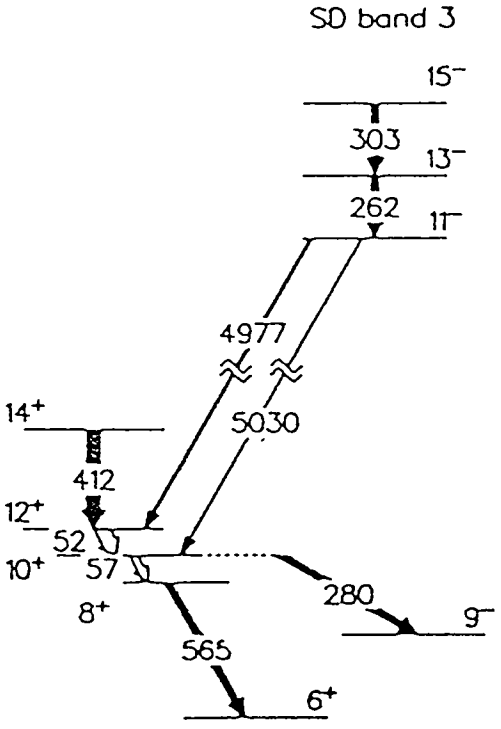

Fig. 3 Level scheme of $^{194}$Hg.

Another important advance coming with the large arrays is the ability to make precise relative lifetime measurements. When comparing recoiling nuclei of the same atomic number, made in the same reaction and

Table 1: Precise Quadrupole Moments of Identical Bands.

| Ref. | Nucleus (band #) | Relative $Q_t$ (exp) | $\beta/\beta_{ref}$ | Deformation |
|---|---|---|---|---|
| * | $^{192}$Hg | 16.6(10) | | |
| ref[9] | $^{194}$Hg (3) | 16.7(10) | 1.00(9) | Same |
| * | $^{192}$Hg | 17.2(13) | | |
| ref[10] | $^{193}$Hg (1-5) | 13.8-14.7(8) | 0.83(8) | Different |
| | $^{152}$Dy | 17.5(7) | | |
| ref[11] | $^{151}$Dy (4) | 17.5(10) | 1.00(7) | Same |
| ** | $^{152}$Dy | 17.5(2) | | |
| | $^{149}$Gd (4) | 17.5(6) | 1.05(4) | Different? |
| ref[12] | $^{148}$Gd (5) | 17.8(13) | 1.07(7) | Different? |
| | $^{132}$Ce | 7.4(3) | | |
| ref[13] | $^{131}$Ce (4) | 8.5(4) | 1.15(7) | Different |
| | $^{131}$Ce | 7.4(4) | | |
| ref[13] | $^{132}$Ce (2) | 7.3(3) | 0.99(7) | Same |

recoiling in the same backing material, the large uncertainties associated with stopping times cancel out and the relative precision can be 5% or better. These lifetimes give the transition quadrupole moments and, assuming axial symmetry, the deformations. Another interesting question about two identical bands is whether they have the same deformations, and we can begin to answer that question. In Table 1 are collected all the precise data on relative lifetimes that are currently available. It is pretty clear that for three pairs of identical bands the deformations are the same within the accuracy of the measurements. In two cases the deformations are very likely different, and in the sixth case, the two gadolinium bands are similar to each other, but probably different than the identical band in $^{152}$Dy. Note that some of these data are still preliminary (*) and for one set (**) the nuclei have different atomic numbers and were made in different reactions. Nevertheless, it seems likely that identical bands do not always have the same deformation.

The conclusion seems to be that identical bands do not necessarily have all properties the same or very similar. This rules out the simplest picture of such bands, namely that essentially nothing changes. In the case of the deformations, the effects of the observed changes on the transition energies must be compensated by other effects, but whether these compensations are accidental or systematic (implying something new) is not clear. The situation for alignments is different. The alignment shifts to a completely different (though integer) value and is not likely the result of compensations of several small effects. Either it is a complete accident or due to some new physics. More data on other cases should tell us which. The identical bands are still a puzzle; however, we are now making progress toward a solution.

***ΔI=2 Staggering.*** One of the exciting recent events in high-spin physics was the announcement by Flibotte et al., [14] of a regular staggerir ; pattern in the transition energies of one of the superdeformed bands in $^{149}$Gd. States differing by four units of angular momentum were found to have small similar shifts in energy of about 60 eV compared to a smooth rotational sequence. Since that time several apparently similar cases were reported in the literature. One

proposed explanation of a long regular staggering of this type was based on a deformed shape with a component having $C_4$ symmetry. However, some of the observed patterns were not so long or regular and might be explained more simply by a crossing of two bands. Since the former explanation involves entirely new and unexpected physics and the latter would be quite puzzling without evidence for the crossing band, it is important to check the data and that has been underway very recently.

Some of the data that gave evidence for long regular staggering sequences came from three superdeformed bands of $^{194}$Hg, which were studied by Cederwall et al [15]. This experiment has been repeated and Krucken will talk about the results tomorrow morning. He concludes that there is no clear evidence in $^{194}$Hg for long regular staggering patterns, although there are very likely short irregularities in some bands. New measurements have also been made on the other cases of staggering reported. These confirmed the original $^{149}$Gd long regular stagger [16], but the other two similar cases were not reproduced. The remaining cases did not involve long sequences and thus look more like band crossings. So up until last week there was only one case of long regular staggering remaining -- the original one.

Today Stephane Flibotte gave me some preliminary results on a new superdeformed band in $^{148}$Eu coming from a Gammasphere experiment run only last week. This nucleus was chosen because it has one proton less than $^{149}$Gd and, if the proton hole is in the [301]1/2 orbital, a band identical to the one with the staggering in $^{149}$Gd should result. Whether this band also has the staggering is an intriguing question. The result is shown in Fig. 4. There appears to be a rather long staggering sequence with, however, a phase opposite to that in $^{149}$Gd. These experiments

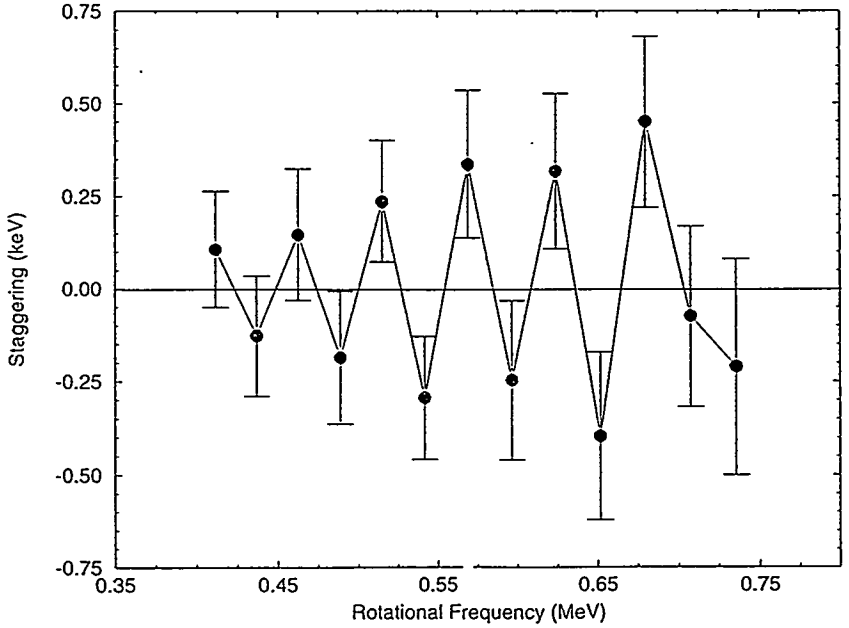


Fig. 4 Staggering plot for $^{148}$Eu from Flibotte et al.

are difficult and it is still very early, but this is a spectacular, albeit puzzling, result.

The cause of such long regular staggering sequences, as well as that of the shorter sequences, is not clear. One problem is that a $C_4$ symmetry in the nuclear shape may not always generate long regular sequences, so that even for the shorter sequences one could not rule out $C_4$ effects. This is a fascinating problem and, with the large arrays, it is progressing rapidly.

## 3. The Future

There are many exciting things going on right now concerning superdeformed nuclei and a lot of open questions. We now have a good idea of configurations for most bands, providing a framework to look for new and unexpected phenomena. The study of linking transitions is just

beginning. Our study of excited collective bands in these nuclei is developing rapidly. I discussed octupole excitations and Peter Twin will tell us about some other types of collective excitations later in this session. We have also taken a big step forward in understanding identical bands and probably have the tools now to solve this long standing puzzle. The mystery of $\Delta I=2$ staggering is deepening, however even if this phenomenon is just band crossing it is interesting. Why do we not see the crossing bands?

There are other still more open questions regarding superdeformed bands. We can study shape evolution, step by step, in the mass 130-150 regions, perhaps helping us understand the decay mechanisms and if or where non-statistical effects show up in these decays. Understanding nuclear pairing is a challenge and the superdeformed nuclei can provide different insights. If there are higher multipoles in the pairing they are likely to show up in superdeformed nuclei due to the different mixture of orbits at the Fermi surface. Dynamic pairing is a real mystery and the large shell gaps coupled with the regular high spin states provide a very different approach to its study. And finally two continua exist; feeding and decay. The feeding is different than that in the normally deformed nuclei -- due to the lower giant dipole resonance, for example. The decay out is a completely new unresolved spectrum. It promises systematic information on mixing matrix elements, level densities and information on both statistical and (perhaps) non-statistical transition probabilities as a function of excitation energy and spin. These continua are a reservoir of new phenomena.

Superdeformed nuclei provide unique information on all the topics mentioned above. It is currently an exciting area with many directions to explore. The new arrays provide the access into these mysteries. For superdeformed nuclei, resolving power delivers!

## Acknowledgments

I am indebted to a number of colleagues for permission to quote data prior to publication and for help and advice in preparing this talk. This work was supported in part by the Director, Office of Energy Research, Office of High Energy and Nuclear Physics, Nuclear Physics Division, of the U. S. Department of Energy under Contract No. DE-AC03-76SF00098.

## References

1. G. de France et al., submitted to Phys. Lett. B
2. B. Mottelson, Proceedings of the Conference on High-Spin Nuclear Structure and Novel Nuclear Shapes, Argonne, Illinois, April 1988, ANL-PHY-88-2 (1988) p1.
3. B. Crowell et al., Phys. Rev. **C51** (1995) R1599
4. T. Nakatsukasa et al., Phys. Rev. **C53** (2213) 1996
5. P, Fallon et al., Proceedings of the Conference on Physics from Large Gamma-Ray Detector Arrays, Berkeley, California, LBL pub-35687 (1994) p89.
6. J.A. Becker et al., Nucl. Phys. A520 (1990) 187c.
7. T.L. Khoo et al., Phys. Rev. Lett., 76 (1996) 1583.
8. F.S. Stephens et al., Phys. Rev. Lett. 64 (1990) 2623; Phys. Rev. Lett. 65 (1990) 301.
9. E.F. Moore et al., to be published.
10. B. Busse et al., to be published.
11. D. Nisius et al., to be published.
12. H. Savajols et al., Phys. Rev. Lett. 76 (1996) 4480.
13. R.M. Clark et al., Phys. Rev. Lett. 76 (1996) 3510.
14. S. Flibotte et al., Phys. Rev. Lett. 71 (1993) 4299.
15. B. Cederwall et al., Phys. Rev. Lett. 72 (1994) 3150.
16. P.J. Twin, reported at the Workshop for Gammasphere Physics, Berkeley, California, Dec. 1995, to be published (World Scientific).

# Microscopic Description of Nuclear Shapes

J.L. Egido, L.M. Robledo, A. Valor and A. Villafranca
Departamento de Física Teórica C-XI
Universidad Autónoma de Madrid, E–28049 Madrid, Spain

**Abstract**

The approximate particle number theory for density dependent forces is sketched, the theory is applied to discuss properties of the superdeformed ground state and excited bands of $^{192}Hg$. The force used in the calculations is the finite range density dependent Gogny force. The agreement with the available experimental results is very satisfactory.

The most popular approaches to describe high spin phenomena -we restrict ourselves to descriptions within the cranking model- have been the mean-field (Woods-Saxon or Nilsson) plus Strutinsky shell corrections [1] and the self-consistent Hartree-Fock-Bogoliubov (HFB) one.

Within the HFB approaches the most successful calculations have been performed with density dependent hamiltonians. The most popular, because of its simplicity, is the Skyrme force, most of the calculations have been performed by Bonche et al. [2, 3, 4] with the SkM* parametrization. Recently the Gogny force [6, 7, 8] has been also applied to high spin problems at normal deformations [9] and to superdeformed shapes [10, 11]. Relativistic mean field calculations [12] has been also very successful in the description of superdeformed bands.

In these calculations Lagrange multipliers were used to adjust on the average the particle number and the angular momentum, the so-called cranked HFB approximation (CHFB). It turned out [9], however, that in spite of the finite range of the force, the condition of conserving the particle number on the average was not enough and a sharp phase transition was found, contrary to what one would expect for a finite system. The same results were obtained with the Skyrme force either with a pure monopole pairing or with a density dependent pairing force in the particle-particle channel. To remedy this problem one has to introduce further correlations as those present in mean field approaches, i.e. ones has to go beyond the mean field approximation. The ideal treatment of pairing correlations in nuclei is particle number projection before the variation [13].

An exact particle number projection at high spin is rather complicated and up to now it has only been applied to separable forces [16]. On the other hand, the semi-classical recipe of solving the mean field equations with a constraint on the corresponding symmetry operator can be derived as the first order approach of a full quantum-mechanical expansion (the Kamlah expansion) [17] of the projected quantities. The second order in this expansion takes into account the particle number fluctuations and might cure some of the deficiencies

of the first order approximation. However, full calculations up to second order are rather cumbersome and just a simple model calculation has been carried out up to now [18]. Most second order calculations have been done using the Lipkin-Nogami (LN) recipe originally proposed in Refs. [19, 20, 21]. We shall now display the corresponding equations for a density dependent hamiltonian. For a derivation see [26].

The projected energy to second order is given by

$$E_{proj} = \langle \hat{H} \rangle - h_2 \langle (\Delta \hat{N})^2 \rangle + h_1 (N - \langle \hat{N} \rangle) + h_2 (N - \langle \hat{N} \rangle)^2, \quad (1)$$

with $\langle \hat{A} \rangle \equiv \langle \Phi | \hat{A} | \Phi \rangle$. In a full variation after projection method one should vary eq. (1). In the Lipkin-Nogami prescription, however, the coefficient $h_2$ is held constant during the variation, the resulting equation is much simpler [15], one has to minimize

$$E_{proj} = \langle \hat{H} \rangle - h_2 \langle (\Delta \hat{N})^2 \rangle \quad (2)$$

with the constraint

$$\langle \hat{N} \rangle = N. \quad (3)$$

For density dependent forces the coefficient $h_2$ takes the form

$$h_2 = \frac{\langle \hat{\mathcal{H}} - \langle \hat{\mathcal{H}} \rangle (\Delta \hat{N})^2 \rangle - \langle \hat{\mathcal{H}} - \langle \hat{\mathcal{H}} \rangle \Delta \hat{N} \rangle \langle (\Delta \hat{N})^3 \rangle / \langle (\Delta \hat{N})^2 \rangle}{\langle (\Delta \hat{N})^4 \rangle - \langle (\Delta \hat{N})^2 \rangle^2 - \langle (\Delta \hat{N})^3 \rangle^2 / \langle (\Delta \hat{N})^2 \rangle} \quad (4)$$

with

$$\hat{\mathcal{H}} = \hat{H} + \frac{\partial \hat{H}}{\partial \rho(r)} \hat{\rho} \quad (5)$$

The last term in this equation is a consequence of the density dependence of the hamiltonian and does not appear in the standard derivation of the Lipkin-Nogami approximation. The presence of this term might be very important for forces with density dependent pairing.

We have applied the LN formalism with the Gogny force to study the superdeformed ground state band and one excited band of the nucleus $^{192}$Hg. These bands have been study experimentally in refs. [22, 23] and theoretically in [24] with the Skyrme force and in [25] with the Wood Saxon plus Strutinsky method. In the calculations we are using the standard DS1 parametrization set [8]. In all our results we shall also present the ones obtained with the plain cranked HFB theory (CHFB) [9].

In fig. 1, left hand side, we show the angular momentum dependence of the charge quadrupole moment, $Q_0$, for the superdeformed ground band of the nucleus $^{192}$Hg. The CHFBLN and the CHFB results differ mostly at low spins where the pairing correlations are larger. As a function of the angular momentum we observe first an increase of the quadrupole moment due to a reduction of the pairing correlations and then a decrease of $Q_0$. This anti-stretching effect is caused by the Coriolis force. In spite of the different values of the CHFB and the CHFBLN approaches, specially at low spins, both predictions coincide with the experimental value ($18.6 \pm 1.4$ eb) [22] within the experimental errors. The nucleus is axially symmetric, i.e. $\gamma = 0$, for all spin values.

In the right hand side of fig. 1 we display the transition energies versus the angular momentum for the superdeformed ground band. The agreement with the experimental data

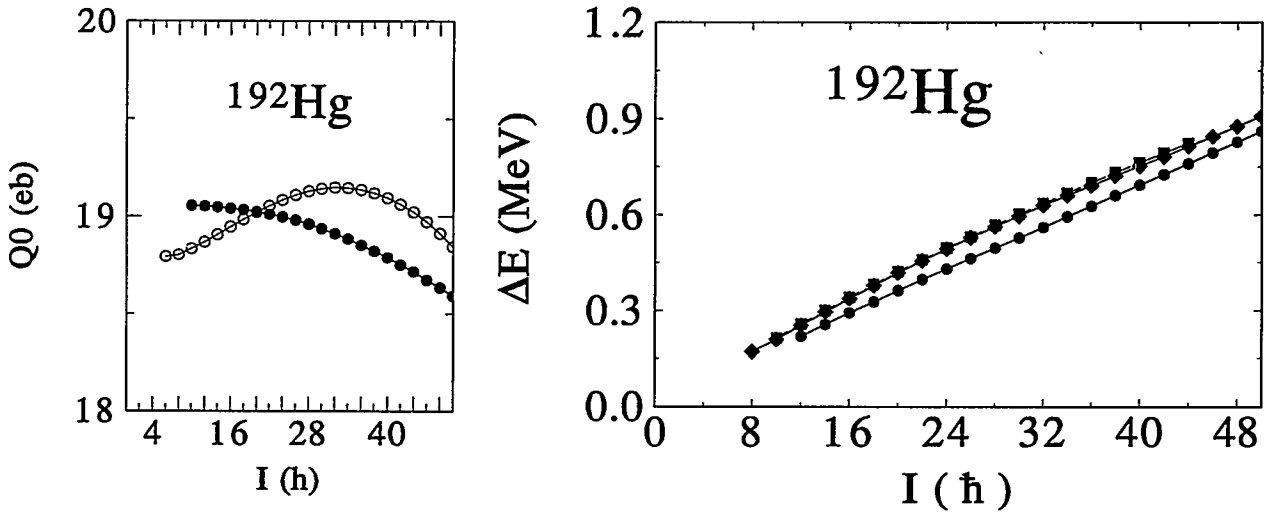


Figure 1: Left hand side, the charge quadrupole moment of the superdeformed ground band for $^{192}$Hg, CHFB (full circles), CHFBLN (open circles), versus de angular moment. Right hand side, the transition energies, CHFB (circles), CHFBLN (diamonds), experiment (squares), [22].

is good in the CHFBLN approach, in the CHFB one obtain too lower values. The reason for it is again the smallness of the pairing correlation in the CHFB approach (the transition energy is inverse proportional to the moment of inertia).

In fig. 2, the second moment of inertia $\mathcal{J}^{(2)}$ as a function of the angular frequency is represented. Here, as in the previous picture, the CHFB results are in poor agreement with the experiment. At small spin values the moment of inertia is too large and the neutron alignment sets in too early. The CHFBLN results, however, are in very good agreement with the experimental results, the correlations induced by the approximate particle number projection produce the desired effect, namely, to diminish the moment of inertia at small spin values and to delay the alignment to higher spin values.

We find that the orbitals responsible for the alignment at $\hbar\omega \approx 0.4$ MeV in $^{192}$Hg is the $\nu[761]\frac{1}{2}$. The proton alignment take place at higher frequencies ($\hbar\omega \approx 0.45$) and it is due to the $\pi[642]\frac{5}{2}orbital$.

Concerning the excited bands of $^{192}$Hg, we shall show CHFBLN results concerning the so-called band 3 in the literature [23], a band of negative parity. The theoretical description is based in the blocked CHFBLN theory. We have found two signature partner bands (we call them $C_1$ and $C_2$), which transition energies agree very well with the experimental data. Band $C_1$ is obtained by blocking of the lowest quasineutron states of negative signature in the positive and negative parity channels, band $C_2$ is obtained by blocking of the lowest positive parity quasineutron with positive signature and the lowest negative parity quasineutron with negative signature. The experimental transition energies agree slightly better with band $C_1$ than with band $C_2$. In fig. 3a we display the charge quadrupole moment of this bands, it is rather constant as compared with the ground band and about 1.5 (eb) smaller than this one. As we can see both bands have almost identical deformation. The bands are also axially

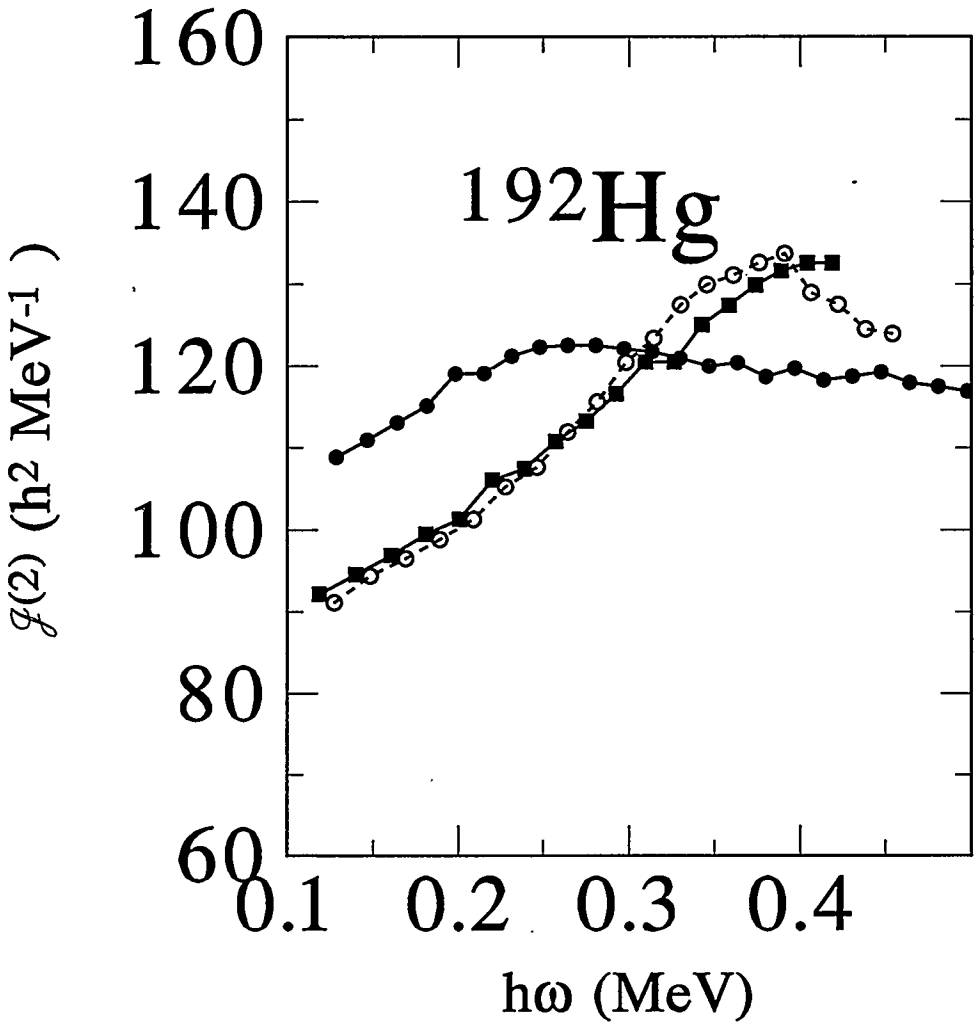


Figure 2: Second moment of inertia for the superdeformed ground band of $^{192}$Hg. Squares for the experimental data [22], full circles for the CHFB approach and open ones for the CHFBLN theory.

symmetric ($\gamma = 0$).

In fig. 3b we show the results for the second moment of inertia as well as the experimental data [23]. Experimentally the moment of inertia grows gradually up to $\hbar\omega = 0.3$ MeV, from this point on a sharp increase take place, producing an upbend at $\hbar\omega = 0.33$ MeV. These features are nicely reproduce by bands $C_1$ and $C_2$. If we identify band $C_1$ with the experimentally measured band 3 it is not clear to us why the signature partner band has not been measured.

In conclusion, the ground state band and the superdeformed band 3 of the nucleus $^{192}$Hg have been study within the approximate particle number projected theory with the density dependent Gogny force. Global properties as well as sensitive properties as the second moment of inertia are very well reproduced, specially within the CHFBLN approximation. We believe that the Gogny forces with the approximate particle number projected mean field theory provides a good description of nuclear properties under a large variety of situations.

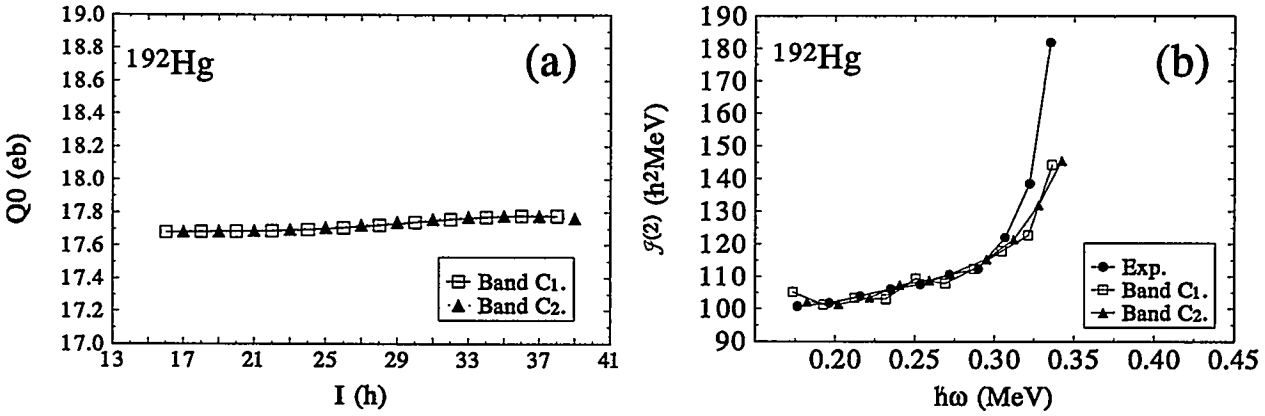


Figure 3: Left hand side, theoretical values of bands $C_1$ and $C_2$ for the charge quadrupole moment of band 3 of $^{192}$Hg. Right hand side, second moments of inertia for band 3 of $^{192}$Hg.

This work was supported in part by DGICyT, Spain under Project PB94–0164.

# References

[1] R. Bensgtsson et al. Phys. Lett. **B57**, 301 (1975); C. G. Anderson et al. Nucl. Phys. **A268**, 205 (1976); K. Neergard, H. Toki, M. Ploszajczak and A. Faessler Nucl. Phys. **A287**, 48 (1977).

[2] P. Bonche, P.H. Heenen and H.C. Flocard. Nucl. Phys. **A467**, 115 (1987).

[3] H.C. Flocard. *Nuclear Structure of the Zirconium Region,* J. Eberth, R.A. Meyer and K. Sistemich (Eds.). Research Reports in Physics. Springer-Verlag, p 143 (1988).

[4] J. Terasaki, P.-H. Heenen, P. Bonche, J. Dobaczewski and H. Flocard, Nucl Phys. **A593** (1995)1

[5] B.R. Mottelson and J.G. Valatin. Phys. Rev. Lett. **5**, 511 (1960).

[6] D. Gogny. *Nuclear Selfconsistent fields.* Eds. G. Ripka and M. Porneuf (North Holland 1975).

[7] J. Dechargé and D. Gogny. Phys. Rev. **C21**, 1568 (1980)..

[8] J.F. Berger, M. Girod and D. Gogny. Nucl. Phys. **A428**,23c (1984).

[9] J. L. Egido and L. M. Robledo, Phys. Rev. Lett. **70**, 2876 (1993).

[10] J. L. Egido, L. M. Robledo and R.R. Chasman, Phys. Lett. **B322** (1994) 22-26

[11] M. Girod, J.P. Delaroche, J. F. Berger and J. Libert, Phys. Lett. **B325** (1994) 1-6

[12] J. Konig and P. Ring, Phys. Rev. Lett. **71**, 3079 (1993)

[13] P. Ring and P. Shuck, *The Nuclear Many Body Problem* (1980), Springer–Verlag Edt. Berlin.

[14] P. Bonche, J. Dobaczewski, H. Flocard, P.-H. Heenen and J. Meyer, Nucl. Phys. **A510**, 466 (1990).

[15] A. Valor, J.L. Egido and L.M. Robledo, Phys. Rev. **C53**, 172 (1996).

[16] J.L. Egido and P. Ring, Nucl. Phys. **A388**, 19 (1982).

[17] A. Kamlah, Z. Phys. **216**, 52 (1968).

[18] D. C. Zheng, D.W.L. Sprung and H. Flocard, Phys. Rev. bf C46, 1335 (1992).

[19] H. J. Lipkin, Ann. Phys. (N.Y.) **12**, 425 (1960).

[20] Y. Nogami, Phys. Rev. **B134**, 313 (1964); Y. Nogami and I.J. Zucker, Nucl. Phys. **60**, 203 (1964).

[21] J. F. Goodfellow and Y. Nogami, Can. J. Phys. **44**, 1321 (1966). and W. Nazarewicz, Phys. Rev. **C48**, 1681 (1993). 2317 (1983).

[22] P. Willsau et al., Nucl. Ohys, **A574**(1994) 560

[23] P. Fallon et al, Phys Rev. **C51** (1995) R1609

[24] G. Gall, P. Bonche, J. Dobaczewski, H. Flocard and P.-H. Heenen, Z. Phys. **A348**, 183 (1994).

[25] W. Satula, S. Cwiok and W. Nararewicz, Nucl. Phys. **529**, 289 (1991)

[26] A. Valor, J.L. Egido and L.M. Robledo, to be published.

# Around the back-bend in an excited $^{150}$Gd Superdeformed Band

P. J. Twin[a], S. Ertürk[a], C. W. Beausang[a], P. Fallon[b],
D. Appelbe[a], S. Asztalos[b], A. Macchiavelli[b], T. Lauritsen[c],
I. Y. Lee[b], F. S. Stephens[b] and M. A. Deleplanque-Stevens[b]

*a* *Oliver Lodge Laboratory, University of Liverpool, Liverpool, L69 3BX, United Kingdom.*

*b* *Nuclear Science Division, Lawrence Berkeley National Laboratory, Berkeley, California 94720, USA.*

*c* *Physics Division, Argonne National Laboratory, Illinois 60439, USA.*

**Abstract:** The excited superdeformed band (band 5) in $^{150}$Gd has a discontinuity (back-bend) in the smooth variation of gamma-ray energy with spin at around 1 MeV. It has been established that the band also has a decay branch that is probably a continuation of band 5 below the back-bend. Gamma-rays have been identified which link band 5 with the yrast superdeformed band in $^{150}$Gd.

## 1. Introduction

There are four strongly excited superdeformed (SD) bands[1]) in $^{150}$Gd. The strongest (SD2) at 50% intensity of the yrast SD band is associated with a proton excitation from the low N [301]½ orbital into the high N $[651]^3/_2$. SD band 3 and 4 are signature parties and they exhibit $\mathcal{J}^{(2)}$ moments of inertia similar to the yrast SD band in $^{149}$Gd and thus they are associated with neutron excitations from the high N [770]½ orbital into the $[402]^5/_2$ orbitals. This report concerns SD band 5 which has an intensity of 38% relative to the yrast SD band and an $\mathcal{J}^{(2)}$ of a large magnitude similar to that of the yrast SD band in $^{152}$Dy. In addition the γ-ray energies are within 1 - 2 keV of those in $^{152}$Dy at the highest energies. These data have led to the proposal [2]) that $^{150}$Gd SD band 5 is associated with a two proton excitation from the [301]½ orbital into the $[651]^3/_2$ orbital. The γ-ray energies slowly diverge from those in $^{152}$Dy as the spin of the band decreases until there is a discontinuity or back-bend at a γ-ray energy of just below 1 MeV. This feature is unusual in SD bands in the A = 150 region, the other examples have been interpreted as neutron pairing effects in $^{150}$Gd band 1 [3]) and $^{149}$Gd band 2 [4,5]); proton pairing alignments [6]) in $^{144}$Gd band 1; and an interaction [7]) between the neutron [651]½ and $[642]^5/_2$ orbitals ($^{146, 147, 148}$Gd). In the case of Gd SD band 5 it has been suggested [2]) that the back-bend is linked to proton pair excitation.

The excited SD bands in $^{150}$Gd have been investigated in an experiment at Gammasphere (with 84 detectors installed) using the $^{130}$Te ($^{26}$Mg, 6n) reaction on 2 tellurium foils of thickness 500μg cm$^{-2}$ on 500μg cm$^{-2}$ gold with a thin layer of aluminium to prevent migration of the tellurium. Over $10^9$ events were recorded with unsuppressed fold greater than 5. Analysis has focussed on setting three selection conditions and thus using data with at least four coincidence γ-rays. Details of the decay scheme around the back-bend have been established and links between SD bands 5 and 1 have been identified [8].

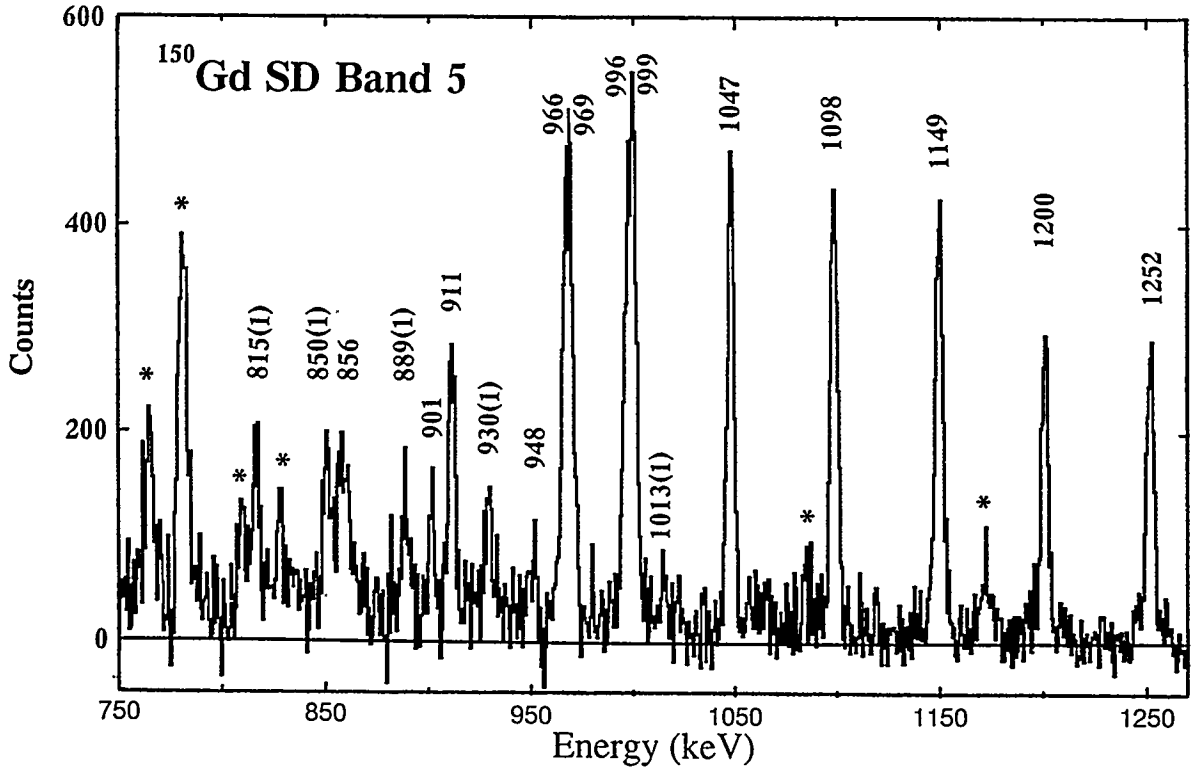


**Figure 1.** Spectrum of SD band 5 in $^{150}$Gd obtained by setting three gates on γ-rays in the band from 1047 keV to 1450 keV. The gamma-rays with energies of 815 keV, 850 keV, 889 keV, 930 keV and 1014 keV are identical to γ-rays in the yrast SD band (band 1) of $^{150}$Gd. Gamma-rays marked with an asterisk (*) are associated with the decay out of the band into normally deformed states.

## 2. The back-bend in $^{150}$Gd

The spectrum of $^{150}$Gd SD band 5 shown in figure 1 has been obtained by setting 3 gates on γ-rays between 1047 keV and 1450 keV (except 1098 keV as this is very similar to the energy of a γ-ray in the yrast SD band). The major intensity flow is via the doublets at 996, 999 keV and 966, 969 keV followed by the 911 keV transition. There are other γ-rays in the spectrum which are not observed in other SD bands and therefore are probably not associated with the decay out via normally deformed states. These include γ-rays with energies identical

to those at the lower spin end of the yrast band which will be discussed later and those at 856, 901 and 948 keV. The later transition is close to the strong 950 keV decay between normally deformed states but this decay is only very weakly seen in spectra obtained for other superdeformed bands in $^{150}$Gd.

A spectrum with two gates on SD band 5 on or above the 1047 keV transition and one gate on the 901 keV transition shows that this γ-ray is in coincidence with the 999 keV member of the higher energy doublet and weakly with the 966 member of the lower - energy doublet. However it is not in coincidence the two other members of those doublets. It is concluded that it is parallel with the 969 keV γ-ray as shown in the decay scheme proposed in figure 2. The 948 keV and 856 keV γ-rays are in coincidence with the 901 keV transition and thus they are placed with the 901 keV as a continuation of SD band 5 below the band crossing. The intensities of the four members of the back-bend doublets have been estimated from a series

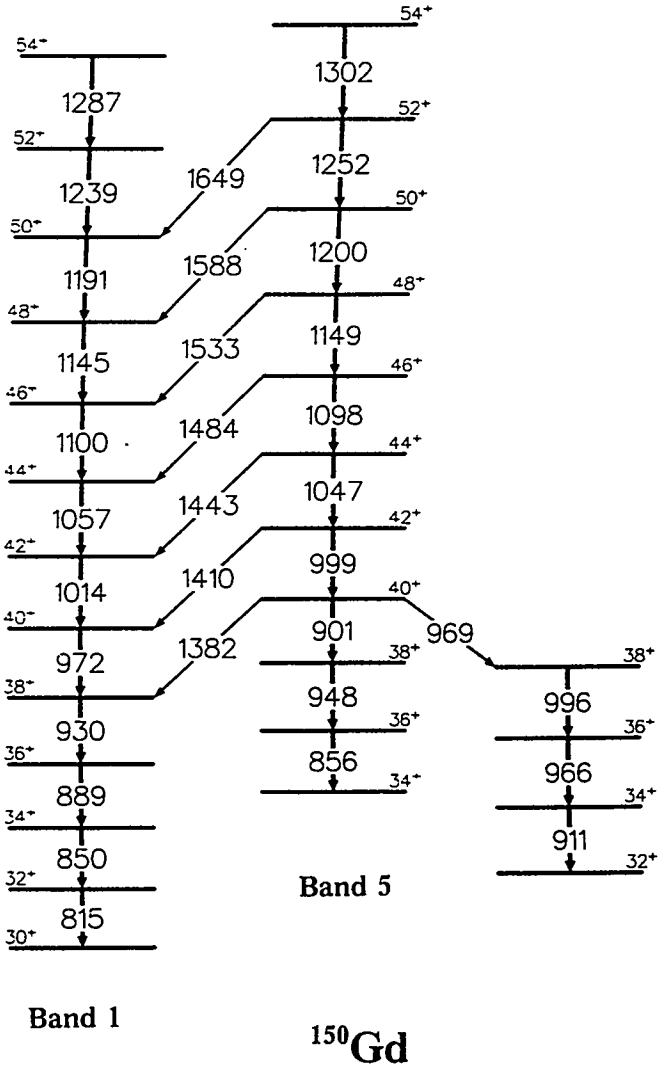


**Figure 2.** Decay scheme of SD band 5 in $^{150}$Gd showing the proposed continuation of the band below the band crossing and the transitions linking SD bands 5 and 1.

of spectra including those with the final condition being a narrow gate on one of the doublet members. These show that the intensities of the 966, 969 and 996 keV transitions are approximately equal and that the difference between these intensities and that of the 999 keV is equal to that of the 901 keV γ-ray. Thus there appears to be no loss of total intensity around the back-bend. The level scheme is consistent with a strong interaction between two levels of spin $38^+$ which are separated by 68 keV (fig. 2) whereas their unperturbed separation is 5 - 10 keV. Adjacent levels in the band would have much larger unperturbed separations and thus have much smaller perturbations of a few keV. Thus the level scheme in figure 2 is consistent with an accidental degeneracy of two states which have different SD configurations and thus it may not be a pairing interaction as previously [2]) suggested.

## 3. Decays between band 5 and band 1

The spectrum (figure 1) of SD band 5 in $^{150}$Gd indicates the presence of the lowest four transitions (815, 850, 889 and 930 keV) of the yrast SD band. The next members are the 972 keV transition, which is not fully resolvable from the 966/969 keV doublet, and the 1014 keV transition which is weaker. Higher energy members are not observable in the spectrum. The intensities of the lowest 4 band 1 γ-rays are each approximately 24% of the intensity of band 5. Gamma-rays linking bands 5 and 1 were identified from spectra generated by setting two gates on band 5 and one gate on band 1. In figure 3a the spectrum has two gates from 999 keV to 1450 keV on band 5 and one gate from 850 keV to 930 keV on band 1 whereas in figure 3b the gates on band 5 have been restricted to 1149 to 1450 keV and that on band 1 extended up to 1057 keV. A series of 7 transitions from 1382 keV up to 1649 keV are observed in these spectra. The 1381 keV γ-ray is much stronger in figure 3a which has gates extending down to 999 keV and the higher energy transitions are stronger in figure 3b where the gates on band 1 are extended to the higher energies. These transitions indicate unambiguously that the bands are linked as shown in figure 2. The γ-ray energies are consistent with this interpretation and it is possible that the links extend to even higher spins. The decay between the bands occurs at spins above the back-bend and it appears to stop at the back-bend. This is at variance with the initial suggestion that the inter-band decays were initiated by the back-bend. The linking transitions are currently being further investigated to establish their intensities and to measure angular correlation information which should give definite information on the multipolarity of the transitions. In fig. 2 the transitions are assumed to be of E2 character and the spins of the states to be even. These assignments are based on the identity of the γ-ray energies with those of the yrast SD band in $^{152}$Dy. However these spin assignments are two lower than currently assumed [7]) for the yrast SD band in $^{152}$Dy. If confirmed by the multipolarity information it shows that the spins of all SD bands with four N = 6 protons should be $2\hbar$ lower relative to Tb and Gd SD bands with two and three N = 6 protons.

The intensity data should enable conclusions about the character of band 5 and that of the linking transitions.

Support for this project is acknowledged from the UK EPSRC and the US DOE Nuclear Physics Division.

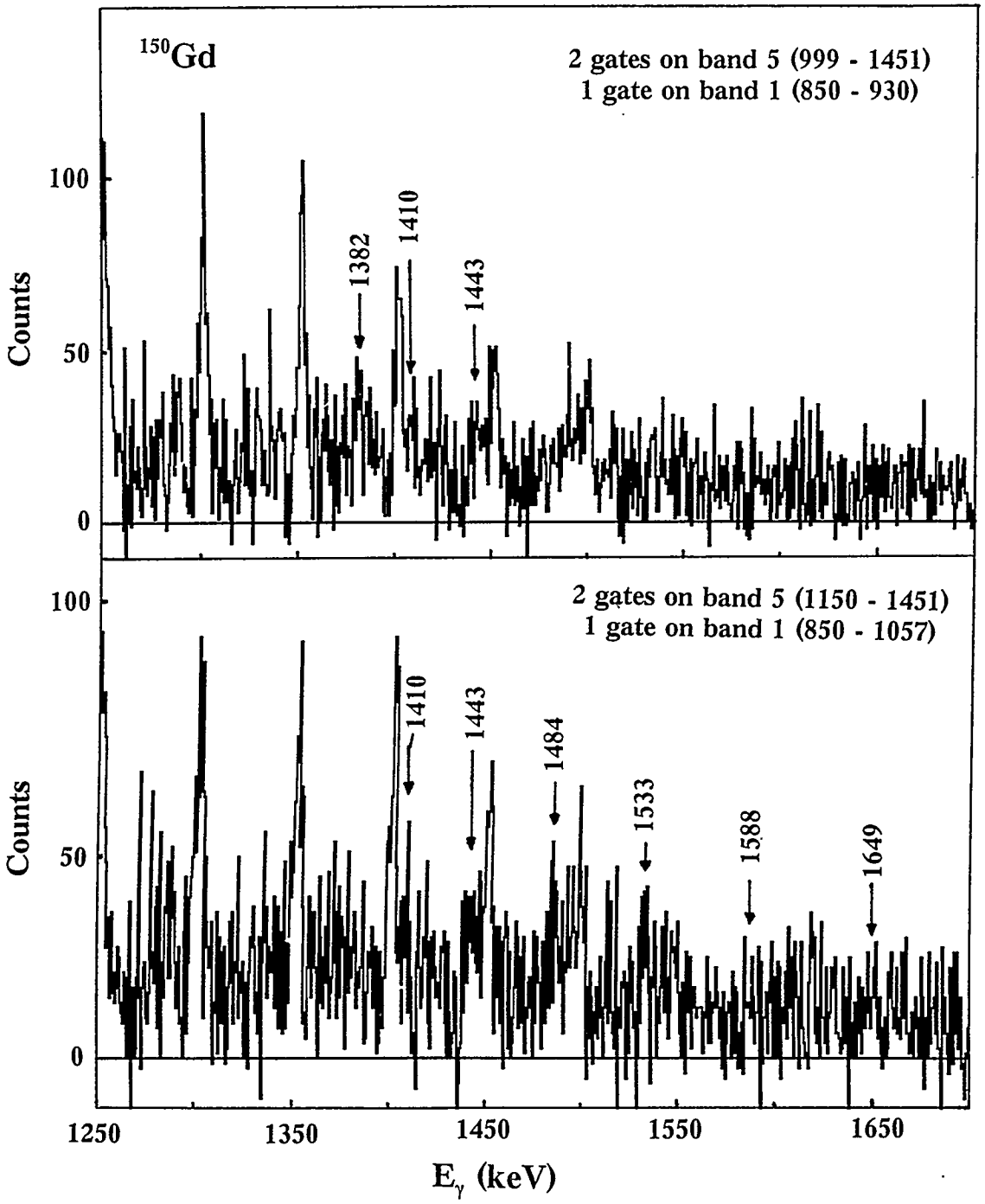


**Figure 3.** Spectra of SD band 5 in $^{150}$Gd showing linking transitions to SD band 1. a) Two gates are set on transitions in band 5 from 999 keV to 1451 keV (except 1098 keV) and one gate on transitions in band 1 from 850 keV to 930 keV. b) Two gates are set on transitions in band 5 from 1150 keV to 1451 keV and one gate on transitions in band 1 from 850 keV to 1057 keV (except 972 keV).

## References


1. C. W. Beausang et. al., Phys. Rev. Lett. **71** (1993) 1800.
2. P. Fallon et. al., Phys. Rev. Lett. **73** (1994) 782.
3. P. Fallon et. al., Phys. Lett. **B218** (1989) 137.
4. B. Haas et al., Phys. Rev. **C42** (1990) R1817.
5. S. Flibotte et. al., Phys. Rev. Lett. **71** (1993) 688.
6. S. Lunardi et. al., Phys. Rev. Lett. **72** (1994) 1427.
7. I. Ragnarsson, Nucl. Phys. **A557** (1993) 167c.
8. P. J. Twin et. al., (to be published).

# *Microscopic study of superdeformation in the A=150 mass region*

C. Rigollet[a], P. Bonche[b], H. Flocard[c], P.-H. Heenen[d] and B. Gall[a]

[a] CRN, IN2P3-CNRS, F67037 Strasbourg, France
[b] SPhT, CEN Saclay, F91191 Gif sur Yvette Cedex, France
[c] IPN, IN2P3-CNRS, F91406 Orsay Cedex, France
[d] Service de Physique Nucléaire Théorique,
ULB - CP 229, B1050 Brussels, Belgium

We are presently investigating the properties of superdeformed (SD) nuclear states in the A=150 mass region. For that purpose, we use the cranked HFB method in which pairing correlations are treated dynamically by means of the Lipkin-Nogami prescription [1]. Our goal is to take advantage of the large amount of experimental data to test the predictive power of our microscopic approach and of the effective interaction.

In the present communication, we focus on $^{152}Dy$ and$^{153}Dy$ for which there are recent experimental data. In particular lifetime measurements have allowed to extract electric quadrupole moments. The new Skyrme effective force SLy4 is used to describe the nucleon-nucleon interaction [2], while for the pairing channel we use a density-dependent zero-range interaction.

The SLy4 interaction is based on a complete study of symmetric and very asymmetric infinite nuclear matters. It improves older Skyrme parametrization with respect to the isospin dependence of nuclear properties. It makes use of more realistic ingredients such as the incompressibility modulus $K_\infty$ which has a too large value in SIII for instance; also, the spin-orbit strength is adjusted on the neutron states of $^{208}Pb$.

Pairing correlations are generated by a density-dependent zero-range interaction. Its intensity is chosen to reproduce the experimental dynamical moment of inertia of the yrast band in $^{150}Gd$. There is also a 5 MeV energy cut-off in the valence single particle space which limits the active pairing field in the vicinity of the Fermi energy.

As in our previous publications we used extensively the Skm* parametrization of the Skyrme force, we first compare the dynamical moment of inertia of $^{150}Gd$ and $^{152}Dy$ calculated both with Skm* and Sly4 to the experimental data. As shown in Fig.1, Sly4 leads to equally good or better results with respect to Skm*. In both cases, the magnitude of the $\mathcal{J}^{(2)}$ moment of inertia is slightly overestimated. Both forces give similar values for the charge quadrupole moments. In $^{152}Dy$ we obtain 17.5 eb, which agrees with experiment [3]. At the present time, there is no experimental value for $^{150}Gd$. For this nucleus, SkM* and SLy4 predict very similar values, 16 eb [1] and 16.2 eb respectively. In what follows, we only present results obtained with Sly4.

In Table 1, we compare calculated charge quadrupole moments with the available experimental data for yrast bands. Indeed lifetime measurements of superdeformed bands in $^{148-149}Gd$ and $^{152}Dy$ have been recently performed through the Doppler Shift Attenuation Method (DSAM) with the Eurogam array in Strasbourg [3]. Yrast

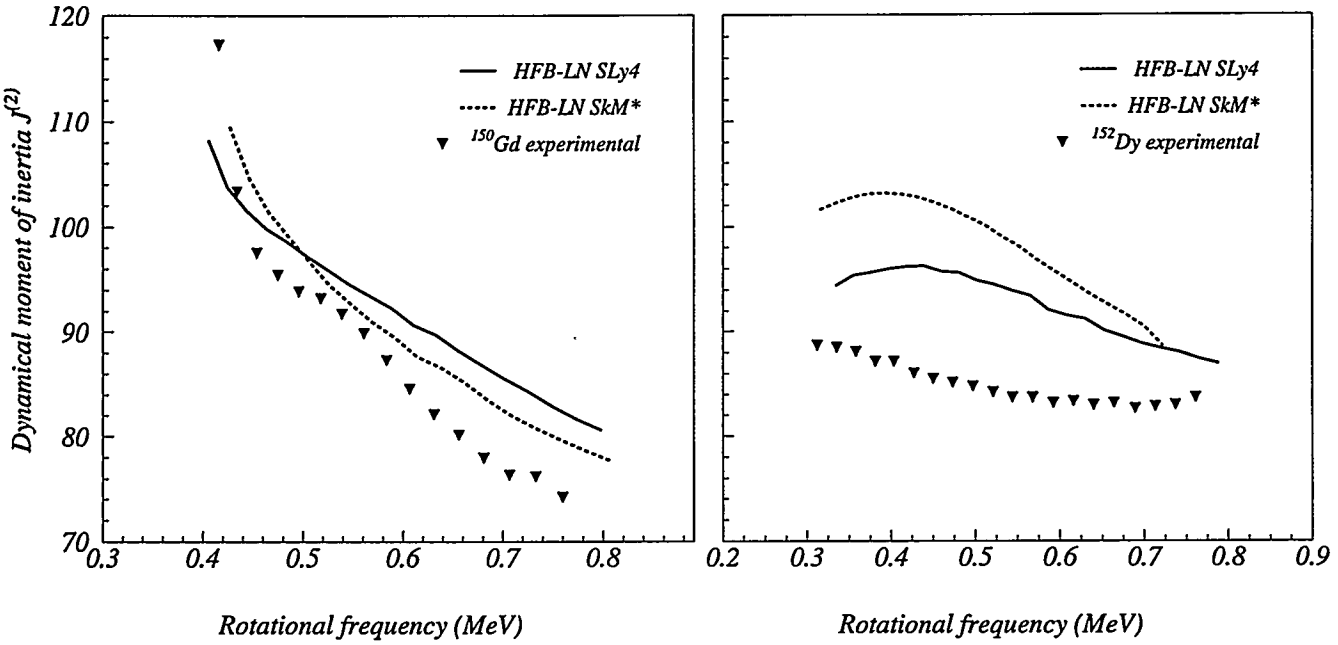


Figure 1: Dynamical moment of inertia calculated with SkM* and SLy4.

bands and some excited bands have been analysed and quadrupole moments were deduced. The different yrast band quadrupole moments are related to the different occupancy of the high-N orbitals [4]. The calculated values agree remarkably well with the data.

| Nucleus | $Q_0^{exp}$ (eb) | $Q_0^{cal}$ (eb) |
|---|---|---|
| $^{152}Dy$ | 17.5 | 17.5 |
| $^{149}Gd$ | 15.0 | 15.5 |
| $^{148}Gd$ | 14.6 | 15.2 |

Table 1.

To extract further informations on deformation, lifetime measurements of SD identical bands belonging to nuclei differing by only one neutron, $^{153}Dy$ and $^{152}Dy$, have been performed with the Gammasphere array in Berkeley [5]. The two nuclei were produced in the same fusion-evaporation reaction $^{124}Sn(^{34}Si, 5n-6n)^{153-152}Dy$ at a beam energy of 175 MeV.

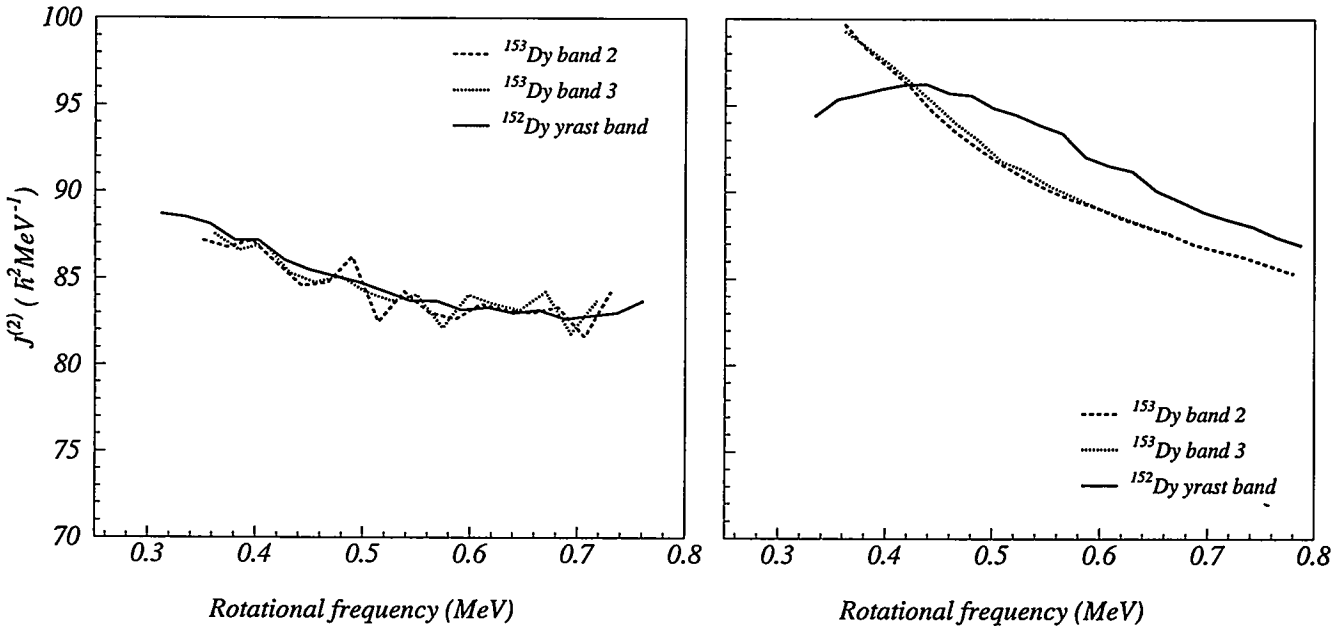


Figure 2: Experimental (left) and calculated (right) dynamical moments of inertia of $^{153}Dy$ (bands 2 and 3) and $^{152}Dy$ (yrast).

The first two excited bands in $^{153}Dy$ (bands 2 and 3) have their moment of inertia identical to that of the yrast band of $^{152}Dy$ (see Fig.2). Their transition energies are lying at the 1/4 and 3/4 points of those of the $^{152}Dy$ yrast band. This feature suggests the same occupancy of intruder orbitals for these 3 bands. Therefore, the last unpaired neutron should lie in an orbital with no signature splitting. Looking to Fig. 3, the best candidates are the [402]5/2±, [514]9/2± and [521]3/2± orbitals. As there is no evidence of band interactions in the $\mathcal{J}^{(2)}$ moment of inertia of those two excited bands in $^{153}Dy$, the most probable orbitals are the [402]5/2± ones.

On the other hand, the yrast band in $^{153}Dy$ has no signature partner. Therefore, its last unpaired neutron most probably occupies the intruder orbital [761]3/2$^-$. For this band, the calculation shows that this configuration lies 400 keV lower than the two excited bands. We found for this band a pattern typical of a band crossing around a rotational frequency of 550 keV, which is not found in the data. This feature is probably related to the large number of negative parity orbitals in the vicinity of the Fermi level. Further analysis is required before drawing any definite conclusions.

On the right-hand side of Fig. 2, we show the calculated moment of inertia of the excited bands of $^{153}Dy$. They are remarkably equal, however they are significantly smaller than that of $^{152}Dy$, in contrast with experiment. This deviation suggests that a careful analysis of other configurations is necessary to confirm the present assignement in $^{153}Dy$.

The quadrupole moments of these three bands are displayed in Fig. 4. As the two excited bands of $^{153}Dy$ are build on degenerate signature partner orbitals, they have the same quadrupole moment. The quadrupole moment of the $^{152}Dy$ yrast

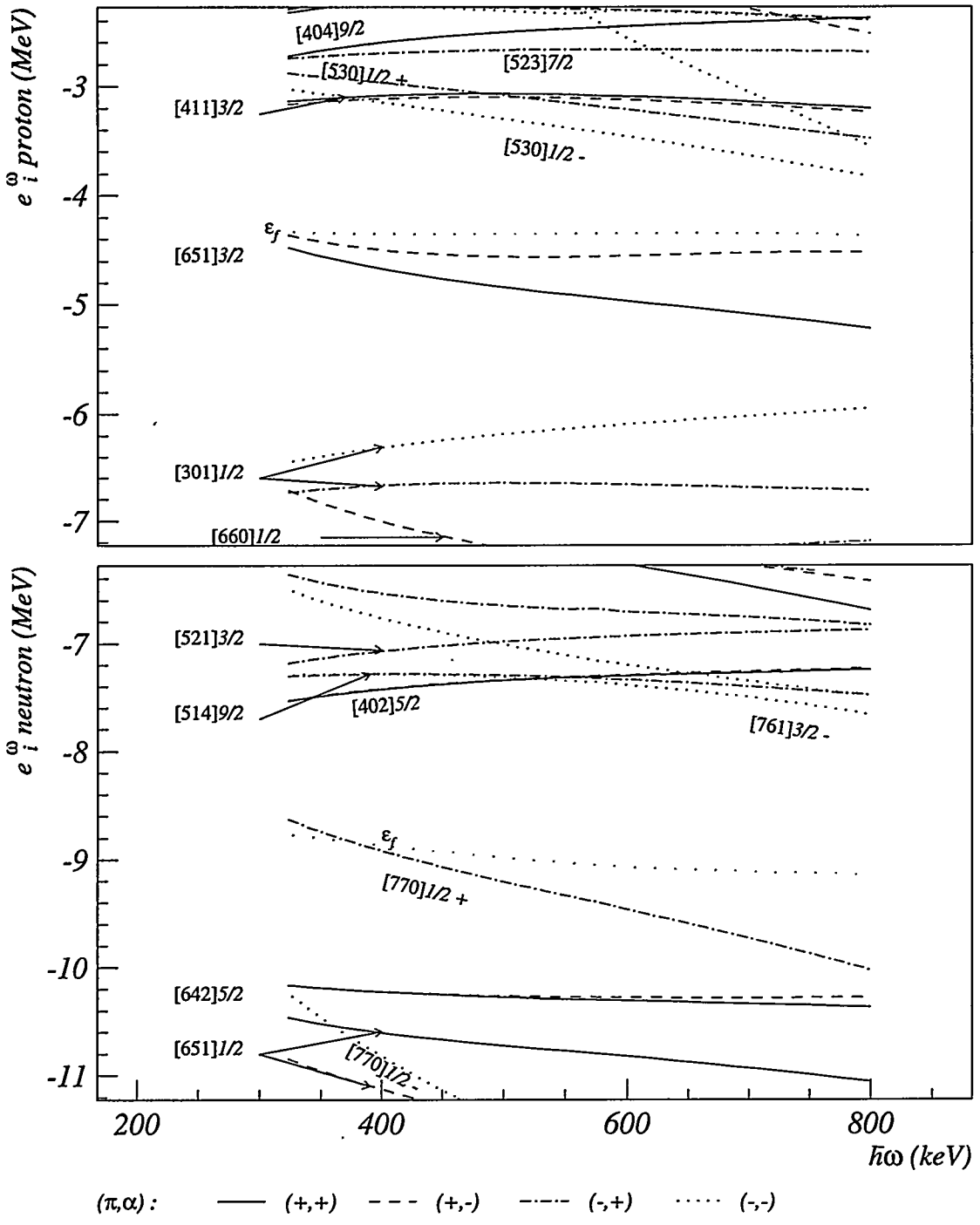


Figure 3: Single particle spectra for $^{152}Dy$.

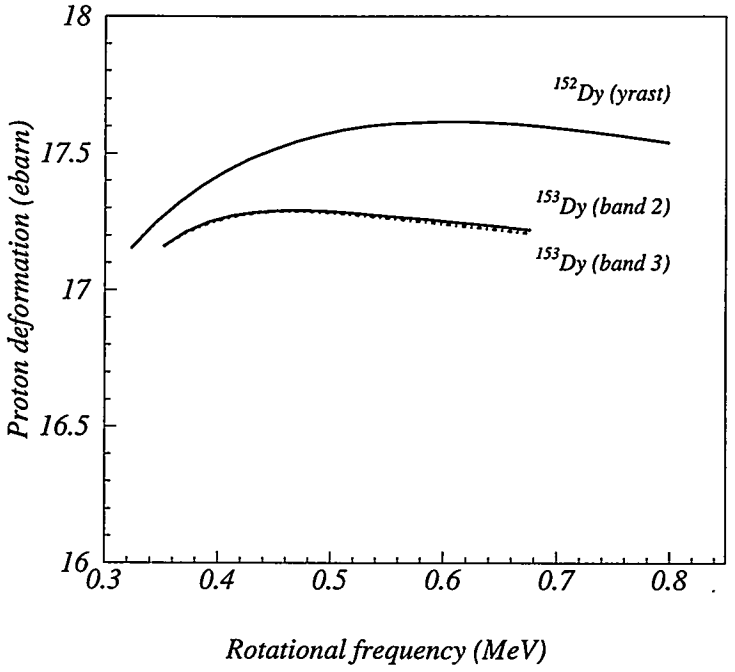


Figure 4: Proton deformations for the identicals bands $^{152}Dy(1)$, $^{153}Dy(2)$, $^{153}Dy(3)$.

band is larger. This can be related to the behavior of the [402]5/2 orbital as a function of deformation.

As the two nuclei were produced in the same reaction, the ratios of quadrupole moments can be extracted unambiguously. The theoretical values agree within the error bars with the experimental numbers, as shown in Table 2.

| Nucleus | $R_{th} = \frac{Q_0^{153Dy}}{Q_0^{152Dy}}\%$ | $R_{exp} = \frac{Q_0^{153Dy}}{Q_0^{152Dy}}\%$ |
|---|---|---|
| $^{153}Dy(yrast)$ | 101.7 | 99.5 (3.4) |
| $^{153}Dy(2)$ | 98.6 | 96.8 (3.4) |
| $^{153}Dy(3)$ | 98.6 | 98.4 (3.4) |

Table 2.

In summary, microscopic calculations based on the SLy4 parametrization of the Skyrme force prove to be very powerful for a detailed analysis of the structure of SD bands in the A=150 mass region.

# References

[1] P. Bonche, H. Flocard and P.-H. Heenen, Nucl. Phys. **A598** (1996) 169; B. Gall, P. Bonche, J. Dobaczewski, H. Flocard and P.-H. Heenen, Z. Phys. **A348** (1994) 183; J. Terasaki, P.-H. Heenen, P. Bonche, J. Dobaczewski, and H. Flocard, Nucl. Phys. **A593** (1995) 1

[2] E. Chabanat, P. Bonche, P. Haensel, J. Meyer and R. Schaeffer Phys. Script. **56** (1995) 231

[3] H. Savajols *et al.*, Phys. Rev. Lett. **76**, 4480 (1996)

[4] C. Baktash, B. Haas, W. Nazarewicz, Annu. Rev. Nucl. Sci. **45**, 485 (1995)

[5] C. Rigollet, Thesis work in progress.

# Lifetime Measurements and Identical SD Bands in the A=190 and A=150 Regions

E. F. Moore[1], D. Nisius[2], R. V. F. Janssens[2], T. L. Khoo[2], T. Lauritsen[2], D. Ackermann[2], I. Ahmad[2], H. Amro[2], D. Blumenthal[2], M. P. Carpenter[2], S. Fischer[2], G. Hackman[2], P. Fallon[3], S. J. Asztalos[3], R. M. Clark[3], M. A. Deleplanque[3], R. M. Diamond[3], R. Krueken[3], I-Y. Lee[3], A. O. Macchiavelli[3], F. S. Stephens[3], F. Hannachi[4], A. Lopez-Martens[4], J. A. Becker[5], L. Bernstein[5], L. P. Farris[5], E. A. Henry[5], A. Korichi[6],P. Chowdhury[7], R. H. Mayer[8], A. V. Afanasjev[9,10], I. Ragnarsson[9]

[1] *North Carolina State University, Raleigh, North Carolina 27695-8202, and Triangle Universities Nuclear Laboratory, Durham, North Carolina 27708-0308*

[2] *Argonne National Laboratory, Argonne, Illinois 60439*

[3] *Lawrence Berkeley National Laboratory, Berkeley, CA 94720*

[4] *Centre de Spectrométrie Nucléaire et de Spectrométrie de Masse, IN2P3-CNRS, bat 104-108, F-91405 Orsay, France*

[5] *Lawrence Livermore National Laboratory, Livermore, CA 94550*

[6] *Institut de Physique Nucléaire, F-91406, Orsay Cedex, France*

[7] *University of Massachussets, Lowell, MA 01854*

[8] *Rutgers University, New Brunswick, NJ 08903*

[9] *Lund Institute of Technology, P. O. Box 118, S-221 00 Lund, Sweden*

[10] *Nuclear Research Center, Latvian Academy of Sciences, LV-2169, Salaspils, Latvia*

(September 3, 1996)

The lifetimes of states in Superdeformed (SD) bands in $^{192,194}$Hg, $^{151,152}$Dy, and $^{151}$Tb have been measured using the Doppler shift attenuation method. Intrinsic quadrupole moments $Q_0$ have been extracted for SD bands in these nuclei. It was found that the quadrupole moments for the "identical" SD bands in these nuclei are the same. In the A=150 region, changes were found in the $Q_0$ values as a function of the number of high-N intruder orbitals. Changes are present also for excited SD bands with the same high-N content. Recent calculations account for most of the observations in the A=150 region.

## I. INTRODUCTION

Following the discovery of a band of coincident $\gamma$ rays with nearly constant energy separation in $^{152}$Dy [1], the large deformation associated with this band was established [2] with a lifetime measurement. With the discovery of similar bands in this mass region, lifetime measurements confirmed their superdeformed character. Similarly, the large deformation associated with a band in $^{191}$Hg [3] was confirmed with lifetime measurements. The limited sensitivity of the early generation of $\gamma$-ray detection arrays, however, restricted lifetime measurements to the most strongly populated (yrast) SD bands. With the new generation detector arrays coming online, the possibility of performing detailed lifetime measurements on excited SD bands has become a reality.

One of the most intriguing aspects of superdeformation is the existence of pairs of "identical" SD bands [4]. These bands have $\gamma$-ray energies that are equal or exhibit a simple relationship to each other (i.e., energies in one band fall at the mid-point energies in the other). Of interest to the present work are two spectacular examples of identical SD bands in both the A=150 and A=190 regions; band 4 of $^{151}$Dy has $\gamma$-ray energies that fall almost exactly at the mid-point energies of band 1 of $^{152}$Dy, and the $\gamma$-ray energies of $^{194}$Hg band 3 are identical to those in $^{192}$Hg band 1 over nearly the entire energy range [4]. The equality of the $\gamma$-ray energies requires that the nuclear moments of inertia to be equal to $\sim 0.2\%$. With the improved resolving power provided by the new arrays, it now becomes possible to perform precise lifetime measurements which may shed light on the properties of the identical bands.

## II. MEASUREMENTS IN THE A=190 REGION

### A. Experimental conditions

In order to establish the relative deformations associated with SD bands, care must be taken to minimize systematic uncertainties, especially those associated with stopping powers. We have used ($^{48}$Ca,4n) reactions on $^{148}$Nd and $^{150}$Nd targets to measure lifetimes in the SD bands of $^{192}$Hg and $^{194}$Hg, respectively. The beams were supplied by the 88 inch cyclotron at Lawrence Berkeley National Laboratory. In each case, the Nd targets were 1.0 mg/cm$^2$ thick and the recoiling nuclei were slowed down and brought

to rest in Au backings. For the $^{192}$Hg measurement, the beam energy of 205 MeV results in a calculated mid-target $v_0/c = 0.0230$, $l_{max} = 47\hbar$, and $E^* = 19$ MeV. In the case of $^{194}$Hg the beam energy of 202 MeV results in $v_0/c = 0.0226$, $l_{max} = 45\hbar$, and $E^* = 21$ MeV. It is important to note that since the same stopping material was used and the velocity profiles and nuclear charges are the same for both $^{192}$Hg and $^{194}$Hg, the difference in stopping powers is negligible.

The $\gamma$ rays were measured at Gammasphere during two separate beamtimes. The first experiment was performed at a time when Gammasphere consisted of 55 detectors arranged into 11 angular rings, ranging from 17° to 163° with respect to the beam direction. Approximately $1 \times 10^9$ triples and higher fold events were recorded for both $^{192}$Hg and $^{194}$Hg. The second experiment was performed when 85 detectors were present in Gammasphere and were arranged into 16 angular rings ranging from 32° to 163° with respect to the beam direction. In this beamtime, some $1.8 \times 10^9$ quadruple and higher fold events were recorded for $^{194}$Hg.

### B. Analysis and results

Angle sorted spectra were constructed by combining double gates set on stopped and nearly stopped transitions at the bottom of each of the SD bands. Care was taken to ensure that consistent gating conditions were applied to each of the SD bands studied. As is customary for this type of measurement, fractions of the full Doppler shift $F(\tau)$ were extracted from the spectra using the first order relation

$$F(\tau) = \frac{\overline{E_\gamma} - E_{\gamma 0}}{E_{\gamma 0}\beta_0 \cos\theta},$$

where $\overline{E_\gamma}$ is the centroid of the $\gamma$-ray energy distribution as measured in a detector located at angle $\theta$ with respect to the beam direction, $E_{\gamma 0}$ is the unshifted $\gamma$-ray energy, and $\beta_0$ is the mid-target initial recoil velocity.

In order to extract the intrinsic quadrupole moments $Q_0$ for the various SD bands, computer simulations of the $\gamma$-decay of the recoiling nuclei were performed using the code FITFTAU. The simulations all used stopping powers obtained from the 1995 version of the code TRIM by Ziegler [5]. The simplest version of the simulation makes the following basic assumptions: (1) the $Q_0$ values are constant within a given SD band, and the partial decay rate T (in $ps^{-1}$) of a band member of spin I is described within the rotational model by the expression:

$$T(I \rightarrow I\text{–}2) = 1.22 E_\gamma^5 Q_0^2 <IK20|(I\text{–}2)K>^2$$

where $E_\gamma$ is the $\gamma$-ray energy in MeV, (2) the sidefeeding into each SD state has exactly the same time structure as the main band, (3) any delay in feeding a band was approximated by a one-step delay. This model (referred to as model I) then describes the band in terms of two fit parameters, namely $Q_0$ and $\tau_{delay}$ and a two-dimensional $\chi^2$ minimization was performed.

In addition to the model described above, a more realistic model (model II) of the sidefeeding was also used in the analysis. In this model, the sidefeeding is assumed to consist of rotational bands having the same moment of inertia ($\gamma$-ray energies) as the main cascade. All sidefeeding cascades were assumed to have a common quadrupole moment $Q_{SF}$ with additional one-step feeding delays ($\tau_{delay}$) at the top. Furthermore, the number of transitions in the sidefeeding cascades was assumed to be proportional to the length of the main cascade above the state of interest. Three fit parameters were therefore used in this case, $Q_0$, $Q_{SF}$, and $\tau_{delay}$, and a three-dimensional $\chi^2$ minimization was performed.

The results of the centroid shift analysis are presented in table I, and examples of fits to $^{192}$Hg band 1 are shown in Fig. 1. From these results it is clear that model II gives much better fits to the data. This is an indication that the simple treatment of sidefeeding used in model I is inadequate to describe the complicated feeding patterns of the SD bands. The values of $Q_{SF}$ obtained from model II fits to the data are significantly lower than those in the main band. However, given the incomplete knowledge of the "true" characteristics of the sidefeeding and the assumptions that went into this model (i.e. same $\mathcal{J}^{(2)}$, number of transitions in SF cascades), it would be premature to assign too much significance to the $Q_{SF}$ values. One should note that the in-band $Q_0$ values increase by $\sim 10\%$ when this model of the sidefeeding is used.

With the exception of $^{194}$Hg band 1, the in-band $Q_0$ values are very similar from band to band. The measured value for band 1 in $^{194}$Hg is larger than that reported by Hughes *et al* [6], while the value obtained for band 2 is similar to that measured previously. A detailed lineshape analysis is in progress for all of the SD bands reported here. Preliminary results for the yrast SD bands in $^{192,194}$Hg indicate that the difference in average $Q_0$ values is somewhat smaller, $17.6 \pm 1.8$ eb versus $18.4 \pm 1.1$ eb for $^{192}$Hg and $^{194}$Hg, respectively. The lineshape fits also indicate that the $Q_0$ values are essentially constant over the range of transition energies measured.

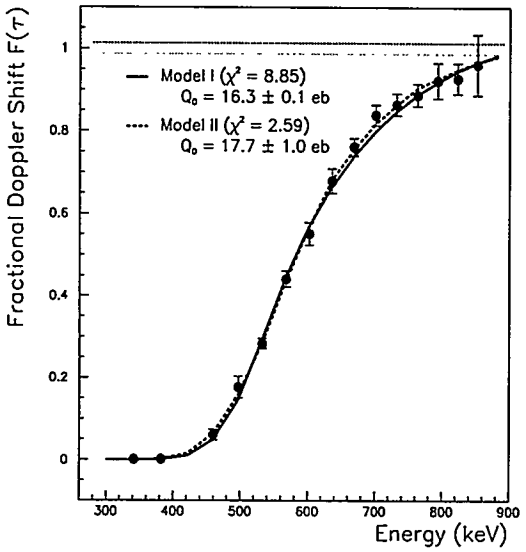


FIG. 1. Fits to the fraction of the full Doppler shift for band 1 in $^{192}$Hg using both models described in the text. The dotted horizontal lines represent the spread in recoil velocities due to the slowing down of the beam through the target.

TABLE I. Summary of centroid shift analysis results for SD bands in $^{192,194}$Hg. The last column for each model lists the total and reduced best-fit $\chi^2$ values.

| Model I Band | $Q_0$ (eb) | $\tau_{delay}$ (fs) | $\chi^2/\chi^2_\nu$ |
|---|---|---|---|
| $^{192}$Hg (1) | $16.2 \pm 0.1$ | $1^{+7}_{-1}$ | 8.85/0.68 |
| $^{194}$Hg (1) | $17.3 \pm 0.2$ | $34^{+8}_{-12}$ | 8.11/0.62 |
| $^{194}$Hg (2) | $17.2^{+0.2}_{-0.3}$ | $24^{+13}_{-19}$ | 4.88/0.44 |
| $^{194}$Hg (3) | $16.3^{+0.3}_{-0.1}$ | $1^{+18}_{-1}$ | 7.13/0.71 |
| **Model II Band** | **$Q_0$ (eb)** | **$Q_{SF}$ (eb)** | **$\tau_{delay}$ (fs)** | **$\chi^2/\chi^2_\nu$** |
| $^{192}$Hg (1) | $17.7 \pm 1.0$ | $10.9 \pm 1.0$ | $6 \pm 6$ | 2.59/0.22 |
| $^{194}$Hg (1) | $19.2^{+0.4}_{-0.8}$ | $10.0^{+1.2}_{-0.4}$ | $39 \pm 6$ | 4.01/0.33 |
| $^{194}$Hg (2) | $17.6 \pm 0.6$ | $11.6 \pm 1.2$ | $28^{+3}_{-6}$ | 3.03/0.28 |
| $^{194}$Hg (3) | $17.7 \pm 0.8$ | $10.8 \pm 0.8$ | $3.5^{+5.0}_{-3.5}$ | 2.95/0.33 |

The most interesting result obtained from this analysis is that the $Q_0$ values for the identical SD bands, $^{192}$Hg (1) - $^{194}$Hg (3), are equal to each other. *This result is independent of the sidefeeding assumptions used in the analysis.* While the experimental errors are too large to determine whether the deformation in $^{194}$Hg (3) is slightly smaller to compensate for the increase in mass with respect to $^{192}$Hg, it is clear that there can be no *large* differences in deformation. As will be shown below, similar results have been obtained from differential DSAM measurements in the A$\sim$150 region. For SD bands in $^{151}$Dy [7] and $^{149}$Gd [8], which are identical to the yrast SD band in $^{152}$Dy, the intrinsic quadrupole moments were all found to have the same value.

## III. MEASUREMENTS IN THE A=150 REGION

### A. Experimental conditions

The differential lifetime measurements in the A=150 region were performed at a time when 56 Compton-suppressed Ge detectors were present in Gammasphere. A 175 MeV $^{34}$S beam was provided by the 88 Inch cyclotron at LBNL on a target which consisted of a 1 mg/cm$^2$ $^{122}$Sn layer evaporated on a 20 mg/cm$^2$ Au backing. In this experiment, $^{151}$Dy nuclei were produced via the dominant ($^{34}$S,5$n$) fusion-evaporation reaction while the $^{152}$Dy and $^{151}$Tb nuclei resulted from the weaker ($^{34}$S,4$n$) and ($^{34}$S,$p4n$) channels, respectively. A total of $1.5 \times 10^9$ triple and higher fold coincidence events were recorded.

The fractional Doppler shifts $F(\tau)$ were obtained for transitions in four SD bands in $^{151}$Dy, as well as for $\gamma$ rays in the yrast SD bands in $^{152}$Dy and $^{151}$Tb. The $F(\tau)$ values were extracted from the data, as described earlier, under the assumption that $F(\tau) = 1.0$ corresponds to the v/c of nuclei formed at the center of the target. For the present experiment, a calculation of the mid-target recoil velocity gives $\beta_0 = 0.0227$. If one assumes isotropic evaporation of particles in the rest frame of the recoiling compound nuclei, all residues should have the same value for $\beta_0$. Furthermore, the velocity profiles for the $^{151,152}$Dy nuclei should be the same over the full stopping range, while that for $^{151}$Tb may be somewhat different due to electronic stopping power differences resulting from the different $Z$ value. The experimental $F(\tau)$ points are presented in Fig. 2. With the exception of $^{152}$Dy, all data points approach $F(\tau) = 1.0$ at the highest $\gamma$-ray energies.

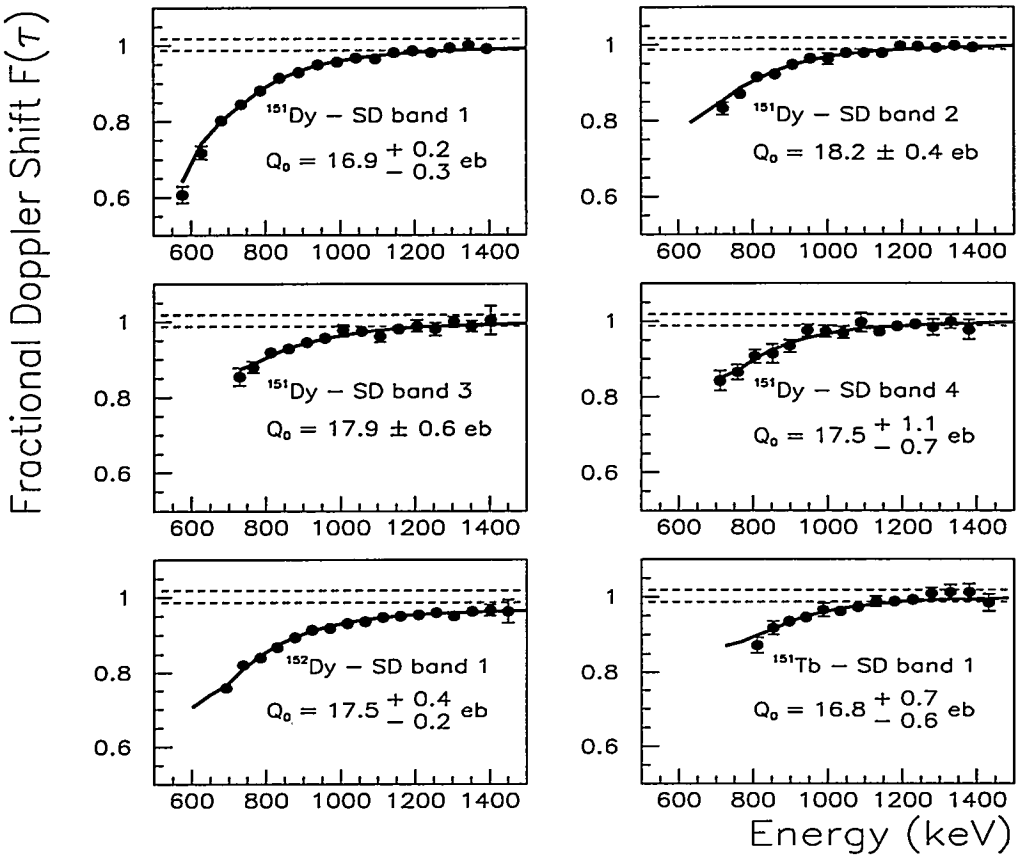


FIG. 2. Fits to the fraction of the full Doppler shift for SD bands in the A=150 region. The dotted horizontal lines represent the spread in recoil velocities due to the slowing down of the beam through the target.

TABLE II. Comparison of the results from this experiment and from the measurement of ref. [8] with recent theoretical calculations described in the text. The quoted errors do not include stopping power uncertainties. Most of the calculated values are taken at a spin value of 40 $\hbar$.

| Nucleus | $Q_0^{exp}$ (eb) | $Q_0^{MO}$ | $Q_0^{WS}$ | $Q_0^{RMF}$ | $Q_0^{SkP}$ | $Q_0^{SKM*}$ | $Q_0^{DD}$ |
|---|---|---|---|---|---|---|---|
| $^{152}$Dy | $17.5 \pm 0.2^a$<br>$17.5\ ^{+0.4}_{-0.2}$ | 18.9 | 18.9 | 18.9 | 18.5 | 18.5 | 17.6 |
| $^{151}$Dy | $16.9\ ^{+0.2}_{-0.3}$ | 18.0 | 18.0 | 18.1 | 17.9 | 18.0 | 16.6 |
| $^{151}$Tb | $16.8\ ^{+0.7}_{-0.6}$ | 18.1 | 18.0 | 18.1 | 17.5 | 17.5 | 17.0 |
| $^{149}$Gd | $15.0 \pm 0.2^a$ | 16.5 | 16.2 | 16.0 | 16.1 | 16.2 | 15.6 |
| $^{148}$Gd | $14.6 \pm 0.3^a$ | 16.0 | 15.6 | 15.7 | 15.5 | 15.8 | 15.2 |

[a]from Savajols *et al.* [8].

### B. Analysis and results

The extraction of intrinsic quadrupole moments $Q_0$ for the various SD bands proceeded in the same manner as described above for the A=190 region. The stopping powers for the various residual nuclei were all calculated using TRIM [5]. The best fit calculated $F(\tau)$ curves are presented in Fig. 2.

In the fit of the $F(\tau)$ values a $\chi^2$ minimization was performed. For the SD bands in $^{151}$Dy and $^{151}$Tb, the sidefeeding delay was well described in terms of the parameters $Q_0$ and $Q_{SF}$ only, (i.e., very good agreement with the data was obtained with $T_{SF} = 0$). However, in the case of $^{152}$Dy, an additional delay of $T_{SF} \simeq 25$ fs was required to fit the data.

We have examined the possibility that this difference in feeding delay might be an artifact of the analysis. We note that these data points were obtained in exactly the same way as those in $^{151}$Dy and $^{151}$Tb. Since all the recoils are formed in the same reaction, it is difficult to see how a change in the condition of the target would produce such a difference. We have also investigated the possible difference in the $4n$ and $5n$ production cross sections across the target thickness. The combination of measured excitation functions [9] and statistical model calculations [10] indicate that this difference is too small to explain the observed deviations. The origin of this sidefeeding delay remains an open question which will be the subject of further investigation. It is important to note that the value of $Q_0$ obtained in the fitting process is most strongly determined by those data point having $F(\tau) < 0.9$, where there is little or no sidefeeding. Finally, we note that the value of $Q_0$ for $^{152}$Dy obtained here is in excellent agreement with that of Savajols *et al.* [8] (see Table 2).

The results of the present analysis show that the quadrupole moment of the "identical" SD band in $^{151}$Dy has the same value of the yrast SD band of $^{152}$Dy. Furthermore, as shown in Tab. 2, our results combined with those of Savajols *et al.* [8] nicely illustrate the effect of the occupation of specific high-N intruder orbitals on the SD quadrupole moments.

Under the usual assumption that the yrast SD band in $^{152}$Dy corresponds to a closed core configuration containing four N=6 protons and two N=7 neutrons ($\pi 6^4 \nu 7^2$), the yrast SD bands can be described as single neutron-hole ($\pi 6^4 \nu 7^1$) and single proton-hole ($\pi 6^3 \nu 7^2$) configurations, respectively. These high-N intruder orbitals are strongly deformation driving and can be expected to have a large influence on the SD $Q_0$ values, as is seen in the data: the $Q_0$ value in $^{152}$Dy is larger than for the yrast SD bands in $^{151}$Dy and $^{151}$Tb. The data also suggest that the influence of proton and neutron intruder orbitals on the $Q_0$ values is similar.

The polarization effects resulting from the occupancy of specific intruder orbitals have recently been calculated in a variety of theoretical approaches, a number of which are compared in Table 2. The results of Nilsson-Strutinsky cranking of the modified oscillator potential with the parameters of ref. [11] are presented as $Q_0^{MO}$ in Table 2, the results for the Gd isotopes and $^{152}$Dy were published previously [8]. Results of cranked Strutinsky calculations with a Woods-Saxon potential [12] are given as $Q_0^{WS}$. The symbol $Q_0^{RMF}$ refers to calculations using the cranked relativistic mean field approach [13]. Finally, the symbols $Q_0^{SkP}$, $Q_0^{SKM*}$, and $Q_0^{DD}$ refer to the Hartree-Fock calculations with SkP and SKM* interactions of Satula *et al.* [14], and with density-dependent zero-range pairing interaction of Bonche *et al.* [15]. Clearly, all of these calculations reproduce the relative changes in $Q_0$ very well. It should be mentioned that the $\sim 10\%$ discrepancies between the experimental values and some of the calculations is not considered serious since they are well within the absolute uncertainties due to stopping powers and the $r_0$ parameter, for example.

The present measurements also probe the possible dependence of the $Q_0$ values on the specific configurations occupied in the $^{151}$Dy SD well. The excited SD bands in $^{151}$Dy are interpreted as excitations in which the the hole (with respect to $^{152}$Dy) can occupy some of the natural parity orbitals in the vicinity of the Fermi surface. In contrast with the yrast SD band in $^{151}$Dy, the intruder content of these excited bands is then the same as in $^{152}$Dy band 1

TABLE III. Calculated $Q_0$ values for three orbitals which may be involved in the configurations of the excited SD bands in $^{151}$Dy. Most of the calculated values are taken at a spin value of 40 $\hbar$. The intruder configuration for band 1 is given for comparison.

| Configuration | $Q_0^{MO}$ | $Q_0^{RMF}$ | $Q_0^{SkP}$ | $Q_0^{SKM*}$ |
|---|---|---|---|---|
| $\nu 7^1$ | 18.0 | 18.1 | 17.9 | 18.0 |
| [651]1/2 | 18.3 | - | 18.1 | - |
| [642]5/2 | 18.4 | 18.7 | 18.3 | 18.3 |
| [411]1/2 | 19.0 | - | 18.7 | 18.7 |

($\pi 6^4 \nu 7^2$) and single-particle Routhians indicate that the neutron holes will most likely be created in the [651]1/2, [642]5/2, or [411]1/2 orbitals [12,16]. From Fig. 1 it is clear that bands 2-4 in $^{151}$Dy are characterized by $Q_0$ values which are larger than that of band 1, as would be expected for bands having an additional $\nu 7$ intruder occupied. More surprising is the observation that the $Q_0$ values for band 2 and, perhaps for band 3, may even be larger than that for $^{152}$Dy SD band 1. In order to investigate this point the Nilsson-Strutinsky calculations described above were extended to some of the proposed orbitals. The results of the calculations are given in Table 3, together with values obtained from other approaches where available.

The "identical" band (band 4) of $^{151}$Dy was assigned [17] to the [411]1/2 orbital as the transition energies in this band lie half-way between those of band 1 in $^{152}$Dy as predicted by Nazarewicz *et al.* [18]. Using the strong coupling picture, these authors showed that, within the pseudospin coupling scheme, the [411]1/2 orbital is associated with a decoupling parameter $a$ having the exact value $a = -1$ (required to obtain transition energies at the halfway point). As shown in Table 3, the $Q_0$ value calculated for the [411]1/2 configuration is almost exactly equal to the value calculated for $^{152}$Dy band 1 (as are the measured values), whereas the values calculated for the [642]5/2 and [651]1/2 orbitals are closer to that of $^{151}$Dy band 1. The data seem to favor the scenario proposed by Ragnarsson [16], which assigns both bands 2 and 4 to the [411]1/2 orbital, although the measured $Q_0$ value for band 2 appears somewhat larger than expected from the calculations. Finally, the calculations of ref. [16] assign band 3 to the [642]5/2 configuration. However, the fact that the measured $Q_0$ value for this band is closer to that of $^{152}$Dy band 1 than that of $^{151}$Dy band 1 stands in contrast to the calculations. Further theoretical investigations may be required to account for these bands properly.

## IV. SUMMARY

Lifetime measurements for identical SD bands in $^{151,152}$Dy and $^{192,194}$Hg have demonstrated that another observable, the intrinsic quadrupole moment, associated with these bands is the same. The results in the A=190 region have also shown that the $Q_0$ values obtained from centroid shift analyses are very sensitive to the treatment of sidefeeding. It is encouraging to note that these types of measurements are no longer limited by the statistical accuracy of the measurement but rather by the fundamental assumptions made in the analysis of the data.

The measurements in the A=150 region combined with those of Savajols *et al.* [8] dramatically illustrate the strong influence that the occupation of specific high-N intruder orbitals have on the $Q_0$ values. In addition, the present investigation indicates that in certain cases, the occupation of other, non-intruder orbitals can also affect the $Q_0$ values. It should be pointed out that while a clear picture appears to emerge for the A=150 region, the situation remains less clear for SD nuclei of the A$\sim$190 region. It is hoped that the results of detailed lifetime measurements in the A=190 region will stimulate detailed calculations of these quantities, similar to those now available for SD nuclei in the A=150 region.

This work was supported in part by the Department of Energy, Nuclear Physics Division under contract nos. DE-FG05-88ER40441, W-31-109-ENG-38, DE-AC03-76SF00098, and W-7405-ENG-48.

[1] P. J. Twin *et al.*, Phys. Rev. Lett. **57**, 811 (1986).
[2] M. A. Bentley *et al.*, Phys. Rev. Lett. **59**, 2141 (1987)
[3] E. F. Moore *et al.*, Phys. Rev. Lett. **63**, 360 (1989).
[4] C. Baktash, B. Haas and W. Nazarewicz, Annu. Rev. Nucl. Part. Sci. **45** (1995) 485.
[5] J.F. Ziegler, J.P. Biersack, and U. Littmark, The Stopping and Range of Ions in Solids (Pergamon, New York,1985), J.F. Ziegler, private communication (1995).
[6] J. R. Hughes *et al.*, Phys. Rev. Lett. **72**, 824 (1994).
[7] D. Nisius *et al.*, to be published.
[8] H. Savajols *et al.*, Phys. Rev. Lett. **76** (1996) 4480.
[9] G. Smith *et al.*, Phys. Rev. Lett. **68** (1992) 158.
[10] F. Puhlhofer, Nucl. Phys. **A280** (1977) 267, and D. Hofmann, private communication.
[11] B. Haas *et al.*, Nucl. Phys. **A561** (1993) 251.
[12] W. Nazarewicz, R. Wyss and A. Johnson, Nucl. Phys. in press.
[13] A. V. Afanasjev, J. J. König and P. Ring, Nucl. Phys. in press.
[14] W. Satula, J. Dobaczewski, J. Dudek and W. Nazarewicz, private communication and to be published.
[15] P. Bonche, H. Flocard and P. -H. Heenen, Nucl. Phys. **A598** (1996) 169.
[16] I. Ragnarsson, Acta Polonica **B27** (1996) 33.
[17] D. Nisius *et al.*, Phys. Lett. **B346** (1995) 15.
[18] W. Nazarewicz et al., Phys. Rev. Lett **64** (1990) 1654.

# RDDS lifetime measurements of low–lying superdeformed states in $^{194}$Hg

R. Kühn[a], A. Dewald[a], R. Krücken[a*] C. Meier[a], R. Peusquens[a], H. Tiesler[a], O. Vogel[a], S. Kasemann[a], P. von Brentano[a], D. Bazzacco[b],C. Rossi-Alvarez[b],G. De Angelis[c] and J. de Boer[d]

[a] *Institut für Kernphysik, Universität Köln, Köln, Germany*
[*] *Present address: LBNL, Berkeley, USA*
[b] *Dipartimento di Fisica, Universita and INFN Sezione Padova, Italy*
[c] *INFN, Laboratori Nationali di Legnaro, Italy*
[d] *Sektion Physik, Universität München, Garching, Germany*

(August 30, 1996)

Abstract: The lifetimes of three low–lying states in the superdeformed (SD) yrast band of $^{194}$Hg were measured by the recoil-distance Doppler-shift method. The deduced transition quadrupole moments,$Q_t$,equal those extracted from a DSAM measurement for the high-lying states of the band corroborate the assumption that the decay out of SD bands does not strongly affect the structure of the corresponding states. By a simple mixing-model the decay can be described assuming a very small admixture of normal-deformed (ND) states to the decaying SD states. The deduced ND mixing amplitudes for the yrast SD bands in $^{192,194}$Hg and $^{194}$Pb are presented along with average transition quadrupole moments for the lower parts of the excited SD bands.

## I. INTRODUCTION

The study of the decay mechanism leading to the abrupt depopulation of superdeformed (SD) bands in the A≈190 mass region at low spins is one of the most exciting topics in present nuclear-structure physics. Recently, discrete $\gamma$–transitions connecting SD bands with the normaldeformed (ND) part of the level scheme were observed first in $^{194}$Hg [1] and later in $^{194}$Pb [2]. It was therefore possible to extract the spins, likely parities and particularly the exact excitation energies of the SD states which thus become favorite candidates for further detailed investigations.

In this work, we report on a RDDS measurement of the lifetimes of low–lying states in the SD bands in $^{194}$Hg. We succeeded to determine the lifetimes of the $12^+$, $14^+$ and $16^+$ states of the SD yrast band. Using branching ratios for the decay out of the SD band from a experiment [3] with high statistics, transition quadrupole moments, $Q_t$ were deduced directly from the measured lifetimes. The comparison of these $Q_t$–values with those extracted from a DSAM measurement [4] for the transitions in the upper part of the band shows that the deformation remains constant down to the bottom of the band and is not appreciably disturbed by the decay out of the band. In addition average transition quadrupole moments for the lower parts of SD bands 2 and 3 were determined.

## II. EXPERIMENT AND ANALYSIS

Superdeformed states of $^{194}$Hg were populated by the reaction $^{150}$Nd($^{48}$Ca,4n)$^{194}$Hg using a beam energy of 209 MeV. The beam was supplied by the XTU tandem accelerator at the Laboratori Nazionali di Legnaro, Italy. The sputter sample used in the ion source contained hydrated $^{48}$Ca and was supplied by the Cologne group. The plunger target consisted of

TABLE I. Lifetimes, reduced transition probabilities and transition quadrupole moments for low–lying states in SD-band 1 in $^{194}$Hg

| $E_i$ [keV] | $I_i^\pi$ [$\hbar$] | $E_\gamma$ [keV] | $I_f^\pi$ [$\hbar$] | $\tau$ [ps] | B($E2$) [$10^3$W.u.] | $Q_t$ [eb] |
|---|---|---|---|---|---|---|
| 6883.1 | $12^+$ | 254.6 | $10^+$ | 2.73 (±0.96) | 2.1 $(^{+1.3}_{-0.6})$ | 20.3 $(^{+5.3}_{-3.1})$ |
| 7179.7 | $14^+$ | 296.6 | $12^+$ | 3.26 (±0.57) | 1.5 $(^{+0.4}_{-0.3})$ | 16.8 $(^{+1.7}_{-1.3})$ |
| 7517.3 | $16^+$ | 337.6 | $14^+$ | 1.47 (±0.42) | 1.8 $(^{+0.8}_{-0.4})$ | 18.3 $(^{+3.4}_{-2.2})$ |

a 1 mg/cm$^2$ $^{150}$Nd layer evaporated onto a 1.6 mg/cm$^2$ thick tantalum foil. The recoiling nuclei with a mean velocity of 2.13 (1) % c were stopped in a 11.6 mg/cm$^2$ gold foil. Target and stopper were mounted in the Cologne plunger apparatus [6] surrounded by the 40 large-volume Compton-suppressed Ge detectors of the GASP array [7] in its configuration II. In this configuration the 80 element BGO ball is replaced by a compact lead collimator which makes it possible to move the detectors closer to the center of the array. This leads to an increase in efficiency by approximately a factor of two. In total $795 \cdot 10^6$ unfolded triple events were recorded at seven target-to-stopper distances ranging from 10 to 83 $\mu$m.

The lifetimes of three low–lying states within SD band 1 were determined using the differential decay-curve method (DDCM) [8,9]. The 40 Ge detectors of the GASP array can be grouped into 7 rings whereby the detectors belonging to one ring have approximately the same azimuth angle. For each distance and each detector ring double-gated spectra with gates set on the shifted components of higher-lying SD transitions were produced. Then, the spectra taken at azimuth angles 145°, 120° and 60° were modified in such a way that the Doppler-shifted peaks came to the same position as those in the spectra taken at 35°while the position of the stop peaks remained unchanged. In this way, it was possible to sum up the complete statistics for each distance in one single spectrum which was then used to determine the shifted and unshifted intensities of the transitions of interest for each distance. Examples of the spectra are given in fig. 1.

The resulting lifetimes as well as the corresponding transition probabilities and transition quadrupole moments of the $12^+$, $14^+$ and $16^+$ state are given in table I. In our calculations we adopted the spin assumptions from ref. [1] and relative intensities from ref. [3]. The transition quadrupole moments almost equal those extracted from DSAM data [4] and thus confirm that the dominant SD configuration of the band remains constant down to the region of its decay. This holds also for $^{192}$Hg and $^{194}$Pb where the lifetimes of low–lying SD states were measured. In fig. 2, the transition quadrupole moments of yrast SD bands for the three nuclei are presented.

Due to insufficient statistics only average transition quadrupole moments could be determined for the lower parts of the excited SD bands 2 and 3 applying the following approach.

For each band we created background-subtracted, double-gated spectra with gates set on the shifted components of the corresponding higher-lying SD transitions. Again, we modified the spectra in such way that all shifted peaks came to the same position as those in the spectra taken under 35°. We then summed up all (modified) spectra to obtain one spectrum for each band containing the complete statistics. Within these spectra, we determined the areas of the Doppler shifted and unshifted peaks of four low–lying transitions for each excited band. Assuming a constant transition quadrupole moment for the lower part of each

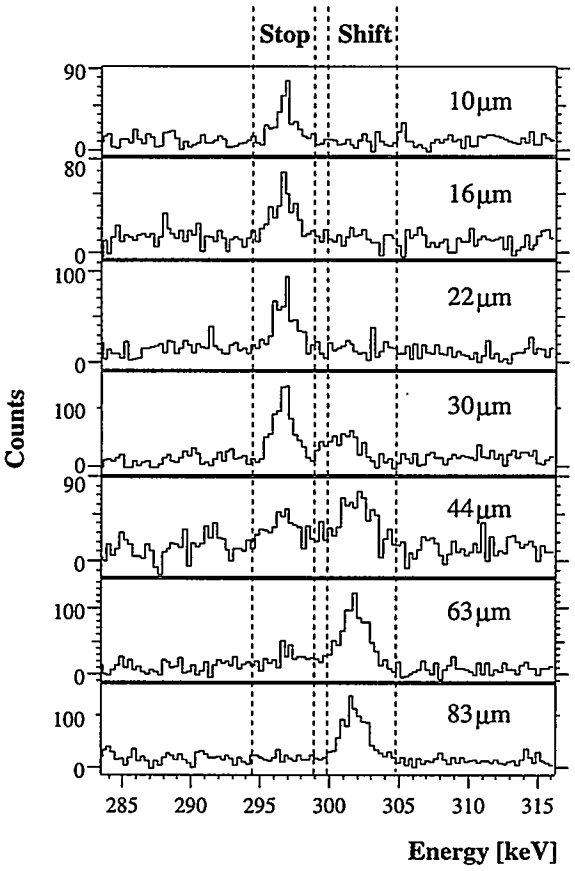


FIG. 1. Doppler shifted and unshifted peaks of the 296 keV transitions of SD band 1 in $^{194}$Hg. The spectra result from summed-up, double gated spectra taken at four different azimuth angles. The Doppler-shifted energies are corrected to correspond to an azimuth angle of 35° .

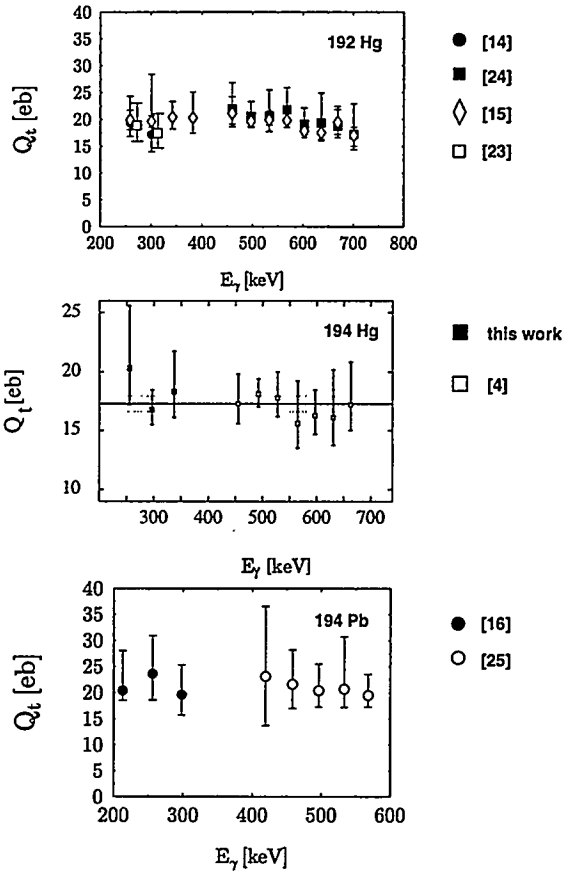


FIG. 2. $Q_t$–values of the yrast SD bands for $^{192,194}$Hg and $^{194}$Pb

band we calculated shifted and unshifted components of the transitions of interest for the corresponding target-to-stopper distances. These values – normalized to the total number of corresponding reaction events – were summed over all distances. Finally, the experimental values were fitted applying a least-$\chi^2$ algorithm to determine the transition quadrupole moments of SD bands 2 and 3.

This procedure yielded average $\overline{Q}_t$-values of 16.5 (31) eb and 15.1 (36) eb for SD band 2 and 3, respectively. A systematic error of 15% is our estimate of the uncertainties arising from this rather complicated procedure.

## III. DISCUSSION

In order to describe the decay out of SD bands we followed the approach proposed by Krücken et al. [10], based on a simple level-mixing model, originally proposed by Vigezzi, Broglia and Døssing [11]. This model has previously been used to describe the situation in $^{152}$Dy, $^{192}$Hg and $^{194}$Pb [12–16].

We calculated the partial decay probabilities for an intraband transition $\lambda_{intra}$ and for the

decay out of the band $\lambda_{out}$ which add up to the total transition probability $\lambda = 1/\tau$, using the relationship:

$$\lambda_{out}(I^\pi) = \frac{1}{\tau} \cdot (1 - N_{intra}(I^\pi)), \tag{1}$$

where $N_{intra}(I^\pi)$ is the branching of the intra-band transition depopulating the ($I^\pi$) state. For the $12^+$ state we calculated a value of $N_{intra}(12^+) = 0.58\,(3)$ using intensities from ref. [3] and deduced a partial decay probability of $\lambda_{out}\,(12^+) = 0.15\,(5)\,ps^{-1}$ for the decay out. The wavefunction of the real state $\Psi$ is assumed to consist of a SD part $|s\rangle$ and a ND part $|n\rangle$, $\Psi = a_s|s\rangle + a_n|n\rangle$ with $a_n^2 + a_s^2 = 1$. Postulating that electromagnetic (EM) transitions between pure SD and ND states are negligible and that the squared ND amplitude $a_n^2$ is small, the probability for the decay out of the band at spin I is given by

$$\lambda_{out}(I^\pi) = a_n^2(I^\pi) \cdot \lambda_n \tag{2}$$

where $\lambda_n$ is the EM transition probability in the ND well. In order to determine $\lambda_n$ only statistical $E1$ transitions were considered for the decay between the ND states. Other types of transitions, magnetic ones and those with higher multipolarities were considered to be small and have been neglected. The $E1$ decay probability was calculated as in refs. [16,10] applying a statistical model.

$$\lambda_n^{E1} = \xi_{E1} \int_0^{U-E_{Yrast}} \frac{\rho(U - E_\gamma)}{\rho(U)}\, f_{GDR}(E_\gamma)\, E_\gamma^3\, dE_\gamma \tag{3}$$

The Fermi-gas approximation was used to describe the level-density at the various excitation energies with a pairing gap of $2\Delta_{12^\pi} = 1.3\,\mathrm{MeV}$ and a level-density parameter of a $22.4\,\mathrm{MeV}^{-1}$ [17]. $\xi_{E1}$ is the $E1$ strength fitted to neutron-resonance data from ref. [18], U is the excitation energy of the decaying SD state taking the pairing gap into consideration and $E_{Yrast}$ is the energy of the corresponding yrast state. We used parameters for the description of the giant dipole resonance (GDR) extracted from photoneutron cross-section measurements on natural mercury from ref. [19] and from references therein.

This gives $\lambda_n = \lambda_n^{E1} = 27.5\,ps^{-1}$ and considering equation (2) a ND squared mixing amplitude $a_n\,(12^+) = 0.5\%, (2)$ for the SD $12^+$ state.

In table II, we give the results of our calculations, in particular the calculated E1 transition probabilities $\lambda_n^{E1}$ and the deduced squared ND mixing amplitudes $a_n^2$. As the intensities of the decay out for $^{194}$Pb [20] and$^{192}$Hg [21] are similar to the ones observed in $^{194}$Hg, we additionally calculated the corresponding values for these nuclei. For $^{194}$Hg and $^{194}$Pb, we used the exact excitation energies from refs. [1,2], whereas for $^{192}$Hg we assumed an excitation energy of 4.3 MeV above yrast (similar to the value in $^{194}$Hg). Note that no lifetimes have yet been measured for the $8^+$ state in $^{194}$Pb and for the $10^+$ states in $^{192}$Hg and $^{194}$Hg. Therefore, in order to estimate the ND contributions to those states we extracted the corresponding lifetimes assuming constancy of the quadrupole moment in each band. As previously shown for $^{194}$Pb and $^{192}$Hg in ref. [10] the behavior of the ND mixing amplitudes with decreasing spin for the three nuclei is rather striking: while $a_n^2$ remains almost constant for $^{194}$Pb, it increases for both mercury isotopes by about an order of magnitude. This can be understood in the framework of a simple two-level mixing-model assuming that the pure SD state $|s_I\rangle$ interacts only with its nearest neighbor ND state $|n_I\rangle$. Let $x_I$ be the energy difference and

TABLE II. Calculated E1 transition probabilities $\lambda_n^{E1}$ and deduced squared ND mixing amplitudes $a_n^2$ for low-lying SD states in $^{192,194}$Hg and $^{194}$Pb which decay to ND states. The calculation of the partial decay probabilities $\lambda_{out}$ involve the lifetime data and intensities from refs. [16,20] ($10^+$, $^{194}$Pb), the weighted average of the lifetime values given in refs. [14,15,22] ($12^+$, $^{192}$Hg) and this work ($12^+$, $^{194}$Hg) as well as the intensities from ref. [21,3]. In order to deduce $\lambda_{out}$ values for the $8^+$ state in $^{194}$Pb and $10^+$ states in $^{192,194}$Hg a constant quadrupole moment was assumed for the bands calculated from the weighted average of the values given in the above references and in refs. [23], [4], [24].

| Nucl. | I | $\lambda_{out}$ | $\lambda_n^{E1}$ | $a_n^2$ |
|---|---|---|---|---|
| | [$\hbar$] | [ps$^{-1}$] | [ps$^{-1}$] | [%] |
| $^{192}$Hg | 12 | 0.026(15) | 15.7 | 0.17(9) |
| $^{192}$Hg | 10 | 0.85 | 15.7 | 5.4 |
| $^{194}$Hg | 12 | 0.147(52) | 27.5 | 0.53(19) |
| $^{194}$Hg | 10 | 1.2 | 27.9 | 4.39 |
| $^{194}$Pb | 10 | 0.012(8) | 2.4 | 0.48(32) |
| $^{194}$Pb | 8 | 0.014 | 2.5 | 0.56 |

$v_I^2 = |\langle n_I|V|s_I\rangle|^2$ the squared matrix element for the interaction V between SD and ND state. The ratio of the amplitudes of the real SD state $|\Psi_I\rangle = a_s(I^\pi)\,|s_I\rangle + a_n(I^\pi)\,|n_I\rangle$ is given by

$$\frac{a_s^2}{a_n^2} = \frac{4v^2}{\left(\sqrt{x^2+4v^2}-x\right)^2}$$

and for $a_n^2 \ll 1$

$$\frac{a_s^2}{a_n^2} \approx \frac{x^2}{4v^2}$$

For small ND amplitudes $a_n^2$ and constant interaction strength $v^2$ one finds $a_n^2 \propto 1/x^2$. The different behavior of $a_n^2$ in the three nuclei is therefore a strong indication that the ND mixing amplitude depends strongly on the arbitrary distance to the nearest-neighbor state in the ND well. This means that the decay pattern of the SD bands in the A≈190 mass region shows clear signs of random behavior.

The members of the Cologne group are very grateful to the INFN for its outstanding hospitality and the permission to use the GASP spectrometer and the Legnaro XTU. This work has been partly funded by the German Federal Minister for Education and Research (BMBF) under Contract No. 06OK602 I, by the Deutsche Forschungsgemeinschaft (DFG) under Contract No. Bo1108/1 and by the Istituto Nazionale di Fisica Nucleare (INFN).

[1] T.L. Khoo et al., Phys. Rev. Lett. **76**, 1583 (1996).
[2] A. Lopez-Martens et al., Phys. Lett. **B380**, 18 (1996).

[3] R. Krücken, submitted to Phys. Rev. C. (1996).
[4] J.R. Hughes et al., Phys. Rev. Lett. **72**, 824 (1994).
[5] M.A. Riley et al., Nucl. Phys. **A512**, 178 (1990).
[6] A. Dewald et al., Nucl. Phys. **A545**, 822 (1992)
[7] D. Bazzacco, in *Proceedings of the International Conference on Nuclear Structure at High Angular Momentum, Ottawa, 1992* (AECL Research, Chalk River, Ontario, 1992), Vol. 2.
[8] Dewald, S. Harissopulos and P. von Brentano, Z. Phys. **A 334**, 163 (1989)

[9] G. Böhm et al., Nucl. Instr. Meth. **A329**, 248 (1993)
[10] R. Krücken, A. Dewald, P. von Brentano, D. Bazzacco, and C. Rossi-Alvarez, accepted by Phys. Rev. C., in press,(1996).
[11] E. Vigezzi, R.A. Broglia, and T. Døssing, Phys. Lett. **B249**, 163 (1990).
[12] Y.R. Shimizu, E. Vigezzi, T. Døssing, and R.A. Broglia, Nucl. Phys. **A557**, 99c (1993)
[13] T.L. Khoo et al., Nucl. Phys. **A557**, 83c (1993).
[14] A. Dewald et al., J. Phys. G. **19** (1993).
[15] P. Willsau et al. Nucl. Phys. **A574**, 560 (1994).
[16] R. Krücken et al., Phys. Rev. Lett. **73**, 3359 (1994).
[17] A. Mengoni and Y. Nakajima, J. Nucl. Sci. Technol. **31**, 151 (1994).
[18] S.F. Mughabghab, *Neutron Cross Sections*, (Academic Press Inc., Orlando, FL, 1984), Vol. 1b.
[19] S.S. Dietrich and B.L. Berman, At. Dat. Nucl. Dat. Tab. **38**, 199 (1988).
[20] M.J. Brinkman et al., Proceedings of the Conference on Physics from Large Gamma-Ray Detector Arrays; Berkeley (1994).
[21] P. Fallon et al., Phys. Rev. C. **51**, R1609 (1995).
[22] I.Y. Lee, C. Baktash, D.M. Cullen, J.D. Garrett, N.R. Johnson, F.K. McGowan, D.F. Winchell, and C.H. Yu, Phys. Rev. C. **50**, 2602 (1994).
[23] E.F. Moore et al., Phys. Rev. Lett. **64**, 3127 (1990).
[24] P. Willsau et al., Z. Phys. **A344**, 351 (1993).
D. Blumenthal, M.P. Carpenter, B. Crowell, D. Gassmann, R.G. Henry, R.V.F. Janssens, and D. Nisius, Phys. Rev. Lett. **75**, 1276 (1995).

# Change of deformation at the backbending in the yrast superdeformed band of $^{144}$Gd

C. A. Ur[1], G. P. Bolzonella[1], L. H. Zhu[2], D. Bazzacco[1] S. Lunardi[1], N. H. Medina[1], C. M. Petrache[1], M. N. Rao[1], C. Rossi Alvarez[1], G. de Angelis[2], D. De Acuna[2], D. R. Napoli[2], W. Gast[3], R. M. Lieder[3], T. Rzaca-Urban[3], S. Utzelmann[3], R. Wyss[4]

[1] *Dipartimento di Fisica dell'Università and INFN, Sezione di Padova, Padova, Italy*
[2] *INFN, Laboratori Nazionali di Legnaro, Legnaro, Italy*
[3] *Institut für Kernphysik, KFA Jülich, Jülich , Germany*
[4] *Royal Institute of Technology, Physics Department Frescati, Stockholm, Sweden*

**Abstract**

A mean lifetime measurement using the Doppler shift attenuation method has been performed at GASP in order to extract the quadrupole moment of the yrast SD band of $^{144}$Gd. The extracted intrinsic quadrupole moments, being $Q_0$=13.7 eb above the backbending and $Q_0$=11.8 eb below the backbending, are consistent with a change of deformation from $\beta_2$=0.51 (at $\beta_4 \approx$0.050) to $\beta_2$=0.45 (at $\beta_4 \approx$0.035). The experimental results are in nice agreement with the theoretical predictions, which revealed that the second well in $^{144}$Gd arises essentially from the very favoured shell structure at N=80 and Z=64. The occupation at higher frequency of the aligned N=6 proton orbitals drives the nucleus to a slightly more deformed shape.

## 1 Introduction

It is known [1] from cranked-Strutinsky calculations using Woods-Saxon potential that some large shell gaps at very elongated shape exist for neutron numbers N=80, 86 and/or proton numbers Z=62, 64, 66. For example, the nuclei $^{144}$Gd and $^{152}$Dy are predicted to be doubly magic at superdeformed shape. Following these predictions several SD bands have been observed experimentally. One of the questions arised in the study of SD nuclei is on the competition between the shell structure and the occupation of the large deformation-driving high-N intruder orbitals in stabilizing SD nuclear shapes. Recent experimental results in the A=130 mass region [2] show the major importance of the shell-gaps with respect to the intruder orbitals occupation.

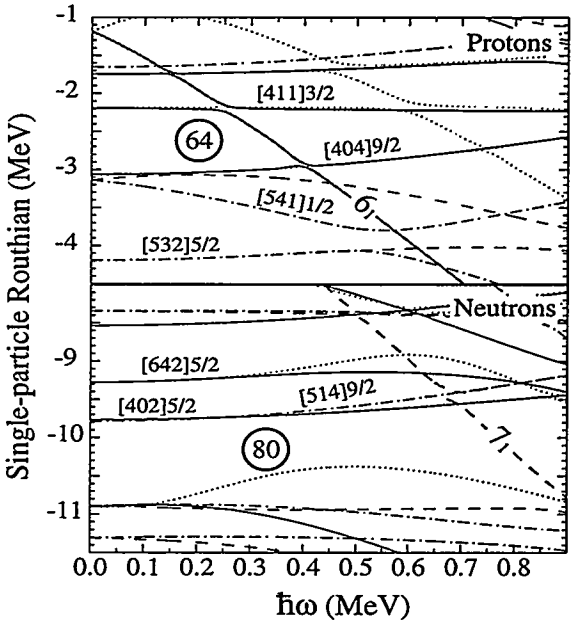


Figure 1: Single particle routhians calculated at $\beta_2$=0.45 ($\beta_4$=0.035) for $^{144}$Gd.

We have now the opportunity to investigate this competition within the SD nucleus $^{144}$Gd. In fact, theoretical calculations tell us that superdeformation in $^{144}$Gd is originally stabilized by the N=80 neutron shell gap at $\beta_2 \approx 0.45$ without occupying the high-N intruder orbitals. This is shown clearly in Fig. 1 by the single particle routhians calculated at $\beta_2$=0.45 ($\beta_4$=0.035). At low frequency, none of the high-N intruder orbitals which characterize the SD bands in the A=150 mass region are occupied. Only when cranking, the N=6 proton intruder orbital decreases in energy and becomes occupied at high frequency. The same calculations predict that at a rotational frequency $\hbar\omega \approx 0.45$ MeV the proton configuration is changing from $\pi 6^0$ to $\pi 6^2$ with a change of deformation from $\beta_2 \approx 0.47$ to $\approx 0.51$ [3]. This would imply a change of deformation less than 10% when two particles are promoted on high-N intruder orbitals.

# 2 Superdeformed bands in $^{144}$Gd

Very recently, five SD bands have been identified in $^{144}$Gd [3, 4] using $^{100}$Mo($^{48}$Ti,4n) reaction. The coincidence $\gamma$–ray spectra of the five SD bands, obtained by setting double gates on clean transitions in each band, are shown in Fig.2. The yrast SD band [3] is one of the few cases which exhibits a backbending, confirming the theoretical prediction [1] of the crossing between $\pi 6^0$ and $\pi 6^2$ configurations due to the alignment of two $i_{13/2}$ protons. The other four excited SD bands [4] are interpreted as proton particle-hole excitation across the Z=64 gap revealing the high stability of the N=80 shell closure at SD shapes. The relative intensity of the yrast SD band with respect to the total population of $^{144}$Gd is reported [4] as a function of the beam energy in $^{100}$Mo($^{48}$Ti,4n) reaction in Fig.3. The data show the well-known saturation pattern (see Fig. 3) in the population of the SD bands. The intensity of the yrast SD band in $^{144}$Gd, being 1.2% of the total population, is comparable to that of the other yrast SD bands in the A = 150 mass region. The results

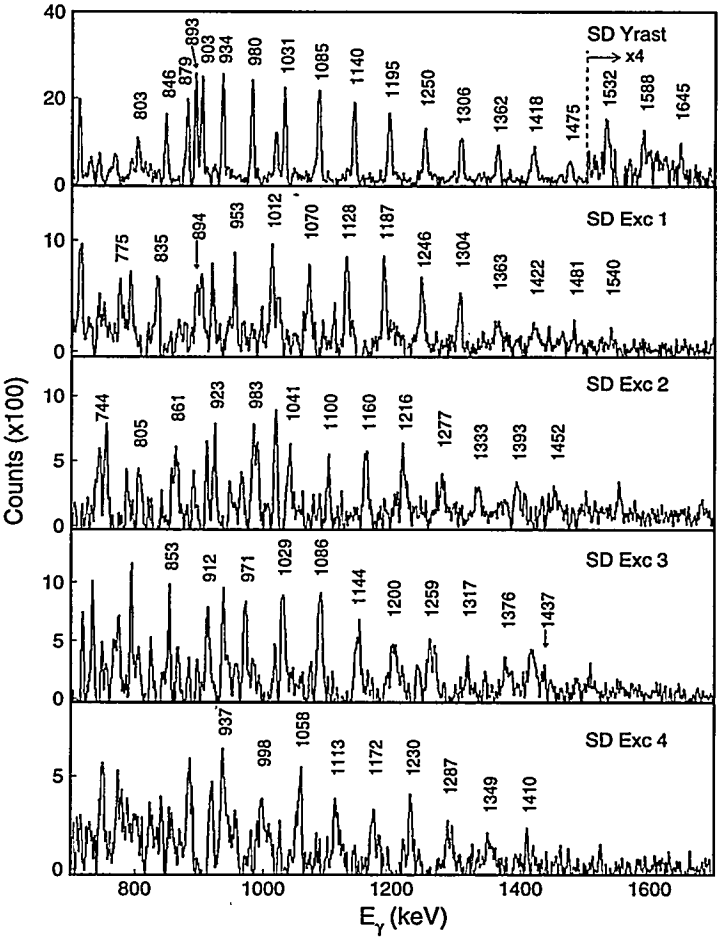


Figure 2: Doubly-gated coincidence spectra of five SD bands of $^{144}$Gd identified in $^{48}$Ti + $^{100}$Mo reaction at 215 MeV. The members of the SD bands are labeled with their energies in keV. Their relative intensities with respect to the total population of $^{144}$Gd are also shown.

therefore exclude a possible configuration-dependence in the population of the SD bands around N=80.

On the other hand, the population of superdeformed (SD) bands has been observed to depend, in few cases, on the mass symmetry of the reaction entrance channel [5, 6]. In order to clarify this issue qualitatively, the completely symmetric reaction $^{74}Ge + ^{74}Ge$ has been recently used where the 318 MeV $^{74}Ge$ beam was provided by the superconducting Linac post-accelerator ALPI in Legnaro. The intensity of the yrast SD band results to be 1.6% of the total population of $^{144}Gd$ channel (open circle in Fig.3) to be compared with the 1.2% obtained with the $^{48}Ti$ beam. For comparison, the x-axis is scaled with the corresponding excitation energy of the compound nucleus. A clear enhancement of the SD band population is observed in the case of the $^{74}Ge + ^{74}Ge$ reaction, which demonstrates the important role played by the reaction entrance channel. In fact, the failure of earlier attempts [7, 8] to populate SD bands in $^{144}Gd$ through $^{28}Si$ induced reactions indicated possibly the importance of entrance channel effects in the population of the SD bands in $^{144}Gd$. Other explanations can be given based on the dynamics of the formation of the equilibrated compound system and/or on the interplay between the fusion-evaporation and fusion-fission channels in the decay of the compound nucleus [9].

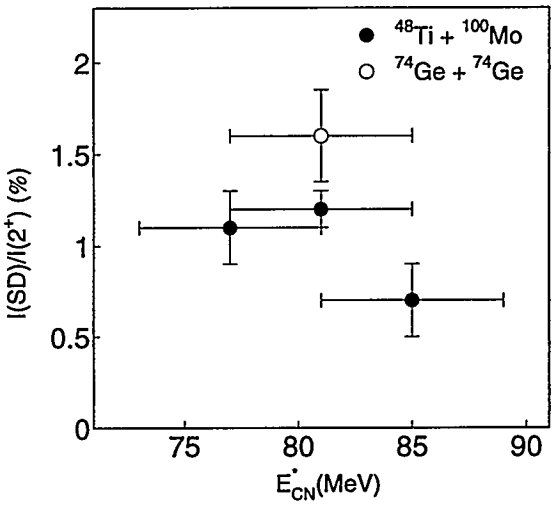


Figure 3: Relative intensities with respect to the total population of $^{144}Gd$ as a function of the excitation energy of compound nucleus. The errors of the intensity are statistics while the ones of the excitation energy correspond to the energy spread due to the thickness of the target.

# 3 DSAM experiment and details

In order to measure the deformation of the nucleus in the SD states a Doppler Shift Attenuation Method (DSAM) experiment has been performed. High spin states in $^{144}Gd$ were populated via the $^{100}Mo(^{48}Ti,4n)$ reaction at a beam energy of 214 MeV. The beam was delivered by the XTU Tandem accelerator at the National Laboratories of Legnaro. The target consisted of a 1 mg/cm$^2$ $^{100}Mo$ foil evaporated on a 10 mg/cm$^2$ gold backing which completely stops the recoiling nuclei. Gamma-rays were detected by the GASP array which consisted of 40 large volume Compton escape-suppressed HPGe detectors and 80 BGO detectors forming the inner ball. Events were collected only when at least 3 Ge detectors and 5 BGO detectors have been fired. A total of $2.13 \times 10^9$ events which after unfolding resulted in $3.94 \times 10^9$ triple events were collected on tape. The Ge detectors in the GASP array are placed symmetrically with respect to the beam direction in seven rings, as follows: 6 at 35°, 6 at 60°, 4 at 72°, 8 at 90°, 4 at 108°, 6 at 120° and 6 at 145°. In the offline

analysis the high spin states of $^{144}$Gd were enhanced by proper gates on the energy sum and the multiplicity from the BGO inner ball. In order to simplify the analysis, the data were reduced by considering only the energy region from 750 keV to 1625 keV where the SD band transitions are located. We enhanced the transitions in the SD band by double gating on in-band transitions and incrementing directly spectra corresponding to the seven rings of detectors in coincidence with all the detectors. In Fig.4 the spectra obtained for the most forward and backward rings of detectors, after background subtraction, are shown.

The experimental fractional Doppler shift, F($\tau$), was calculated according to the following relation:

$$F(\tau) = \frac{\Delta E_\gamma}{2 \cdot \beta \cdot \overline{E}_\gamma \cdot \cos\theta_{forward}} \qquad (1)$$

where $\Delta E_\gamma$ is the energy difference between the centroids of the shifted $\gamma$–rays corresponding to the forward and backward angles ($\theta_{forward}$ and $\pi - \theta_{forward}$, respectively), $\overline{E}_\gamma$ is their mean value and $\beta$=$v_0$/c where $v_0$ is the mean initial recoil velocity. The experimental F($\tau$) curve is represented in Fig. 5, where the errors are only from the statistics of the spectra of the rings at forward and backward direction and the points corresponding to the 1084 keV and 1134 keV transition are taken only from the forward ring in order to avoid the strong contaminants in the backward ring.

The slowing down process of the recoils and, accordingly, the velocity profile has been simulated with the Monte Carlo procedure developed on the basis of the code of Bacelar *et al.* [10] using a number of 5000 histories and up to 1600 time steps of $\approx$ 1.0 fs. The electronic stopping power was calculated according to the formalism of Braune [12]. The calculation of the theoretical F($\tau$) value depends on the mean time of the decay of the state (often called "apparent lifetime"), which is defined by the mean lifetime of the state and the entire decay history above the state, including the unknown sidefeeding. The program we used is a modified version with respect to the one reported in [13] and is dealing with a rotational cascade, having a constant intrinsic quadrupole moment $Q_0$, where each state has a sidefeeding provided by a rotational sideband with the same dynamical moment of inertia $\Im^{(2)}$ as the SD

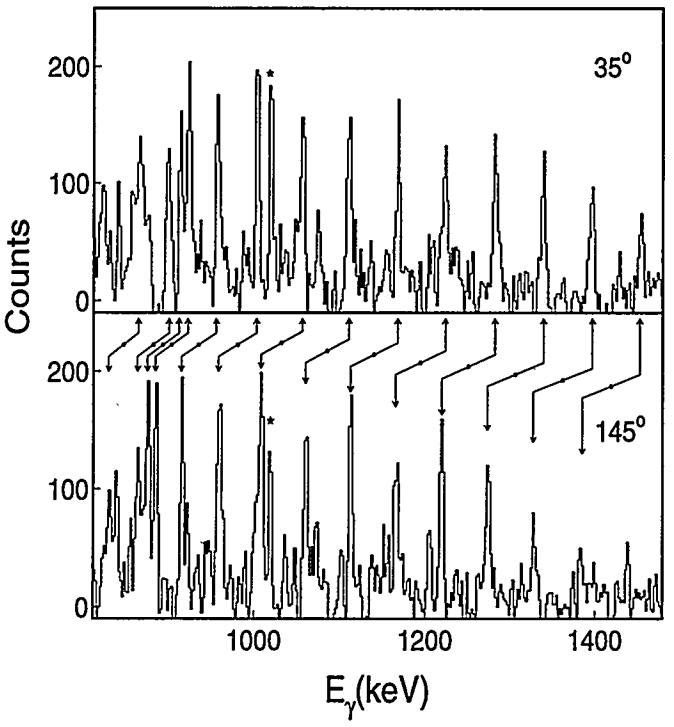


Figure 4: Coincidence spectra corresponding to the ring of detectors at 35° and 145° related to the beam direction respectively, double gated on the members of the yrast SD band in $^{144}$Gd. The shifts of the $\gamma$–rays are positioned with the arrows. The lines marked with asterisk indicate the unshifted $\gamma$–ray of ND states.

band and an intrinsic quadrupole moment $(Q_0)_{SF}$.

The calculations were performed under the assumption that $(Q_0)_{SF}$ has the same value for all the sidebands, as it was suggested in previous works [11, 13] for this mass region. The values for $Q_0$ are extracted by minimizing the $\chi^2$ of the calculated curve fit to the experimental points. The best fit of the experimental data above the backbending (see Fig.5) was obtained for $Q_0$=13.7±1.2 eb. Below the backbending there is no sidefeeding but we have to consider the decay out of the states. For this part the data indicate a value of $Q_0$=11.8 eb. Since the number of points below the backbending is low it was not possible to make a fit of the data and, consequently, it was difficult to evaluate the error for this value. We estimated the limits of $Q_0$ to be ≈±1.5 eb as suggested by the error bars for the F($\tau$) experimental points. We have to notice at this point that the results are subjected to 10-15% of errors due to the uncertainties on the stopping power. However, this does not affect the relative deformation below and above the backbending. The corresponding axial deformation was calculated using the exact expansion of liquid drop model expression for $Q_0$ in terms of the $\beta_2$ and $\beta_4$ and under the assumption that $\beta_4$=0.5$\beta_2$-0.19 for 0.45 < $\beta_2$ < 0.60 [1]. We obtained that the deformation of the nucleus is changing from $\beta_2$=0.45±0.05 to $\beta_2$=0.51±0.04, which agrees with what is expected theoretically when two protons occupy N=6 intruder orbitals [3].

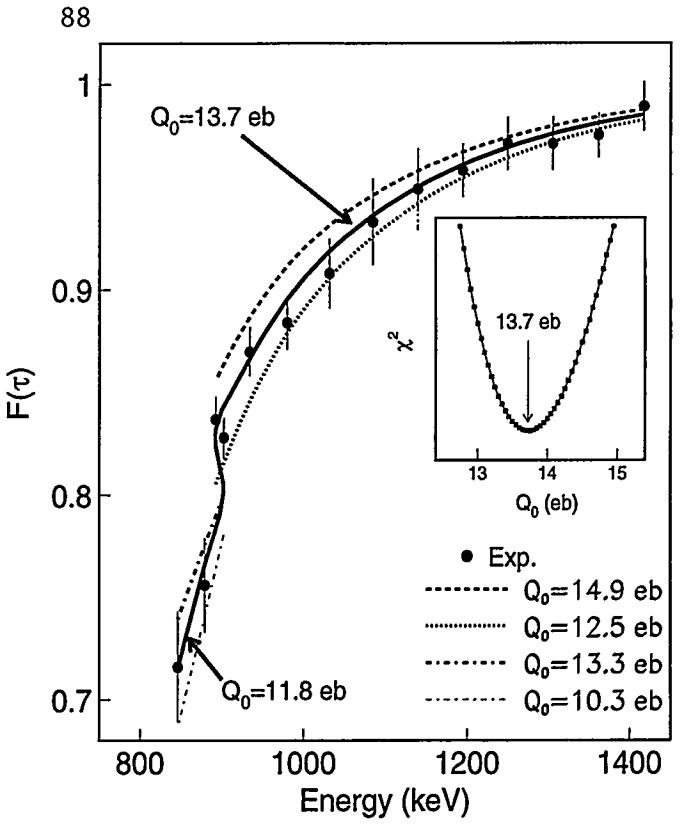


Figure 5: Experimental fractional Doppler shift extracted from the spectra corresponding to the most forward and backward rings of detectors. The solid line indicated with the $Q_0$ values gives the best description of the data under the assumption that the sidefeeding has the same time structure as the in-band feeding. The inset shows the $\chi^2$ minimization for the part above the crossing.

# 4 Conclusions

We have measured the deformation along the yrast SD band of $^{144}$Gd by means of the DSAM technique and obtained for the quadrupole deformation $\beta_2$=0.45 and $\beta_2$=0.51 below and above the backbending, respectively. This results is nicely confirming the theoretical prediction that the change of configuration from $\pi 6^0$ to $\pi 6^2$ induces a change of deformation of about 10%. The major contribution to the deformation in the second minimum of $^{144}$Gd is due therefore to the very favoured shell structure at N=80 and Z=64, without involving the

occupation of the high N intruder orbitals which are not present in the SD band configuration below the backbending.

# References


[1] W.Nazarewicz, R.Wyss and A.Johnson, Nucl. Phys. A **503**, 285 (1989).

[2] A.Galindo-Uribari *et al.* (to be published).

[3] S.Lunardi *et al.*, Phys. Rev. Lett. **72**, 1427 (1994).

[4] S.Lunardi *et al.* (to be published).

[5] G. Smith et al. Phys. Rev. Lett. **68** (1992) 158.

[6] S. Flibotte et al. Phys. Rev. **C45** (1992) R889.

[7] J.P. Vivien et al., Phys. Rev. **C33** (1986) 2007.

[8] Y. Schutz et al., Phys. Rev. **C35** (1987) 348.

[9] G. Viesti et al. Nucl. Phys. **A579** (1994) 225.

[10] J.C.Bacelar *et al.*, Nucl. Phys. A **442**, 509 (1985).

[11] M.A.Bentley *et al.*, J. Phys. G **17**, 511 (1991).

[12] K.Braune, MPI Heidelberg Diploma, 1977; D.Pelte and D.Schwalm, in *Heavy Ion Collisions*, ed. R.Bock (Nord Holland, Amsterdam, 1982), Vol. 3, Chap. 1.

[13] H.Savajols *et al.*, Phys. Rev. Lett. **76**, 4480 (1996).

# Superdeformation in the Mass A~80 Region

Cyrus Baktash

*Physics Division, Oak Ridge National Laboratory, Oak Ridge, TN 37831-6371*

A new island of superdeformed nuclei with major-to-minor axis ratio of 2:1 has recently been discovered in the A~80 medium-mass region, confirming the predictions for the existence of a large SD gap at particle number N,Z~44. The general properties of more than 20 bands observed so far will be reviewed here, and compared with those of the superdeformed bands in the heavier nuclei.

## 1. Introduction

Superdeformation was first discovered in the actinide fission isomers [1], and was explained as resulting from a secondary minimum at superdeformed (SD) shapes [2]. In the actinide region, the sum of the macroscopic liquid drop term, and the microscopic shell correction to the total energy gives rise to a second minimum at SD even at very low spins. However, with the weakening of the Coulomb force in lighter systems, SD minima are stabilized only at high spins and for certain nuclei close to SD magic numbers. Studies of these high-spin SD structures, and especially their mass dependence, provide an important insight into the competition between the microscopic and macroscopic effects, the role of the odd-time terms in the Hamiltonian, as well as certain aspects of the effective interactions such as the spin-orbit force.

The first high-spin SD band was observed in $^{152}$Dy in 1986 [3], and was followed in 1989 by discovery of another island of superdeformation around $^{192}$Hg [4]. These findings were in excellent agreement with the results of the earlier calculations which had predicted the existence of superdeformed magic particle numbers N,Z ~44, 64, 86, and 116 [5,6]. Encouraged by these experimental successes, numerous searches were undertaken to verify the existence of the predicted superdeformed shell gaps near particle number 44. However, largely due to experimental difficulties, these efforts were not successful until recently. Among the problems specific to this mass region which hinder the observation of these weakly populated bands are the following:

(i) Due to the $A^{-5/3}$ scaling, the gamma rays associated with the medium-mass nuclei (and particularly those in the SD bands) have high energies and, thus, poor detection efficiency;

(ii) Reactions used to populate the high-spin states result in large velocities and angular spread of the recoiling nuclei which cause excessive Doppler broadening and poor energy resolution;

(iii) Because of the low Coulomb barrier and high excitation energy needed to populate the high-spin states, light charged-particle emission fragments the yields of the fusion-evaporation products into a large number (typically 20 or more) of exit channels.

Therefore, the $\gamma$ rays from a variety of reaction products can easily mask and interfere with those from the SD bands which are usually populated with less than 0.1% of the total cross section.

The first of these difficulties may be alleviated by the use of large Ge detectors, while the second problem may be overcome in part by segmenting the Ge crystals. Therefore, the observation of the first SD in $^{83}$Sr [7] had to await the advent of arrays of large Ge detectors such as Eurogam-I. Another breakthrough, which made the systematic studies of SD bands in the mass A~80 region possible, was to combine the charged-particle detector array

Microball [8] with the Gammasphere array. Full detection of the evaporated proton and α particles and their energies helps in two ways. First, it serves to select and identify the exit channels of interest which are usually produced weakly at the beam energies optimal for the population of SD bands. Second, it allows the reconstruction of the recoil momenta which results in considerable improvements in the Doppler correction and, hence, gamma-ray energy resolution. This is best illustrated in Fig. 1, which compares gated γ-ray spectra for the yrast SD band in $^{83}$Sr from two experiments. Panel (a) is the sum of several singles gates on the transitions in the band from the Eurogam-I experiment which produced the first example of superdeformation in this region [7]. Figure 1(b) was obtained by summing several double-gated spectra from a Gammsphere+Microball experiment which selected the $^{83}$Sr channel by requiring that all of the four emitted protons be present in the data stream [9]. It shows a significant improvement in both the peak-to-background ratio (a factor of ~8) and the energy resolution of the gamma rays. Furthermore, the clean channel selection afforded by the Microball allowed detailed characterization of the band properties, including a better assignment of the spins and the point it intersects the normally-deformed (ND) yrast band [9].

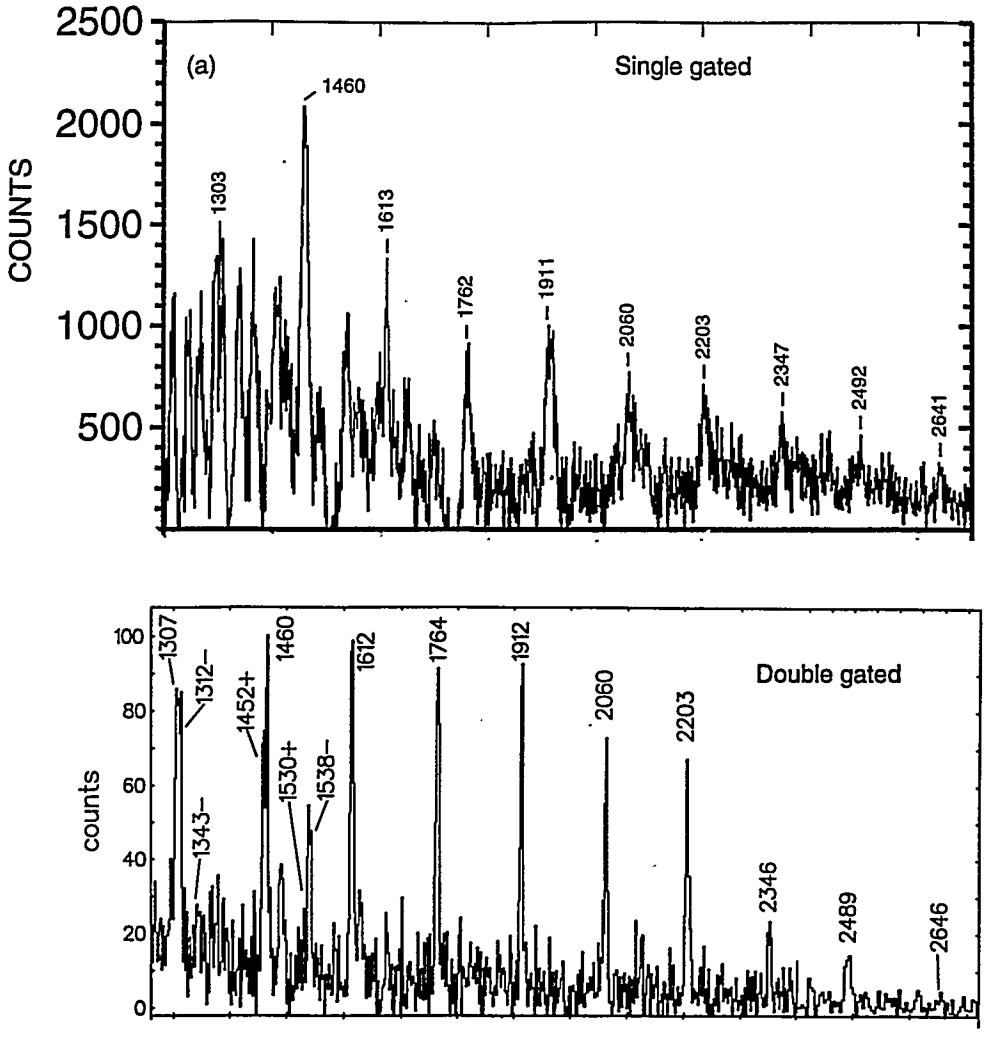


**Fig. 1.** Comparison of the gated spectra of the SD band in $^{83}$Sr obtained in two experiments [7,9] (See text for explanation).

As a result of these advancements, more than 20 SD bands in ten medium-mass nuclei have been found in the past two years. They include multiple bands in $^{80,81,82}$Sr [10,11,12], $^{83,84}$Y [13], $^{83}$Zr [14], $^{87}$Nb [15], as well as the yrast SD bands in $^{83}$Sr [7,9], $^{82}$Y [16], and $^{84}$Zr [17]. In this paper, we review the general properties of these bands and compare their characteristics with those of the SD bands in the heavier mass resigns.

## 2. Experimental observables and their systematics

Some of the general properties of SD bands that may be experimentally studied to test various theoretical models are: the $\mathcal{J}^{(2)}$ moments of inertia and their variations with rotational frequency, transition quadrupole moments ($Q_t$), measurements of the g-factors either directly or indirectly from the B(M1)/B(E2) ratios, and identification of the excited bands and their relative spins and excitation energies with respect to the yrast SD band. To varying degrees, all these observables are sensitive to, and help identify the single-particle configurations of the SD bands. Other observables which are also relevant to this question are the *relative* alignments of different SD bands, either in the same nucleus or in neighboring isotopes and isotones. This quantity may be simply deduced from the $\gamma$-ray energies and determines the fractional change in the $\mathcal{J}^{(2)}$ of the pair of bands as discussed in Ref. [18].

The feeding pattern of the SD bands and their variations (if any) with reaction may shed some light on the fusion-evaporation reaction mechanism, and factors which limit both population and retention of the high partial waves in compound nuclei. The decay pattern is related to the quantum-mechanical tunneling through the barrier which separates the SD and ND states, and depends on such factors as the barrier height, level density, and pairing interaction.

**2.1 Population and Decay:** The first SD in this mass region was observed [7] using the Eurogam-I array and the $^{56}$Fe($^{30}$Si, 2*pn*)$^{83}$Sr reaction at a beam energy of 128 MeV. This and similar reactions, which form compound nuclei at ~70 MeV excitation energy and >50$\hbar$ angular momentum, have been found to be optimal for the population of SD bands in the 4*p*, 3*p*, 2*pn*, and in particular the $\alpha 2p$ and $\alpha pn$ exit channels. Our studies indicate that emission of alpha particles, which originate from the highest angular momentum states in these compound nuclei, is very effective in populating the high-spin states [19] and SD bands in medium-mass nuclei. It should be noted that since such a relatively high excitation energy corresponds to the maximum production of the four-particle emission channels, the above three-particle channels are populated with only modest cross sections.

Similar to the SD bands in heavier nuclei, these bands are fed over a range of several transitions and generally reach a saturation intensity of <2% of the total. The exceptions are the yrast bands in $^{83}$Zr [14] and $^{84}$Zr [17], which are populated with intensities of more than 5% and 4%, respectively. Both of these values are about a factor of 2 larger than the intensities of the yrast SD bands in their Y isotones that were populated via the 3*p* channel in the same reactions. In the case of $^{84}$Zr, significant differences were observed in the feeding saturation point when the band was populated by two different reactions, namely 2*pn* and $\alpha 2p$ [17]. This is the only known example of this effect and points to an important new factor that influences the population of SD bands. Also, the common assumption that the half-intensity point (i.e., the level which receives 50% of the total intensity of the band) coincides with the point where SD bands become yrast is called into question due to the fact that this point was observed to vary with reaction.

The decay of these bands is sudden and is completed within a narrow range of one to three transitions. As is the case in the heavier nuclei, these SD bands decay statistically to

several ND bands of both parities. From the intensities of the feeding-out (of the SD) and feeding in (to the ND) transitions, one can estimate the approximate spins of the SD bands. The spins of the lowest-lying states have been estimated to be approximately $15\hbar$ in the N=43 nuclei $^{81}$Sr [11] and $^{83}$Zr [14], and close to $20\hbar$ in the more neutron-rich nuclei $^{82,83}$Sr [12,9] and $^{84}$Zr. Many of these bands extend to a maximum spin of ~$40\hbar$. Assuming that the yrast SD and ND bands cross each other at a point where their sidefeeding intensities are nearly equal, it is estimated that these SD bands become yrast at ~$30\hbar$. Interestingly, this spin corresponds to the onset of band termination that has long been predicted [6] to occur in many of the ND bands in this region. Band termination was recently observed in several nuclei such as $^{83}$Sr [20], $^{83}$Y[21], and $^{84}$Zr [17], as evidenced in their rapidly decreasing $\mathcal{J}^{(2)}$ (see Fig. 2a) and $Q_t$ values [22].

**2.2 Systematics of the moments of inertia and identical bands:** A very distinctive feature of these bands is the high energies of their gamma rays which typically range from about 1300 to more than 2600 keV. This may be compared with a maximum gamma-ray energy of approximately 700 and 1500 keV for the SD bands in the A~190 and 150 regions, respectively [23]. The energy differences of the consecutive gamma rays in the SD bands of the A~80 nuclei are approximately 150 keV, which imply a dynamical moment of inertia $\mathcal{J}^{(2)}$~$27\hbar^2$/MeV, corresponding to that of a rigid rotor with a quadrupole deformation of $\beta_2$~0.5, or major-to-minor axis ratio of 2:1.

Figure 2b shows a plot of the $\mathcal{J}^{(2)}$ versus rotational frequency ($\omega$) for the SD band in $^{83}$Sr, along with those in $^{240}$Pu, $^{192}$Hg, and $^{152}$Dy, which represent typical SD bands in their respective mass regions [23]. To better demonstrate the similarity of these bands, all moments of inertia were scaled by $A^{5/3}$ to factor out the average mass-number dependence. Apart from the A~190 region, where the values rise continuously with $\omega$, the scaled moments of inertia of the other three SD bands have comparable values and are nearly constant as a function of $\omega$. The band in $^{83}$Sr extends to a maximum rotational frequency of about 1.3 MeV, nearly twice as high as the frequencies encountered in the A~150 region. Thus, the SD bands in the A~80 region represent the highest collective rotational frequency observed so far.

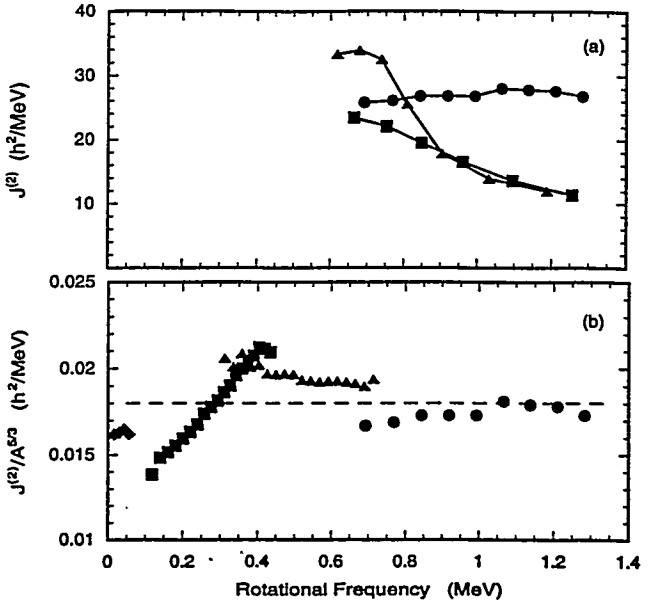


**Fig. 2.** Plots of scaled $\mathcal{J}^{(2)}$ vs. rotational frequency. (a) The SD band in $^{83}$Sr (circles) and two ND bands in $^{83}$Y (squares) and $^{82}$Sr ( triangles). (b) SD bands in $^{240}$Pu (diamonds), $^{192}$Hg (squares), $^{152}$Dy (triangles), and $^{83}$Sr (circles). The dashed line shows the corresponding plot for a SD rigid rotor with $\beta_2$=0.5.

Figure 3 shows the systematics of the $\mathcal{J}^{(2)}$ of the SD bands in ten nuclei in this region. Apart from a few cases (e.g., $^{81}$Sr or $^{83}$Zr) where discontinuities due to band crossing are present, the majority of the $\mathcal{J}^{(2)}$ values fall in the range of ~25-$30\hbar^2$/MeV.

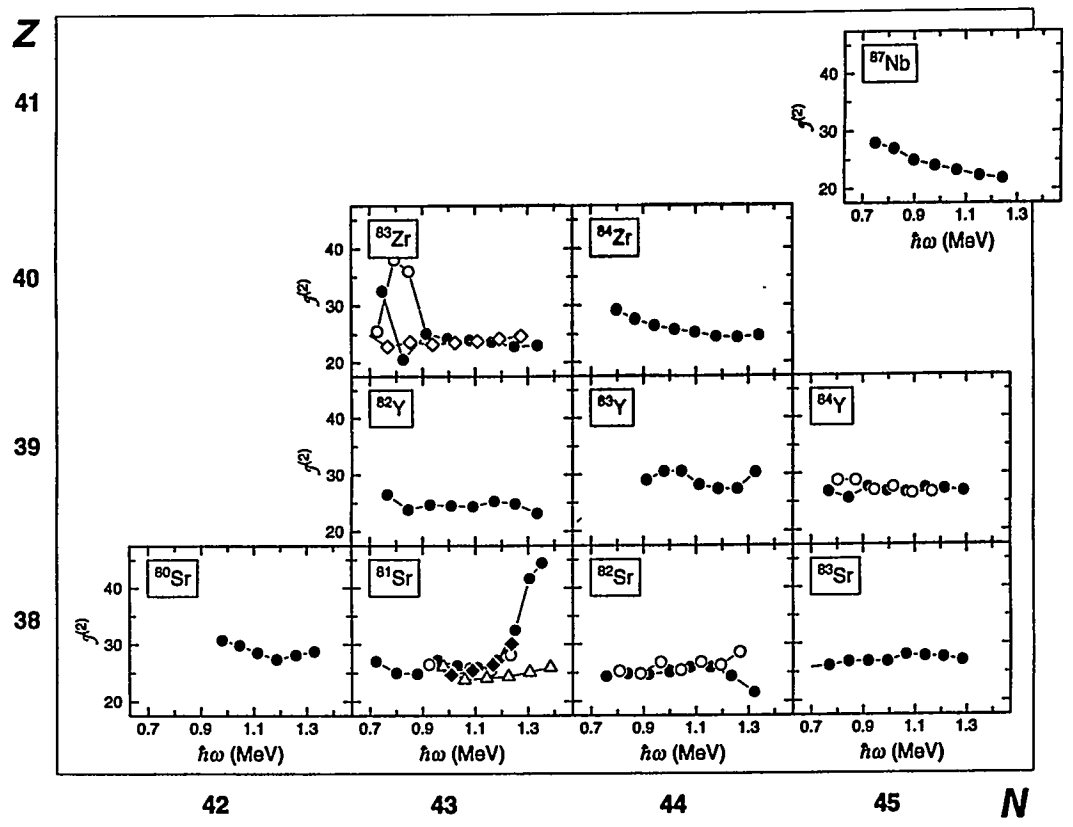


**Fig. 3.** Systematics of the $J^{(2)}$ moments of inertia for the SD bands in the A~80 region.

A convenient way to compare the $J^{(2)}$ values of these bands is to calculate the fractional changes $\Delta J^{(2)}/J^{(2)}$ of pairs of bands as described in Ref. [18]. A histogram of the fractional changes in moments of inertia is shown in Fig. 4, which compares all bands vs. all others (solid), and all bands vs. the yrast bands in their adjacent A+1 nuclei (dashed). In the latter category, nearly 16% of the bands are identical, as compared with ~12% and 4% for the SD bands in the A~150 and 190 regions, respectively [24]. Special among these identical bands are two pairs of twinned bands (i.e., bands with similar gamma-ray energies) in $^{82}$Sr vs. $^{83}$Y and $^{83}$Sr vs. $^{84}$Y [13], which imply the existence of a single-particle routhian with a slope of -0.5$\hbar$ at Z=39. As discussed in

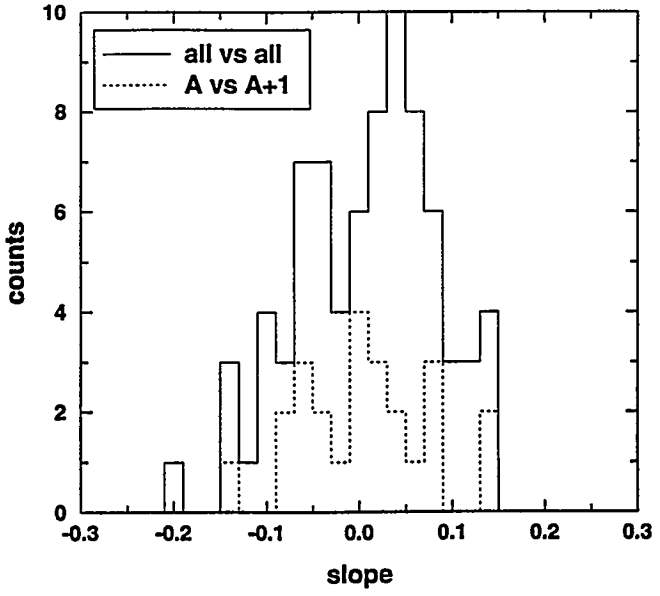


**Fig. 4.** Histogram of frequency distributions of the fractional changes $\Delta J^{(2)}/J^{(2)}$ of pairs of SD bands in the A~80 region (see text).

Sec. 3, this information may be used to test theoretical models and to constraint their parametrs. Other experimental observations which may be used for the same purpose are the rotational frequencies where band crossings take place and their interaction strengths. A particularly interesting case is the band crossing encountered in $^{87}$Nb [15]. The observed interband transitions and their branching ratios indicate that the crossing between the neutron [420]1/2 and [413]7/2 orbitals is responsible for this interaction [15]. This fact may be used to infer the relative position of these orbitals. Furthermore, a second band interaction observed in only one of the two bands may be interpreted as due to the crossing with the neutron $i_{13/2}$ orbital which originates from the N=6 shell. This is the first evidence for the involvement of a "superintruder" ($\Delta$N=3) in the configuration of a SD structure and represents a Coriolis interaction ($\hbar\omega$~8.25 MeV) which is about 35% larger than anything observed upto now. What makes this unique situation possible is a combination of the large deformation and extremely high rotational frequency which lowers the energy of this superintruder orbital.

**2.3 Transition quadrupole moments and deformations:** Because of both the large B(E2) values and high energies of the intraband transitions, the SD states have very short lifetimes. For example, the sum of the feeding and decay times for the top few states is typically a few fs, while the whole band decays in about 50 fs which is comparable to the transit times of the recoils through a thin (~400 $\mu$g/cm$^2$) target foil. Therefore, the traditional DSAM technique with backed targets is too slow to be useful for the measurements of the lifetimes of these states. On the other hand, since the recoils do experience detectable reductions in their velocities as they traverse through the thin target foil, their velocity profiles provide a useful clock to measure the decay times. Thus, by measuring the centroids of the Doppler-shifted gamma rays in the forward and backward Ge detectors, one can obtain average fractional shifts $F(\tau)=\langle v(\tau)/v_0\rangle$ which can be compared with the calculated values to obtain the $Q_t$ of the band [25]. ($v(\tau)$ is the instantaneous recoil velocity of the nucleus as deduced from the observed centroid shifts and $v_0$ is the maximum recoil velocity in the experiment.) This method was successfully used to measure an average $Q_t$ of 5.2$\mp$0.8 eb for the SD band in $^{84}$Zr [17], which corresponds to a B(E2) strength of 440 W.u. or a quadrupole deformation of $\beta_2$=0.53 for an axially symmetric prolate shape. This and other $Q_t$ measurements clearly establish the SD character of these bands.

An important question to be addressed by future $Q_t$ measurements is what are the particle numbers that give rise to the largest SD gaps. The present data (which are admittedly of poor statistical quality) indicate a gradual increase of $Q_t$ for the Sr isotopes from N=42 toward N=44 [10,11,22], and a larger $Q_t$ for $^{84}$Zr than either $^{82}$Sr or $^{83}$Y for the N=44 isotones [22,13,17]. The latter trend is shown in Fig. 5, which is a plot of

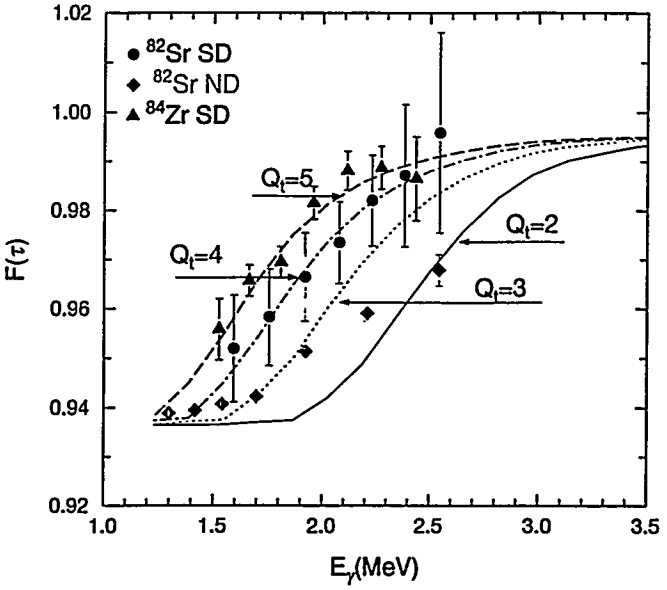


**Fig. 5.** Plots of $F(\tau)$ curves vs. $\gamma$-ray energies for the SD and some ND states in $^{82}$Sr and $^{84}$Zr.

the F(τ) vs. γ-ray energy for the transitions from the ND states in $^{82}$Sr, and from the SD levels in $^{82}$Sr and $^{84}$Zr. It is worth noting that the data points for the longer-lived ND states cluster around the dashed line at $v/v_0$=0.94, which corresponds to the velocity of the recoils after they have left the target. Nearly all the data points for $^{84}$Zr band lie above those for $^{82}$Sr, indicating shorter lifetimes for the former band.

Although $Q_t$ values are sensitive to other variables (e.g., the number of the high-j intruder orbitals involved in their configurations [26]), these preliminary results suggest that N=44 and Z=40 are optimal particle numbers for the formation of SD structures. As noted in Sec. 2.1, the SD bands in $^{83,84}$Zr are populated twice as strongly as other SD bands studied so far which also supports the idea that Z=40 is an optimal proton number. Nevertheless, these early conclusions await confirmation by future precision measurements which would populate these bands under *identical* conditions. For example, the bands in the $^{82}$Sr, $^{83}$Y, and $^{84}$Zr (N=44) isotones may be studied via (α2p) reactions induced by the $^{30}$Si, $^{31}$P, and $^{32}$S beams on the *same* $^{58}$Ni target and at beam energies that produce the same entry-state distributions in the corresponding compound nuclei. Similarly, the N=44 to 46 Sr isotopes may be produced by the reactions of $^{28,29,30}$Si beams on the same $^{60}$Ni target. A comparison of the feeding patterns, total intensities, and the $Q_t$ values of these bands populated under similar conditions would provide valuable insight into the relative contributions of the N~45 and Z~39 orbitals to their structures.

**2.4 Forking and unusual decays:** One of the SD bands in each of the $^{83}$Zr [14] and $^{87}$Nb [15] nuclei fork out to two branches near the bottom of the cascade. Their $\mathcal{J}^{(2)}$ moments of inertia indicate that the close-lying levels in the two branches interact with each other. Evidence has also been presented that two levels in one of the bands in $^{81}$Sr [11] interact with two other states which lie only ~10 keV away. More interestingly, in the case of the N=83 Sr and Zr isotones, the routhians of the bands curve down and reapproach those of the ND states, allowing for their mutual interaction. (This unusual situation cannot be avoided for any reasonable values of the bandhead energies which are consistent with the sidefeeding intensities.) A similar situations has not been encountered in the heavier SD regions. The proximity of these SD bands to the ND bands may provide a favorable condition for the observation of the direct linking transitions.

## 3. Comparisons with theoretical calculations

Many of the observed properties of the SD bands in the A~80 region are in good agreement with the predictions made using the cranked Strutinsky method (see, e.g., Refs. [7,9,11,12,17] for comparisons of $\mathcal{J}^{(2)}$, $\beta_2$, and the calculated low-lying SD bands). These calculations incorporate the Woods-Saxon potential for the microscopic part and the Yukawa-plus-exponential mass formula for the macroscopic part of the total energy. For a given configuration, the equilibrium deformations at fixed values of ω were determined by minimizing the total energy at each ($\beta_2$,$\gamma$) grid point with respect to the hexadecapole deformation. Pairing correlations were neglected, as they are expected to play a minor role at high-spins in the A~80 mass region. Details of the calculational procedure and technique are given in Refs. [6,27]. These calculations predict a number of low-lying SD structures that have deformations ranging from $\beta_2$~0.45 to 0.55, depending on how many $h_{11/2}$ intruder orbitals are involved in their configurations (see, e.g., Refs. [7,11,12]). At high spins, they generally have one proton in the $h_{11/2}$ orbital, symbolized as $\pi 5^1$. The neutron configurations of the yrast SD bands contain one to three $h_{11/2}$ orbitals for N=43-45, respectively. Therefore, a gradual increase in deformation is expected in going from N=42 in $^{80}$Sr to N=45 in $^{83}$Sr, in good agreement with the preliminary $Q_t$ measurements. On the other hand, some disagreements with data have also been encountered. For example,

theoretical proton single-particle routhians do not show a significant energy gap at Z~40 which could account for the large population intensity and quadrupole moments observed in the Zr isotopes. Similarly, the twinned bands observed in the $^{82}$Sr-$^{83}$Y and $^{83}$Sr-$^{84}$Y isotones can be explained only for a large deformation of $\beta_2$~0.58, which is in disagreement with the measured transition moments. It seems that some modifications of the single-particle energy spectra are called for to accommodate these experimental observations.

In general, results of other models [e.g., Refs. 28,29] share many similarities with these calculations, but they also differ in some details. For example, while cranked relativistic mean field calculations [29] for the SD band in $^{83}$Sr predict the same $\nu 5^3 \pi 5^1$ configuration, they calculate a larger equilibrium deformation ($\beta_2$~0.65 vs. 0.57). Future lifetime measurements using the completed Gammasphere array will be able to distinguish between these models.

## 4. Summary and Outlook

Thanks to the development of a new generation of powerful $\gamma$-ray detector systems, a new region of SD nuclei in the mass A~80 was recently discovered. The identification and characterization of the properties of these bands have been greatly facilitated by the use of the Microball charged-particle detector system. So far, more than 20 SD bands have been observed in 10 nuclei which span N=42-46 and Z=38-41, thus confirming the earlier predictions for the existence of a large SD gap at N~44. In general, the properties of these bands are in good agreement with the predictions of the cranking models. However, the presence of several disagreements point to possible shortcomings in the single-particle energy spectra at large deformations and rotational frequencies. The high rotational frequencies sustained by these bands correspond to the largest Coriolis force encountered so far, and allow for the observation of the $i_{13/2}$ superintruder orbital in these medium-mass nuclei. Another consequence of the high rotational frequency and large SD energy gaps is that the T=1 pairing correlations become negligibly small. This paves the way to observe the influence of the T=0 p-n interaction in the SD bands of the N=Z~30 nuclei which are yet to be discovered. Finally, because of the dominance of charged-particle emission in this region, it is now possible to probe possible nuclear structure effects on the energies and angular distributions of the emitted protons and alpha particles. This will open up new and exciting opportunities to study nuclear structure and reaction at their interface.

## Acknowledgments

Much of the experimental work reviewed here is the result of a large collaboration involving researchers from ORNL, Washington University, University of Pittsburgh, LBNL, and Florida State University [7-11, 13-15, 17-22]. I am greatly indebted to the members of this collaboration group, especially Y. Akovali, M.J. Brinkamn, B. Cederwall, F. Cristancho, D.M. Cullen, J. Doring, M. Devlin, C.J. Gross, H.-Q. Jin, D.R. LaFosse, I.-Y. Lee, F. Lerma, A.O. Macchiavelli, D. Rudolph, J.X. Saladin, D.G. Sarantites, D.W. Stracener, G. Sylvan, S.L. Tabor, D.F. Winchell, and V. Wood, and C.-H. Yu. Theoretical support by T. Werner and W. Nazarewicz are gratefully acknowledged. Oak Ridge National Laboratory is managed by Lockheed Martin Research Corp. for the U.S. Department of Energy under contract No. DE--AC05-96OR22464.

## References


[1] S.M. Polikanov *et al.*, Sov. Phys. JETP **15**, 1016 (1962).
[2] V.M. Strutinsky, Nucl. Phys. **A95**, 420 (1967), **A122**, 1 (1968).
[3] P.J. Twin *et al.*, Phys. Rev. Lett. **57**, 811 (1986).
[4] E.F. Moore *et al.*, Phys. Rev. Lett. **63**, 360 (1989).
[5] I. Ragnarsson, S.G. Nilsson, and R.K. Sheline, Phys. Rep. **45**, 1 (1978).
[6] W. Nazarewicz *et al.*, Nucl. Phys. **A435**, 397 (1985).
[7] C. Baktash *et al.*, Phys. Rev. Lett. **74**, 1946 (1995).
[8] D.G. Sarantites *et al.*, Nucl. Inst. and Meth. A (in press).
[9] D.R. LaFosse *et al.*, Phys. Lett. **B354**, 34 (1995).
[10] M. Devlin *et al.*, this conference and to be published.
[11] F. Christancho *et al.*, Phys. Lett. **B357**, 281 (1995).
[12] A.G. Smith *et al.*, Phys. Lett. **B355**, 32 (1995).
[13] H.-Q. Jin *et al.*, Bull. Am. Phys. Soc. **41**, 881, (1996); and to be published.
[14] D. Rudolph *et al.*, Phys. Lett. **B** (in press).
[15] D.R. LaFosse *et al.*, Phys. Rev. Lett. (submitted).
[16] P.J. Dagnall *et al.*, Z.Phys. **A353**, 251 (1995).
[17] H.-Q. Jin *et al.*, Phys. Rev. Lett. **75**, 1471 (1995).
[18] C. Baktash, B. Haas, and W. Nazarewicz, Annu. Rev. Nucl. Part. Sci. **45**, 485 (1995).
[19] D. Rudolph *et al.*, Phys. Rev. C (submitted).
[20] D.M. Cullen *et al.*, in *Proc. Conf. on Physics from Large γ-Ray Detector Arrays, Berkeley*, Aug. 1994, Vol. I, p.44.
[21] H.-Q. Jin *et al.*, to be published
[22] C.-H. Yu *et al.*, Phys. Rev. C (submitted).
[23] X.-L. Han and C.-L. Wu, At. Data Nucl. Data Tables **52**, 43 (1992).
[24] G. deFrance *et al.*, Phys. Rev. C**53**, R1070 (1996).
[25] B. Cederwall *et al.*, Nucl. Instrum. Meth. Phys. Res. A**354**, 591 (1995).
[26] W. Satula *et al.*, this conference and to be published.
[27] J. Dudek, W. Nazarewicz, and N. Rowley, Phys. Rev. C **35**, 1489 (1987).
[28] S. Aberg, H. Flocard, and W. Nazarewicz, Annu. Rev. Nucl. Part. Sci. **40**, 439 (1995).
[29] A.V. Afanasjev, J. Konig, and P. Ring, Phys. Lett. **B367**, 11 (1966).

# Systematic Description of Superdeformed Bands in the Mass-190 Region

Yang Sun[1,2,3], Jing-ye Zhang[2], and Mike Guidry[2,3]
[1] *JIHIR, Oak Ridge National Laboratory, Oak Ridge, Tennessee 37831*
[2] *Department of Physics and Astronomy, University of Tennessee, Knoxville, Tennessee 37996*
[3] *Physics Division, Oak Ridge National Laboratory, Oak Ridge, Tennessee 37831*

## Abstract

Superdeformed bands for the mass-190 region are described by the Projected Shell Model. Even–even, odd mass and odd–odd nuclei are equally well described. Good agreement with available data for all isotopes studied is obtained. Our calculation of electromagnetic properties and pairing correlations provides an understanding of the observed gradual increase of dynamical moments of inertia with angular momentum observed in many bands in this mass region.

In the superdeformed (SD) mass-190 region, data show that both kinematical ($\mathcal{J}^{(1)}$) and dynamical ($\mathcal{J}^{(2)}$) moments of inertia (MoI) for many SD bands exhibit a gradual increase as a function of increasing rotational frequency, with a more pronounced increase in $\mathcal{J}^{(2)}$. The usual explanation using the cranking model is that this behavior is caused by a gradual rotation alignment of pairs from high-$j$ intruder orbitals [1]. Although the role played by high-$j$ intruders for many phenomena in a normally deformed system is well understood, it is not obvious that such knowledge translates simply to the SD case for at least two reasons: (1) At the static level, high-$j$ intruder orbitals are no longer of unique parity at larger deformation as they are in the normally deformed case [2,3]. (2) At the dynamical level, the larger quadrupole moment for a SD band implies more mixing among different configurations through the two-body hamiltonian, which includes explicitly a quadrupole–quadrupole term. This mixing will reduce the influence from any particular orbital.

In order to further understand the issues raised above, we have performed calculations using the projected shell model. The calculations that we describe provide a full description of the SD spectrum, electromagnetic properties, and pairing properties. We shall demonstrate that all the observed quantities are reproduced by this calculation, and that a gradually decreasing pairing caused by the Coriolis Antipairing (CAP) effect acting on both low and high-$j$ orbitals is responsible for the observed smooth increase of the MoI.

Our theoretical analysis for SD nuclei is based on the Projected Shell Model (PSM) [4], which has been generalized from its description of normally deformed systems [5]. The configuration space and the interaction strengths in the Hamiltonian used for the description of the SD mass-190 region are given in Ref. [2].

In Fig. 1, we compare calculated transition energies $E_\gamma$ and dynamical MoI $\mathcal{J}^{(2)}$ with the available measurements for yrast SD bands in even–even $^{188-196}$Hg isotopes. The agreement

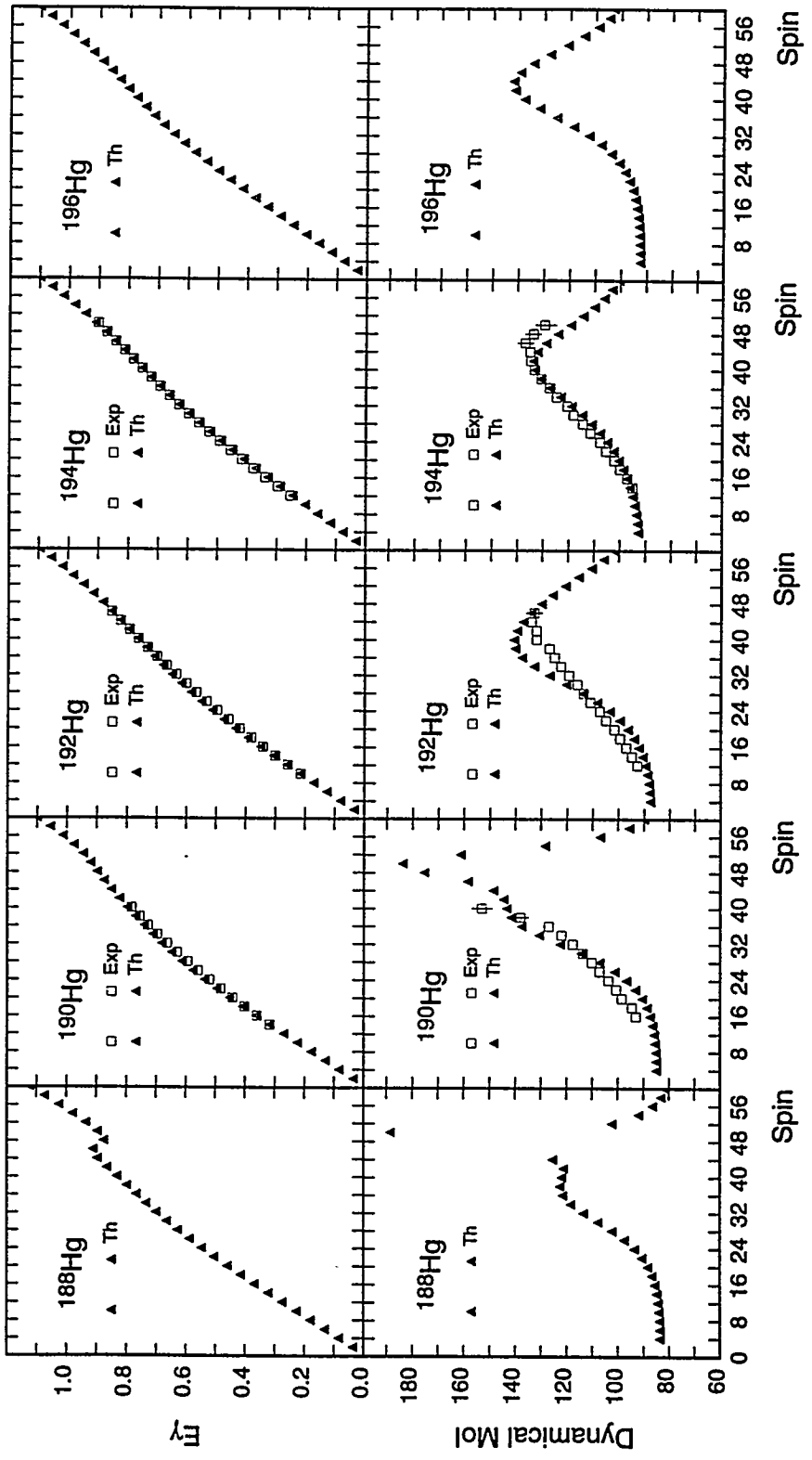


FIG. 1. Comparison of calculations with experimental data for even–even $^{188-196}$Hg: a) $\gamma$-ray energies defined by $E_\gamma(I) = E(I) - E(I-2)$ (MeV); b) Dynamical MoI defined by $\mathcal{J}^{(2)}(I) = 4/[E_\gamma(I) - E_\gamma(I-2)]$ ($\hbar^2$MeV$^{-1}$).

with data is extremely good, with even the sensitive dynamical MoI being reproduced well. The MoI rises gradually with angular momentum for all nuclei in this mass region; however, the rate of increase (slope of $\mathcal{J}^{(2)}$) varies from nucleus to nucleus. The calculations reproduce these variations well without adjustment of parameters, indicating the potential of the model to give a quantitative description of SD nuclei. The differences in slope arise from the variation of effective interaction strengths and band crossing spin for different nuclei, which is a common occurrence in normally deformed bands [6,7]. It is clear that extension of data in known SD nuclei by even a few spin units, or observation of SD states in Hg isotopes 2 neutron numbers larger or smaller than presently known, could provide strong tests of these calculations. We predict a backbending at $I = 48\hbar$ in $^{188}$Hg.

Generally, we predict a gradually decreasing $\mathcal{J}^{(2)}$ for the highest spins. The whole pattern forms a smooth bump with the maximum at about $I = 42\hbar$. At this spin the SD ground-state band (g-band) crosses, simultaneously, a 2-qp proton band and a 2-qp neutron band. After the crossing, the 2-qp proton band is lower in energy and thus has larger weight in the yrast band for $I > 42\hbar$. We note that changing the quadrupole pairing will shift the band crossing, thereby shifting the peak in the $\mathcal{J}^{(2)}$ curve. If the quadrupole pairing employed in Fig. 1 is decreased (increased) by 30%, the $\mathcal{J}^{(2)}$ peak for $^{194}$Hg is shifted to $I = 38\hbar$ ($I = 46\hbar$), but the $E_\gamma$ values are displaced by only a few keV. Thus, the location of the maximum in $\mathcal{J}^{(2)}$ is sensitive to the quadrupole pairing strength, but our other results do not depend significantly on this parameter. In particular, the quadrupole pairing force is not found to be responsible for the gradual increase behavior of $\mathcal{J}^{(2)}$, as claimed in Ref. [8].

The angular momenta for experimental states in Fig. 1 are those proposed by the corresponding experimentalists, but only for $^{192,194}$Hg are these measured quantities. For $^{192,194}$Hg the agreement with data is excellent, with the experimental and theoretical $E_\gamma$ values virtually indistinguishable on the scale of the plot. This provides strong theoretical support for recently-measured spin values in these nuclei. This indicates also that the present model could be a powerful tool to predict unknown spins for SD nuclei.

Comparisons of our results with data for odd-mass nuclei are shown in Fig. 2, where we take the recent SD measurements for $^{193}$Pb and $^{193}$Tl as representative examples for odd-$N$ and odd-$P$ nuclei, respectively. In the left part of Fig. 2, the calculated $\mathcal{J}^{(2)}$ for the $[761]\frac{3}{2}$ band in $^{193}$Pb starts at a higher value, deceases rapidly until $I = 16\hbar$, and finally increases again at $I = 36\hbar$. Thus, $\mathcal{J}^{(2)}$ is observed to be approximately constant for the spin region $I = 16 - 36\hbar$, but predict that it should increase at higher spins. One observes also that for the signature partner bands 1 and 2, our calculation predicts a larger $\mathcal{J}^{(2)}$ for band 1 until $I = 36\hbar$, as found in the data. After that spin, $\mathcal{J}^{(2)}$ for band 2 has a larger value. Very good agreement with data for the $E_\gamma$'s is obtained, particularly for higher spins, and the signature splitting between the partners is also reproduced. Thus, our calculations support the present spin assignment.

The right part of Fig. 2 shows our results, together with data, for the $[642]\frac{5}{2}$ band of $^{193}$Tl. The present data stop at the point where the theoretical $\mathcal{J}^{(2)}$ curve turns downward at $I = 44\hbar$. Again, extension of the data to higher spins will test our prediction. For the $E_\gamma$'s, there is good overall agreement between data and calculations, with the right phase and amplitude in the splitting of signature partners.

Fig. 3 compares the same data [9] with two sets of calculations. A nearly constant $\mathcal{J}^{(2)}$ is observed in the measured spin interval. In the left part of Fig. 3, we performed a calculation by using the configuration proposed in Ref. [9], $\nu[761]\frac{3}{2} + \pi[642]\frac{5}{2}$. However, we obtained a decreasing $\mathcal{J}^{(2)}$. The other configuration, $\nu[642]\frac{3}{2} + \pi[642]\frac{5}{2}$, reproduces the data much

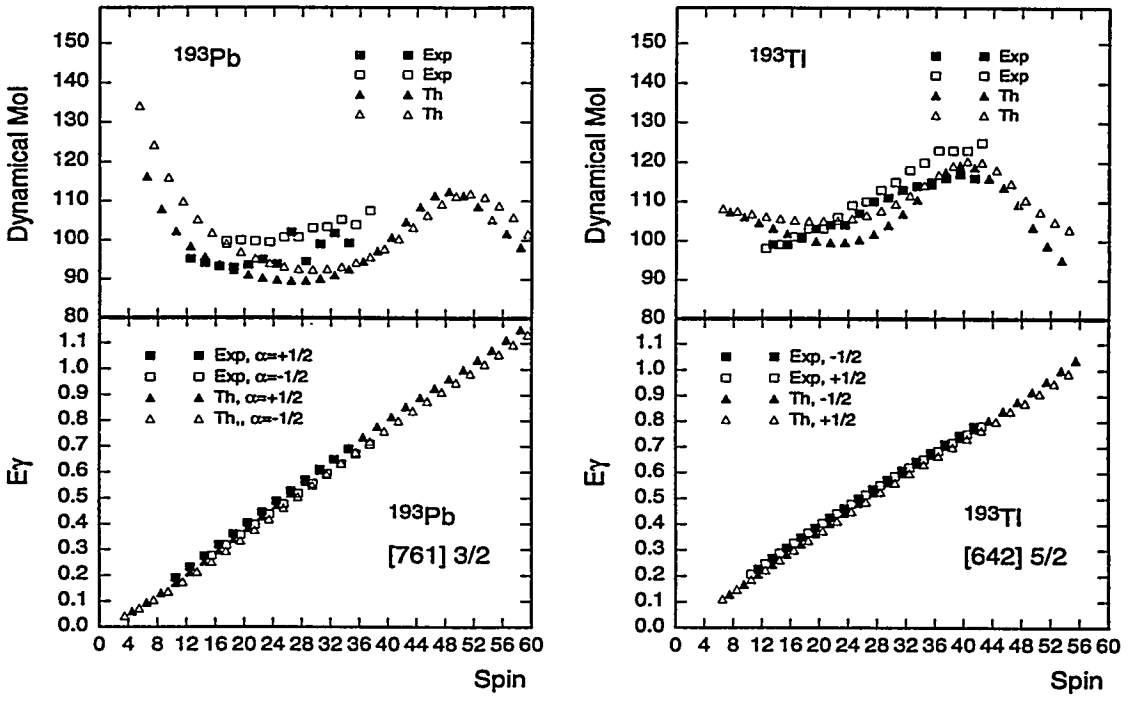


FIG. 2. Comparison of calculations with experimental data for $^{193}$Pb (left part), and for $^{193}$Tl (right part).

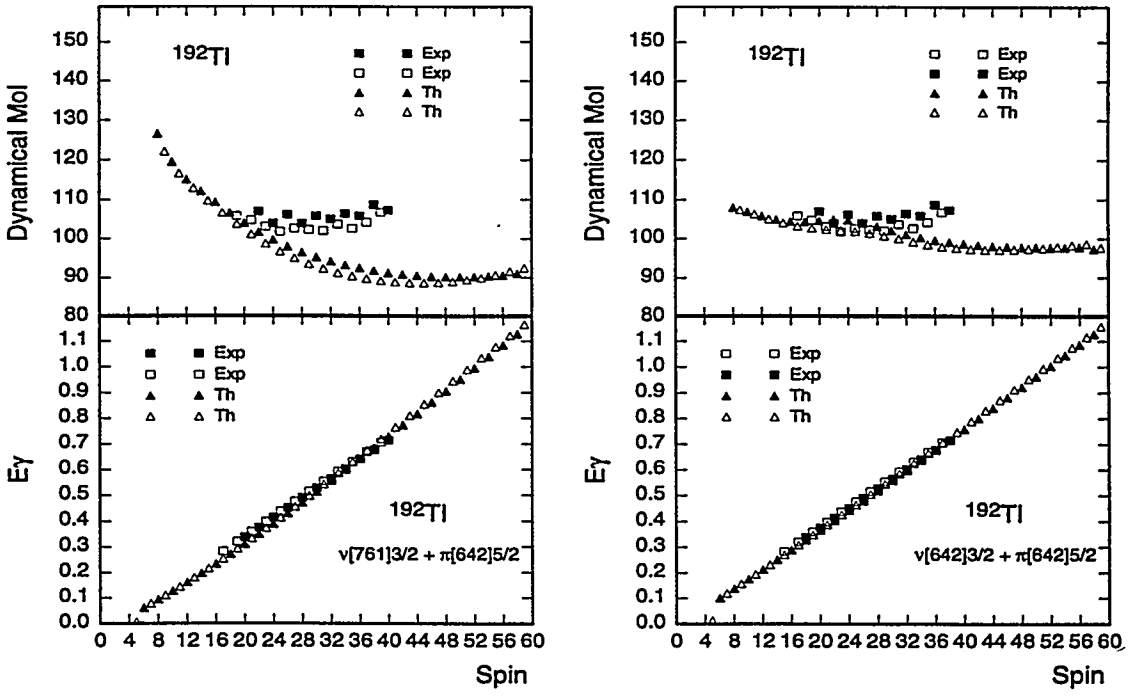


FIG. 3. Comparison of calculations with experimental data for $^{192}$Tl. See text for theoretical configurations.

better, with excellent agreement in $\mathcal{J}^{(2)}$ up to $I = 32\hbar$ — see the right part of Fig. 3. (The deviation beyond that spin is due to the absence of 4-qp states in our odd–odd calculations.) A better agreement in $E_\gamma$ for the latter configuration is also observed.

Since our wavefunctions are eigenfunctions of angular momentum, we can calculate unambiguously the transition quadrupole moment $Q_t$, $g$-factor, and pairing gaps ($\Delta_n$ and $\Delta_p$), as a function of angular momentum. These quantities are defined in Ref. [10]. In Fig. 4 we show the theoretical values of these quantities for the SD yrast band in $^{194}$Hg. Rather constant $Q_t$ (Fig. 4a) is found up to $I \approx 24\hbar$, with a value of 16.8 eb that is comparable to the measured average $Q_t$ of 17.2 $\pm$ 2.0 eb. Above that spin, the theoretical values are gradually and smoothly quenched because of gradual alignment processes that lead to a small reduction of collectivity. Therefore, this calculation indicates that stretching in deformation is negligible for the range of measured angular momenta in the $^{194}$Hg yrast band.

The calculated $g$-factors are presented in Fig. 4b. There are as yet no experimental data available for comparison. These quantities are sensitive to the alignment of individual nucleon pairs. Proton and neutron $g$-factors are plotted separately, as is their sum. We observe a rather constant, small, and negative value for neutrons. The behavior of the total $g$-factor is governed by that of the protons, which shows a gradual increase with angular momentum in the range $I = 24 - 44\hbar$. At $I = 44\hbar$, the total $g$-factor reaches $Z/A \approx 0.41$ and saturates thereafter. The g-factors suggest that the rotation alignment of high-$j$ orbitals enhances the MoI, but the alignment contribution seems insufficient to cause the pronounced increase in the MoI seen in Fig. 1 for $^{194}$Hg. In particular, this cannot easily explain the increase in the MoI before $I = 24\hbar$, where the high-$j$ pair alignment is small.

We show calculated pairing gaps in Fig. 4c. Note that the quantities displayed are not BCS gaps; they are computed from the many-body wavefunctions, which incorporate dynamical effects in the pair field [10]. We observe steady quenching of proton and neutron pairing with increasing spin across the entire spin range. This smooth decrease of $\Delta$ corresponds to a collective CAP effect that enhances the MoI with increasing angular momentum. A somewhat steeper decrease in the gap is found for protons in the range $I = 24 - 44\hbar$. This additional contribution comes from the increasing importance of high-$j$ pair alignment, in accord with discussions given above.

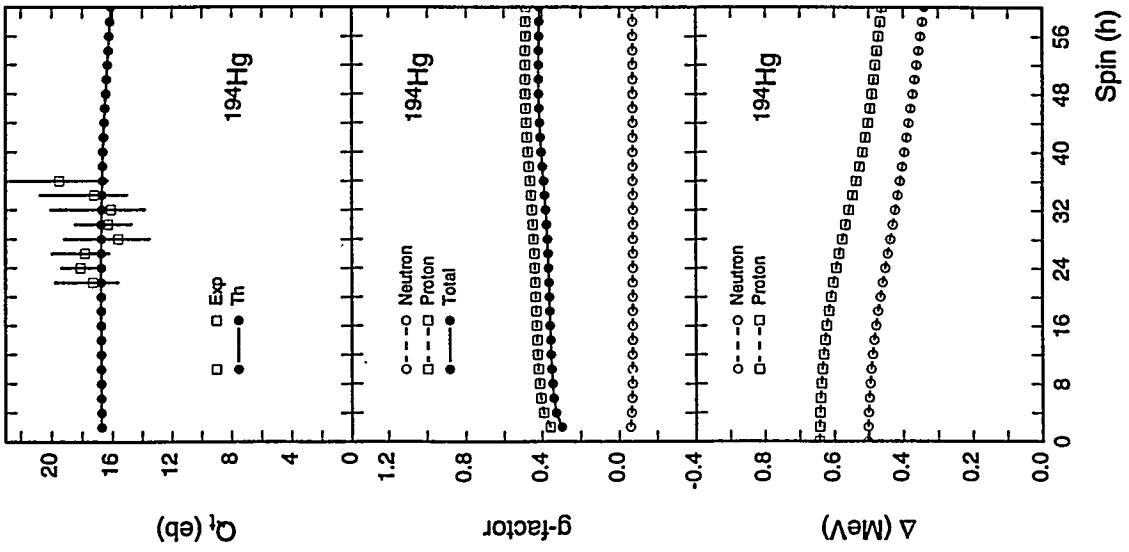


FIG. 4. For $^{194}$Hg: a) Comparison of the calculated transition quadrupole moments (in eb) with the data. b) Theoretical $g$-factors; c) Theoretical pairing gaps (in MeV).

Thus we conclude that the gradual increase of the MoI for SD bands in the mass-190 region is due to smooth quenching of pairing correlations by the CAP effect, which receives contributions from all orbitals and only becomes dominated by gradual rotation alignment of high-$j$ particles at higher spins. In previous discussions [1,8], the gradual rotation alignment of quasiparticles from high-$j$ orbitals was stressed, but the important average contribution of *all orbitals* through the CAP effect has not been emphasized. This observation is implicit in previous studies where it was noticed [1] that treatment of the collective motion in a cranking model with shell-correction calculations could have difficulties for a quantitative description of the MoI of a SD band.

In conclusion, the Projected Shell model has been used to provide the first comprehensive theoretical description of the SD bands in the mass-190 region that simultaneously describes all observables, including the angular momentum. The increase of the MoI is caused by a smooth decrease of the pairing correlation within the nucleus due to a combination of the CAP effect and rotation alignment of high-$j$ pairs, with no evidence of deformation stretching. These conclusions are supported by calculations of transition quadrupole moments, $g$-factors, and pairing gaps. We notice in this connection the recently observed relative transition quadrupole moments for SD bands in $^{132}$Ce and $^{131}$Ce [11], indicating a negligible polarization effect induced by the high-$j$ particles. Finally, these calculations provide a variety of predictions that could be tested by extension of existing SD data to somewhat higher spins and to other nuclei in this region, and by measurement of g-factors.

## ACKNOWLEDGMENTS

The Joint Institute for Heavy Ion Research has as member institutions the University of Tennessee, Vanderbilt University, and the Oak Ridge National Laboratory; it is supported by the member institutions and by the U. S. Department of Energy through Contract No. DE–AS05–76ER04936 with the University of Tennessee. Theoretical nuclear physics research at the University of Tennessee is supported by the U. S. Department of Energy through Contract No. DE–FG05–87ER40361 and DE–FG05–93ER40770. Oak Ridge National Laboratory is managed by Lockheed Martin Energy Research Corp. for the U. S. Department of Energy under Contract No. DE–AC05–96OR22464.

## REFERENCES

[1] M.A. Riley, *et al.*, Nucl. Phys. **A512**, 178 (1990)

[2] Yang Sun, Jing-ye Zhang, and M. Guidry, subm. Phys. Rev. Lett. April, 1996.

[3] C.-L. Wu, D. H. Feng, and M. W. Guidry, Ann. Phys. **222**, 187 (1993)

[4] Y. Sun and M. Guidry, Phys. Rev. **C52**, R2844 (1995)

[5] K. Hara and Y. Sun, Int. J. Mod. Phys. **E4**, 637 (1995)

[6] R. Bengtsson, I. Hamamoto, and B. Mottelson, Phys. Lett. **73B**, 259 (1978)

[7] Y. Sun, P. Ring and R.S. Nikam, Z. Phys. **339**, 51 (1991)

[8] W. Satula and R. Wyss, Phys. Rev. **C50**, 2888 (1994); R. Wyss and W. Satula, Phys. Lett. **B351**, 393 (1995)

[9] S.M. Fischer, *et al.*, Phys. Rev. **C53**, 2126 (1996)

[10] Y. Sun and J.L. Egido, Phys. Rev. **C50**, 1893 (1994); Nucl. Phys. **A580**, 1 (1994)

[11] R.M. Clark, *et al.*, Phys. Rev. Lett. **76**, 3510 (1996).

# NEW RESULTS ON THE SUPERDEFORMED $^{196}$Pb NUCLEUS : THE DECAY OF THE EXCITED BANDS TO THE YRAST BAND

S. Bouneau[1], F. Azaiez[1], J. Duprat[1], I. Deloncle[2], M-G Porquet[2], U.J. van Severen[3], T. Nakatsukasa[4], M.M. Aleonard[5], A. Astier[6], S. Baldsiefen[3], C.W. Beausang[7], F.A. Beck[8], C. Bourgeois[1], D. Curien[8], N. Dozie[2], L. Ducroux[6], B. Gall[8], H. Hubel[3], M. Kaci[2], W. Korten[3], M. Meyer[6], N.Redon[6], H. Sergolle[1] and J.F. Sharpey-Schafer[9]

[1] *IPN Orsay (France),* [2] *CSNSM Orsay (France),* [3] *ISKP Bonn (Germany),*
[4] *AECL Research, Chalk River Laboratories, Chalk River, Ontario (Canada),*
[5] *CENBG Gradigan (France),* [6] *IPN Lyon (France),* [7] *Univ. Liverpool (UK),*
[8] *CRN Strasbourg (France),* [9] *National Accelerator Centre Faure (South Africa)*

**Abstract**

The study of the superdeformed (SD) $^{196}$Pb nucleus has been revisited using the EUROGAM phase 2 spectrometer. In addition to the known yrast and two lowest excited SD bands, a third excited SD band has been seen. All of the three excited bands were found to decay to the yrast SD band through, presumably, E1 transitions, allowing relative spin and excitation energy assignments. Comparisons with calculations using the random-phase approximation suggest that all three excited bands can be interpreted as octupole vibrational structures.

## 1 - INTRODUCTION

Nearly all excitations observed in SD minima have been identified as particle, hole or (multi-) particle-hole excitations. Calculations [1] suggested that the octupole vibrational mode is the lowest of the possible vibrational modes for superdeformed shapes in both the mass 150 and 190 regions. Recently the excited SD band 6 [2] in $^{152}$Dy has been put forward [3] as having properties characteristic of an octupole vibration. However, the experimental evidence for octupole vibrational states in $^{190}$Hg [4] is somewhat clearer. Cowell et al. [4] have reported the observation of E1 transitions connecting the first excited SD band of $^{190}$Hg, band 2, to the yrast SD band 1. We report here another case where the three observed excited SD bands, in $^{196}$Pb were found to decay to the yrast SD band through, presumably, E1 transitions. This result suggests that the inclusion of the octupole vibrational degree of freedom may be important to give a satisfactory description of the properties of the excitations of SD nuclei.

## 2 - EXPERIMENT AND RESULTS

The results presented here are from an experiment performed with the Eurogam Phase 2 $\gamma$-ray spectrometer [5], which consists of 54 escape-suppressed Ge detectors. Of these, 30 are large-volume Ge detectors located in rings at the forward and backward hemispheres; the remaining 24 detectors around 90 degrees, are so-called "clover" detectors, each consisting of four closely packed Ge crystals within a single cryostat and inserted in the same escape-suppression shield. The experiment was performed using the reaction $^{186}$W($^{16}$O,6n) on a stack of three isotopically pure 0.2 mg/cm$^2$ W targets. The Vivitron accelerator was set at a beam energy of 110 MeV. A total of $10^9$ triple and higher-fold events was acquired. The data were subsequently analysed by sorting and extracting triple-gated spectra with background subtraction. The known yrast [6] and two first excited SD bands [7] in $^{196}$Pb were seen in the data. In addition to the three known bands a forth SD band was discovered in $^{196}$Pb. The spectra of the four observed SD bands are displayed in figure 1 and their transition energies are listed in table 1. Their assignement to $^{196}$Pb is firmly confirmed, by the observation of gamma transitions between low-lying $^{196}$Pb yrast states, in coincidence with the bands (see figure 1). The intensities, relative to the yrast SD band (band 1), were found to be approximately 20%, 20% and 5% for band 2, band 3 and band 4, respectively. A very unusual feature of the three excited bands was observed. Each of them decays to the yrast SD band with intensities ranging from a few per cent to a few tens of per cent. In the following, we are going to present the results concerning the decay of each of the three excited bands to the yrast SD band.

## 2.1 - Band 2 and Band 3

In addition to their firm assignment to $^{196}$Pb, band 2 and band 3 have been extended to higher rotational frequencies, compared to what has been reported previously by Van Severen et al.[7]. More importantly, the coincidence spectra obtained by requiring triple-gates on the highest members of band 3 contain the low-lying gamma-transitions belonging to the yrast SD band 1. Figure 2 exhibits a spectrum, where band 3 shows a smooth increasing pattern of de-excitation to the yrast SD band, starting around the rotational frequency $\hbar\omega \approx 0.20$ MeV. This pattern of decay is unlike those of almost all previously observed SD bands in the A=150 and A=190 regions, in which the nucleus remains in the SD band until finally decaying to the normally deformed states. Only the $^{190}$Hg first excited band which has been interpreted as due to an octupole vibrational state built on top of a SD nucleus, shows a similar de-excitation pattern to the yrast SD band. At the higher energy part of the spectrum of figure 2, one can see a clustering of $\gamma$-lines around 944 keV. This series of unresolved lines was found to be in coincidence with the higher part of band 3 and the lower part of band 1, suggesting that the lines are the connecting transitions between the two SD bands. The coincidence pattern between the $\gamma$-transitions in band 1 and in band 3 allows us to propose the decay scheme shown in figure 4. The relative placement of the two bands is uniquely determined by the sums and differences of the $\gamma$-rays involved. It is worth pointing out that the clustering of the connecting transitions around a unique value (944 keV) is due to the fact that in the region where band 3 decays to band 1, the two bands have very close transition energies.

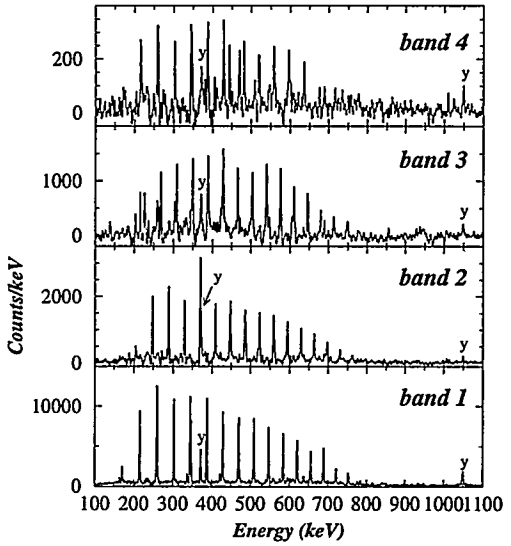


*Figure 1 : Triple gated spectra on the four observed SD bands in $^{196}$Pb. $\gamma$-transitions connecting normally deformed states in $^{196}$Pb are labeled by "y".*

In order to determine the relative spins of the two SD bands, DCO (directional correlations from oriented nuclei [8]) ratios were extracted for the interband transitions. These were defined simply as the number of counts in the clover detectors (located around 90 degrees) divided by the number of counts in the large volume detectors (at forward and backward angles), after correction for efficiency. These ratios were calibrated using transitions of known multipolarity and were found to be approximately 1.3 for $\Delta$ L = 1 transitions and 0.8 for $\Delta$ L = 2 transitions. Only one ratio was extracted for the entire 944 keV composite line (assuming that all of its components are of the same nature). This ratio was deduced from triple gated spectra, under the assumption that the requirement of a gating transition did not significantly perturb the orientation of the nuclear mo-

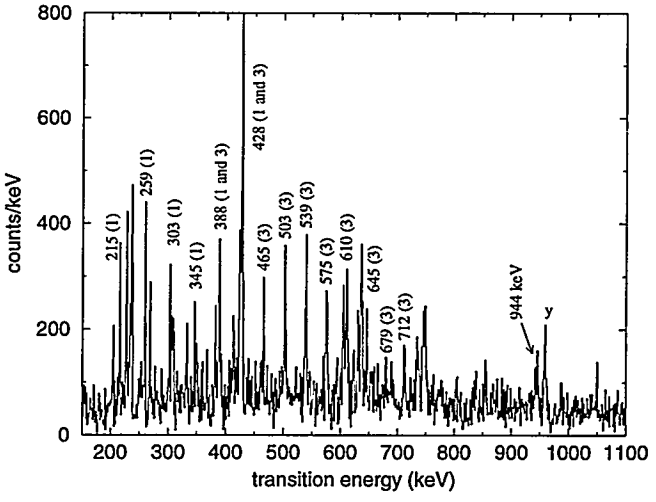


*Figure 2 : Triple gated spectrum obtained by requiring 1 gate on the lowest members of band 1 and 2 gates on the highest members of band 3. $\gamma$-lines are indicated by the energy and the number of the band to which they belong.*

mentum (this is quite a good assumption because of the quasi-spherical symmetry of the array's geometry and because of the large angular momentum J of the states considered compared to the multipolarity $\lambda$ of the transitions). The measured value of the DCO ratio 1.2 (2) for the broad 944 keV line, is found to be in agreement with a dipole character. Thus it is very likely that the two SD bands (band 1 and band 3) differ by one unit of angular momentum as indicated in figure 4. Because of the limited statistics, it was unfortunately not possible to extract a polarisation measurement for this group of connecting transitions (by using the set of clover detectors as a polarimeter). Similarly but less firmly band 2 has been found to be in coincidence with band 1 and no connecting transitions have been found. The relationship between the transitions energies in band 2 and band 3 is that between strongly coupled bands (namely the transition energies of band 2 lie at the mid-points of those of band 3). Thus band 2 and band 3 could be considered as signature partner bands. This assumption allows the placement of band 2 in the level scheme as shown in figure 3. In this level scheme the unobserved transitions are indicated by dashed arrows.

## 2.2 - Band 4

In addition to the two known excited SD bands (band 2 and band 3), a third excited SD band (band 4) has been observed. This band appears very clearly in a spectrum gated on the lowest transitions of band 1. This can be taken as evidence that this new SD band decays very strongly to the Yrast SD band 1. This is also very well illustrated in figure 3, where a spectrum obtained by requiring a double gate on the highest members of band 4 and one gate on the lowest members of band 1, is shown. This spectrum exhibits the same behaviour as band 3, namely a rapid loss of intensity from band 4 to band 1. In the case of band 4 the depopulation to the yrast band occurs at relatively higher rotational frequency ($\hbar\omega \approx 0.25$ MeV) than band 3. Only a very weak candidate at 1241 keV for the connecting transitions between SD states in band 4 and band 1 was observed. Despite the weakness of this line, a clear coincidence was observed between the lowest transitions in band 1, the highest transitions in band 4 and the 1241 keV transition. The observed coincidence relationship suggests the tentative part of the level scheme involving the decay of band 4 (see figure 4). Because of the weakness of the observed interband transition (two other interband transitions are tentatively added to the level scheme) it was not possible to extract any information on its nature and multipolarity.

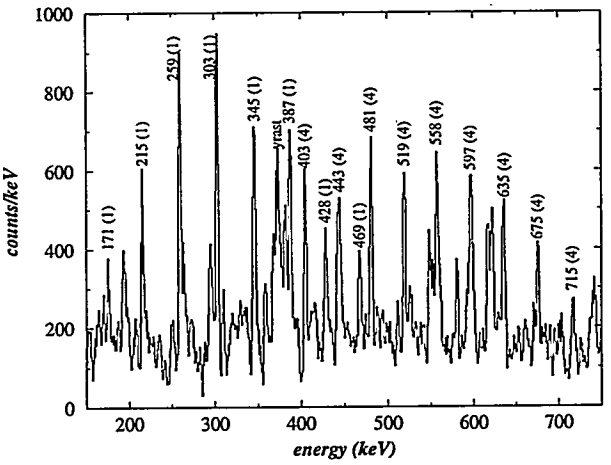


*Figure 3 : Triple gated spectrum obtained by requiring 1 gate on the lowest members of band 1 and 2 gates on the highest members of band 4. $\gamma$-lines are indicated by the energy and the number of the band to which they belong.*

# 3 - INTERPRETATION

As mentioned earlier, band 2 and band 3 could be considered as two strongly coupled signature partner bands. If we assume for the two bands the spins indicated in the level scheme of figure 4 (based on the assumption that the connecting transitions between band 3 and band 4 are stretched dipoles and that band 2 and band 3 are signature partners), the alignment of the two bands with respect to the yrast SD band in the $^{194}$Pb core could be calculated as a function of rotational frequency. These alignments are shown in figure 5 together with those of the two excited SD bands in $^{194}$Hg for which the yrast SD band in $^{192}$Hg is taken as a reference. The spins of the bands in $^{194}$Hg and $^{194}$Pb are suggested by recent measurements of linking transitions between the SD states and the normally deformed states in those nuclei [9, 10, 11]. For the yrast SD bands in $^{196}$Pb and in $^{192}$Hg, the spins are deduced from the fits of the $J^{(2)}$ moment of inertia, using the Harris expansion. The first observation which may be made

from figure 5 is that, independently of any spin values, the $J^{(2)}$ dynamical moments of inertia of band 2 and band 3 are identical to that of the yrast band in $^{194}$Pb (for rotational frequency $\hbar\omega$ higher than 0.2 MeV). The same feature is observed between the excited bands in $^{194}$Hg and the yrast SD band in $^{192}$Hg. One possible interpretation for the two first exited SD bands in $^{194}$Hg and $^{196}$Pb is that they are due to a two quasi-particle excitation involving the two strongly coupled [624]9/2 and [512]5/2 neutron orbitals located above the N=112 SD shell gap. It is now known, from the study of the SD $^{193}$Hg nucleus [12] that occupancy of such orbitals do not affect the behaviour of the $J^{(2)}$ moment of inertia , relative to the neighbouring core. Furthermore, the lack of M1 transitions between band 2 and band 3, could be taken as an indication that they correspond to the two signature partner bands with the value K=2 [13]. The same interpretation has been already proposed for the two excited SD bands in $^{194}$Hg [14]. Concerning band 4, a striking similarity was found between the $J^{(2)}$ of that band and the $J^{(2)}$ of band 1 in $^{195}$Pb [15]. They are both fairly constant around a value of 105 $\hbar^2$ MeV$^{-1}$. This behaviour of the $J^{(2)}$ moment of inertia is typical of SD lead isotopes where the $j_{15/2}$ intruder orbital is occupied by a single neutron [15, 16]. Thus band 4 could be due to a two quasi-particle excitation involving the neutron $j_{15/2}$ and the lowest strongly coupled neutron orbital (presumably the [624]9/2 orbital). This interpretation in terms of a two quasi-particle excitation accounts for the observed $J^{(2)}$ behaviour of the three excited SD bands in $^{196}$Pb, but not for their relatively strong decay to the yrast SD band 1. Furthermore, the excitation energies of these SD bands, relative to the yrast SD band, were found to be approximately 1 to 1.2 MeV, which is fairly low for a two quasi-particle excitation (if one assumes a typical 1 MeV energy gap $\Delta$). If we assume that the connecting transitions of band 3 and band 4 to the yrast band are of E1 character, an alternative interpretation invoking octupole vibrational excitations is suggested by recent microscopic RPA calculations by Nakatsukasa et al [17, 18]. The details of this theoretical approch are discussed in this conference by Nakatsukasa. The calculated $J^{(2)}$ moment of inertia from this model are shown in figure 6 together with measured ones for the three excited SD bands. A striking agreement is found between experimental and theoretical results. The success in reproducing the measured $J^{(2)}$ moment of inertia of the two first excited SD bands suggests that band 2 and band 3 are the two signature partners of the K=2 octupole vibrational bands. The agreement for band 4 is not as good, but still could indicate that this band is the unique signature of the K=0 octupole vibrational band. The experimental B(E1) values extracted from the data were found to be approximately $10^{-6}$, $10^{-5}$ and $10^{-4}$ Wu for band 2, band 3 and band 4, respectively. While the calculated values are systematically one order of magnitude lower for the three bands, their relative increase within the three bands is well reproduced[18].

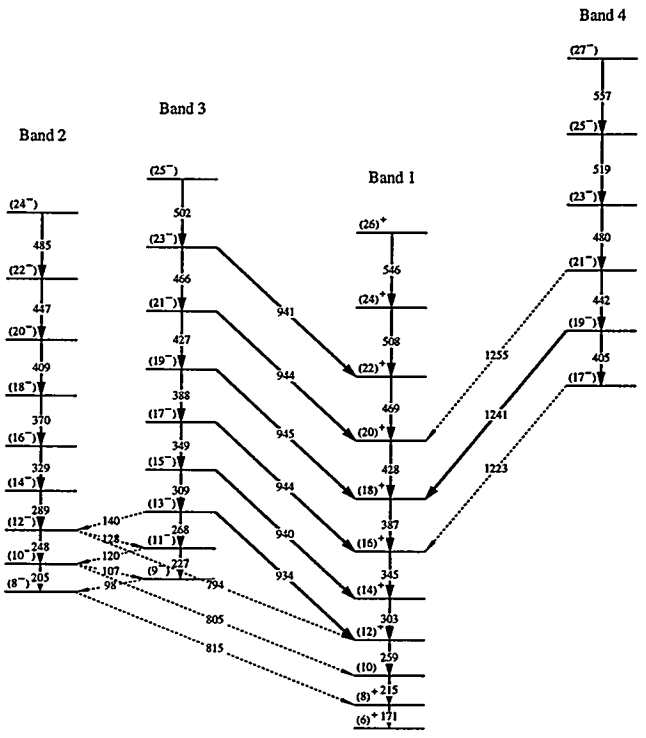


*Figure 4 : Tentative level scheme including the yrast SD band and the three excited bands in $^{196}$Pb.*

# 4 - CONCLUSION

The three excited SD bands in $^{196}$Pb show an unusual decay to the yrast SD band through presumably E1 transitions. This suggests that an alternative to the quasi-particle interpretation of the bands could be an interpretation in terms of octupole vibrational states built on top of the SD nucleus. Further experiments should be done in order to establish the E1 character of the interband transitions. A similar interpretation for almost all the excited SD bands observed in even-even nuclei of the mass-190 region is suggested by Nakatsukasa et al [17, 18]. This again raises the question related to the origin of the one unit of alignment of the excited bands in $^{194}$Hg with respect to the $^{192}$Hg core and the even more puzzling half unit of alignment of the excited bands in $^{196}$Pb with respect to the $^{194}$Pb core (see figure 5). For exemple to what extend octupole vibration in SD $^{194}$Hg and $^{196}$Pb could account for the observed constant alignment ($1\hbar$ or $1/2\hbar$ with respect to the corresponding core ($^{192}$Hg and $^{194}$Pb). Finally, other results concerning the decay of the yrast SD band to the normally deformed states in $^{196}$Pb and a possible fourth excited band with even stronger decay to the yrast SD band, have been obtained in this experiment and will be discussed in a forthcoming paper.

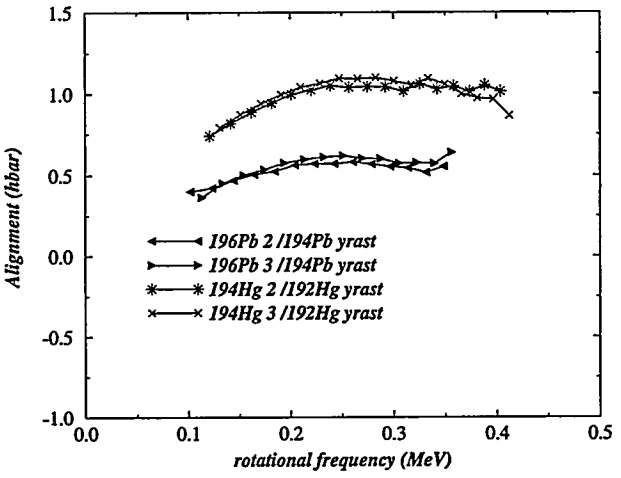


*Figure 5 : Alignment plot of the first two excited SD bands in $^{196}$Pb and in $^{194Hg}$Hg with respect to the yrast SD band in $^{194}$Pb and in $^{192Hg}$Hg, respectively.*

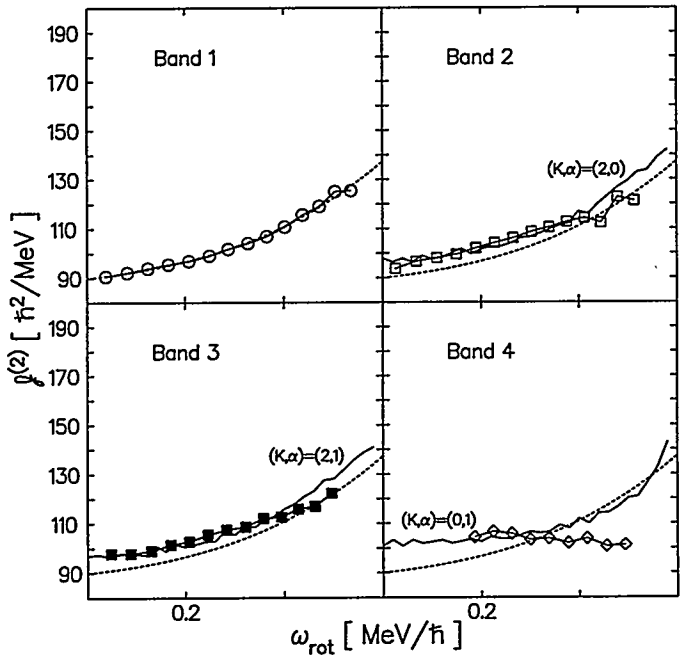


*Figure 6 : Results from RPA calculations based on the cranked shell model: Calculated (solid lines) and experimental (symbols) $J^{(2)}$ moments of inertia for the four SD bands in $^{196}$Pb. The dotted lines indicate the yrast $J^{(2)}$.*

Table 1: Energies of the four SD bands in $^{196}$Pb. Uncertainties range from 0.2 keV to 0.5 keV

| Band 1 | Band 2 | Band 3 | Band 4 |
|---|---|---|---|
| 170.9 | 204.9 | 227.2 | 367.0 |
| 215.5 | 247.9 | 268.1 | 405.3 |
| 259.6 | 289.0 | 309.0 | 442.8 |
| 303.0 | 329.7 | 349.4 | 480.6 |
| 345.5 | 369.9 | 388.6 | 519.3 |
| 387.4 | 409.0 | 427.2 | 557.8 |
| 428.6 | 447.4 | 465.3 | 597.0 |
| 469.0 | 485.1 | 502.7 | 635.4 |
| 508.3 | 522.0 | 539.6 | 675.2 |
| 546.7 | 558.3 | 575.1 | 714.4 |
| 584.1 | 593.9 | 610.5 | |
| 620.1 | 628.7 | 645.0 | |
| 654.9 | 663.2 | 679.4 | |
| 688.1 | 697.0 | 712.2 | |
| 720.6 | 730.0 | | |
| 752.3 | 764.0 | | |
| 783.5 | | | |

# References


[1] J. Dudek, T.R. Werner and Z Szymanski; Phys. Lett. B248 (1990) 235, S.Mizutori, Y.R. Shimizu and K. Matsuyangi ; Prog. Theor. Phys. 83 (1990) 666 and 86 (1991) 131, J. Holler and S. Aberg; Z. Phys. A336 (1990) 363, P. Bonche et al; Phys. Rev. Lett. 66 (1991) 876, J. Skalski et al. Nucl.Phys. A551 (1993) 109 and, J. Meyer et al. Nucl. Phys. A588 (1995) 597

[2] P. Dagnall et al.; Phys. Lett. B335 (1994) 313

[3] T. Nakatsukasa et al.; Phys. Lett. B343 (1995) 19

[4] B. Crowell et al.; Phys. Rev. C51 (1995) 1599

[5] P.J. Nolan, Nuc. Phys. A520 (1990) 657c

[6] M.J. Brinkman et al. Z. Fur Phys. A336 (1990) 115

[7] U.J. van Severen et al. Z. Fur Phys. A353 (1995) 15

[8] K. S. Krane et al. Nucl. Data Tables 11 (1973) 351

[9] T. L Khoo et al., Phys. Rev. Lett. 76 (1996) 1583

[10] A. Lopez-Martens et al, Phys. Lett. B380 (1996) 18

[11] D. Ackermann et al., this proceedings

[12] M. J. Joyce et al., Phys. Rev. Lett. 71 (1993) 2176

[13] P. B. Semmes et al., Phys. Lett. B345 (1995) 185

[14] M. Riley et al., Nucl. Phys. A512 (1990) 178

[15] L. P. Farris et al., ys. Rev. C51 (1995) R2288

[16] J. R. Hughes et al. Phys. Rev. C51 (1995) 447

[17] T. Nakatsukasa et al. Phys. Rev. C53 (1996) 2213

[18] T. Nakatsukasa et al, this proceedings, and private communication

# Microscopic Structure of High-Spin Vibrational States in Superdeformed A=190 Nuclei

Takashi Nakatsukasa
*AECL, Chalk River Laboratories, Chalk River, Ontario K0J 1J0, Canada*

Kenichi Matsuyanagi
*Department of Physics, Kyoto University, Kyoto 606-01, Japan*

Shoujirou Mizutori
*JIHIR, Oak Ridge National Laboratory, P.O.Box 2008, Oak Ridge, TN 37831, U.S.A.*

Yoshifumi R. Shimizu
*Department of Physics, Kyushu University, Fukuoka 812, Japan*

Microscopic RPA calculations based on the cranked shell model are performed to investigate the quadrupole and octupole correlations for excited superdeformed (SD) bands in even-even A=190 nuclei. The $K = 2$ octupole vibrations are predicted to be the lowest excitation modes at zero rotational frequency. The Coriolis coupling at finite frequency produces different effects depending on the neutron and proton number of nucleus. The calculations also indicate that some collective excitations may produce $\mathcal{J}^{(2)}$ moments of inertia almost identical to those of the yrast SD band. An interpretation of the observed excited bands invoking the octupole vibrations is proposed, which suggests those octupole vibrations may be prevalent in even-even SD A=190 nuclei.

## I. INTRODUCTION

Superdeformed (SD) rotational bands provide us with an opportunity of studying a finite quantum many-body system at the limits of a strong Coriolis field and large deformation. As an example of elementary excitations in rapidly rotating nuclei, low-frequency vibrational motion at high spin is of great interest. Since the large deformation and the rapid rotation of SD bands may produce a novel shell structure, we expect features of surface vibrational motions quite different from those of spherical and normal-deformed (ND) nuclei. In this paper quadrupole and octupole vibrations built on the SD yrast band are discussed in terms of a microscopic model based on the cranked mean field extended by the random-phase approximation (RPA).

In a recent paper [1] (to which we refer hereafter as NMMS), we have discussed the quadrupole and octupole correlations in excited SD bands in $^{190,192,194}$Hg. We have found that the $K = 2$ octupole vibrations are the lowest excitation modes in these SD nuclei and the interplay between rotation and vibrations produces different effects depending on neutron number. From a comparison with the experimental $\mathcal{J}^{(2)}$ moments of inertia, we have proposed a new interpretation that most of the observed excited bands are the ($K = 2$) octupole vibrations. In this paper, we extend this work to all even-even SD nuclei observed in A=190 region and compare our theoretical results with new experimental data. Assuming that the observed excited SD bands correspond to the lowest octupole vibrations, the observed properties (Routhians, $\mathcal{J}^{(2)}$ moments of inertia, and linking transitions into the yrast SD bands) will be consistently explained for all even-even A=190 nuclei.

## II. COLLECTIVE EXCITATIONS IN RAPIDLY ROTATING SUPERDEFORMED NUCLEI

Before discussing explicit examples of excited SD bands, let us discuss the characteristics of elementary excitation modes in high-spin SD and ND states in even-even nuclei.

ND nuclei belong to a family of nuclei with "open-shell" configurations. At low spin, since the pairing correlations produce an energy gap $\Delta$ (typically 1 MeV), the excitation energies of the lowest two-quasiparticle (2QP) states are at least $2\Delta \approx 2$ MeV and the collective (isoscalar) excitations become the lowest excitation modes which have been universally observed in experiments. However, this situation is changed at high spin by many rotationally aligned 2QP states coming down rapidly with frequency. These aligned 2QP bands erase the energy gap and become the dominant modes of low-energy excitation. Thus, at present, very few experimental data are available for the collective modes of excitation at high spin.

On the other hand, SD nuclei are characterized as "closed-shell" nuclei with a large shell gap near the Fermi surface. In addition, the large deformation tends to reduce the aligned angular momenta of high-$j$ orbitals. These properties of the SD shape keep an energy gap in the quasiparticle spectra even in the high-spin region. (see quasiparticle Routhians in NMMS and compare them with those of ND nuclei, e.g., in Ref. [2]). As a result, the collective states may be still the lowest modes

even at high spin. In this sense, the SD nuclei could provide an observatory of the collective excitations in rapidly rotating systems.

In the A=150 region, the behavior of excited SD bands have been well accounted for as single-particle excitations except for a few cases in $^{152}$Dy [3,4], $^{148}$Gd [5], and $^{150}$Gd [6]. This may be because the pairing correlations are extremely suppressed in the A=150 region. Since the pairing correlations may increase the quadrupole and octupole collectivity, we expect the different feature of near-yrast excitation spectra in the A=190 region.

In even-even SD A=190 nuclei, most of excited bands have $\mathcal{J}^{(2)}$ moments of inertia very similar to those of the yrast SD bands, which show a gradual increase with frequency. On the other hand, atypical $\mathcal{J}^{(2)}$ moments almost constant with frequency have been observed universally in odd-A SD nuclei and have been explained by invoking occupation of a quasiparticle state associated with neutron $N = 7$ ($j_{15/2}$) orbitals [7–10]. These experiments provide important information on the quasiparticle spectra around the $N = 112$ SD shell gap, which tells us the $N = 7$ orbitals is the lowest at high frequency and the blocking of the $N = 7$ orbitals leads to the lack of alignment producing a constant $\mathcal{J}^{(2)}$. If we try to interpret the excited bands in even-even nuclei as the simple 2QP states, it is a puzzle why the similar atypical $\mathcal{J}^{(2)}$ have not been observed in the even-even cases. We will show in the next section that the collective excitations can provide a possible answer to this mystery.

## III. MICROSCOPIC STRUCTURE OF COLLECTIVE EXCITATIONS

In this section, we give a brief review of our theoretical model and discuss the $\mathcal{J}^{(2)}$ moments of inertia for the excited bands. See NMMS for a complete description of the model and details of numerical calculations.

In the cranked shell model extended by the RPA theory, vibrational excitations built on the rotating vacuum are microscopically described by superpositions of a large number of 2QP states. The RPA also allows us to describe non-collective 2QP excitations and weakly collective states which are difficult to discuss by means of macroscopic models. Effects of the Coriolis force on these various modes of excitation are automatically taken into account in RPA solutions since the mean field is affected by the cranking term $-\omega_{\rm rot} J_x$.

The model Hamiltonian is assumed to be of the form:

$$H' = h'_{\rm s.p.} + H_{\rm int} \ , \tag{3.1}$$

where $h'_{\rm s.p.}$ is a cranked single-particle Nilsson Hamiltonian including the pairing field. The quadrupole deformation and pairing gaps are determined by the standard Strutinsky procedure at $\omega_{\rm rot} = 0$. We have adopted the phenomenological prescription given in Ref. [11] for the pairing gaps at finite frequency (which is characterized by a "critical" frequency $\omega_c$). The residual interactions are separable multipole interactions,

$$H_{\rm int} = H_{\rm pair} - \frac{1}{2}\sum_{\lambda K} \chi_{\lambda K} Q^\dagger_{\lambda K} Q_{\lambda K} \ , \tag{3.2}$$

where $H_{\rm pair}$ is a residual pairing interaction consistent with the mean field and $Q_{\lambda K}$ are multipole operators defined in doubly-stretched coordinates $r''_i = (\omega_i/\omega_0) r_i$ ($i = x, y, z$) [12]. The coupling strengths of the interactions $\chi_{\lambda K}$ are determined in the same way as in NMMS. However, since we do not know exactly the self-consistent interactions in a realistic Nilsson potential, we have done the calculations with two different values of the octupole coupling strengths; the "harmonic-oscillator" value ($f_3 = 1$) [12] and the one increased by 5% ($f_3 = 1.05$). We use this symbol $f_3$ as a scaling factor of the coupling strengths. See eq.(3.13) in NMMS.

After diagonalizing the Hamiltonian (3.1) with the RPA theory, it is written as

$$H' = \text{const.} + \sum_{\alpha, n} \hbar\Omega^\alpha_n X^{\alpha\dagger}_n X^\alpha_n \ , \tag{3.3}$$

for even-even nuclei at finite rotational frequency. Here $\alpha$ (=0,1) indicates the signature quantum number. $X^{\alpha\dagger}_n$ and $\hbar\Omega^\alpha_n$ are the n-th RPA-normal-mode creation operator and its excitation energy, respectively. Since we take the yrast SD band as the RPA vacuum, $\hbar\Omega^\alpha_n$ gives the Routhian (excitation energy in the rotating frame) relative to the yrast SD band.

From the RPA eigenenergies, we calculate the $\mathcal{J}^{(2)}$ moments of inertia for excited SD bands as follows (see NMMS for detail): The relative difference between the excited and yrast bands is given by $j^{(2)} = -d^2\hbar\Omega_n/d\omega^2_{\rm rot}$, and added to the experimental $\mathcal{J}^{(2)}_0$ of the yrast band, $\mathcal{J}^{(2)}_0 + j^{(2)}$. This procedure allows us to take into account the complex correlations which are implicitly included in $\mathcal{J}^{(2)}_0$; e.g., the pairing fluctuation, the higher-order pairing.

In the RPA theory, excited states $|n\rangle$ ($n \neq 0$) are described by superposition of 2QP excitations,

$$|n\rangle = \sum_{\mu\nu} \left\{ \psi_n(\mu\nu) a^\dagger_\mu a^\dagger_\nu + \varphi_n(\mu\nu) a_\nu a_\mu \right\} |0\rangle \ , \tag{3.4}$$

where $|0\rangle$ is the RPA vacuum and $\psi_n(\mu\nu)$ ($\varphi_n(\mu\nu)$) are the RPA forward (backward) amplitudes. The backward amplitudes are generally smaller than the forward amplitudes if the mean field is stable enough. A non-collective state has a single dominant 2QP component, namely $|\psi_n(\sigma\rho)|^2 \approx 1$ and $|\psi_n(\mu\nu)|^2 \approx 0$ for $(\mu\nu) \neq (\sigma\rho)$. On the other hand, a collective state may be characterized by the coherent contributions from many different 2QP components and substantial contributions from backward amplitudes.

As is discussed in sec.II, the lowest $N = 7$ neutron quasiparticles change $\mathcal{J}^{(2)}$ moments of inertia most significantly. Therefore, the observed excited bands in even-even nuclei, which show the $\mathcal{J}^{(2)}$ identical to those of the

yrast $\mathcal{J}_0^{(2)}$, cannot be the lowest 2QP states associated with these orbitals. A possible explanation for this similarity of $\mathcal{J}^{(2)}$ is interpreting them as 2QP excitations invoking high-$K$ orbitals. For instance, bands 2 and 3 in $^{194}$Hg have been originally assigned as two-quasineutron excitations [624 9/2]⊗[512 5/2] [13]. However, this does not explain why we have not observed 2QP excitations associated with the neutron $N = 7$ orbitals which should be lower in energy at high frequency (see discussion in sec.II).

Instead, we presume those excited bands could be the collective states. First of all, the excitation energies of collective states may be lower than any 2QP state. In addition, some collective bands may produce the $j^{(2)} \approx 0$ (which means $\mathcal{J}^{(2)} \approx \mathcal{J}_0^{(2)}$) because of the spreading of the RPA amplitudes over many 2QP's. In a highly collective state, the amplitude $|\psi_n(\mu\nu)|$ of each 2QP component is small and the peculiar effect of the neutron $N = 7$ orbitals can be *smeared* by the other components. This "smearing" has been actually demonstrated for $^{194}$Hg in NMMS, and will be also done for Pb isotopes in sec. V.

## IV. COLLECTIVE EXCITATIONS IN Hg NUCLEI

In this section, results of the RPA calculations are presented for the excited states in SD Hg nuclei. Since we have already published this result in NMMS, here we briefly review the main results of NMMS and discuss new experimental data on $^{194}$Hg. The main conclusions of NMMS are summarized as follows.

1. The $K = 2$ octupole vibrations are the lowest excitation modes ($E_x \approx 1$ MeV, B($E3$; $0^+ \to 3^-$) $\approx 10$ s.p.u.) in these Hg isotopes at $\omega_{\rm rot} = 0$.
2. The $\gamma$ vibrations are higher in energy and less collective ($E_x \geq 1.4$ MeV, B($E2$; $0^+ \to 2^+$) $< 2 \sim 3$ s.p.u.) than the lowest octupole vibrations at $\omega_{\rm rot} = 0$.
3. In $^{190}$Hg, two observed excited SD bands, bands 2 and 4, are assigned to the lowest octupole bands with signature $\alpha = 1$ and 0, respectively. The $\alpha = 1$ octupole vibration is rotationally aligned, while the $\alpha = 0$ is crossed by a two-quasineutron band at high frequency.
4. In $^{192}$Hg, bands 2 and 3 are assigned to the lowest ($K = 2$) octupole bands with signature $\alpha = 1$ and 0, respectively. Both bands are crossed by a two-quasineutron band at high frequency.
5. In $^{194}$Hg, bands 2 and 3 are assigned to the lowest ($K = 2$) octupole bands with signature $\alpha = 0$ and 1, respectively.
6. The strongest mixture of low-$K$ components ($K =$ 0 and 1) at finite frequency is predicted for band 2 of $^{190}$Hg, which explains why strong dipole decay into the yrast SD band has been observed only for this band.

For $^{194}$Hg, recent GAMMASPHERE experiments have revealed the excitation energies and spins of the yrast [14] and excited (band 3) SD bands [15]. The experimental Routhians of band 3 relative to the yrast SD band have been extracted from these experimental data [15]. The experiments indicate that band 3 is very low-lying, $E'_x \approx 0.8$ MeV at $\omega_{\rm rot} = 0$, which seems to support our interpretation of collective vibrations because the lowest 2QP states have been predicted to be at $E'_x \approx 1.5$ MeV in NMMS.

In Fig. 1 we compare the experimental Routhians with the theoretical results presented in NMMS and Ref. [16] (indicated by (1) and (2), respectively) and with Routhians calculated with slightly different parameters (indicated by (3)). The parameter sets used for the calculations are; (1) the same parameters as in NMMS (dynamically reduced pairing and $f_3 = 1$), (2) the same as in Ref. [16] (constant pairing gaps and $f_3 = 1.05$), and (3) the same as (1) except $f_3 = 1.057$ and $\hbar\omega_c = 0.5$ MeV for protons (see eq.(3.4) in NMMS). It turns out that the previous calculation (2) had predicted the experimental Routhians very nicely, while the calculation (1) had overestimated the excitation energy by about 200 ~ 300 keV. The parameters (3) are chosen to reproduce the experiments: it seems to suggest that the reduction of proton pairing is smaller than expected in NMMS and the optimal octupole coupling strengths are slightly larger than the harmonic-oscillator values. This is consistent with the discussion in NMMS in which we have shown the slightly larger coupling strengths ($f_3 = 1.05$) reproduce the experimental $\mathcal{J}^{(2)}$ even better.

Experimental information has also been obtained on the signature splitting of bands 2 and 3 (assuming they are signature partners). This is discussed in a paper by F. Stephens in this proceedings [17]. Again, the agreement becomes better for the result with the slower pairing reduction and the larger octupole coupling.

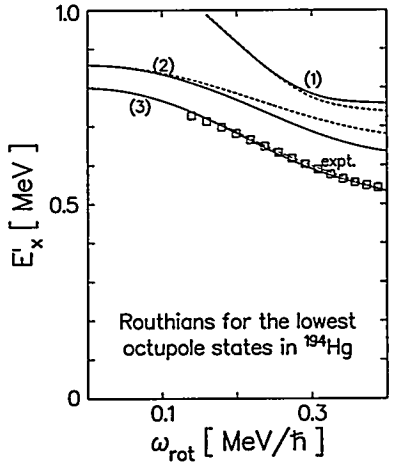


FIG. 1. The RPA eigenenergies for the lowest octupole states in $^{194}$Hg. Solid (dashed) lines correspond to states with signature $\alpha = 1$ (0). Experimental data for band 3 ($\alpha = 1$) are shown by open squares.

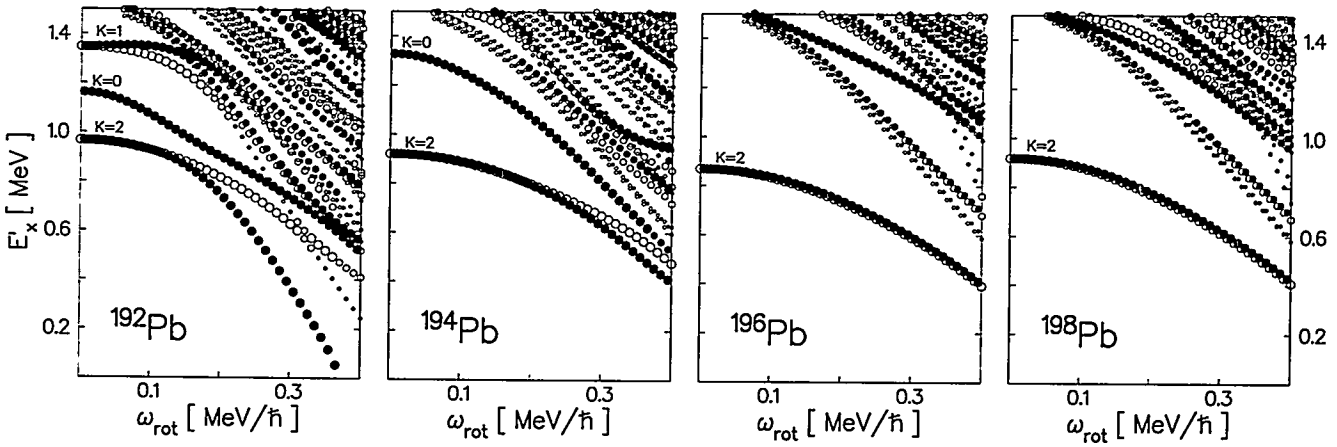


FIG. 2. RPA eigenenergies of negative-parity states for $^{192,194,196,198}$Pb calculated with $f_3 = 1.05$. Open (solid) circles indicate states with $\alpha = 0$ (1). Large, medium, and small circles indicate RPA solutions with $E3$ transition amplitudes larger than 200 $e$fm$^3$, larger than 100 $e$fm$^3$, and less than 100 $e$fm$^3$, respectively. If we take $f_3 = 1$, the excitation energy of the lowest octupole states will be around 1.2 MeV at $\omega_{rot} = 0$.

## V. COLLECTIVE EXCITATIONS IN Pb NUCLEI

In this section, the results are presented for excited states in SD even-even Pb nuclei. In $^{192,194,196,198}$Pb, the predicted properties of $\gamma$ vibrations are similar to those in Hg nuclei (see the previous section and NMMS); the excitation energy ($E_x \approx 1.5 \sim 1.6$ MeV) is higher than the lowest octupole state and their weak collectivity will be dissipated at high spin. Therefore, the observation of the $\gamma$ vibration is expected to be more difficult than the octupole vibrations. Hereafter, let us focus our discussion on the collective octupole excitations.

Figure 2 shows the calculated Routhians with negative parity relative to the yrast SD bands for even-even Pb nuclei. The quadrupole deformation $\epsilon = 0.44$, the pairing parameters $\Delta(0) = 0.8$ (0.7) MeV with $\hbar\omega_c = 0.5$ (0.5) MeV for neutrons (protons), and $f_3 = 1.05$ are used throughout (cf. sec.III-A in NMMS). The lowest states are again the $K = 2$ octupole vibrations for all nuclei.

### A. $^{194}$Pb and $^{196}$Pb

The excited SD bands in even-even Pb nuclei have been observed in $^{194}$Pb (bands 2 and 3) [18] and $^{196}$Pb (bands 2, 3, and 4) [19]. We assume the lowest octupole bands ($\alpha = 0$ and 1) correspond to the observed excited bands (bands 2 and 3) in $^{194}$Pb and $^{196}$Pb. Unfortunately we could not give unique assignment to band 4 in $^{196}$Pb (see below).

The calculated $\mathcal{J}^{(2)}$ moments of inertia are shown in Fig. 3(a) together with the experimental data. The signature of excited bands is determined by following the experimental suggestions [18,19]. As is discussed in sec.III, the $\mathcal{J}^{(2)}$ identical to those of the yrast SD band are reproduced by means of the "smearing" effect. The results calculated with $f_3 = 1.05$ agree with the experiments especially well. There is an experimental suggestion that

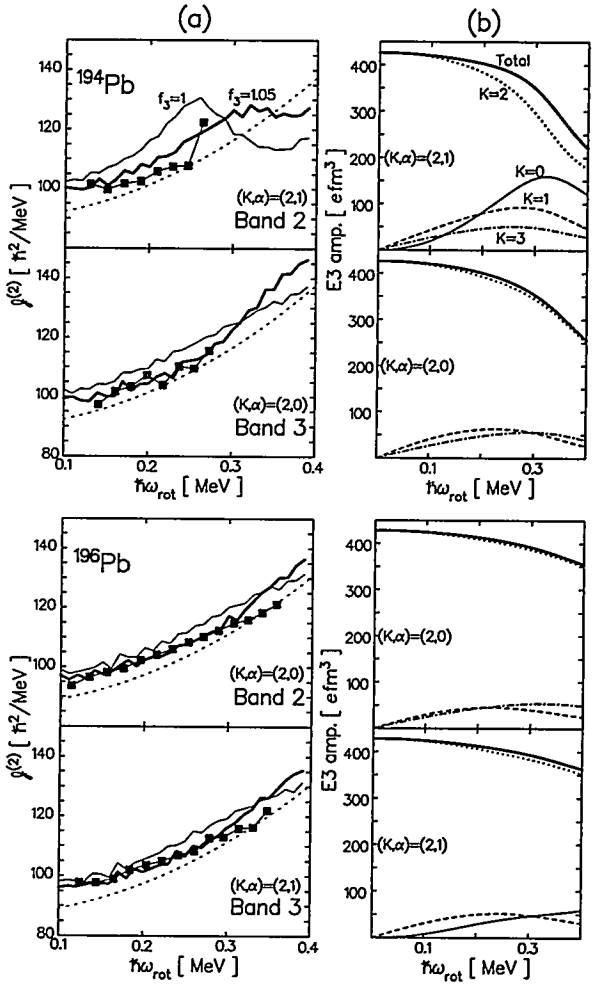


FIG. 3. (a) Calculated (solid lines) and experimental (symbols) $\mathcal{J}^{(2)}$ moments of inertia for excited SD bands in $^{194}$Pb (upper) and $^{196}$Pb (lower). Thin solid lines are the results with $f_3 = 1$ while the thick lines indicate the results with $f_3 = 1.05$. Dotted lines indicate the yrast $\mathcal{J}^{(2)}$. Experimental data are taken from Ref. [18,19].
(b) $E3$ transition amplitudes of the corresponding octupole states calculated with $f_3 = 1.05$.

the band-head energy of bands 2 and 3 in $^{196}$Pb is around 870 keV [19], which again indicates better agreement with the results with $f_3 = 1.05$ (Fig. 2).

In order to clarify how the "smearing" works, we show examples of RPA amplitudes calculated with $f_3 = 1.05$ for the lowest $\alpha = 1$ octupole state in $^{196}$Pb: At $\omega_{\rm rot} = 0$, the largest component is a two-quasineutron $\nu(56)$ (occupying $N = 5$ and $N = 6$ orbitals) with $|\psi|^2 = 0.14$, while it will be a two-quasiproton $\pi(56)$ with $|\psi|^2 = 0.12$ at $\hbar\omega_{\rm rot} = 0.3$ MeV. As you can see, even the largest component occupies less than 10% of the total sum of forward amplitudes $\sum_{\mu\nu} |\psi(\mu\nu)|^2 \approx 1.48$. As is discussed before, the neutron $N = 7$ orbitals give the most significant effect on $\mathcal{J}^{(2)}$ moments of inertia. The largest component associated with neutron $N = 7$ is $|\psi|^2 = 0.04$ (0.02) at $\hbar\omega_{\rm rot} = 0$ (0.3) MeV. Therefore, the blocking of $N = 7$ orbitals turns out to be extremely weak in this collective excitation, which results in the $\mathcal{J}^{(2)}$ almost identical to those of the yrast band.

The experiment [19] has also observed decay transitions from excited SD bands (bands 2, 3, and 4) into the yrast SD band in $^{196}$Pb (the dipole character of decays from band 3 was confirmed). Assuming the $E1$ transitions, the experimental B($E1$) values have been extracted from the branching ratio; B($E1$)$_{\rm exp} \approx 10^{-6}$, $10^{-5}$, and $10^{-4}$ W.u. for bands 2, 3, and 4, respectively. Using the $E1$ recoil charge ($-Ze/A$ for neutrons and $Ne/A$ for protons), the calculations with $f_3 = 1.05$ at $\hbar\omega_{\rm rot} = 0.3$ MeV have suggested B($E1$)$_{\rm cal} \approx 10^{-7}$, $10^{-6}$ W.u. for bands 2 and 3, respectively. If we assume band 4 is an either $K = 0$ or 1 octupole band, the B($E1$)$_{\rm cal}$ would be about $10^{-5}$ W.u. Although the calculation underestimates the absolute magnitude by a factor of 10, the relative difference among bands 2, 3, and 4 is well reproduced. However, the band-head energies of $K = 0$ and 1 octupole states are predicted to be around 1.5 MeV which is much higher than the experimental suggestion ($\approx$ 1 MeV); this weakens our interpretation of band 4 as an octupole state. Note that, since we could not make the reliable prediction about $\beta$ vibrations, we cannot deny a possibility that band 4 is a $\beta$ vibration. Besides, if the transitions from band 4 are $M1$, it could be a 2QP band, because the $\mathcal{J}^{(2)}$ moments of this band show the atypical behavior which might suggest effects of the neutron $N = 7$ orbitals.

Figure 3(b) shows the $E3$ amplitudes ($K = 0$, 1, 2, and 3) of the lowest octupole states as functions of frequency. The $K$-mixing turns out to be weak for both bands 2 and 3 in $^{196}$Pb. Since the $E1$ strength is supposed to be carried by the low-$K$ component ($K = 0$ and 1), it provides the small B($E1$) for bands 2 and 3 ($10^{-7} \sim 10^{-6}$ W.u.). The calculation suggests the relatively strong Coriolis mixing for $(K, \alpha) = (2, 1)$ octupole band in $^{194}$Pb. This leads to B($E1$)$_{\rm cal} \approx 10^{-6} \sim 10^{-5}$ W.u. which is the largest among the octupole states shown in Fig. 3. Further experimental investigation about the linking transitions between excited and yrast SD bands in $^{194}$Pb may clarify the octupole collectivity of this band.

### B. $^{192}$Pb and $^{198}$Pb

Although the excited SD bands in even-even A=190 nuclei have been observed so far only in $^{190,192,194}$Hg and $^{194,196}$Pb, we expect this will be significantly extended in near future by means of the new generation $\gamma$-ray detectors. Among those candidates, $^{192}$Pb and $^{198}$Pb may be relatively easy to access because the yrast SD bands have been already observed. In this section, we make a prediction on the properties of octupole bands in these nuclei.

The octupole states in $^{192}$Pb are similar to those (bands 2 and 4) in $^{190}$Hg; the lowest octupole phonon with signature $\alpha = 1$ is rotationally aligned, and the second lowest with $\alpha = 0$ is crossed by a 2QP band (Fig. 2). In Fig. 4, we show the calculated $\mathcal{J}^{(2)}$ moments of inertia for the lowest octupole bands in each signature sector. The $\alpha = 1$ band shows the large and almost constant $\mathcal{J}^{(2)}$, while the $\alpha = 0$ shows a bump at frequency $\hbar\omega_{\rm rot} \approx 0.3$ MeV (if we take $f_3 = 1$, the position of this bump will be shifted to $\hbar\omega_{\rm rot} \approx 0.23$ MeV). Since the aligned octupole phonon is a result of strong Coriolis mixing, the $\alpha = 1$ band has substantial amounts of $K = 0$ and 1 components at finite frequency, which will lead to the relatively strong $E1$ decays into the yrast SD band (B($E1$)$_{\rm cal} \approx 10^{-6} \sim 10^{-4}$ W.u.).

In $^{198}$Pb, the lowest $K = 2$ octupole states ($\alpha = 0$ and 1) are predicted to have no signature splitting. Their $\mathcal{J}^{(2)}$ moments of inertia are identical to each other and similar to those of the yrast SD band (Fig. 4). In this case, since the Coriolis mixing is very weak, the $E1$ strengths are predicted to be small (B($E1$)$_{\rm cal} \approx 10^{-7} \sim 10^{-6}$ W.u.).

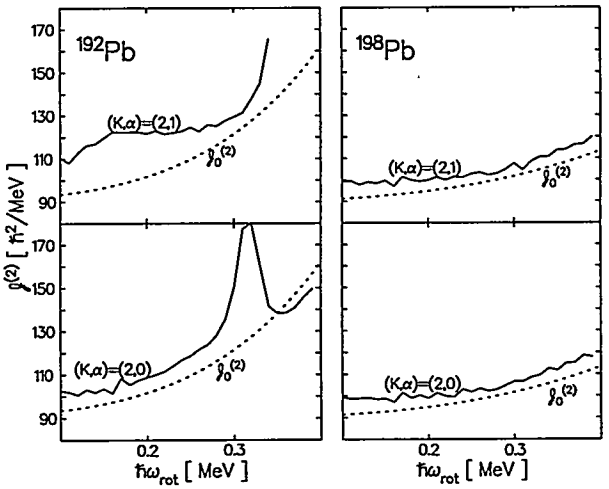


FIG. 4. Calculated $\mathcal{J}^{(2)}$ moments of inertia for the lowest octupole bands with $\alpha = 0$ (lower) and $\alpha = 1$ (upper) in $^{192}$Pb (left) and $^{198}$Pb (right). $f_3 = 1.05$ is used in the calculations. Dotted lines indicate the yrast $\mathcal{J}^{(2)}$. Experimental data are taken from Ref. [20,21].

## VI. CONCLUSIONS: "OCTUPOLE PARADISE"

The microscopic structure of the $\gamma$ and the octupole vibrations built on the SD yrast bands in $^{190,192,194}$Hg and $^{192,194,196,198}$Pb were investigated by means of the RPA based on the cranked shell model. For all these even-even nuclei, the $K = 2$ octupole vibrations are predicted to be the lowest.

New experimental data on SD $^{194}$Hg [15] seem to support our interpretation in NMMS that bands 2 and 3 may be $K = 2$ octupole vibrational states. The results in Ref. [16] calculated with slightly different parameters agreed better with the experimental Routhians for band 3, which may suggest the pairing reduction at finite frequency should be smaller and the optimal octupole coupling strengths be larger than the ones used in NMMS.

For the observed excited bands in SD Pb isotopes, the following configurations have been assigned:

$^{194}$Pb Band 2 : the $(K, \alpha) = (2, 1)$ octupole vibration.
Band 3 : the $(K, \alpha) = (2, 0)$ octupole vibration.
$^{196}$Pb Band 2 : the $(K, \alpha) = (2, 0)$ octupole vibration.
Band 3 : the $(K, \alpha) = (2, 1)$ octupole vibration.
Band 4 : indefinite.

With these assignments, our calculation accounted for the $\mathcal{J}^{(2)}$ moments of inertia and the observed decays of excited bands into the yrast SD band ($^{196}$Pb). It is also suggested that the relatively strong Coriolis mixing in the $(K, \alpha) = (2, 1)$ octupole vibration in $^{194}$Pb may lead to the strong $E1$ decay into the yrast SD band. It would be interesting for the experiment to search for these decay transitions in this nucleus.

We have also done the calculations on excited SD bands in $^{192}$Pb and $^{198}$Pb. The following octupole bands are predicted (possible experimental signatures are indicated in [*italics*]):

$^{192}$Pb (i) the $\alpha = 1$ aligned octupole vibration
[*large* $\mathcal{J}^{(2)}$ *and* $E1$ *linking transitions*].
(ii) the $(K, \alpha) = (2, 0)$ octupole vibration crossed by a 2QP band
[*a bump of* $\mathcal{J}^{(2)}$ *at* $\hbar\omega_{\rm rot} = 0.2 \sim 0.3$ *MeV*].
$^{198}$Pb the signature-paired $K = 2$ octupole vibrations
[$\mathcal{J}^{(2)}$ *similar to those of the yrast*].

As mentioned above, the $K = 2$ octupole vibrations are predicted to be the lowest in the region where the SD bands have been observed so far ($79 \leq Z \leq 83$, $109 \leq N \leq 116$). Since the $E1$ strengths only come from the Coriolis mixing of the $K = 0$ and 1 components, the most direct evidence of octupole correlations, namely the strong decays into the yrast SD band, have been observed in limited cases (band 2 in $^{190}$Hg and band 4 in $^{196}$Pb). However, if future experiments extend this region into $N < 108$ or $N > 116$, the $K = 1$ octupole vibrations are predicted to become the lowest (or close to the lowest). Then, strong $E1$ decay should be observed, and would be good experimental evidence for octupole collectivity. This lowering of $K = 1$ octupole states at open shell configurations is a result of the striking shell structure at superdeformation and has been discussed in Ref. [22–24].

From these calculations and from a comparison with available experiments, we would like to conclude that the octupole vibrations are prevalently observed in even-even SD A=190 nuclei ("*Octupole Paradise*"). The observation of the high-spin collective excitations is very difficult in ND nuclei, because the energy gaps at the Fermi surface quickly disappear due to many aligned 2QP states, so that non-collective modes of excitation become dominant at high spin. The large deformation and large shell gap in SD nuclei may overcome this situation and provide us with a valuable opportunity to observe a variety of collective excitations in rapidly rotating quantum systems.

We would like to acknowledge F. Azaiez, P. Fallon, G. Hackman, M.A. Riley, M.-G. Porquet, F. Stephens for offering us new experimental data and for valuable discussions.

[1] T. Nakatsukasa, K. Matsuyanagi, S. Mizutori and Y.R. Shimizu, Phys. Rev. **C53**, 2213 (1996).
[2] R. Bengtsson, S. Frauendorf and F.-R. May, At. Data and Nucl. Data Tables, **35**, 15 (1986).
[3] P.J. Dagnall et al., Phys. Lett. **B335**, 313 (1995).
[4] T. Nakatsukasa, K. Matsuyanagi, S. Mizutori and W. Nazarewicz, Phys. Lett. **B343**, 19 (1995).
[5] G.de Angelis et al., Phys. Rev. **C53**, 679 (1996).
[6] P. Twin et al., this proceedings.
[7] M.J. Joyce et al., Phys. Lett. **B340**, 150 (1994).
[8] M.P. Carpenter et al., Phys. Rev. **C51**, 2400 (1995).
[9] J.R. Hughes et al., Phys. Rev. **C51**, R447 (1995).
[10] L.P. Farris et al., Phys. Rev. **C51**, R2288 (1995).
[11] R. Wyss, W. Satula, W. Nazarewicz and A. Johnson, Nucl. Phys. **A511**, 324 (1990).
[12] H. Sakamoto and T. Kishimoto, Nucl. Phys. **A501**, 205 (1989).
[13] M.A. Riley et al., Nucl. Phys. **A512**, 178 (1990).
[14] T.L. Khoo et al., Phys. Rev. Lett. **76**, 1583 (1996).
[15] G. Hackman et al., this proceedings.
[16] T. Nakatsukasa, Act. Phys. Pol. **B27**, 59 (1996).
[17] F.S. Stephens et al., this proceedings.
[18] J.R. Hughes et al., Phy. Rev. **C50**, R1265 (1994).
[19] F. Azaiez et al., this proceedings.
[20] E.A. Henry et al., Z. Phys. **A338**, 469 (1991).
[21] R.M. Clark et al., Phys. Rev. **C50**, 1222 (1994).
[22] S. Mizutori, Y.R. Shimizu and K. Matsuyanagi, Prog. Theor. Phys. **86**, 131 (1991).
[23] T. Nakatsukasa, S. Mizutori and K. Matsuyanagi, Prog. Theor. Phys. **87**, 607 (1992).
[24] S. Mizutori, T. Nakatsukasa, K. Arita, Y.R. Shimizu and K. Matsuyanagi, Nucl. Phys. **A557**, 125c (1993).

# Selfconsistent Calculations for Hyperdeformed Nuclei

H. Molique, J. Dobaczewski *, J. Dudek and W.D. Luo

*Centre de Recherches Nucléaires, $IN_2P_3$–CNRS/ Université Louis Pasteur*
*F-67037 Strasbourg Cedex 2, France*

*Abstract: Properties of the hyperdeformed nuclei in the $A \sim 170$ mass range are re-examined using the self-consistent Hartree-Fock method with the SkM* parametrization. A comparison with the previous predictions that were based a non-selfconsistent approach is made. The existence of the "hyper-deformed shell closures" at the proton and neutron numbers Z=70 and N=100 and their very weak dependence on the rotational frequency is suggested; the corresponding single-particle energy gaps are predicted to play a role similar to that of the Z=66 and N=86 gaps in the super-deformed nuclei of the $A \sim 150$ mass range. Selfconsistent calculations suggest also that the $A \sim 170$ hyperdeformed structures have neglegible mass asymmetry in their shapes. Very importantly for the experimental studies, both the fission barriers and the "inner" barriers (that separate the hyperdeformed structures from those with smaller deformations) are predicted to be relatively high, up to the factor of ~2 higher than the corresponding ones in the $^{152}$Dy superdeformed nucleus used as a reference.*

An interest in the possible existence of the *hyperdeformed* nuclei at high spins has constantly accompanied the fast progress in understanding the structure of the *superdeformed* nuclei during the last ten years. An early prediction of an existence of a hyperdeformed minimum in the $^{152}$Dy nucleus [1], has been followed by several Conference reports about a possible experimental evidence of it (see article [2] as one of the references); yet the problem of obtaining an unambigous experimental evidence of an existence of the hyperdeformed nuclear shapes seems to be a very difficult one. This difficulty can be viewed as one of the important motivations for our theoretical study whose preliminary results will be presented below.

We would however like to stress yet another and a much more profound motivation for studying the hyperdeformed structures in nuclei. As it has been predicted in Ref. [3], the abundance of the super- and hyper-deformed nuclei in nature should follow certain rules manifested by "cycles" or "chains" in terms of the proton and neutron numbers (cf. Ref. [4] for more precision and details) and not merely a more or less random pattern. It has been suggested in the same reference that the cyclic pattern is merely a manifestation of an existence of an (approximate) pseudo $SU_3$ symmetry of the nuclear interactions that should also be obeyed by an average nuclear field (cf. Ref. [5] in which some, both mathematical

*Permanent address: Institute of Theoretical Physics, Warsaw University, Hoża 69, PL-00681 Warsaw, Poland

and physical concepts related to the pseudo $SU_3$ mechanism, have been introduced). Consequently, the possible future experimental discovery of the hyperdeformed nuclei should be viewed as directly related to the study of the very basic properties of the nuclear interactions - and in particular of their pseudo $SU_3$ symmetry. (Let us also recall here that the adjective "pseudo" carries by no means any pejorative meaning and has been introduced in order to differentiate from the name "$SU_3$ symmetry" introduced earlier in a different context).

In the following we are going to concentrate on discussing some particular nuclear structure properties of hyperdeformed nuclei that follow from our calculations. Let us begin by recalling the prediction in Ref. [4] where the (non-selfconsistent) Strutinsky type calculations with the deformed Woods-Saxon potential have been performed. In these calculations addressing the nuclei around Z $\sim$ 70 and N $\sim$ 100 (cf. Fig.2 of the above paper) the total nuclear energies have been minimised in terms of the ($\beta_2, \gamma$ and $\beta_4$)-deformations. The overall total energy landscapes seemed particularly interesting from the nuclear hyperdeformation point of view: at the limit of high spins I$\sim$(80-to-90)$\hbar$ several nuclei manifested very deep total energy minima at the nuclear elongations corresponding to those with the axis ratio 3:1. According to those predictions, both the barriers against fission and those separating the hyperdeformed minima from the normal-deformed ones reached as much as 8 MeV or even more. In addition, those hyperdeformed minima were predicted to become the yrast at the above spin range.

Although optimistic, the predictions of the calculations based on the Strutinsky method had at least two drawbacks. First of all, in such an approach the deformation space must be defined prior to the calculations and only then the total energy minimisation over the predefined space can be performed. Since for purely technical reasons deformation spaces of more than three or four dimensions are difficult to treat due to computing-time limitations, by using such a method one can never be sure that the space actually used is totally adequate for the problem in question. This becomes a particularly important problem at the very exotic elongations where the nuclear shapes are *a priori* less well known. For instance in the quoted article [4] no octupole type degrees of freedom have been included and their possible importance remained an open question. Moreover, by using the Strutinsky method one is inevitably confronted with the question of an adequate shape parametrisation of the average field potential, again especially at the very strong elongations where, for example, the "necking" degrees of freedom themselves may require a use of a few shape variables to be correctly accounted for.

To become independent of the above drawbacks we have employed the Hartree-Fock approach using the code *HFODD* of Ref. [6]. Not to introduce here too many technical details related e.g. to the stability tests with respect to the basis cut off etc., let us only mention that the method used allows us to treat *all* the shapes corresponding to the standard expansion of the nuclear surface $\Sigma$ : $R(\theta,\phi) \sim [1 + \sum_{\lambda=0}^{\lambda_{max}} \sum_{\mu=-\lambda}^{\lambda} \alpha_{\lambda\mu} Y_{\lambda\mu}(\theta,\phi)]$, in terms of spherical harmonics, where all the $\alpha_{\lambda\mu}$ are permitted to be non-zero and real. The calculations discussed below account therefore for the following degrees of freedom: 2 quadrupole ones ($Q_{20}$ and $Q_{22}$), 4 octupole ($Q_{30}$, $Q_{31}$, $Q_{32}$ and $Q_{33}$), 5 hexadecapole ($Q_{40}$, $Q_{41}$, ... $Q_{44}$) etc. We have calculated all the multipole moments up to $\lambda_{max}$=9 within the selfconsistent solutions. This is equivalent to controlling the deformation space of the dimension equal to 51 in terms of the multipole moments, a space clearly unreachable in terms of the Strutinsky

approach.

Since according to a comparison of the predicted properties for several nuclei from the A $\sim$ 170 mass region the $^{170}$Yb nucleus seems to be a good case for the hyperdeformation studies, we are going to illustrate the predicted shape properties using this particular case as an example. Table 1 illustrates an ensemble of the 51 multipole moments corresponding to the selfconstitent solution at spin I=92$\hbar$. As it is directly seen, at its hyperdeformed minimum the nucleus in question has essentially four deformations contributing; all the so-called mass-asymetric degrees of freedom ($\lambda$ = *odd*) are orders of magnitude smaller than the neighboring even ones. One may conclude that the mass-asymetric moments are of no importance in the hyperdeformed nuclei from the discussed mass range.

Table 1: *Multipole moments $Q_{\lambda\mu}$ in units of (10 Fm)$^\lambda$ for the $^{170}$Yb nucleus at spin I=92$\hbar$ at the selfconsistent solution corresponding to the hyperdeformed minimum. The only significantly large values have been written in boldface. Note that out of 51 deformation degrees of freedom represented here only four can be considered non-neglegible.*

| $\lambda$ | $\mu=0$ | $\mu=1$ | $\mu=2$ | $\mu=3$ | $\mu=4$ | $\mu=5$ | $\mu=6$ | $\mu=7$ | $\mu=8$ | $\mu=9$ |
|---|---|---|---|---|---|---|---|---|---|---|
| 2 | **88.62** | | 0.065 | | | | | | | |
| 3 | 1.2(-4) | 0.066 | 1.2(-5) | 3.9(-4) | | | | | | |
| 4 | **14.01** | 0.005 | 0.081 | 2.8(-5) | -9(-4) | | | | | |
| 5 | 1.7(-4) | 0.061 | 2.5(-5) | -3.3(-4) | -2(-7) | -4(-9) | | | | |
| 6 | **6.414** | 0.002 | 0.064 | 2.1(-5) | 4(-3) | 1(-6) | -3(-5) | | | |
| 7 | 1.7(-4) | 0.035 | 2.5(-5) | -5.9(-4) | -6(-7) | 2(-5) | 1(-8) | 5(-7) | | |
| 8 | **2.498** | 0.000 | 0.018 | -1.3(-5) | 1(-2) | 6(-6) | 5(-5) | 4(-8) | -2(-7) | |
| 9 | 1.5(-4) | 0.012 | 1.6(-5) | -9.2(-4) | -9(-7) | 1(-4) | 8(-8) | 2(-6) | 2(-9) | 5(-9) |

It is important to reveal the single particle (shell) structure underlying the stability of the hyperdeformed nuclei in question. The corresponding illustration is given in the following Figs. 1 and 2 where the single-particle levels (routhians) for neutrons and protons, respectively, are plotted in function of the rotational frequency. We would like to emphasize the fact that varying the proton or neutron numbers will generally modify also the single-particle spectra much more significantly as it would have been the case when using the Nilsson or the Woods-Saxon average fields. However, the explicit calculations for the nuclei in the vicinity of the $^{170}$Yb indicate that the gaps Z=70 and N=100 visible from the two Figures remain relatively stable, i.e. persist in the self-consistent spectra of neighboring nuclei. Refering in particular to the proton spectra, let us observe an existence of four close-lying levels just above the Z=70 gap. The presence of such close lying states suggests that in the case of Z=71 nuclei each of the HD bands would be ($\sim$ 4 times) weaker populated thus rendering a possible observation of the hyperfdeformation in the neighboring Lutetium nuclei more difficult than those in the Ytterbium.

There are several other features in those single-particle spectra which deserve noticing, first of all the relatively weak slopes of the corresponding curves. Since the aligned angular momenta are directly proportional to the slopes (first derivatives -de$^\omega_\nu/d\omega$), from the above

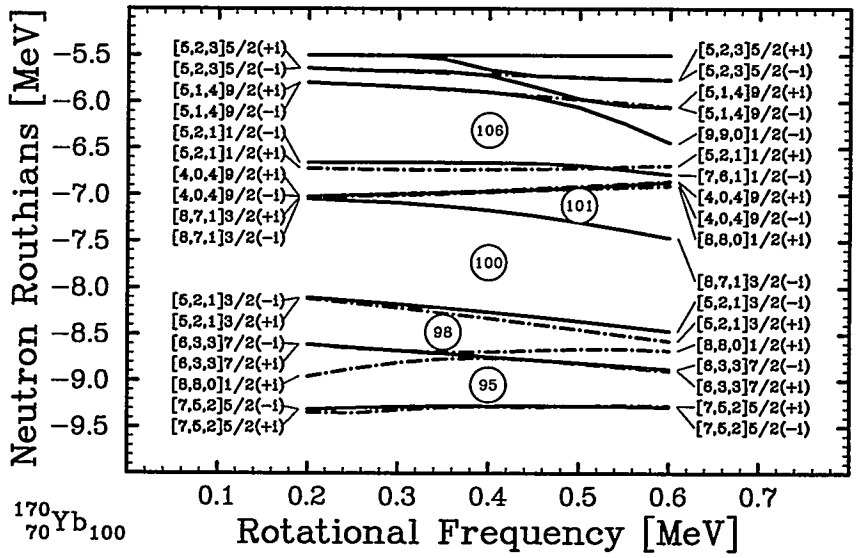


Figure 1: *Hartree-Fock single-particle neutron routhians illustrating a shell-structure around the N=100 gap in the hyperdeformed $^{170}Yb$. Nilsson labels are given at the extremes of the $\omega$-axis. The eigenvalues of the simplex operator $\hat{S}_y=\hat{R}_y(\pi)\cdot\hat{\pi}$ where $\hat{\pi}$ denotes the parity operator and $\hat{R}_y(\pi)$ the rotation through an angle of $\pi$ about the $\mathcal{O}_y$-axis are given in parentheses.*

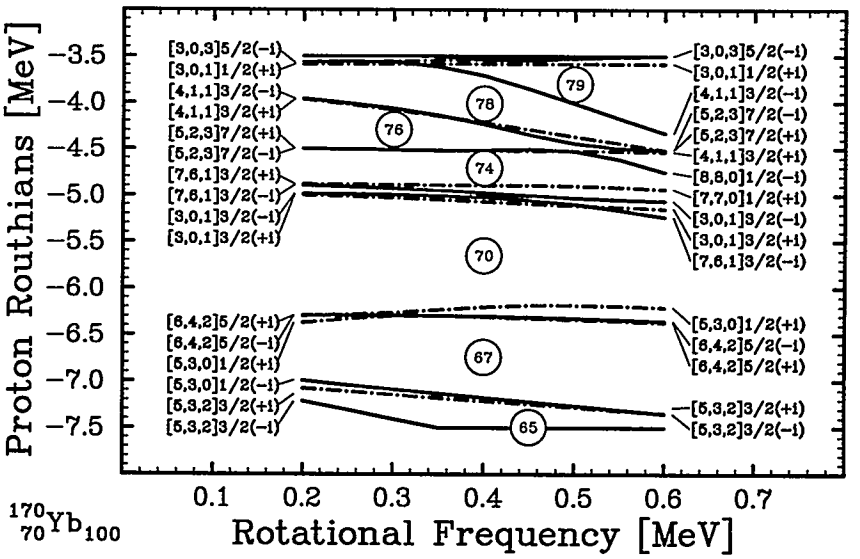


Figure 2: *Similar to that in Fig. 1 but for the protons illustrating the shell structure around the gap at Z=70.*

observation it follows that the angular momentum contributions from otherwise highly alignable orbitals such as e.g. [770]1/2, [761]1/2 or [880]1/2 etc. are very small. Indeed, the exact calculations of the corresponding individual alignments show that they are very seldomly greater than 1 $\hbar$.

Let us return to the problem of the stability of the predicted hyperdeformed Ytterbium nuclei against fission or against decay into minima with the smaller deformations. It is very

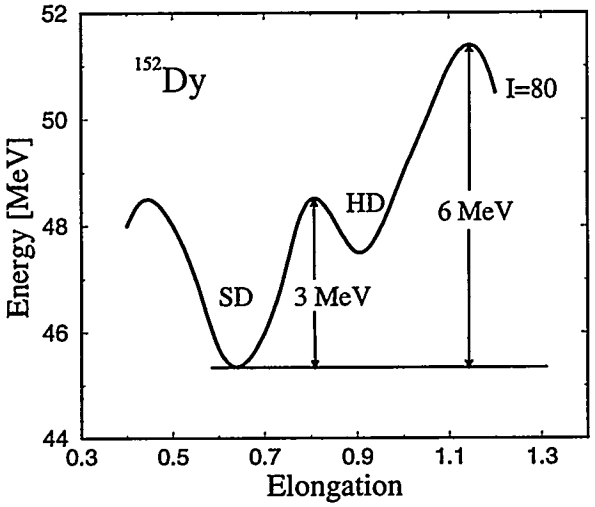


Figure 3: *The total Strutinsky-energy cut for* $^{152}Dy$*; parameter* $\alpha_{20}$ *represents elongation.*

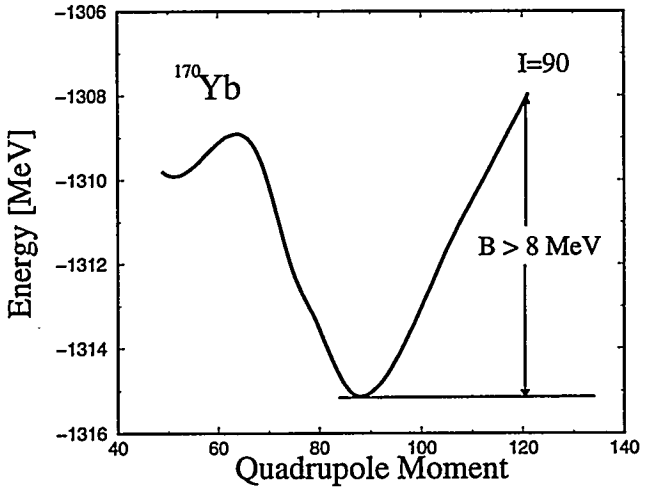


Figure 4: *Preliminary results of the HF calculations for the hyperdeformed* $^{170}Yb$.

difficult to give here an absolute estimate; instead we would like to give a comparison between the corresponding illustrations for the rather well known $^{152}$Dy nucleus and the $^{170}$Yb predicted to be of a special interest in the hyperdeformation context. The Figs. 3 and 4 above provide such a comparison. The height of the fission barrier in the hyperdeformed $^{170}$Yb is larger than that corresponding to the *superdeformed* one in $^{152}$Dy, although the spin is 10 $\hbar$ higher. Similarly, the inner barrier in the $^{170}$Yb is markedly higher than that in $^{152}$Dy.

Consequently we may conclude, that the theoretical predictions for the stability of the hyperdeformed minima at high spins are quite optimistic: the hyperdeformed nuclei in the mass A $\sim$ 170 range should be more stable than the superdeformed nuclei in the A $\sim$ 150 mass range. However, our preliminary calculations indicate that the *rotational bands* in the hyperdeformed nuclei in question may be much shorter, composed of up to 10 transitions rather than about 20 (a number typical for the mass A $\sim$ 150 range).

The problem of the mass-asymmetric degrees of freedom is by no means generally trivial and the corresponding couplings may become important in other mass regions as it illustrate Tables 2 and 3.

Table 2: *Octupole moments $Q_{3\mu}$ in units of (10 Fm)$^3$ for the $^{152}$Dy nucleus at spin I=80$\hbar$ for the selfconsistent solutions in function of the quadrupole deformation. Table illustrates the behavior of the octupole moments corresponding to the vicinity of the superdeformation (the mass quadrupole moment* $\sim$ 40 units).

| $Q_{20}$ | $Q_{30}$ | $Q_{31}$ | $Q_{32}$ | $Q_{33}$ |
|---|---|---|---|---|
| 35.7 | 0.087 | 0.025 | 0.000 | -3(-3) |
| 40.2 | 0.385 | 0.019 | 0.009 | 9(-4) |
| 52.5 | 0.380 | 0.002 | -0.021 | -7(-5) |
| 73.0 | 1.096 | 0.003 | -0.058 | 8(-6) |
| 83.3 | 4.593 | 0.193 | 0.173 | -8(-4) |
| 91.9 | 3.475 | 0.012 | -0.393 | -5(-5) |

Table 3: *Octupole moments $Q_{3\mu}$ in units of (10 Fm)$^3$ for the $^{168}$Yb nucleus at spin I=80$\hbar$ for the selfconsistent solutions in function of the quadrupole deformation varying around the hyperdeformed minimum. When comparing these results with those for $^{152}$Dy in Table 2, a very different type of behavior in terms of the octupole moments should be observed.*

| $Q_{20}$ | $Q_{30}$ | $Q_{31}$ | $Q_{32}$ | $Q_{33}$ |
|---|---|---|---|---|
| 67.7 | 0.637 | 1.520 | -0.034 | -0.018 |
| 75.7 | 0.189 | 1.262 | 0.014 | 0.002 |
| 86.1 | 0.030 | 0.574 | 0.087 | 0.002 |
| 91.7 | 0.016 | 0.370 | 0.035 | 0.001 |
| 102.4 | -0.007 | -0.081 | -6(-5) | -1(-4) |
| 109.0 | 0.007 | -0.093 | -5(-5) | -2(-4) |
| 122.2 | -0.021 | -0.069 | -2(-5) | -3(-4) |

Our study can be summarized and concluded in the following way:

- The hyperdeformed strong shell closures at Z=70 and N=100, predicted in Ref. [4] using Woods-Saxon technique are confirmed using selfconsistent Hartree-Fock method with the Skyrme interactions (SkM*);
- In hyperdeformed nuclei in the vicinity of $^{170}$Yb the fission barriers are predicted to be "enormous" - up to 8 MeV at spins from (80-to-100)$\hbar$; these are significantly larger than those in the $^{152}$Dy SD nucleus at spins (60-to-80)$\hbar$;
- It should be noted, however, that although the hyperdeformed nuclei discussed should be relatively very stable, the corresponding rotational bands may be significantly "shorter" as compared to the superdeformed bands known in the mass A $\sim$ 150 range;
- An analysis corresponding to the space of 51 deformation degrees of freedom ($Q_{\lambda,\mu}$ multipoles with $\lambda$ = 2 to 9 and all $\mu$) performed, indicates that the mass-asymmetric degrees of freedom are neglegibly small at the hyperdeformed minima of nuclei in the vicinity of the $^{170}$Yb nucleus;
- The nonaxial deformations are also predicted to be neglegibly small and consequently the hyperdeformed nuclei in the vicinity of the $^{170}$Yb are expected to be probably "the most axial" known in the nuclear world;
- The individual angular momentum contributions from most of the high-j orbitals are minute (usually smaller than 1 $\hbar$, except for two orbitals). This implies, when employing a classical language, the most coherent collective rotation known so far in the nuclear world;
- Out of an analysis of the structure of individual-nucleonic levels near the Fermi level in the nuclei studied one may predict an existence of numerous iso-spectral bands.

*Acknowledgments:* We would like to express our thanks to the *Institut du Développement et de Ressources en Informatique Scientifique* (IDRIS) of the CNRS, France, which provided us with the computing facilities under Project no. 940333. This research was supported in part by the Polish Committee for Scientific Research under Contract No. 2 P03B 034 08.

# References

[1] J. Dudek, presentation at the Gordon Conference on Nuclear Chemistry (1988)

[2] A.Galindo-Uribarri et al., Phys. Rev. Lett. **71**, 231 (1993)

[3] J. Dudek et al., Phys. Rev. Lett. **59**, 1405 (1987)

[4] J. Dudek, T. Werner and L. Riedinger, Phys. Lett. **B 211**, 252 (1988)

[5] A. Arima, M. Harvey, and K. Shimizu, Phys. Lett. **B 30**, 517 (1969)

[6] J. Dobaczewski and J. Dudek, to be submitted to the Comp. Phys. Comm.

# How close are hyperdeformed states to the scission point?

L.M. Robledo[†], R.R. Chasman[††] and J.L. Egido [†]
[†] Departamento de Física Teórica C-XI
Universidad Autónoma de Madrid, 28049 Madrid, Spain
[††] Physics Division, Argonne National Laboratory
Argonne, IL 60439, USA

**Abstract**

The HFB method with the Gogny force is used to study the effects of reflection asymmetry at $I = 0\hbar$ on the barriers separating superdeformed and hyperdeformed minima from fission in the $^{176}$ W and $^{168}$ Yb nuclei. The fission barrier for the HD minimum is reduced by 5 MeV in $^{176}$ W when reflection asymmetry is taken into account.

Since the discovery in 1986 of the first superdeformed band in $^{152}$ Dy [1], more than a hundred and fifty superdeformed bands have been observed [2]. The reason for the existence of superdeformed bands are the strong shell effects showing up for prolate shapes with axis ratios near 2:1. One can understand this very easily by looking at the behavior of the energy levels of a deformed harmonic oscillator as a function of deformation (see for instance [3]): they bunch together when the ratio of the harmonic oscillator frecuencies, $\omega_\perp$:$\omega_z$ is a rational number giving rise to new energy gaps that favor deformation. For instance, the ratio 2:1 favors superdeformed (SD) prolate shapes. A 3:1 ratio also yields a bunching of levels that favors very extended shapes, the so-called hyperdeformed (HD) shapes. Therefore, one would expect that if many SD bands have been observed there would be also experimental evidence for HD bands but unfortunately such is not the case up to now. One may argue that the preceding argument is based on a pure harmonic oscillator and the spin-orbit coupling might wash out the shell effects giving rise to hyperdeformation. However, there are calculations with the Woods-Saxon potential [4] indicating that the strong shell effects giving rise to the HD states still remain. Realistic Woods-Saxon plus Strutinsky calculations predict HD minima in several rare earth nuclei that usually become yrast at $I \sim 70 - 90\hbar$. The question now is whether such minima could be populated in heavy-ion induced reactions, since the fission barriers are estimated [5] to vanish at spins around $75 - 85\hbar$ for rare earth nuclei. In the work of ref. [4] HD minima are obtained for several Yb, Er and Hf isotopes. Among them, the best candidates are $^{168}$ Yb, $^{166}$ Er and $^{170}$ Hf. In these nuclei the HD minimum ($\beta_2 \sim 0.9$) becomes yrast at spin $80\hbar$, a value which is compatible with the presence of a fission barrier thus favoring the population of such states. More recently, using a different

parameterization of the shape of the nucleus that includes a necking degree of freedom, extensive studies have been carried out in the $A \sim 180$ region with the Strutinsky method [6] looking for very extended shapes beyond SD. In this calculation several HD minima with axis ratios $(\langle z^2 \rangle / \langle x^2 \rangle)^{1/2}$ of the order of 2.2 and higher are found at high spins. For some isotopes they become yrast already at $I = 62\hbar$ as is the case for $^{182}$ Os. The reliability of the shape parametrization used in [6] has been assessed by more fundamental Cranked HFB calculations with the Gogny force for the test case of $^{182}$ Os [7]. In these studies the octupole degree of freedom, i.e. reflection asymmetric shapes, were not taken into account. However, there are studies in the $A \sim 180$[8] at I=0, indicating that octupole deformation plays an important role in stabilizing hyperdeformed minima found in this region. When we extended our high spin studies [6] to include the octupole degree of freedom, we found [9] a substantial lowering of the energy of the nuclear surface in the vicinity of the fission barrier. The most significant one is that of $^{176}$W at $I = 70\hbar$ where a lowering of $\sim 7$ MeV is found for shapes with axis ratios of 3.7:1. The significance of this results becomes clear if one takes into account that in the absence of reflection asymmetry $^{176}$ W had a HD minimum (axis ratio 2.2:1) which became yrast at $I = 70\hbar$ and had an outer barrier (i.e. the barrier to fission) 6.3 MeV high, making it a possible candidate for an experimental search [6]. The lowering in energy due to the octupole degree of freedom means that the outer barrier may be substantially lowered in all these nuclei making it less likely that HD states will be observed. Our [9] study did not indicate that this was a serious problem in $^{182}$ Os.

The most important shortcoming of the Strutinsky method is that the shape of the nucleus has to be characterized in terms of a few parameters. This is not a serious drawback for moderately deformed nuclei, but in the region of very extended shapes in the vicinity of fission, it can be a problem. Therefore, it is particularly desirable here to compare the Strutinsky calculations with HFB studies, in which such shape parameterization restrictions are not present. With this in mind we decided to carry out HFB calculations for $^{176}$ W using the Gogny force. Our objectives are to determine if this large lowering in energy is an artifact of the Strutinsky method and also to consider the impact of the onset of fission on the possibility of populating very extended shapes. It is important to consider fission, as the shapes in which this effect is manifest have surface areas that are close to those of two separated spherical fragments.

Because we wish to study shapes that are extremely elongated, shapes extended to the point that fission occurs, we must use a very large oscillator basis in our HFB calculation (with shells in the $z$-direction of the order of 30). In principle, one would like to study hyperdeformation at high spins allowing for the possibility of asymmetric shapes. The large basis space needed in this case as well as the number of operators involved in the relevant constraints make such calculations extremely time-consuming, even with present day computers [10]. Therefore we restrict ourselves to *axially symmetric*, i.e. $I = 0\hbar$, calculations. In order to perform calculations in a large basis space a new code has been written. The need for the new code arose from instabilities in the standard calculation of the matrix elements of the force for large values of the harmonic oscillator quantum numbers of the basis - see [13] for details. This code fully implements the HFB method with the Gogny force for axially symmetric systems; including shapes that are reflection asymmetric. The flexibility of the gradient method used in the solution of the HFB equations allows us to handle many constraints such as any multipole operator $\hat{Q}_{\lambda 0}$ or the asymmetric necking [11] operator

$\hat{Q}_{\rm nk} = \exp(-(\hat{z} - z_0)^2/a_0^2)$ . In the calculations the DS1 parameter set of the Gogny force has been used. This set of parameters was fitted to yield a lower surface coefficient $a_s$ in seminfinite nuclear matter; giving theoretical fission barriers for $^{240}$ Pu and other actinides in very good agreement with the experimental data [12]. Therefore we believe that this set is well suited for the study of very extended shapes.

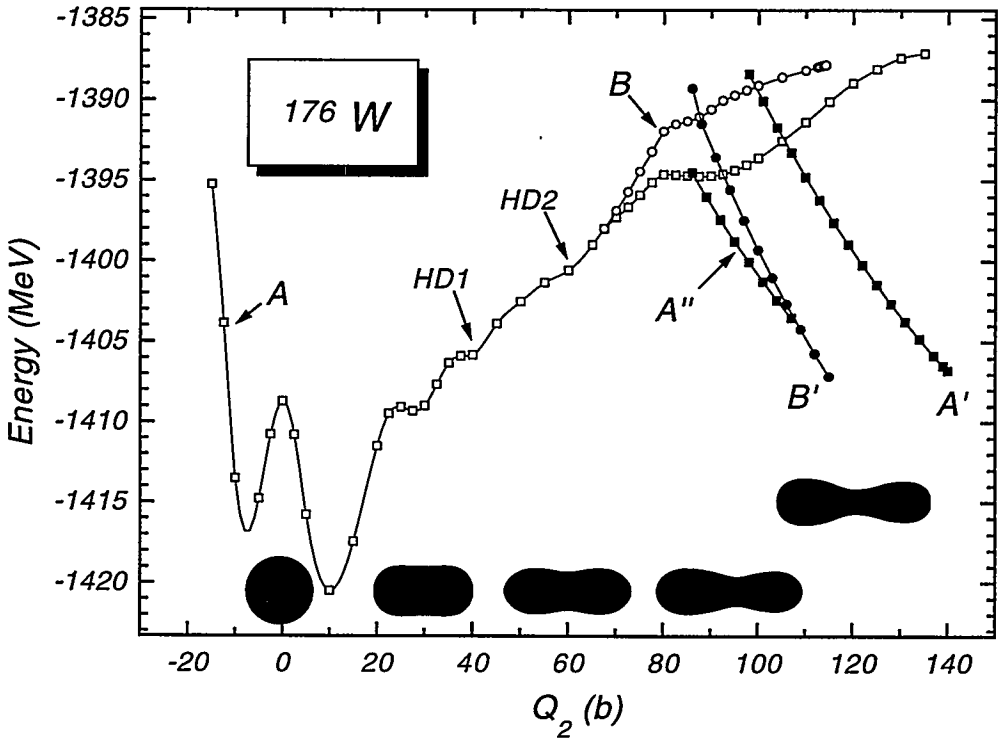


Figure 1: The HFB energy in MeV versus the mass quadrupole moment $Q_2$ given in barns. The open squares curve (A) stands for the unconstrained calculation. The open circles curve (B) correspond to the reflection symmetric ($Q_3 = 0$) calculation. The two-fragment solutions are represented by full squares (A' and A") and full circles (B') corresponding to reflection asymmetric and reflection symmetric solutions respectively. In the bottom part of the figure the shape of the nucleus for the unconstrained calculation (defined as the isosurface at $\rho_0 = 0.08\text{fm}^{-3}$) is depicted for several values of $Q_2$ (from left to right $Q_2 = 0b$, $30b$, $60b$, $95b$ and $120b$).

We have performed HFB calculations in the $^{176}$ W and $^{168}$ Yb nuclei using the mass quadrupole moment $Q_2 = z^2 - \frac{1}{2}(x^2 + y^2)$ as the main constraint. In Fig. 1 we present the major results for the nuclide $^{176}$ W. Five different curves are displayed that correspond to different physical situations: The open squares curve labeled A is obtained by constraining the quadrupole moment of the nucleus. The open circles curve (labeled B) is obtained making the additional constraint of having reflection symmetric (i.e. $Q_3 = 0$) shapes. The curves labeled A' and A" (full squares) correspond to reflection asymmetric *two-fragment*

solutions while the one labeled B' is for the reflection symmetric one. Curve A present three minima at $Q_2 \sim -7.5b$, $Q_2 \sim 10b$ and $Q_2 \sim 28b$ corresponding to an oblate solution, the ground state ($\beta_2 = 0.31$ [1] ) and a superdeformed state ($\beta_2 = 0.73$), respectively. The three minima are reflection symmetric. In addition to these minima there are also two shoulders in the energy curve for $Q_2$ values of $40b$ and $60b$. The one at $Q_2 = 40b$ (labeled as HD1 in Fig. 1) has an axis ratio of 2.2 that roughly correspond to the one of the HD solution becoming yrast at $I = 70\hbar$ in the Strutinsky calculation of ref. [6]. The shoulder at $Q_2 = 60b$ (labeled as HD2) has an axis ratio of 2.8 that could be associated to the second HD minimum seeing in the calculation of ref. [6], the one that becomes yrast at $I = 76\hbar$. For $Q_2$ values higher than $70b$ the energy levels off and is lower than the one of curve B indicating that for this range of $Q_2$ the system becomes reflection asymmetric (with $\beta_3$ values in the range of 0 to 0.3). Comparing curves A and B we observe that the maximum energy gain due to reflection asymmetry is 4.66 MeV and correspond to $Q_2 = 95b$. This result is in good agreement with the lowering of 6.2 MeV obtained for this nucleus at $I = 0\hbar$ [9]. To better compare our results with the ones of [9] one first has to define the concepts of elongation $\eta_2$ and necking in $\eta_{nk}$ shape parameters for the HFB results where the density is not a sharp one. To this end, we define the HFB shape as the isosurface corresponding to roughly half density, i.e. $\rho = 0.08\mathrm{f}m^{-3}$. The region with $Q_2$ larger than $70b$ (where reflection asymmetry is important) has $\eta_2$ values in the range 1.0 to 1.3 and $\eta_{nk}$ ones in the range -0.14 to -0.3 in good agreement with the Strutinsky results [9]. The agreement of our results with those obtained with the Strutinsky method [9] for $^{176}$ W indicate that the strong octupole effects seen in the $A \sim 176$ region for very extended shapes are genuine effects and not artifacts of the Strutinsky method. The implication is then that the outer barriers observed in that region are going to be strongly suppressed, making it less likely that very extended shapes in those nuclides can be populated.

The end points of curves A and B correspond to configurations which are no longer stable against fission: increasing the quadrupole moment slightly results in solutions with two fragments lying on curves A' and B' respectively. The curve B' corresponds to symmetric fission (two $^{88}$ Rb nuclei) while the curve A' is for a mass asymmetric split ($^{66}$ Ni and $^{110}$ Pd). These two end points are saddle points of the corresponding fission paths. The energy differences between the HD minimum HD1 and these saddle points are 19 MeV and 21 MeV, respectively.

The octupole moments of the constrained solutions of curve A' are very similar to the ones of curve A for the same values of the quadrupole moment but these solutions differ in their hexadecapole moments. The ones of curve A' are typically about $20b^2$ lower than the ones of curve A. Therefore it is possible to reach the two-fragment curve A' from the one-fragment one (A) by constraining the hexadecapole moment. The corresponding energy curve shows a maximum that corresponds to another saddle point before fission. This saddle point is 20 MeV above the HD1 minimum. On the other hand, curve A" correspond to a very asymmetric mass split of $^{50}$ Ti and $^{126}$ Te. The octupole deformation of the two fragments as a whole is rather high with $\beta_3$ values of the order of 0.7. Therefore, we can reach curve A" from curve A by constraining the octupole moment. The energy difference between the maximum of this octupole constrained curve (that corresponds to the scission point) and

[1]The definition is $\beta_2 = \sqrt{20\pi}Q_2/(5\langle r^2\rangle)$

the HD1 minimum (i.e. the fission barrier of HD1 along the very mass asymmetric fission chanel) is only 15 MeV, that is, around 5 MeV lower than the other fission barriers mentioned before. The effect of reflection asymmetry is, therefore, to reduce the fission barrier as was previously suggested. A more detailed analysis of these solutions and their properties can be found in [13].

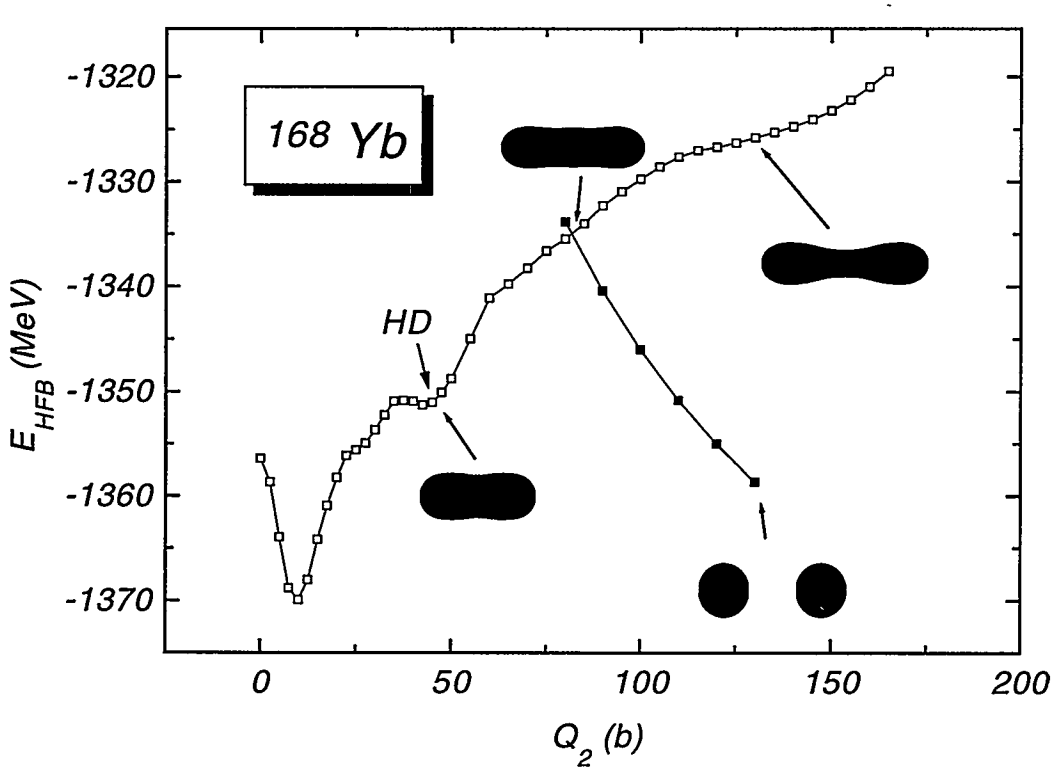


Figure 2: The HFB energy in MeV versus the mass quadrupole moment $Q_2$ given in barns for $^{168}$ Yb. The open squares curve correspond to the one-fragment solutions while the filled squares curve is for the reflection symmetric two-fragment solution. The shape of the nucleus as defined in Fig. 1 is also depicted for some values of the quadrupole moment.

In Fig.2 we have plotted the energy as a function of the mass quadrupole moment for $^{168}$ Yb. The most important result of this calculation is that in the whole range of $Q_2$ considered the nucleus remains reflection symmetric. In addition to the prolate ground state minimum located at $Q_2 = 10b$ there is another, very shallow, minimum at $Q_2 = 45b$ with $\beta_2 = 1.01$, $\beta_4 = 0.61$ and an axis ratio of 2.5. The shape parameters of this minimum agree quite nicely with the ones of the HD minimum found by Dudek et al. [4] at high spins. In the same plot we also represent the reflection symmetric two-fragment solution (full squares). This solution has $Q_4$ values much lowers than the one fragment solution in contrast to $^{176}$ W. For instance, in the crossing point at $Q_2 = 80b$ the values for $Q_4$ are $62b^2$ and $34b^2$ for the one-fragment and two-fragment solutions, respectively. This means that we can force symmetric fission by constraining in $Q_4$. The maximum of this energy curve

corresponds to the scission point and is located $\sim 25MeV$ higher in energy than the HD minimum found in our calculation. This barrier energy is 10 MeV larger than in the $^{176}$ W case. If the HD minima were to become yrast at the same spins, we would estimate that it is more likely to populate the HD minimum of $^{168}$ Yb than that of $^{176}$ W .

The work of (JLE) and (LMR) has been supported in part by DGICyT, Spain under project PB94–0164. Some of the calculations reported here were carried out on the SP computer of the MCS division of Argonne National Laboratory and on the NERSC computers at the Lawrence laboratories. The work of (RRC) is supported by the U.S. Dept. of Energy, Div. of Nuclear and High Energy Physics under contract W31-109-ENG-38. We thank NATO for the collaborative research grant 921182, which has facilitated our research.

# References

[1] P.J. Twin et al. Phys. Rev. Lett. **57**, 811 (1986).

[2] See, for instance, the WWW address `http://isotopes.lbl.gov/isotopes/hspin.html`

[3] A. Bohr and B.R. Mottelson, *Nuclear Structure* Vol. 2, pg 592. W. A. Benjamin, (1975). 1975

[4] J. Dudek, T. Werner and L.L. Riedinger, Phys. Lett. **B211**, 252 (1988).

[5] A.J.Sierk, Phys. Rev. **C33**, 2039 (1986).

[6] R.R. Chasman, Phys. Lett. **B302**, 134 (1993).

[7] J.L. Egido, L.M. Robledo, and R.R. Chasman, Phys. Lett. **B322**, 22 (1994).

[8] W. Nazarewicz, Phys. Lett. **B305**, 195 (1993).

[9] R.R. Chasman, and L.M. Robledo, Phys. Lett. **B351**, 18 (1995).

[10] In a HF or HFB calculation the number of two-body matrix elements to be computed grows as the fourth power of the number of basis states. It means that in a high spin calculation with spatial asymmetry one is confronted with the calculation and/or handling of $\sim 10^{10}$ matrix elements. The computer memory requirements are of the order of 100 Gb. An alternative way to tackle this problem is to compute in each iteration the two body matrix elements. Taking into account that in the calculation of each matrix element one has to do of the order of 100 floating point operations (flops) it means that in *each iteration* one has to do $\sim 10^{12}$ (around 3 hours in a computer with a sustained throughput of 100 Mflops )

[11] J.F. Berger, J.D. Anderson, P. Bonche and M.S. Weiss, Phys. Rev. **C41**, R2483 (1990).

[12] J.F. Berger, M. Girod and D. Gogny Nucl. Phys. **A428**, 23c (1984).

[13] J.L. Egido, L.M. Robledo and R.R. Chasman, to be published.

# Test of $\Delta I = 2$ Staggering in the superdeformed bands of $^{194}$Hg

R. Krücken[1], G. Hackman[2], M.A. Deleplanque[1], R.V.F. Janssens[2], I.Y. Lee[1], D. Ackermann[2], I. Ahmad[2], H. Amro[2], S. Asztalos[1], D.J. Blumenthal[2], M.P. Carpenter[2], R.M. Clark[1], R.M. Diamond[1], P. Fallon[1], S.M. Fischer[2], B. Herskind[3], T.L. Khoo[2], T. Lauritsen[2], A.O. Macchiavelli[1], R.W. MacLeod[1], D. Nisius[2], G.J. Schmid[1], F.S. Stephens[1], and K. Vetter[1]

[1] *Nuclear Science Division, Lawrence Berkeley National Laboratory, Berkeley CA 94720, U.S.A.*

[2] *Argonne National Laboratory, Argonne IL 60439, USA.*

[3] *The Niels Bohr Institute, University of Copenhagen, Denmark.*

Superdeformed (SD) nuclei are some of the best quantum rotors known. Their characteristic long sequences of equally spaced transition energies provide a unique opportunity to search for unexpected effects on an energy scale rarely achieved elsewhere in nuclear physics. In this context the recent observation of a regular staggering pattern of the transition energies in the yrast SD band in $^{149}$Gd [1], where states differing by four units of angular momentum show a similar energy shift of about 60 eV relative to a (smooth) rotational sequence, is particularly intriguing. Evidence for similar effects has been reported in $^{194}$Hg [2], $^{148}$Gd [3], $^{192}$Tl [4] and in some Ce nuclei [5]. These observations have triggered an intense theoretical effort to understand this phenomenon [6, 7, 8, 9, 10, 11]. Some discussions connect this effect with the presence of a $C_4$ symmetry of the nuclear Hamiltonian [6, 7, 8]. Other studies [9, 10, 11] argue that the measured energy differences could be related to band-crossings. Since the observed energy shifts are only of the order of 100 eV or less it is essential to confirm the reported effects by new measurements with higher statistics utilizing the currently available detector arrays, like Gammasphere [12] and Eurogam II [13]. In this contribution we report results from a new experiment on the known SD bands in $^{194}$Hg [14, 15] investigating the previously reported [2] staggering in those bands. The very high statistics obtained in this experiment has made possible the determination of the relative transition energies for these bands with a precision of 60 eV or better for most transitions. No extended regular $\Delta I = 2$ staggering was found in the three SD bands of $^{194}$Hg and the new results do not confirm those previously reported in Ref. [2]. However, deviations of the $\gamma$-ray energies from a smooth reference have been established for the two excited SD bands in $^{194}$Hg.

Superdeformed states in $^{194}$Hg were populated in the reaction $^{150}$Nd($^{48}$Ca,4n) using a 201 MeV $^{48}$Ca beam provided by the 88-inch Cyclotron of the Lawrence Berkeley National Laboratory. The emitted $\gamma$ rays were detected by the Gammasphere array which at the time of the experiment consisted of 70 Compton-suppressed Ge detectors. A stack of two 500 $\mu$g/cm$^2$ thick Nd targets was used with both sides of each target foil covered with a thin layer of gold (450 $\mu$g/cm$^2$ facing the beam and 220 $\mu$g/cm$^2$ on the other side). A total of $1.4 \times 10^9$ coincidence events with fold $\geq 4$ were recorded on magnetic tape. A gain of 0.125 keV per ADC channel was chosen in order to achieve a high resolution..

The effects we were looking for are only of the order of 100 eV and consequently the analysis plays an important role. Therefore we give hereafter a brief description of the analysis performed

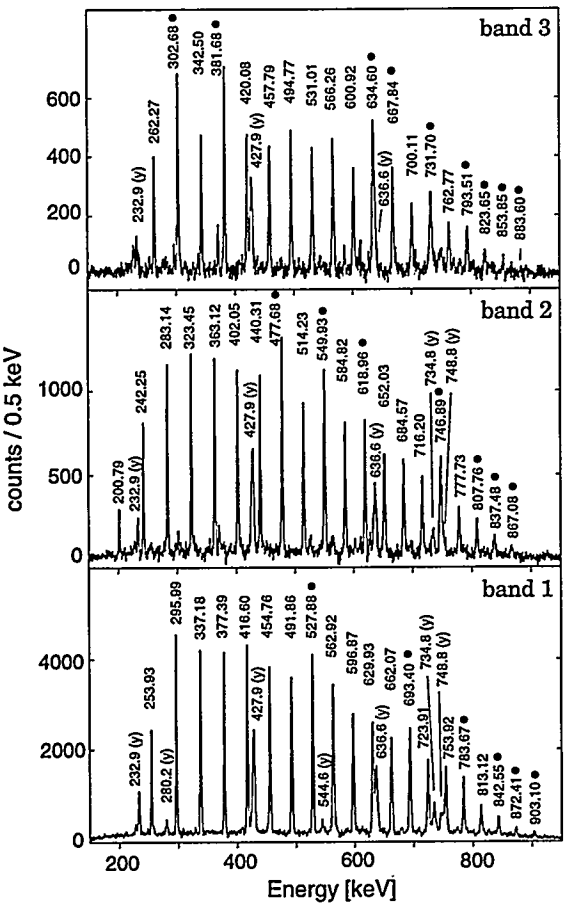


Figure 1: Triple gated and background subtracted coincidence with spectra for the three superdeformed bands. The transitions marked with filled circles were not used as gates. Strong yrast transitions in $^{194}$Hg [17] are labeled with their energy and the symbol "y".

to extract the transition energies of the SD bands in $^{194}$Hg. An off-line correction of drifts in the ADC gains was performed for each individual detector and they were gain-matched by using $\gamma$ rays from a $^{152}$Eu calibration source. Gated coincidence spectra were created for each of the three known SD bands in $^{194}$Hg using in each case several sets of gating transitions, all leading to very clean spectra of the SD bands. Using the sorting method described in Ref. [16] was used to create triple-gated spectra as well as spectra with at least four gates satisfied, which, hereafter, we will call quadruple-gated spectra. Figure 1 shows triple-gated spectra for the three SD bands in $^{194}$Hg. This procedure avoids the overweighting of single channels (so-called *spikes*) in the spectra due to the unfolding of high-fold events. To avoid such spikes is crucial for the correct determination of the transition energies, specifically in the quadruple-gated spectra. Different backgrounds were subtracted from the triple-gated spectra in order to test for systematic effects arising from these subtractions. For the present analysis no background was subtracted from the quadruple-gated spectra.

The Doppler-shift for SD transitions above 700 keV was found to vary from the average recoil velocity (v/c=0.0200(5)) for the lower energy transitions due to the fact that these decays occur in the target foils and their thin gold backing while the recoiling nuclei are still slowing down. The correction method proposed by Cederwall et al. [18] was used to take these effects into account and this improved the peak resolution for those high-energy transitions by 10-15%. The transition energies $E_\gamma$ were determined by using a conventional fitting routine from the triple- and quadruple-gated spectra corresponding to different gating conditions.

Table 1 summarizes the transition energies and relative intensities derived in the present experiment for the three SD bands in $^{194}$Hg. The uncertainties given in Table 1 are dominated by the uncertainties arrising from possible or observed contaminats but also take into account the uncertainties arising from different background subtractions and gating conditions as well as the possible statistical fluctuations. The improvement in the overall precision of the present measurement compared with that in Ref. [2] is more than a factor of two.

For each band the deviation of the $\gamma$-ray energies from a smooth reference $\Delta E_\gamma$ was determined

Table 1: Transition energies $E_\gamma$ and relative intensities $I$ for all transitions of the three superdeformed bands in $^{194}$Hg as determined in this work. The intensities are corrected for detector efficiency and internal conversion.

| $^{194}$Hg-1 | | $^{194}$Hg-2 | | $^{194}$Hg-3 | |
|---|---|---|---|---|---|
| $E_\gamma$ (keV) | I (%) | $E_\gamma$ (keV) | I (%) | $E_\gamma$ (keV) | I (%) |
| | | 200.79 (6) | 36 (5) | | |
| 253.93 (4) | 58 (3) | 242.25 (6) | 75 (5) | 262.27 (6) | 76 (5) |
| 295.99 (3) | 97 (3) | 283.14 (6) | 100 (5) | 302.68 (6) | 90 (5) |
| 337.18 (3) | 95 (3) | 323.45 (6) | 97 (5) | 342.50 (6) | 90 (5) |
| 377.39 (3) | 97 (3) | 363.12 (6) | 100 (5) | 381.68 (6) | 97 (5) |
| 416.60 (3) | 100 (3) | 402.05 (6) | 100 (5) | 420.08 (6) | 100 (5) |
| 454.76 (3) | 99 (3) | 440.31 (6) | 102 (5) | 457.79 (6) | 99 (5) |
| 491.86 (5) | 101 (3) | 477.68 (6) | 101 (5) | 494.77 (6) | 102 (5) |
| 527.88 (3) | 100 (3) | 514.23 (6) | 100 (5) | 531.01 (7) | 104 (5) |
| 562.92 (3) | 94 (3) | 549.93 (6) | 102 (5) | 566.26 (6) | 105 (5) |
| 596.87 (5) | 89 (3) | 584.82 (6) | 99 (5) | 600.92 (6) | 95 (5) |
| 629.93 (3) | 87 (3) | 618.96 (6) | 89 (5) | 634.60 (11) | 91 (5) |
| 662.07 (4) | 82 (3) | 652.03 (6) | 86 (5) | 667.84 (7) | 89 (5) |
| 693.40 (4) | 76 (3) | 684.57 (7) | 84 (5) | 700.11 (6) | 86 (5) |
| 723.91 (6) | 68 (3) | 716.20 (6) | 71 (5) | 731.70 (17) | 72 (5) |
| 753.92 (6) | 56 (3) | 746.89 (19) | 54 (5) | 762.77 (6) | 61 (5) |
| 783.67 (8) | 48 (3) | 777.73 (6) | 44 (5) | 793.51 (6) | 48 (5) |
| 813.12 (3) | 33 (3) | 807.76 (8) | 35 (5) | 823.65 (13) | 30 (5) |
| 842.55 (6) | 19 (3) | 837.48 (7) | 18 (5) | 853.85 (12) | 13 (5) |
| 872.41 (13) | 10 (3) | 867.08 (24) | 8 (5) | 883.60 (22) | 9 (5) |
| 903.10 (18) | 5 (3) | | | | |

by calculating the fourth derivative[1] of the $\gamma$-ray energies $E_\gamma(I)$ at a given spin $I$ by:

$$\Delta E_\gamma(I) = \frac{3}{8}\left[E_\gamma(I) - \frac{1}{6}\left[4E_\gamma(I-2) + 4E_\gamma(I+2) - E_\gamma(I-4) - E_\gamma(I+4)\right]\right] \qquad (1)$$

This expression was previously used in Ref. [2] and is identical to the expression for $\Delta^4 E_\gamma(I)$ in Ref. [11]. We chose to use the expression above in order to be able to follow higher order changes in the moments of inertia of the SD bands. The effects discussed below are certainly also visible in all lower derivatives. Figure 2 shows the resulting values of $\Delta E_\gamma$ for the entire frequency range of the three SD bands in $^{194}$Hg from the present experiment on the left side and the results from Ref. [2] on the right side. The uncertainties for $\Delta E_\gamma$ given in Fig. 2 are calculated using the standard error propagation method. We are aware that the given uncertainties of the individual $\Delta E_\gamma$-values do not account for the correlations induced in the staggering pattern by the change of individual $E_\gamma$-values. The effect of these correlations will be discussed later in this paper.

To evaluate the statistical significance of the staggering pattern an analysis was performed in terms of the confidence level defined in Ref. [2]. In this method the distribution of $\Delta E_\gamma$ values around their average is compared to the distribution obtained when the sign of every other data point is changed. The separation of these distributions in terms of their standard deviation (by

[1]The expression given is in fact the finite difference approximation to the forth derivative $d^4E_\gamma/dI^4$ of the transition energies.

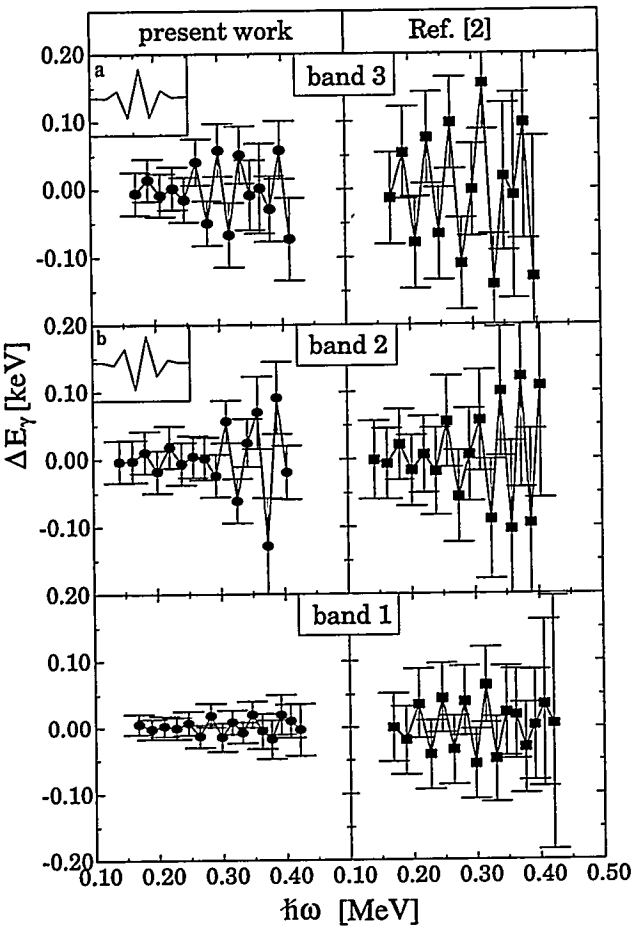


Figure 2: Fourth derivative $\Delta E_\gamma$ (see eq. 1) of $E_\gamma$ for the three superdeformed bands in $^{194}$Hg versus rotational frequency $\hbar\omega$ from present work (left) and Ref. [2](right). The insets show staggering patterns expected from a band crossing scenario (see text for details).

definition the standard deviations of both distributions are equal), gives a measure of the significance of the observed effect (including amplitude and regularity). Assuming a regular staggering over the whole frequency range, we have determined the confidence levels for the three SD bands in $^{194}$Hg. The confidence level for band 1 is $0.7\,\sigma$, which cannot be called statistically significant and reflects that all $\Delta E_\gamma$-values are within their uncertainties consistent with $\Delta E_\gamma = 0$. For band 2, a confidence level of $1.4\,\sigma$ was found for a regular staggering over the whole range. We also investigated the significance of those short regular oscillations which differ from the smooth reference outside their uncertainties. In band 2 the two frequency ranges $\hbar\omega = 0.29 - 0.35\,\mathrm{MeV}$ and $\hbar\omega \geq 0.35\,\mathrm{MeV}$ exhibit larger confidence levels of $2.5\,\sigma$ if analyzed individually. But the opposite phases of the oscillations in these regions lead to a small overall confidence level. However, each of these frequency ranges exhibits a significant deviation from a smooth reference. Band 3 exhibits the most regular pattern, which is represented by a $3.1\,\sigma$ confidence level.

However, this large confidence level is mainly due to the oscillations observed in the frequency range $\hbar\omega = 0.25 - 0.325\,\mathrm{MeV}$. The region below exhibits only very small confidence levels of about $0.5\,\sigma$, while a value of $1.3\,\sigma$ is obtained for frequencies $\hbar\omega > 0.325\,\mathrm{MeV}$. This leads to the conclusion that there is no clear evidence for a regular oscillation extending outside the frequency range $\hbar\omega = 0.25 - 0.325\,\mathrm{MeV}$.

An additional statistical analysis was performed in order to investigate the fact that changes of individual $E_\gamma$-values will have a correlated influence on the $\Delta E_\gamma$-plot, since each $\gamma$-ray energy is used in the calculation of five $\Delta E_\gamma$-values (see eq. 1). In this analysis we have determined the probability that the observed staggering plots can be produced by a smooth rotational sequence of $\gamma$-ray energies that obey the experimental uncertainties. We find that there is a 47.8% probability that the staggering plot of band 1 is produced by a smooth rotational sequence. For bands 2 and 3 this probability is 10.8% and 0.4%, respectively. One may therefore conclude that the statistical analyses support the presence of significant deviations from a smooth reference in bands 2 and 3. Though not necessarily over the whole band, as discussed above.

The following conclusions can be drawn about the individual bands.
*(i)* Within the quoted uncertainties, band 1 shows no significant deviation from a smooth behavior over the entire frequency range.
*(ii)* A deviation from a smooth behavior of the $\gamma$-ray energies is obvious in band 2 for rotational frequencies above 0.3 MeV. However, this deviation does not correspond to a regular oscillation pattern, since a phase inversion is observed at $\hbar\omega = 0.35$ MeV.
*(iii)* A short regular staggering pattern of the order of $\pm 50$ eV is visible in band 3 in the frequency range $\hbar\omega = 0.25 - 0.325$ MeV. Whether the observed pattern continues or not at higher and/or lower frequencies remains an open question due to the magnitude of the uncertainties involved.

We now want to discuss the present data in relation to some suggested interpretations. The results from Ref. [2] have been interpreted as evidence for a possible $C_4$ symmetry in the Hamiltonian [6, 7, 8]. This interpretation was originally based on the observation of an extended regular $\Delta I = 2$ staggering in the yrast SD band of $^{149}$Gd [1]. We have no clear evidence for such extended staggering in the SD bands of $^{194}$Hg. However, it is not clear that $C_4$ symmetry must always generate extended regular staggering [19]. So, in fact, we are unable to use our new results to discuss the possible presence of a $C_4$ symmetry in $^{194}$Hg. Many more systematic studies must be done in order to establish the presence or absence of $C_4$ symmetry.

Alternatively, we may compare the observed deviations with the patterns expected from a band-crossing, as discussed in refs. [9, 10, 11]. The insets in Figure 2 show the deviations from a smooth reference that one would expect for the crossing of two bands. Two extreme cases were chosen where the crossing occurs either near levels in the bands (a) or at the midpoint between levels (b). The interaction between the bands is assumed to be so weak that the configuration mixing is extremely small and, as a result, no measurable cross talk between the bands occurs. Situation (a) can be approximated by the shift of only one level in the band and (b) by the shift of two levels. It is obvious that the staggering patterns in the insets are very similar to parts of the staggering plots for band 2 and 3. However, no single pattern can account for the experimentally observed deviations from the smooth reference. In addition, no evidence was found for additional SD bands which could be involved in a band crossing. Therefore there is no experimental evidence for bands whose possible crossings could account for the observed deviations in bands 2 and 3.

In summary, we have performed a high statistics experiment to test for the previously reported [2] evidence for a $\Delta I = 2$ staggering in the three SD bands in $^{194}$Hg. The transition energies have been determined in this work with a precision of at least 60 eV for most transitions. With an improvement in the precision by a factor of two with respect to Ref. [2] we cannot confirm evidence for an extended regular $\Delta I = 2$ staggering in any of the three SD bands of $^{194}$Hg. However, we observe deviations from a smooth reference in the SD bands 2 and 3 which differ from those previously reported. We are unable to discuss the possible presence of a $C_4$ symmetry, since no extended staggering was observed, which was the basis of earlier discussions of this symmetry and no specific predictions are available for bands in $^{194}$Hg. The oscillation patterns of the $\gamma$-ray energies that can be induced by a simple band-crossing or level-shift have been briefly discussed. While the similarities of these patterns with parts of the observed effects are significant, at least two such crossings or level-shifts would be required in each band to explain the data. Even though such level-shifts seem to provide a simple and straightforward explanation of the observed effects, it is apparent that other experimental signatures, such as a crossing band, are needed to fully understand the results of the present work. No such band has been found in the present data set. Thus the data does not settle the question of the origin of the observed effects.

This work is supported in part by the Department of Energy, Nuclear Physics Division, under contract no. DE-AC03-76SF00098 and W-31-109-ENG-38.

# References


[1] S. Flibotte *et al.*, Phys. Rev. Lett. **71**, 4299 (1993).

[2] B. Cederwall *et al.*, Phys. Rev. Lett. **72**, 3150 (1994).

[3] G. de Angelis *et al.*, Phys. Rev. **C 53**, 679 (1996).

[4] S.M. Fischer *et al.*, Phys. Rev. **C53**, 2126 (1996).

[5] A.T. Semple *et al.*, Phys. Rev. Lett. **76**, 3671 (1996).

[6] I. Hamamoto and B. Mottelson, Phys. Lett. **B 333**, 294 (1994).

[7] I.M. Pavlichenkov and S. Flibotte, Phys. Rev. C **51**, R460 (1995).

[8] A.O. Macchiavelli, D. Cederwall, R.M. Clark, M.A. Deleplanque, R.M. Diamond, P. Fallon, I.Y. Lee, F.S. Stephens and S. Asztalos, Phys. Rev. C **51**, R1 (1995).

[9] Y. Sun, J. Zhang, M. Guidry, Phys. Rev. Lett. **75**, 3398 (1995).

[10] M.A. Riley at the Workshop on Gammasphere Physics, Berkeley Dec. 1995, to be published. (World Scientific)

[11] W. Reviol, H.-Q. Jin and L.L. Riedinger, Phys. Lett. **B 371**, 19 (1996).

[12] Gammasphere Proposal, March 1988, LBL-PUB-5202; I.Y. Lee, Nucl. Phys. **A520**, 641c, (1990).

[13] F.A. Beck, Prog. Part. Nucl. Phys **28**, 443 (1992); C.W. Beausang *et al.*, Nucl. Instr. Meth. **A313**, 37 (1992).

[14] M.A. Riley *et al.*, Nucl. Phys. **A512**, 178 (1990).

[15] C.W. Beausang *et al.*, Z. Phys **A335**, 325 (1990); E.A. Henry *et al.*, Z. Phys **A335**, 361 (1990).

[16] C.W. Beausang, D. Prevost, M.H. Bergstrom, G. deFrance, B. Haas, J.C. Lisle, Ch. Theisen, J. Timár, P.J. Twin, J.N. Wilson, Nucl. Instr. Meth. **A364**, 560 (1995).

[17] H. Hübel, A.P. Byrne, S. Ogaza, A.C. Stuchbery, G.D. Dracoulis, Nucl. Phys. **A453**, 316 (1986).

[18] B. Cederwall *et al.*, Nucl. Instr. Meth. **A354**, 591 (1995).

[19] B. Mottelson in Proceedings of the Conference on Physics from Large Gamma-Ray Detector Arrays; Berkely CA Aug 2-6 1994; LBL-35687;p.2

# $\Delta I = 2$ Energy Staggering in Normal Deformed Dysprosium Nuclei.

M.A. Riley[1], J. Simpson[2], T.B. Brown[1], D.E. Archer[1], J. Döring[1], P. Fallon[3], C. Kalfas[5], J.F. Sharpey-Schafer[4] and S.L. Tabor[1]

*1) Department of Physics, Florida State University, Tallahassee, Florida 32306*
*2) CCLRC, Daresbury Laboratory, Daresbury, Warrington, WA4 4AD, U.K.*
*3) Nuclear Science Division, Lawrence Berkeley Laboratory, Berkeley, CA 94720*
*4) Oliver Lodge Laboratory, University of Liverpool, Liverpool L69 3BX, U.K. and National Accelerator Centre, Faure, PO Box 72, ZA-7131 South Africa.*
*5) Institute of Nuclear Physics, NCSR Demokritos, 15310 Athens, Greece*

Very high spin states ($I \geq 50\hbar$) have been observed in $^{155,156,157}$Dy. The long regular band sequences, free from sharp backbending effects, observed in these dysprosium nuclei offer the possibility of investigating the occurence of any $\Delta I = 2$ staggering in normal deformed nuclei. Employing the same analysis techniques as used in superdeformed nuclei, certain bands do indeed demonstrate an apparent staggering and this is discussed.

The recent discovery of a bifurcation or $\Delta I = 2$ staggering in certain superdeformed bands [1,2,3], where sequential transition energies are alternatively pushed up and down in energy by a small amount (~100 eV) with respect to the anticipated smooth rotational behavior, is currently attracting a great deal of attention. This small effect, corresponding to a perturbation of 1 part in ~6000 in the transition energies has become observable because of the greatly increased sensitivity of the new generation of gamma-ray arrays. (Please see the contribution of Krücken et al., to these proceedings for the most recent results on $^{194}$Hg.) This surprising effect may possibly be related to an unexpected invariance with respect to rotation of the nucleus by 90° [1,4,5,6]. Other interpretations have suggested that it could be generated within a collective model involving quantized intrinsic vortical motion [7], or by mixing of multiple K bands [6], or by an interference effect between close lying rotational bands [8,9].

The weak signature of this effect, has so far only been seen cleanly in superdeformed nuclei, owing to the exceptional spin range and regularity of the rotational sequences involved. There is no reason however to exclude the presence of this effect from rotational bands of nuclei of lower (normal) deformation. Indeed, the first suggestion of a $\Delta I = 2$ staggering was made by Peker et al. [10] for the low spin ground bands of certain actinide nuclei. However, the persistence of the effect over a long spin sequence could not be established. Such an observation in other normal deformed nuclei over a longer spin range would be useful since the intensity of any such band is likely to be much higher than in the usual superdeformed bands and also its spin and excitation energy will probably be known. Finding such long regular sequences in normal deformed nuclei, free from the effects of sudden backbending, is unfortunately, very rare. However, the dysprosium nuclei near N = 90, namely $^{155,156,157}$Dy, in which some of the highest spin states in normal deformed nuclei are observed (I~50), are found to fulfill these requirements. Many regular high spin sequences are observed in these nuclei which show smooth rotational behavior. These sequences have been examined for evidence of $\Delta I = 2$ staggering using the same criteria and tests as performed on the superdeformed cases. In this analysis it is found that certain bands in $^{156}$Dy do show evidence of staggering.

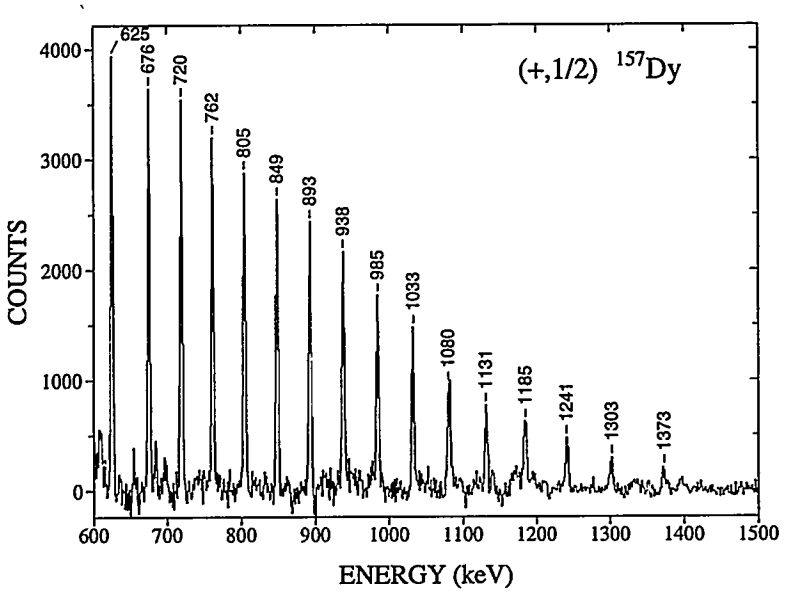


Figure 1: Coincidence spectrum for the positive parity yrast band in $^{157}$Dy.

Very high spin states in $^{155,156,157}$Dy were populated using the $^{124}$Sn($^{36}$S,xn) reaction at a beam energy of 160 MeV. The beam was provided by the 88" Cyclotron at Lawrence Berkeley Laboratory. The target consisted of two stacked foils of $^{124}$Sn each of thickness 500$\mu$g.cm$^{-2}$. Approximately 1.5×10$^9$ $\gamma^3$ coincidence events were collected using the E.I. Gammasphere array with 34 escape suppressed Ge detectors. Analysis has been performed using RADWARE in particular utilizing the cube inspection program LEVIT8R [11].

Figure 1 illustrates one of the long uninterrupted series of $\gamma$-rays typical of a rotational band sequence in the N $\sim$ 90 Dy nuclei. Previously [15] this structure, the yrast band of $^{157}$Dy, had been observed up to the 1131 keV ($81/2^+ \rightarrow 77/2^+$) transition. This regular spectrum is very reminiscent of superdeformation. Indeed, the dynamical moment of inertia of this band is very close to that of some superdeformed bands in the A$\sim$150 region. In this case however, (and other similar bands in $^{155,156,157}$Dy) the large apparent moment of inertia is not due to large deformation but caused by the gradual alignment of a pair of $i_{13/2}$ neutrons and $h_{11/2}$ protons over an extended spin range. These strong interactions between certain crossing multi-quasiparticle bands are a common feature in the N $\sim$ 90 Dy nuclei and have been discussed in ref. [12,14,15]. These smooth alignments are demonstrated in figure 2 where the $^{157}$Dy$_{91}$ yrast band is compared with the same configuration in $^{161}$Yb$_{91}$ [16] in which the interaction strengths at the same band crossings are weaker and thus distinctly observed.

Techniques used to search for oscillating effects in superdeformed nuclei have been, to look for signs of staggering in the dynamical moment of inertia values, and/or to use a local reference method [1,2]. In this latter approach, the transition energy between two states (I and I−2), is compared with the energy expected from a smooth interpolation of the observed transition energies from states above and below spin I within the same band. For regular rotational behavior, no divergence should be observed. Figure 3 shows the results of this approach applied to a selection of smoothly behaving rotational bands in $^{155,156,157}$Dy which are observed to high spin. Although, in several Dy bands

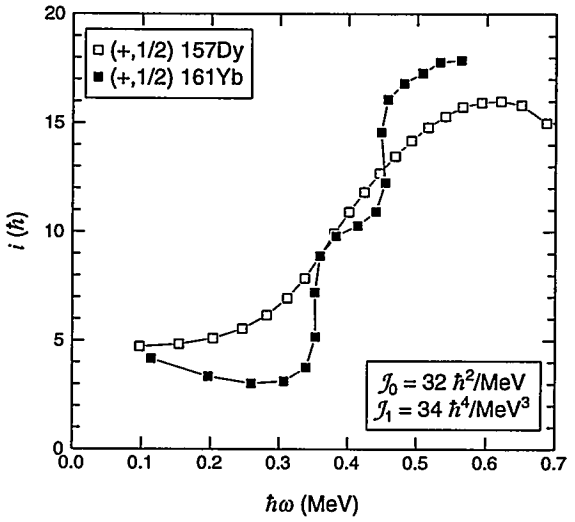


Figure 2: Alignment plot for the positive parity yrast bands in $^{157}$Dy and $^{161}$Yb illustrating the strong interaction strengths in the Dy N = 91 isotope but weak interaction strengths in the Yb N = 91 isotope at the BC neutron ($\hbar\omega \sim 0.35$ MeV) and $A_pB_p$ proton ($\hbar\omega \sim 0.45$ MeV) crossings.

there are brief signs of a staggering effect, these do not last for a significantly extended period, $\geq$6 oscillations, except in the case of the $(-,0)_2$ band in $^{156}$Dy. To investigate further, this latter band has the fortunate property that it is one member of a strongly coupled band sequence[12]. Thus, there is the possibility of using the signature partner $(-,1)_2$ as a natural reference for the $(-,0)_2$ band (as long as it is itself smoothly behaving), which will not suffer from the weaknesses in the local reference method. It is well known that one problem of the local reference method is that, if a perturbed state does occur or a slightly incorrect transition energy is used, then its effects are carried over to the analysis of transitions up to 4 spin units higher and lower. Figure 4 shows the dynamical moment of inertia of the $(-,0)_2$ band in $^{156}$Dy along with its partner $(-,1)_2$ band showing the zig-zag oscillation of the $(-,0)_2$ band about the smooth behavior of its partner at high rotational frequency.

Thus the $(-,0)_2$ band in $^{156}$Dy would appear to show similar characteristics of $\Delta I = 2$ staggering as displayed in the superdeformed examples. The size of the perturbations are however much larger, ~keV as opposed to ~ tenths of keV for the superdeformed cases, but seem to occur over just as extended a spin range ($\geq$6 oscillations). Whether there is a common connection between the explanation of the staggering effect in this normal deformed example to the superdeformed cases remains to be seen. Of value is the fact that, much more experimental information is known about the $(-,0)_2$ band in $^{156}$Dy, such as its excitation energy and spin and perhaps more importantly the exact presence of rotational bands of the same parity and signature close in excitation energy [12,13,18].

Figure 5 shows a plot of excitation energy (minus a rigid rotor reference) versus spin for bands of the same parity $\pi$ and signature $\alpha$ as the $(-,0)_2$ band in $^{156}$Dy. Its strongly coupled signature partner is also shown. It can be seen that the trajectory of the $(-,0)_2$ band lies very close indeed to that of the $(-,0)_1$

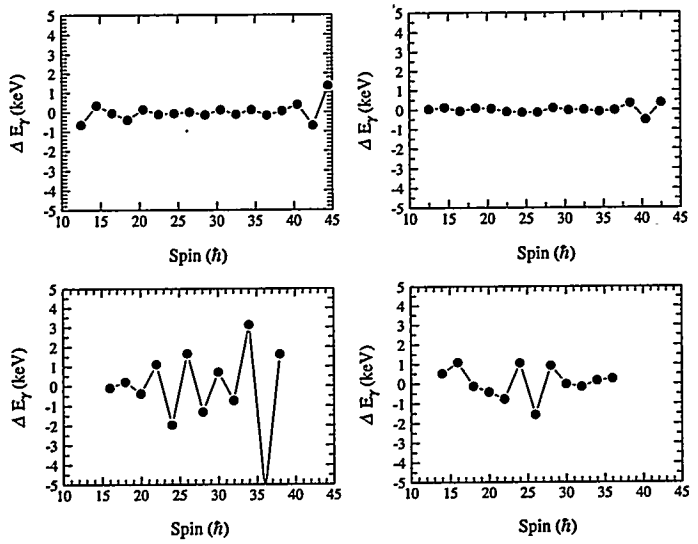


Figure 3: Plots of $\Delta E_\gamma$ for transitions in selected rotational bands in $^{155,156,157}$Dy compared with the expectations of a local reference versus spin (see ref. [2]). Top: right and left are the yrast (+,1/2) bands in $^{157}$Dy and $^{155}$Dy respectively. Bottom: right and left are the $(-,0)_1$ and $(-,0)_2$ bands in $^{156}$Dy respectively. Note their out of phase behavior near I = 25ħ. Error bars are similar or less than that of the symbol size.

band for a large range of spin values with the two bands crossing near spins 15 and 25. There is also the possibility of a further intersection slightly above spin 36. Some details of the lower spin crossings between these bands were discussed in ref. [12], where it was noticed that while an obvious perturbation ($V_{int}$ ~4 keV) occurs between the I = 24 levels the interaction at I = 16 was very much weaker. It was suggested that the latter could be explained by a large difference in K values at low spins between the bands. Note that ΔK=4 between these two bands, a situation consistent with the suggestions of Macchiavelli et al. [6]. This K value difference however may tend to be gradually lost with increasing spin and quasiparticle seniority.

A natural explanation for the apparent ΔI = 2 staggering in the $(-,0)_2$ band would then seem to include its crossing and interaction with the $(-,0)_1$ band. Indeed the maximum of the first perturbation envelope, see Fig. 3, occurs near spin I = 25, a crossing point of the two bands. Note that the perturbations in the $(-,0)_1$ band are found to be out of phase with those of the $(-,0)_2$ band at this point. The continuation of the oscillations in the $(-,0)_2$ band to higher spins and the possible increase in amplitude also seems correlated with the fact that further quasiparticle alignments occur and that these two (-,0) bands seem (along with a third (-,0) band) to be heading for a further intersection above I = 36.

This scenario discussed above for the $(-,0)_2$ band in $^{156}$Dy, ie, close lying bands of the same parity and signature over an extended spin range which cross in a rather gently manner is remarkably similar to the proposal put forth in Ref. [8,9] as a possible explanation of ΔI = 4 bifurcation. These latter authors suggest that the ΔI = 4 bifurcation observed in superdeformed nuclei, (and which they suggest should also occur in normal deformed nuclei) does not necessarily signal the presence of an explicit fourfold symmetry but may alternatively arise due to an interference effect between different quasiparticle orbitals (or bands) near the yrast line. The shallowness of any crossing between

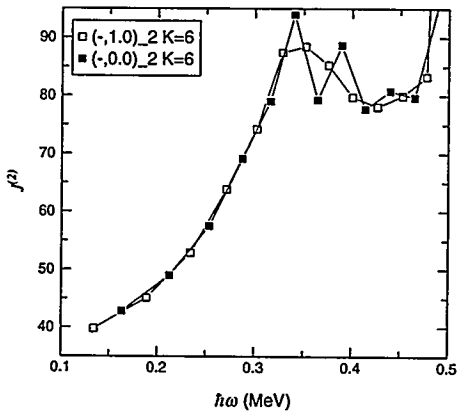


Figure 4: Plot of dynamical moment of inertia for the $(-,0)_2$ band in $^{156}$Dy compared with the smooth behavior exhibited by its signature partner band. Note that the oscillations begin in the $(-,0)_2$ band at the peak of the $J^{(2)}$ curve which corresponds not only to the crossing point between the $(-,0)_2$ and $(-,0)_1$ bands but also the occurrence of the BC neutron crossing.

the two bands determining the range of spins over which the staggering effect persists. In addition, our same example in $^{156}$Dy has been used in ref. [17] to also point out the possibility of $\Delta I = 2$ staggering caused by simple band mixing. In the latter the suggestion is made that an extension of the oscillation pattern could result if a further crossing of levels occurred at the right number of spin units higher than the first crossing, a suggestion in tune with our discussion of the bands in $^{156}$Dy above and that contained in ref. [19].

In summary, a number of smooth rotational cascades extending over an extended spin range in normal deformed Dy nuclei have been investigated for any apparent $\Delta I = 4$ bifurcation, or $\Delta I = 2$ staggering effect. Certain bands in $^{156}$Dy were singled out for special attention. It was shown that the $(-,0)_2$ band exhibited many of the features consistent with the possible interpretation of this phenomenon as an interference effect between bands of the same signature and parity which lie close and cross in excitation energy. However, further experimental work, and extra examples, both in superformed and normal deformed systems, together with more detailed theoretical work are required before a really satisfactory understanding of this interesting phenomenon is reached.

## Acknowledgments

Special thanks to D. C. Radford, H.Q. Jin, R. McCleod and W.T. Milner for their software support and to R. Darlington for making the targets. The Gammasphere staff and Cyclotron crew at LBL are thanked for their help in making our experiment run so magnificently. Useful discussions with Y. Sun, J.Ye Zhang and M. Guidry are acknowledged. Support for this work was provided by the U.S. Department of Energy, the National Science Foundation, the State of Florida, the U.K. Engineering and Physical Science Research Council and the Greek Scientific Research Council. MAR and JS acknowledge the receipt of a NATO Collaborative Research Grant.

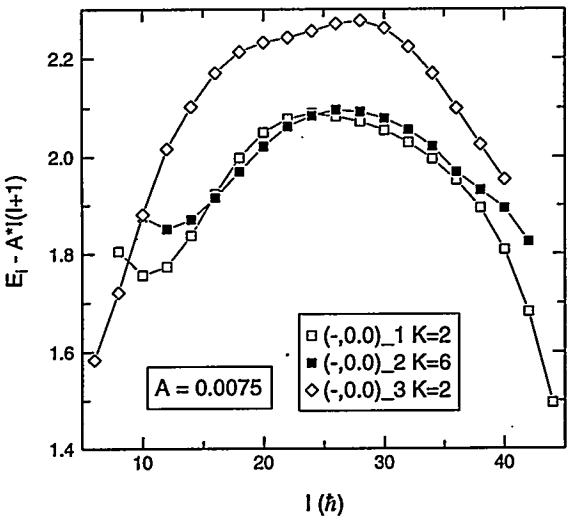


Figure 5: Excitation energy minus a rigid rotor reference as a function of spin for selected negative parity bands in $^{156}$Dy.

## References


1. S. Flibotte *et al.*,, Phys. Rev. Lett. **71**, 4299 (1993).
2. B. Cederwall *et al.*,, Phys. Rev. Lett. **72**, 3150 (1994).
3. A.T. Semple *et al.*, Phys. Rev. Lett. **76**, 3671 (1996).
4. I. Hamamoto and B.R. Mottelson, Phys. Lett. **B333**, 294 (1994).
5. I.M. Pavlichenkov and S. Flibotte, Phys. Rev. **C51**, R460 (1995).
6. A.O. Macchiavelli *et al.*,, Phys. Rev. **C51**, R1 (1995).
7. I.N. Mikhailov and P. Quentin, Phys. Rev. Lett. **74**, 3336 (1995).
8. Y. Sun, J.Ye Zhang and M. Guidry, Phys. Rev. Lett. **75**, 3398 (1995)
9. Y. Sun, J.Ye Zhang and M. Guidry, Phys. Rev. **52**, R2844 (1995).
10. L.K. Peker *et al.*,, Phys. Rev. Lett. **50**, 1749 (1983).
11. D.C. Radford, Nucl. Instr. and Meth. **A361** 297 (1995).
12. M.A. Riley *et al.*, Nucl. Phys. **A486**, 4546 (1988).
13. J.D. Morrison *et al.*, Europhys. Lett. **6(6)**, 493 (1988).
14. R. Vlastou *et al.*, Nucl. Phys. **A580**, 133 (1994).
15. M.A. Riley *et al.*, Zeit Phys. **A345**, 121 (1993).
16. C. Teneiro *et al.*, Daresbury Annual Report 1989-90, Nuclear Structure Appendix, page 61.
17. W. Reviol, H.Q. Jin and L.L. Riedinger, Phys. Lett. **B371**, 19 (1996).
18. M.A. Riley *et al.*, (to be published).
19. M.A. Riley *et al.*, Proc. of Workshop on Gammasphere Physics, Berkeley, Dec. 1995, World Scientific, (in press).

# Evidence for 'Magnetic Rotation' in Nuclei: New Results on the M1–bands of $^{198,199}$Pb

R.M.Clark

*Lawrence Berkeley National Laboratory, Berkeley, California 94720*

**Abstract**

Lifetimes of states in four of the M1–bands in $^{198,199}$Pb have been determined through a Doppler Shift Attenuation Method measurement performed using the Gammasphere array. The deduced B(M1) values, which are a sensitive probe of the underlying mechanism for generating these sequences, show remarkable agreement with Tilted Axis Cranking (TAC) calculations. Evidence is also presented for the possible termination of the bands. The results represent clear evidence for a new concept in nuclear excitations: 'magnetic rotation'.

The observation of long cascades of magnetic dipole (M1) transitions in the neutron deficient Pb nuclei [1, 2] has prompted great interest. The properties of the bands are extremely unusual: i) most of the structures follow the rotational I(I+1) rule over many states despite very low deformations; ii) the levels show no signature splitting; iii) the levels are linked by strong M1 transitions with a typical reduced transition probability, B(M1), of the order of several Weisskopf units; iv) the B(M1)/B(E2) ratios are very large (typically $\geq$20–40 $(\mu_N/\mathrm{eb})^2$); v) the ratio $\Im^{(2)}$/B(E2) is roughly an order of magnitude larger than that for normal or superdeformed bands, indicating that a substantial portion of the inertia is generated from effects other than quadrupole collectivity.

The initial interpretations of the bands [1, 2] suggested that they were based on high–K proton configurations (involving $h_{9/2}$ and $i_{13/2}$ orbitals) which induce a small oblate deformation ($\beta_2 \simeq$–0.1). These protons are coupled to neutron holes in the $i_{13/2}$ sub–shell which carry angular momentum aligned with the collective rotational axis. While this picture accounts reasonably well for the occurrence of the structures, their most perplexing characteristic remained unexplained: how can long, regular cascades, which appear rotational, occur when the nucleus develops only a small deformation?

An intuitively appealing description of the behaviour of the M1–bands arises naturally from the Tilted Axis Cranking (TAC) model [3], and is schematically illustrated in Fig. 1. Near the band–head the proton angular momentum vector, $\underline{j}_\pi$, is nearly parallel to the symmetry axis while the neutron angular momentum vector, $\underline{j}_\nu$, is perpendicular to it. The total angular momentum vector, $\underline{J}$, then lies along a tilted axis at an angle $\theta$ with respect to the symmetry axis. To generate angular momentum $\underline{j}_\pi$ and $\underline{j}_\nu$ gradually align along the direction of $\underline{J}$ with $\theta$ remaining approximately constant. Only a small component of the total angular momentum is from collective rotation (denoted by $\underline{R}$ in Fig. 1). If the spin vectors are long and rigid enough then regular I(I+1) sequences are predicted. Since the behaviour of $\underline{j}_\pi$ and $\underline{j}_\nu$ is reminiscent of the closing of a pair of shears this process has been dubbed the 'shears mechanism' [2].

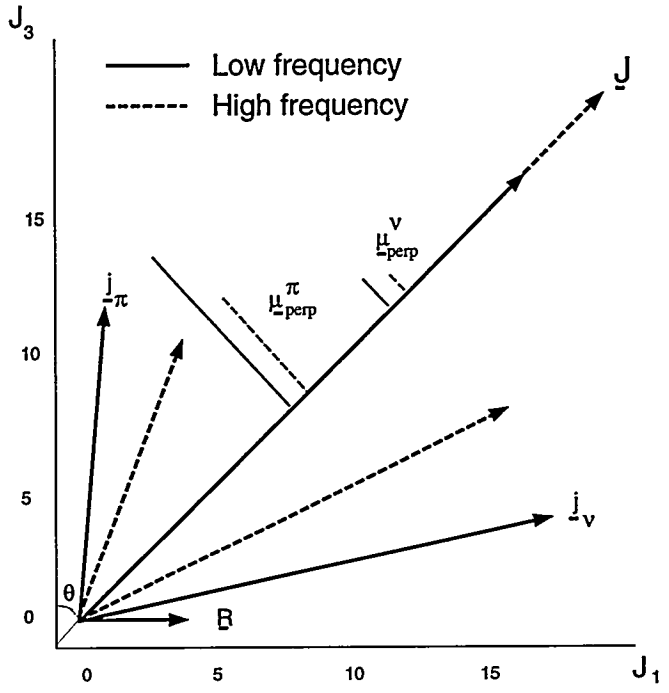


Figure 1: Schematic representation of the angular momentum coupling scheme and the mode of generating angular momentum (the 'shears mechanism') as suggested by the TAC model.

The regular sequences of strongly enhanced M1 transitions (sometimes called 'shears bands') and the TAC picture suggest a new concept – 'magnetic rotation' [4, 5]. This arises as a consequence of breaking the intrinsic rotational symmetry by a long magnetic dipole vector (which rotates about $\underline{J}$ in the TAC picture described above). This is in direct analogy to the familiar concept of ('electric') rotation when the symmetry is broken by an electric quadrupole resulting from the deformed nuclear charge distribution.

Experimental routhians, angular momenta, and moments of inertia for the bands are well reproduced in the TAC model [2, 3, 4]. However, there is a crucially important prediction of the model that remained unconfirmed. Since the B(M1) is determined by the components of the magnetic moments perpendicular to $\underline{J}$, a characteristic drop in the magnitude of B(M1) is expected with increasing rotational frequency. Previous attempts at deducing B(M1) values through lifetime measurements [6, 7, 8, 9, 10] proved inconclusive. In order to test the TAC model, with the underlying concept of magnetic rotation, we have performed an experiment to determine lifetimes of states in the M1–bands of $^{198,199}$Pb. High–spin states in these nuclei were both populated using the $^{186}$W($^{18}$O,xn) reactions at 99 and 104 MeV. The beam, which was accelerated by the 88–Inch Cyclotron of the Lawrence Berkeley Laboratory, was incident on a 12.2mg/cm$^2$ thick $^{186}$W target for the higher beam energy, while the run at the lower beam energy used a 500$\mu$g/cm$^2$ $^{186}$W foil on a 700 $\mu$g/cm$^2$ Al backing. Gamma rays were detected with the Gammasphere array [11] which for this experiment consisted of 60 large–volume (~75–80% efficient) Ge detectors situated at various angles relative to the beam. Totals of $4.7\times10^8$ (four and higher fold) and $1.9\times10^9$ (three and higher fold) events

were collected using the thick $^{186}$W and Al–backed targets, respectively.

For the data taken with the Al–backed target, Doppler–broadened lineshapes were observed for in–band transitions with $E_\gamma \geq 350$ keV. A standard lineshape analysis was performed. The complete stopping was modelled using the prescription discussed in detail by Gascon et al. [12]. The tabulations of Northcliffe and Schilling [13] with shell corrections were used for the electronic stopping powers. Estimates for the lifetimes of the energy levels in four bands were obtained (these bands are labelled according to the conventions of [1, 2]). The B(M1) and B(E2) transition rates were deduced from the standard formulae [14]:

$$B(M1) = \frac{0.05697 B_\gamma}{E_\gamma^3 \tau\,(1+\alpha_{TOT})}\ [\mu_N^2]\,; B(E2) = \frac{0.08156(1-B_\gamma)}{E_\gamma^5 \tau (1+\alpha_{TOT})}\ [e^2b^2] \qquad (1)$$

where $\tau$ is the lifetime of the state in ps, $E_\gamma$ is the energy of the transition in MeV, and $B_\gamma$ is the branching ratio for the M1 transition. The $\Delta$I=1 transitions were assumed to be pure M1's. This assumption is supported by previous studies [1, 2] which generally found very small negative mixing ratios. The conversion of the crossover E2 transitions was also neglected.

Fig. 2 shows the resultant B(M1)'s plotted as a function of transition energy for each of the bands. For comparison, B(M1) values calculated by means of the TAC model using the parameters given in [10] are also shown for the suggested configurations of each band. The deformation is kept constant close to the equilibrium value for $\omega = 0.3 MeV$. The abbreviation used in Fig. 2 to label the configurations is described in [2, 10]: A, B, C, D denotes the $i_{13/2}$ quasi–neutrons, E, F the natural parity quasi–neutrons and the proton configuration is denoted by its aligned spin. Note, from previous studies the spins and the configuration assignments, of $^{199}$Pb(1,2) are firmly established [2] while those of $^{198}$Pb(1,3) are tentative [1, 6]. Also shown in Figs. 2c, 2d are estimates of the B(M1)'s calculated using the semi–classical Dönau and Frauendorf formula [15], using parameters as discussed in [8]. Clearly, the B(M1) values deduced from experiment are in excellent agreement with the TAC model predictions. They are at variance with the results of the standard semi–classical treatment, which assumes that the K value is fixed and the alignment is perpendicular to the symmetry axis (no shears mechanism). Both the magnitude and slope of the results are well reproduced by TAC theory. The experimentally deduced B(E2)'s are shown in Fig. 3. Using these values and the TAC formula [3, 10]:

$$B(E2) = \frac{15(eQ_0 sin^2\theta)^2}{128\pi} \qquad (2)$$

(where $Q_0$ is the intrinsic quadrupole moment and $\theta$ is the tilting angle – see Fig.1 and [3, 10]) we obtain values of $Q_0 \simeq 3$ eb, which corresponds to an average deformation parameter of $\beta_2 \simeq 0.1$ [16], confirming the very low deformation of these structures.

Moreover, the B(E2) values drop with increasing frequency. This can also be understood qualitatively in terms of the shears mechanism since one will approach the point at which the proton and neutron angular momentum vectors will be fully aligned. If the vectors are aligned, the density distributions of the proton and neutron wavefunctions will be axially symmetric with respect to the axis of the total spin, $\underline{J}$, and B(E2) tends to zero. At this point the band will terminate.

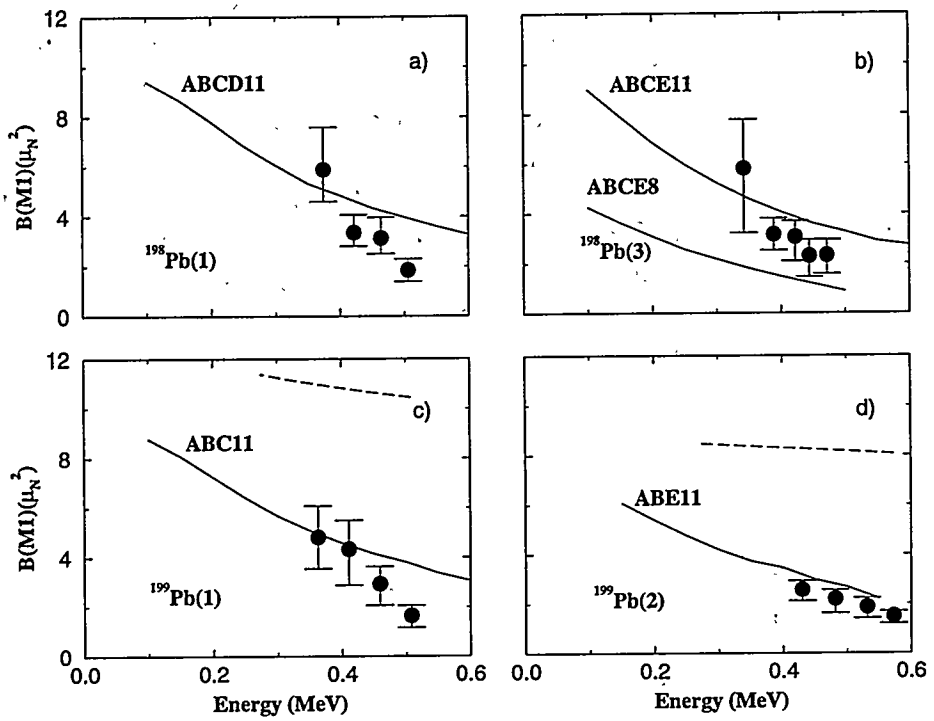


Figure 2: Experimentally deduced B(M1) ($\mu_N^2$) values. The solid lines are the results of TAC model calculations [10] for the suggested configurations of the bands. The dashed lines in c) and d) are B(M1) estimates calculated using the semi–classical treatment of Dönau and Frauendorf [15].

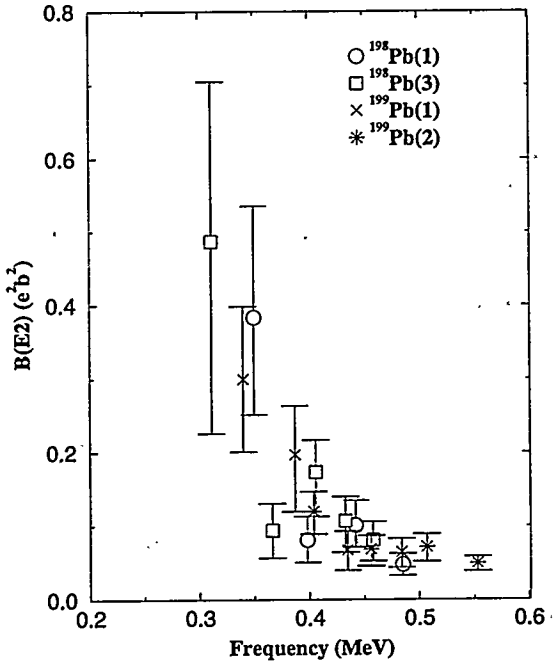


Figure 3: Experimentally deduced B(E2) ($e^2b^2$) values.

To look for further evidence of the termination, transitions extending the bands to higher spin have been searched for and found [17]. For instance, at the spin the TAC model predicts the termination to occur for $^{199}$Pb(2) ($57/2\hbar$) we see that the band becomes irregular and above this one sees a new, weaker M1 structure extending to higher spins. What may have happened is that at the point of termination, the band is crossed by a new structure involving an additional pair of $i_{13/2}$ quasineutrons. A plot of angular momentum versus M1–transition energy is shown in Fig. 4 and one can see that the experimental alignment is roughly $7\hbar$ in agreement with expectations. Above this frequency, the proton and neutron angular momentum vectors will re–orient, and the shears mechanism continues, resulting in the higher lying M1–band as observed.

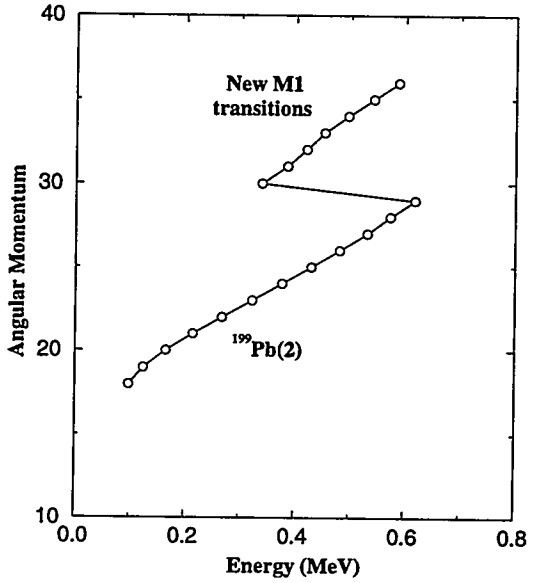


Figure 4: Plot of the angular momentum as a function of transition energy for $^{199}$Pb(2).

Our results show that, despite low quadrupole collectivity, regular 'rotational' sequences with strongly enhanced magnetic dipole transitions can be explained within the framework of the TAC model. The 'shears mechanism' provides both a qualitatively appealing and quantitatively accurate description of the behaviour of the bands in the neutron–deficient Pb nuclei. Moreover, we suggest that our results represent evidence for the concept of magnetic rotation as implied by the shears mechanism. This novel idea extends our conception of the possible modes for nuclear excitations.

**Acknowledgements** We would like to express our gratitude to Dr. John Wells, for his help in setting–up and running the lineshape analysis package, and to Dr. Stefan Frauendorf for invaluable discussions. The crew and staff of the 88–Inch Cyclotron are thanked. The experimental data presented in this contribution involved a collaboration of groups from LBNL, LLNL, Bonn and York.

# References

[1] R.M.Clark et al., Nucl. Phys. A 562 (1993) 121, and references therein

[2] G.Baldsiefen et al., Nucl. Phys. A 574 (1994) 521, and references therein

[3] S.Frauendorf, Nucl. Phys. A 557 (1993) 259c

[4] S.Frauendorf, in 'Proceedings of the Conference on Physics from Large Detector Arrays', Berkeley (August 1994), LBL–35687, Vol. 2, 52

[5] S.Frauendorf, J.Reif, and G.Winter, Nucl. Phys. A, in print

[6] T.F.Wang et al., Phys. Rev. Lett. 69 (1992) 21

[7] J.R.Hughes et al., Phys. Rev. C 48 (1993) R2135

[8] R.M.Clark et al., Phys. Rev. C 50 (1994) 84

[9] E.F.Moore et al., Phys. Rev. C 51 (1995) 115

[10] M.Neffgen et al., Nucl. Phys. A 595 (1995) 499

[11] I.Y.Lee, Nucl. Phys. A 520 (1990) 641c

[12] J.Gascon et al., Nucl. Phys. A 513 (1990) 344

[13] L.C.Northcliffe and R.F.Schilling, Nucl. Data Tables 7 (1970)

[14] H.Ejiri and M.J.A. de Voigt, 'Gamma Ray and Electron Spectroscopy in Nuclear Physics' (Oxford University Press, Oxford, England, 1987), p. 504

[15] F.Dönau and S.Frauendorf in 'Proceedings of the International Conference on High Angular Momentum Properties of Nuclei', Oak Ridge (July 1982), Nucl. Sci. Res. Conf. Series, Vol. 4 (Harwood, New York, 1983) p. 143

[16] K.E.G.Löbner, M.Vetter, and V.Hönig, Nucl. Data Tables A7 (1970) 465

[17] H.Hübel et al., to be published, Z. Phys. A

# Multi-quasiparticle Isomers near stability and Reduced Pairing

G.D. Dracoulis
*Department of Nuclear Physics, R.S.Phys.S.E, The Institute of Advanced Studies, Australian National University, Canberra ACT 0200, Australia*

*Aspects of the formation of multiquasiparticle isomers, massive-transfer reactions for reaching nuclei close to stability, and analysis of the seniority-dependent stepwise reduction in pairing from the rotational properties of multiquasiparticle bands are outlined.*

This report draws on work in progress by a number of colleagues including Filip Kondev, Simon Mullins, Chris Purry and Phil Walker, which will be published in full elsewhere.

The proximity of high-$\Omega$ orbitals near both proton and neutron Fermi surfaces in nuclei near Z = 74 and N = 104 results in high-K states competing with collective rotation of low-seniority configurations to generate the yrast line. In favorable situations it is possible to observe both the intrinsic states and associated rotational bands. The band properties allow characterisation of the configurations and evaluation of orbital and seniority-dependent effects, including pairing reduction and consequent loss of nuclear superfluidity.

## *Isomers near Stability*

The low excitation energy and the inhibited decays imposed by the K-selection rules mean that many such intrinsic states will be metastable, enabling time-correlated $\gamma$-$\gamma$ studies which allow unambiguous temporal ordering and give high sensitivity for weakly populated states and for identification of weak branches, *providing* the lifetimes fall in the region betwen tens of nanoseconds and a few microseconds. Longer lifetimes result in the effective isolation of the states from other structures in the same nucleus. Although the region near A$\sim$ 180 is replete with examples of isomers with lifetimes ranging up to the 31 year $16^+$ isomer in $^{178}$Hf, many more are predicted [1] , some with K as high as 30 $\hbar$, but they cannot be reached at present because of the limitations of fusion evaporation reactions. Some will become accessible immediately beams such as $^{6}$He and $^{8}$Li etc. become available.

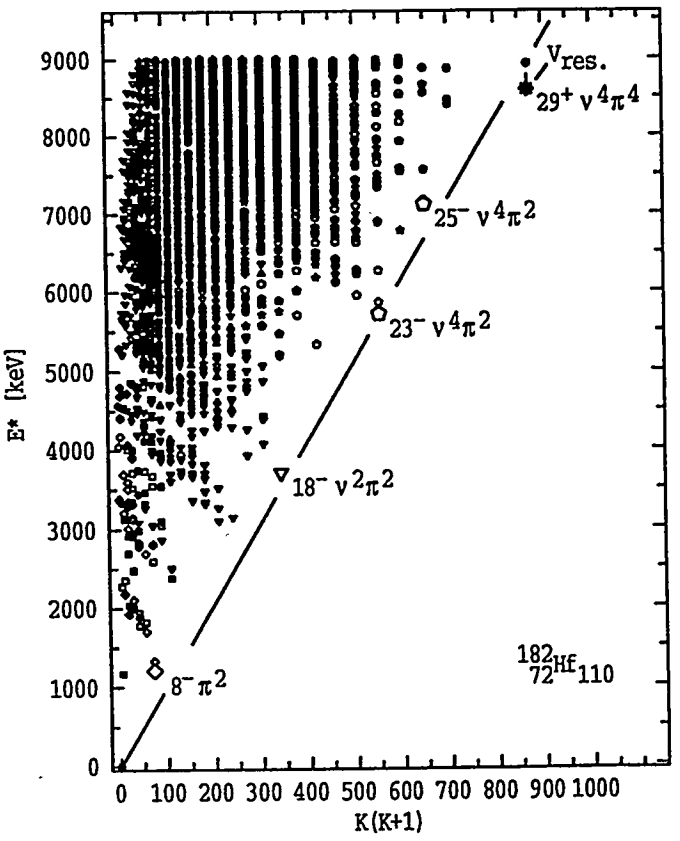


*Figure 1: Calculated states in $^{182}$Hf*

Predictions are shown in fig. 1 for $^{182}$Hf which could be reached by the reaction $^{176}$Yb($^{11}$Be,$\alpha$n)$^{182}$Hf or by transferring two neutrons to the heaviest stable hafnium isotope, $^{180}$Hf. High-K multi-quasiparticle states are predicted to form the yrast line. A 61.5 m $8^-$ state was found many years ago [2] and was shown to $\beta$-decay to medium-spin states in $^{182}$Ta, that path being in fact a primary source of information on such states in $^{182}$Ta. Relatively more-yrast, higher-spin states are predicted with $K^\pi = 18^-$, $23^-$ and $29^+$ which, because of their high-K and low energy will have severely inhibited decays within $^{182}$Hf. There is a prospect of identifying new high-spin structures both within the parent nucleus via the $\gamma$-decay branch, and in its daughter if $\beta$-decay competes, although there will be technical demands because of the very long lifetimes implied.

*Massive Transfer*

Even before such beams become available, massive transfer or incomplete fusion reactions offer the possibility of studying the spectroscopy of a number of lutetium, hafnium, tantalum and tungsten isotopes near or at stability. We have pursued these recently using a particle-detector ball in association with CAESAR to select the $\alpha$-emission channel in $^{11}$B bombardments of $^{176}$Yb. In these $^{180}$Ta and $^{181}$Ta are populated by the $\alpha$3n and $\alpha$2n exit channels, respectively [3].

Such reactions correspond to about 12% of the fusion cross-section and the reaction process is to first order a breakup, where the heavy fragment proceeds to fuse with the target with an energy corresponding to sharing of the beam velocity [4,5]. These reactions lend themselves to spectroscopy because the energy dependence of the cross-section follows that approximately for fusion-evaporation, offset by the additional energy required for the breakup (about 8 MeV in the case of $^{11}$B $\rightarrow$ $\alpha$ + $^{7}$Li); because of the higher angular momentum input which is somewhere between that of fusion of the heavy fragment and the angular momentum of the projectile + target system at grazing. This is much more favourable than if a $^{7}$Li projectile were used directly because it would be effectively sub-barrier. (In the case above, leading to $^{180}$Ta, the optimum $^{7}$Li energy for 3n evaporation is at the barrier of $\sim$ 29 MeV.); because of a

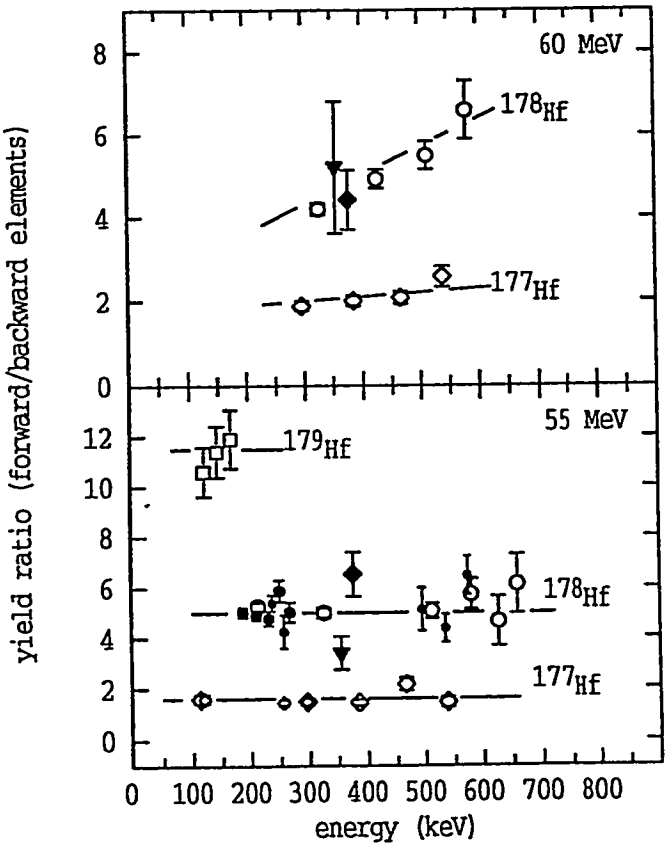


*Figure 2: Yield ratios*

distinctive correlation between forward or backward emission of the $\alpha$-particle and the population of specific nuclei, consistent with a rapid change in the grazing angle as the beam energy is raised from near to well above the Coulomb barrier.

This technique has allowed recently the independent identification [6] of the rotational band based on the $16^+$ isomer in $^{178}$Hf which extends up to spin $22\hbar$ and whose properties confirm the suggested configuration for the isomer as the $\nu^2 7/2^-[514]9/2^+[624] \otimes \pi^2 7/2^+[404]9/2^-[514]$ combination. The transitions agree with the level energies for the $17^+$ and $(18^+)$ states identified from (d,d') of the isomer itself [7]. The ratios of yields for different products are shown in figure 2, for two beam energies and the $^{176}$Yb($^9$Be,$\alpha$ $x$n)$^{181-x}$Hf reactions. It demonstrates clear separation into regions with different numbers of neutrons emitted.

*Time evolution*

Although delayed coincidences are obviously the preferred mode for identification and placement of transitions above isomers, once the lifetimes exceed the tens of microsecond region, they are not viable unless prompt and delayed components can be physically separated between detector components. In some cases, however, the history contained in the time evolution has sufficient information to make unambiguous placements.

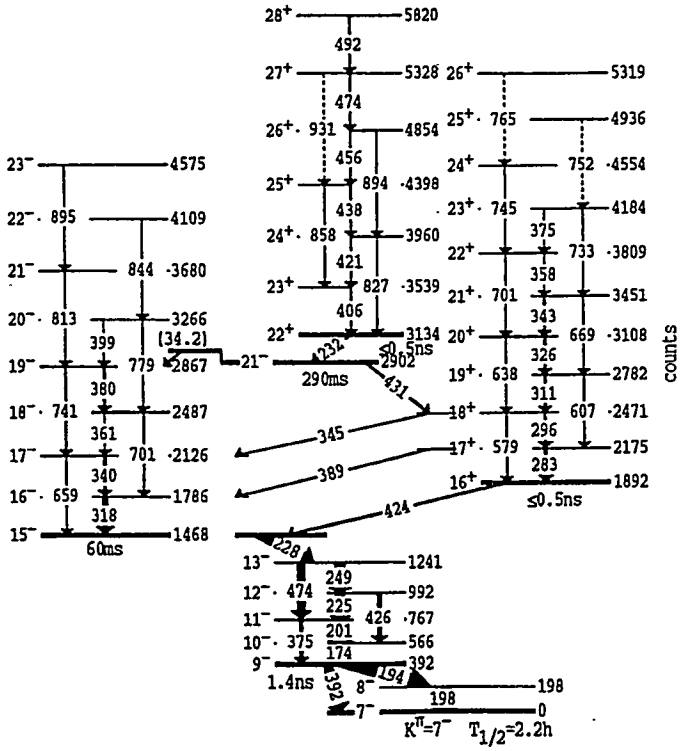


*Figure 3: $^{178}$Ta partial scheme*

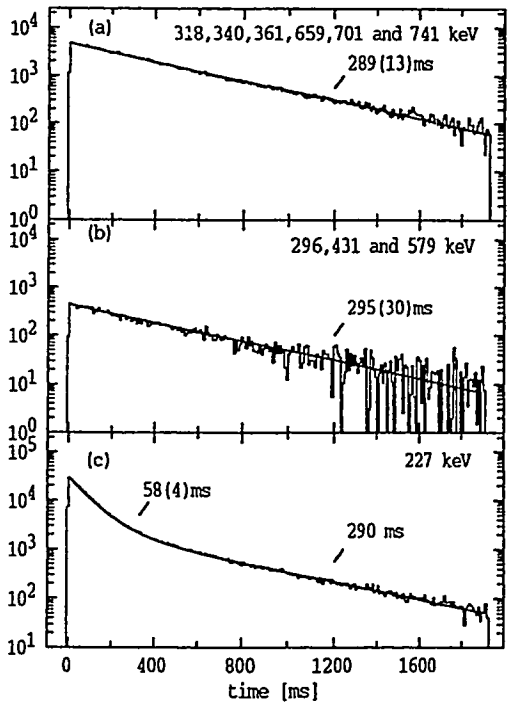


*Figure 4: time spectra*

As part of our mapping of the intrinsic and collective states, aimed in part at a systematic evaluation of pairing, we have recently identified high-spin states in $^{178}$Ta [8] . A $15^-$ isomer was known previously but its lifetime of 58 ms is too long to allow direct

identification of states feeding it. These are of importance for a number of reasons, including characterisation of the configuration of the isomer itself. The new level scheme shown in figure 3 incorporates an even longer-lived $21^-$ isomer, which on the basis of excitation functions etc. has been placed above the $15^-$ isomer. The validity of this assignment is confirmed directly by the time curves in figure 4 which show that the high-spin delayed feeding which proceeds through two separate paths (via the $15^-$ band and also a $16^+$ band) arises from the same 290 ms isomer, while the two component curve observed for the subsequent decay shows that the 290 ms isomer feeds the known $15^-$, 58ms isomer.

*Stepwise Pairing Reduction*

Pairing has played a seminal role in understanding nuclear properties such as explaining why moments-of-inertia are one-third of that for rigid rotation of a deformed body – a result of a superfuidity analagous to superconductivity in metals. However, the corresponding first-order phase transition often discussed is not now expected, either as a function of rotational frequency, or of orbital blocking. The change in pairing by blocking is illustrated in figure 5, estimated using the Lipkin-Nogami prescription, for neutrons in $^{178}$W. Even with six orbitals blocked near the Fermi surface the neutron pairing remains at $\sim$ 40% of the unblocked value. A similar result is obtained for the protons. Since it is usually energetically favourable to balance the neutron and proton contributions, it is doubtful that intrinsic states of sufficiently high seniority to quench the pairing in either protons or neutrons, and certainly not in both, are likely to be within reach.

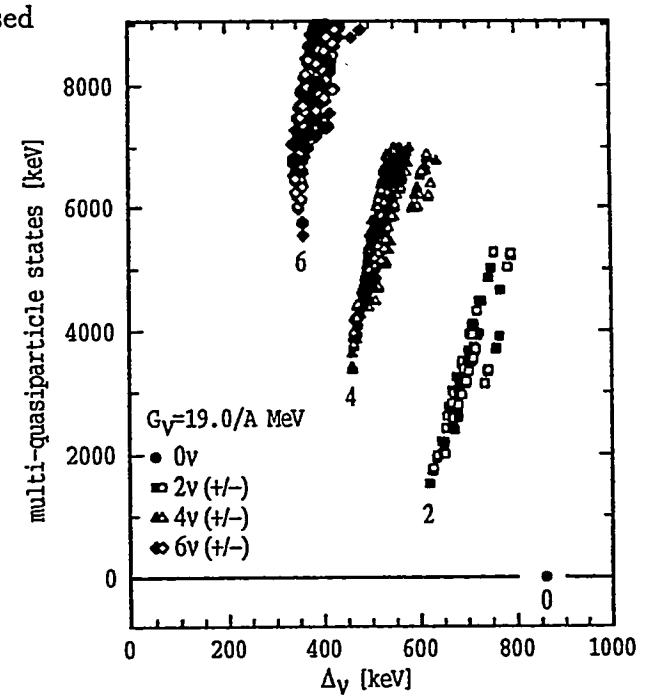


*Figure 5: Calculated neutron pairing in $^{178}W$*

The highest seniority state which also has an associated rotational band known is the $K^\pi = 25^+$, $\nu^4\pi^4$ state in $^{178}$W . Purry *et al* [10] have also identified a suite of multi-quasiparticle states and associated rotational bands in this nucleus, with different seniorities and different combinations of the same subset of proton and neutron orbitals near the Fermi surface. The rotational behaviour of a number of these is shown in fig. 6 in a plot of the projection of the total angular momentum $I_x$ against the rotational frequency, obtained including the nominal K-value in the usual prescriptions. From this figure it is apparent that with increasing seniority the curves become more linear and increase in magnitude at any given frequency, indicating the addition of more aligned angular momentum as the number of contributing particles increases.

However, a) the effective moment-of-inertia remains well below that for a rigid body although it is appreciated that the rigid value is only expected to be reached on average [11].) b) the curves do not cross a "barrier" exemplified by the $25^+$ band. Although it is not possible to cover the details here, examination of the configurations involved, (all contain one or two $i_{13/2}$ neutrons but of the ones shown only the $19^-$, $25^+$ and the $45/2^-$ in $^{179}$W also contain the $h_{9/2}$ proton), and also knowing that, with reduced pairing, the alignment expected in bands with $i_{13/2}$ neutron will be reduced

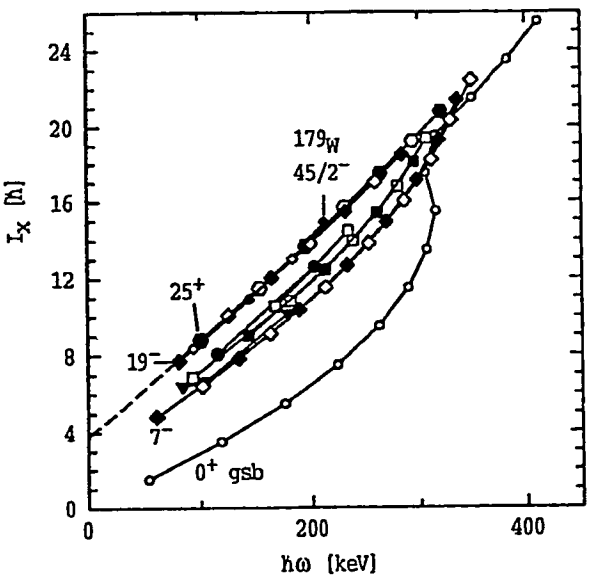


*Figure 6: Total alignments in $^{178}W$*

(its Fermi level is midshell where Coriolis effects are more sensitive to spacing of the *quasi*particle levels whereas for the $h_{9/2}$ proton, the Fermi level is near the $\Omega = 1/2$ orbital and hence its alignment is persistent [11]), allows one to assert that the results do show the effects of reduced pairing in the sense that there is a loss of additivity, so that

$$i_{tot} < \sum (i(\pi h_{9/2}) + i(\nu i_{13/2}) + i(the\ \ rest))\ \ and;\ \ i_{tot} \rightarrow i(\pi h_{9/2})$$

Partial confirmation of this assertion is provided by the comprehensive set of bands identified in $^{178}$Ta [8] most of which do *not* contain the $h_{9/2}$ proton. Two pairs of these are compared in figure 7 in the form of a net alignment obtained by subtracting a common reference. This is not meant to be a precise measure of the alignment since in this situation the reference cannot be defined, but is meant to provide an amplified scale. The absence of the $h_{9/2}$ proton allows underlying changes to be revealed – the $15^-$ $\pi\nu^3$ state is obtained by adding the $6^+$ $\nu^2$ component to the

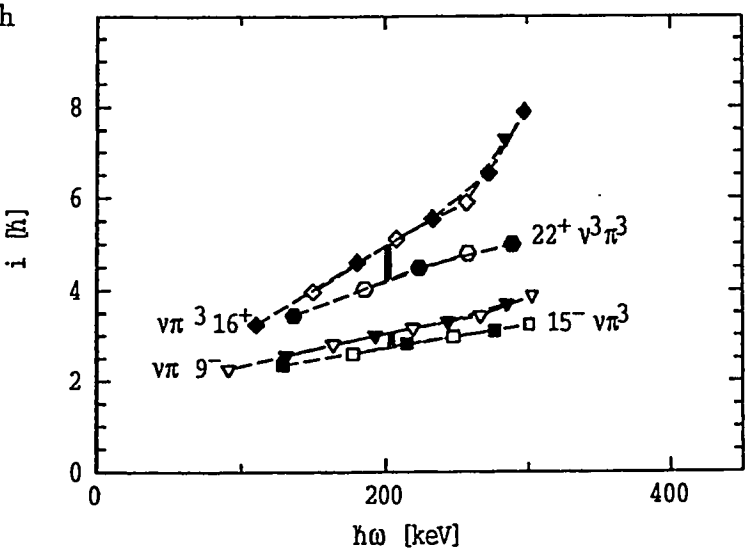


*Figure 7: Net alignments in $^{178}Ta$*

$9^-$ $\pi\nu$ state but despite the extra particles, the apparent alignment is lower. The same situation prevails for the $22^+$ $\pi^3\nu^3$ band and the $15^+$ $\pi\nu^3$ configuration, the former having an additional $6^+$ $\pi^2$ component but less apparent alignment than the latter. The implication to be drawn from this is that the alignment contribution from the particles because of reduced pairing falls faster than the collective moment-of-inertia increases, from the same factor.

*Quantitative Comparison*

What is required to evaluate these effects precisely is a *many*-particles-plus-rotor model. A semi-quantitative step we have followed is to fit each band over a region where there are no alignment *gains* with the generalised Harris formula $I_x(\omega) = i + \Im_0\omega + \Im_1\omega^3$ and then examine the parameters. As implied earlier, the expectation as pairing decreases is that $\Im_1$ will decrease and $\Im_0$ will increase, leading to the the more linear and higher curves in figure 5 We have combined the calculated values of the proton and neutron pairing for each configuration in the two-fluid formula of Migdal [12] with $\Im_{tot} = \frac{N}{A}\Im_n(\Delta_n) + \frac{Z}{A}\Im_p(\Delta_p)$; $\Im_{p,n} = \Im_{rig}(1 - \frac{ln(x\sqrt{1+x^2})}{x\sqrt{1+x^2}})$ and $x = \delta\frac{\hbar\omega_0}{2\Delta_{p,n}}$ for comparison with the extracted values of $\Im_0$. These values are compared for cases of different seniority etc. drawn from $^{176}$Ta, $^{178}$Ta and $^{178}$W. For the $^{178}$W cases, there is a measure of agreement, given the approximate nature of the formulation. The tantalum cases are more problematic. Independent of the general arguments presented earlier, it is apparent that the moments-of-inertia extracted in this way only partly conform to the expectation that the increase would follow seniority.

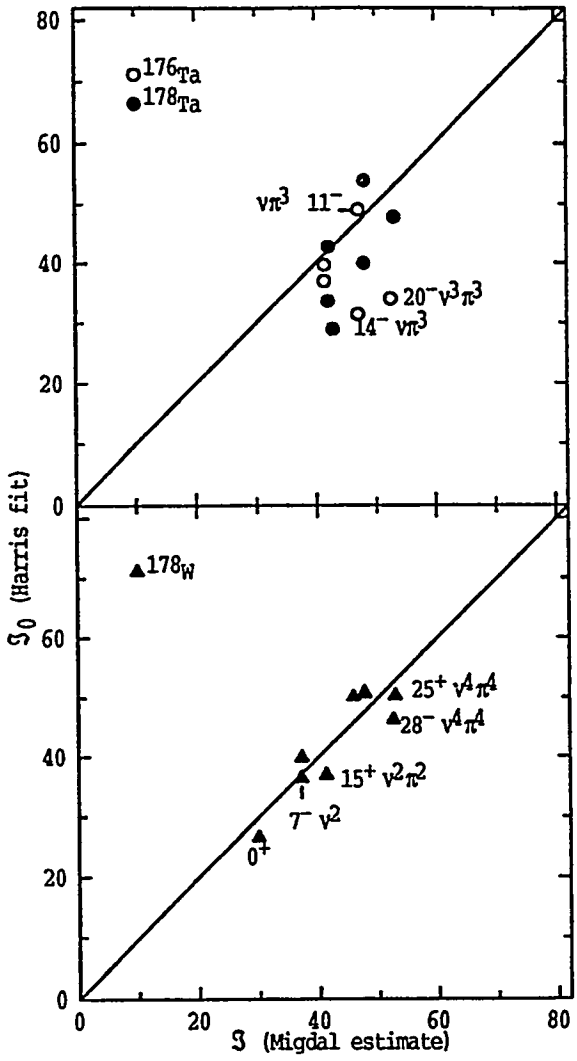


*Figure 8: Experimental and calulated moments*

## References


[1] P.M. Walker, Kiran Jain and G.D. Dracoulis, contribution to this conference

[2] T.E. Ward, P.E. Haustein, J.B. Cumming and Y.Y. Chu, Phys. Rev. C 10(1974)1983

[3] G.D. Dracoulis *et al* Phys. Rev. C. 53(1996)1205 and to be published

[4] T. Inamura, M.Ishihara, T. Fukuda, T. Shimoda and H.Hiruta Phys. Lett. 68B(1977)51

[5] D.R. Zolnowski *et al* H. Phys. Rev. Lett. 41(1978)92

[6] S.M. Mullins *et al* to be published

[7] S. Deylitz *et al* Phys. Rev. C 53(1996)1266

[8] F.G. Kondev *et al* Phys. Rev. C in press and to be published

[9] C.S. Purry *et al* Phys. Rev. Lett. 75(1995)406 and to be published

[10] V.V. Pashkevich and S. Frauendorf Sov.J.Nucl. Phys., 20(1975)588

[11] G.D. Dracoulis Proceedings of Conference on Physics from Large $\gamma$-ray Arrays, 1994 LBL-35687 CONF-940888 UC-413, Vol 2, p179

[12] A.B. Migdal , Nucl. Phys. 13 (1959) 655.

# Return of $K$ selection at high spin: decay of bandheads in $^{178}$W

P.M. Walker[1], C.S. Purry[1], G.D. Dracoulis[2], T. Kibédi[2], F. Kondev[2]
S. Bayer[2], A.M. Bruce[3], A.P. Byrne[2], M. Dasgupta[2], W. Gelletly[1]
P.H. Regan[1] and C. Thwaites[3]

[1] *Department of Physics, University of Surrey, Guildford GU2 5XH, United Kingdom*
[2] *Department of Nuclear Physics, Research School of Physical Sciences and Engineering, Australian National University, Canberra ACT 0200, Australia*
[3] *Department of Mechanical and Manufacturing Engineering, Cockcroft Building, University of Brighton, Brighton BN2 4GJ, United Kingdom*

**Abstract:** In contrast to the de-excitation of the low-seniority states in $^{178}$W, the decay of the $K^\pi = 25^+$, 8-quasiparticle isomer is strongly hindered. This is seen to be related to its yrast status.

The $A \approx 180$ region of deformed nuclei is structurally unique in containing multi-quasiparticle $K$ isomers with four or more unpaired nucleons and half lives greater than $10^{-9}$ s. The observed variation of half life with $Z$ and $N$ is illustrated in fig.1 for the most energetically favoured 4- and 5-quasiparticle isomers. The high-$K$ states and their rotational bands are able to compete to form the yrast line due to strong shell effects: with a quadrupole deformation of $\beta \approx 0.25$, both the neutron and proton Fermi surfaces are close to high-$\Omega$ orbitals, where $\Omega$ is the projection of the intrinsic angular momentum on the nuclear symmetry axis. The quantum number $K = \Sigma\Omega$ is approximately conserved and bandheads generally decay by the minimum possible change in $K$ (the $K$-selection rule).

Recently, isomer decays have been observed which violate the $K$-selection rule, in the sense that significant fractions of the decays bypass available high-$K$ states [1, 2, 3, 4, 5, 6, 7]. These "anomalous" decays have been interpreted in terms of rotational $K$ mixing [2, 3] and tunneling through a potential barrier in the $\gamma$ plane [1, 4, 8, 9], but the relative importance of these mechanisms remains to be clarified.

We have made an extensive study of the nucleus $^{178}$W, which was produced at high spin by the $^{170}$Er($^{13}$C,5n) reaction. Pulsed beams of 80 MeV $^{13}$C were provided by the ANU 14UD tandem accelerator. Numerous multi-quasiparticle bands and bandheads were observed, including a band based on a 220 ns, 8-quasiparticle yrast isomer [10]. The lowest 4- and 6-quasiparticle bandheads in $^{178}$W, with $K^\pi = 11^-$, $12^+$ and $18^-$, are far above the yrast line, as illustrated in fig.2. They have short half lives and fragmented decays, which include anomalous branches with low reduced-hindrance values, as detailed in table 1. In short, $K$ does not appear to be a good quantum number. (The reduced hindrance is defined as $f_\nu = (T^\gamma_{1/2}/T^W_{1/2})^{1/\nu}$, where $T^\gamma_{1/2}$ is the partial $\gamma$-ray half life, $T^W_{1/2}$ is the corresponding Weisskopf single-particle estimate, $\nu = \Delta K - \lambda$, and $\lambda$ is the transition multipolarity.)

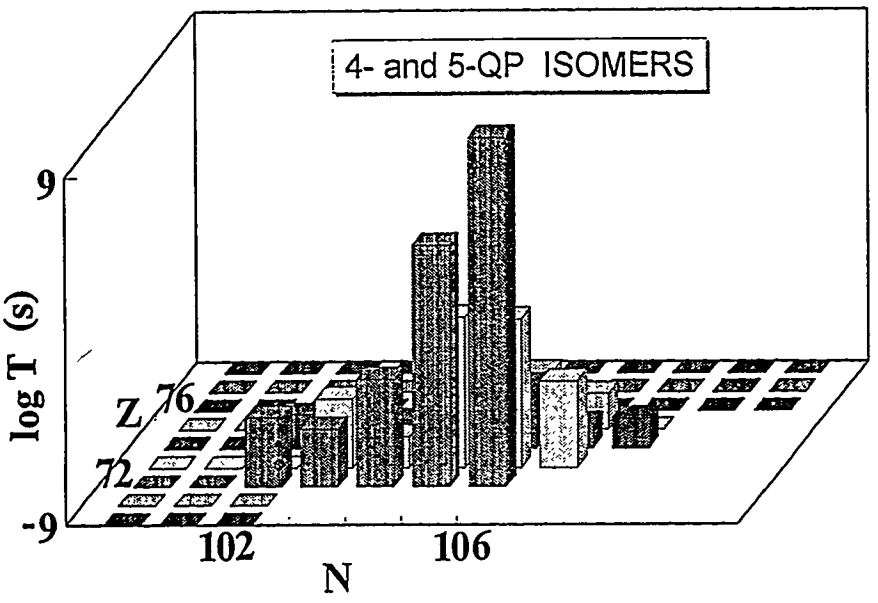


Figure 1. The region of the $N - Z$ plane where high-$K$ multi-quasiparticle isomers are found. The vertical scale is $log_{10}T_{1/2}$ where $T_{1/2}$ is measured in seconds. It covers half lives from $10^{-9}$ to $10^{9}$ seconds. The longest half life is that of $^{178}$Hf, with $T_{1/2} = 31\ y \approx 10^{9}$ s. Squares at the $10^{-9}$ s level represent nuclei for which data are available, but where no isomers with $T_{1/2} > 10^{-9}$ s have been found. There is, as yet, no corresponding experimental information for the open foreground area of the figure, with low $Z$ and high $N$, but energetically favoured isomers are predicted [11].

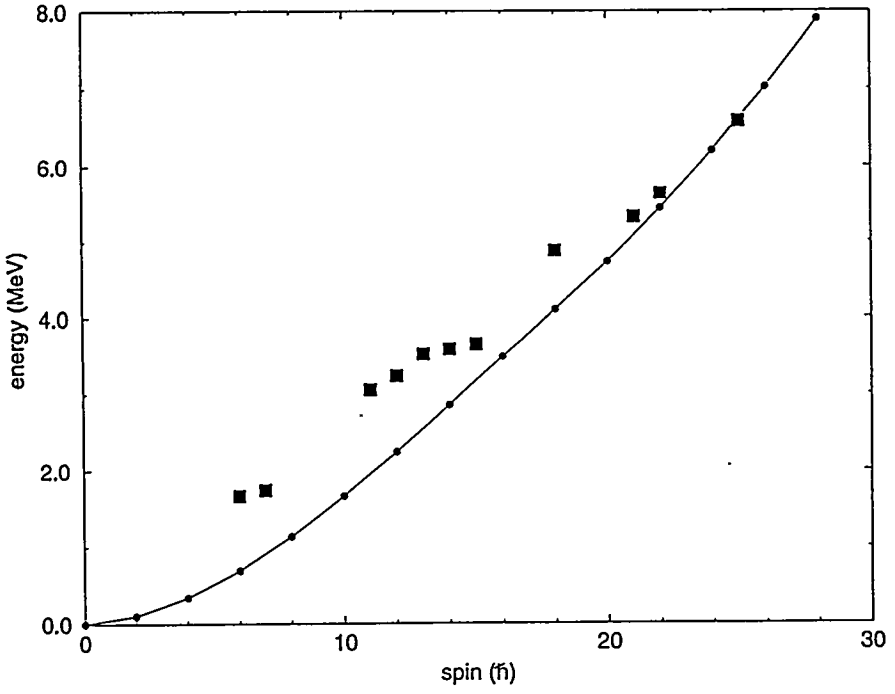


Figure 2. Multi-quasiparticle bandhead energies in $^{178}$W (squares) shown as a function of angular momentum, compared with the ground-state band and its extension (dots).

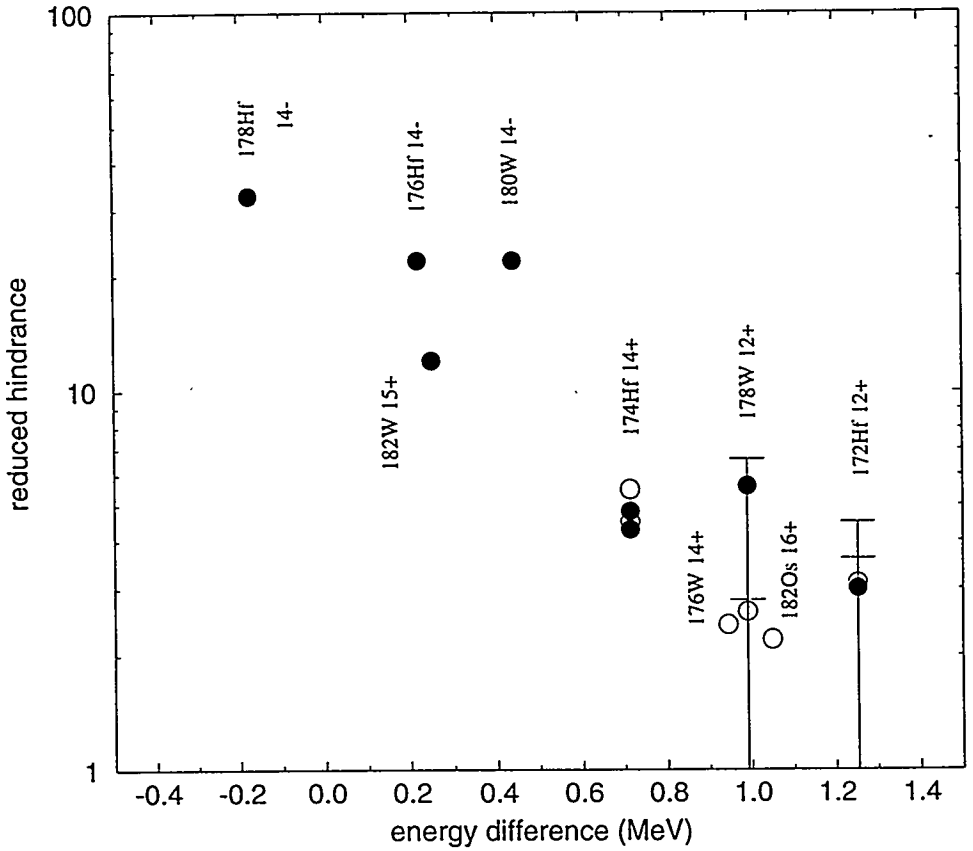


Figure 3. Reduced hindrance, $f_\nu$, as a function of energy above the yrast line (or below the yrare line, for yrast isomers) for $\Delta K > 4$, E2 decays from 4-quasiparticle states. Open circles correspond to anomalous decays. The data points for $^{172}$Hf [5] and $^{178}$W are for (arbitrary) 1 ns state half lives; their experimental upper limit half lives (corresponding to the upper error bars) are 5 ns and 2 ns, respectively. The values for the other nuclei have statistical uncertainties that are smaller than the data points.

The decay of the 8-quasiparticle yrast isomer, however, is strongly hindered and obeys the $K$-selection rule. This $K^\pi = 25^+$ bandhead decays only by a $\Delta K = 3$, 183 keV E1 transition, with $f_\nu^* = 25$ (where the E1 hindrance has been divided by $10^4$ before taking the $\nu$th root, to facilitate comparison with other multipolarities [3]).

The variation in decay pattern can be understood in terms of bandhead excitation energies relative to the yrast line. The reduced hindrances for all known $\Delta K > 4$, E2 ($I \rightarrow I - 2$) decays from 4-quasiparticle isomeric states in even-even nuclei are compared in fig.3. It is seen that the reduced hindrance declines as the excitation energy increases relative to the the yrast line, for both normal and anomalous decays. This systematic feature [12] applies also to higher-seniority isomers, including the value of $f_\nu^* = 25$ for the E1 decay of the $K^\pi = 25^+$ yrast isomer in $^{178}$W. Angular momentum does not, in itself, appear to destroy the $K$ quantum number, an observation which is supported by a new covariance analysis of spectrum fluctuations in $^{163}$Er [13]. Rather, a statistical effect related to the density of states above the yrast line is here implicated in the decline of $K$, and may serve as a test to discriminate between rotational $K$-mixing and $\gamma$-tunneling models.

TABLE 1

**Decays from 4- and 6-quasiparticle states in $^{178}$W**

(a) $K^\pi = 11^-$, $T_{1/2}^{level} < 2$ ns, $E^{level} = 3053$ keV

| $E^\gamma$ (keV) | $T_{1/2}^\gamma$ | $\Delta K$ | Multipolarity | $f_\nu$ |
|---|---|---|---|---|
| 269 | < 56 ns | 4 | E2 | < 2.9 |
| 476 | < 18 ns | - | | |
| 508 | < 22 ns | 4 | M1 | < 51 |
| 564 | < 56 ns | 9 | M1 | < 5.1 |
| 727 | < 74 ns | 4 | M1 | < 109 |
| 921 | < 7 ns | 4 | M1 | < 63 |
| 1012 | < 110 ns | 9 | E2 | < 3.8 |
| 1090 | < 5 ns | 4 | E2 | < 29 |
| 1389 | < 56 ns | 11 | E1 | < 3.1* |

(b) $K^\pi = 12^+$, $T_{1/2}^{level} < 2$ ns, $E^{level} = 3235$ keV

| $E^\gamma$ (keV) | $T_{1/2}^\gamma$ | $\Delta K$ | Multipolarity | $f_\nu$ |
|---|---|---|---|---|
| 181 | < 3 ns | 1 | E1 | |
| 431 | < 48 ns | 12 | M1 | < 3.0 |
| 552 | < 26 ns | - | E2 | |
| 564 | < 54 ns | 6 | M1 | < 13 |
| 689 | < 220 ns | 5 | E1 | < 14* |
| 791 | < 60 ns | 6 | E2 | < 6.6 |
| 908 | < 220 ns | 5 | E1 | < 17* |
| 991 | < 36 ns | 12 | M1 | < 3.7 |
| 1571 | < 26 ns | 12 | E2 | < 2.8 |

(c) $K^\pi = 18^-$, $T_{1/2}^{level} < 2$ ns, $E^{level} = 4878$ keV

| $E^\gamma$ (keV) | $T_{1/2}^\gamma$ | $\Delta K$ | Multipolarity | $f_\nu$ |
|---|---|---|---|---|
| 168 | < 15 ns | 1 | E1 | |
| 363 | < 3.5 ns | 5 | M1 | < 9.3 |
| 671 | < 8.8 ns | 5 | E2 | < 5.0 |
| 967 | < 59 ns | 11 | M1 | < 4.4 |
| 1267 | < 88 ns | 11 | E2 | < 3.1 |

Note: * To compare with other multipolarities, the E1 hindrance has been divided by $10^4$ before calculating $f_\nu$.

# References


[1] P. Chowdhury *et al.*, Nucl. Phys. A485 (1988) 136

[2] P.M. Walker *et al.*, Nucl. Phys. A568 (1994) 397

[3] N.L. Gjørup *et al.*, Nucl. Phys. A582 (1995) 369

[4] B. Crowell *et al.*, Phys. Rev. C 53 (1996) 1173

[5] D.M. Cullen *et al.*, this conference

[6] C. Thwaites *et al.*, this conference

[7] T. Shizuma *et al.*, this conference

[8] K. Narimatsu *et al.*, Nucl. Phys. A601 (1996) 69

[9] Y.R. Shimizu *et al.*, this conference

[10] C.S. Purry *et al.*, Phys. Rev. Lett. 75 (1995) 406

[11] P.M. Walker, K. Jain and G.D. Dracoulis, this conference

[12] P.M. Walker, in *Proc. Conf. on Physics from Large Gamma-Ray Detector Arrays* (Berkeley, August 1994), Vol. II, (LBL Report No. 35687, 1994) p. 63

[13] P. Bosetti et al., Phys. Rev. Lett. 76 (1996) 1204, and this conference

# Direct Transitions from High-$K$ Isomers to Low-$K$ Bands — $\gamma$ Softness or Coriolis Coupling —

Yoshifumi R. Shimizu, Kanako Narimatsu, Shin-Ichi Ohtsubo and Toshiyuki Shizuma†

*Department of Physics, Kyushu University, Fukuoka 812, Japan*

† *Institute of Physics and Tandem Accelerator Center, University of Tsukuba, Ibaraki 305, Japan*

**Abstract:** Recent measurements of direct transitions from high-$K$ isomers to low-$K$ bands reveal severe break-down of the $K$-selection rule and pose the problem of how to understand the mechanism of such $K$-violation. Our recent systematic calculations by using a simple $\gamma$-tunneling model reproduced many of the observed hindrances, indicating the importance of the $\gamma$ softness. However, there are some data which cannot be explained in terms of the $\gamma$-degree of freedom. In this talk, we also discuss the results of conventional Coriolis coupling calculations, which is considered to be another important mechanism.

## § The $\gamma$-Tunneling Model Analysis

In this talk we have discussed the direct (or one-step) transitions from high-$K$ isomers to low-$K$ bands, for which we have recently performed systematic calculations[1]. The motivation of our work came from the recent accumulation of precise measurements of week transitions from the high-$K$ isomers, which clearly shows break-down of the so-called $K$-selection rule[2]. Especially, the data that attracted our attentions are $\gamma$ decays of the $14^+$ isomer in $^{174}$W measured here at Argonne[3]; the transitions to low-$K$ bands are the main branch and indicate two-to-three orders of magnitudes smaller hindrance than those of the same $14^+$ isomer in neighboring nucleus $^{174}$Hf. The authors in Ref.3) attributed the large break-down of $K$ quantum number to the $\gamma$-softness. We wanted to check whether it is true or not, and calculated the transition probabilities systematically in this Hf, W, Os region by using a simple model of tunneling in the $(\epsilon_2, \gamma)$ coordinate.

The essential idea of the model was already discussed in Refs.4,5) some time ago, but the detail of the model should be fixed to calculate the absolute values of transition probability. The idea is simple: it is assumed that there are two groups of states separated by a potential barrier with respect to some collective coordinates. Assuming no direct communications between these two groups (because of large difference of internal structure), the transitions between states in the two wells occur through a mixing between particular states in each well. Then the transition probability is written as a product of the transitions rate inside each well and the squared mixing amplitude. Since the in-band transitions are rather well-known, remaining task is to estimate the mixing amplitude, for which we use the interaction strength $v$ given by the semi-classical tunneling estimate;

$$v^2 = \Big(\frac{\hbar\omega_0}{2\pi}\Big)^2 T, \quad \text{with} \quad T = [1 + \exp(2W/\hbar)]^{-1} \approx \exp(-2W/\hbar), \tag{1}$$

where $\omega_0$ is the zero point frequency of the higher well corresponding to the isomer and $W$ is the (imaginary time) action. To be more specific, we have used $(\epsilon_2, \gamma)$ as collective coordinates, and the transmission coefficient $T$ is calculated as a tunneling from a isomer minimum ($\gamma \approx -120°$) to a low-$K$ minimum ($\gamma \approx 0°$). We do not go into details here (see

Ref.1)), but we would like to mention that the same model has been successfully applied to the problem of decay of the superdeformed bands[6], where the prefactor $(\hbar\omega_0/2\pi)^2$ is replaced by $\hbar\omega_{\rm SD}D_n/(2\pi)^2$ with $\hbar\omega_{SD}$ being the frequency of the superdeformed well and $D_n$ being the mean level distance in the normal deformed well.

Now we concentrate on $E2$ and $M1$ transitions where no ambiguity exits for in-band transitions. Then there are no adjustable parameters in the sense that they are determined by different data or calculations. This is an important point for the systematic analysis. It is found that not only the relative difference of hindrance of decays of $14^+$ isomers in $^{174}$Hf and $^{176}$W mentioned above but also the absolute values of their partial life-times are rather well accounted for by the $\gamma$-tunneling calculation[1]. After finishing Ref.1), we have noticed or analyzed some other data and they are listed in Table 1 in the same form as in Ref.1). Including the new results in Table 1, I show in Fig.1 the summary of comparisons of calculated and measured partial life-times of the low-$K$ branches of transitions. They are plotted in terms of the so-called hindrance factor defined as $F \equiv T^{\gamma}_{1/2}/T^{\rm W}_{1/2}$, where $T^{\gamma}_{1/2}$ is calculated or measured one and $T^{\rm W}_{1/2}$ is it's Weisskopf estimate. The left part is for $\Delta I = 2$ ($E2$) transitions and the right part for $\Delta I = 0, 1$ ($M1$ and $E2$). The abscissa is the calculated hindrance factor and the ordinate is the measured one, so the point on the diagonal line means that the agreement is perfect. Considering the simplicity of the model, it is surprising that there are so many points sitting near diagonal. If one has a closer look, it is seen that most of the transitions with large $\Delta K$ value can be well explained by this $\gamma$-tunneling mechanism.

Table 1 Comparison of the calculated and experimental hindrance factors for some transitions of isomers which are not shown in Ref.1). See Ref.1) for detailed explanation.

| Nucl. | $K^{\pi}_{\rm i}$ | | $T_{1/2}$ | $g_{K_{\rm i}} - g_R[\mu_{\rm N}]$ | $Q_{K_{\rm i}}$[eb] | $W$ [$\hbar$] | $\hbar\omega_0$ [MeV] | Refs. |
|---|---|---|---|---|---|---|---|---|
| | $K^{\pi}_{\rm f}$ | $\lvert\Delta K\rvert$ | | $g_{K_{\rm f}} - g_R[\mu_{\rm N}]$ | $Q_{K_{\rm f}}$[eb] | | | |
| | | $I^{\pi}_{\rm f}$ $E_\gamma$ [keV] | | $B(M1)$ [$\mu^2_{\rm N}$] | $B(E2)$ [e$^2$b$^2$] | $F_{\rm cal}$ | $F_{\rm exp}$ | |
| $^{174}$Yb | $6^+$ | | 830 $\mu$s | $-0.30$ | 7.9 | 10.66 | 1.66 | 7) |
| | $0^+_{\rm g}$ | 6 | | | 8.0 | | | |
| | | $4^+_{\rm g}$ 1265 | | — | $7.7\times10^{-11}$ | $7.5\times10^{7}$ | $1.2\times10^{10}$ | |
| | | $6^+_{\rm g}$ 992 | | $2.6\times10^{-11}$ | $4.1\times10^{-10}$ | $6.0\times10^{9}$ | $3.8\times10^{10}$ | |
| | | $8^+_{\rm g}$ 628 | | — | $1.1\times10^{-10}$ | $5.5\times10^{7}$ | $2.9\times10^{8}$ | |
| $^{177}$W | $\frac{29}{2}^+$ | | $<1$ ns | 0.17 | 6.5 | 6.89 | 1.35 | 8) |
| | $\frac{7}{2}^+$ | 11 | | 0.48 | 7.3 | | | |
| | | $\frac{25}{2}^+$ 1764 | | — | $3.7\times10^{-9}$ | $1.1\times10^{5}$ | $<3.7\times10^{5}$ | |
| | | $\frac{27}{2}^+$ 1386 | | $9.8\times10^{-9}$ | $1.3\times10^{-8}$ | $6.5\times10^{7}$ | $<9.3\times10^{5}$ | |
| | | $\frac{29}{2}^+$ 1224 | | $5.9\times10^{-8}$ | $2.9\times10^{-7}$ | $4.9\times10^{6}$ | $<1.4\times10^{5}$ | |
| $^{178}$W | $12^+$ | | $<2$ ns | 0.02 | 7.4 | 7.40 | 1.41 | 8) |
| | $0^+_{\rm g}$ | 12 | | | 7.3 | | | |
| | | $10^+_{\rm g}$ 1570 | | — | $3.5\times10^{-8}$ | $1.7\times10^{5}$ | $<3.0\times10^{4}$ | |
| | | $12^+_{\rm g}$ 992 | | $2.4\times10^{-10}$ | $2.0\times10^{-7}$ | $1.3\times10^{7}$ | $<1.5\times10^{6}$ | |

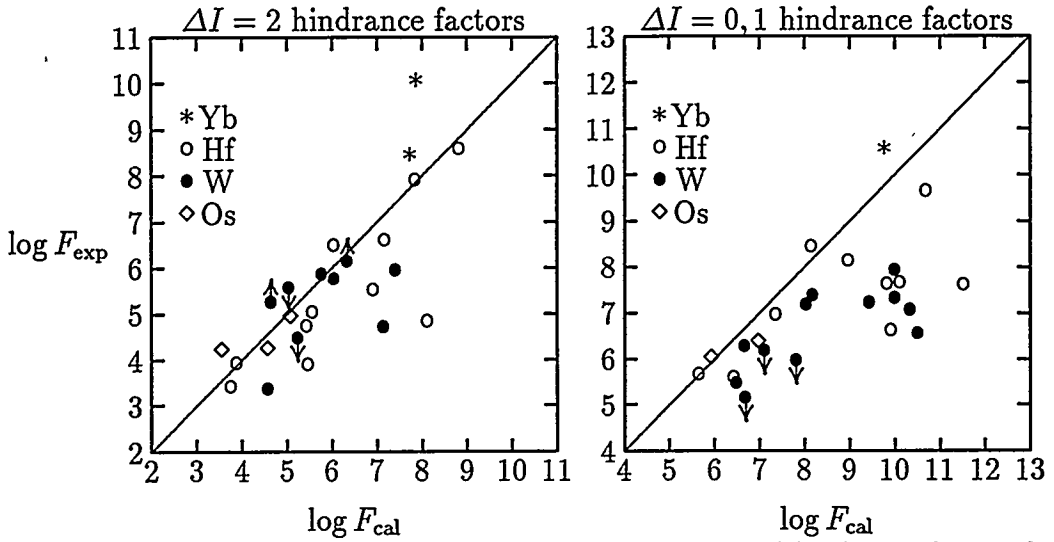


Fig.1 Summary of comparison between calculated and observed hindrance factors for $K$ isomers in the Yb, Hf, W, Os region. Data in Ref.1) and Table 1 are included.

## § $\gamma$ Softness vs. Coriolis Coupling

Though a large body of observed hindrances can be explained by the $\gamma$-tunneling model, there are still a lot of points in Fig.1 for which the $\gamma$-degree of freedom is not enough to account for the observed small hindrances. So we must look for another mechanism; e.g. the spin-orientation-degree of freedom. In place of changing the shape in the $(\epsilon_2, \gamma)$ coordinate, one can think of the change of orientation of the deformed body with respect to the angular momentum axis to reach the final state; note that the deformations of the high-$K$ isomer and the low-$K$ band are very similar in this nuclear region. This situation is schematically depicted in Fig.2 (left). This kind of collective coordinate are nothing else but the one describing the tilted axis cranking (TAC)[9]. Although we are trying to do the large amplitude TAC calculations (see Fig.2 (right)), we could not get convincing results mainly because of numerical difficulties. Alternatively, we here show the results of more conventional calculations; i.e. the higher-order Coriolis coupling, which is suppose to incorporate the same physical effects as the change of the spin-orientation.

The calculation is, in principle, simple and the formula is given in the Bohr-Mottelson's textbook[10]; our case is the so-called $K$-forbidden transitions, Eq.(4-95). The problem is how to calculate the intrinsic matrix element in it with large difference of $K$, $\Delta K \equiv K_{\rm f} - K_{\rm i}$. We have recently developed a general method to calculate the intrinsic moments appearing in the intensity relations by using the cranking approach. Within the lowest order the relevant intrinsic moment with the $K$-forbiddenness, $n = |\Delta K| - \lambda$, is written,

$$\langle K_{\rm f}|m_{\Delta K=-n-\lambda,\nu=-\lambda}|K_{\rm i}\rangle = \frac{1}{n!\mathcal{J}^n}\left[\frac{d^n\langle\langle K_{\rm f}(\omega_{\rm rot})|Q_{\lambda,-\lambda}|K_{\rm i}(\omega_{\rm rot})\rangle\rangle}{d\hbar\omega_{\rm rot}^n}\right]_{\hbar\omega_{\rm rot}\to 0}, \qquad (2)$$

where $Q_{\lambda\nu}$ is the transition operator and its matrix element is calculated by the cranking model at infinitesimal frequency. Although the general evaluation is still difficult, this matrix element can be relatively easily calculated for pure two-quasiparticle transitions. A good

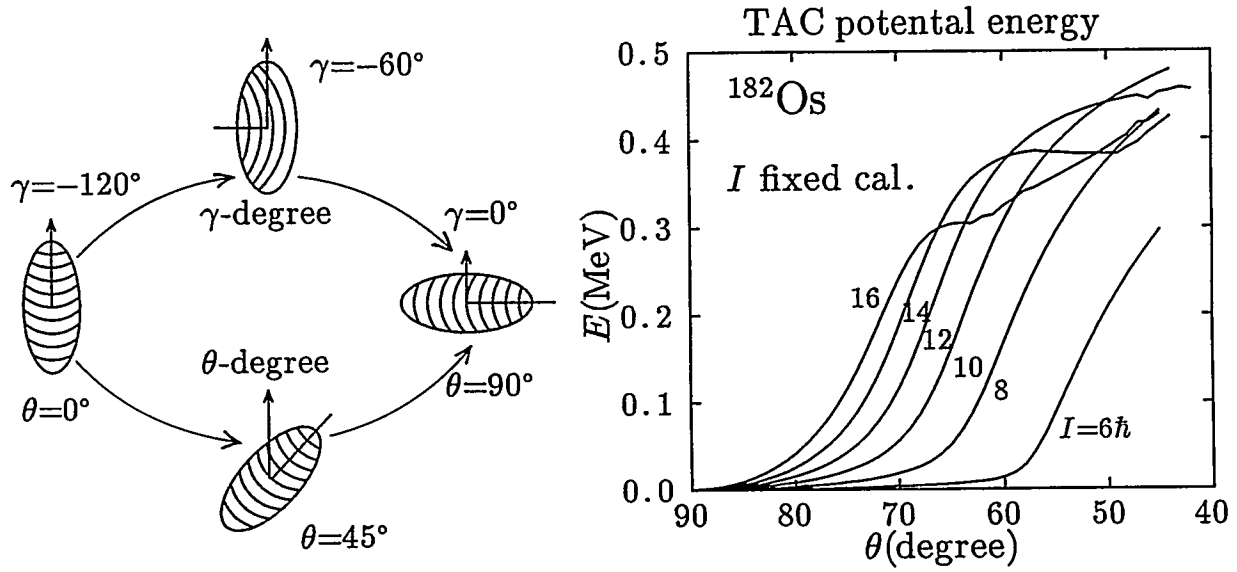


Fig.2 Left: Schematic drawing of the two possible mechanisms for the decay of high-$K$ isomer to low-$K$ band. Right: An example of potential energy in $^{182}$Os with respect to the tilting angle $\theta$ obtained by TAC calculations. Here the energy is calculated by fixing the total $I$ and the energy for each $I$ value is shifted so that the minimum energy is zero. The mean-field parameters, $\epsilon_2 = 0.219$, $\epsilon_4 = 0.049$ and $\Delta_n = 0.890$, $\Delta_p = 0.871$, are fixed for simplicity.

example, for which we can apply the formula, is the $6^+$ isomer systematically observed in this region. For the $6^+$ isomer, the transitions to $8^+, 6^+$ and $4^+$ members of the ground state band are measured with $E2$ or $M1$ property, for which fourth or fifth order of Coriolis coupling is responsible, see Eq.(4-194) and Fig.4-27 in Ref.10). In such a case, the initial and final states in (2) are written as

$$|K_{\rm i}\rangle\!\rangle = U(\omega_{\rm rot})[a^\dagger a^\dagger]_{K^\pi=6^+}|0\rangle,\ |K_{\rm f}\rangle\!\rangle = U(\omega_{\rm rot})|0\rangle,\ U(\omega_{\rm rot}) = \exp\Big(\sum_{ij} g(ij)a_i^\dagger a_j^\dagger - {\rm h.c.}\Big), \quad (3)$$

where $a^\dagger$ is the creation operator of the Nilsson quasiparticle state at $\omega_{\rm rot} = 0$. The collective rotation is generated by $U(\omega_{\rm rot})$ and can be calculated by the cranked mean-field theory.

Before showing the results of Coriolis coupling, let us discuss the $\gamma$-tunneling calculations for the $6^+$ isomers. In Fig.3 (left) we show the isotope dependence of the hindrance factors of the $6^+ \to 6_g^+$ transitions for Yb, Hf, W, Os nuclei. Experimental points are also shown by filled symbols if available. As is seen, the calculations fit the data rather well for lighter Hf or W isotopes including the strong isotope dependence, but they are far off the measured hindrances for heavier isotopes (N $\geq$ 106). The difference of the hindrances in isotopes mainly comes from the change of softness of the potential energy surface, especially in the barrier region, $\gamma \approx -60°$, just as in the case of $14^+$ isomers in $^{174}$Hf and $^{176}$W; see Ref.1) for potential energy surfaces in the $(\epsilon_2, \gamma)$ plane or along the paths.

Now how about the results of Coriolis coupling. In order to calculate the transition probabilities according to Eqs.(2)-(3), one must specify which two quasiparticle configurations are responsible for the actual $6^+$ isomers. In this mass region, $\pi[404]\frac{7}{2}[402]\frac{5}{2}$, $\nu[514]\frac{7}{2}[512]\frac{5}{2}$, $\nu[514]\frac{7}{2}[523]\frac{5}{2}$, and $\nu[633]\frac{7}{2}[642]\frac{5}{2}$ are possible low-lying $K^\pi = 6^+$ excitations. In fact it is

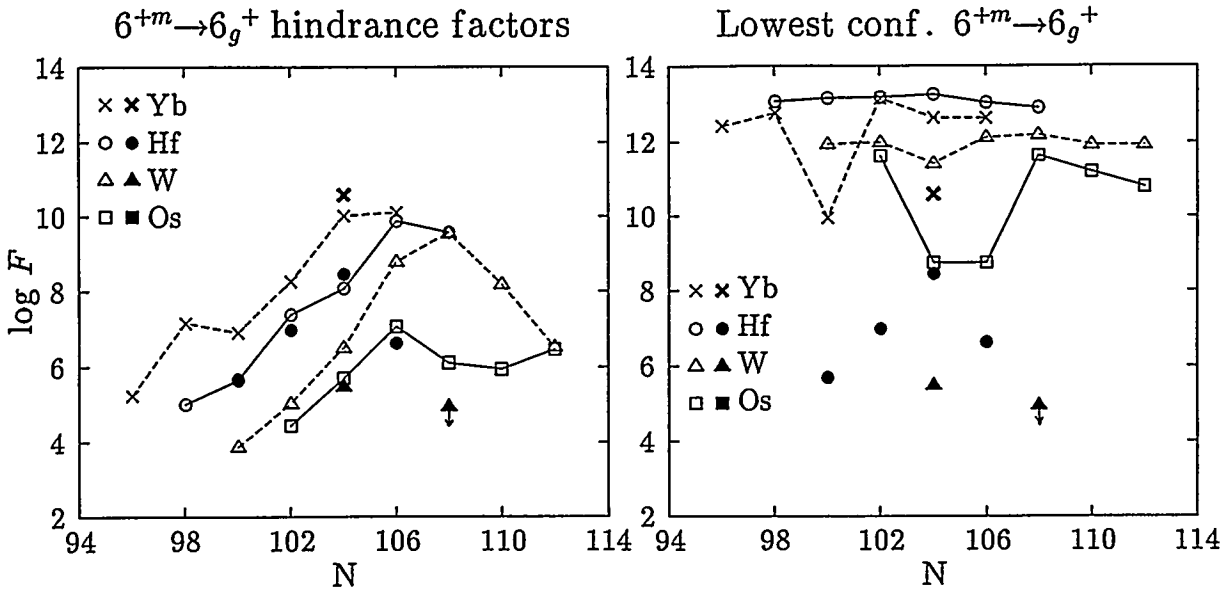


Fig.3 Left: the hindrance factors of the $6^+ \rightarrow 6^+_g$ transitions for Yb, Hf, W, Os isotopes calculated by the $\gamma$-tunneling model. Right: the same but calculated by the higher-order Coriolis coupling. The measured values are also shown by filled symbols if available.

believed that the observed $6^+$ isomer is not a pure configuration from the measured $g$-factors. Although the mixing probabilities are assigned in some cases, we need the amplitude including sign in the calculation. Moreover the main concern here is the order of magnitude one can obtain form this type of simple Coriolis coupling calculations. Therefore we stick to the possible pure configurations. In Fig.3 (right) we show the results for the lowest-lying two quasiparticle configurations. Here we have used a standard Nilsson potential (Bengtsson-Ragnarsson 1985 parameters) and $\epsilon_4$ deformation is neglected. The deformation parameters $\epsilon_2$ and the pairing gaps are taken from the experimentally deduced values. Effective spin $g$-factor $g_s^{\rm eff} = 0.7 g_s^{\rm free}$ is used for $M1$ transitions, and effective charge $\delta e = e$ is used for $E2$ transitions. It is found that the isotope dependence is rather weak within the same configuration, but the resultant hindrance factors considerably depend on the configurations. The configuration dependence in Fig.3 (right) mainly comes from the difference of configurations: e.g. the lowest-configuration is always $\pi[404]\frac{7}{2}[402]\frac{5}{2}$ in the Hf isotopes, while it is changing between $\nu[633]\frac{7}{2}[642]\frac{5}{2}$ (N=104,106) and $\nu[514]\frac{7}{2}[512]\frac{5}{2}$ in the Os isotopes.

In any case these simple Coriolis-coupling calculations give much larger hindrances (or smaller transition rates) compared with the measured values. Note that we have used Eq.(3) in accordance with the conventional Coriolis coupling picture: Namely only the collective (i.e. $a^\dagger a^\dagger$ and $aa$) part of the cranking term, $-\omega_{\rm rot} J_x$, is used for $n$-th order perturbations. One can include the full cranking term in the same way as in Eq.(3), but we have found that the result of such calculations is unstable in the sense that the obtained matrix element in Eq.(2) is very sensitive to the detail of the mean-field parameters, e.g. the chemical potential, the deformation parameters and the pairing gap. This is because the inclusion of $a_i^\dagger a_j$ term is accompanied by the energy denominator $1/(E_i - E_j)$, which diverges at Fermi surface, in contrast to the $a_i^\dagger a_j^\dagger$ and $a_j a_i$ terms which are accompanied by $1/(E_i + E_j)$.

## § Summary and Discussions

Systematic calculations by using the $\gamma$-tunneling mechanism can explain surprisingly large amount of measured hindrance factors, which are ranging more than five order of magnitudes. However, there are many other data which remain to be understood by other mechanisms. Thus, we have performed conventional Coriolis coupling calculations for $6^+$ isomers assuming pure two quasiparticle configurations. The result indicates too large hindrance factor or too small transition rates, which just recover the usual $K$-selection rule. Therefore some "collective" effects, i.e. mixing of pure configurations, are necessary.

The large-amplitude TAC-type calculations for the spin-orientation-degree ($\theta$-degree in Fig.2) of freedom is certainly desired. It is not so easy to obtain the potential energy surface with respect to the $\theta$ coordinate in its full range; note that magnitude of the angular momentum should be fixed during the change of $\theta$ coordinate. In Fig.2 (right) an example of our present status of calculations is shown for $^{182}$Os: It is clearly seen that the fluctuation in the $\theta$ direction decreases as the mean spin value increases. The low-spin motion of this nucleus is prolate-collective rotation, and so the energy is minimum at $\theta = 90°$. Approaching the $\theta = 0°$ isomer configuration, it is progressively become difficult to keep the spin value (and the neutron and proton numbers) because of sharp and frequent level-crossings with respect to the $\theta$ coordinate. We must use e.g. the gradient method to obtain the full surface, which is a future problem.

We have restricted to the transitions from high-$K$ isomers to the low-$K$ bands. But there are many other data decaying to the intermediate $K$ values and show similar break-down of the $K$-selection rule. In order to investigate such cases the TAC type calculation is inevitable. Finally, we would like to mention that the TAC is supposed to be the large amplitude version of Coriolis coupling though semi-classical in its nature. Therefore, it is an another important issue how to compromise the conventional Coriolis coupling picture, which recovers the $K$-selection rule as discussed above, and the TAC picture, which hopefully gives its large break-down.

## References


1) K. Narimatsu, Y. R. Shimizu and T. Shizuma, Nucl. Phys. **A601** (1996), 69.
2) P. Walker, the talk in this conference.
3) B. Crowel, et al., Phys. Rev. Lett. **72** (1994), 1164; Phys. Rev. **C53** (1996), 1173.
4) P. Chowdhury, et al., Nucl. Phys. **A485** (1988), 136.
5) T. Bengtsson, et al., Phys. Rev. Lett. **62** (1989), 2448.
6) Y. R. Shimizu, et al., Nucl. Phys. **A557** (1993), 99c.
7) J. Borggreen et al., Nucl. Phys. **A96** (1967), 561;
   E. Browne, Nucl. Data Sheet **62** (1991), 1.
8) T. Shizuma et al., in preparation.
9) S. Frauendorf, Nucl. Phys. **A557** (1993), 259c.
   T. Horibata and N. Onishi, Nucl. Phys. **A596** (1996), 251.
10) Å. Bohr and B. R. Mottelson, *Nuclear Structure*, Vol. II, (Benjamin, New York, 1975), Chapter 4.
11) Y. R. Shimizu and T. Nakatsukasa, preprint *nucl-th/960618*.

# Tilted Axis Rotation in odd-odd $^{164}$Tm

W. Reviol, L. L. Riedinger, X. Z. Wang, and J.-Y. Zhang
*University of Tennessee, Knoxville, TN 37996-1200, USA*

H. J. Jensen, G. B. Hagemann, R. A. Bark, P.O. Tjøm, S. Leoni, T. Lönnroth, H. Schnack-Petersen, T. Shizuma, and J. Wrzesinski
*Niels Bohr Institute, DK 4000 Roskilde, Denmark*

## Abstract

Ten band structures are observed in $^{164}$Tm, among them sets of parallel and anti-parallel couplings of the proton and neutron spins. The Tilted Axis Cranking scheme is applied for the first time to an odd-odd nucleus in a prominent region of nuclear deformation.

## I. INTRODUCTION

Multiple band structures have been observed in $^{164}$Tm. These provide a wealth of information, particularly on: *(i)* high-$K$ bands in a well deformed rare-earth nucleus at low excitation energy; *(ii)* differences between the parallel (high-$K$) and anti-parallel (low-$K$) couplings of certain high-$j$ proton and neutron orbitals, which are both present in some cases ($\pi h_{11/2} \otimes \nu i_{13/2}$, $\pi g_{7/2} \otimes \nu i_{13/2}$); *(iii)* alignment processes probing neutron pair correlations (blocking of $\nu i^2_{13/2}$ excitations); *(iv)* energies, signature splittings and inversions of low-$K$ bands ($\pi h_{9/2} \otimes \nu i_{13/2}$, $\pi d_{5/2} \otimes \nu i_{13/2}$) probing p-n correlations and deformation effects.

Here we focus on the bands with high $K$ or/and large magnetic moments, as indicated by $B(M1)/B(E2)$ ratios, to test the Tilted Axis Cranking (TAC) scheme [1]. Indeed, these bands in $^{164}$Tm are signature partner $E2$ sequences but with an energy splitting near zero, a possible indication for TA rotation. This model has been successfully applied to high-$K$ bands in the neighboring $^{163}$Er [2] and $^{166}$Yb [3] nuclei which are found, however, at high excitation energies ($E_x > 1500$ keV). Thus, the low-lying bands in an odd-odd rare-earth nucleus are a natural choice to further test and discuss the importance of the TAC model.

## II. EXPERIMENTAL TECHNIQUES AND RESULTS

The experiment was performed with the Nordball detector system at the Niels Bohr Institute Tandem Accelerator using the $^{150}$Nd($^{19}$F,5n) reaction at 85 MeV to populate $^{164}$Tm. For a part of the experiment, two of the coaxial Ge detectors were replaced by LEP Ge detectors to ensure sensitivity for important low-energy transitions at the bottom parts of band structures. In total, 2 billion two- and higher fold coincidences between the Ge

detectors were recorded. The two-fold coincidences were analysed for appropriate software-gates for the inner $BaF_2$ ball and for different time conditions to search for delayed transitions (within a 10 – 250 ns interval). An analysis of the triples data was also performed.

A part of the level scheme obtained from the present work is presented in Fig. 1. All bands can be related to either the $K^\Pi = 1^+$ ground state or the low-lying $K^\Pi = 6^-$ isomeric state ($t_{1/2}$ = 5.1 m) [4]. The bands labeled 6 (yrast band), and 5 have been observed previously [4], the latter however not as a signature partner band. Multipolarities of $\gamma$-ray transitions are inferred from directional correlations (DCO ratios). Delayed transitions are found at some band heads, *e.g* band 5 ($E_\gamma$ = 110 keV) and band 6 ($E_\gamma$ = 124 keV).

## III. CONFIGURATION ASSIGNMENTS AND DISCUSSION

The configuration assignments proposed for the band structures in $^{164}$Tm rest on energy considerations, signature splittings, band crossings and interactions, and the magnetic properties deduced from in-band $\gamma$-ray transitions. The starting point for these assignments is a "first-order" level scheme for $^{164}$Tm based on the lowest lying single-proton and neutron states in the neighboring odd-$A$ nuclei $^{163,165}$Tm [5,6] and $^{163}$Er [2], respectively. In Table I, these configurations are summarized and it is indicated by band labels partially introduced in Fig. 1 which assignments for the level scheme are proposed. Perhaps most interesting are the configurations $7/2[523]_p 5/2[642]_n$ ($\pi h_{11/2} \otimes \nu i_{13/2}$) and $7/2[404]_p 5/2[642]_n$ ($\pi g_{7/2} \otimes \nu i_{13/2}$) where bands corresponding to both parallel and anti-parallel couplings of the proton and neutron spins are observed. For these cases, the Gallagher-Moszkowski rule [7] specifies that the coupling with parallel intrinsic spins is lower in energy than the anti-parallel coupling (the rotational part of the energy $\sim (I^2 - K^2)$ needs to be considered as well).

*Alignments of $i_{13/2}$ neutrons.* Rotational alignment of an $i_{13/2}$ (AB) neutron pair at a rotational frequency $\hbar\omega \sim 0.25$ MeV is only observed for bands 7 and 8. In contrast, in most of the bands this excitation from a two- to a four-quasiparticle configuration is delayed by the odd neutron. Thus, for all these bands configurations with a $\nu i_{13/2}$ content are proposed.

*Signature splittings.* Only the bands 4 and 5 exhibit a significant energy signature splitting ($\Delta E' > 20$ keV) in the frequency range $\hbar\omega < 0.25$ MeV. By systematics, the $1/2[541]_p 5/2[642]_n$ ($\pi h_{9/2} \otimes \nu i_{13/2}$) and $1/2[411]_p 5/2[642]_n$ ($\pi d_{3/2} \otimes \nu i_{13/2}$) configurations are assigned to bands 4 and 5, respectively. For all the other bands no signature splitting is observed. This striking feature of the multi-band spectrum of $^{164}$Tm justifies an application of the TAC model.

*Interband transitions.* Special attention should be paid to band 3 in the low-$K$ part of the level scheme. Interlinking $E2$ transitions between bands 3 and 4 indicate that both structures have the same parity. The interaction strength deduced is on average $V_I \sim 5$ keV, in agreement with corresponding $\pi h_{11/2} - \pi h_{9/2}$ bandcrossings in $^{163,165}$Tm [5,6]. In addition, the $B(M1)/B(E2)$ ratios observed for band 3 are among the largest measured, indicating the presence of the $h_{11/2}$ proton (see below). Thus, the assignment of a $\pi h_{11/2} \otimes \nu i_{13/2}$ (low-$K$) configuration for band 3 is most reasonable. In the case of band 8, most of the population strength is carried away by pronounced $E1$ transitions to the yrast band. Consequently, the lower spin range of the band (below the AB crossing) is not observed. The links between bands 6 and 8 resemble a situation in the level scheme of the isotone $^{163}$Er [2], where the negative-parity neutron levels (E,F) decay to the $\nu i_{13/2}$ band (A,B). Because of an interaction

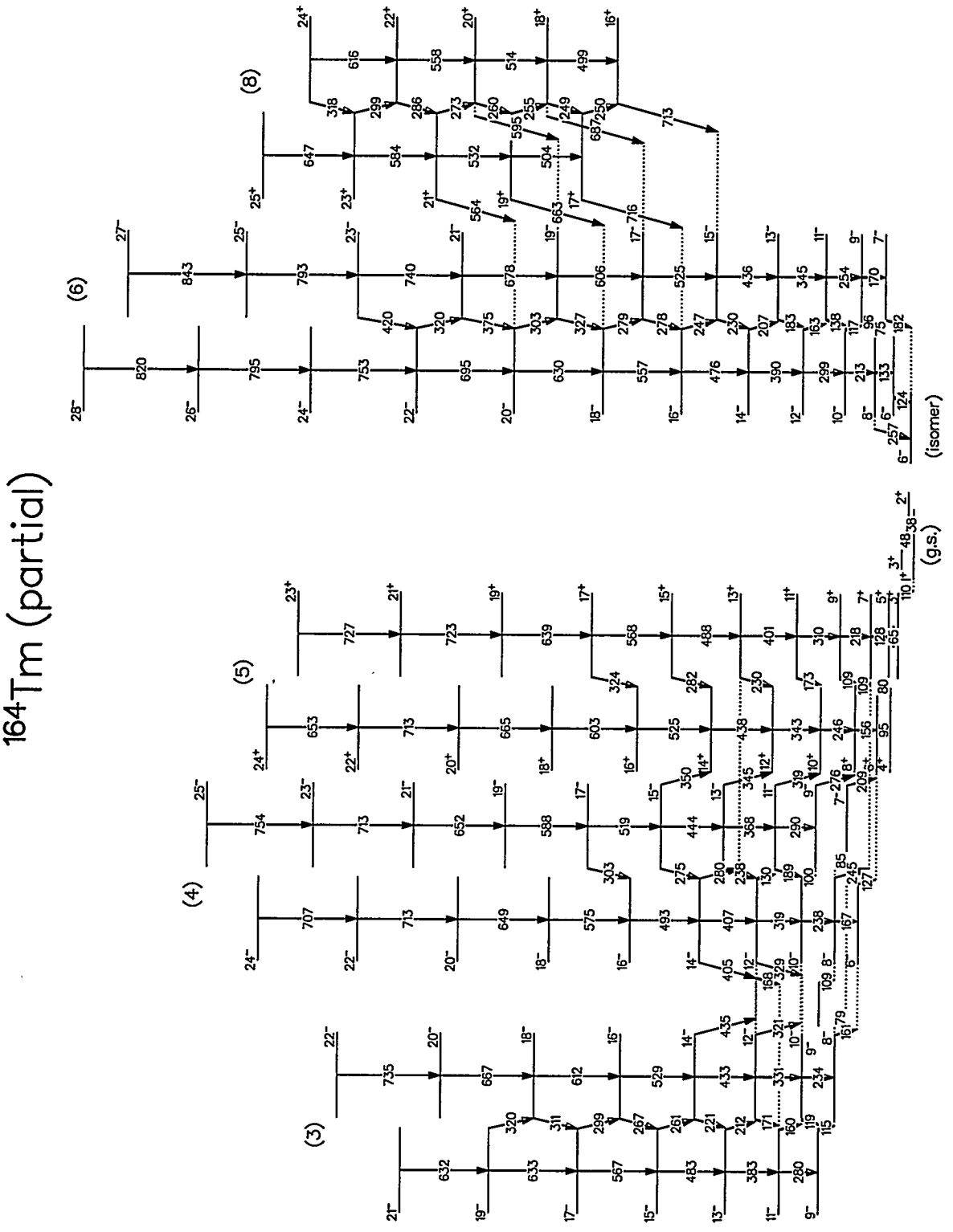


FIG. 1. Partial level scheme for $^{164}$Tm. The bands shown in the left half of this scheme feed directly the $K^{\Pi} = 1^{+}$ ground state, while the bands to the right are associated with the known $6^{-}$ isomer at $E_x \sim 30$ keV. Other sets of bands were observed (*cf.* Table I), which are excluded here due to space limitations. Band labels are introduced to ease the discussion.

between bands 6 and 8 it is reasonable to propose that their configurations have a $\pi h_{11/2}$ part in common (*cf.* Table I).

TABLE I. Expected proton-neutron configurations in $^{164}$Tm and proposed assignments to the bands observed. Left colums: Known proton and neutron levels in neighboring odd-$A$ nuclei labeled by their Nilsson quantum numbers and a symbol for spin "up" or "down" of the $j$-orbital. Right columns: Doublets of couplings for parallel and anti-parallel proton and neutron spins labeled by the $K = K_p \pm K_n$ value at the bandhead. Number in parenthesis is the label of the assigned band. Asterisk marks bands shown in Fig. 1.

| Couplings | | | |
|---|---|---|---|
| | | odd-odd $K^\pi$ | |
| p | n | lower ↑↑ | higher ↑↓ |
| 7/2[523] ↑ | 5/2[523] ↓ | $1^+$ (g.s.) | $6^+$ (8)* |
| 7/2[404] ↓ | 5/2[523] ↓ | $6^-$ (isomer, 7) | $1^-$ |
| 1/2[411] ↓ | 5/2[523] ↓ | $3^-$ | $2^-$ |
| 5/2[402] ↑ | 5/2[523] ↓ | $0^-$ | $5^-$ |
| 1/2[541] ↓ | 5/2[523] ↓ | $3^+$ | $2^+$ |
| 7/2[523] ↑ | 5/2[642] ↑ | $6^-$ (6)* | $1^-$ (3)* |
| 7/2[404] ↓ | 5/2[642] ↑ | $1^+$ (2) | $6^+$ (1) |
| 1/2[411] ↓ | 5/2[642] ↑ | $2^+$ (5)* | $3^+$ |
| 5/2[402] ↑ | 5/2[642] ↑ | $5^+$ | $0^+$ |
| 1/2[541] ↓ | 5/2[642] ↑ | $2^-$ (4)* | $3^-$ |
| 7/2[523] ↑ | 3/2[521] ↑ | $5^+$ (9) | $2^+$ |

*Magnetic properties of in-band transitions.* In Fig. 2, experimental $B(M1)/B(E2)$ ratios for four prominent bands are shown. The following observations can be made: *(i)* The bands 3 and 6, based on configurations containing $h_{11/2}$ protons, exhibit larger $B(M1)/B(E2)$ ratios than the other set of bands as is expected due to the larger proton g-factor ($g_K(h_{11/2}) > g_K(g_{7/2})$). *(ii)* The $M1$ strength is significantly larger for band 3 than for band 6. This demonstrates the effect of coupling the proton and neutron spins in different directions with a constructive or destructive effect on the $M1$ rates. Such a $B(M1)/B(E2)$ difference between bands 1 and 2 is not seen, likely because the g-factor for the $g_{7/2}$ proton orbital is small. For comparison, the results of TAC calculations assuming an axially symmetric nuclear shape with a deformation parameter $\epsilon_2 = 0.25$ are presented. The observed trend that the low-$K$ coupling yields larger $B(M1)/B(E2)$ ratios than the high-$K$ coupling is nicely reproduced by the TAC calculations over the full frequency range. Particularly for the low-$K$ coupling, the agreement between data and calculations is excellent, emphasizing that TAC predictions for the relative contributions of particle spins to the total spin $I$ are very reliable. For the two $\pi h_{11/2} \otimes \nu i_{13/2}$ couplings under discussion, significant tilt angles between the spin axis and the symmentry axis are suggested *i.e.* $\Theta \sim 66^\circ$ (high-$K$) and $77^\circ$ (low-$K$) at a representative frequency $\hbar\omega = 0.2$ MeV. The tilt angles predicted for the $\pi g_{7/2} \otimes \nu i_{13/2}$ couplings are very similar. In addition, the measured $B(M1)/B(E2)$ ratios for

bands 7 and 8, which are based on two- and four-quasiparticle configurations, are equally well reproduced by tilted solutions [8]. These examples show that for couplings of high-$K$ proton orbitals and medium or low-$K$ neutron orbitals tilted rotation is favored.

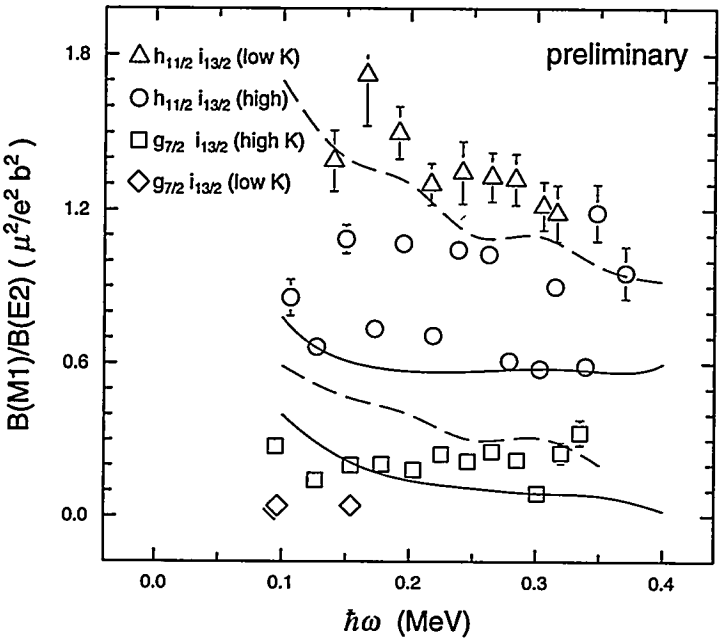


FIG. 2. Sample $B(M1)/B(E2)$ ratios as a function of rotational frequency and comparison with calculations using the TAC model. Data points: $\Delta$ (band 3), O (#6), $\square$ (#1), $\diamond$ (#2). Theoretical curves: dashed for low-$K$, full lines for high-$K$ configurations.

*Unexpected signature effect in the yrast band.* The $B(M1)/B(E2)$ ratios for band 6 show a staggering between even and odd spins with an inversion at $I = 16$. Such an effect at low frequency and spin ($I < 16$) in the band is unexpected, since there is no indication for any other difference between the signatures ($\Delta E' \sim 0$). While this staggering of branching ratios seems not to be explainable by a rotational model, one might speculate that vibrational degrees of freedom are responsible for the effect. In fact, the $E1$ transitions between bands 8 and 6 observed over a rather large spin range are indicative of significant octupole strength ($B(E1) \sim 1-5\times10^{-3} e^2 fm^2$) [8]. Perhaps an admixture of a *e.g.* $K = 1$ octupole component in the $\pi h_{11/2} \otimes \nu i_{13/2}$ configuration could affect the in-band transition rates.

## IV. CONCLUSIONS

Ten band structures each consisting of two signatures are observed in $^{164}$Tm. The rare observation of both $K = K_p \pm K_n$ couplings for the $\pi h_{11/2} \otimes \nu i_{13/2}$ and $\pi g_{7/2} \otimes \nu i_{13/2}$ configurations serves as an important test for model predictions at medium to high spin. The TAC model explains the main features of the near-yrast energy spectrum, *i.e.* the presence of low-lying bands with no signature splitting, and the closeness of two high-$K$ bands (#6 and 1) to the yrast line. For these bands, the TAC model reaches a level of

agreement with the measured $B(M1)/B(E2)$ branching ratios and spins barely achievable with other rotational models (*e.g.* particle+rotor). The calculations indicate angles of tilt (between the axes of symmetry and spin) as extreme as 66° at $\hbar\omega = 0.2$ MeV, where 90° is expected for a band with significant decoupling. A problem is the presence of a signature dependent staggering in the $B(M1)/B(E2)$ values for the $\pi h_{11/2}\nu i_{13/2}$ band (#6) in the absence of an energy splitting. This disagreement illustrates a shortcoming of the TAC model, which cannot account for any signature differences. But, other rotational models seem to have the same difficulty in explaining a signature difference in transition rates but not in energies. The present work on $^{164}$Tm is the first example for a successful application of the TAC model to a deformed odd-odd nucleus. Together with the high-$K$ bands of non-yrast states in neighboring Er and Yb nuclei, a consistent picture for tilted axis rotation in the region near $Z = 70$ is obtained.

Valuable discussions with S. Frauendorf and P.B. Semmes are gratefully acknowledged.

[1] S. Frauendorf, Nucl. Phys. A 557 (1993) 259c; and references therein.
[2] A. Brokstedt et al., Nucl. Phys. A 571, 337 (1994).
[3] A. Oliviera et al., Phys. Rev. C 47, R926 (1994).
[4] S. Drissi et al., Nucl. Phys. A 466, 385 (1987); and references therein.
[5] H.J. Jensen et al., Z. Phys. A 340, 335 (1991).
[6] H.J. Jensen et al., to be published.
[7] C.J. Gallagher and S.A. Moszkowski, Phys. Rev. 111, 1282 (1958).
[8] W. Reviol et al., to be published.

Work supported in part by U.S. DOE under contract No. DE-FG05-87ER40361.

# Properties of Rotational Bands at the Spin Limit in $A \sim 50$, $A \sim 65$ and $A \sim 110$ Nuclei

V.P. Janzen,[1] A.V. Afanasjev,[2,*] H.R. Andrews,[1] G.C. Ball,[1] J.A. Cameron,[3] M. Cromaz,[4] J. DeGraaf,[4] T.E. Drake,[4] S. Flibotte,[3] A. Galindo-Uribarri,[1] G. Hackman,[3,†] D.M. Headly,[5] J. Jonkman,[3] S. Mullins,[3‡] D.C. Radford,[1] I. Ragnarsson,[2] J.L. Rodriguez,[3] C.E. Svensson,[3] J.C. Waddington,[3] D. Ward[1] and G. Zwartz[4].

[1] *AECL, Chalk River Laboratories, Chalk River, ON, K0J 1J0 Canada*
[2] *Department of Mathematical Physics, Lund Institute of Technology, Lund, S-221 Sweden*
[3] *Department of Physics & Astronomy, McMaster University, Hamilton, ON, L8S 4M1 Canada*
[4] *Department of Physics, University of Toronto, Toronto, ON, M5S 1A7 Canada*
[5] *Department of Physics, Florida State University, Tallahassee, FL, 32306 U.S.A.*

**Abstract**

There is now widespread evidence for the smooth termination of rotational bands in $A \simeq 110$ nuclei at spins of 40-to-50$\hbar$. The characteristics of these bands are compared to those of bands recently observed to high spin in $^{64}$Zn and $^{48}$Cr, studied with the $8\pi$ $\gamma$-ray spectrometer coupled to the Chalk River miniball charged-particle-detector array.

A necessary requirement for establishing nuclear deformation and the associated collective rotational bands at low spin is the presence of a minimal number of valence particles (or particles and holes) outside a closed, spherical shell. The nucleus $^{122}_{54}Xe_{68}$, for example, has four protons and 18 neutrons outside the $^{100}$Sn doubly closed shell. This combination is sufficient to build up the strong correlations between valence nucleons which are necessary for deformation to occur, and which lead to a collective, rotational band built on the ground-state configuration. In nuclei which lie near closed shells the number of valence particles may be insufficient for collective rotational motion to be the favoured excitation mode producing low-lying states. This is the case for Sn and Sb nuclei ($Z = 50$ and 51, respectively), in which the states of lowest spin and excitation energy arise from combinations of the single-particle orbitals at near-spherical deformation. Nonetheless, if particle-hole excitations across the shell gap are not too costly in energy, it may be possible for the nucleus to deform and consequently for rotational bands to appear at modest spins and excitation energy. These structures are well known in $Z \approx 50$ nuclei [1] where they are known as "intruder-type" bands, since they spring from particle-hole configurations involving orbitals which intrude from high-lying shells. The spectrum shown in Fig. 1 illustrates the yrast intruder band in $^{109}$Sb, discovered [2] with the $8\pi$ spectrometer at Chalk River and subsequently studied [3, 4] in more detail with the Gammasphere spectrometer. The proton valence configuration in this case consists of an odd $h_{11/2}$ proton coupled to a deformed two-particle-two-hole (2p-2h) excited Sn core, *i.e.*, $\pi h_{11/2} \otimes (g_{9/2}^{-2} \otimes g_{7/2}^{2})$.

In a classical system, this type of rotational motion can continue to arbitrarily high spin. In atomic nuclei, the intrinsic motion of a finite number of nucleons places constraints on the quantum-mechanical observables, in particular the spin of the nucleus. In the modified-oscillator description, the maximum spin possible in a given ground-state band

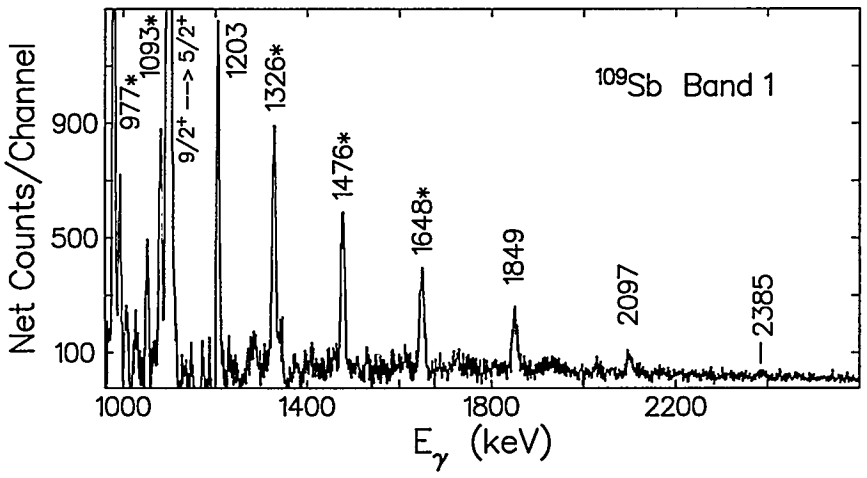


Figure 1: Gamma-ray spectrum of the yrast rotational band in $^{109}$Sb. Band members are labelled by energy; gating transitions are denoted by *. From Ref. [2].

can be obtained simply by summing the available oscillator quanta of Nilsson orbitals appearing between the nearest closed shell and the Fermi surface [5]. For heavy nuclei near the middle of closed shells this spin limit is relatively large, of order $A$ of the nucleus [5], and one would expect to observe rotational bands extending to extremely high spins.

Nevertheless, there are a number of cases where the ground-state rotational band appears to be interrupted at only modestly high spins, *e.g.*, $40\hbar$ in $^{158}$Er [6], and only $22\hbar$ in the above-mentioned $^{122}$Xe [7]. These occurences can be understood as a crossing of the yrast band with a very different sequence of states, terminating in a non-collective state (or states) of maximal spin which is (are) energetically favoured. For this reason, one can refer to such a process as "favoured band termination" [8]. It is often accompanied by sudden changes in the yrast line of the nucleus, as illustrated in Fig. 2 for the positive-parity states in $^{122}$Xe.

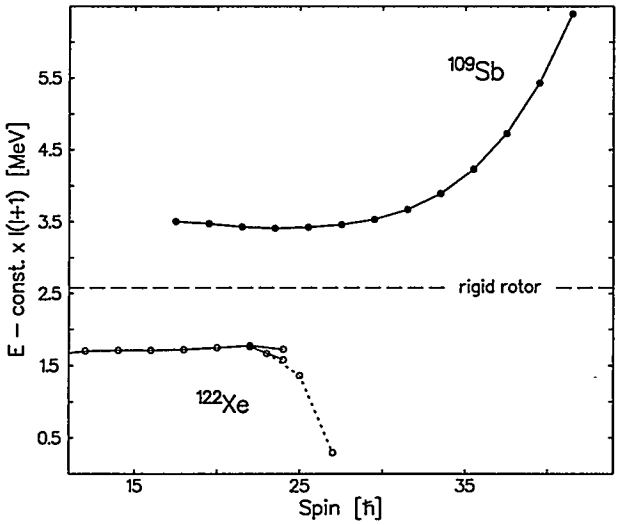


Figure 2: Comparison between the positive-parity states in $^{122}$Xe [7] and the yrast intruder band in $^{109}$Sb [3, 4]. A rigid-rotor reference, chosen to make the trajectories approximately flat close to spin $20\hbar$, has been subtracted in each case.

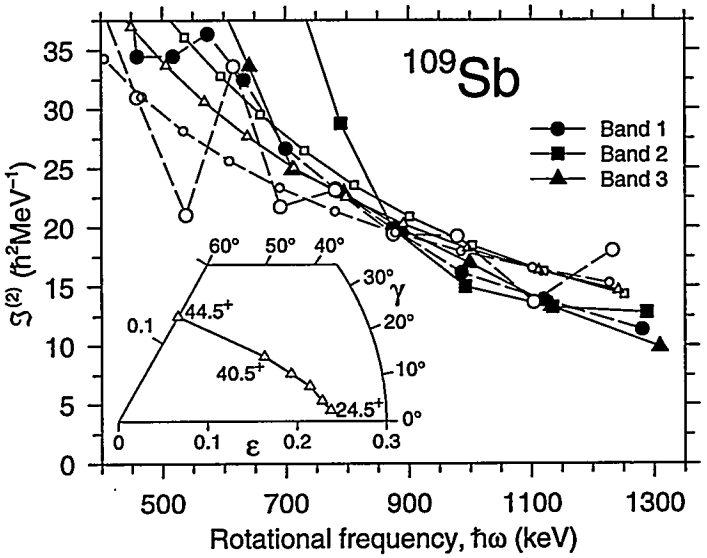


Figure 3: Comparison between experimental (filled) and theoretical (open symbols) $\mathcal{J}^{(2)}$ moments for the three most strongly populated bands in $^{109}$Sb. The theoretical values are smoothed by fitting a four-parameter $I(I+1)$ expansion to the 13 highest calculated energies in the band. For one of the bands the unsmoothed values are also shown as larger symbols. Inset: plot of the calculated intrinsic shape of the nucleus as a function of spin, in steps of $4\hbar$, for the rotational band predicted to be yrast at the highest spins observed. At intermediate spins the calculated shape is approximately prolate, while with increasing spin it gradually moves in the direction of increasing $\gamma$-deformation, becoming oblate non-collective ($\gamma = 60°$) at termination. From Ref. [8].

The intruder bands of $A \simeq 110$ Sb and Sn nuclei do not undergo the same process. Indeed, inspection of the $^{109}$Sb spectrum in Fig. 1 reveals an obvious feature which is inconsistent with the behaviour of $^{122}$Xe at high spin: the spacing between consecutive $\gamma$-ray peaks is smoothly increasing as a function of increasing $\gamma$-ray energy and thus as a function of spin. Consequently, when plotted relative to a rigid-rotor reference energy, as in Fig. 2, the trajectories of $^{109}$Sb and $^{122}$Xe are quite different.

Another way of illustrating the changes which occur at high spin is to invoke the dynamic moment of inertia, $\mathcal{J}^{(2)} = dI/d\omega \approx 4/\Delta E_\gamma$, as in Fig. 3. This quantity is constant for an ideal rigid rotor, and is sensitive to changes in structure and deformation; an added advantage is that the spins need not be known. The $\mathcal{J}^{(2)}$ moments in Fig. 3 undergo a substantial but smooth decrease with increasing $\gamma$-ray energy (and thus with increasing rotational frequency and spin). At the highest spins, the dynamic moments of inertia are only 1/2-to-1/3 the magnitude of the static moments, which are themselves comparable to the rigid-body moments for a deformation $\beta_2 \approx 0.25, \gamma \approx 0°$. Comparison with Nilsson-Strutinsky cranking calculations has led us to conclude that this smooth decrease signifies a continuous transition from high collectivity to a noncollective state [8]. In contrast to the behaviour of $^{122}$Xe, this change occurs gradually and with no change in the valence configuration; it is the "smooth termination" of a collective band in which the spin available from the constituent valence nucleons is gradually exhausted. The inset to Fig. 3 illustrates the changes in deformation which are predicted to occur during this process. A detailed description of "smooth band termination" from a theoretical perspective can be found in

Ref. [9]. For $^{109}$Sb, as well as for neighbouring $^{108}$Sn [10] and $^{110}$Sb [11], the agreement between theory and experiment is remarkably good, notably for the latter two which do have firm spin and parity assignments.

The excellent agreement between theory and experiment is satisfying, yet several questions arise. Amongst them are:

- Why don't we see more of this phenomenon, and in different mass regions?
- If there are more cases, what are the similarities and/or differences?
- Can we directly measure the decline in collectivity as a band smoothly terminates?

To begin with, bands with very similar $\mathcal{J}^{(2)}$ features have now been found in 13, possibly 14, $A \simeq 110$ nuclei, as shown in Fig. 4. There is evidence in 4 of these that at least one band has been observed up to the terminating state. Results for $^{110}$Sb, which are in very good agreement with theory, are discussed by Lane *et al.* in a contribution to these proceedings. Ragnarsson and Afanasjev discuss the evidence for band termination in the $A = 80$ mass region and in $^{117,118}$Xe, also in these proceedings.

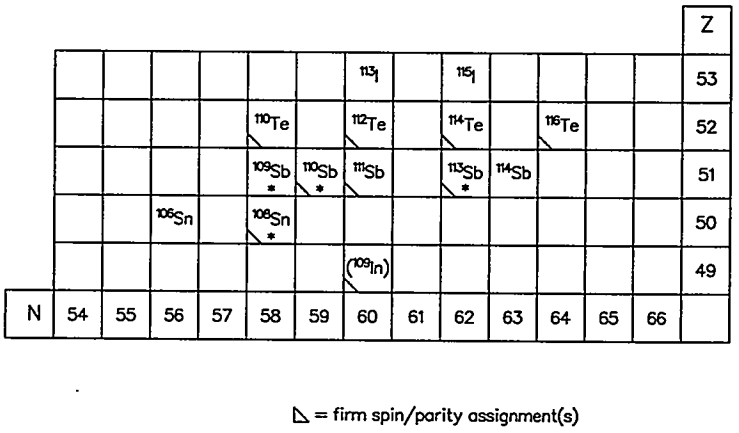


Figure 4: Known cases of smooth band termination in the $A \simeq 110$ mass region. A * denotes nuclei for which there is evidence of at least one terminating state.

Additional information, from lighter nuclei, comes from recent $8\pi$-spectrometer experiments concerning $A \simeq 65$ and $A \simeq 48$ nuclei. As it turns out, the primary conditions for smoothly terminating bands in $A \simeq 110$ nuclei, namely, enough valence particles (and/or holes) to generate collective bands at low spin, but not so many that the terminating spin is out of experimental reach, can be met in nuclei which are close to the $^{56}_{28}Ni_{28}$ and $^{40}_{20}Ca_{20}$ doubly closed-shell nuclei. Galindo-Uribarri *et al.* have studied $^{64}_{30}Zn_{34}$ [12] at high spins, using the $^{40}$Ca($^{28}$Si,4p) reaction at a beam energy of 115 MeV; the Chalk River miniball array [13], which comprises 44 CsI charged-particle detectors in near-$4\pi$ geometry, was used to detect the evaporated protons. In this nucleus, for which only non-collective states were previously known, they discovered a strongly coupled excited rotational band which extends from spin $(10)\hbar$ to $(22)\hbar$. The dynamic moment of inertia, shown in Fig. 5, undergoes the gradual decrease to very low values at high frequency which is characteristic of smooth band termination. Theoretical calculations, of the type used so successfully in the $A \simeq 110$ mass

region, suggest that the valence proton configuration is $\pi(f_{7/2}^{-1} \otimes g_{9/2}^{1}) \otimes p_{3/2}^{2}$, in other words, a 1p-1h proton excitation across the $Z = 28$ spherical shell gap. The six valence neutrons are in orbitals which lie above the corresponding $N = 28$ gap. In this case, it appears that experiment has not reached the point of termination which, according to theory, occurs at spin $26\hbar$.

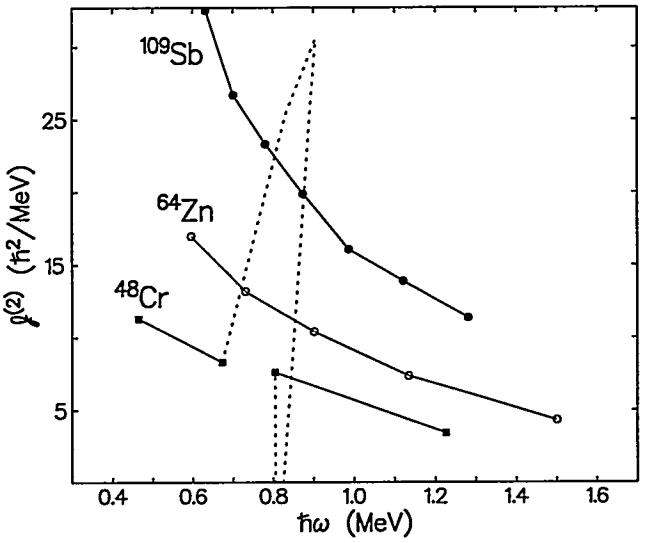


Figure 5: Dynamic moments of inertia for the yrast smoothly terminating bands in $^{109}$Sb, $^{64}$Zn and $^{48}$Cr. The dashed line indicates a band-crossing region in $^{48}$Cr (see text).

There is recently obtained data for the $N = Z$ nucleus $^{48}$Cr [14], from an $8\pi$-spectrometer experiment which also used the miniball to detect charged particles. The reaction $^{28}$Si($^{28}$Si,$2\alpha$) was used at a beam energy of 125 MeV. This nucleus differs from $^{109}$Sb and $^{64}$Zn in that $^{48}$Cr is known to be well deformed in its ground state, and to possess a collective ground-state rotational band. Attention has recently been drawn to the high-spin properties of this nucleus, primarily because it is the first instance in which a "heavy" collective nucleus has been analysed within a microscopic full shell model [15], with the results compared to the mean-field cranking approach used as the standard for interpretating rotational structures in heavier systems. Cameron *et al.* [14] have now observed the ground-state band up to $16\hbar$, which is the limiting spin within a $\pi \otimes \nu\, f_{7/2}$ shell space. The results have been confirmed [16] by a subsequent experiment with the Ga.S.P. spectrometer. The plot of $\mathcal{J}^{(2)}$ is complicated in this case by a rotational alignment which occurs at a frequency $\hbar\omega = 0.8$ MeV, giving rise to large fluctuations in the dynamic moments. Nevertheless, as shown in Fig. 5, it is clear that the overall trend in the $\mathcal{J}^{(2)}$ values is similar to that shown by the bands in $^{109}$Sb and $^{64}$Zn.

The similarities between smoothly terminating bands in the three different mass regions are may be summarized as follows:

- The dynamic moments of inertia gradually fall to very low values, 1/2-to-1/3 of the static moments. Another way of describing this is that the level energies *increase* rapidly as termination is approached, giving rise to the term "unfavoured" termination [8].

- Related to this, the $\gamma$-ray energies approaching termination become unusually high, approximately 3 MeV.

- Based on theory, the deformation gradually changes from collective prolate (little or no $\gamma$-deformation) to single-particle oblate ($\gamma = 60°$), and termination is reached when these bands exhaust the spin available from the valence configuration (*e.g.*, see inset to Fig. 3).

The third question raised above concerns the possibility of a direct measurement of the expected decline in collectivity during termination. Experiments aimed at measuring the lifetimes of these states are difficult. Although the bands are well populated at moderate spin (*e.g.*, the lowest-spin member of band 1 in $^{109}$Sb has approximately 30 % of the intensity of the strongest ground-state transition) the intensities drop off dramatically at high spin [3, 4]. In addition, the $\gamma$-ray energies are unusually high, approximately 3 MeV, so that detection efficiencies are low and lifetimes are relatively short, even if the highest states have little or no collectivity. So far, the best evidence comes from the lightest nucleus, $^{48}$Cr, as shown in Fig. 6. The $B(E2)$ values, as obtained from the Doppler shifts of $\gamma$ rays emitted from the recoiling residues, reflect considerable collectivity at low spin, in reasonable agreement with shell-model (SM) theory. The fluctuations in the middle of the band are not understood although it has been suggested that they are related to the alignment process mentioned above. At the highest spins, approaching the band's limit, the $B(E2)$ values drop off to a level which corresponds to approximately 5 single-particle units, again in agreement with theoretical predictions. It should be noted that experiments have been recently performed which are designed to measure lifetimes at high spin in heavier nuclei, notably $^{109}$Sb and $^{108}$Sn, but the results are unavailable at this writing.

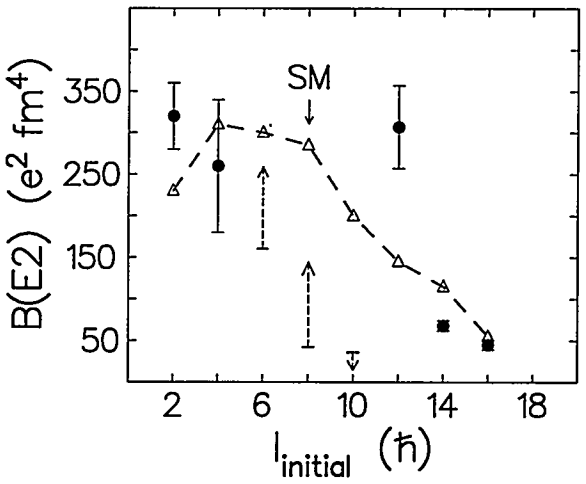


Figure 6: Measured and shell-model calculated (SM) [15] B(E2) values for $^{48}$Cr. The data above spin $I = 8$ are taken from Cameron *et al.* [14]. For $I = 6, 8$ and 10, only experimental limits are available.

In summary, there are now a considerable number of examples of smooth band termination in the $A \simeq 110$ region, and, most recently, good evidence for similar occurrences in

$^{64}$Zn and $^{48}$Cr. We anticipate that further experimental results will shed light on the existence of such bands in even more nuclei, and provide direct evidence for the expected loss of collectivity as termination is reached.

The efforts of the staff at the TASCC acccelerator laboratory in Chalk River are gratefully acknowledged. This work has been supported by the Canadian NSERC and Swedish NSRC.

* *Permanent address: Nuclear Research Center, Latvian Academy of Sciences, LV-2169 Salaspils, Latvia*

† *Present address: Physics Division, Argonne National Laboratory, Argonne IL 60439, U.S.A.*

‡ *Present address: Department of Nuclear Physics, RSPhysSE, Australian National University, Canberra ACT 0200, Australia*

# References

[1] V.P. Janzen, Phys. Scripta **T56** (1995) 144.

[2] V.P. Janzen *et al.*, Phys. Rev. Lett. **72** (1994) 1160.

[3] D.B. Fossan *et al.*, Proc. of the Conf. on Physics from Large $\gamma$-ray Detector Arrays, Berkeley, CA, August, 1994 (LBL Report No. LBL-35687, 1995) Vol. 2, p.194.

[4] H. Schnare *et al.*, Phys. Rev. C (in press).

[5] A. Bohr and B.R. Mottelson, *Nuclear Structure* (Benjamin, New York, 1975), Vol. 2.

[6] J. Simpson *et al.*, Phys. Lett. B **327** (1994) 187, and references therein.

[7] J. Simpson, H. Timmers, M.A. Riley, T. Bengtsson, M.A. Bentley, F. Hanna, S.M. Mullins, J.F. Sharpey-Schafer and R. Wyss, Phys. Lett. B **262** (1991) 388.

[8] I. Ragnarsson, V.P. Janzen, D.B. Fossan, N.C. Schmeing and R. Wadsworth, Phys. Rev. Lett. **74** (1995) 3935.

[9] A.V. Afanasjev and I. Ragnarsson, Nucl. Phys. **A591** (1995) 387.

[10] R. Wadsworth *et al.*, Phys. Rev. C **53** (1996) 483.

[11] G.L. Lane *et al.*, contribution to these proceedings.

[12] A. Galindo-Uribarri, G.C. Ball, V.P. Janzen, D.C. Radford, D. Ward, I. Ragnarsson and D.M. Headly, abstract submitted to this conference, and to be published.

[13] A. Galindo-Uribarri, Prog. Part. Nucl. Phys. **28** (1992) 463.

[14] J.A. Cameron *et al.*, Phys. Lett. B (in press).

[15] E. Caurier, J.L. Egido, G. Martinez-Pinedo, A. Poves, J. Retamosa, L.M. Robledo and A.P. Zuker, Phys. Rev. Lett. **75** (1995) 2466.

[16] S. Lenzi *et al.*, Z. Phys. **A354** (1996) 117.

# First Excited States in Doubly-Odd $^{110}$Sb: Smooth Band Termination in the $A \approx 110$ Region.

G.J. Lane[1], D.B. Fossan[1], I. Thorslund[1], P. Vaska[1], R.G. Allat[2], E.S. Paul[2], L. Käubler[3,4], H. Schnare[4], I.M. Hibbert[5], N. O'Brien[5], R. Wadsworth[5], W. Andrejtscheff[6], J. de Graaf[7], J. Simpson[8], I.Y. Lee[9], A.O. Macchiavelli[9], D.J. Blumenthal[10], C.N. Davids[10], C.J. Lister[10], D. Seweryniak[10], A.V. Afanasjev[11,12] and I. Ragnarsson[11]

[1] Department of Physics, State University of New York at Stony Brook, NY 11794-3800
[2] Oliver Lodge Laboratory, University of Liverpool, Liverpool L69 3BX, United Kingdom
[3] Institut für Kern- und Teilchenphysik, TU Dresden, Mommsenstr. 13, D-01062 Dresden, Germany
[4] Institut für Kern- und Hadronenphysik, FZ Rossendorf, Postfach 510119, D-01314 Dresden, Germany
[5] Department of Physics, University of York, Heslington Y01 5DD, United Kingdom
[6] Institute for Nuclear Research and Nuclear Energy, Bulgarian Academy of Sciences, Tzarigrad Chaussee 72, BG-1784 Sofia, Bulgaria
[7] Department of Physics, University of Toronto, ON M55 1A7, Canada
[8] CCLRC Laboratory, Daresbury, Warrington WA4 4AD, United Kingdom
[9] Lawrence Berkeley National Laboratory, Berkeley, CA 94720
[10] Argonne National Laboratory, Argonne, IL 60439
[11] Department of Mathematical Physics, Lund Institute of Technology, Box 118, S-22100 Lund, Sweden
[12] Nuclear Research Centre, Latvian Academy of Sciences, LV-2169, Salaspils, Miera str. 31, Latvia

**Abstract**

Excited states have been identified for the first time in $^{110}$Sb in a comprehensive series of $\gamma$-spectroscopy experiments, including recoil-mass and neutron-fold measurements. Three high-spin decoupled bands with configurations based upon 2p-2h excitations across the $Z = 50$ shell gap, are observed to show the features of smooth band termination, the first such observation in an odd-odd nucleus. The yrast intruder band has been connected to the low spin levels and is tentatively identified up to its predicted termination at $I^{\pi} = (45^{+})$. Detailed configuration assignments are made through comparison with configuration-dependent cranked Nilsson-Strutinsky calculations; excellent agreement with experiment is obtained. The systematic occurrence of smoothly terminating bands in the neighbouring isotopes is discussed.

## 1 Introduction

The $Z = 50$ region exhibits a wealth of collective structures, coexisting with the expected single-particle features. For example, prolate collective bands have long been known to occur at moderate excitation energies in the antimony [1] and tin [2] isotopes, built upon configurations involving the excitation of protons across the shell gap via the $\pi g_{9/2} - \pi g_{7/2}$ level crossing at $\beta \sim +0.2$. Perhaps the best example is $^{117}$Sb [3], in which a rather complete set of rotational structures based upon 1p-1h and 2p-2h excitations are known. More recently, the lighter isotopes with $Z \geq 50$ and $A \approx 110$ have been studied with heavy beams and the new generation of arrays, extending our knowledge of the collective intruder bands to very high spin. It has been found that most of the decoupled bands built upon 2p-2h excitations exhibit a decrease in the dynamic moment-of-inertia with spin to unusually low values, typically one-third to one-half of the rigid-body value. This has been interpreted as a gradual alignment of the valence nucleons outside of the $Z = N = 50$ closed shells, resulting in the nuclear shape crossing the $\gamma$-plane, smoothly changing over a sequence of many transitions from a collective prolate shape ($\gamma = 0°$) to a non-collective oblate shape ($\gamma = +60°$) [4, 5]. When all the valence particles (and holes) have aligned, the band sequence terminates. Due to the gradual nature of the process and the fact that a single configuration

is followed all the way from the low-spin collective regime up until the point where the band terminates, this feature has been called smooth band termination.

So far, smoothly terminating bands have been observed to near termination spins in $^{106,108}$Sn [6, 7], $^{109,111,113}$Sb [8, 9, 10] and $^{114}$Te [11]. Of all the bands seen in these nuclei, few have been connected to the low spin states and thus most do not have firm spin assignments. Nevertheless, estimates of the spin values can be obtained from feeding arguments, giving excellent agreement with theoretical calculations for a number of cases, in particular for $^{109}$Sb, in which four bands have been observed up to their smooth terminations [8].

Recent calculations predicted that the neighbouring nucleus, $^{110}$Sb, should exhibit a smoothly terminating band that would be yrast over a large range of spins [5]. The current paper reports the first observation of excited states in this neutron deficient nucleus[a], including three decoupled bands showing the features of smooth termination, one of which is the previously predicted yrast configuration.

[a]Pan *et al.* have also identified excited states in $^{110}$Sb, as evidenced by their abstract submitted to this conference.

## 2 Experimental Method and Results

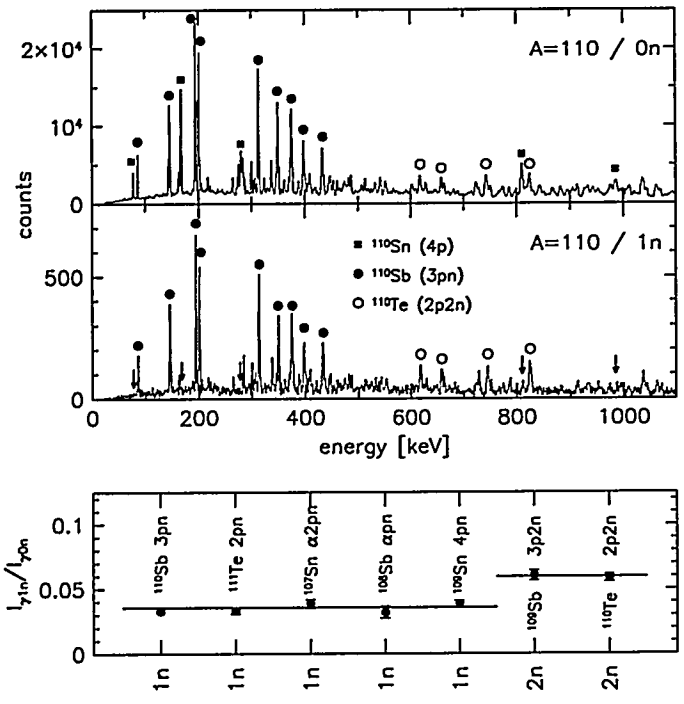


Figure 1: Spectra measured in coincidence with $A = 110$ residues and zero or one neutron. The lowest panel shows the intensity ratios measured for $\gamma$-rays in coincidence with zero and one neutron.

High spin states in $^{110}$Sb were populated in three different experiments as summarised in Table 1. The upper panels of Figure 1 show the $\gamma$-ray spectra measured (at Argonne) in coincidence with $A = 110$ residues and zero or one neutron. Note how the neutron coincidence requirement removes the $\gamma$-rays from $^{110}$Sn (4p channel) in the lower spectrum. The relative intensity ratios for the $\gamma$-rays in the zero and one-neutron gated spectrum give a measure of the neutron fold associated with the different reaction channels, as shown in the bottom panel. The ratio averaged over the different $\gamma$-rays assigned to $^{110}$Sb clearly indicates a single neutron is evaporated, and, since $A = 110$, a 3pn reaction channel.

With the positive assignment of $\gamma$-rays to $^{110}$Sb, the high-fold GAMMASPHERE data set was predominantly used to construct the level scheme. The data were unfolded into $\sim 2.3 \times 10^9$ $\gamma\gamma\gamma$ coincidences and incremented into a RADWARE cube, while the LEVIT8R software was used to project background-subtracted, gated coincidence spectra. Data from a third backed target experiment performed at the Hahn-Meitner Institute provided important lifetime information.

Fig. 2 presents a partial level scheme for $^{110}$Sb showing three decoupled bands at high spin feeding into both an intensely populated strongly coupled band and a number of irregularly spaced spherical states. The labelled spins and parities are deduced from a DCO analysis in

Table 1: Experiments performed

| Reaction | Energy [MeV] | Target [mg/cm$^2$] | Location | Detectors |
|---|---|---|---|---|
| $^{54}$Fe($^{59}$Co,2pn) | 230 | 2 × 0.440 | Berkeley | EI-GAMMASPHERE (36 × 80% dets) |
| $^{56}$Fe($^{58}$Ni,3pn) | 240 | 0.590 | Argonne | AYEBALL (9 × 25% and 7 × 80% dets) + FMA + 15 neutron dets. |
| $^{55}$Mn($^{58}$Ni,2pn) | 240 | 2.0 + 23 of Au | Hahn-Meitner Institute | OSIRIS (11 × 25-35% dets) |

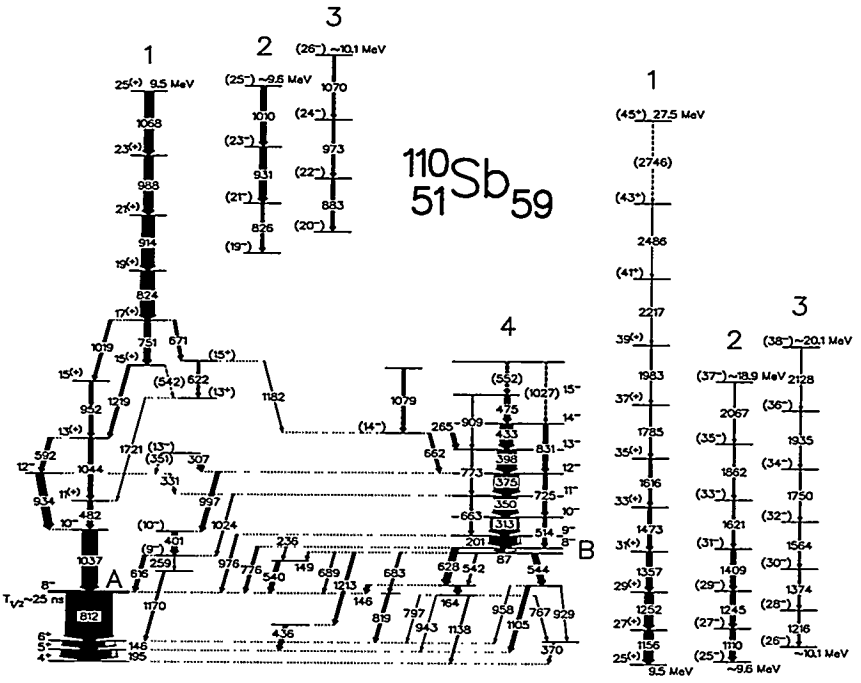


Figure 2: Partial level scheme for $^{110}$Sb with the high-spin extensions of bands 1, 2 and 3 on the right drawn to half-scale. All the spins and parities are tentative since the ground state spin is not definitively known (see text).

which the levels marked A and B are assumed to have $J^\pi = 8^-$. These two assignments follow from systematic features known in the heavier odd-odd antimony isotopes. Firstly, all the heavier odd-odd antimony isotopes exhibit an isomer with spin and parity $8^-$ [12], formed from the $\pi h_{11/2} \otimes \nu d_{5/2}$ and $\pi h_{11/2} \otimes \nu g_{7/2}$ spherical configurations in the lighter and heavier isotopes, respectively. The isomeric state identified in $^{110}$Sb in the present experiments has similarities with the $8^-$ isomer in the heavier isotopes. Another feature common to the heavier isotopes is a strongly coupled band with a $9^- \rightarrow 8^-$ transition of around 200 keV [12], formed from a rotation-aligned $h_{11/2}$ neutron coupled to the high-$\Omega$ $g_{9/2}$ proton hole; band 4 in Fig. 2 is just such a structure.

Using the $8^-$ assignment to the isomer as a starting point, the DCO analysis has determined the spins of band 1, although the band parity assignment rests upon the assumed E1 character of the 592 and 482 keV transitions. The spins and parities of bands 2 and 3 have been estimated from their observed decay patterns. Note also that the authors of Ref. [13] assign $3^+$ ground states to both $^{108}$Sb and $^{110}$Sb, deduced from the observed feeding of the $2^+$ and $4^+$ levels in $^{108,110}$Sn during the $\beta^+$ and EC decay of $^{108,110}$Sb. However, Ref. [14] gives the ground state spin and parity of $^{108}$Sb as $4^+$ on the basis of measured angular correlations for some of the low-spin transitions and comparison with shell model calculations. For $^{110}$Sb, assuming the isomer has $J^\pi = 8^-$, the DCO analysis also gives a $4^+$ ground state.

## 3 Discussion

For nuclei in the $A \approx 110$ region and configurations involving only a few holes in the $\pi g_{9/2}$ subshell, calculations with a configuration-dependent cranked Nilsson-Strutinsky model predict that,

due to the limited valence space, the collective bands built on a particular configuration eventually terminate [4, 5]. As discussed in the introduction, such bands undergo a gradual shape change as the valence particles and holes align. This results in a decrease of the dynamic moment-of-inertia with spin, and, since $\mathcal{J}^{(2)} \propto 1/\Delta E_\gamma$, an increase in the $\gamma$-ray energy spacings within the band. Bands 1, 2 and 3 all exhibit this phenomenon. It is also found that the building of the last spin units before termination has a large energy cost, determined mainly from (i) the difficulty of aligning the high-$\Omega$, $\pi g_{9/2}$ holes and (ii) the fact that the neutron $(d_{5/2}/g_{7/2})$ sub-shells are essentially half-filled [5]. This unfavoured band termination is manifest as a characteristic minimum when the excitation energy relative to a rigid rotor reference is plotted versus spin $(E - E_{RLD})$.

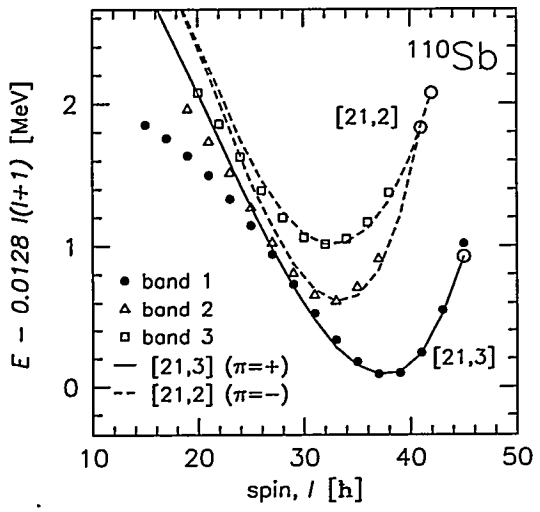


Figure 3: Theoretical $E-E_{RLD}$ curves for the three bands calculated to be most favoured in the spin range $25 - 45\hbar$ (lines), compared to the three decoupled bands experimentally observed in $^{110}$Sb (symbols). Large open circles indicate the predicted terminating states.

This can be seen in Fig. 3, where the solid and dashed lines are the results of calculations within the formalism of Ref. [5] for the three rotational bands predicted to lie lowest in energy in the spin region $25-45\hbar$. Note that the theoretical results for the [21,3] configuration had been presented prior to the experimental results being obtained (see Fig. 13 of Ref. [5]). The notation used here to describe the configurations is the same as Ref. [5], namely $[p_1 p_2, n]$ where $p_1$ is the number of $g_{9/2}$ proton holes, $p_2$ the number of $h_{11/2}$ protons and $n$ the number of $h_{11/2}$ neutrons.

The data points in Fig. 3 are the experimental energies of the three decoupled bands. Since the pairing correlations are neglected in the calculations, when comparing theory and experiment, the absolute energies relative to the ground state should not be considered, but rather the energy relative to some high spin state. Thus the excitation energies of the theoretical bands have been adjusted in Fig. 3 so that the predicted [21,3] configuration agrees with band 1 at $I = 37\hbar$. Excellent agreement between theory and experiment for the region above $25\hbar$ is obtained. Note that the tentative 2746 keV transition would decay from the terminating state with $I^\pi = 45^+$.

The states which bands 2 and 3 feed suggest that these bands have the opposite parity to band 1, making it natural to associate them with the two signatures of the [21,2] configuration. Since linking transitions connecting the bands to the low spin states have not been found it is necessary to estimate their spins. Experimentally it is found that bands 2 and 3 feed into states with known spins of up to $18\hbar$ (full level scheme to be published), so that the suggested spins in Fig. 2 are reasonable. To make a comparison with theory, the experimental bandheads for bands 2 and 3, which have unknown energies, are adjusted so that the minimum of the $E - E_{RLD}$ curves agrees with the energies of the theoretical predictions. With this reasonable choice there is again excellent agreement with theory in the region above $25\hbar$, as shown in Fig. 3. Furthermore, the measured intensities for the three bands are in qualitative agreement with their predicted relative excitation energies. In contrast to band 1, neither bands 2 nor 3 are observed up to termination, probably because at high spin they are predicted to rise above the yrast line (see Fig. 3), with a consequent loss in feeding. Note also, that for all three bands the theory begins to deviate from experiment at low spin where pairing becomes increasingly important [5, 8].

With the detailed configuration assignments it is now possible to compare the smoothly ter-

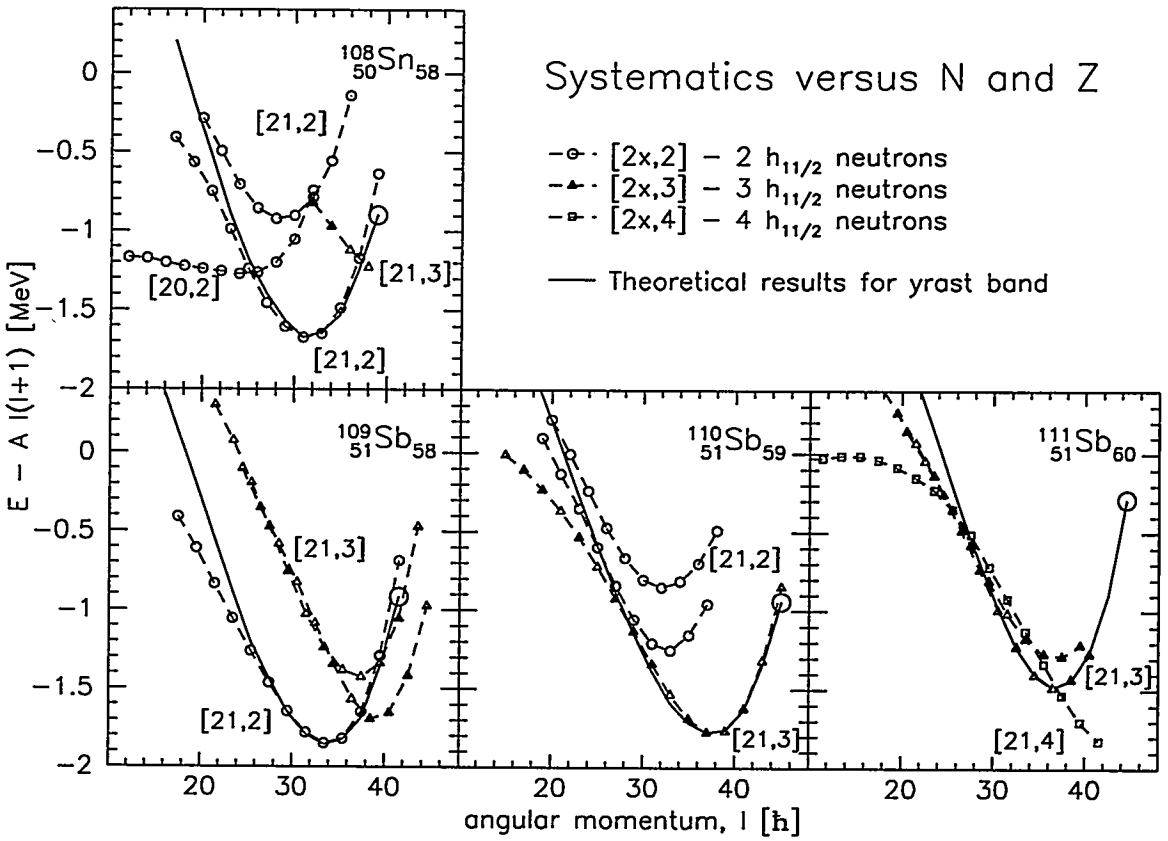


Figure 4: Experimental systematics of smoothly terminating bands observed in the isotopes neighbouring $^{110}$Sb. The overall energy scales for the different isotopes have been shifted to bring them all into the same energy region, while the solid lines are the results of theoretical calculations for the yrast band in each case. Of the bands plotted, only the favoured signatures of the following configurations have known spins: [20,2] and [21,2] in $^{108}$Sn, [21,3] in $^{110}$Sb and [21,4] in $^{111}$Sb.

minating bands observed in $^{110}$Sb to those observed in the neighbouring nuclei, building upon the summary previously presented in Ref. [15]. Figure 4 shows the three smoothly terminating bands most intensely populated in four different isotopes, together with their assigned configurations. The results of theoretical calculations for the yrast band are shown as solid lines for each isotope.

The yrast terminating bands which are observed in $^{108}$Sn are the [20,2], [21,2] and [21,3] configurations, going from lower to higher spins, respectively [7]. Thus we see that the simple $(g_{7/2})^2(g_{9/2})^{-2}$ proton excitation occurs at lower spin, while to form the yrast line at higher spins, the $(g_{7/2}h_{11/2})(g_{9/2})^{-2}$ excitation is more favourable. At the very highest spins observed, an extra $h_{11/2}$ neutron is needed to create the necessary angular momentum.

In the $N = 58$ isotone, $^{109}$Sb, the yrast neutron configurations are exactly analogous, with the [21,2] occurring at lower spin than the [21,3] configuration [8]. Since the $(g_{7/2}h_{11/2})(g_{9/2})^{-2}$ proton excitation begins to dominate at higher spin in $^{108}$Sn, it is not surprising that with the slightly higher Fermi level in the antimony isotope, the extra valence proton prefers to go into the $h_{11/2}$ sub-shell. Indeed calculations for the antimony isotopes show that the [20,n] configurations generally lie far above the yrast line.

In $^{110}$Sb, the [21,3] configuration begins to dominate over the [21,2] configuration due to the rise of the neutron Fermi level within the $h_{11/2}$ sub-shell. Along a similar vein, in $^{111}$Sb the [21,3] and [21,4] configurations are both observed to lie at the yrast line [5, 9]. In all cases the theoretical

calculation for the yrast band gives excellent detailed agreement for spins above $25\hbar$, but deviates at lower spins due to the increase in the pairing correlations.

Moving on to nuclei not shown in Figure 4, $^{112}$Sb currently provides a gap in the systematics. However, $^{113}$Sb is known, with the [21,4] configuration forming the yrast line and the [21,3] configuration lying somewhat above it [10, 15]. The observed configurations in the $N = 62$ isotone, $^{114}$Te [11], are identical to $^{113}$Sb except with the addition of the extra valence proton in the $h_{11/2}$ sub-shell, i.e. [22,4] and [22,3]. In these heavier isotopes, which have more valence particles and a higher level density, the calculations begin to lose the detailed agreement which is seen in Figure 4. Thus for the $N = 62$ isotones, the position in spin of the minima of the $E - E_{RLD}$ curves is well reproduced by calculations; however, the slopes of the curves around the minima are not, as can be seen in Figs. 5 and 6 of Ref. [15] and Fig. 2 of LaFosse's abstract to this conference [10].

## 4 Conclusions

Excited states have been observed in $^{110}$Sb for the first time, including three decoupled bands with configurations based upon 2p-2h intruder excitations, which show the characteristic properties of smooth band termination. The yrast band, which has been linked to the low spin states and has known spins, is in excellent agreement with the results of prior calculations for the [21,3] configuration, while the other two unlinked bands are believed to be the two signatures of the [21,2] configuration. The changing structure of the smoothly terminating bands seen in the neighbouring isotopes can be understood in terms of the varying proton and neutron Fermi levels.

**Acknowledgements:** This work was supported by the NSF (U.S.A.), EPSRC (U.K.), DOE (U.S.A.), BMBF (Germany) and the Swedish Natural Science Research Council. A.V.A. and I.R. are grateful for financial support from the Crafoord Foundation (Lund, Sweden) and the Royal Swedish Academy of Sciences. The authors are grateful to many colleagues at Berkeley, Argonne and the H.M.I. for their help in the various experiments.

## 5 References

[1] A.K. Gaigalas *et al.*, Phys. Rev. Lett. **35**, 555 (1975); R.E. Shroy *et al.*, Phys. Rev. C **19**, 1324 (1979).
[2] J. Bron *et al.*, Nucl. Phys. **A318**, 335 (1979).
[3] D.R. LaFosse *et al.*, Phys. Rev. Lett. **69**, 1332 (1992).
[4] I. Ragnarsson *et al.*, Phys. Rev. Lett. **74**, 3935 (1995); I. Ragnarsson, these proceedings.
[5] A.V. Afansjev and I. Ragnarsson, Nucl. Phys. **A591**, 387 (1995).
[6] R. Wadsworth *et al.*, Phys. Rev. C **50**, 483 (1994).
[7] R. Wadsworth *et al.*, Phys. Rev. C **53**, 2763 (1996).
[8] V.P. Janzen *et al.*, Phys. Rev. Lett. **72**, 1160 (1994); H. Schnare *et al.*, Phys. Rev. C, in press.
[9] D.R. LaFosse *et al.*, Phys. Rev. C **50**, 1819 (1994).
[10] V.P. Janzen *et al.*, Phys. Rev. Lett. **70**, 1065 (1993); D.R. LaFosse *et al.*, abstract submitted to this conference and to be published.
[11] I. Thorslund *et al.*, Phys. Rev. C **52**, R2839 (1995).
[12] *Table of Isotopes,* 7th ed., edited by C.M. Lederer and V.S. Shirley, (Wiley, New York, 1978).
[13] K. Oxorn *et al.*, Z. Phys. **A279**, 289 (1976).
[14] J. Cederkäll *et al.*, Nucl. Phys. **A581**, 189 (1995).
[15] D.B. Fossan, *Workshop on Gammasphere Physics*, Berkeley, 1995, (World Scientific), in press.

# Rotational bands terminating at maximal spin in the valence space

I. Ragnarsson and A.V. Afanasjev[1]

Department of Mathematical Physics, Lund Institute of Technology,
PO Box 118, S-22100, Lund, Sweden

**Abstract:** For nuclei with mass $A \lesssim 120$, the spin available in "normal deformation configurations" is experimentally accessible with present detector systems. Of special interest are the nuclei which show collective features at low or medium-high spin and where the corresponding rotational bands with increasing spin can be followed in a continuous way to or close to a non-collective terminating state. Some specific features in this context are discussed for nuclei in the $A = 80$ region and for $^{117,118}$Xe.

The nucleus $^{158}$Er and its neighbours were the first heavy nuclei where terminating bands were predicted [1] and subsequently discovered [2]. The concept of terminating bands has then also been introduced for $Z \sim 54, A \sim 120$ nuclei but for a long time, no very high spin states were observed in this region and no convincing example of a *band* which terminates was found. Subsequently, the rotational bands which are formed for nuclei around $^{109}$Sb in configurations with typically 2 holes in the $Z = 50$ core were explored. In experiment, these bands can be followed [3] when they gradually lose collectivity with increasing spin up to termination at $I \geq 40\hbar$ [4, 5]. Recently, it has become possible to study rotational bands in even lighter nuclei up to spin around $I = 30\hbar$ or more. A study of the available single-particle orbitals reveals that this is close to the maximum spin which can be built in the valence space for nuclei with $A \lesssim 100$. Therefore, as illustrated in fig. 1, for nuclei with $A = 40 - 120$, there are now many examples where the notion of band termination is appropriate.

In fig. 1, we indicate regions where nuclear rotational bands have been studied to termination or close to termination. Furthermore, the orbitals available for $Z, N = 20-28, 28-50$ and beyond $Z, N = 50$ are indicated on the left hand side of this figure. In this contribution, we will discuss some nuclei in the middle of the deformed $28 \leq Z, N \leq 50$ region and the $^{117,118}$Xe nuclei in the outskirts of the $50 \leq Z, N \leq 82$ region. Indicated in fig. 1 is also the $^{102}_{46}$Pd$_{56}$ nucleus which falls in the $Z < 50$, $N > 50$ deformed region but which is still on the left side of $\beta$-stability so that it can be studied to high spin in (HI,$xn$,...) reactions. In a recent Eurogam II experiment, the terminating spin in the ground band, $I = 32^+$, and other bands which appear to terminate for $I \sim 40$ have been observed [6]. The nucleus $^{48}$Cr also shows collectivity at low spin with a definite termination at $I = 16^+$ corresponding to the maximal spin in the $\pi(\mathrm{f}_{7/2})^4\ \nu(\mathrm{f}_{7/2})^4$ valence configuration [7]. The excitation energies are described to a high precision in shell model calculations including the full $N = 3$ shell [8]. Also in the Nilsson-Strutinsky cranking formalism considered here, it is straightforward to follow this band to termination. The termination is described in a more illustrative way than in the shell model but with considerably larger discrepancies between calculations and

[1]Perm. address: Nucl. Res. Center, Latvian Acad. of Sciences, LV-2169, Salaspils, Miera str. 31, Latvia

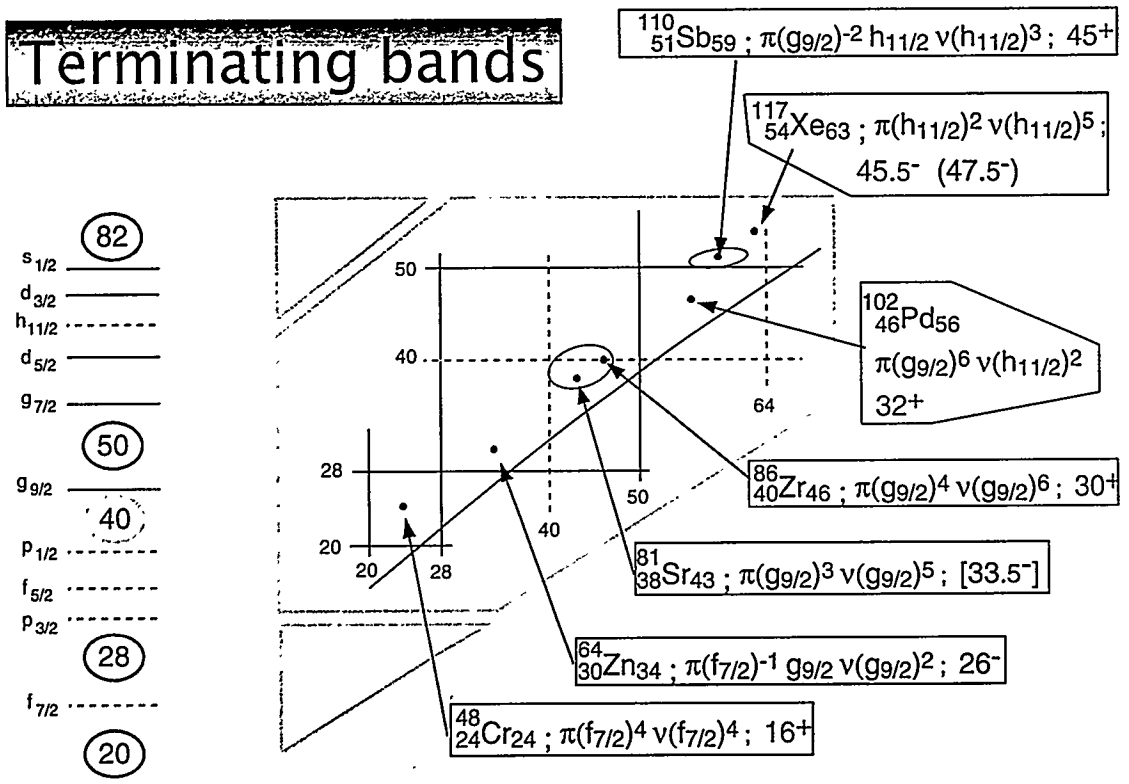


**Fig. 1.** Regions where nuclear rotational bands have been studied to termination or close to termination. Typical terminating configurations in representative nuclei and their maximum spin are indicated. Some of these nuclei are discussed by V.P. Janzen and G.J. Lane in their contributions to this conference. The orbitals available in the mass regions of interest are indicated on the left hand side.

experiment.

The theoretical results presented here have been obtained within the configuration-dependent shell-correction approach with the cranked Nilsson potential as described in [9], see also [4, 5]. The pairing correlations are neglected in the present calculations, so the results can be considered as realistic at reasonably high spin which, in general, depends on the mass region, say $I \gtrsim 15\hbar$ in the $A \sim 80$ region and $I \gtrsim 25\hbar$ in the $A \sim 120$ mass region. In the calculations, the full Nilsson Hamiltonian is diagonalized so when a configuration is described from the filling of different $j$-shells, this only corresponds to the main components of the wave-functions.

**$^{86}$Zr.** Let us now turn to the region of nuclei with $28 \leq Z, N \leq 50$. Terminating bands in this region were discussed from a theoretical point of view long ago [10] while it was only rather recently that experimental evidence for terminations in this region was reported for the nucleus $^{82}$Sr [11]. Here we will first consider the nucleus $^{86}_{40}Zr_{46}$ [12] which is on the borderline between deformed and transitional nuclei. This has the "advantage" that the maximal spin is somewhat lower than for the more collective nuclei in the middle of the region. The natural neutron configuration is $\nu(g_{9/2})^6$ relative to a $N = 40$ core with

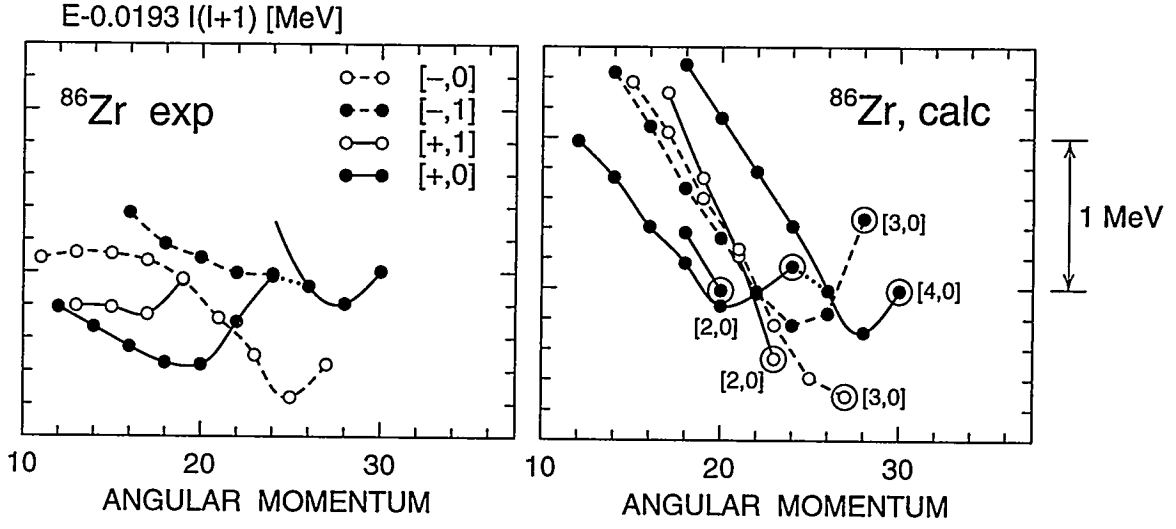


**Fig. 2.** Observed low-lying states in $^{86}$Zr compared with the calculated configurations. The energies are given relative to a $(\hbar^2/2J_{rig})I(I+1)$ reference, where the moment of inertia parameter $A = (\hbar^2/2J_{rig})$ is 0.0193 MeV. The same symbols as defined in the figure are used for the experimental bands and their theoretical counterparts. Terminating states are encircled. Configurations are labelled by [p,n] where p (n) is the number of proton (neutron) holes in the $N = 3$ orbitals. The figure is taken from ref. [12].

all $N = 3$ orbitals filled. This neutron configuration has a maximal spin of $I^n_{max} = 12^+$. Considering that the nucleus is somewhat deformed, the favoured proton configurations are $\pi(p_{3/2}f_{5/2}p_{1/2})^{-n}(g_{9/2})^n$ with $n = 2, 3$ and 4. The maximal proton spin in these configurations is $I^p_{max} = 12^+$ for $n = 2$, $15^-$ or $16^-$ for $n = 3$ and $18^+$ for $n = 4$. We also note that if for $n = 2$, both proton holes are in the $p_{1/2}$ subshell, the maximum proton spin is $I^p_{max} = 8^+$. Combining neutrons and protons in $^{86}$Zr, we do then expect low-lying configurations which terminate for $I_{max} = 20^+, 24^+, 27^-, 28^-$ and $30^+$. The energies of these configurations are illustrated in the right panel of fig. 2 where selected calculated bands [12] are shown relative to a rigid rotor reference. In the left panel, the most low-lying experimental sequences [12] are shown vs. the same reference. The general agreement between experiment and calculations is partly obtained by a slight adjustment of the modified oscillator parameters. The comparison with calculations suggests that one configuration terminates for $I = 24^+$ and that a new one takes over at $I = 26^+$.

While we do not expect the configuration which terminates for $I = 24^+$ to be strongly collective, the configuration which terminates for $I = 30^+$ is calculated as a smooth rotational band which, however, has lost pretty much of its collectivity when it is first observed experimentally at $I = 26^+$. Of special interest is the fact that requiring signature $\alpha = 0$ (even spin) for protons and neutrons separately, $I = 30^+$ is the highest spin which can be formed in the valence space for $^{86}$Zr. For negative parity, the terminating spin of the $\alpha = 1$ branch, $27^-$, is calculated much lower in energy than the $28^-$ state of the $\alpha = 0$ branch. This is consistent with the fact that the signature $\alpha = 1$ branch is observed to termination at $27^-$ while the signature $\alpha = 0$ branch is observed only to $I = 24^-$. We also note that for odd spins and positive parity, we calculate a low-lying $23^+$ state where the two $N = 3$ holes are in $f_{5/2}$ and $p_{1/2}$, respectively. This state is not observed in experiment, which is not too

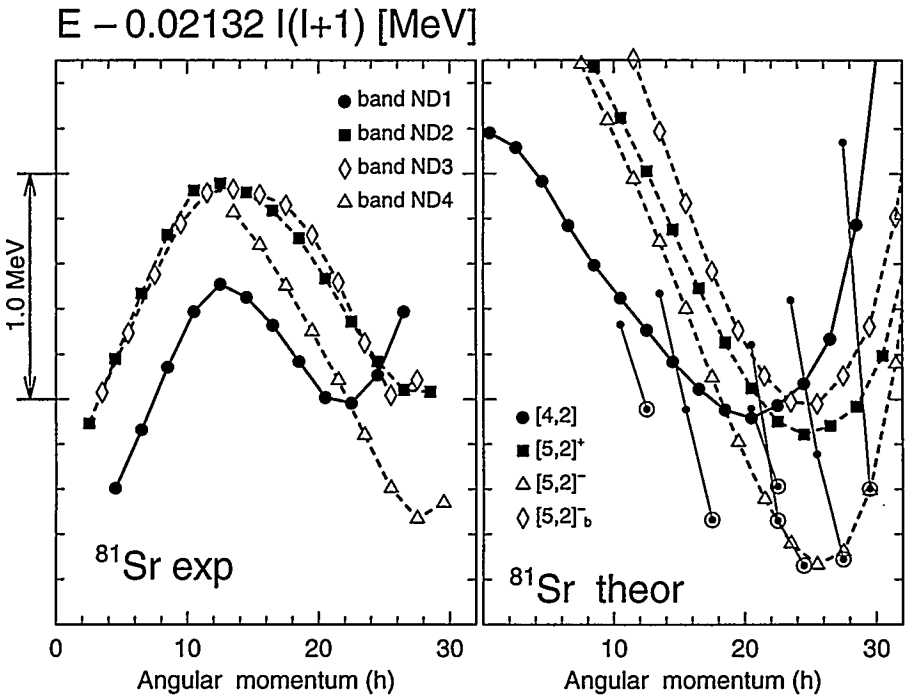


**Fig. 3.** The bands ND1-ND4 observed in $^{81}$Sr [13] compared with the calculated configurations, in a similar way as for $^{86}$Zr in fig. 2 but with the parameter $A = (\hbar^2/2J_{rig})$ equal to 0.02132 MeV. The same symbols are used for experimental bands and their theoretical counterparts. The bands which terminate in favoured way are shown by thin lines and their terminating states are encircled. Configurations are labelled by [p,n] where p (n) is the number of proton (neutron) holes in the $N = 3$ orbitals.

surprising considering the fact that the corresponding band is calculated to go away from yrast very quickly with decreasing spin.

**$^{81}$Sr.** Another interesting nucleus is $^{81}$Sr where, in addition to superdeformed bands, four rotational bands at normal deformation have recently been observed to spin values close to $30\hbar$ [13]. In fig. 3, these rotational bands are compared with the most low-lying calculated [14] bands where we have used the $A = 80$ parameters of Galeriu *et al.* [15]. The good agreement strongly suggests that our description is essentially correct. For spin values $I = 10 - 20\hbar$, these bands are triaxial close to oblate with $\gamma \approx -40°$ and $\varepsilon_2 \approx 0.25 - 0.30$. The corresponding potential energy minimum is mainly caused by a large gap in the neutron single-particle orbitals for the $\nu(f_{5/2}p_{1/2})^{-2}(g_{9/2})^5$ configuration. The most favoured $Z = 38$ proton configurations at this deformation are $\pi(p_{3/2}f_{5/2}p_{1/2})^{-4}(g_{9/2})^2$ and $\pi(p_{3/2}f_{5/2}p_{1/2})^{-5}(g_{9/2})^3$. It is then easy to calculate the maximum spin in these configurations which is in the range $I_{max} \approx 30.5 - 33.5\hbar$. The experimental bands are observed to typically $4\hbar$ below $I_{max}$ where the calculated deformation is $\gamma \approx -40°$ and $\varepsilon_2 \approx 0.15$. The bands appear to approach termination in a smooth way with the terminating state at rather high energy, possibly so high that it will be impossible to follow these bands to their respective $I_{max}$ spin. Indeed, it is questionable if these bands can be described as terminating because according to the calculations, the energy of the aligned $I = I_{max}$ state is so high that it is possible to build a

"collective" state at this spin at a somewhat lower energy. Then it is also possible to build even higher spin states at very high cranking frequencies in a similar way as has previously been discussed for the pure oscillator by Troudet and Arvieu [16].

In addition to the bands discussed above, we do also calculate other less collective configurations which terminate at low energy cost (*favoured termination*) as shown in fig. 3. They have similar excitations across the $Z, N = 40$ gap, however, the termination takes place at $\gamma = 60°$ and at a large quadrupole deformation $\varepsilon_2 \approx 0.2 - 0.25$. In fig. 3, one especially notes $I = 17.5^+$ state with the configuration $\pi(p_{1/2}\, f_{5/2}\, p_{3/2})^{-4}_2 (g_{9/2})^2_8 \otimes \nu(p_{1/2}\, f_{5/2}\, p_{3/2})^{-2}_0 (g_{9/2})^5_{7.5}$. This band has small collectivity connected with positive $\gamma$ deformation ($\gamma \sim 40°$) of several states before termination which might explain why it is not seen in experiment.

**$^{117}$Xe, $^{118}$Xe.** High spin structures of nuclei in the $A \approx 120$ region have generally been described as neutron particle-hole excitations relative to a $^{114}$Sn (semi-)closed core. Configurations with few excitations of this kind do often give low-lying aligned states but no real *bands* which can be said to terminate in these aligned states. With more particle-hole excitations, the spins of the fully aligned states become higher and, as illustrated below, terminating bands are formed. Then, it also seems more natural to describe the configurations relative to the $^{100}$Sn core. The nucleus $^{117}$Xe is then described by 4 protons and 13 neutrons relative to this core. In this nucleus, a rotational band has recently been observed to $I^\pi = 45.5^-$ [17]. It is natural to assume that this band is formed from a positive parity proton configuration in which case the odd parity is formed from an odd number of $h_{11/2}$ neutrons. Then, from the available single-particle orbitals, as illustrated in fig. 1, we see that the highest proton spin we can make is $16^+$ for the $(g_{7/2})^2(h_{11/2})^2$ configuration. Using only the $g_{7/2}$, $d_{5/2}$ and $h_{11/2}$ subshells, the highest neutron spin is $29.5^-$ for the $(g_{7/2}d_{5/2})^8(h_{11/2})^5$ configuration while if one (or two) neutrons are lifted to $d_{3/2}$ subshell, the highest neutron spin is $31.5^-$. Consequently, the maximum total spin in the valence space is then $45.5^-$ or $47.5^-$ suggesting that the experimental band has been observed to termination or $2\hbar$ below. This is under the assumption that no core excitations are involved. Considering that calculated bands involving core excitations are generally high in energy and showing very different properties than the observed band, such an assumption appears well founded.

In fig. 4, the observed and calculated bands are compared. In the calculations, we cannot easily trace excitations from the $(g_{7/2}d_{5/2})$ subshells to the $d_{3/2}$ subshell [18] so we cannot distinguish between the bands terminating at $I = 45.5^-$ and $I = 47.5^-$ discussed above. We do however note that the lowest energy $I = 45.5^-$ state is calculated as non-collective ($\gamma = 60°$) which means that it corresponds to the configuration with no $d_{3/2}$ neutrons. An interesting observation following from experiment is that the highest spin states are neither built at a very high energy cost nor at a very low energy cost. Instead, the $E$ vs. $I$ curve approximately follows what would be expected from rigid rotation. Indeed, $\mathcal{J}^{(2)}$ is approximately equal to $\mathcal{J}^{(1)}$ in the rotational frequency range $\hbar\omega = 0.5 - 0.8$ MeV, fig. 4, with subsequent decrease at higher frequencies. As a result, it is difficult to draw the conclusion that the observed band is near termination from the energies alone. This then corresponds to how bands terminate in the rotating oscillator [19] but is rather different from what has been discussed in nuclei where the main emphasis has been put on either favoured or unfavoured terminations.

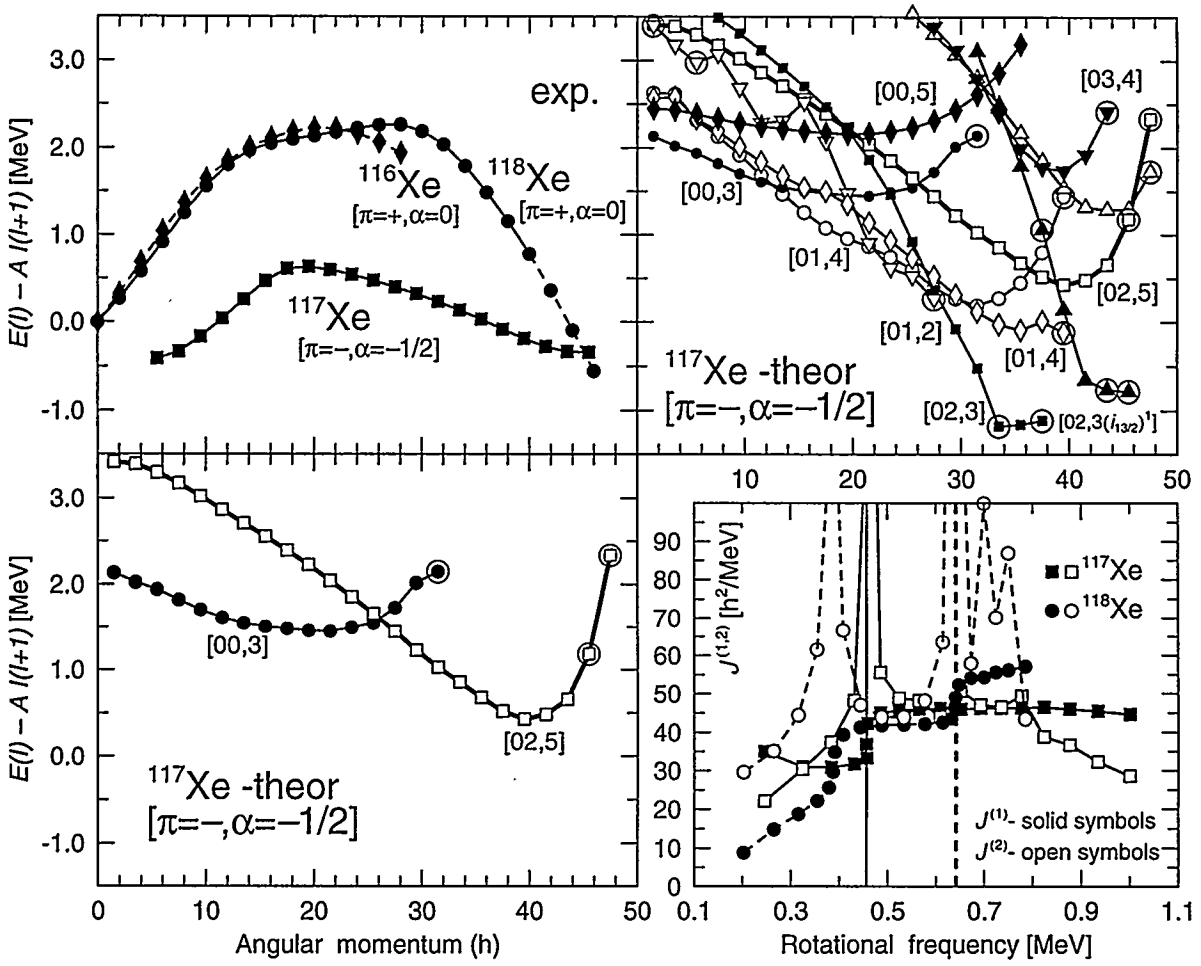


**Fig. 4.** *Upper left panel:* experimental collective rotational bands in $^{116,117,118}$Xe taken from ref. [17]. The energies are given in a similar way as in fig. 3, with the moment of inertia parameter $A = (\hbar^2/2J_{rig})$ equal to 0.01172 MeV, 0.01155 MeV and 0.01139 MeV for the bands in $^{116,117,118}$Xe nuclei, respectively. *Upper right panel:* calculated configurations in the yrast region of $^{117}$Xe. They are labelled according to ref. [5] by $[p_1p_2, n_1]$, where $p_1$ is the number of proton holes in the $g_{9/2}$ orbitals, $p_2$ ($n_1$) is the number of protons (neutrons) in the $h_{11/2}$ orbitals. The parameter set from ref. [20] is used. *Lower left panel:* two selected calculated configurations which can be associated with the observed collective band in $^{117}$Xe. *Lower right panel:* the kinematic, $\mathcal{J}^{(1)}$, and dynamic, $\mathcal{J}^{(2)}$, moments of inertia of observed bands in $^{117,118}$Xe.

Our results for $^{117}$Xe do also raise some questions about our description of very high spin states. The problem is illustrated in the upper right panel of fig. 4 where also other calculated configurations of $^{117}$Xe are shown. It turns out that for spins $I \approx 20 - 40\hbar$, the configuration identified with the observed band in $^{117}$Xe is far from yrast in the calculations. This puts some doubts on our interpretation but provided that the band indeed continues to $I^\pi = 45.5^-$, it is very difficult to imagine any other interpretation. The calculated spectrum does then suggest that the parameters we use for $^{117}$Xe are not optimal. One

should note that if the parameters are changed within reasonable range, the relative energies of different configurations could be rather strongly affected while the $E$ vs. $I$ curves for specific configurations are much less sensitive to parameter changes. Furthermore, it is not unreasonable that some states of low collectivity are indeed lower in energy than the observed band because, in experiment, it is much easier to follow long collective sequences than to identify isolated non-collective states.

In the nucleus $^{118}$Xe, the ground band has tentatively been observed to $I = 46^+$ as illustrated in fig. 4. The high spin part of this band shows very different properties relative to the band in $^{117}$Xe. Indeed, the very low energy cost of the highest spin units above $I \approx 40\hbar$ appears impossible to reproduce in calculations. Confining ourselves to the valence space, the maximum spin is indeed $I = 46^+$ but the calculated energy cost for the highest spin units is similar to the cost in $^{117}$Xe, in strong disagreement with the tentative experimental spectrum. We would thus suggest that one would perform a new experiment for this nucleus (and its neighbours) using a state-of-the-art detector system so that the valence space spectrum configurations could really be followed to termination and other configurations with core excitations could hopefully be identified at very high spin.

We are grateful for financial support from the Swedish Natural Science Research Council, the Crafoord Foundation and the Royal Swedish Academy of Sciences. We also thank the authors of ref. [12] for generous access to unpublished experimental data on $^{86}$Zr and J. Döring for helpful discussions and suggestions. The help of C.J. Ragnarsson in preparing fig. 1 is appreciated.

# References

[1] T. Bengtsson and I. Ragnarsson, Phys. Scripta T 5 (1983) 165.
[2] P.O. Tjøm *et al.*, Phys. Rev. Lett. 55 (1985) 2405.
[3] V.P. Janzen *et al.*, Phys. Rev. Lett. 72 (1994) 1160; G.J. Lane *et al.*, these proceedings.
[4] I. Ragnarsson *et al.*, Phys. Rev. Lett. 74 (1995) 3935.
[5] A.V. Afanasjev and I. Ragnarsson, Nucl. Phys. A 591 (1995) 387.
[6] J. Gizon *et al.*, to be publ.
[7] J.A. Cameron *et al.*, Phys. Rev. C49 (1994) 1347 and to be publ.; S.M. Lenzi *et al.*, Z. Phys. A354 (1996) 117; V.P. Janzen *et al.*, these proceedings.
[8] E. Caurier *et al.*, Phys. Rev. Lett. 75 (1995) 2466.
[9] T. Bengtsson and I. Ragnarsson, Nucl. Phys. A 436 (1985) 14.
[10] W. Nazarewicz *et al.*, Nucl. Phys. A 435 (1985) 397.
[11] D.M. Cullen *et al.*, Proc. Conf. on Physics from Large $\gamma$ ray Detector Arrays, Berkeley, CA, 1994 (LBL, Berkeley, 1994), vol. I, p. 44; C. Baktash, Bull. Am. Phys. Soc. 39 (1994) 1156 and C. Baktash *et al.*, Phys. Rev. Lett. 74 (1995) 1946.
[12] J. Döring *et al.*, to be publ.
[13] F. Cristancho *et al.*, Phys. Lett. B 357 (1995) 281.
[14] A.V. Afanasjev and I. Ragnarsson, to be publ.
[15] D. Galeriu, D. Bucurescu and M. Ivaşcu, J. Phys. G 12 (1986) 329.
[16] T. Troudet and R. Arvieu, Z. Phys. A 291 (1979) 183.
[17] E.S. Paul *et al.*, Phys. Rev. C 51 (1995) R2857.
[18] A.V. Afanasjev, I. Ragnarsson and J. Sears, Acta Physica Polonica B27 (1996) 187.
[19] I. Ragnarsson, Phys. Lett. B 199 (1987) 317.
[20] Jing-ye Zhang *et al.*, Phys. Rev. C 39 (1989) 714.

# Status of Development of the Gamma Ray Energy Tracking Array (GRETA)

I.Y. Lee, G.J. Schmid, K. Vetter, M.A. Deleplanque, R.M. Diamond, P. Fallon, A.O. Macchiavelli, R.W. Macleod, F.S. Stephens, R.M. Clark, and R. Krücken
*Lawrence Berkeley National Laboratory, Berkeley, California 94720*

## I. Introduction

The current generation of large gamma-ray detector arrays, Gammasphere, Eurogam and GASP, are based on modules of Compton suppressed Ge detectors. Due to the solid angle occupied by the Compton shields and to gamma rays escaping the detector, the total peak efficiency of such a design is limited to about 20% for a 1.3 MeV gamma ray. A shell consisting of closely packed Ge detectors has been suggested as the solution to the efficiency limitation. In this case, the entire solid angle is covered by Ge detectors, and by adding the signal from neighboring detectors, the escaped energy is recovered and much higher efficiency can be achieved (e.g. 60% for a 1.3 MeV gamma ray). However, for high multiplicity cascades, the summing of two gamma rays hitting neighboring detectors reduces the efficiency and increases the background. In order to reduce this summing, a large number of detectors is required. For example, with a multiplicity of 25, we need about 1500 detectors to keep the probability of false summing below 10% and the cost of such a detector array will be prohibitive.

Rather than such an approach, we are developing a new concept for a gamma-ray array; a shell of closely-packed Ge detectors consisting of 100-200 highly-segmented elements. The high granularity of the segmented Ge detector enables us to resolve each of the scattering interactions and determine its position and energy. A tracking algorithm, using the position and energy information, will then identify the interactions belonging to a particular gamma ray and its energy is obtained by summing only these interactions. Such an array can reach a total efficiency about 60%, with a resolving power 1000 times higher than that of current arrays. This large increase in power will provide many new opportunities for exciting physics which will be discussed later. To realize such a detector array, R&D efforts are being pursued in three areas. They are: 1) manufacture of segmented detectors which can give high energy resolution and 3-D position information; 2) electronics based on pulse shape digitization and digital processing of signals to give the energy and coordinates of the interaction points; and 3) an algorithm to identify interaction points belonging to a particular gamma ray.

## II. Segmented detector development

A detector with three dimensional position information can be achieved by segmenting one of the electrodes in two dimensions to provide two of the coordinates and the third coordinate derived from the drift time of the charges. There are many possible segmentation and packing schemes. One possibility is using tapered hexagonal or pentagonal shaped detectors with a segmented outside surface. A prototype detector of this type is designed and ordered. As shown in Figure 1, this detector has a tapered hexagonal shape with a flat-to-flat distance at the base of 7 cm and a length of 9 cm. It has six longitudinal segmentations and one transverse segmentation which divide the outer surface into 12 segments. Signals from each of the segments as well as from the center electrode will be read out. This prototype will be tested together with electronics, data processing methods and the tracking algorithm. After testing, further transverse segmentation will be carried out to produce a 6-by-6 configuration which gives 36 segments.

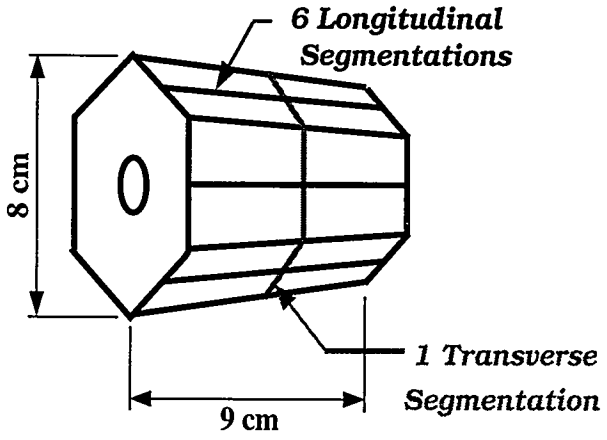


Figure 1. Prototype GRETA detector has a tappered hexagonal shape with six longitudianl segmentations and one transverse segmentation.

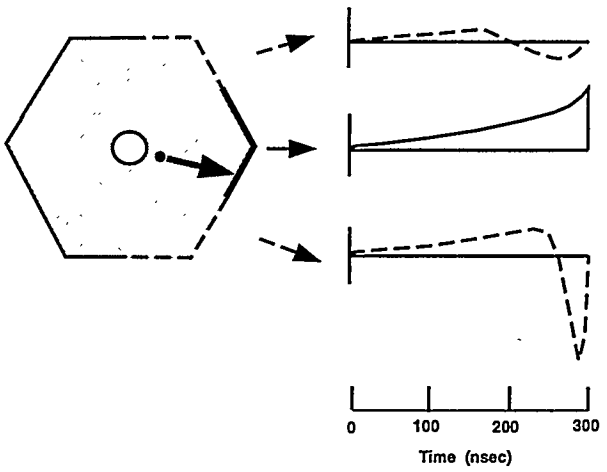


Figure 2. Current signal on three electrodes from a charge drifting toward the outside electrodes.

## III. Signal processing

To determine the position in three dimensions accurately, a detailed understanding of the signal shape is necessary. A signal is produced when electrons and holes formed by the slowing down of the photo- or Compton-electrons induce image charge of opposite sign on the electrodes. As the charge drifts toward the electrodes, the amount of the image charge changes and it causes current to flow in or out of the electrodes. Figure 2 shows a schematic diagram of the current signal expected from a segmented detector. When the charge is at a large distance from the electrodes, the induced charge is distributed over several electrodes and their current signals are similar. As the charge moves closer to the destination electrode, the induced charge on this electrode increases and charge on the other electrode decreases. The current continues to increase on the destination electrode until the charge finally reaches the electrode and neutralizes the image charge and the current stops. The duration of the current signal (drift time) can be used to determine the drift distance. The integral of the current gives the charge which provides the energy measurement. The signal from the neighboring electrode has a bipolar shape with a zero net charge. This fact can be used to identify the electrode where the charge is collected which gives a position resolution of the size of the electrode. Actually, a better position resolution can be obtained by analyzing the shape of the induced signal from the neighboring electrodes. As shown in Figure 2, the maximum amplitude and time of zero crossing of these signal are sensitive to the transverse position and they can be used as parameters for the shape analysis.

In order to use this information, the pulse shape has to be digitized in small time steps and with sufficient resolution in amplitude for further processing. We have started testing digital pulse shape acquisition electronics and processing methods on a two-fold segmented Gammasphere detector. Using a four-channel waveform digitizer, we collected charge and current pulse shapes from the center electrode and charge signals from the two outer segments. Collimated gamma ray sources were used to scan the front surface of the Ge detector. Figure 3 shows the histograms of drift time for gamma ray source at radii of 10, 20 and 30 mm respectively. These results indicate that a radial position resolution of about 5 mm can be obtained from the charge drift time.

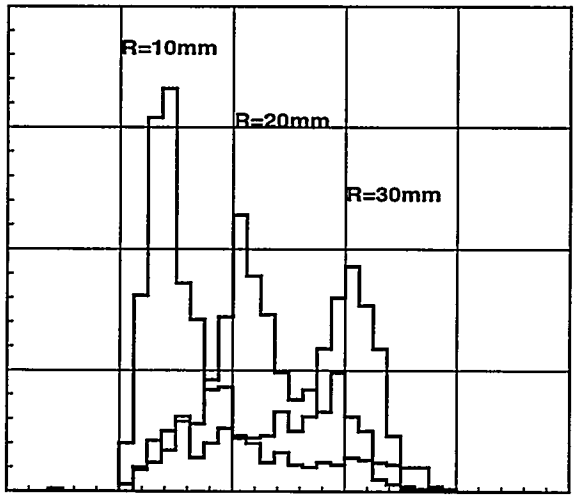


Figure 3. Histograms of signal rise time for collimated gamma rays incident at 10,20, and 30 mm from the center of a Gammasphere Ge detector.

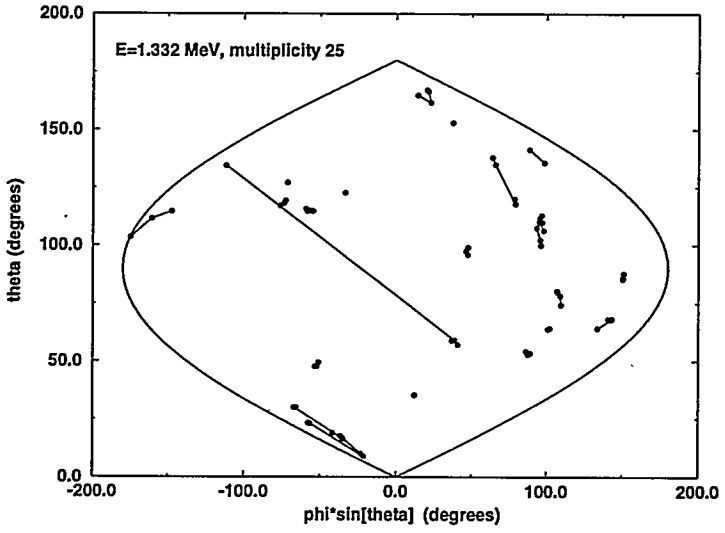


Figure 4. Projection of the interaction points from 25 gamma rays each with an energy of 1.33 MeV in a shell of Ge with an inner radius of 12 cm and an outer radius of 21 cm. Points belonging to a given gamma ray are connected with straight lines.

## IV. Tracking algorithm

Algorithms are being developed for identifying interaction points belonging to a given gamma ray. Compton scattering events were generated using a Monte Carlo method in a shell of Ge with an inner radius of 12 cm and an outer radius of 21 cm. Figure 4 shows the projection on a sphere of the interaction points of 25 gamma rays each with an energy of 1.33 MeV. The interaction points belonging to a gamma ray were connected by straight lines. This figure indicated that about half of the gamma rays have interaction points isolated from that of other gamma rays such that they can be identified easily. Thus, we use cluster identification as the first step of the algorithm . The interaction points within a given angular separation as viewed from the target are grouped in to a cluster. In the second step, each cluster was evaluated by tracking to determine whether it contains all the interaction points belonging to a single gamma ray. The tracking algorithm uses the angle-energy relation of the Compton scattering to determine the most likely scattering sequence from the position and energy of the interaction points. If the interaction points have infinite position and energy resolution, the tracking would be exact and the proper identified full energy cluster will show no deviation from the scattering formula. But the wrongly identified cluster or partial energy cluster will deviate from the formula and the separation of the good and bad clusters could be done easily. However, with finite resolutions the good cluster will also have a non-zero deviation and they can not be separated cleanly from the bad clusters. Any cut will have different effects on the efficiency and peak-to-total ratio. For example, a cut at a smaller deviation value will give a lower efficiency and a higher P/T value. Therefore, we have to determine the optimal cutting procedure based on experimental conditions such as gamma ray multiplicity and energy distribution. One type of incorrectly identified cluster is a gamma ray being separated in to two clusters. These clusters can be identified by tracking two cluster together. If the result gives a small deviation the gamma ray is recovered by adding the two clusters. Figure 5 shows the flow diagram of the current version of the algorithm. The bad cluster which did not satisfy the tracking criteria for either an isolated cluster or a cluster that can be added are rejected. This simulation was carried out for a number of events and spectra of accepted gamma rays were generated. Figure 6 shows the efficiency and P/T achieved so far for simulated events with 25 gamma rays each with an energy of 1.33 MeV and a detector position resolution of 1 mm. Several improvements of this algorithm are being developed. Information such as the energy dependence of the angular distribution of the Compton scattering cross section and the distribution of the distance between two interaction points will be used in the tracking. Methods for separating overlapping clusters are also being developed.

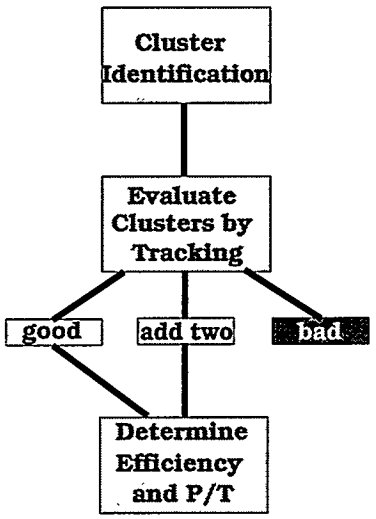


Figure 5. Flow diagram of the current version of cluster identification and tracking algorithm.

## V. Physics opportunities

If GRETA can achieve the maximum efficiency of 60% and a P/T of 90%, the corresponding resolving power will be 3500 times higher than the current generation of arrays such as Gammasphere and

Euroball phase III. If the efficiency is 50% and the P/T is 80%, the factor will be about 1000. Figure 7 compares the resolving power of HERA, Gammasphere and GRETA. This high resolving power will enable us to study weaker and exotic features of nuclear structure such as hyperdeformation and a wider range of neutron- and proton-rich nuclei. If one produces these nuclei by deep inelastic or fragmentation reactions, the intensity of the product falls off roughly by a factor of three for every neutron away from the

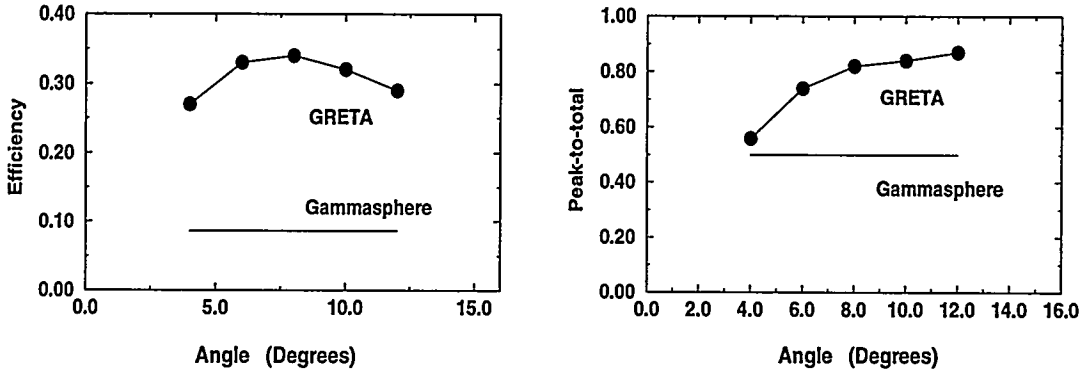


Figure 6. Efficiency and peak-to-total ratio achieved so far for simulated events of 25 gamma rays with energy of 1.33 MeV and a detector position resolution of 1 mm. The curvers are ploted as function of the angle parameter used in the cluster identification.

stability line. Thus a factor of 1000 means one can study six additional isotopes on either side of the stability line. This would increase the total number of nuclei available for study by about 500. Because of its large volume of monolithic Ge, GRETA gives a high efficiency for high energy energy gamma rays and in the same time provides a high energy resolution. For example, a 15 MeV gamma ray will have an efficiency of 35% (compare to 1% for Gammasphere) and an energy resolution of 15 keV. The study of the detailed shape of giant resonances and the study of giant resonances selected by discrete gamma ray transitions will be benefited by using such a detector array.

The tracking will determine the position of the first hit of the gamma ray with a position resolution of a few mm which gives an accuracy of about one degree for the direction of the gamma rays. This will reduce the Doppler broadening due to the finite detector opening angle especially important for nuclei produced with large velocity such as those from heavy ion Coulomb excitation reactions and beam fragmentation reactions. Another benefit of tracking is that the azimuthal angle between the first and second interaction points provides a measure of the linear polarization of the gamma ray. Compton polarimeters based on current generation arrays have low polarization efficiency due to multiple scattering and absorption in the large crystal

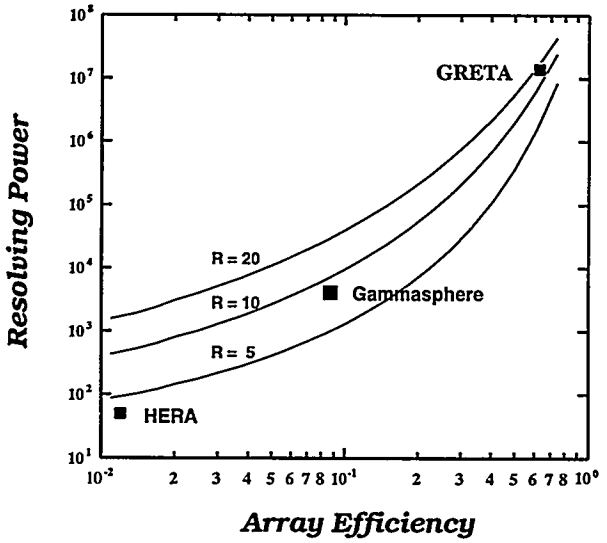


Figure 7. Resolving power of three generations of arrays, HERA, Gammasphere and GRETA. The three curves correspond to resolving power per fold R of 5, 10 and 20, respectively.

used as a scatterer.

Such a detector would also have considerable impact outside the area of nuclear structure. For example, the detection of the weak branches of multi-photon decay of positronium will be improved by more than the increase in detector efficiency. The detailed reconstruction of each photon would distinguish, for example, a four-photon event from a Compton scattered 3-photon event. These precision measurements would be a sensitive test of higher-order QCD effects and of time reversal invariance.

## VI. Conclusion

The power of a true $4\pi$ gamma-ray detector with the precise characterization of each photon is enormous. In nuclear structure studies it will bring the intensity levels we can study from $10^{-4}$ down to $10^{-7}$. While some extensions of our present studies have been outlined above, there is little doubt that completely new phenomena will become observable. Such a detector will also be a great resource for other fields of physics. The development work carried out so far indicates that there is no major problem with the GRETA concept. However, more detailed studies need to be carried out before all the technical aspects of this detector are understood. We hope in about a year or so to establish the feasibility of such detector and the detailed design work could begin in 1997 and construction in 1998.

# THE HOLIFIELD RADIOACTIVE ION BEAM FACILITY AT OAK RIDGE NATIONAL LABORATORY

J. D. Garrett*
*Physics Division, Oak Ridge National Laboratory, Oak Ridge, Tennessee 37831-6368, U.S.A.*

The status of the new Holifield Radioactive Ion Beam Facility at Oak Ridge National Laboratory (ORNL), which is slated to start its scientific program late this year is discussed, as is the new experimental equipment which is being constructed at this facility. Information on the early scientific program also is given.

## 1. Background

The fast on-line isotope separator technology developed[1] at CERN and other facilities has progressed to the extent that it is feasible to produce and accelerate beams of isotopes not occurring in terrestrial matter with sufficient intensity to address a myriad of nuclear structure, nuclear astrophysics, and material science questions[2-4]. First-generation isotope separator on line (ISOL) radioactive ion beam (RIB) facilities are being constructed in North America, Europe, and Japan based on this technology and existing accelerators and reactors. The Holifield Radioactive Ion Beam Facility[5] (HRIBF) at ORNL will be the first such ISOL RIB facility operational devoted completely to such scientific studies with accelerated radioactive ions. The present paper describes the status of this facility, which will become operational later this year. The plans for the early scientific program and some future possibilities for the HRIBF also will be discussed. At this nuclear structure conference the nuclear structure program of the HRIBF will be emphasized.

## 2. Present Status of the Facility

The HRIBF is based on a reconfiguration of the accelerators and experimental facilities available since the early 1980s at the Holifield Heavy Ion Research Facility. A High Voltage RIB Injector, as shown in Figure 1, has been constructed where intense beams of light ions from the Oak Ridge Isochronous Cyclotron (ORIC) will be utilized to produce radioactive atoms. After defusion from the target, ionization, and mass and isobaric separation, these radioactive ions will be accelerated in the 25-MV Tandem Accelerator.

The construction of the HRIBF and the associated radiation handling system, also shown in Figure 1, is complete. ORIC has provided beams to the target on the RIB Injection Platform, and stable beams of several elements, produced at the target position of the target-ion source on the injection platform, have been ionized, mass analyzed, charge exchanged, accelerated from the injection platform, isobaric analyzed, accelerated through the tandem accelerator, and identified.

---

* This paper is a group report made on behalf of more than 50 scientists, engineers, technicians, and craft personnel who over the past 5 years have participated in planning, engineering, constructing, and commissioning the HRIBF and its associated experimental equipment.

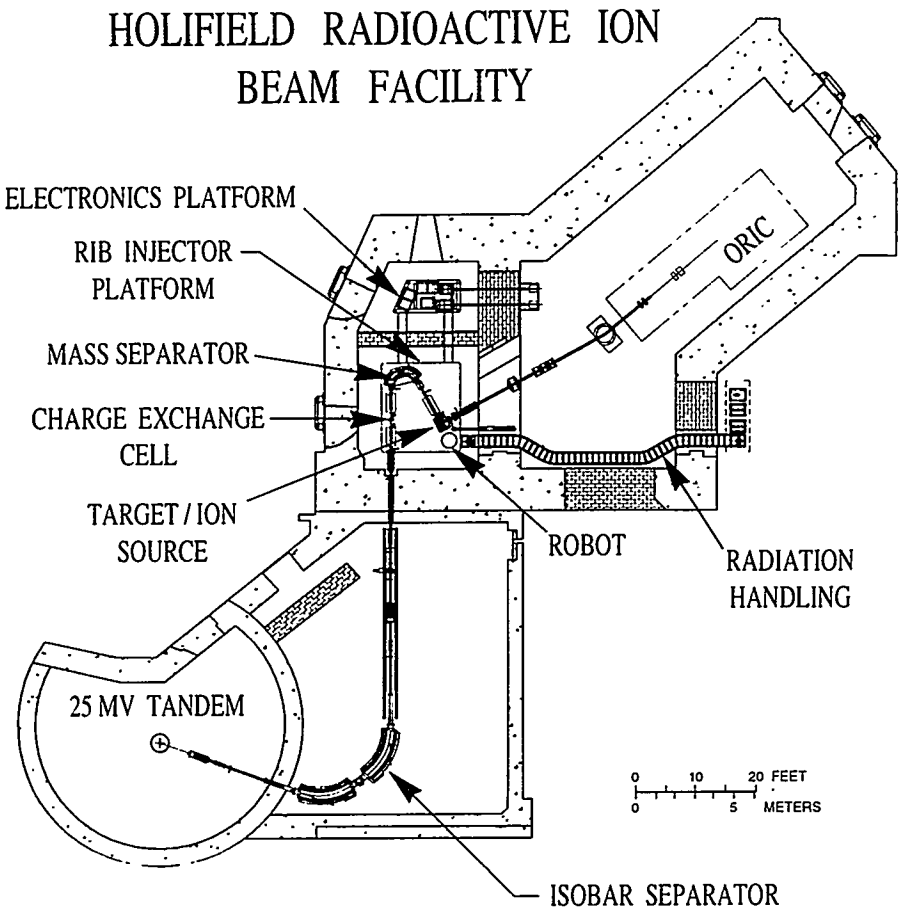


Figure 1 Layout of the HRIBF showing ORIC, the RIB Injector Platform, the magnetic analysis system for the selection of the RIB of interest, the 25-MV Tandem Accelerator, and the radiation handling system.

Likewise at a separate location (the UNISOR mass identifier) a liquid germanium target has been developed and tested with beams from the Tandem Accelerator in a target ion source assembly identical to that which will be used on the RIB Injection Platform. For example, both radioactive $^{69}$As and $^{70}$As have been produced in the $^{70}$Ge(p,xn) reactions with 40 MeV protons, ionized, extracted, mass analyzed, and identified. The measured intensities when scaled to the 20 μA proton beam of ORIC, isotopically pure $^{70}$Ge targets, and realistic charge exchange fractions and transmission should provide beams of radioactive $^{69}$As and $^{70}$As with intensities of greater than 3 x $10^7$ and $10^8$ particles per second, respectively. In mid-August the liquid germanium target will be moved to the RIB Injection Platform and a demonstration radioactive arsenic beam will be produced on the platform and accelerated through the Tandem. Beams of heavier radioactive arsenic ions produced by (p,xn) reactions on heavier germanium isotopes and gallium ions produced in the Ge(p,αxn) reactions also have been identified in these target tests and could be provided as future RIBs. Similarly radioactive isotopes of selenium could be produced with ($^3$He,xn) and (α,xn) reactions and a slightly-modified liquid germanium target. However, such selenium beams have not been demonstrated. Due to the thinner effective target, associated with the larger energy loss of helium atoms than for protons, the selenium RIBs are expected to be somewhat less intense than the arsenic RIBs.

Presently, the liquid germanium target has been moved to the RIB Injector Platform, and an $Al_2O_3$ target for the development of radioactive $^{17}F$ and $^{18}F$ (using the $^{16}O(d,n)$ and $^{18}O(p,n)$ reactions, respectively) has been installed at the UNISOR separator. Previous tests have demonstrated that essentially all of the radioisotopes of fluorine produced from proton bombardments can be released from a 3 micron $Al_2O_3$ gauze fiber target.

Proton-rich radioactive isotopes of other volatile elements, such as sulfur, sodium, potassium, copper, and gallium, which can be produced with hydrogen and helium beams, and refractory targets also are being considered for future beam development of the HRIBF.

## 3. Experimental Apparatus

There is a tradition for nuclear structure studies with accelerated beams of heavy ions at ORNL, dating from the 1950s. Therefore, an assortment of experimental apparatus for such studies exists. Examples include an array of 20 Compton-suppressed germanium detectors, a $4\pi$ array of 72-NaI detectors, an array of 96 $BaF_2$ detectors for detecting high energy gamma rays, an Enge split pole magnetic spectrograph, the UNISOR on-line isotope separator featuring a helium dilution refrigerator, and a variety of scattering chambers. In addition new experimental stations especially suited for nuclear structure studies with RIBs and for the new ORNL nuclear astrophysics program have been constructed and are described in the ensuing paragraphs.

### 3.1 The Recoil Mass Spectrometer (RMS)

The focal point of the nuclear structure experimental station is a newly-designed recoil mass spectrometer[7] (RMS) located in Robinson Hall, a recent addition to the Holifield Facility. This instrument is designed to select rare reaction products from the beam and other reaction channels at the level of one part in about $10^{13}$. Besides the usual electric-magnetic-electric dipole arrangement for such mass separators, the "front end" of the RMS is designed so that the beam is stopped prior to the mass analysis. A position sensitive avalanche counter (PSAC) for establishing the horizontal and vertical positions of the recoiling reaction products is located at the RMS focal plane, and an ionization chamber is located "downstream" of the PSAC. The ionization chamber is used to establish the Z of the reaction products by an energy loss measurement. This Z "measurement" should be effective for $Z < 50$.

The construction of the RMS and its basic compliment of focal plane detectors is complete. It is presently being commissioned. Preliminary measurements[8] for the products of the reaction of 220 MeV $^{58}Ni$ and $^{60}Ni$ yielded a mass resolution of $M/\Delta M \approx 450$ for A = 114 with essentially no background at the focal plane, see Figure 2.

Ancillary instrumentation provides information on both the prompt and delayed decay properties of the reaction products and their daughters. The transit time of a typical reaction product for the nearly 25 meter flight path from the target to the RMS focal plane, 1 - 5 μs, divides the experimental possibilities for this instrument into two types: "prompt" events in which the radiation is detected near the target and "delayed" events in which the radiation is detected at the focal plane. Detectors being installed at the RMS focal plane include double-sided silicon-strip detectors for proton and α-particle decay studies as well as a moving tape collector with germanium detectors and a pair spectrometer to study the gamma decay of the reaction products.

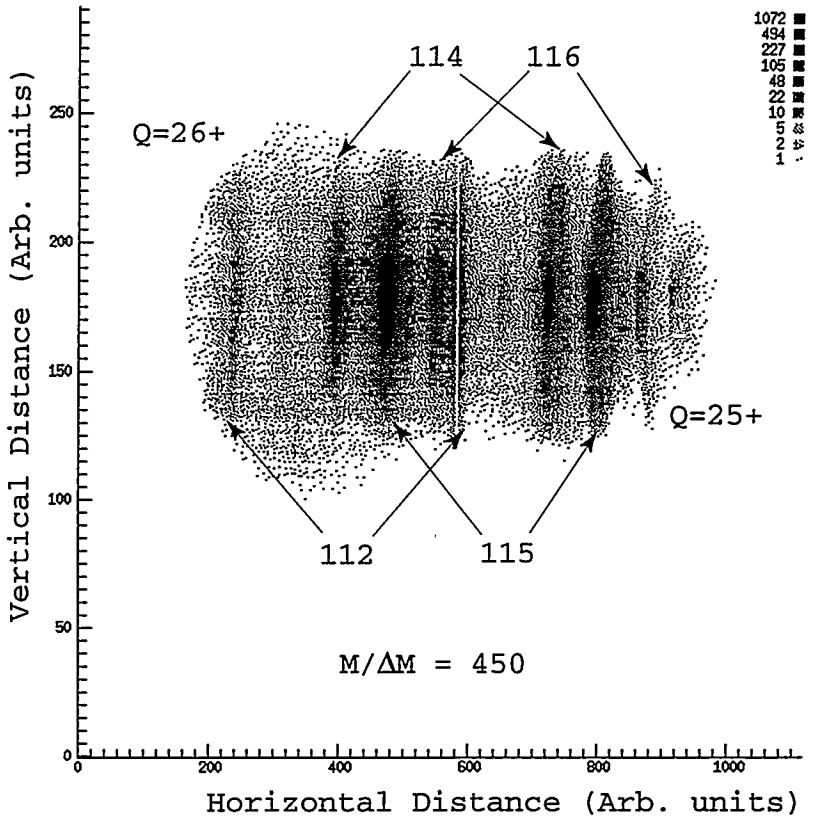


Figure 2 Experimental x and y position spectrum at the RMS focal plane for the products of the reaction of 220 MeV $^{58}$Ni and $^{60}$Ni.

## 3.2 Gamma-ray and Particle Arrays for Nuclear Structure

Arrays of gamma-ray, light-charged-particle, and neutron detectors[9], optimized for the study of weakly populated nuclei lying far from the valley of stability, are being constructed at the target position of the nuclear structure experimental station. A schematic diagram of this array is shown in Figure 3. Also shown in this figure is the "fantail" scattering chamber, designed to shield the germanium detectors from the buildup of scattered radioactive particles from the beam thereby minimizing the background gamma-ray activity.

The heart of this array is eleven "clover" detectors. Each "clover" consists of four individual germanium crystals, sharing a common cryostat. The four crystals may be operated either as four independent detectors, or as a single large detector by summing their signals. In 10 of the 11 planned "clovers" each germanium crystal is electronically subdivided ("segmented") into halves, providing a lateral spatial resolution of less than 2 cm. In addition to providing excellent efficiency for detecting high-energy gamma rays (150% relative to a 3" x 3" NaI crystal), these detectors maintain good energy resolution even for gamma rays emitted from fast-moving recoiling nuclei by minimizing the effects of Doppler broadening. Such an arrangement also provides a means for measuring the linear polarization of the detected gamma rays.

The twelve high-purity 25% germanium detectors with their associated bismuth germinate anti Compton shields from the existing ORNL germanium array and three "clover" detector are

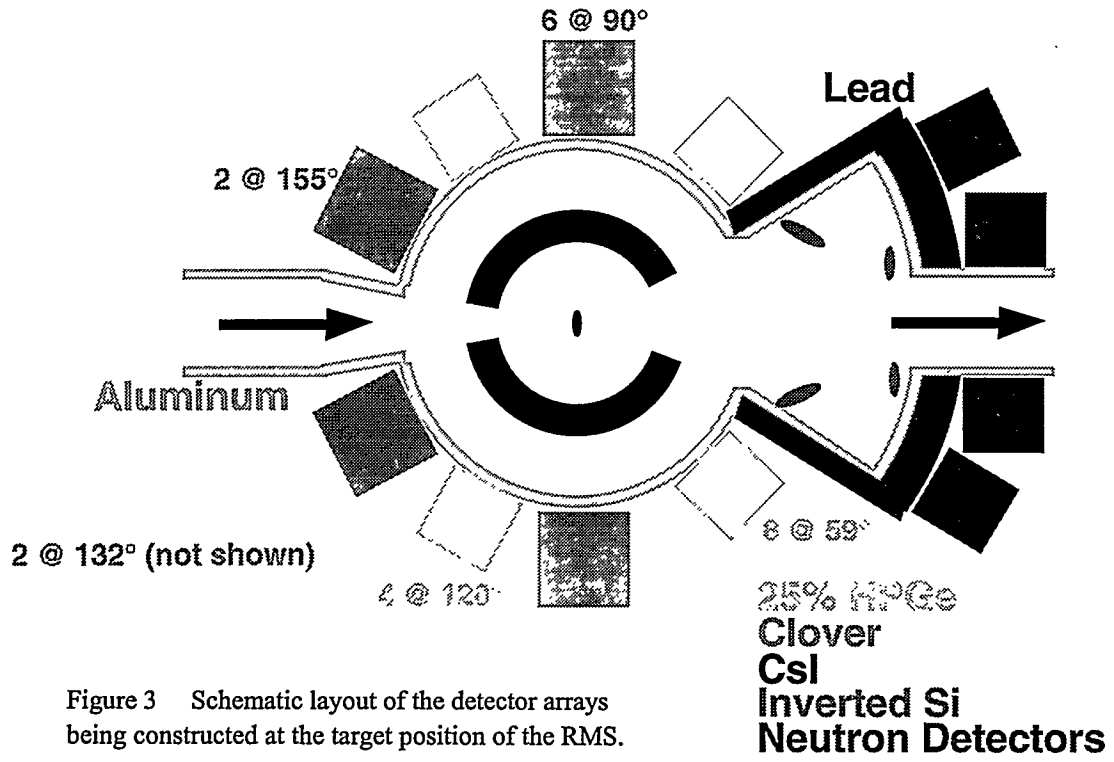


Figure 3 Schematic layout of the detector arrays being constructed at the target position of the RMS.

presently available. By the beginning of 1997 the target chamber, new detector support system and six "clover" detectors should be available; however, only five "clover" detectors will be operational with existing electronics prior to May 1997 when the new electronics becomes available. The completion of this array is slated for late in 1997 if sufficient capital funds are available in fiscal year 1997.

The construction[9] of a microball (a 4 $\pi$ CsI detector array) for detecting light charged particles is scheduled for completion in mid-1997. This instrument, similar in design[10] to the microball currently in use with the GAMMASPHERE, also is shown in Figure 3 together with an array of neutron detectors at the most forward angles with respect to the beam.

### 3.3 The Astrophysics Experimental Station

The foci of the astrophysics experimental station and indeed the newly established nuclear astrophysics program[11] at the HRIBF is the Daresbury Recoil Separator (DRS). This instrument was given to ORNL by the British Natural Science and Engineering Council (SERC), when the Nuclear Structure Facility at Daresbury Laboratory was closed. It was moved to the HRIBF late in 1994, where it is currently being installed. Its design as a velocity filter makes it well-suited for studying inverse (p,$\gamma$) reactions which occur in stellar explosions. This instrument and its associated detectors should be ready for commissioning late in 1996.

**Table I Scientific Topics Represented in the Letters of Intent**

| Topic | Number of Letters |
|---|---|
| Astrophysics | |
| rp-process & CNO breakout* | 5 |
| Solar neutrinos | 1 |
| Nuclear Structure | |
| Light nuclei | 2 |
| Self-conjugate nuclei | 7 |
| $^{100}$Sn region | 2 |
| A = 110 - 130 nuclei* | 6 |
| Heavy nuclei | 1 |
| Coulomb excitation* | 1 |
| Proton & $\alpha$ decay* | 3 |
| Giant dipole resonances | 1 |
| Ion traps | 1 |
| Reactions | |
| Transfer reactions* | 3 |
| Subbarrier fusion* | 1 |

*Denotes topics which can be addressed with radioactive arsenic and fluorine beams.

## 4. Experimental Program

The scientific program of the HRIBF has been discussed previously (see *e.g.,* reference[6]). Thirty-four letters of intent for using this facility were received in August 1995 from 99 scientists at 36 institutions. The scientific content of these letters of intent are characterized in Table 1, where the programs that can start with radioactive arsenic and fluorine beams also are indicated. The distribution of the institutions represented on the letters of intent is shown in Figure 4.

In response to a call for proposals for research with beams of radioactive $^{69}$As and $^{70}$As, 960 hours of running were recently requested for nuclear structure studies. Two thousand eight hours of associated experiments with beams of stable ions also were requested. On August 6, 1996, the HRIBF Program Advisory Committee met and granted 800 hours of running time with radioactive $^{69}$As and $^{70}$As beams and 1000 hours of associated experiments with stable beam. A list of approved experiments can be obtained on the HRIBF web site (www.phy.ornl.gov).

The production and acceleration of neutron-rich RIBs also are feasible at the HRIBF. Intense proton beams from ORIC can be used to produce neutron-rich fission fragments from a $^{238}$U target. For example, preliminary projections indicate that up to about $10^7$ particles per second of "doubly magic" $^{132}Sn_{82}$ could be accelerated above the Coulomb barrier with the addition of an actinide target to the present facility. Of course, the radiation handling system would have to be adequate to deal with the additional long-lived radioactivity of the fission fragments. Neutron-rich RIBs from such an actinide target are planned for 1998.

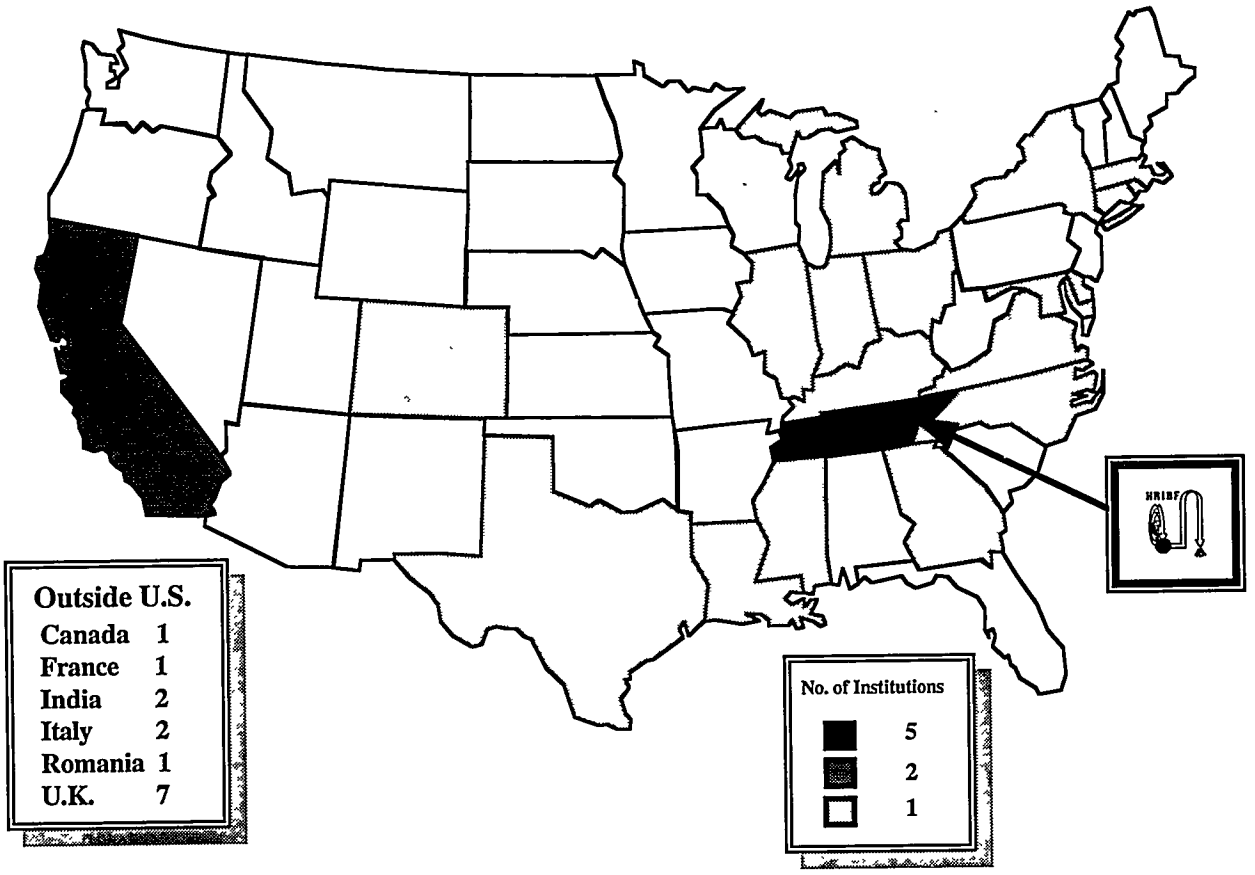


Figure 4 Distribution of the 36 institutions represented on the 34 letters of intent to use the HRIBF. The distribution of the 12 institutions outside of the U.S. is tabulated in the lower left-hand corner of the figure.

**Note added in proof:** On August 30 the first $^{69}$As and $^{70}$As beams were produced on the RIB Injection Platform and accelerated through the 25-MV Tandem Accelerator. Recent measurements indicate that radioactive $^{17}$F and $^{18}$F can be produced and released from the $Al_2O_3$ gauze fiber target and can be ionized. When intense beams of radioactive $^{17}$F and $^{18}$F have been demonstrated, a call for proposals for experiments utilizing these beams, which are ideal for a variety of nuclear astrophysics and nuclear reaction studies, will be issued.

## Acknowledgements

The participation of more than 50 scientists, engineers, technicians, and craft personnel who have participated in the planning, engineering, constructing, and commissioning of the HRIBF and its associated experimental equipment is gratefully acknowledged. This research was sponsored by the Oak Ridge National Laboratory, managed by Lockheed Martin Energy Research Corporation for the U.S. Department of Energy under contract number DE-AC05-96OR22464.

# High Spin Isomer Beam Line at RIKEN

T. Kishida[1], Y. Gono[2], E. Ideguchi[1], T. Morikawa[2], M. Kidera[3], M. Shibata[2], H. Tsuchida[2], K. Miyazaki[2], H. Watanabe[2], H. Y. Wu[1], A. Tanokura[4], S. S. Yamamoto[4], A. Yoshida[1], S. Mitarai[2], A. Odahara[2], T. Murakami[5], M. Oshima[3], H. Kusakari[6], M. Sugawara[7], M. Kubo[4], T. Murata[4], M. Shimura[4], H. Kumagai[1], M. Ishihara[1]

1 The Institute of Physical and Chemical Research (RIKEN), Saitama 351-01, Japan
2 Department of Physics, Kyushu University, Fukuoka 812, Japan
3 Japan Atomic Energy Research Institute (JAERI), Ibaraki 319-11, Japan
4 Department of Physics, Sophia University, Tokyo 102, Japan
5 National Institute of Radiological Science, Chiba 263, Japan
6 Faculty of Education, Chiba University, Chiba 263, Japan
7 Chiba Institute of Technology, Chiba 275, Japan

## 1. INTRODUCTION

Nuclear high spin states have been the subject of extensive experimental and theoretical studies. For the production of high spin states, fusion reactions are usually used. The orbital angular momentum brought in the reaction is changed into the nuclear spin of the compound nucleus. However, the maximum induced angular momentum is limited in this mechanism by the maximum impact parameter of the fusion reaction and by the competition with fission reactions. It is, therefore, difficult to populate very high spin states, and as a result, large $\gamma$-detector arrays have been developed in order to detect subtle signals from such very high spin states.

The use of high spin isomers in the fusion reactions can break this limitation because the high spin isomers have their intrinsic angular momentum, which can bring the additional angular momentum without increasing the excitation energy. There are two methods to use the high spin isomers for secondary reactions: the use of the high spin isomers as a target and that as a beam. A high spin isomer target has already been developed and used for several experiments. But this method has an inevitable shortcoming that only "long-lived" isomers can be used for a target: $^{178}Hf^{m2}$ ($16^+$) with a half-life of 31 years in the present case.[1-3] By developing a high spin isomer beam, we can utilize various short-lived isomers with a short half-life around 1 $\mu$s.

The high spin isomer beam line of RIKEN Accelerator Facility is a unique apparatus in the world which provides a high spin isomer as a secondary beam.[4,5] The combination of fusion-evaporation reaction and inverse kinematics are used to produce high spin isomer beams; in particular, the adoption of "inverse kinematics" is essential to use short-lived isomers as a beam.

In general, the intensity of a secondary beam is supposed to be much smaller than a primary beam. It is, therefore, very important to study some characteristics of high spin isomer beam and to develop a beam line with a high transport efficiency. Thus, this report put stress on some general requirements for the construction of a high spin isomer beam line and the present status of our beam line.

## 2. RIKEN ACCELERATOR FACILITY AND HIGH SPIN ISOMER BEAM LINES

RIKEN Accelerator Facility has two beam lines which has been used as a high spin isomer beam line: E1C and RIPS.

E1C was a gas filled beam line in the first stage. A gas filled system makes it possible to transport several different charge states efficiently to the experimental area. It was used as a high spin isomer "separator" for the search of new isomer states. And then, it was found that this beam line could be used as a "secondary beam" because the separated isomer has a sufficient energy and intensity for secondary reactions. But the problem of this system was its beam size. The diameter of the beam spot was more than 40 mm. It does not fit for secondary reactions.

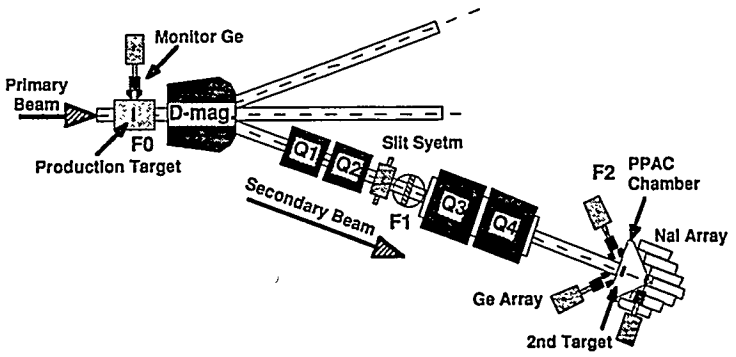


Fig.1 Schematic layout of E1C beam line

By evacuating the beam line, the diameter of the beam spot became much less than 10 mm. Figure 1 shows the schematic layout of E1C beam line. In order to make a dispersive focal plane, two quadrupole magnets (Q1 and Q2) were added. E1C has an angular acceptance of ±7 mr.

In order to improve the transmission efficiency, a large acceptance beam line, RIPS, was recently used as a high spin isomer beam line. Though RIPS is well known as a high energy RI beam line by using projectile fragmentation, it can also successfully be used as a low energy isomeric beam line by using fusion-evaporation. Figure 2 shows the schematic layout of RIPS beam line. RIPS has an angular acceptance of ±40 mr.

The detailed characteristics of the both beam lines are presented in Chapter 4.

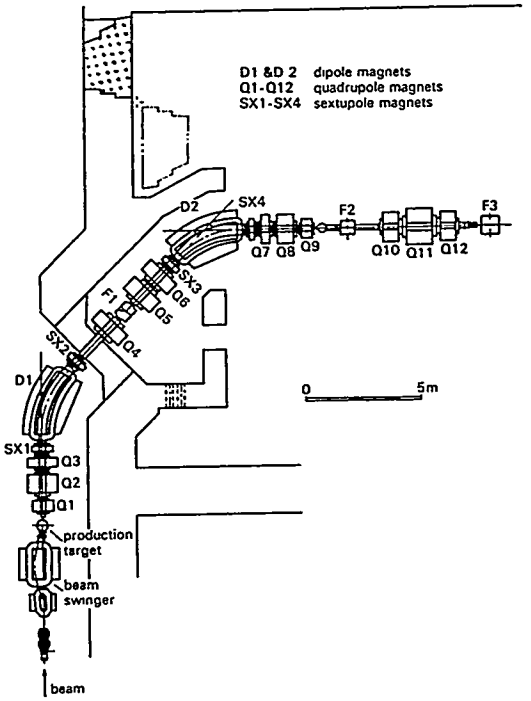


Fig.2 Schematic layout of RIPS beam line

## 3. RECIPE FOR HIGH SPIN ISOMER BEAM LINE

In this chapter, discussions are made on some general requirements for the construction of high spin isomer beam line.

First, on the requirement for the primary beam. The mechanism of inverse kinematics is used, which means that a heavy ion is the incident and a light atom is the target. In this case, the reaction products recoil in the forward direction maintaining kinetic energies high enough to induce secondary reactions. Figure 3 shows the recoil energy of the compound nucleus as a function of mass-number of the target nucleus with the incident

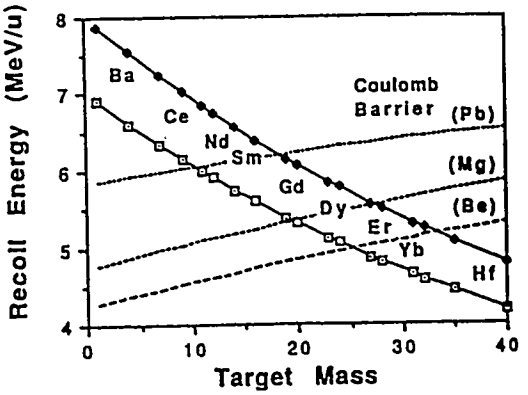


Fig.3 Recoil energy vs target mass number

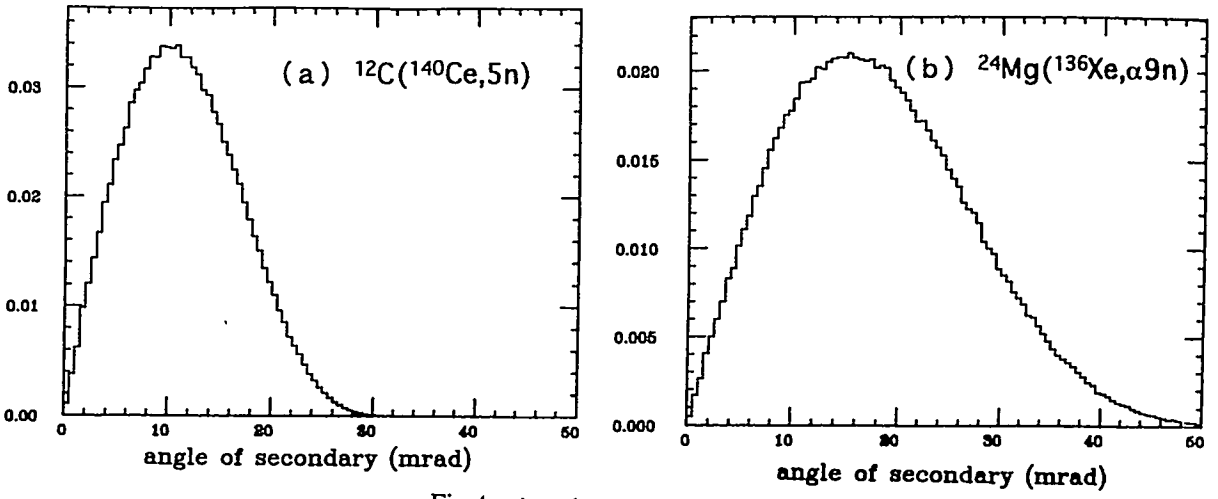


Fig.4 Angular distributions of $^{147}$Gd

$^{136}$Xe beam energy of 7 MeV/nucleon (open square) and 8 MeV/nucleon (filled circle). The dashed curves are Coulomb barrier energies for the compound nuclei in the case with the secondary target of Be, Mg and Pb. In general, the required energy range for the primary beam is 6 - 10 MeV/nucleon around the mass region of 140. This energy range is almost minimum available energy of the RIKEN Ring Cyclotron. The beam from ATLAS also satisfy this requirement around this mass region.

Next, on the requirement for the reaction mode. There are many reaction modes for the production of high spin isomer states. In general, when the production target is heavy, separation between the primary beam and the reaction product by their magnetic rigidity becomes good, and the angular divergence of the reaction product becomes large; and vice versa. To see them more quantitatively, some results of calculations are shown for $^{147}$Gd produced by the reaction of $^{12}$C($^{140}$Ce,5n) and $^{24}$Mg($^{136}$Xe,α9n) in the following. Figures 4a and 4b show the angular distributions of $^{147}$Gd in these two cases. From this result, we conclude that the angular acceptance of ±50 mr is large enough to transport Gd efficiently even when the production target is heavy. Figures 5a and 5b show the charge state distributions of $^{147}$Gd and the primary beam as functions of the magnetic rigidity. When the production target is heavier, separation between $^{147}$Gd and the primary beam by the magnetic rigidity becomes better. And in our energy region, it is concluded that a high spin isomer beam line must cover the magnetic rigidity in the range of about 0.8 - 1.3 Tm.

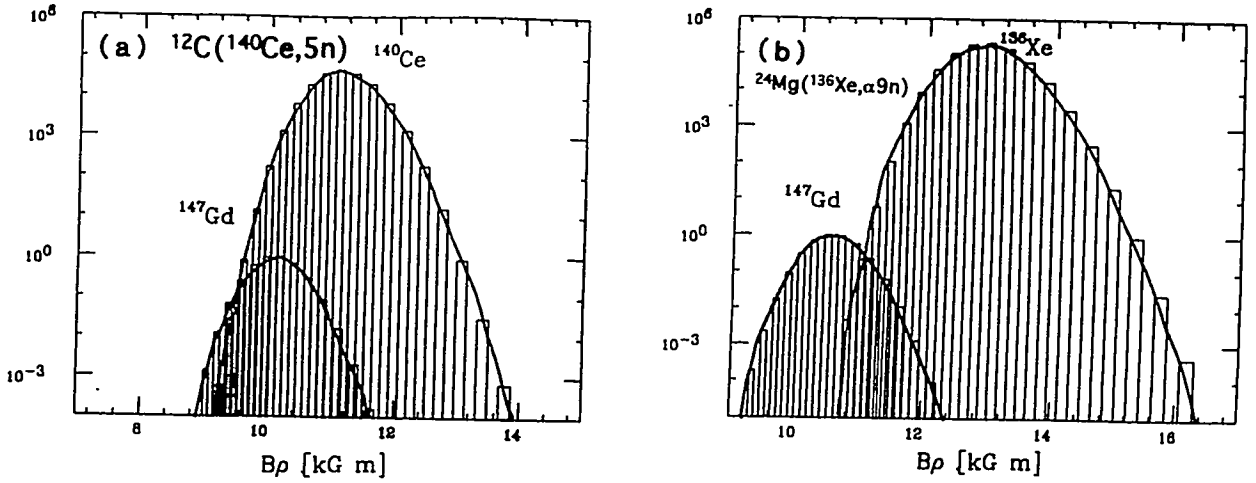


Fig.5 Charge state distributions of $^{147}$Gd and the primary beam

Finally, there are some other requirements for high spin isomer beams. 1) The optics should be dispersive at the first focal plane. It is for the separation of the reaction product from the primary beam. 2) The optics should have small dispersion after the first focal plane. It is for the efficient transport of the reaction product and for the small beam spot. 3) Double stage spectrometer system is desirable to remove serious background due to the primary beam scattered by the beam pipe. 4) The path length of the beam line should be as short as possible for the efficient transport of short-lived isomers.

## 4. PRESENT STATUS AND FUTURE IMPROVEMENTS

The main characteristics of E1C and RIPS are tabulated in Table 1. By considering the requirements described in Chapter 3, it is concluded that RIPS is more suitable for a high spin isomer beam line than E1C. RIPS has an advantage in all the characteristics except the path length between the production target and the final focal plane. RIPS has a long path length, which corresponds to the flight time of about 860 ns, while that of E1C is about 220 ns.

| | RIPS | E1C |
|---|---|---|
| Geometrical Acceptance | ±40mr (circle) 《5msr》 | ± 7mr(v) ±15mr(h) 《0.42msr》 |
| Momentum Acceptance | ±3%(full) (±4.5%) | ±<2%(full) (±<3.4%) |
| Max Bρ | 5.76Tm | ~1.8Tm |
| Focus | 《F1》 dispersive 2.4cm/% 《F2》 double achromatic 《F3》 double achromatic | 《F1》 dispersive 0.45cm/% 《F2》 small dispersion |
| Flight Path | F1: 10.4m F2: 21.3m F3: 27.5m | F1: 3.65m F2: 7.63m |

Table 1 Main characteristics of E1C and RIPS

For a quantitative comparison, some considerations are made here in the case of $^{12}C(^{140}Ce,5n)$. The comparison by using this reaction mode might be more profitable for E1C than for RIPS. This is because the high spin isomer state of $^{147}Gd$ has a relatively short half-life and the angular divergence of $^{147}Gd$ is small for this reaction mode. When the magnetic rigidity is set at the value corresponding to 48+ charge state of $^{147}Gd$, the acceptance for each charge state is calculated as (47+ : 5.1 %, 48+ : 29 %, 49+ : 5.1 %) for E1C and (46+, 47+, 48+, 49+, 50+ : 100 %) for RIPS. Then, by taking into account of the charge state distribution presented in Fig.5a, the total acceptance of E1C becomes 9.4 %, and that of RIPS becomes 89 %, which is almost 10 times larger than E1C. But, due to the flight decay of the isomer ($^{147m}Gd$; $t_{1/2}$=0.55μs), the resulting transmissions are 6.4 % and 19 % respectively. Then the ratio of transmission between RIPS and E1C is calculated to be 3. The experimental value of the ratio was 4, which agrees with the calculation. Because this value is obtained by using an unfavorable reaction mode for RIPS, this ratio is usually much larger (about 10 or more). The beam intensity of high spin isomers at E1C is about $10^3$ - $10^4$ $sec^{-1}$, and that at RIPS is about $10^4$ - $10^5$ $sec^{-1}$.

These beam lines are used for the secondary reactions of high spin isomers. One of the reactions is Coulomb excitation of isomer states. By using E1C beam line, the Coulomb excitation of 8⁻ *K*-isomer of $^{174}Hf$ was observed successfully.[6] In this experiment, the intensity of the isomer was $5\times10^3$ $sec^{-1}$. Such experiment is possible only by using isomer beams. Another secondary reaction is the secondary fusion of high spin isomers to investigate very high spin states. Such experiments are planned by using RIPS beam line.

In order to perform the latter experiments, however, the statistics has to be 1 or 2 oder of magnitude larger than that in the case of Coulomb excitation. It is fortunate that the RIKEN beam will become $10^2$ or $10^3$ times as intense as the present at the end of 1996. And the window-less gas target with differential pumping system is now under construction in order to produce productin target which is never destroyed by the intense primary beam. The beam intensity of high spin isomer is, then, expected to be $10^6$ - $10^7$ $sec^{-1}$.

REFERENCES

[1] G. Rotbard *et al.*, Phys. Rev. C **48**, R2148 (1993).
[2] N. Boos *et al.*, Phys. Rev. Lett. **72**, 2689 (1994).
[3] S. Deylitz *et al.*, Phys. Rev. C **53**, 1266 (1996).
[4] Y. Gono *et al.*, Nucl. Phys. A **557**, 341c (1993).
[5] Y. Gono *et al.*, Nucl. Phys. A 588 , 241c (1995).
[6] T. Morikawa *et al.*, Phys. Lett. B350 , 169 (1995).

# High Spin Spectroscopy Near The N=Z Line: Channel Selection and Excitation Energy Systematics

C.E. Svensson, J.A. Cameron, S. Flibotte, G. Gervais, D.S. Haslip, J.M. Nieminen, J.C. Waddington, J.N. Wilson
*Department of Physics and Astronomy, McMaster University, Hamilton, Ontario, Canada L8S 4M1*

G.C. Ball, A. Galindo-Uribarri, V.P. Janzen, D.C. Radford, D. Ward
*AECL, Chalk River Laboratories, Chalk River, Ontario, Canada K0J 1J0*

M. Cromaz, T.E. Drake
*Department of Physics, University of Toronto, Toronto, Ontario, Canada M5S 1A7*

The total $\gamma$-ray and charged-particle energies emitted in fusion-evaporation reactions leading to N=Z compound systems in the A = 50-70 mass region have been measured with the $8\pi$ $\gamma$-ray spectrometer and the miniball charged-particle detector array. A new method of channel selection has been developed which combines particle identification with these total energy measurements and greatly improves upon the selectivity possible with particle detection alone. In addition, the event by event measurement of total $\gamma$-ray energies using the BGO ball of the $8\pi$ spectrometer has allowed a determination of excitation energies following particle evaporation for a large number of channels in several different reactions. The new channel selection procedure and excitation energy systematics are illustrated with data from the reaction of $^{24}$Mg on $^{40}$Ca at $E_{lab} = 80MeV$.

## 1. Introduction

One of the major problems plaguing the high spin $\gamma$-ray spectroscopy of light ($A < 100$) proton-rich nuclei produced in fusion-evaporation reactions is the fragmentation of the total cross section into a large number of exit channels. A low Coulomb barrier in these systems, combined with strong pressures for decay towards stability, cause proton and alpha emission to dominate over neutron evaporation and the population of 10-20 nuclear species in a single reaction is common. In principle, the spectroscopic difficulties resulting from a large number of open exit channels can be solved by detecting the charged evaporation particles in coincidence with the $\gamma$ rays [1–5]. In practice, however, channel selection by charged-particle detection is limited by the efficiency of the particle detection system. Even with near $4\pi$ coverage by the particle detector array, some fraction of the charged evaporation particles inevitably escape detection. The result is that low particle multiplicity gated spectra are contaminated by events from higher particle multiplicity channels in which some of the particles have escaped detection. For example, a $\gamma$-spectrum in coincidence with the detection of 3 protons will contain not only real 3p events, but also 4p, $\alpha$3p and 3pn events where the extra particle was not detected. If a low particle multiplicity channel of interest is populated very weakly in a reaction, while higher particle multiplicity channels have much larger cross-sections, the high particle multiplicity contaminants can completely dominate the low particle multiplicity gated spectra. In this situation, the channel selection provided by charged-particle gating is not sufficient to permit an accurate spectroscopic study of the weakly populated low particle multiplicity channel.

## 2. Channel Selection Method

A detailed description of the new channel selection procedure has been given in [6]. Here we present a brief summary of the method. In order to discriminate between events from different channels for which the same charged particles are *detected*, we consider the different total energies available in the center of mass system for different exit channels:

$$E_{CM} = T_{CM} + Q \tag{1}$$

where $T_{CM}$ is the kinetic energy of the collision in the center of mass system (the same for all channels) and $Q$ is the Q-value for the specific reaction channel.

This total CM energy is emitted as $\gamma$-ray energy and particle kinetic energy:

$$E_{CM} = H_\gamma + T_{part} \tag{2}$$

where $H_\gamma$ is the total $\gamma$-ray energy and $T_{part}$ is the sum of the proton, alpha, and nuclear recoil kinetic energies in the CM system.

The BGO ball of the $8\pi$ spectrometer acts as an efficient $\gamma$-ray calorimeter to measure $H_\gamma$ for each fusion reaction, and the miniball [1] charged-particle detector array gives $T_{part}$ on an event by event basis. The position of each event can thus be plotted in a Total Energy Plane (TEP) where $H_\gamma$ is the $x$ coordinate and $T_{part}$ is the $y$ coordinate of the event. If we ignore loss of beam energy in the target for the moment, $E_{CM}$ is a constant for a given channel and thus equation (2) constrains all events from this channel to lie on a line of constant energy in the TEP (ie. a line with slope negative one and $x$ and $y$ intercepts equal to $E_{CM}$).

For channel selection purposes, we are concerned with events in which one or more particles escape detection. Consider a 3-proton particle gated data set. As noted above, the real 3p events in this data must all lie on a line of constant energy in the TEP. Now, consider a 4p event that appears in the 3p-gated data because one of the protons was missed. Firstly, the Q-value for the 4p channel is less than for the 3p channel by the binding energy of the fourth proton and thus there is less total CM energy available in the 4p channel. Secondly, the kinetic energy of the missed proton is absent from the sum in equation (2). These two effects add constructively and permit discrimination between 4p events in which a proton is missed and real 3p events. Similar arguments apply for the $\alpha$3p and 3pn events in the 3p-gated data. Given a 3p-gated TEP plot like that shown in Fig. 1, the channel selection achieved by charged-particle gating alone can be greatly improved by setting a two-dimensional gate in the TEP around the 3p line and taking the real 3p events inside this gate, while eliminating the background from the higher particle multiplicity channels that appear in the data set because particles were missed.

## 3. Channel Selection Results

In order to illustrate the effectiveness of the Total Energy Plane method of channel selection, we present here results from an experiment at TASCC in which a beam of $^{24}$Mg at $E_{lab} = 80MeV$ was directed onto a self-supporting $\sim 460\mu g/cm^2$ target of $^{40}$Ca enriched to 99.8% purity. In Fig. 2 a) we show a portion of the $\gamma$-spectrum in coincidence with the detection of 3 protons. Due to the imperfect particle detection efficiencies (the proton and alpha detection efficiencies in this experiment were $\epsilon_p = 0.56$ and $\epsilon_\alpha = 0.42$ respectively) strong peaks appear in this spectrum from all of the 3p, 4p, $\alpha$3p, and 3pn exit channels. The channel selection achieved with particle coincidence gating can be improved significantly, however, using the Total Energy Plane method. In Fig. 1 we show a shading contour plot in the TEP for all events in which 3 protons were detected. The real 3p events have considerably larger total detected energy and are cleanly separated from the contaminating 4p, $\alpha$3p, and 3pn events. As noted in Section 2, channel selection is achieved by taking a two-dimensional gate in the TEP that includes the majority of the events from the desired channel but little contamination from the higher particle multiplicity channels. In Fig. 2 b) we show a $\gamma$-spectrum produced by taking a gate in the 3-proton TEP around the real 3p events. All of the strong peaks in this spectrum are now from the real 3p channel ($^{61}$Cu). While 90% of the real 3p events pass the TEP gate, only 14% of the 4p events survive, and both the $\alpha$3p and 3pn contaminants are almost completely eliminated - less than 4% of these events pass the TEP gate. While real 3p events constitute only 53% of the 3-proton gated spectrum (Fig 2a), the TEP gated spectrum (Fig. 2b) is 95% pure 3p channel.

In the above, the 3-proton gated data, in which the desired channel, 3p, as well as the contaminating channels (4p, $\alpha$3p, and 3pn) were all strongly populated, has been used to illustrate clearly the effectiveness of the TEP method of channel selection. The real power of this method, however, lies in the isolation of very weakly populated low particle multiplicity channels - the channels which leave the nucleus with the highest spin and excitation energy. For example, in our reaction of $^{24}$Mg on $^{40}$Ca at $E_{lab} = 80MeV$ the nucleus observed with the most excitation energy was $^{62}$Zn. This nucleus, populated via the 2p exit channel, constituted only $\sim 0.3\%$ of the total reaction cross section. In Fig. 4a) we show the $\gamma$-spectrum in coincidence with the detection of 2 protons. Due to the very weak population of the 2p channel and the imperfect particle detection efficiencies, this spectrum is completely dominated by contamination from much more strongly populated higher particle multiplicity channels (4p, $\alpha$3p, $\alpha$2pn, 2$\alpha$2p, 3pn, 3p, $\alpha$2p, and 2pn). Of the transitions in $^{62}$Zn only the $2^+ \rightarrow 0^+$ at 954 keV is visible in the 2p-gated spectrum, and this peak is an order of magnitude smaller than those from the contaminating channels.

In Fig. 3 we show the Total Energy Plane for all events in which 2 protons were detected. Although the 2p channel is sufficiently weak compared to the contaminating channels that it does not show up as a peak in this plot, the calculated line of constant energy for the 2p channel focuses our attention on the high energy "bulge" in this TEP that is produced by the real 2p events. Taking the gate shown in Fig. 3 around this bulge we obtain a $\gamma$-spectrum dominated by real 2p events. Using the higher particle multiplicity gated spectra to subtract the remaining small contaminating peaks we obtain the $\gamma$-spectrum shown in Fig 4 b). All of the peaks in this spectrum belong to the real 2p channel ($^{62}$Zn). The TEP gate (before subtraction) improves the channel-to-total ratio for the real 2p channel by a factor of 46 over that obtained by gating on 2 detected protons. With this huge improvement in channel selection, spectroscopic study of this very weakly populated channel becomes possible.

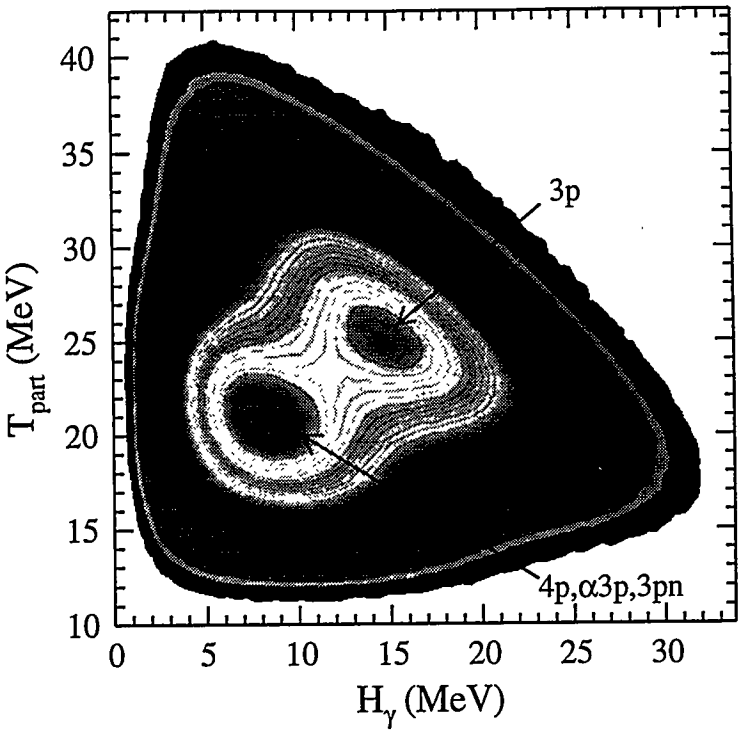


Fig. 1. Total Energy Plane contour plot for all events in which 3 protons were detected. The real 3p events are cleanly separated from the contaminating four-particle channels.

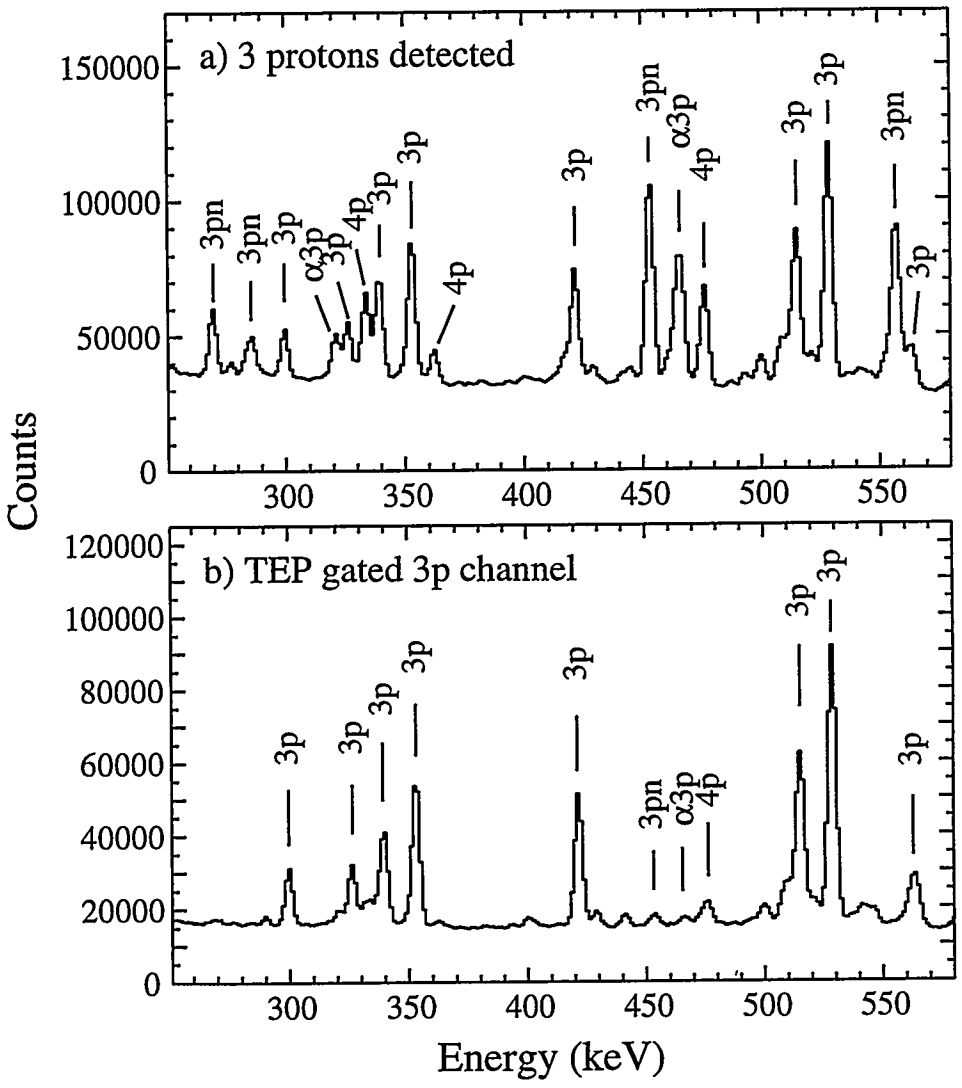


Fig. 2. Portion of the γ-spectra produced by a) gating on 3 detected protons, and b) setting a gate around the real 3p region of the 3p gated Total Energy Plane (Fig.1).

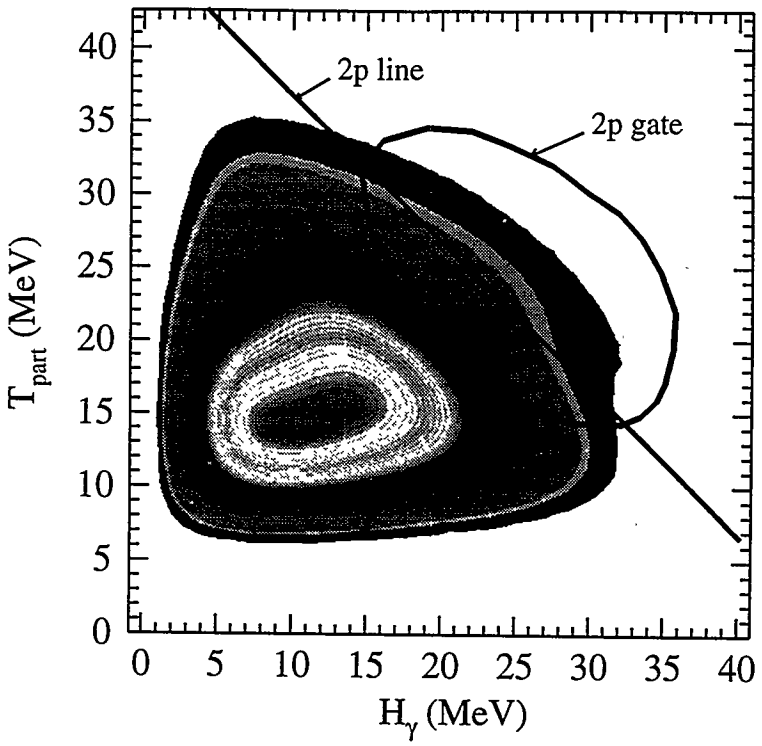


Fig. 3. Total Energy Plane plot for all events in which 2 protons were detected. The high energy "bulge" is produced by events from the very weakly populated 2p channel.

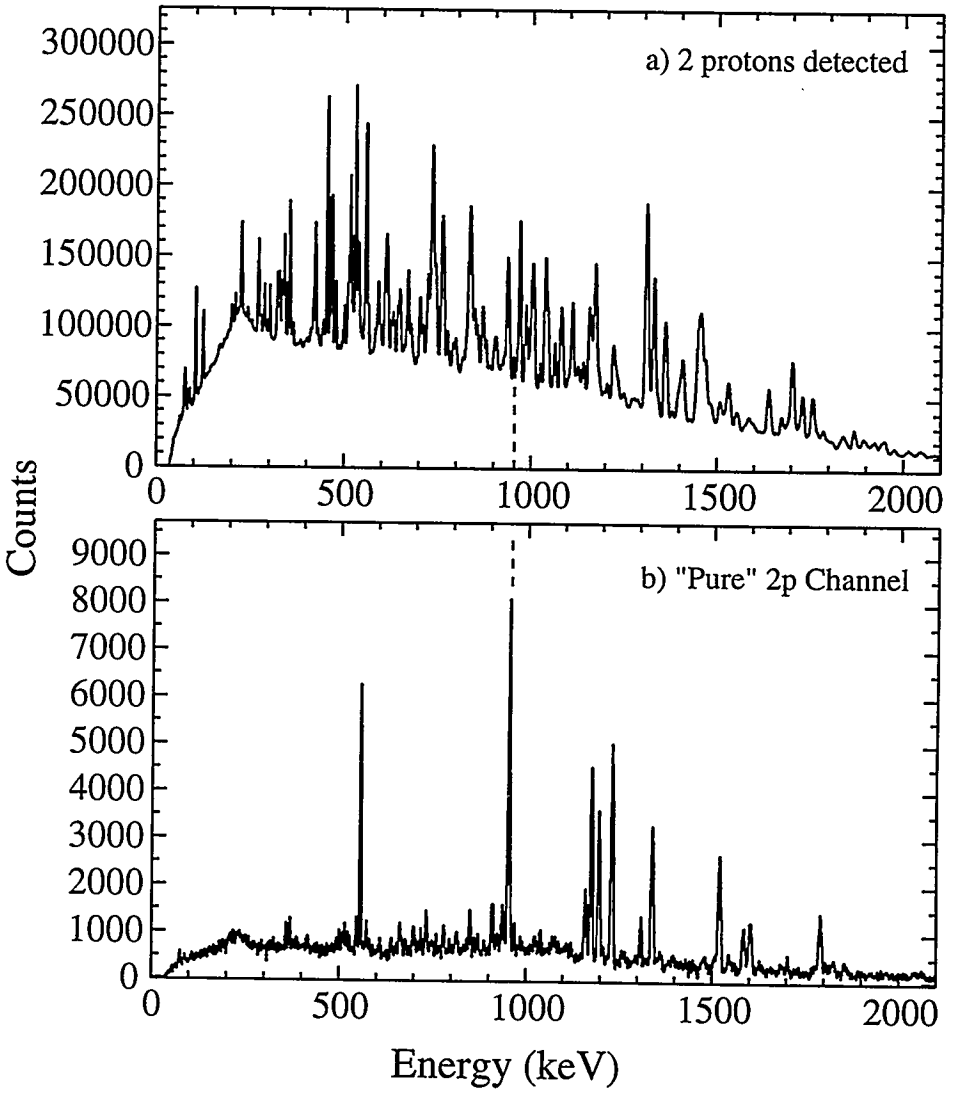


Fig. 4. Comparison of a) the γ-spectrum in coincidence with the detection of 2 protons, and b) a "pure" 2p channel ($^{62}$Zn) spectrum produced by gating in the TEP (Fig.3) and then subtracting remaining contaminants.

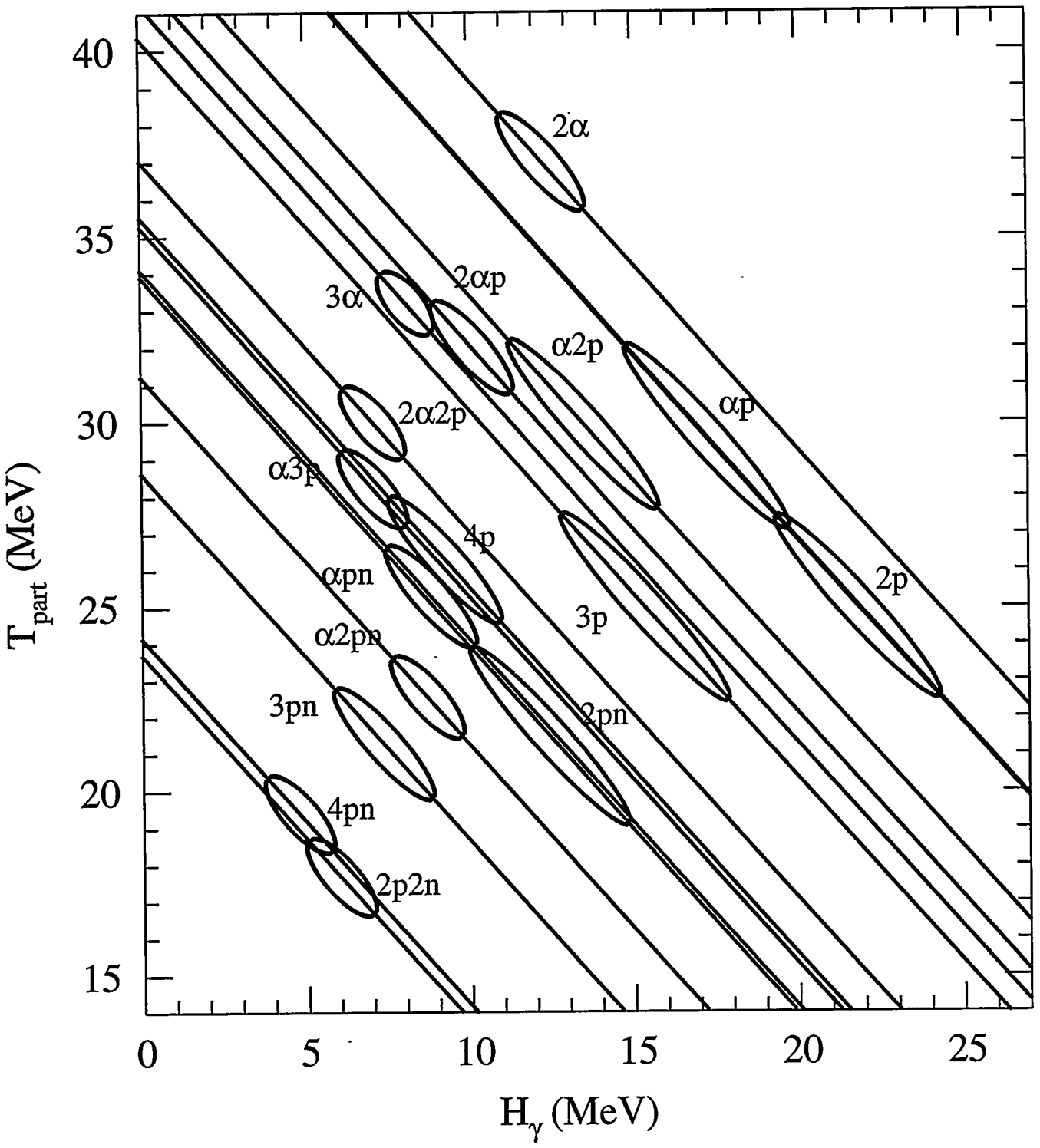


Fig. 5. Entry regions in the Total Energy Plane for the 16 exit channels observed in the reaction of $^{24}Mg$ on $^{40}Ca$ at $E_{lab}$ = 80 MeV. See text for details.

## 4. Excitation Energy Systematics

In Section 2 it was noted that the real 3p events in the 3-proton gated Total Energy Plane must all lie on a line of constant total energy. These events will not, of course, be uniformly distributed along this line. The division of the total CM energy between the kinetic energies of the evaporation particles and the excitation energy left in the final nucleus is determined by the statistical pressures which govern the decay of the compound nucleus. In Fig. 1 we see that the peak in the entry distribution for $^{61}$Cu (the 3p channel) is at a total particle kinetic energy $T_{part} = 25.0MeV$ and a final nucleus excitation energy $H_\gamma = 15.3MeV$. By making TEP plots similar to Fig 1 for all exit channels (gates on discrete $\gamma$-ray transitions are required for weaker channels) the division of the total CM energy can be mapped out for all nuclei produced in a reaction.

In Fig. 5 we show entry regions in the TEP for all 16 exit channels observed in the $^{24}$Mg + $^{40}$Ca experiment. The diagonal lines are the lines of constant total energy for the 16 channels. The semimajor axes of the ellipses (corrected for $T_{part}$ and $H_\gamma$ resolutions) are such that 68% of the channel populations are enclosed, and the semiminor axes represent the spreads in total available CM energy due to beam loss through the target. One interesting feature that is immediately apparent from Fig. 5 is that the sum of the particle kinetic energies is almost identical for the 2p,3p, and 4p exit channels. In other words, the differences in excitation energy left in the final nucleus for these channels are simply the binding energies of the last proton removed. This pattern is also observed for the $\alpha$p, $\alpha$2p, $\alpha$3p and 2pn, 3pn, 4pn exit channel chains. Fig. 5 also shows that of the four N=Z exit channels observed in this experiment (2p2n, $\alpha$pn, 3$\alpha$, and 2$\alpha$) the 2$\alpha$ exit channel leaves the final nucleus with the greatest excitation energy. Although the cross sections are low for pure alpha exit channels in these systems, alpha particles are often emitted from the highest angular momentum components of the compound system [8,9] and these channels provide the best opportunity to study high spin states in even-even N=Z nuclei using stable beams and targets.

## 5. Summary and Outlook

In addition to mapping out excitation energy systematics, the Total Energy Plane has been shown to provide a powerful method for improving channel selection in reactions where charged-particle evaporation from the compound system dominates. This method is presently being employed in the analysis of a series of experiments conducted at the TASCC facility producing the even-even N=Z compound systems in the A = 50-70 mass region. Although this method has been developed to take advantage of the total energy measuring capabilities of the $8\pi$ spectrometer + miniball charged-particle detector array, it is also applicable to other large $\gamma$-ray spectrometer + charged-particle detector arrays. The method could be employed in the analysis of data taken with GASP + ISIS [3], and when combined with the sensitivity of GAMMASPHERE + the microball [2] and the $H_\gamma$ response of GAMMASPHERE with the Hevimet shielding removed [7], the Total Energy Plane method will provide a powerful tool to increase the sensitivity of high spin spectroscopic studies of very proton-rich nuclei far from $\beta$-stability.

## Acknowledgements

This work was partially supported by the Natural Sciences and Engineering Research Council of Canada (NSERC) and Atomic Energy of Canada Limited (AECL). We thank the staff at TASCC for supplying the beam.

---

### References

[1] A. Galindo-Uribarri, Prog. Part. Nucl. Phys. 28 (1992) 463.
[2] D.G. Sarantities et al., Nucl. Instr. and Meth. A, in press.
[3] E. Farnea et al., LNL - INFN (Rep) - 095/95 189.
[4] T. Kuroyanagi et al., Nucl. Inst. and Meth. A316 (1992) 289.
[5] D.W. Stracener et al., Nucl. Inst. and Meth. A294 (1990) 485.
[6] C.E. Svensson et al., submitted to Nucl. Inst. and Meth. A.
[7] M. Devlin et al., this conference and preprint, 1996.
[8] J. Gilat and J.R. Grover, Phys Rev C 3 (1971) 734.
[9] C. Baktash, this conference.

# ALPHA PARTICLE SPECTRA IN COINCIDENCE WITH NORMAL AND SUPERDEFORMED STATES IN $^{150}$Tb

G. Viesti[1], M. Lunardon[1], D. Bazzacco[1], R. Burch[1], G. de Angelis[2], M. Cinausero[2], D. Fabris[1] E. Farnea[2], E. Fioretto[2], S. Lunardi[1], N. H. Medina[1], G. Nebbia[1], G. Prete[2], C. Rossi Alvarez[1], G. Vedovato[2]

[1] *Dipartimento di Fisica dell'Universitá and INFN, Sezione di Padova, Padova, Italy*
[2] *INFN, Laboratori Nazionali di Legnaro, Legnaro, Italy*

## 1. Introduction

The study of correlations between particle evaporation from highly excited compound nuclei at large angular momenta and the states in the final evaporation residues (ER) is a field of investigation which has been opened, in the last years, with the advent of the new large $\gamma$-ray arrays [1-5]. It is now possible to correlate the evaporation spectra to various bands with shapes ranging from spherical to superdeformed (SD) in the same final nucleus.

It is generally accepted that the particle evaporation from the compound nucleus is chaotic and that only in the near-yrast $\gamma$ cascade, where the feeding of different classes of states takes place, the ordered motion is restored [6]. The sensitivity of the particle spectra on the feeding of specific states in the residual nuclei can be taken as an indication that additional degrees of freedom might be important in the evaporation process or that particular regions of the phase space open to the decay populate preferentially some selected structures in the final cold nucleus. This latter point is important for the understanding of the feeding mechanism of SD states.

Several experiments performed so far did not find a clear dependence of the shapes of the particle spectra on the excited states having different deformations in the ER. For example, the proton spectra in coincidence with transitions in the SD bands of $^{133}$Nd [4] and $^{152}$Dy nuclei [4,5] were found to be similar to those in coincidence with transitions in the normal deformed (ND) bands.

Alpha particles have been proposed since long as a sensitive probe of the deformation of the emitting nucleus [7]. Results are presented here of an experiment in which we have measured the energy spectra of alpha particles associated with different classes of states (ND and SD) in the $^{150}$Tb nucleus populated in the reaction $^{37}$Cl($^{120}$Sn,$\alpha$3n$\gamma$)$^{150}$Tb.

## 2. Experimental details

The experiment was performed at the XTU Tandem facility of the Laboratori Nazionali di Legnaro using a beam of 187 MeV $^{37}$Cl (intensity $\sim$8 pnA) and a target made of two foils (0.5 mg/cm$^2$+0.4 mg/cm$^2$) of $^{120}$Sn. Gamma-rays were detected using the GASP spectrometer [8]. Charged particles were detected with the ISIS silicon ball which is made of 40 $\Delta$E-E telescopes (130 $\mu$m and 1000 $\mu$m thick, respectively) covering a geometrical solid angle of about 90% of $4\pi$. The event trigger was determined by any three or more Compton suppressed Ge detectors and five or more BGO scintillators of the GASP inner ball firing in coincidence with the charged particle detectors.

A total of $5.5\times10^8$ events in coincidence with alpha particles were recorded. The $\alpha$ spectra shown in the following are those measured in the first forward ring of the silicon ball

(six telescopes at $\theta_{lab}$~34°) for which the threshold due to the thickness of the ΔE detector is unimportant. The energy spectra of the telescopes were summed, after gain matching.

Fig.1.

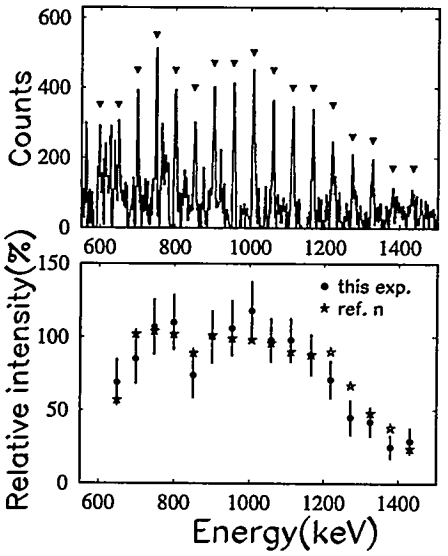


The data in coincidence with $\alpha$-particles have been sorted into various matrices and cubes, with proper conditions on the fold k and sum energy H measured in the inner ball.

The $\gamma$-ray spectra in coincidence with alpha particles and associated with long $\gamma$-ray cascades selected in the inner ball ( fold k>10 and sum energy H>14 MeV) are very clean and show practically only the residual nuclei $^{149,150}$Tb. With the mentioned conditions on fold and sum energy, the total number of events is only $1.6\times10^8$.

The spectrum of the known yrast SD band in $^{150}$Tb [9,10] extracted from the $\gamma$-$\gamma$-$\gamma$ data in coincidence with $\alpha$-particles is shown in Fig.1. The intensity of the band is ~0.7% of the $^{150}$Tb total population, a figure which compares well with the data of the ($^{31}$P,5n) reaction reported in ref.10. The feeding pattern of the band seems to be scarcely affected by the reaction used, as shown in the lower panel of Fig.1.

### 3. Alpha particle spectra.

The $\alpha$ particle spectra in coincidence with ND states in $^{149,150}$Tb nuclei and with the yrast SD band of $^{150}$Tb are shown in Fig.2. For comparison, Monte Carlo CASCADE Statistical Model calculations [11,12] are presented in the same figure.

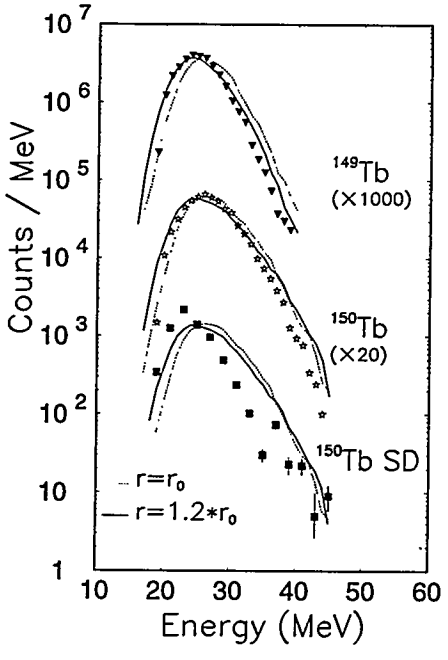


Fig.2

The spectral shapes of the alpha particles in coincidence with ND states are reproduced by calculations in which standard input parameters [5] are used, with the exception of the emission barrier which is lowered. This is achieved by increasing the radius in the Optical Model potential ($r=1.2\times r_0$, where $r_0$ is the radius of the spherical nucleus). The radius expansion has been introduced often in the past in order to simulate the emission from a deformed nucleus [12].

A decrease of the mean alpha particle energy associated with the $^{149}$Tb nucleus ($\alpha$4n decay, $<E_\alpha>$=25.24 MeV) with respect to $^{150}$Tb ($\alpha$3n decay, $<E_\alpha>$=26.90 MeV) is evident from Fig.2. This effect is well accounted for by the statistical model calculations which give $<E_\alpha^{calc}>$=25.6 MeV and $<E_\alpha^{calc}>$=26.8 MeV, respectively.

The $\alpha$-spectrum in coincidence with the yrast SD band of $^{150}$Tb has been derived from the $\gamma$-$\gamma$-$E_\alpha$ cube by carefully selecting the gates on the transitions of the band in order to avoid contaminations from other structures. This is possible since detailed level schemes of both the $^{149}$Tb and

$^{150}$Tb nuclei are available [13,14]. We have also verified in the $\gamma$-$\gamma$-$\gamma$ cube that, by double gating on the selected SD transitions, none of the lines appearing in the resulting $\gamma$-ray spectrum belong to the $^{149}$Tb nucleus. The alpha particle spectrum in coincidence with the $^{150}$Tb yrast SD band was constructed using the following procedure: first a $\gamma$-$E_\alpha$ matrix was created from the $\gamma$-$\gamma$-$E_\alpha$ cube without background subtraction. A $\gamma$-$E_\alpha$ background matrix was then created selecting proper background regions for each SD transition. This background matrix was subtracted from the previous one. The final spectrum of Fig.2 was obtained using only the SD band transitions with energies of 954, 1007, 1112, 1166, 1219 and 1272 keV. The average energy of this spectrum is $<E_\alpha>=25.06\pm0.01$ MeV, which is about 2 MeV lower than that derived for the ND states of $^{150}$Tb.

Fig.3

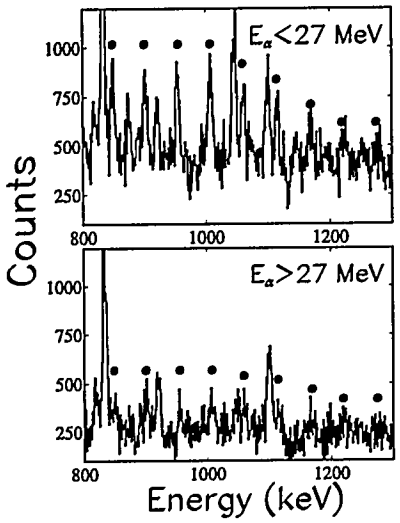


As a cross check of this result, two $\gamma$-$\gamma$ matrices were also created from the $\gamma$-$\gamma$-$E_\alpha$ cube requiring a coincidence with $\alpha$-particles of energy larger than or lower than the average energy of the spectrum in coincidence with the ND states of $^{150}$Tb. Gates have then been set on the SD transitions in both $\gamma$-$\gamma$ matrices. The results reported in Fig.3, confirm that the SD band is preferentially populated (a factor 1.9 larger) by alpha particles having lower energies. This means that the optimal conditions for observing weak SD structures populated in an $\alpha xn$ decay chain in this mass region is the simoultaneus requirement of high fold conditions in the inner ball and low energy in the charged particle detectors.

Fig.4

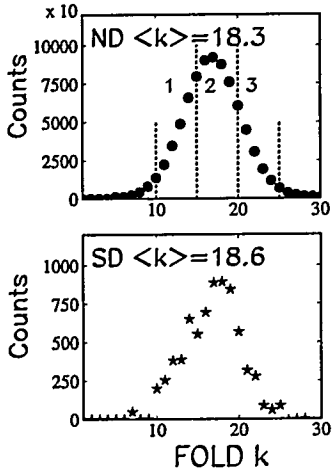


In order to explain the shift in energy between the alpha particles associated with the ND and SD bands we have explored their angular momentum dependence and how this is reflected by the average energy $<E_\alpha>$. For this purpose, we have extracted the k-fold distributions of the events associated with the spectra of Fig.2 by double gating on a $\gamma$-$\gamma$-k cube. The fold distributions themselves do not exhibit sizeable differences when selecting ND ($<k_{ND}>=18.3$) and SD ($<k_{SD}>=18.6$) transitions in the $^{150}$Tb nucleus, as shown in Fig.4. This does not imply a similarity in the associated angular momentum, because the average multipolarity of the gamma-rays cascade in coincidence with ND and SD states is not the same [15].

The feeding of the yrast SD band of $^{150}$Tb is known to occur at spins $I_{ER}\sim48$-$58\hbar$ [9,13] and this is confirmed by the feeding pattern obtained in the present experiment. Therefore, we may associate to the measured mean fold $<k_{SD}>$ in coincidence with the SD band an angular momentum of at least $I_{ER}\sim53\hbar$. Taking into account a correction $\Delta J\sim8\ \hbar$ for the angular momentum carried away by the alpha particles [16], the average value of the compound nucleus angular momentum correlated with the SD spectrum is estimated to be $<J_{SD}>\geq61\ \hbar$. On the other hand, the value $<k_{ND}>=18.3$ for the ND states of

$^{150}$Tb nucleus can be associated with a much lower angular momentum value, $<J_{ND}>\approx 47\ \hbar$, using an empirical spin-fold calibration for ND states in this mass region [17] and the above defined correction for the $\alpha$-particles evaporation.

Fig.5

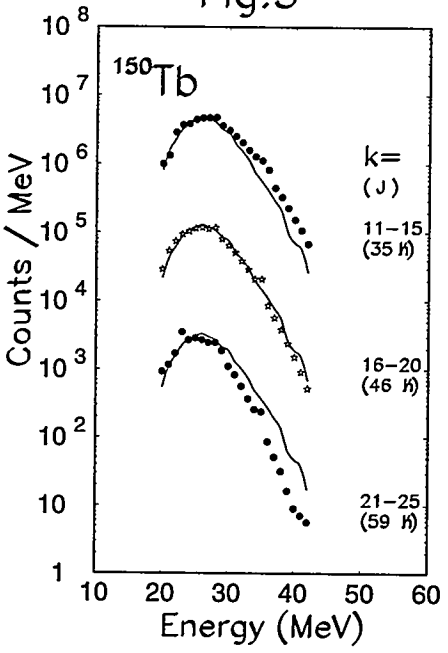


In order to understand better the role of the angular momentum in the observed effects, we have derived the $\alpha$ spectra feeding the ND states in $^{150}$Tb for three different fold conditions k=11-15, k=16-20 and k=21-25, which correspond roughly [17] to $J_{ND}\approx 35\hbar$, $46\hbar$ and $59\hbar$, respectively. In Fig.5 the latter spectra are compared with the total $\alpha$-particle spectrum with no condition in fold (solid line). The energy distribution exhibit, with increasing fold, a shift toward lower energies becoming also narrower. Qualitatively, the same effect was observed in the proton spectra of Refs. 1,2,5 where it was reproduced by statistical model calculations and explained in terms of the reduction of the thermal energy available to the decay chain when increasing the fold k (or equivalently the angular momentum).

Fig.6

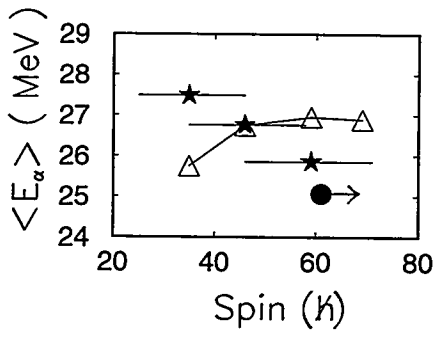


The correlation between $<E_\alpha>$ and the average angular momentum (stars) is reported in Fig.6, where the value in coincidence with the SD band (heavy dot) is also included. The experimental data feature a continuous decrease of the average energy with increasing angular momentum without a marked distinction between the ND and SD data. Furthermore, from the CASCADE calculations reported also in Fig.6 (triangles), it appears clearly that the statistical model does not describe correctly the angular momentum dependence of $<E_\alpha>$. In fact, the average energy is predicted to increase with the angular momentum. The energy of the charged particles emitted from an equilibrated compound nucleus depend on the nuclear temperature $T$ of the daughter nucleus, on the emission barrier $B$ and on the channel orbital angular momentum. The energy associated to the orbital angular momentum is often indicated as the so-called spin-off contribution [18]. In the actual CASCADE statistical model calculations the barrier $B$ does not depend on the angular momentum of the compound nucleus, whereas the balance between the reduction of $T$ with increasing angular momentum and the spin-off depends on the phase space open to the decay. Results reported in Fig.6 suggest that the reduction in thermal energy is overwhelmed in the model by the spin-off contribution.

## 4. Conclusions.

From the results reported here, it seems that the $\alpha$ energy spectra in coincidence with a given decay channel are, as those of protons, affected by the different selection of the $\gamma$-ray fold k and therefore of the angular momentum.

In contrast with earlier investigations of the proton spectra, a clear difference in energy is observed between the $\alpha$ spectra in coincidence with states having different deformation in a given decay channel, the SD channel being shifted to lower energies. Despite the uncertainties in deriving the angular momentum from the measured k-fold in the case of the ND and SD structures, the present work strongly suggests that the bulk of this effect is related to the differences in the angular momenta associated with the two classes of states.

The standard statistical model (CASCADE code) fails in reproducing quantitatively and qualitatively the angular momentum dependence of the $\alpha$ spectra. A further lowering of the emission barriers, with respect to the Optical Model ones, seems to be required to describe the spectra at the higher angular momenta. The failure of the model predictions was not evidenced in earlier studies because of the lower sensitivity of the energy spectra of protons to angular momentum induced effects (as the spin-off energy and changes in the emission barrier).

The modelling of the statistical decay at large angular momenta, especially in the region of competition between evaporation and fission (J$\sim$70$\hbar$ in the present case) should be further pursued as it is particularly important for the understanding of the feeding mechanism of the SD bands and of the dynamics of the fission process.

1) D.G. Sarantites et al., Phys. Rev. Lett. 64 (1990) 2129.
2) D.J. Blumenthal et al., Phys. Rev. Lett. 66 (1991) 3121.
3) K. R. Phol et al., Phys. Rev. C49 (1994) 1372.
4) A. Galindo-Uribarri, Prog. Part. Nucl. Phys. 28 (1992) 463.
5) G. Viesti et al., Phys. Rev. C51 (1995) 2385.
6) T. L. Khoo et al., Nucl. Phys. A557 (1993) 83.
7) R. G. Stokstadt, Treatise on Heavy-Ion Science, edited by D.A. Bromley (Plenum, New York, 1985) Vol 3, p.83 and references therein.
8) D. Bazzacco et al. Phys. Lett. B309 (1993) 235.
9) M.A. Deleplanque et al., Phys. Rev. C39 (1989) 1651.
10) P. Fallon et al., Phys. Rev. C52 (1995) 93.
11) F. Pulhofer, Nucl. Phys. A280 (1977) 267.
12) R. K. Choudhury et al., Phys. Lett. 143B (1984) 74.
13) G. Duchene et al., Z. Phys. A350 (1994) 39
14) Z. Meliani et al., Nucl.Phys. A575 (1994) 221.
15) see for example F. Soramel et al. Phys. Lett. B350 (1995) 173.
16) average value estimated by the statistical model code PACE2.
17) M. Lops, Thesis, University of Padova 1994, unpublished.
18) N.N. Ajitanand et al. Phys. Rev. C34 (1986) 877.

# The Microball and Gammasphere: Research Highlights and Future Directions

M. Devlin, D.G. Sarantites, D.R. LaFosse, and F. Lerma
Chemistry Department, Washington University, Saint Louis, MO 63130

August 27, 1996

**Abstract**

The Microball, a compact, $4\pi$ charged-particle detector array, has been used in conjunction with Gammasphere for numerous physics experiments, and more are planned in the near future. A summary of this research program is presented, and the device and its capabilities are described. An example of its use in the study of the population and entry state excitation energy distributions of normal and superdeformed bands in $^{82}$Sr is presented.

## 1 Introduction

The Microball [1] is a 95 element array of CsI(Tl) detectors designed as an exit channel and particle spectroscopy device to be used in conjunction with Gammasphere. To date, it has been used in over twenty physics experiments, and many more are planned. The topics addressed by these studies include superdeformation in the $A = 80$ region [2], reaction mechanism studies of the population of superdeformed bands [3, 4], spectroscopy of $N = Z$ nuclei [5], identification of new SD bands in Eu [6], Sm [7], and numerous $A = 130$ [8, 9] isotopes, investigations of identical bands in $A = 150$ [6] and 80 [10] nuclei, investigations of $\Delta I = 4$ staggering [11], studies of the decay out of SD bands in Eu [6], spectroscopy in the $A = 80$ region [12, 14, 15, 16], and searches for hyperdeformation in Gd [17, 18] and Sm [7] isotopes.

The capabilities and performance of the Microball will be discussed in the following section. An example of a current application of the Microball and Gammasphere will then be presented, namely a study of the entry states for superdeformed and normal deformed bands in $^{82}$Sr. This example is chosen because it illustrates the use of the Microball to study the connection between reaction dynamics and nuclear structure, and because it is atypical in that it involves using Gammasphere as an auxiliary device for the Microball.

## 2 Performance of the Microball

The coincident detection of both evaporated particles and de-excitation $\gamma$-rays in fusion-evaporation reactions offers the possibility of studying both nuclear structure and reaction dynamics in detail. Charged particle detection provides both exit channel selection and recoil momentum reconstruction, allowing accurate event-by-event Doppler correction and hence improving the resolving power. Central to such a detection system are the technical requirements for evaporated particle identification, high detection efficiency ($\approx 4\pi$ coverage), low total mass, and the ability to function with high counting rates. The Microball accomplishes these tasks with an array of 95 CsI(Tl) scintillation detectors with photodiode readout. Pulse-shape and rise-time discrimination between protons

and alpha particles is used, and the array has 96% geometric coverage and high granularity. The particle identification is sufficient to cleanly discriminate between protons, deuterons and tritons at reasonable counting rates, and provides proton/alpha particle discrimination for all of the detectors at count rates in excess of 3-4000 counts/detector/s. For the near-barrier energies typically used at Gammasphere, excellent channel selection is obtained, with single proton detection and

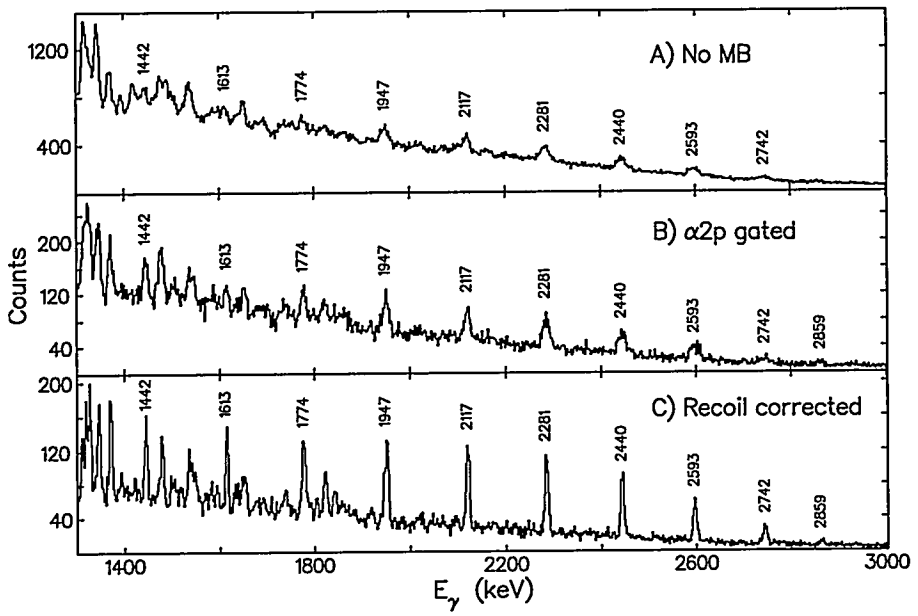


Figure 1: Yrast superdeformed band in $^{80}$Sr, double-gated on the labeled lines, A) without exit channel selection, B) with the $\alpha$ 2p channel selected, and C) with the recoil-momentum residual Doppler shift correction applied. No background subtracted in used.

identification efficiencies of up to 0.9. The performance of the array has continually improved with each use, and is now capable of keeping up with Gammasphere data rates in most experiments without compromising the particle identification.

As an example of the capabilities of the Microball, figure 1 shows the improvement in resolving power obtained with the Microball in the case of the yrast superdeformed band in $^{80}$Sr [13]. Channel selection improves the peak to background ratio in this case, and applying a recoil momentum reconstruction correction to the Doppler shift further improves both the peak to background ratio and the peak width, from $\approx$ 20 keV to $\approx$ 8 keV at $E_\gamma = 2$ MeV.

The channel selection properties of the Microball are sufficiently powerful to allow the extraction of detailed spectroscopic information even for weak charged-particle channels. For example, the $3\alpha$ channel was studied in a recent experiment at Gammasphere (with 57 Ge detectors), and provided new data on high spin states in $^{76}$Kr [14]. The cross section for this channel was about 2 mb. The ultimate limit in cross section that can be studied in such a manner is certainly well below a millibarn, though for channels close to or past the $N = Z$ line, the addition of neutron detectors and/or recoil separators are needed.

The cost of using the Microball inside Gammasphere is that the additional mass of the Microball reduces the $\gamma$-ray response of Gammasphere. Detailed simulations [19] indicate that this loss is severe at low $\gamma$-ray energies (below $\approx$150 keV), less than 10% at $E_\gamma = 500$ keV, and decreases with increasing $E_\gamma$.

# 3 The population of SD bands

A topic of current interest is the correlation between the population of specific bands or shapes in nuclei following heavy ion fusion-evaporation reactions, and the spectra of the evaporated particles. Such studies have been reported both for normal deformed bands [20, 21, 22, 23] and for superdeformed bands [24]. The combination of the Microball and Gammasphere provides high-quality data with which to pursue these issues, and a study of the evaporated proton spectra in the $^{28}$Si($^{58}$Ni,4$p$)$^{82}$Sr reaction has recently been carried out. A similar study for the residual nucleus $^{145}$Tb is also being carried out with the Microball and Gammasphere [3].

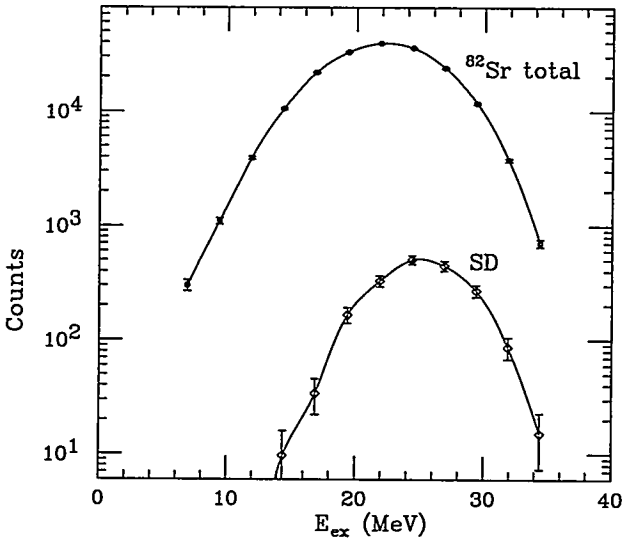


Figure 2: Entry state excitation energy distributions for the total and SD population of $^{82}$Sr

The motivation behind this study is two-fold: first, to investigate previous reports of difference in proton spectra correlated with the population of side bands in $^{82}$Sr [20, 22], and secondly to extend such studies to include the population mechanism of superdeformed (SD) states. $^{82}$Sr has been reported to possess a SD band populated at about the 1% level [15, 25]. A distinct advantage of studying an exit channel which consists only of evaporated, charged particles is that the sum of the particle energies is a direct measure of the resulting excitation energy ($E^*$) in the residual nucleus, provided no $\gamma$-emission occurs prior to particle emission. In the present case the exit channel consists of four protons.

Figure 2 shows the extracted entry-state excitation distributions for both the total $^{82}$Sr population and SD population. The SD band is populated at an average excitation energy ($E^*$) approximately 3 MeV greater than that characteristic of the (predominantly) normal-deformed population. As expected from this result, cuts on $E^*$ produce $\gamma$-ray spectra which have different SD intensities. Figure 3 shows four such $\gamma$-ray spectra, obtained from the $E^*$ cuts shown and single gates on the SD band members. The SD intensity is seen to decrease relative to the normal deformed lines with decreasing $E^*$, and the population of the highest spin states in the SD band is seen to be particularly effected by the $E^*$ cuts. This energy shift in the evaporated particle spectra associated with SD population is consistent with measurements in other systems [6, 24, 26, 27], though not with all prior measurements [28].

The decrease in SD feeding spin with decreasing $E^*$ cuts hints at an explanation for the SD–ND excitation energy shift: SD is fed differently than ND because it has a higher average spin, and the

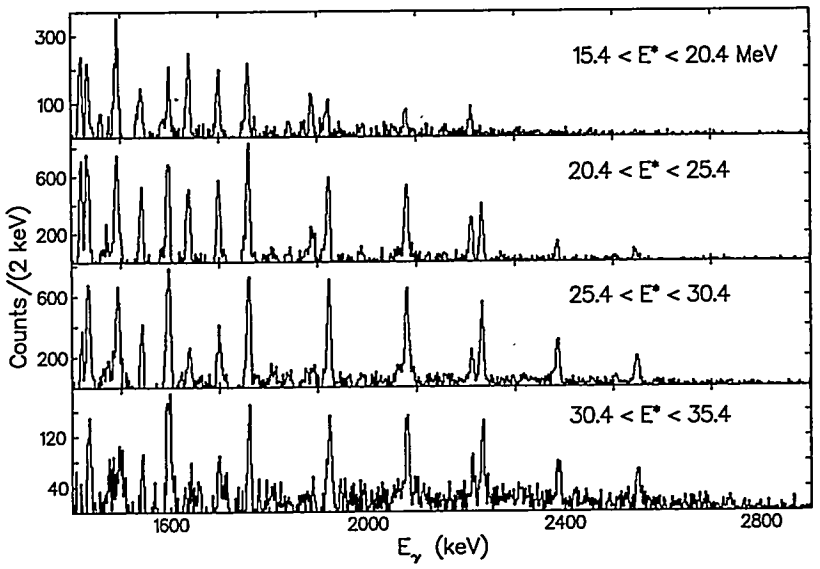


Figure 3: Single-gated SD spectra for the yrast SD band in $^{82}$Sr, for the ranges in excitation energy shown.

average entry $E^*$ is correlated with the entry spin. The quality of the Microball–Gammasphere data is sufficient to investigate this directly by gating on individual transitions and extracting the sum proton energy ($\Sigma E_p$). Figure 4 shows the average summed proton energy ($\Sigma E_p$) corresponding to the feeding of a state at spin $I$ (bottom) and $E_I$ (top) for various bands, obtained by double-gating on the two transitions below each state in the band. These data represent the average entry-state $E^*$ for each state, including both direct and side feeding, and therefore give a cumulative measure of the total $E^*$ distribution. All of the bands shown, including the SD band, conform to the same trend, indicating that the entry state spin distributions are positively correlated with $E^*$ distributions.

The differences among ND levels and bands in figure 4 are currently being studied; since no background was subtracted in producing the results shown, contaminations from other channels may either mask small systematic differences or make others appear larger. From the general trend of the SD band it is seen that, at least on average, the population mechanism of SD states is not different from that of normal deformed states. The spins of the SD band are determined from the measured feeding into normal deformed states, and the lowest SD level is put at an excitation energy of 10 MeV, so that the top half of figure 4 is consistent with the bottom half, as one would expect.

The interesting subject of whether other degrees of freedom influence the subsequent population of particular bands can be investigated in detail with Gammasphere and the Microball. In particular, the question of the possible influence of deformation at the time of fusion on SD population is being studied. The present results imply that such effects will likely be small, and in order to study them it is essential that $\gamma$-ray multiplicity ($k$) and sum energy ($H$) information be obtained with Gammasphere, in order to separate the dominant phase space effects from more subtle effects. The use of Gammasphere, without the Hevimet collimators, as a sum spectrometer has been investigated in simulations [19], and data have been taken in this mode already in two experiments.

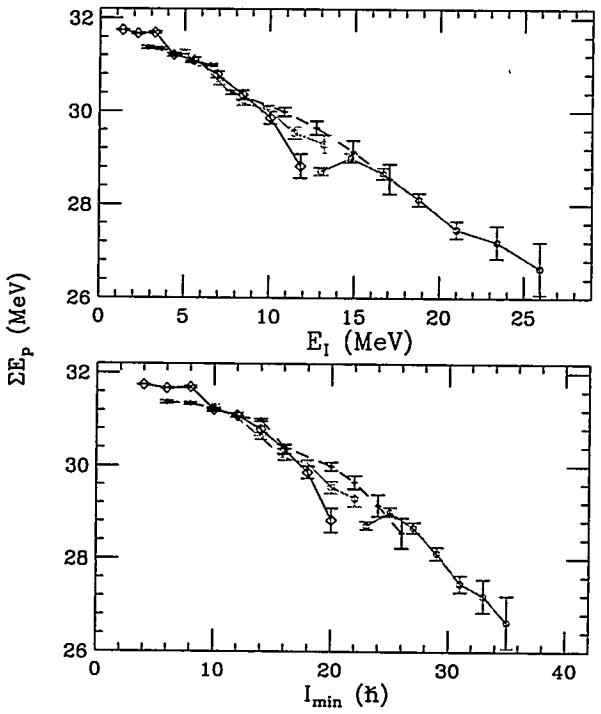


Figure 4: Sum-proton energy centroids for individual states as a function of the level energy (top) and spin (bottom). Four separate bands are shown, including the ground band (diamonds) and SD band (circles). The other two bands are normal-deformed side bands.

## 4 Future directions

The current capabilities of the Gammasphere and the Microball have produced a considerable amount of interesting physics, and will continue to do so, both in the exploration of SD and normal deformed spectroscopy and in studies of reaction mechanisms. The additional capabilities provided by the use of Gammasphere as a sum spectrometer will also undoubtedly be exploited, as will the coupling of neutron detectors to the Gammasphere-Microball arrangement to study the most neutron-deficient nuclei.

Future improvements in the design of $4\pi$ charged particle detector arrays are being considered. One such plan for a next-generation device, the "Nanoball", has been produced. Its major improvement is increased segmentation, in order to better keep up with the high counting rates typical at Gammasphere.

When Gammasphere is coupled with the FMA at ANL, the Microball will be able to augment the mass identification provided by the FMA with accurate, high efficiency $Z$ identification. The coupling of the FMA and the Microball has already been accomplished in a recent experiment to measure evaporation residue cross sections at 10 MeV/nucleon, demonstrating the technical feasibility of the combination [30].

## References

[1] D.G. Sarantites, P.-F. Hua, M. Devlin, L.G. Sobotka, J. Elson, J.T. Hood, D.R. LaFosse, J.E. Sarantites, and M.R. Maier, Nucl. Instr. and Meth. A, in press.

[2] C. Baktash, et al., these proceedings, and references therein.
[3] J.N. Wilson, et al., these proceedings, vol. 1, p. 51, and to be published.
[4] M. Devlin, et al., to be published.
[5] M. Leddy, et al., these proceedings, vol. 1, p. 121, and to be published; P. Hausladen, et al., to be published.
[6] F. Lerma, et al., these proceedings and to be published
[7] H.-Q. Jin, et al., these proceedings, vol. 1, p. 19, and to be published.
[8] J. Pfohl, et al., these proceedings, vol. 1, p. 38. and to be published.
[9] D.T Joss, et al., Phys. Rev. C, in press.
[10] H.-Q. Jin, et al., these proceedings, vol. 1, p. 18. and to be published.
[11] S. Flibotte, et al., to be published.
[12] J. Döring, et al., these proceedings, vol. 1, p. 73. and to be published.
[13] M. Devlin, et al., these proceedings, vol. 1, p. 9, and to be published.
[14] D. Rudolph, et al., these proceedings, vol. 1, p. 98. and to be published.
[15] C.-H. Yu, et al., these proceedings, vol. 1, p. 54. and to be published.
[16] G.N. Sylvan, et al., BAPS 41, (1996), 899. and to be published.
[17] D.R. LaFosse, et al., Phys. Rev. Lett., 74, (1995), 5186.
[18] D.R. LaFosse, D.G. Sarantites, C. Baktash, S. Asztalos, M.J. Brinkman, B. Cederwall, R.M. Clark, M. Devlin, P. Fallon, C.J. Gross, H.-Q. Jin, I.Y. Lee, F. Lerma, A.O. Macchiavelli, R. MacLeod, D. Rudolph, D.W. Stracener, and C.-H. Yu, Phys. Rev. C, in press.
[19] M. Devlin, L.G. Sobotka, D.G. Sarantites, and D.R. LaFosse, Nucl. Instr. and Meth. A, in press.
[20] D.G. Sarantites, C. Baktash, N.G. Nicolis, G. Garcia-Bermudez, V. Abenante, J.R. Beene, N.R. Johnson, M.L. Halbert, D.C. Hensley, F.K. McGowan, H.C. Griffin, I.Y. Lee, Z. Majka, M.A. Riley, T.M. Semkow, D.W. Stracener, and A. Virtanen, Phys. Rev. Lett. 64 (1990) 2129.
[21] D.J. Blumenthal, C.J. Lister, P. Chowdhury, B. Crowell, P.J. Ennis, Ch. Winter, T. Drake, A. Galindo-Uribarri, G. Zwartz, H.R. Andrews, G.C. Ball, D. Radford, D. Ward, and V.P. Janzen, Phys. Rev. Lett. 66 (1991) 3121.
[22] K.R. Pohl, P.H. Regan, J.W. Arrison, D.P. Balamuth, Phys. Rev. C49 (1994) 1372.
[23] D.W. Stracener, Ph.D. thesis, Washington University, 1993, unpublished.
[24] G. Viesti, M. Lunardon, D. Bazzacco, D. Fabris, S. Lunardi, N.H. Medina, G. Nebbia, C. Rossi Alvarez, G. de Angelis, M. Cinausero, E. Farnea, E. Fioretto, G. Prete, and G. Vedovato, Phys. Lett. B382 (1996) 24; also G. Viesti, et al., these proceedings.
[25] A.G. Smith, P. Dagnall, J.C. Lisle, D.H. Smalley, T.R. Werner, R. Chapman, C. Finck, B. Haas, M. Leddy, W. Nazarewicz, D. Prévost, N. Rowley, and H. Savajols, Phys. Lett. B355 (1995) 32.
[26] T.L. Khoo, R.V.F. Janssens, E.F. Moore, K.B. Beard, Ph. Benet, I. Ahmad, M.P. Carpenter, R.R. Chasman, P.J. Daly, M.W. Drigert, U. Garg, Z.W. Grabowski, F.L.H. Wolfs, and D. Ye, Nulc. Phys. A520 (1990) 169c.
[27] T. Lauritsen, Ph. Benet, T.L. Khoo, K.B. Beard, I. Ahmad, M.P. Carpenter, P. Daly, M.W. Drigert, U. Garg, P.B. Fernandez, R.V.F. Janssens, E.F. Moore, F.L.H. Wolfs, and D. Ye, Phys. Rev. Lett. 69 (1992) 2479.
[28] D. Ward, Nucl. Phys. A520 (1990) 139c.
[29] N.G. Nicolis, D.G. Sarantites, and J.R. Beene, computer code EVAP, unpublished.
[30] R.J. Charity, et al., to be published.

# STRUCTURE AND REACTIONS OF DRIP-LINE NUCLEI

P.G. Hansen
National Superconducting Cyclotron Laboratory
and
Department of Physics and Astronomy
Michigan State University, East Lansing MI 48824-1322

## 1. Introduction

Secondary radioactive beams produced at intermediate-energy heavy-ion accelerators have in a short time span added a new dimension to the research on nuclear species at the limits of particle stability, and new detection techniques have made it possible to study reactions caused by incident beams of as little as one particle per second. Imminent developments such as the M.S.U. Coupled-Cyclotron Facility [1] are expected to extend the range and to permit the observation of many previously inaccessible species. For a perspective on the progress in this area we only need to go about fifteen years back to a time when it had just become possible to study the radioactivity of rare nuclear species such as $^{11}$Li. In presenting early experiments with secondary beams produced in fragmentation James Symons [2] said "... In the introduction to this paper we questioned the applicability of high-energy heavy-ion accelerators to this field. Our experience at the Bevalac leads us to believe that this question does indeed have a positive answer. If the physics interest justifies it, then high-energy heavy-ion beams can certainly be expected to play a role in the study of nuclei at the limits of stability." At the time, very few, if any, realized how prophetic this remark was.

In the present paper the interpretation of the longitudinal-momentum distributions from the nuclear fragmentation of single-nucleon halos is discussed. It is pointed out that these measurements, at least for the cases studied so far, directly reflect the halo wave function, and that there is no direct contribution from the reaction mechanism. This is an important difference from the radial momentum distributions, for which diffractive processes play an important role.

Let me mention in passing that while final-state interactions seem relatively unimportant for the cases to be discussed in the following, they are essential for understanding the continuum states in $^{10}$Li. The latter are, in turn, the key to understanding the three-body system $^{11}$Li. The importance of this aspect was first identified by Barranco et al. [3], and the influence of both nn and n-$^{9}$Li final-state interactions has been the subject of an interesting series of papers by Garrido et al. [4].

## 2. Stripping and Diffraction Dissociation of Nuclear Halos

It has commonly been assumed that the longitudinal momentum distributions of the core fragment in reactions such as ($^{11}$Be, $^{10}$Be) and ($^{8}$B, $^{7}$Be) on light targets represented the true momentum distribution of the halo state. This would imply that experiments on a single-nucleon halo measured the square of the Fourier transform of the total wave function. A series of papers [5-10]

have now shown that the information actually obtained is more specific and, in fact, more interesting. The essential point is that the reactions that remove the halo nucleon can only sample the halo proper, i.e. the region of space outside of the nuclear core. The core-target collisions at small impact parameters lead to other exit channels, mainly complex fragmentation reactions. When this geometrical selection is taken into account, the calculations agree well with the measured [11-13] momentum widths and cross sections.

Owing to a number of favorable circumstances, the analysis of dissociation reactions of halo states is much simpler than that of the more familiar deep-inelastic reactions of other intermediate-energy ions. First of all, the weakly bound and spatially extended halo states can be approximated by a wave function $\psi_0$ based on a single-particle potential-well model. The reactions producing a fast core fragment have contributions from two reaction channels, and because the beam velocity is much higher than that of the halo nucleon, both can be treated in the sudden approximation. In the first channel, referred to as nucleon stripping (or absorption), the halo nucleon has interacted strongly with the target and disappears from the beam. In the second channel, referred to as diffraction dissociation, the nucleon and the core fragment move forward with essentially beam velocity.

The high projectile energies, 0.5-12 GeV, imply that the collision may be described in terms of a classical impact parameter, so that the dissociation reactions are characteristic of impact parameters greater than $b_{min}=R_C+R_A$, defined as the sum of the (energy-dependent) core and target interaction radii. The high energy also means that the eikonal approximation is applicable, so that the target trajectory is a straight line and the range of the nuclear interaction (which does not have to be weak) is of the order of the target radius $R_a$. The result is that the wave function of the halo state remains unchanged throughout all space except for a region corresponding roughly to a cylinder of radius $R_a$ The more detailed dependence is taken into account by the choice of the profile function, but the results [5-10] are not strongly dependent on the details and they agree well with each other and with experiments.

## 3. Results for Parallel-Momentum Distributions

As a transparent illustration [5] we cite here a simple model valid for large target radii. In this, the profile function is approximated by a planar cut-off parallel to the beam direction and tangential to the target surface, a model originally due to Glauber. Assume further that the total spatial wave function appropriate for a halo neutron in an $s$ state is a Yukawa, so that the corresponding intrinsic momentum distribution along the $z$ axis is a one-dimensional Lorentzian

$$\frac{dW}{dp_z} = \frac{\Gamma}{2\pi} \frac{1}{(\Gamma^2/4 + p_z^2)}$$

where the width $\Gamma=(8\mu S_n)^{1/2}$ is defined in terms of the reduced mass and the neutron separation energy. Exploiting that the Fourier transform of the severed wave function can be expressed

analytically [14], it is found after integration over the $x$ and $y$ momentum components that the momentum distribution in the $z$ direction equals the intrinsic one given above multiplied by the correction factor

$$C_1(w) = \frac{1}{2}\int_0^{\pi/2} \cos(\vartheta)\exp\left[-2w/\cos(\vartheta)\right] d\vartheta$$

where the parameter is defined as $w = b_1(\Gamma^2/4+p_z^2)^{1/2}/\hbar$, expressed in terms of the distance $b_1$ from the center of the halo system to the cutoff plane. The usual definition of the impact parameter corresponds to $b=R_T+b_1$, where $R_T$ is the effective target radius. For the value of $b_1 = 0$ (not realizable in experiments) half of the halo wave function would be removed and the distribution would be unchanged in shape. The actual minimum value of $b_1$ is given by the core radius, about 2.5 fm, and larger values of the impact parameter lead to increasingly narrow distributions. For the case of $^{11}$Be there is good agreement the experimental findings, essentially for two reasons, (i) the Yukawa is, apart from a normalization factor, identical to the exact solution in the region sampled, and (ii) the target radius is comparable to the decay length of the wave function.

A better approximation [8], exact for small target radii, is to assume that the wave function inside the reaction zone may be replaced by its value along the axis of the target trajectory as seen from the halo's coordinate system. For neutron halos this approximation leads to convenient analytical expressions. The corresponding momentum distributions for halo protons were calculated numerically with a Woods-Saxon single-particle wave functions In both cases the differential cross sections can be estimated by integrating over impact parameter. Results obtained with this model are shown in Fig. 1. For the case of $^{11}$Be there is good agreement between the experimental parallel momentum width [11] and the calculation. In view of the strong dependence on impact parameter that underlies this result, it must be considered a numerical coincidence that the distribution corresponding to the total wave function has a very similar width. This is underscored by the fact that the plateau at 80-160 MeV/c is entirely absent in the momentum distribution of the localized wave function. To see why this is so, we note that the high momentum components in the wave function in momentum space are the counterpart of the inner lobe peaking at 0.7 fm in the spatial wave function. This is a region of space that is not sampled in the experiment. For the case of $^{11}$Be, the absence of an outer plateau is presumably too weak an effect to be observable, but it is likely that it could be discernible in the momentum distributions from stripping of $s$-state proton halos in the light phosphorus isotopes [15].

For the case of $^{8}$B, the calculated intrinsic parallel-momentum width corresponding to the total wave function is 153 MeV/c. The calculated value of 75 MeV/c obtained when the selection due to localization [8] is taken into account agrees well with the experimental value [12] of 81±6 MeV/c. The apparent discrepancy between the widths of the total momentum distribution and that of the experiment originally led to the claim [12] that an interpretation in terms of single particle model was not possible.

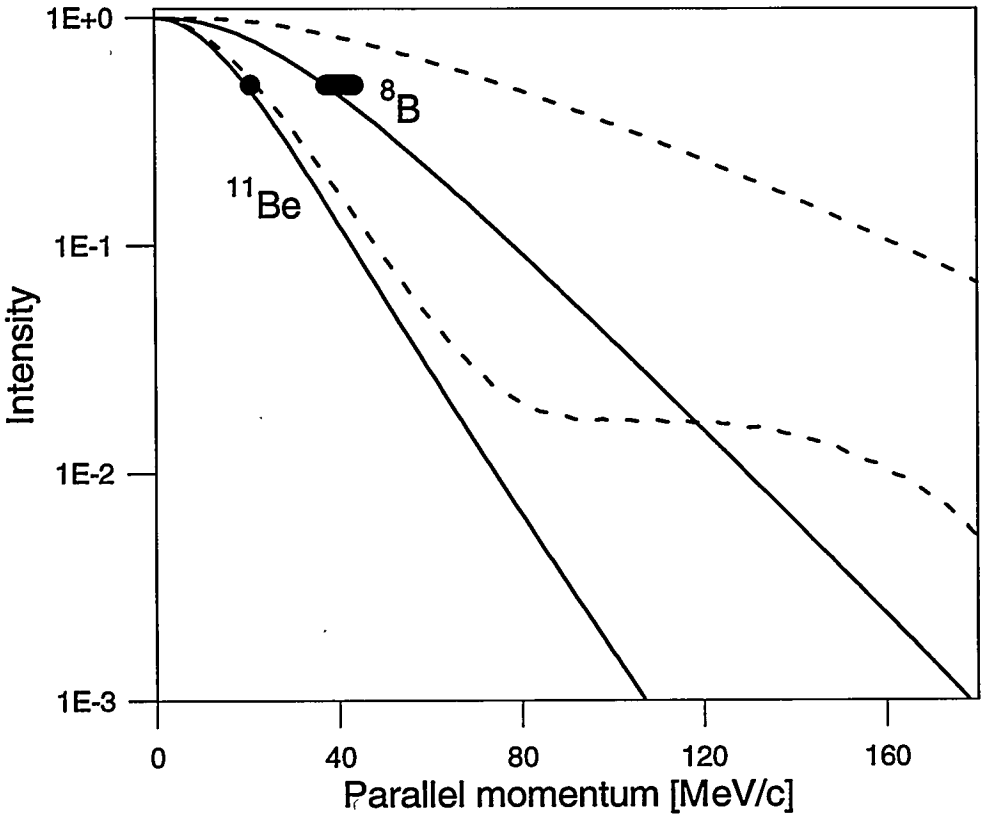


*Fig. 1*

*The parallel momentum distributions of the core fragment from the single-nucleon stripping reactions of $^{11}$Be ($s_{1/2}$ ground state) and $^{8}$B ($p_{1/2}$ ground state). The dashed lines are those of the total momentum wave functions and the full-drawn lines correspond to the external spatial part selected in the stripping reaction. The shaded areas are the measured [11,12] values of the half width at half maximum.*

The experiments underlying Fig. 1 do not distinguish the stripping and diffraction-dissociation mechanisms and analyses such as the two sketched above assume that the final-state interaction between the nucleon and the core fragment is negligible. Hencken et al. [10] find that this is indeed a valid approximation for $^{11}$Be, for which a similar conclusion was reached in Coulomb-excitation experiments [14], where plane-wave and Woods-Saxon final states gave almost identical results. On the other hand, Barranco et al. [9] using a simpler model for $^{11}$Be find that the final-state interactions increase the full width at half maximum of the parallel-momentum distribution to 79 MeV/c for diffraction dissociation as compared with 49 MeV/c for the stripping reaction.

An independent verification of the estimates given here is provided by the measured cross sections. The calculated $^{11}$Be cross section of 316 mb at 41 MeV/u is roughly one third of the free-nucleon value and agrees well with the experimental value [14] of 290±40 mb. The $^{8}$B cross sections are calculated as 111 mb at 40 MeV/u and 54 mb at 1471 MeV/u are roughly one tenth of the free-

nucleon values and are qualitatively in good agreement with the measured [16,12] values of 80±15 and 94±4 mb, respectively. The overall agreement must be considered satisfactory, but it is probably worth noting that the tendency of the model [8] must be to underestimate the widths and, more so, the cross sections. This tendency will be most pronounced for the case of $^{8}$B for which the external wave function falls off rapidly. The cross sections and longitudinal-momentum widths agree well with a more refined recent calculation with a profile function calculated from an optical model and a microscopic Glauber model [10] at low and high energies, respectively. In this calculation it is interesting to see that the stripping and diffraction-dissociation cross sections come out identical at low energies, just as for a black-disc model, whereas the former is far bigger at high energies. The reaction and elastic cross sections for free nucleons behave in the same way.

The interpretation given here suggests, contrary to what is often assumed, that the longitudinal momentum distributions measured with a light target should not be affected appreciably by the acceptance of the spectrometer. Basically this may be seen from the uncertainty principle, which allows an exact measurement of the momentum along the $z$-axis for a precisely known (x,y) coordinate. For an infinitesimal target it follows that all information about the original momentum in the $xy$ plane will be destroyed by the measurement. For a small target the radial momentum distribution of the neutron in the approximation leading to the expressions above becomes proportional to $[J_1(k_r R_a)/k_r R_a]^2$, the usual diffraction pattern, depending only on the radius of the target. This means that the wave function at the moment of the collision takes a form that factorizes, so that the $k_z$ distribution will not be changed by an incomplete detection of the $k_x$ and $k_y$ components.

## 4. Concluding Remarks

The parallel momentum distributions of the heavy fragment in processes such as ($^{11}$Be,$^{10}$Be) and ($^{8}$B,$^{7}$Be) on light targets reflect the halo wave function in a localized region outside of the nuclear core. When this is taken into account, the calculated longitudinal momentum widths and reaction cross sections are in good agreement with the experiments. The transverse momentum components and also the momentum distributions of the halo nucleon(s) provide interesting complementary information [17].

The author appreciated interesting discussions with many colleagues during the Argonne Conference on Nuclear Structure at the Limits, and comments made by Henning Esbensen and Enrico Vigezzi have been taken into account in this written version of my presentation.

**References**


1. The K500⊗K1200: Construction of a Coupled Cyclotron Facility at the National Superconducting Cyclotron Laboratory, Michigan State University, MSUCL-949, September 1994.
2. T.J.M. Symons in Proc. 4th Int. Conf. on Nuclei Far From Stability, Helsingør, 1981, CERN-81-09, p.668.
3. F. Barranco, E. Vigezzi and R.A. Broglia, Phys. Lett. B **319**, 387 (1993).
4. E. Garrido, D.V. Fedorov and A.S. Jensen, Phys. Rev. C **53**, 3159 (1996).
5. P.G. Hansen *in* Proc. Int. Conf. Exotic Nuclei and Atomic Masses (ENAM), Arles June 1995, (M. de Saint Simon and O. Sorlin, eds.) Editions Frontieres, Gif-sur-Yvette 1995, p. 175.
6. B.A. Brown, A. Csótó, and R. Sherr, Nucl. Phys. A **597**, 66 (1996).
7. H. Esbensen, Phys. Rev. C **53**, 2007 (1996).
8. P.G. Hansen, Phys. Rev. Lett. **77**, 1016 (1996).
9. F. Barranco, E. Vigezzi and R.A. Broglia, Momentum Distributions in Halo Nuclei, Z. Ph. A, in press.
10. K. Hencken, G. Bertsch and H. Esbensen, Breakup Reactions of the Halo Nuclei, to be published.
11. J.H. Kelley et al., Phys. Rev. Lett. **74**, 30 (1995).
12. W. Schwab et al., Z. Phys. A **350**, 283 (1995).
13. J.H. Kelley et al., to be published.
14. R.Anne et al., Nucl. Phys. A **575**, 125 (1994); Phys. Lett B **304**, 55 (1993).
15. B.A. Brown and P.G. Hansen, Phys. Lett. B **381**, 391 (1996).
16. I. Pecina et al., Phys. Rev. C **52**, 191 (1995).
17. P.G. Hansen, A.S. Jensen and B. Jonson, Nuclear Halos, Ann. Rev. Nucl. Part. Sci. **45**, 591 (1995).

# Shell-Model Monte Carlo Calculations Near $N = Z$

D. J. Dean
*Physics Division, Oak Ridge National Laboratory, P.O. Box 2008, Oak Ridge, Tennessee 37831 USA*
(August 30, 1996)

The pairing and structure of nuclei near $N = Z$ is described in the framework of shell-model Monte Carlo (SMMC) calculations. Principal results include the enhancement of J=0 T=1 proton-neutron pairing at N=Z nuclei, and the marked difference of thermal properties between even-even and odd-odd N=Z nuclei. Additionally I will present a study of the rotational properties of the T=1 (ground state), and T=0 band mixing seen in $^{74}$Rb.

## I. INTRODUCTION AND FORMALISM

As new radioactive beam facilities become operational, a wealth of information on nuclei near the N=Z line has emerged. Several physical features in these nuclei are of interest. First, proton-neutron pairing is enhanced for $N = Z$ nuclei as compared to $N = Z + 2$, $N = Z + 4$,..., nuclei. This enhancement can be seen when computing the $\Delta_{pp}$, $\Delta_{nn}$, and $\Delta_{pn}$ residual pairing from the experimental masses [1]. Empirical mass formulae (see e.g. Ref. [2]) indicate that the enhancement of p-n pairing is partially due to the Wigner term, and partially due to p-n pairing within the mass formula itself. Exact calculations of the pairing operators unambiguously indicate the nature of the pair condensates within a nucleus, and will be one of the focuses of this presentation.

A second interesting property is that of T=1 ground states for odd-odd N=Z systems. The p-n pairing plays a major role here. One way to approach the p-n pairing in odd-odd N=Z nuclei is to consider the rotational spectrum, as was done experimentally in Ref. [3]. In that work, the ground-state band was proposed to consist of T=1 isobaric analog states seen in $^{74}$Kr, while the T=0 odd-spin states became yrast at about 1.5 MeV of excitation energy.

In this contribution, I will attempt to elucidate several of these interesting properties using the tools of shell-model Monte Carlo (SMMC) [4]. SMMC offers an alternative way to calculate nuclear structure properties, and is complementary to direct diagonalization. SMMC cannot find, nor is it designed to find, every energy eigenvalue of the Hamiltonian. It is designed to give thermal or ground-state expectation values for various one- and two-body operators. Indeed, for larger nuclei, SMMC may be the only way to obtain information on the thermal properties of the system from a shell-model perspective. We are interested in finding the partition function of the imaginary-time many-body propagator $U = \exp(-\beta\hat{H})$ where $\beta = 1/T$ and $T$ is the temperature of the system in MeV. We calculate expectation values of any observable $\hat{\Omega}$ with

$$\langle\hat{\Omega}\rangle = \frac{\mathrm{Tr}\hat{U}\hat{\Omega}}{\mathrm{Tr}\hat{U}} . \tag{1}$$

Since $\hat{H}$ contains many terms that do not commute, we must discretize $\beta = N_t\Delta\beta$. Finally, two-body terms in $\hat{H}$ are linearized through the Hubbard-Stratonovich transformation, which introduces auxiliary fields over which one must integrate to obtain physical answers. The method can be summarized as

$$\begin{aligned} Z = \mathrm{Tr}\hat{U} = \mathrm{Tr}\exp(-\beta\hat{H}) &\rightarrow \mathrm{Tr}\left[\exp(-\Delta\beta\hat{H})\right]^{N_t} \\ &\rightarrow \int \mathcal{D}[\sigma]G(\sigma)\mathrm{Tr}\prod_{n=1}^{N_t}\exp\left[\Delta\beta\hat{h}(\sigma_n)\right] , \end{aligned} \tag{2}$$

where $\sigma_n$ are the auxiliary fields (there is one $\sigma$-field for each two-body matrix-element in $\hat{H}$ when the two-body terms are recast in quadratic form), $\mathcal{D}[\sigma]$ is the measure of the integrand, $G(\sigma)$ is a Gaussian in $\sigma$, and $\hat{h}$ is a one-body Hamiltonian. Thus, we have transformed the shell-model problem from diagonalization of a large matrix to one of large dimensional quadrature. Dimensions of the integral can reach up to $10^5$ for rare-earth systems, and it is thus natural to use Metropolis random walk methods to sample the space. Such integration can most efficiently be performed on massively parallel computers. Further details are discussed in [4].

Realistic interactions often have a Monte Carlo sign problem, that is they have complex actions. We have found that a certain class of Hamiltonians has good Monte Carlo sign properties, and we perform calculations with these Hamiltonians. Fortunately in nuclear physics good Hamiltonians, such as pairing plus quadrupole, are not too far removed from realistic Hamiltonians so that the extrapolation is a gentle function of the coupling constant, $g$ [5].

The residual nuclear interaction builds up pairing correlations in a nucleus. A measure of these correlations may be studied using the operator

$$A^\dagger_{JM}(j_aj_b) = \frac{1}{\sqrt{1+\delta_{ab}}}\left[a^\dagger_{j_a}\times a^\dagger_{j_b}\right] \tag{3}$$

for like-nucleons (proton-proton or neutron-neutron pairs), and

$$A^\dagger_{JM}(j_aj_b) = \frac{1}{2\sqrt{1+\delta_{ab}}}\left\{\left[a^\dagger_{pj_a}\times a^\dagger_{nj_b}\right] \pm \left[a^\dagger_{nj_a}\times a^\dagger_{pj_b}\right]\right\} , \tag{4}$$

where "+(-)" is for T=0 (T=1) p-n pairing. A convenient measure of the pair correlations is the trace of the pair matrix which is given by

$$M^J_{\alpha\alpha'} = \sum_M \langle A^\dagger_{JM}(j_a j_b) A_{JM}(j_c j_d) \rangle \ . \qquad (5)$$

Correlations are determined after a mean-field component is subtracted from this matrix, as discussed in [4].

In the following I will describe some of the initial calculations for $pf$ shell nuclei, and more recent results in the $0f_{5/2}1p0g_{9/2}$ space. I will conclude with a future outlook for large calculations within the SMMC framework.

## II. INTERACTIONS AND MODEL SPACES

SMMC calculations of $pf$ shell nuclei were performed for ground-state [6] and thermal [7,8] properties of nuclei using the Kuo-Brown [9] interaction modified in the monopole terms [10]. (The interaction has subsequently been dubbed KB3.) Excellent agreement between theory and experiment was observed, indicating the usefulness of this interaction for $pf$ shell nuclei up to $A = 60$. The KB3 interaction also successfully reproduces many of the ground-state properties and spectra of nuclei in the lower $pf$ shell [11]. As an example, Fig. 1 displays the mass excesses in this model space, relative to the $^{40}$Ca core (top panel), and the deviation between theory and experiment (bottom panel). Investigations of B(E2)'s, B(M1)'s, and Gamow-Teller operators were also carried out, and good agreement in comparison to experimental data has been demonstrated [4,6].

In order to investigate heavier systems, the $0g_{9/2}$ was included in the $pf$ model space [9]. However, we found that the coupling between the $0f_{7/2}$ and $0g_{9/2}$ causes fairly significant center-of-mass contamination to the ground state, and we therefore close the $0f_{7/2}$. The model space is thus $0f_{5/2}1p0g_{9/2}$. This appears to be a good approximation in systems where both the neutrons and protons completely fill the $f_{7/2}$ level. The monopole terms of this new interaction were modified [12] to give a good description of the spectra of nuclei in the Ni isotopes. Since $^{56}$Ni is the core of this model space, the single-particle energies were determined from the $^{57}$Ni spectrum. Mass excesses (top panel) and differences between experiment and theory (bottom panel) are shown in Fig. 2 for this new interaction.

## III. PAIR CORRELATIONS NEAR N=Z

It has long been anticipated that $J = 0^+$ proton-neutron correlations play an important role in the ground states of $N = Z$ nuclei. These correlations were explored with SMMC for $N = Z$ nuclei in the mass region $A = 48 - 58$ in the $pf$-shell, and $A = 64 - 74$ in the $0f_{5/2}1p0g_{9/2}$ space. As the even-even $N = Z$ nuclei have isospin $T = 0$, the expectation values of $A^\dagger A$ are identical in all three isovector $0^+$ pairing channels. This symmetry does not hold for the odd-odd $N = Z$ nuclei in this mass region, which usually have $T = 1$ ground states, and $\langle \hat{A}^\dagger \hat{A} \rangle$ can be different for proton-neutron pairs than for like-nucleon pairs. (The expectation values for proton and neutron pairs are identical.)

We find the proton-neutron pairing strength significantly larger for odd-odd $N = Z$ nuclei than in even-even nuclei, while the $0^+$ proton and neutron pairing shows the opposite behavior, in both cases leading to a noticeable odd-even staggering, as displayed in Fig. 3, for the $pf$ shell. Due to the strong pairing of the $f_{7/2}$, all three isovector $0^+$ channels of the pairing matrix essentially exhibit only one large eigenvalue which is used as a convenient measure of the pairing strength in Fig. 3.

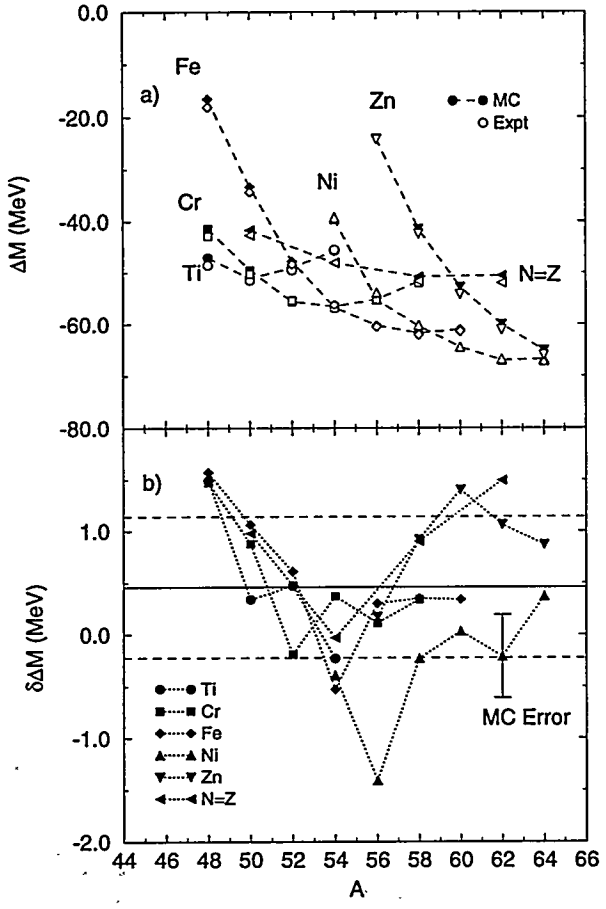


FIG 1. Upper panel (a): Comparison of the mass excesses $\Delta M$ as calculated within the SMMC approach with data. Lower panel (b): Discrepancy between the SMMC results for the mass excesses and the data, $\delta\Delta M$. The solid line shows the average discrepancy, 450 keV, while the dashed lines show the rms variation about this value (from [6]).

This staggering is caused by a constructive interference of the isotensor and isoscalar parts of $\hat{A}^\dagger \hat{A}$ in the odd-odd $N = Z$ nuclei, while they interfere destructively in the even-even nuclei. The isoscalar part is related to the

pairing energy and is found to be about constant for the nuclei studied here.

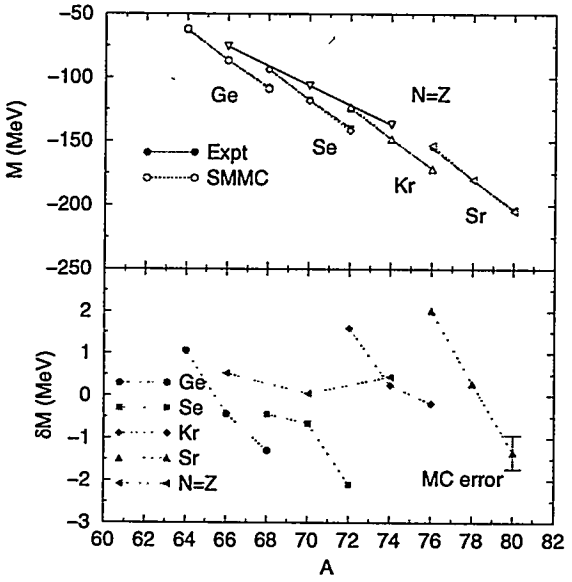


FIG 2. Calculated mass excesses are compared with experiment (top panel), and the difference between experiment and theory is shown (bottom panel).

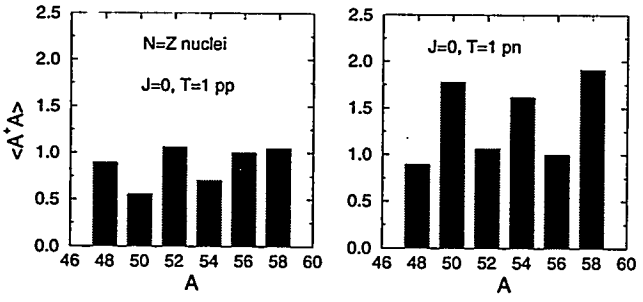


FIG 3. Largest eigenvalues for the $J = 0$, $T = 1$ proton-proton (left) and proton-neutron (right) pairing matrix as a function of mass number.

Fig. 4 shows the correlated pairs for $N = Z$ nuclei in the $A = 64 - 74$ region of the $0f_{5/2}1p0g_{9/2}$ space. Correlated pairs are calculated by summing over the full $M_{\alpha\alpha'}$ matrix and subtracting the mean field which is determined by calculating the pairing matrix in the absence of the two-body interaction. Note that $^{64}$Ge exhibits little $J = 0$ pairing, indicating that the $p_{3/2}$ subshell is relatively closed for this system. The correlated pairs exhibit a strong $J = 0$, $T = 1$ like-particle staggering for the even-even and odd-odd $N = Z$ systems, while the number of correlated proton-neutron pairs is much larger than the like-particle pairing for the odd-odd systems. The correlated pairing behavior of $N = Z$, $N = Z + 2$, $N = Z + 4$ nuclei is shown in Fig. 4, where one clearly sees the decrease in T=1 proton-neutron pairing as one moves away from $N = Z$.

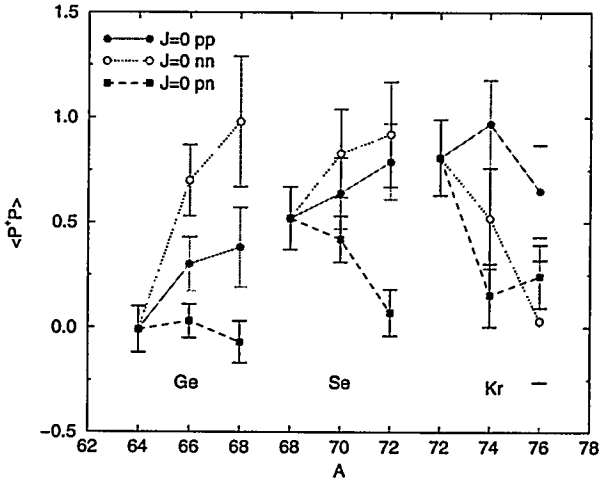


FIG 4. Correlated $J = 0$, $T = 1$ pairs in the proton-proton and proton-neutron channel for $N = Z$ nuclei in the $0f_{5/2}1p0g_{9/2}$ model space.

Another striking feature of proton-neutron pairing can be found through studying the thermal properties of these systems [4,7,8]. In the case of $^{52}$Fe $J = 0$, proton-neutron and like-particle pairing decrease quickly to fermi-gas values at a temperature of approximately 1.1 MeV (corresponding to an excitation energy of approximately 4 MeV). This decrease in pairing behaves like $P(T) = P_0 \left(1 + \exp\left\{\frac{T-T_0}{\alpha}\right\}\right)^{-1}$, where $T_0 \approx 1.1$ MeV, and $\alpha = 0.25$ MeV, and is the same for both like-particle and proton-neutron T=1 pairing. For the case of $^{50}$Mn, the proton-neutron pairing decreases much more quickly, and is almost zero at approximately a temperature of 0.75 MeV, while the like-particle pairing remains until 1.1 MeV. One also sees a dramatic drop in the dependence of the isospin $< T^2 > [= T(T+1)]$ on temperature. Since $^{50}$Mn has a $T = 1$ ground-state, $< T^2 >= 2$ at very low temperatures, but decreases towards zero as the system is heated, indicating a thermal mixture of T=1 and T=0 states.

## IV. PAIR CORRELATIONS IN $^{74}$RB

The band mixing seen in $^{74}$Rb can be measured within SMMC by adding a cranking term to the shell-model Hamiltonian. Thus $H \leftarrow H + \omega J_z$. Note that since $J_z$ is a time-odd operator, the sign problem is reintroduced, and good statistical sampling requires the cranking to be carried out only to finite $\omega$. For the calculations shown in Fig. 5, the largest cranking frequency was $\omega = 0.4$. A signature of the band mixing is a change in the isospin $< T^2 >$ as a function of $< J_z >$, which is shown in the figure. We see that at about a spin of $J_z = 4\hbar$, $< T^2 >$ moves away from its initial value of 2. A mixing of $T = 0$ and $T = 1$ states forces the expectation value to decrease. Thus in a full shell-model calculation, we predict the onset of this mixing at approximately $J_z = 4\hbar$, consistent with the spectrum found in Ref. [3].

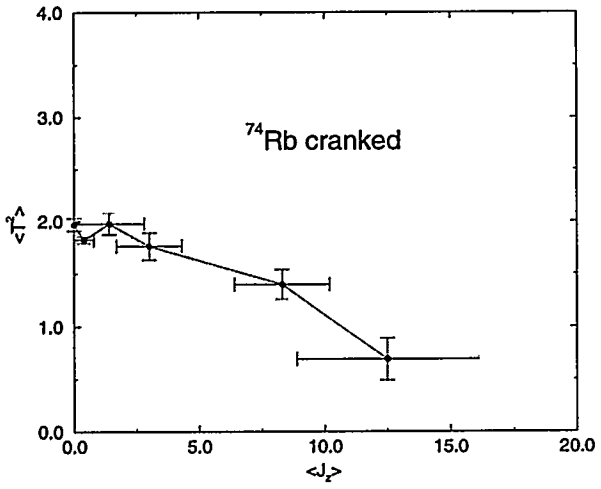


FIG 5. $< T^2 >$ as a function of $J_z$ for $^{74}$Rb.

## V. CONCLUSIONS AND FUTURE PROSPECTS

In these Proceedings I have indicated some of the studies of pairing that are accessible using SMMC techniques. As the above results indicate, strong $J = 0$, $T = 1$ proton-neutron correlations exist for odd-odd $N = Z$ nuclei, and die off quickly as one adds neutrons. Thermal studies of $N = Z$ even-even and odd-odd systems indicate that proton-neutron pairs break more readily with increasing temperature than do the like-particle pairs. Finally, an odd-odd $N = Z$ system such as $^{74}$Rb should exhibit a $T = 1$ to $T = 0$ band mixing as one cranks the system.

I would like to close with a forward glimpse into the near future of SMMC. Two directions relevant to this conference are currently being pursued. The first deals with deformations in the mass 80 region. Obviously, inclusion of the $0g_{9/2}$ cannot describe the deformation of nuclei such as $^{80}$Sr, and one must also include more single-particle states from the *sdg* subspace. The simplest way to do this is to include the $1d_{5/2}$ into the subspace, and use a collective quadrupole interaction between the $0g_{9/2}$ and $1d_{5/2}$. The upward B(E2)'s are shown in units of $e^2fm^4$ in the table with and without the inclusion of the $1d_{5/2}$. The effective charges are $e_p = 1.5$ and $e_n = 0.5$. Although the lighter nuclei (such as $^{66}$Ge) are slightly affected, $^{80}$Sr is describable in this manner, and thus these preliminary calculations indicate a possible way to consistently describe nuclei in the entire mass 60-90 region.

| Nucleus | no $d_{5/2}$ | with $d_{5/2}$ | expt |
|---|---|---|---|
| $^{66}$Ge | $1181 \pm 40$ | 1938 | 960 |
| $^{72}$Se | 1854 | 2800 | 1750 |
| $^{80}$Sr | 1526 | 7804 | 8400 |

The second new development concerns SMMC calculations in two major oscillator shells. The difficulty that must be overcome concerns the center-of-mass motion that comes about due to the stationary nature of the mean-field potential. We use the Glockner-Lawson technique to remove the center-of-mass component. We use the WBMB interaction [13] with the *pf* shell single-particle energies adjusted downward by 3 MeV relative to the sd-shell. Results of these calculations are shown in Fig. 6.

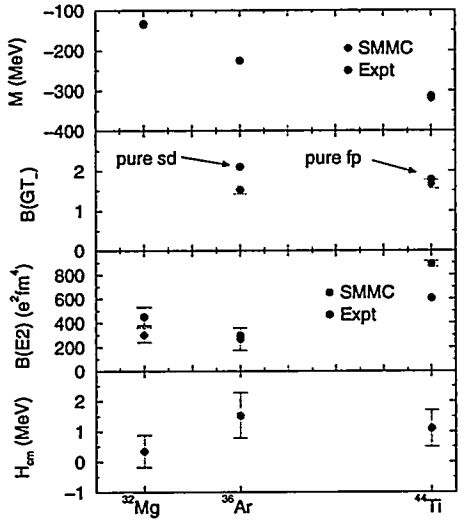


FIG 6. Calculations of $< H >$ (upper) , $B(GT)$ (upper middle), $B(E2)$ (lower middle), and $< H_{cm} >$ (lower) for three nuclei in the full *sd-pf* shells.

The collaborative efforts of S.E. Koonin, K. Langanke, W. Nazarewicz, F. Nowacki, A. Poves, P.B. Radha, and T. Ressell are gratefully acknowledged. Oak Ridge National Laboratory is managed by Lockheed Martin Energy Research Corp. for the U.S. Department of Energy under contract number DE-AC05-96OR22464. Computational cycles were provided by the Center for Computational Sciences at ORNL. DJD acknowledges an E. P. Wigner Fellowship from ORNL.

---

[1] P. Moller and J.R. Nix, Nucl. Phys. **A536**, 20 (1992)
[2] H.J. Krappe, J.R. Nix, and A.J. Sierk, Phys. Rev. **C20**, 992 (1979)
[3] D. Rudolph et al, Phys. Rev. Lett. **76**, 376 (1996)
[4] S.E. Koonin, D.J. Dean, and K. Langanke, Phys. Repts., in press (1996)
[5] Y. Alhassid, D. J. Dean, S.E. Koonin, G. Lang, and W.E. Ormand, Phys. Rev. Lett. **72**, 613 (1994)
[6] K. Langanke, D.J. Dean, P.B. Radha, Y. Alhassid, and S.E. Koonin, Phys. Rev. **C52**, 718 (1995)
[7] D.J. Dean, S.E. Koonin, K. Langanke, P.B. Radha, and Y. Alhassid, Phys. Rev. Lett. **74**, 2909 (1995)
[8] K. Langanke, D.J. Dean, P.B. Radha, and S.E. Koonin, Nucl. Phys. **A602**, 244 (1996)
[9] T.T.S. Kuo and G.E. Brown, Nucl. Phys. **85**, 40 (1966)
[10] A. Poves and A.P. Zuker, Phys. Rep. **70**, 235 (1981)
[11] E. Caurier, A.P. Zuker, A. Poves and G. Martinez-Pinedo, Phys. Rev. **C50**, 225 (1994)
[12] A. Nowacki, Ph.D. Thesis, Madrid, Spain, 1995
[13] E.K. Warburton and B.A. Brown, Phys. Rev. **C46**, 923 (1992)

# A NUMBER-PROJECTED MODEL WITH GENERALIZED PAIRING INTERACTION IN APPLICATION TO ROTATING NUCLEI

W. Satuła[a–d] and R. Wyss[d]

[a] *Institute of Theoretical Physics, Warsaw University, ul. Hoża 69, PL-00-681 Warsaw, Poland*
[b] *Joint Institute for Heavy Ion Research, Oak Ridge, TN 37831, USA*
[c] *Department of Physics, University of Tennessee, Knoxville, TN 37996, USA*
[d] *The Royal Institute of Technology, Physics Department Frescati, Frescativägen 24, S–104 05 Stockholm, Sweden*

A cranked mean-field model that takes into account both T=1 and T=0 pairing interactions is presented. The like-particle pairing interaction is described by means of a standard seniority force. The neutron-proton channel includes simoultanously correlations among particles moving in time reversed orbits (T=1) and identical orbits (T=0). The coupling between different pairing channels and nuclear rotation is taken into account selfconsistently. Approximate number-projection is included by means of the Lipkin-Nogami method. The transitions between different pairing phases are discussed as a function of neutron/proton excess, $T_z$, and rotational frequency, $\hbar\omega$.

The development of highly efficient detector arrays and radioactive ion beam facilities will open up new avenues to study the nature of nuclear interactions at the proton drip line. In particular, it will allow to access heavy, self-conjugate nuclei and nuclei in the vicinity of the N=Z line, the *kingdom* of neutron-proton (*np*) pairing correlations. Phenomena related to the onset of *np*-pairing, competition between different pairing modes as a function of $|T_z|$ and rotational frequency, $\hbar\omega$, including possible phase transitions, the influence of *np*-pairing on the position of the proton drip line and stability of the nuclei along the proton drip line due to the additional binding energy emerging from *np*-pairing are becoming highly exciting topics in nuclear structure.

The study of *np*-pairing dates back to the sixties when Goswami and coworkers [1–3] and Goodman [4] worked out the necessary generalizations of the Bogolyubov transformation allowing to include *np*-pairing correlations in the framework of the mean-field theory. These early studies were limited to light, self-conjugate nuclei, suggesting that the T=0 and T=1 pairing phases are exclusive [5,6]. It was also pointed out that *np*-pairing appears to be important only in close vicinity of the N=Z line [7]. The formalism has been extended to include nuclear rotation in Ref. [8], suggesting a possible phase transition between the two pairing modes at high spin [9].

The aim of this paper is to related to basic physics of *np*-pairing correlations. We present a model applicable for pairing-and-deformation selfconsistent cranking calculations with approximate restoration of particle-number symmetry. As a starting point of our considerations we chose the eigenstates of a *deformed* phenomenological single-particle potential. The main goal is to construct a formalism which accounts for simultaneous scattering of ($i$) the nucleonic pairs where both particles occupy states belonging to different

signature ($\boldsymbol{\alpha\tilde{\beta}}$ mode) and (*ii*) pairs where both particles occupy states of the same signature ($\boldsymbol{\alpha\beta}$ mode). Starting with the most general Bogolyubov transformation, we enforce the so called *antilinear simplex symmetry*, $\hat{S}_z^A = \hat{P}\hat{T}\hat{R}_z$ [8] as selfconsistent symmetry (SCS) [10]. The $\hat{S}_z^A$ symmetry considerably simplifies the structure of the density matrix, $\boldsymbol{\rho} = \boldsymbol{V}^*\boldsymbol{V}^T$, and pairing tensor $\boldsymbol{\kappa} = \boldsymbol{V}^*\boldsymbol{U}^T$:

$$\boldsymbol{\rho} = \begin{pmatrix} \Re(\rho_{\alpha\beta}) & 0 \\ 0 & \Re(\rho_{\tilde{\alpha}\tilde{\beta}}) \end{pmatrix} + i \begin{pmatrix} 0 & \Im(\rho_{\alpha\tilde{\beta}}) \\ \Im(\rho_{\tilde{\alpha}\beta}) & 0 \end{pmatrix} \tag{1}$$

$$\boldsymbol{\kappa} = \begin{pmatrix} 0 & \Re(\kappa_{\alpha\tilde{\beta}}) \\ \Re(\kappa_{\tilde{\alpha}\beta}) & 0 \end{pmatrix} + i \begin{pmatrix} \Im(\kappa_{\alpha\beta}) & 0 \\ 0 & \Im(\kappa_{\tilde{\alpha}\tilde{\beta}}) \end{pmatrix} \tag{2}$$

and consequently the structure of Hartree-Fock-Bogolyubov (HFB) equations.

Our two-body *np*-pairing interaction is an extension of the standard seniority pairing interaction. It is separable in the particle-particle channel, $\bar{v}_{\alpha\beta\gamma\delta} \propto g_{\alpha\beta}g^*_{\gamma\delta}$, with $g_{\alpha\beta}$ proportional (up to a phase factor) to the overlap $\langle\alpha_\tau|\beta_{\tau'}\rangle$ between single-particle wave functions. Beyond weak modifications due to the isovector part of our mean-field, like the static Coulomb field, the interaction is dominated by $\boldsymbol{\alpha\tilde{\alpha}}$ and $\boldsymbol{\alpha\alpha}$ types of pairing. The structure of $\boldsymbol{\alpha\tilde{\alpha}}$ and $\boldsymbol{\alpha\alpha}$ types of pairing correlations can be related to the isospin quantum numbers. Under the assumption of the time-reversal invariance and isospin symmetry the $\boldsymbol{\alpha\tilde{\alpha}}$ pairs are of isospin T=1 while the $\boldsymbol{\alpha\alpha}$ pairs are of isospin T=0. The T=0 component of $\boldsymbol{\alpha\tilde{\alpha}}$ pairing is ruled out through the $\hat{S}_z^A$ symmetry as well the T=1 component of the $\boldsymbol{\alpha\alpha}$ pairing. This simple analysis shows that *symmetries* play an *important* role in the theoretical description *np*-pairing [7] that deserve more systematic study.

To avoid a sudden collapse of the mean-field pairing correlations induced by e.g. fast nuclear rotation we introduce an approximate particle-number projection by extending the Lipkin-Nogami (LN) method [12]. This method is equivalent to a restricted HFB-type variation, $\delta\langle HFB|\hat{\mathcal{H}}^\omega|HFB\rangle = 0$, for the Routhian:

$$\hat{\mathcal{H}}^\omega = \hat{H}^\omega - \sum_\tau \lambda_\tau^{(1)}\Delta\hat{N}_\tau - \sum_{\tau\tau'} \lambda_{\tau\tau'}^{(2)}\Delta\hat{N}_\tau\Delta\hat{N}_{\tau'}. \tag{3}$$

with linear constraints treated variationaly and quadratic constraints calculated selfconsistently using three additional subsidiary conditions [11]. The LN equations are similar to the HFB equations but for Routhian (3).

An open question in mean-field calculations relates to the strength of the *np*-pairing interaction. Whereas the strength of the seniority pairing force is well established by fit to the odd-even mass differences, very little is known concerning the *np*-pairing force. Based on isospin-symmetry argument, it seems well justified to assume that at N$\sim$Z line $G_{p(n)} \sim G_{np}^{T=1}$. Our results will therefore be presented either as a function of or at a given value of the parameter $x^{T=0}$ that scales the strength of T=0 *np*-pairing with respect to the average strength calculated for *nn*- and *pp*- correlations i.e. $x^{T=0} = G_{np}^{T=0}/G_{np}^{T=1}$, $G_{np}^{T=1} = (G_n + G_p)/2$.

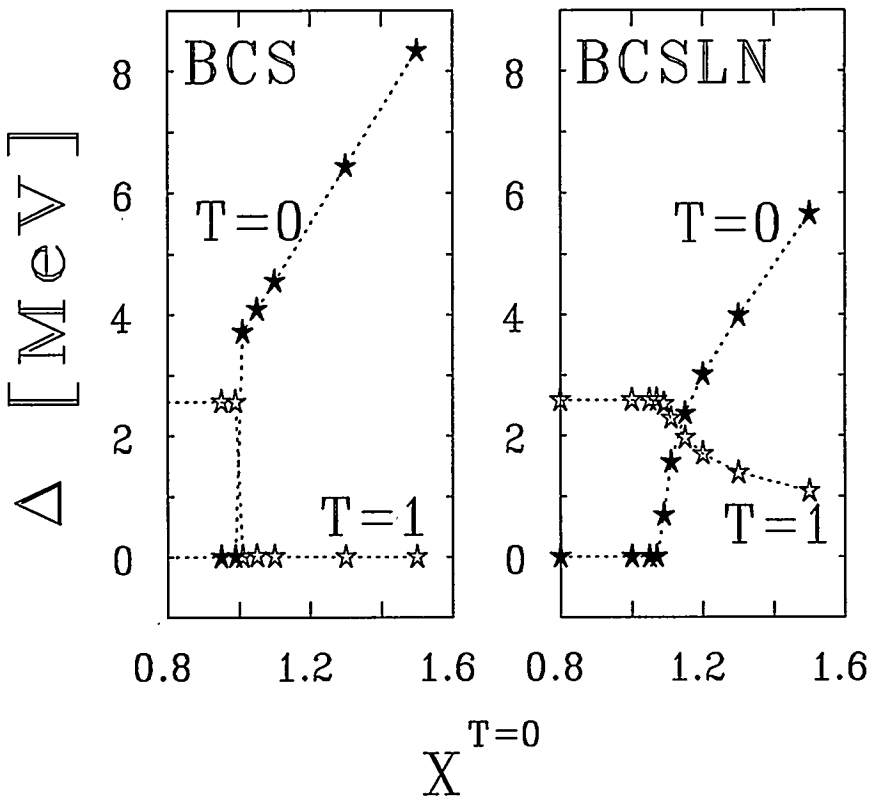


FIG. 1. *Average pairing gaps for a self-conjugate nucleus, N=Z, as a function of* $x^{T=0} = G_{np}^{T=0}/G_{np}^{T=1}$. *Left (right) panel shows the results of calculations without (with) particle number projection.*

Fig. 1 shows the pairing gaps at zero frequency calculated with (BCSLN) and without (BCS) approximate number projection for a self-conjugate, N=Z, nucleus. The BCS version of our model has been discussed in the literature [4] and the solutions can be characterized as follows:* (*i*) For $x^{T=0} < 1$ ($G_{np}^{T=0} < G_{np}^{T=1}$) the T=1 pairing is energetically favoured over the T=0 pairing. The pairing energy depends only on $\Delta^2 \equiv 2\Delta_0^2 + (\Delta_{np}^{T=1})^2$ and *no* energy is gained by activating the T=1 *np*-pairing. (*ii*) The solution at $x^{T=0} = 1$ ($G_{np}^{T=0} = G_{np}^{T=1}$) is highly degenerate. The HFB energy depends only on $\Delta^2 \equiv 2\Delta_0^2 + (\Delta_{np}^{T=1})^2 + |\Delta_{np}^{T=0}|^2$. Also in this case, no energy is gained due to *np*-pairing. (*iii*) The solution at $x^{T=0} > 1$ ($G_{np}^{T=0} > G_{np}^{T=1}$) corresponds to a pure T=0 *np*-pairing phase.

As shown in Fig. 1, the results from the number-projected calculations are quite different. The critical value of the strength necessary to activate T=0 *np*-pairing is larger, $x_{crit}^{T=0} \approx 1.1$. The LN-method introduces different modifications of the pairing potential for the T=1 *pp*- (*nn*-) and T=1 *np*-pairing field. It causes that at $x^{T=0} < x_{crit}^{T=0}$ and under the assumption of $G_{np}^{T=1} = G_{\tau\tau}^{T=1}$ the pairing gap for the T=1 *np*-pairing, $\Delta_{np}^{T=1}$, becomes zero. It implies that the LN method has an isovector component, that requires further investigation. However, at $x^{T=0} > x_{crit}^{T=0}$ the T=0 *np*-pairing correlations *coexists* with the T=1, $|T_z|$=1 pairing. The exclusivness of T=0 and T=1 pairing phases in N=Z

*In this case we disregard Coulomb energy and therefore $G_n = G_p$ and $\Delta_n = \Delta_p = \Delta_0$

nuclei is a generic feature of the BCS method and is smeared out in the number-projected calculations.

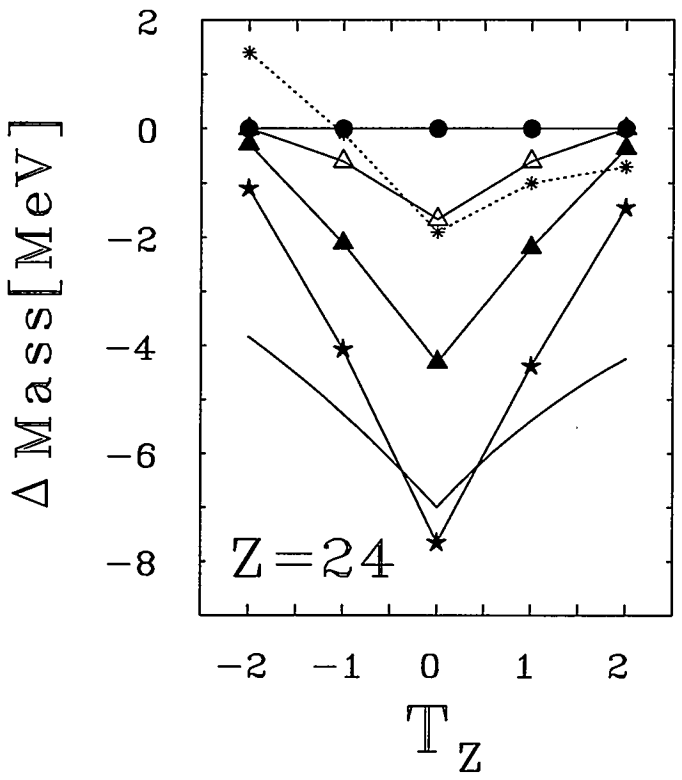


FIG. 2. *Calculated additional binding energy, $E(x^{T=0}) - E(x^{T=0} = 1)$, arising from the presence of T=0 pairing for a number of Cr-isotopes in the vicinity of the $T_z$=0 line. Different curves denote results for: $x^{T=0}$=1.1 (•), 1.2 (△), 1.3 (solid triangles) and 1.4 (⋆). The solid line without symbols denotes the Wigner energy term due to [14] and the dotted line (∗) marks the result of the ETFSI-model [15].*

For N≠Z both BCS and BCSLN models provide solutions which are qualitatively similar to the $T_z$=0, BCSLN case i.e. the T=0 *np*-pairing correlations coexist with the T=1 *pp*- and *nn*-pairing correlations. It is worth stressing that the value of $x_{crit}^{T=0}$ is strongly $T_z$ dependent i.e. increases quite rapidly with neutron/proton excess or, alternatively, *np*-correlations are restricted to small $|T_z|$. In consequence, our calculations suggest a critical value of $|T_z^{crit}|$ beyond which, i.e., for $|T_z| > |T_z^{crit}|$, there is no collective solution to *np*-pairing, see Fig. 2. The narrow range of *np*-pairing correlations with respect to $|T_z|$ suggests that they might give a possible microscopic explanation of the Wigner energy in even-even nuclei [13].

Fig. 3 illustrates the response of different pairing phases to nuclear rotation, see also [8,9]. These are qualitative calculations at constant deformation and as such should not be directly compared to the experimental data. The standard calculations with $|T_z|$=1 pairing force are compared to the case with T=0 *np*-pairing. At $\hbar\omega = 0$, the strength of the T=0 force is undercritical and T=0 pairing is not active. At a certain critical frequency, $\hbar\omega_{crit}$, there is a sudden *onset* of T=0 pairing, see also [9]. The latter effect can be viewed as either a phase transition or as band crossing.

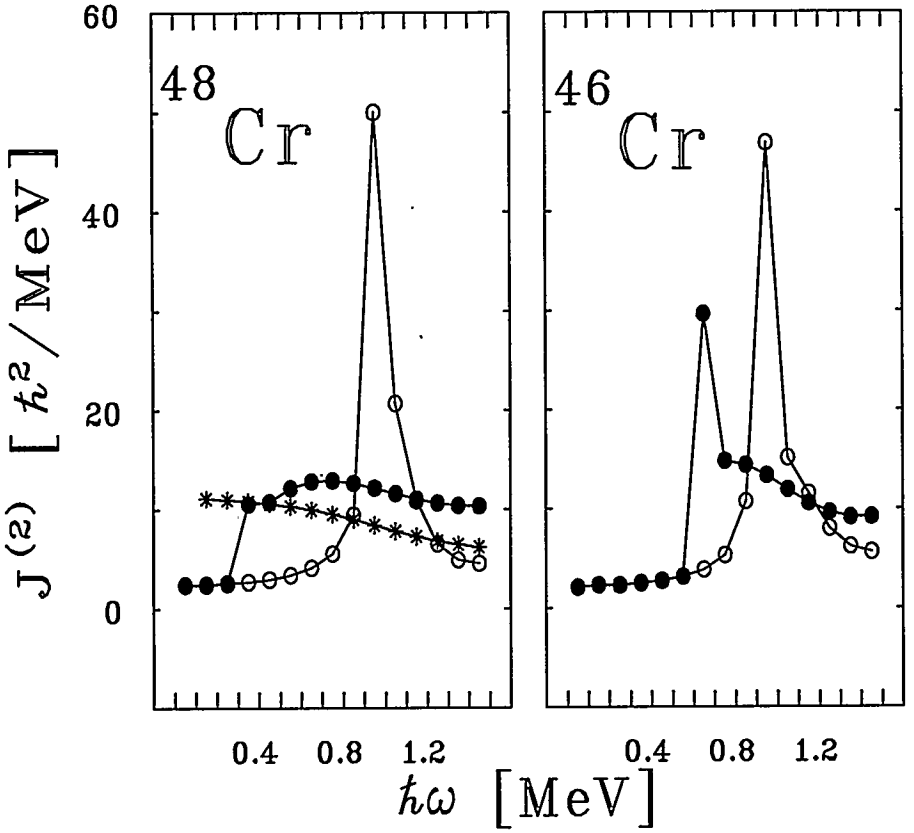


FIG. 3. *The calculated dynamical moments of inertia for $^{46}Cr$ and $^{48}Cr$. Open circles correspond to the case of pure T=1, $T_z$=±1 pairing and the sharp peak in $\mathcal{J}^{(2)}$ is due to the breaking of the $f_{7/2}$ pairs. The curve marked by solid dots indicate calculations with undercritical T=0 np-pairing strength at $\hbar\omega$=0. The sudden rise of the moment of inertia corresponds to the critical frequency, where the T=0 pairing correlations switch on. Note the entirely different behaviour of the moment of inertia for the two cases. The dotted line (∗) denotes the calculations without pairing.*

The influence of the T=0 *np*-pairing on the dynamical moment of inertia is apparent. It reflects the basic difference between the mechanisms of building angular momentum for the cases of T=1, $|T_z|$=1 pairing and T=0 *np*-pairing, respectively. For the case of T=1 pairing the well known pair breaking mechanism dominates. For the case of T=0 pairing, angular momentum is built up by smoothly aligning *np*-pairs along the rotational axis without involving any pair breaking mechanism. In fact, the T=1 pair breaking and alignment of angular momenta of quasi-particles along the rotational axis due to centrifugal and Coriolis forces effectively increases the number of nucleons with parallely coupled angular momenta enhancing T=0, $\alpha\alpha$, *np*-pairing correlations. The result is a phase transition at high spins, illustrated in Fig. 3. Note, that nuclear rotation in the presence of this phase resembles rigid-body like rotation even though T=1 *pp*- and *nn*-pairing correlations are present. The moments of inertia in the presence of T=0 pairing actually exceed the value obtained for a system without pairing.

The classes of solutions discussed above appear to be generic for all even-even nuclei with N∼Z, i.e. do not depend qualitatively on A. Our results can be summarized as follow: The previously suggested exclusiveness of the T=0 and T=1 pairing phases [5,6,9]

does not find support in our calculations. The sudden phase transition between the T=0 and T=1 pairing modes is a generic feature of the BCS approximation for N=Z nuclei. This phase transition becomes smeared out in number-projected LN calculations. There, the T=0 *np*-pairing correlations coexist with T=1 *nn*- and *pp*-pairing correlations over a broad range of the strength $G_{np}^{T=0}$ as well as rotational frequency $\hbar\omega$, when $x^{T=0} > x_{crit}^{T=0}$. However, pairing correlations of $\boldsymbol{\alpha\alpha}$ and $\boldsymbol{\alpha\tilde{\alpha}}$ type counteract. For N≠Z, the T=0 *np*-pairing correlations and T=1 *nn*- and *pp*-pairing correlations do coexist in both BCS and number-projected LN calculations. The T=0 *np*-pairing correlations are confined to a narrow region along the N=Z line. The additional binding arising from these correlations may be viewed as a microscopic origin of the Wigner term in even-even nuclei. Even in the cases where *np*-pairing correlations are not present in the ground state one can generate T=0 *np*-pairing correlations at large rotational frequencies. An onset of $\boldsymbol{\alpha\alpha}$ *np*-pairing quite dramatically influences the mechanism of building angular momenta. The T=0 *np*-pairs can easily be decoupled from the deformed core by the Coriolis force and consequently nuclear rotation resembles rigid-body like rotation though *pp*- and *nn*-pairing correlations are present. In both BCS and number-projected calculations, the T=0 and T=1 phases of *np*-pairing are exclusive at $\hbar\omega \neq 0$. We believe that this exclusiveness is an artifact related to our schematic interaction and/or the assumed self-consistent symmetries.

We wish to thank J. Dobaczewski, A. Goodman and W. Nazarewicz for many stimulating discussions. Financial support from the Göran Gustafsson Foundation, Swedish Natural Science Research Council (NFR) and Polish State Committee for Scientific Research (KBN) under Contract No. 2 P03B 034 08 is gratefully acknowledged. One of us (W.S.) would like to express his sincere thanks to the Joint Institute for Heavy Ion Research and University of Tennessee for postdoctoral scholarschip.

---

[1] A. Goswami, Nucl. Phys. **60** (1964) 228.
[2] A. Goswami and L.S. Kisslinger, Phys. Rev. **140** (1965) B26.
[3] H.T. Chen and A. Goswami, Phys. Lett. **B24** (1967) 257.
[4] A.L. Goodman, Nucl. Phys. **A186** (1972) 475.
[5] A.L. Goodman, G.L Struble and A. Goswami, Phys. Lett. **B**26 (1968) 260.
[6] A.L. Goodman, G.L Struble, J. Bar-Touv and A. Goswami, Phys. Rev. **C**2 (1970) 380.
[7] H. Wolter, A. Faessler and P. Sauer, Nucl. Phys. **A167** (1971) 108.
[8] K. Nichols and R.A. Sorensen, Nucl. Phys. **A309** (1978) 45.
[9] E.M. Müller, K. Mühlhans, K. Neergård and U. Mosel, Nucl. Phys. **A383** (1982) 233.
[10] A.L. Goodman, Nucl. Phys. **A230** (1974) 466.
[11] W. Satuła and R. Wyss, submitted to Phys. Lett. **B**.
[12] H.C. Pradhan, Y. Nogami and J. Law, Nucl. Phys. **A201** (1973) 357.
[13] E. Wigner, Phys. Rev. **51** (1937) 106.
[14] W. Myers and W. Swiatecki, Nucl. Phys. **81** (1966) 1.
[15] Y. Aboussir, J.M. Pearson, A.K. Dutta and F. Tondeur, Atomic Data and Nuclear Data Tables **61**, (1995) 127.

# IN-BEAM STUDIES OF $^{98}$Cd AND $^{102}$Sn

M. Lipoglavšek[a,b], M. Górska[c], J. Nyberg[a], A. Ataç[a], A. Axelsson[a], R. Bark[d], J. Blomqvist[e], J. Cederkäll[e], B. Cederwall[e], G. de Angelis[f], C. Fahlander[a,f], H. Grawe[c], A. Johnson[e], S. Leoni[d], A. Likar[b], M. Matiuzzi[d], S. Mitarai[g] L.-O. Norlin[e], M. Palacz[h], J. Persson[a], H.A. Roth[i], R. Schubart[c], D. Seweryniak[j], T. Shizuma[g] D. Sohler[e], G. Sletten[d], W.B. Walters[k], M. Weiszflog[a]

[a] *The Svedberg Laboratory and Department of Radiation Sciences, Uppsala University, Box 533, S-75121 Uppsala, Sweden*
[b] *J. Stefan Institute, Ljubljana, Slovenia*
[c] *GSI, Darmstadt, Germany*
[d] *Niels Bohr Institute, University of Copenhagen, Copenhagen, Denmark*
[e] *Department of Physics, Royal Institute of Technology, Stockholm, Sweden*
[f] *INFN, LNL, Legnaro, Italy*
[g] *Department of Physics, Faculty of Science, Kyushu University, Japan*
[h] *Sołtan Institute for Nuclear Studies, Swierk, Poland*
[i] *Chalmers University of Technology, Gothenburg, Sweden*
[j] *Argonne National Laboratory, Argonne, IL, USA*
[k] *Department of Chemistry, University of Maryland, College Park, MD, USA*

## Abstract

For the first time excited states of the neutron deficient nuclei $^{98}$Cd and $^{102}$Sn were identified using in-beam spectroscopy following fusion evaporation reactions. Half lives of long lived isomeric states in both nuclei were also measured. Due to very low cross sections for producing $^{98}$Cd and $^{102}$Sn with stable beams and targets, a special detector setup utilizing NORDBALL ancillary detectors and a recoil catcher device was used. High $\gamma$-ray detection efficiency was achieved with two EUROBALL Ge cluster detectors.

# 1. Introduction

The region of nuclei around $^{100}$Sn has been the subject of many experimental and theoretical studies in the past due to its importance for the Nuclear Shell model. Recently a substantial progress was achieved in experimental studies of excited states of nuclei in the vicinity of $^{100}$Sn. Nuclei with only three quasiparticles away from the doubly closed shell were reached by the studies of excited states in $^{97}$Ag[1], $^{99}$Cd[2] and $^{101}$In[3]. In the continuation of these efforts this work reports on studies of excited states of the two proton-hole nucleus $^{98}$Cd and its two neutron-particle counterpart $^{102}$Sn.

# 2. Experiment

Two experiments were performed at the Tandem Accelerator Laboratory of the Niels Bohr Institute in Denmark. The first 8 days long experiment aimed at studies of excited states in $^{98}$Cd. A 215 MeV $^{58}$Ni beam was used to bombard a 1 mg/cm$^2$ thick $^{46}$Ti target enriched to 86 %. The compound nucleus was $^{104}$Sn and $^{98}$Cd was populated in the 1$\alpha$2n exit channel. In the second experiment the beam energy was raised to 225 MeV and a 1 mg/cm$^2$ thick $^{50}$Cr target enriched to 99.0 % was used. This 10 days long experiment aimed at excited states of $^{102}$Sn populated via the reaction $^{50}$Cr($^{58}$Ni,1$\alpha$2n).

Due to very low cross sections for producing $^{98}$Cd and $^{102}$Sn in the 1$\alpha$2n reaction channel and since there were indications for long lived isomeric states expected in both nuclei[4], a special detector setup was assembled, see figure 1. The setup consisted of two parts. A $4\pi$ Silicon ball with 31 elements[5], a $2\pi$ Neutron wall with 15 elements[6] and 5 large $BaF_2$ detectors were placed around the target. The ancillary detectors were used for identification of the reaction channel and for obtaining a precise time reference signal for each event. By carefully aligning the time signals from all ancillary detectors a resolution (FWHM) of about 2 ns was achieved for the time reference signal. Such a good time resolution was essential for good neutron-$\gamma$ separation in the neutron detectors, which was done by means of a combined time-of-flight and pulse shape discrimination technique. Besides a fairly high neutron detection efficiency of 27%, the neutron-$\gamma$ separation also turned out to be very good. Only 0.2% of the events not connected with neutron emission were misinterpreted as if one neutron was detected. About 1% of the events, where one neutron was emitted were found in the 2n gated spectra due to neutron scattering from one detector to another. Protons and $\alpha$ particles were detected in silicon detectors with detection efficiencies of 64 and 42%, respectively. The separation between protons and $\alpha$ particles was done according to the energy deposited in the detectors. Low energy $\alpha$ particles emitted mainly in the backward angles relative to the beam direction deposit the same amount of energy as protons, which caused about 9% of the emitted $\alpha$ particles to be misinterpreted as protons. A small fraction, less than 0.1%, of the emitted protons were misinterpreted as $\alpha$ particles.

The second part of the experimental setup consisted of an exchangeable recoil catcher foil[7] and two EUROBALL Ge cluster detectors[8], placed 60 cm downstream from the target. The recoil catcher foil had a diameter of 10 cm. In the center it had a 1 cm wide hole for beam. It was exchanged once every hour in order to decrease the background from long lived radioactivity. The Ge detectors were placed around the catcher foil. Therefore, only $\gamma$-ray decays, that occurred after the recoils were stopped in the catcher foil, were detected. The

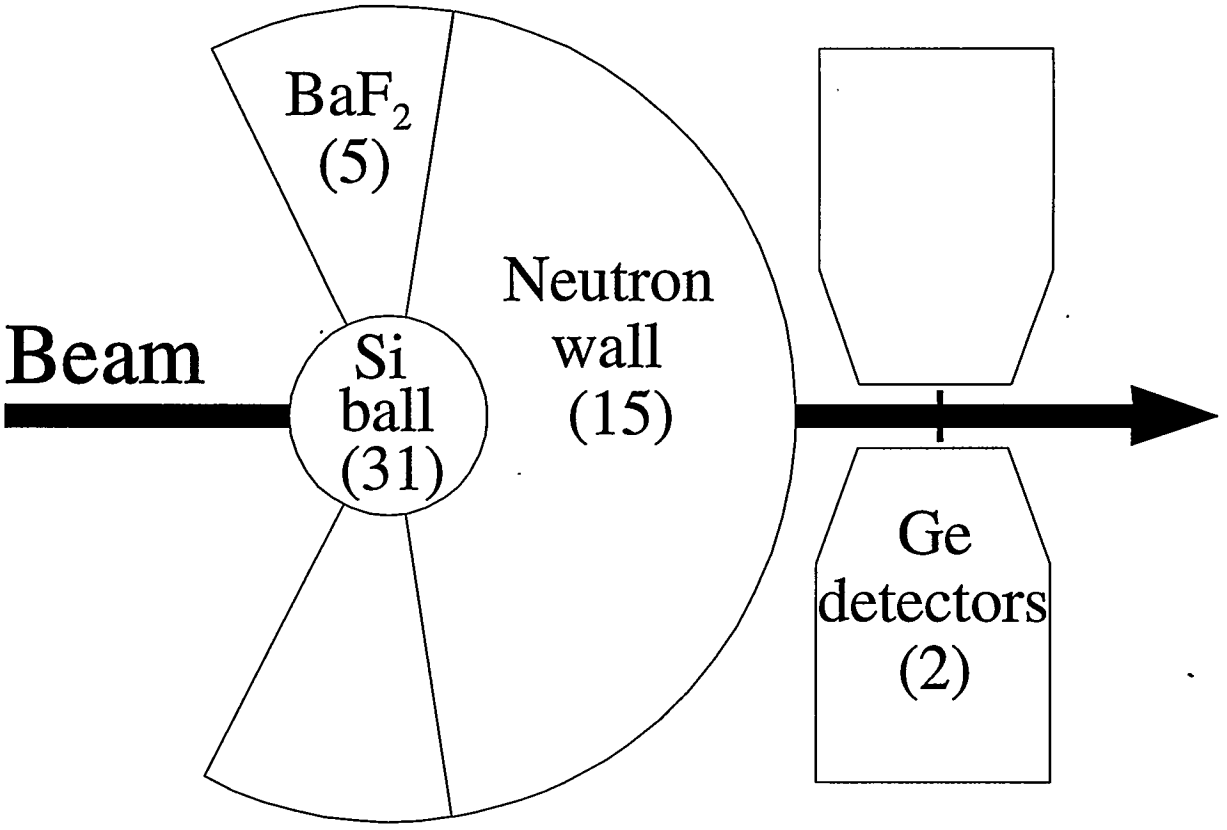


Figure 1: Experimental setup used for studying nuclei with long lived isomeric states.

flight time of the recoils was about 50 ns. With this setup the background originating from prompt $\gamma$ radiation could be decreased by more than an order of magnitude compared to our previous in beam experiments[2,3]. The BGO shields of the Ge cluster detectors, except for the back catchers, were not used, and thus the detectors could be placed very close to the recoil catcher foil. The distance between the center of the catcher foil and the front face of the central Ge crystal in the cluster detector was 78 mm, which resulted in a $\gamma$-ray detection efficiency of about 6% at 1.3 MeV.

The trigger system was also specially adjusted to suit studies of long lived isomeric states. Events were accepted if there was at least one signal from the Ge detectors between 30 and 880 ns after the reaction. The time of the reaction was determined by the ancillary detectors. The energy and time signals from the Ge and Si detectors, the time-of-flight and zero-cross-over time signals from the neutron detectors and the time signals from $BaF_2$ detectors were written to tape for each accepted event.

## 3. Results

The analysis is still in progress and therefore all the results are preliminary. We have identified four $\gamma$ rays belonging to $^{98}$Cd with the energies 1395, 688, 199 and 148 keV. A half life of approximately 480 ns was measured for the expected isomeric $8^+$ state. The cross section for the $^{46}$Ti($^{58}$Ni,1$\alpha$2n)$^{98}$Cd reaction was approximately 20 $\mu$b.

Two $\gamma$ rays with energies 1472 and 497 keV were identified to belong to $^{102}$Sn. The half life of the expected isomeric $6^+$ state was measured to be approximately 1 $\mu$s. We expected to find three E2 transitions between the $6^+$ state and the $0^+$ ground state. However, it is very probable that a low energy transition between the $6^+$ and $4^+$ states was not observed due to low statistics and due to the internal conversion of such a low energy E2 transition. The measured relative cross section for the reaction $^{50}$Cr($^{58}$Ni,1$\alpha$2n)$^{102}$Sn compared to the reaction $^{50}$Cr($^{58}$Ni,1$\alpha$2p)$^{102}$Cd was approximately 0.02%. Assuming that the cross section for the reaction leading to $^{102}$Cd is 50 mb, as obtained from the CASCADE[9] code, and that the isomeric $8^+$ state in $^{102}$Cd is populated in only 20% of the reactions leading to $^{102}$Cd[10], the cross section for the reaction leading to $^{102}$Sn is about 2 $\mu$b.

## 4. References

1) D. Alber et al., *Z. Phys.* **A335** (1990) 265.
2) M. Lipoglavšek, et al., *Phys. Rev. Lett.* **76** (1996) 888.
3) J. Cederkäll et al., *Phys. Rev.* **C53** (1996) 1955.
4) R. Grzywacz et al., Proceedings of the International Conference on Exotic Nuclei and Atomic Masses, Arles, France, 1995. Editions Frontieres, 1995, p. 561.
5) T. Kuroyanagi et al., *Nucl. Instr. Meth.* **A316** (1992) 289.
6) S. E. Arnell et al., *Nucl. Instr. Meth.* **A300** (1991) 303.
7) R. Schubart et al., *Physica Scripta* **T56** (1995) 311.
8) J. Eberth et al., Proceedings of the Conference on Physics from Large Gamma-Ray Detector Arrays, August 2 – 6, 1994, Berkeley, Ca., USA, Vol. II, LBL–35687, p. 160.
9) F. Pühlhofer, *Nucl. Phys.* **A280** (1977) 267.
10) J. Persson et al., to be published.

# First in-beam observation of excited states in $^{156}_{72}Hf_{84}$ using the Recoil-Decay Tagging Method

D. Seweryniak, I. Ahmad, H. Amro, D.J. Blumenthal, L.T. Brown, M.P. Carpenter, C.N. Davids, S. Fischer, D.J. Henderson, R.V.F. Janssens, T.L. Khoo, C.J. Lister, D. Nisius
*Argonne National Laboratory*

T. Davinson, R.J. Irvine, P.J. Woods
*University of Edinburgh*

W.B. Walters
*University of Maryland*

I. Hibbert, C. Parry, R. Wadsworth
*York University*

Excited states in the proton rich nuclide $^{156}_{72}Hf_{84}$ were observed for the first time using the $^{102}Pd(^{58}Ni,2p2n)^{156}Hf$ reaction at 270 MeV. Gamma rays were detected with the AYEBALL array of Compton suppressed Ge detectors, placed in front of the Fragment Mass Analyzer, and were assigned to individual reaction channels using the Recoil-Decay Tagging Method. Prompt $\gamma$-ray cascades were associated with the alpha decay of both the ground state and the $8^+$ isomeric state in $^{156}Hf$. The level scheme constructed for $^{156}Hf$ is compared with level schemes of lighter even-even N=84 isotones and is discussed within the framework of the Shell Model.

## I. INTRODUCTION

The structure of nuclei situated along the N=82 neutron shell closure, above the Z=64 line have for a long time been an aim of numerous studies. Interest in this region of the chart of nuclides increased after the discovery that $^{146}_{64}Gd_{82}$ can be regarded as a doubly magic core [1]. This has been attributed to the presence of a large energy gap between the $g_{7/2}$, $d_{5/2}$ proton orbitals, which are filled in $^{146}Gd$, and the remaining proton orbitals of the Z=50-82 major shell, i.e. $h_{11/2}$, $s_{1/2}$ and $d_{3/2}$. The immediate neighbors of $^{146}Gd$ can be produced with relatively large cross sections using heavy-ion induced fusion-evaporation reactions and there exists a vast amount of experimental data on their structure. For a summary of a large body of experimental work see ref. [2]. Deduced single-particle energies and two-body matrix elements, with respect to the $^{146}Gd$ core, have been used in several shell-model calculations which successfully reproduce excited states observed in nuclei which have more than two valence nucleons outside the $^{146}Gd$ core [2,3].

The N=82 isotones heavier than $^{146}_{64}Gd_{82}$ are an ideal testing ground for studying the proton-proton residual interaction, and it is worth noting that their yrast high spin states, can be accurately described using the $(\pi h_{11/2})^n$ configuration space. The N=84 isotones heavier than $^{148}_{64}Gd_{84}$ on the other hand are crucial for determining both the interaction between neutrons in the $f_{7/2}$ and $h_{9/2}$ orbitals (which are the two lowest neutron orbitals) and the interaction of these neutrons with protons gradually filling the $h_{11/2}$ orbital. In addition, the $i_{13/2}$ neutron orbital also plays a significant role at higher excitation energies, due to its large angular momentum which effectively contributes to the total spin.

Another interesting aspect of studies of light nuclei with N$\geq$82 and Z$\geq$64 is the close proximity of the proton drip-line. This presents an opportunity to address questions related to the interplay between $\gamma$ decay and proton decay, the formation of proton halos in heavy nuclei, and the impact of the continuum on loosely bound states. In fact, a number of new proton emitters have been recently identified in this region in a series of experiments performed at the ATLAS accelerator using the Fragment Mass Analyzer (FMA) [4]. Every odd-Z element between Ta and Bi has been found to have at least one isotope which decays by proton emission. In addition, there exists a vast amount of data on alpha decay in this region (see [5] and references therein).

However, studies of the level structure of proton rich nuclei in the N$\geq$82, Z$\geq$64 region are impeded by very small reaction cross sections due to the lack of suitable stable target and beam combinations, strong competition from fission and fragmentation of the fusion-evaporation cross section. The nucleus $^{154}_{72}Hf_{82}$ is the heaviest N=82 isotone with known excited states. The decay of its $10^+$ isomer has been observed using the Daresbury Recoil Separator [7]. Excited states of even-even N=84 isotones through $^{154}_{70}Yb_{84}$ [8] and odd N=84 isotones through $^{153}_{69}Tm_{84}$ [9] have been investigated in a series of in-beam experiments summarized in ref. [3].

A procedure, termed the Recoil-Decay Tagging (RDT) method, has recently been employed for identifying in-beam prompt $\gamma$ rays in nuclei which undergo $\alpha$ or proton decay. The method was successfully used for the first time for $\alpha$ and proton emitters in the $^{100}Sn$ region and yielded very promising results [6].

In the present work, prompt $\gamma$-ray cascades correlated with the two $\alpha$ lines, previously assigned to $^{156}Hf$, were identified using the RDT method. The level scheme obtained for $^{156}Hf$ will be discussed in the framework of the Shell Model and compared with the excited states observed in neighboring nuclei.

## II. EXPERIMENT

A 270 MeV $^{58}$Ni beam from the ATLAS accelerator was used to bombard a 1 mg/cm$^2$ $^{102}$Pd target in order to populate excited states in $^{156}_{72}Hf_{84}$ via the 2p2n fusion-evaporation channel. Gamma rays were detected with AYEBALL [10], an array of 16 HPGe detectors and 2 LEP spectrometers surrounding the target, placed in front of in the FMA. Detected $\gamma$ rays were assigned to individual reaction channels using the RDT method [6]. Residual recoiling nuclei were dispersed in the FMA according to their mass to charge state ratio and implanted into a Double-Sided Silicon Strip Detector (DSSD) placed behind the focal plane of the FMA. The subsequent characteristic $\alpha$ decays observed in the same pixel of the DSSD as the implantation allowed complete identification of the implanted residues and thus of $\gamma$ rays detected at the target position.

The ground state of $^{156}$Hf has a half life of 23 ms and is known to decay predominantly by emitting an $\alpha$ particle with an energy of 5.87 MeV. Another $\alpha$ line with an energy of 7.78 MeV and a half-life of 0.52 ms has been assigned to the decay of an isomeric state in $^{156}$Hf [5]. The isomeric state has been found to be populated following the $\beta$ decay of the $[\pi h_{11/2}\nu f_{7/2}]_{9+}$ state in $^{156}$Ta, and, as a result, has been assigned as a $[\nu h_{9/2}\nu f_{7/2}]_{8+}$ configuration in analogy to heavier N=84 isotones [11]. In the present experiment, prompt $\gamma$-ray cascades could be associated with both $^{156}$Hf alpha lines.

The energy spectrum of $\alpha$ particles collected in the DSSD during the experiment is shown in Fig. 1.

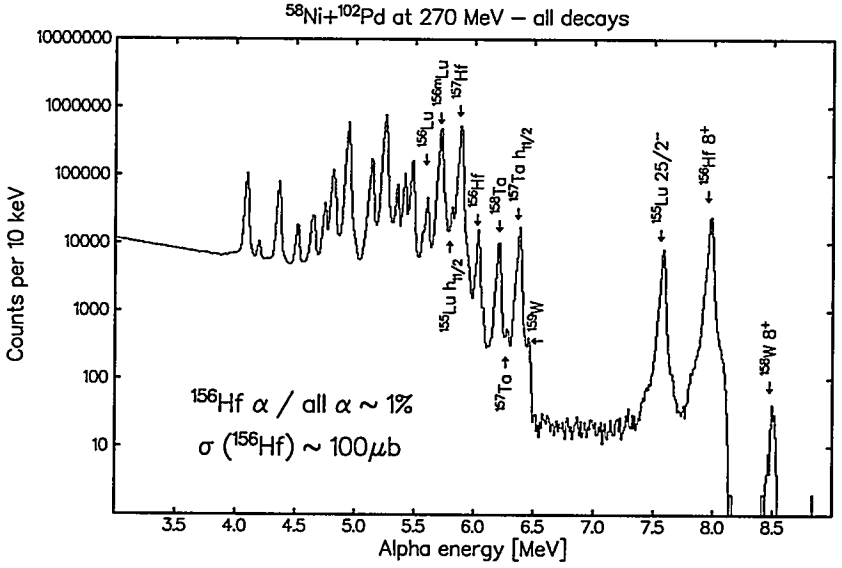


FIG. 1. Energy spectrum of alpha particles measured in the DSSD.

Both $^{156}$Hf $\alpha$ lines represent about 1% of the entire spectrum. Singles $\gamma$-ray spectra tagged on the $^{156}$Hf alpha lines are presented in Fig. 2. Three strong $\gamma$-ray lines are correlated with the ground state $\alpha$ decay of $^{156}$Hf. The spectrum correlated with the $\alpha$ particles emitted from the isomeric state is somewhat more complicated, indicating fragmentation of the decay path at higher excitation energies. A preliminary level scheme for $^{156}$Hf is proposed in fig. 3.

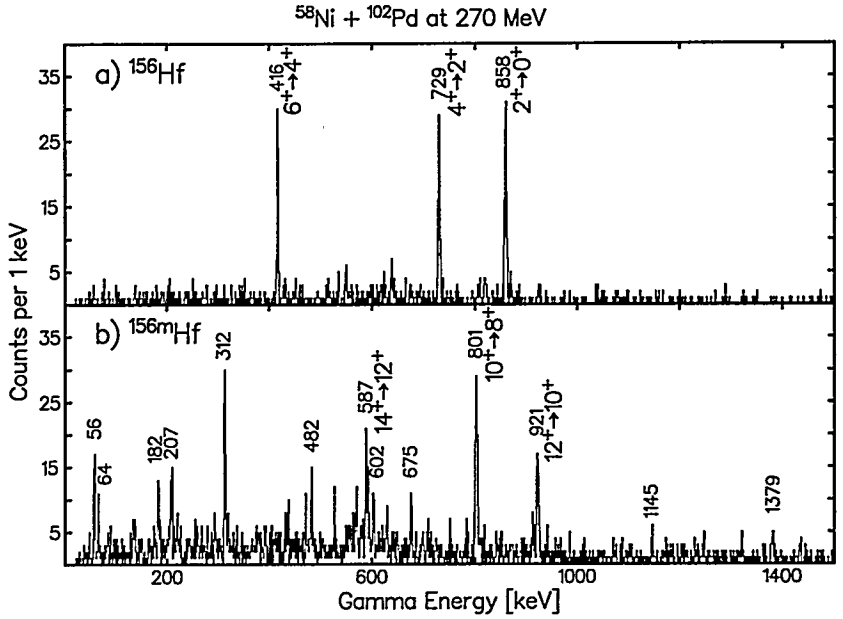


FIG. 2. Gamma-ray singles spectra tagged on a) the ground state $\alpha$ decay of $^{156}$Hf and b) the $\alpha$ decay of the $8^+$ isomeric state in $^{156}$Hf.

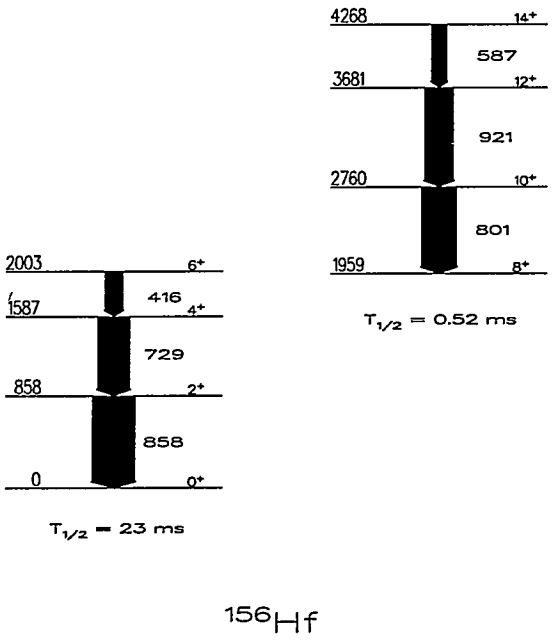


FIG. 3. A preliminary level scheme for $^{156}$Hf.

Gamma-ray transitions were ordered solely on the basis of the measured $\gamma$-ray intensities in the singles recoil-decay tagged spectra. Because of the low statistics, only the strongest transitions have been placed in the level scheme. The spins and parity assignments of the proposed levels were obtained using fragmentary angular distribution information. These assignments are, however, supported by comparison with the systematic behavior of states in the lighter known even-even N=84 isotones. They should nevertheless be regarded as preliminary.

## III. DISCUSSION

The three strong $\gamma$-ray transitions feeding the ground state are placed in a cascade of stretched E2 transitions forming a $6^+ \rightarrow 4^+ \rightarrow 2^+ \rightarrow 0^+$ sequence of states. As shown in fig. 4, the resulting $2^+$, $4^+$ and $6^+$ excitation energies follow the systematics of the lighter known even-even N=84 isotones and, together with the ground state, are proposed to form the $(\nu f_{7/2})^2$ multiplet.

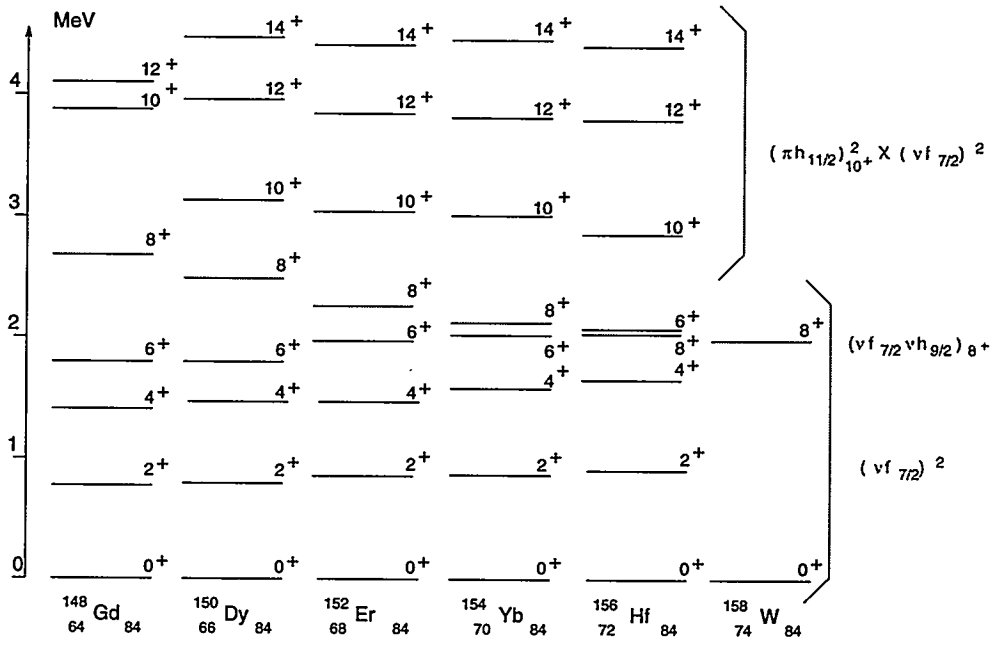


FIG. 4. Systematics of yrast states in even-even N=84 isotones. The configuration assignments proposed in this work are indicated on the right hand side of the figure. The $8^+$ state shown for $^{158}$W has only been oberved in $\alpha$-decay studies.

The energy sum of these three $\gamma$-ray transitions places the $6^+$ state above the $8^+$ isomer. An E4 $\gamma$-ray transition is the only competition for the $\beta$ and $\alpha$ decays from this state. The $8^+$ state is thus a classical yrast trap. The lowering of the $8^+$ state with respect to the $6^+$ level as Z increases is mainly a consequence of the narrowing of the energy gap between the two lowest lying neutron orbitals, $\nu f_{7/2}$ and $\nu h_{9/2}$, as illustrated in fig. 5. In the heavier N=84 isotones this trend has been associated with the strong attractive interaction between the $h_{11/2}$ proton and the $h_{9/2}$ neutron when coupled to spin I=1$\hbar$ [3]. This attraction is taken advantage of by each successive proton pair added to the $^{146}$Gd core.

The three strongest transitions correlated with the $\alpha$ decay of the $8^+$ isomer have also been assigned as stretched quadrupole transitions forming a cascade reaching a spin of 14$\hbar$ and an excitation energy of about 4.3 MeV. This sequence resembles the cascades seen in the lighter N=84 isotones, and the proposed $10^+$, $12^+$ and $14^+$ states can be interpreted as the $(\nu f_{7/2})^2_{0^+,2^+,4^+}$ states coupled to the aligned proton pair $(\pi h_{11/2})^2_{10^+}$. Gamma-ray lines remaining in fig. 2b have not yet been placed in the level scheme. They are most likely situated above 4 MeV excitation energy where the decay path is fragmented, as has been observed in $^{154}$Yb [8].

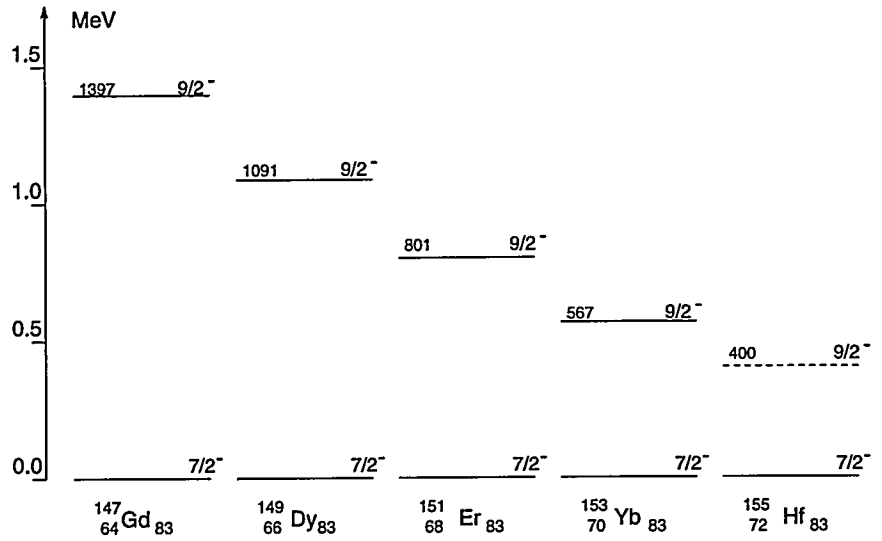


FIG. 5. Systematics of the neutron single-particle states in odd N=83 isotones. The $9/2^-$ state in $^{155}$Hf was extrapolated.

Although the interpretation of the $^{156}$Hf level structure proposed in this work appears to be quite strightforward, more in depth shell-model analysis may shed some light on the growing role of the $h_{9/2}$ neutron orbital. A simple extrapolation from known nuclei places this orbital only 200 keV above the $f_{7/2}$ neutron orbital in $^{156}$Hf and both orbitals are almost degenerate in $^{158}$W, a nuclues which has only 2 protons more than $^{156}$Hf. One of the consequences of this degeneracy would be the mixing of the members of the $(\nu h_{9/2})^2_{0^+,2^+,4^+,6^+,8^+}$ multiplet with the yrast $(\nu f_{7/2})^2$ band. Also any attempt to find footprints of the interaction between the continuum and the observed states requires data with much better statistics, which is necessary to extend the level scheme of $^{156}$Hf to higher excitation energies, both along the yrast line and above it.

In the same experiment, excited states in the odd-Z proton-rich N=84 isotones $^{155}$Lu and $^{157}$Ta were also observed for the first time. It is also worth mentioning that evidence was found that one of the states in $^{157}$Ta, most likely the $\pi d_{3/2}$ state which have not been seen before, undergoes direct proton decay. Prompt $\gamma$-ray cascades were correlated with the $\alpha$ decays of the $h_{11/2}$ proton states in both nuclei and with the $25/2^-$ isomer in $^{155}$Lu. Preliminary analysis of the $\gamma$-ray spectra correlated with $\alpha$ particles emitted from the $\pi h_{11/2}$ states revealed yrast bands similar to these observed in heavier odd-Z N=84 isotones (see fig. 6).

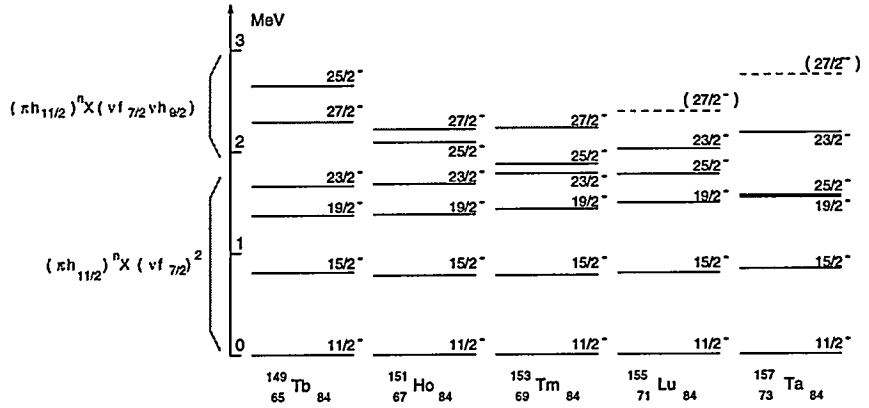


FIG. 6. Systematics of yrast bands built on the $h_{11/2}$ proton states in odd-Z N=84 isotones. The states shown for $^{155}$Lu and $^{157}$Ta are proposed for the first time from the present work. The suggested configurations are indicated on the left hand side of the figure.

The proposed E2 cascades feeding the $\pi h_{11/2}$ state reach spin $23/2^-$. The resulting $23/2^-$, $19/2^-$, $15/2^-$, $11/2^-$ sequence resembles the $6^+$, $4^+$, $2^+$, $0^+$ sequence in $^{156}$Hf, and can be interpreted as the $(f_{7/2})^2$ multiplet aligned with the $h_{11/2}$ odd proton. In addition, possible $27/2^-$ states are suggested for both nuclei which would correspond to the maximum spin state of the $\pi h_{11/2} \otimes (\nu f_{7/2} \otimes \nu h_{9/2})_{8+}$ configuration. In the $25/2^-$ state neutrons occupy the same orbitals as in the $27/2^-$ state but one proton $(h_{11/2})^2$ pair is broken. The results show that the yrast $25/2^-$ state drops below the yrast $23/2^-$ already in $^{155}$Lu and comes down even more in $^{157}$Ta forming an yrast trap. The lowering of the $25/2^-$ state with respect to the $23/2^-$ state simply mimics the drop of the $\nu h_{9/2}$ orbital with respect to the $\nu f_{7/2}$ orbital.

## IV. SUMMARY

In this work results for excited states in three N=84 isotones, i.e. $^{156}$Hf, $^{155}$Lu and $^{157}$Ta, are presented for the first time. Despite low statistics, the proposed $\gamma$-ray transitions were unambiguously assigned to the individual reaction channels using the RDT method and yrast cascades feeding the ground states, and the $8^+$ isomer in $^{156}$Hf, were proposed. The resulting level schemes, to a large extent, follow the systematics of the lower-Z N=84 isotones, allowing shell-model interpretation similar to that proposed in ref. [3]. More in-depth analysis requires data with better statistics.

The RDT method used in the present experiment, is seen to be a very powerful tool to identify in-beam $\gamma$-ray transitions associated with very weakly populated reaction channels at and even beyond the proton drip-line. Indeed, in another experiment, $\gamma$-ray transitions correlated with the ground state and isomeric state proton decay in $^{147}$Tm were identified, truly representing in-beam $\gamma$-ray spectroscopy beyond the proton drip line. A large array of Ge detectors such as GAMMASPHERE, placed in front of the FMA, would increase the $\gamma$-$\gamma$ coincidence efficiency by a factor of about 50 compared to AYEBALL, This would allow the extension of already known level schemes to higher excitation energies and studies even further beyond the proton drip-line. For example, the heavier even-even N=84 isotone $^{158}$W, where the neutron orbitals $f_{7/2}$ and $h_{9/2}$ are almost degenerate, would be well within the range of such a detection system.

The excellent support of the ATLAS crew is greatly appreciated. This work is supported by the U.S. Department of Energy, Nuclear Physics Division, under contract No. W-31-109-ENG-38. T.D. and P.J.W. wish to acknowledge travel support from NATO under Grant No. CRG 940303.

---

[1] P. Kleinheinz, R. Broda, P.J. Daly, S. Lunardi, M. Ogawa, and J. Blomqvist, Z. Phys., **A290**, 279 (1979)
[2] M. Lach, P. Kleinheinz, M. Piiparinen, M. Ogawa, S. Lunardi, M.C. Bosca, J. Styczen, and J. Blomqvist, Z. Phys. **A341**, 25 (1991)
[3] C.T. Zhang, P. Kleinheinz, M. Piiparinen, R. Broda, R. Collatz, P.J. Daly, K.H. Maier, R. Menegazzo, G. Sletten, J. Styczen, and J. Blomqvist, Phys. Rev. **C54**, R1 (1996)
[4] C.N. Davids, D.J. Blumenthal, D.J. Henderson, H.T. Penttilä, D. Seweryniak, A.H. Wuosmaa, P.J. Woods, T. Davinson, R.J. Irvine, R.D. Page, J.C. Batchelder, C.R. Bingham, B.E. Zimmerman, L.T. Brown, A.V. Ramayya, B.C. Busse, L.F. Conticchio, W.B. Walters, S.J. Freeman, M. Freer, and K.S. Toth, Proceedings of the Internat. Conf. on Exotic Nuclei and Atomic Masses, 1995, Arles, France, Eds. M. de Saint Simon and O. Sorlin, Editions Frontieres, p. 263
[5] R. Page, P.J. Woods, R.A. Cunningham, T. Davinson, N.J. Davis, A.N. James, K. Livingston, P.J. Sellin, and A.C. Shotter, Phys. Rev. **C53**, 660 (1996)
[6] E.S. Paul, P.J. Woods, T. Davinson, R.D. Page, P.J. Sellin, C.W. Beausang, R.M. Clark, R.A. Cunningham, S.A. Forbes, D.B. Fossan, A. Gizon, J. Gizon, K. Hauschild, I.M. Hibbert, A.N. James, D.R. LaFosse, I. Lazarus, H. Schnare, J. Simpson, R. Wadsworth, and M.P. Waring, Phys. Rev. **C51**, 78 (1995).
[7] J.H. McNeill, J. Blomqvist, A.A. Chishti, P.J. Daly, W. Gelletly, M.A.C. Hotchkis, M. Piiparinen, B.J. Varley, and P.J. Woods, Phys. Rev. Lett. **63**, 860 (1989)
[8] C.T. Zhang, R. Broda, R. Menegazzo, P. Kleinheinz, R. Collatz, H. Grawe, S. Hofmann, M. Lach, K.H. Maier, M. Schramm, R. Schubart, and J. Blomqvist, Z. Phys. **A345**, 327 (1993)
[9] C.T. Zhang, P. Kleinheinz, M. Piiparinen, R. Collatz, T. Lonnroth, . Sletten, and J. Blomqvist, Z. Phys., **A348**, 249 (1994)
[10] P.H. Reagan et al., to be published
[11] S. Hofmann, P. Armbruster, G. Berthes, T. Faestermann, A. Gillitzer, F.P. Hesberger, W. Kurcewicz, G. Münzenberg, K. Poppensieker, H.J. Schott, and I. Zychor, Z. Phys. **A333**, 107 (1989)

# COLLECTIVE PROPERTIES OF DRIP-LINE NUCLEI

**I.Hamamoto[a] and H.Sagawa[b]**

[a] Department of Mathematical Physics, Lund Institute of Technology, University of Lund, Lund, Sweden. [b] Center for Mathematical Sciences, University of Aizu, Fukushima, Japan.

Performing the spherical Hartree-Fock (HF) calculations with Skyrme interactions and, then, using RPA solved in the coordinate space with the Green's function method, we have studied the effect of the unique shell structure as well as the very low particle threshold on collective modes in drip line nuclei [1-3]. In this method a proper strength function in the continuum is obtained [4,5], though the spreading width of collective modes is not included. We have examined also one-particle resonant states in the obtained HF potential. Unperturbed particle-hole (p-h) response functions are carefully studied, which contain all basic information on the exotic behaviour of the RPA strength function in drip line nuclei.

An appreciable amount of transition strength appears in the very low energy region (just above the particle threshold) of neutron drip line nuclei, if small angular momenta of particles are possible in combination with neutron hole orbitals with small binding energies. If no one-particle resonant states with the required quantum numbers are present for a particle excitation, the threshold strength consumes the major part of the transition strength, which is obtained by exciting particles in the given hole orbital. The presence of neutrons with a few MeV binding energies is sufficient for obtaining a clear exhibition of this low-energy threshold strength, and the phenomena are differentiated from the socalled soft multipole excitations in halo nuclei. In our present case the distribution of the whole response strength including giant resonances can be drastically changed compared with that of $\beta$-stable nuclei.

Towards the proton drip line except very light nuclei one may expect, in general, no such drastic change in either proton one-particle shell-structure or nuclear collective properties, compared with the case of $\beta$-stable nuclei. The expectation comes from the presence of a high Coulomb barrier, which hinders the occurrence of the phenomena uniquely connected with very small binding energies of protons. On the other hand, proton drip line nuclei are relatively easy to reach experimentally. Thus, we will have an opportunity for testing our understanding of the structure of nuclei far from $\beta$-stability, for exmaple, microscopic models with some effective interactions.

In order to illustrate clearly the low-energy threshold strength in neutron drip line nuclei, we take the nucleus ${}^{28}_{8}O_{20}$ as a very simple and easily understandable example, since ${}^{28}O$ is an $\ell$-s doubly closed-shell nucleus, in which p-h excitations within the major shell is available neither for monopole nor quadrupole excitations. In the harmonic oscillator model all unperturbed strength of monopole as well as quadrupole excitations in ${}^{28}O$ lies at $2\hbar\omega_0$=27 MeV, using $\hbar\omega_0$=$41A^{-1/3}$ MeV. Though in Skyrme HF calculations ${}^{28}O$ lies inside the neutron drip line, there is an experimental indication of the nucleus being outside. In the case that ${}^{28}O$ turns out to lie indeed outside of the neutron drip line, the physics described in our present work is applicable, for example, to ${}^{24}O$ instead of ${}^{28}O$.

In fig.1 the calculated one-particle levels (including the sharp one-particle resonant states) of $^{28}O$ are shown. The last occupied orbital for neutrons is $1d_{3/2}$ at -1.8 MeV, while that for protons is $1p_{1/2}$ at -27.0 MeV. For reference, the major one-particle excitations for the monopole operator are indicated by arrows. For protons all three excitations are from a bound to a bound level and the excitation energies are 27-29 MeV. In contrast, for neutron monopole excitations there is no available one-particle bound or resonant levels. Then, the unperturbed response strength starts to appear at $E=\epsilon_B$ , with the $(\ell+1/2)$ power of the available energy, $(\mathrm{E}\text{-}\epsilon_B)^{\ell+1/2}$, in which E expresses the excitation energy and $\epsilon_B$ denotes the binding energy of hole levels. In fig.2 the neutron unperturbed strength is shown for respective hole orbitals. Since the operator is monopole, the particle state, for example, with the $1d_{3/2}$-hole has to have the quantum number $d_{3/2}$, and, then, the strength is seen to rise as $(\mathrm{E}\text{-}1.8)^{5/2}$ . No appreciable monopole strength of neutron excitations is found for $E>40$ MeV. It is seen that the predominant part of the whole neutron transition strength appears at the energy much lower than $2\hbar\omega_0$=27 MeV.

In fig.3 the sum of all the unperturbed neutron strength in fig.2 is expressed by the dotted line. The proton unperturbed strength at 27-29 MeV is not shown, since the width of the excitations is zero. In fig.3 the RPA strength function for the isoscalar (IS) and the isovecotr (IV) monopole mode is shown as a function of excitation energy. It is seen that neither the IS nor IV RPA strength is concentrated in a narrow energy region around, say, $65\mathrm{A}^{-1/3}$=21.4 MeV or $170\mathrm{A}^{-1/3}$=56.0 MeV, which is the energy of the respective giant resonance expected for $\beta$-stable nuclei with A=28. In particular, a considerable strength appears in a surprisingly low-energy region. It is clear that the low-energy strength originates from the unperturbed neutron strength in the same energy region.

In fig.4 the calculated result of monopole modes of a proton drip line nucleus, $^{100}_{50}Sn_{50}$ , is shown. In a clear contrast to fig.3 there is no appreciable low-energy threshold strength, though the proton threshold energy (=the binding energy of the last occupied proton orbital, $1g_{9/2}$ ) is 3.15 MeV. The calculated peak energy of the IS monopole giant resonance is 17.5 MeV, which may be compared with the energy of the IS monopole giant resonance observed for a $\beta$-stable nucleus $^{100}_{42}Mo_{58}$ , 16.0 MeV.

In fig.5 the result of quadrupole modes for $^{28}O$ is shown. Due to the same reason as in monopole modes, the RPA quadrupole strength coming mainly from neutron excitations starts to appear just above the neutron threshold energy, 1.8 MeV. The calculated energy of the IS quadrupole giant resonance is 15.1 MeV, which is appreciably lower than the systematic value for $\beta$-stable nuclei, $\mathrm{E}_x=58\ \mathrm{A}^{-1/3}$ MeV = 19.1 MeV. This lower frequency of the IS quadrupole giant resonance is a feature in nuclei near the neutron drip line.

From our knowledge of $\beta$-stable nuclei, the core polarization charge ($e_{pol}$) is expected to be large, when a collective quadrupole mode appears in the low energy region of the excitation spectra of the core. Thus, at first sight one might imagine that $e_{pol}$ would be large in the neutron drip line nuclei. The question is how much the low-energy threshold strength contributes to $e_{pol}$ and whether or not the contribution is constructive to the one by the giant resonance. On the other hand, from a general argument one might expect small $e_{pol}$ values for light very neutron-rich nuclei, since the very small proton core, which cannot contribute anyway so much to $e_{pol}$ , may not be efficiently polarized by neutrons. Thus, we

estimate $e_{pol}$(E2) values taking the neutron drip line nucleus $^{28}O$ and the proton drip line nucleus $^{100}Sn$ as examples. The method to estimate $e_{pol}$ values is basically the same as the one employed in ref.[6].

The estimated static $e_{pol}(E2)$ values due to the polarization of $^{28}O$ turn out to be very small. Using the SkM* interaction, we have obtained $e^{IS}_{pol}(E2)$=0.14 and $e^{IV}_{pol}(E2)$=0.06 , when averaged over one-particle orbitals. That means, $e^{p}_{pol}(E2)$=0.08 $e$ and $e^{n}_{pol}(E2)$=0.20 $e$. We find that in addition to the smallness expected in general for light very neutron-rich nuclei, a considerable amount of further reduction on the $e_{pol}(E2)$ values comes from an appreciable cancellation between the contributions by the low-lying threshold strength and those by the higher-lying giant resonance. For example, $e^{IS}_{pol}(E2)$ receives -0.06 $e$ from the excitations below 9 MeV and +0.20 $e$ from those above 9 MeV in fig.5, while $e^{IV}_{pol}(E2)$ gets -0.04 $e$ from the excitations below 15 MeV and +0.10 $e$ from those above 15 MeV. It is also seen that in the case of $^{28}O$ the cancellation occurs uniquely for $e_{pol}(E2)$ and not for either $e_{pol}(E1)$ or $e_{pol}(E3)$, for example.

In order to understand the cancellation mechanism, in fig.6 we show examples of IS quadrupole transition densities of the low-energy threshold strength in $^{28}O$. The shape of the transition density in fig.6, which has two radial nodes and a large tail, is very different from that of a collective surface mode. The unique shape of the radial transition densities of the threshold strength leads to the destructive contribution to the $e^{IS}_{pol}(E2)$.

Using the same model, we estimate the $e_{pol}(E2)$ values for $^{100}Sn$. The polarization charge in the j-j closed shell nucleus $^{100}Sn$ is, in general, much larger than that in $\ell$-s closed shell nuclei, due to the contribution by the low-energy p-h excitations within the same major shell. Furthermore, we have no low-energy threshold strength in this nucleus and, thus, no cancellation between various contributions to $e_{pol}(E2)$. On the average, we have obtained $e^{p}_{pol}(E2)$=1.0 $e$ and $e^{n}_{pol}(E2)$=1.35 $e$, using the SkM* interaction. The polarization charges estimated by using the SG2 (SIII) interaction are about 10 percent larger (up till 15 percent smaller) than those obtained by the SkM* interaction. The dependence of calculated $e_{pol}(E2)$ values on Skyrme interactions comes mainly from the variation of the calculated energy of the lowest sharp collective $2^+$ state of $^{100}Sn$ , which indeed varies from 4.3 to 5.2 MeV.

The values of $e_{pol}(E2)$ estimated for $^{100}Sn$ are consistent with the available empirical information obtained from the shell model analysis of the measured half-life of a $17/2^+$ level in $^{99}_{48}Cd_{51}$ [7], though the estimated $e_{pol}(E2)$ values depend appreciably on Skyrme interactions used.

## References


[1 ] I.Hamamoto, H.Sagawa and X.Z.Zhang, Phys. Rev. **C53**, 765 (1996) ; I.Hamamoto and H.Sagawa, Phys. Rev. **C53**, R1492 (1996).
[2 ] I.Hamamoto and H.Sagawa, Phys. Rev. **C**, to be published.
[3 ] I.Hamamoto and H.Sagawa, submitted to Phys. Lett. **B**.
[4 ] S.Shlomo and G.Bertsch, Nucl.Phys. **A243**, 507 (1975).
[5 ] N.Van Giai and H.Sagawa, Nucl.Phys. **A371**, 1 (1981).
[6 ] H.Sagawa and B.A.Brown, Nucl.Phys. **A430**, 84 (1984).
[7 ] M.Lipoglavsek et al., Phys.Rev.Lett.**76**, 888 (1996).

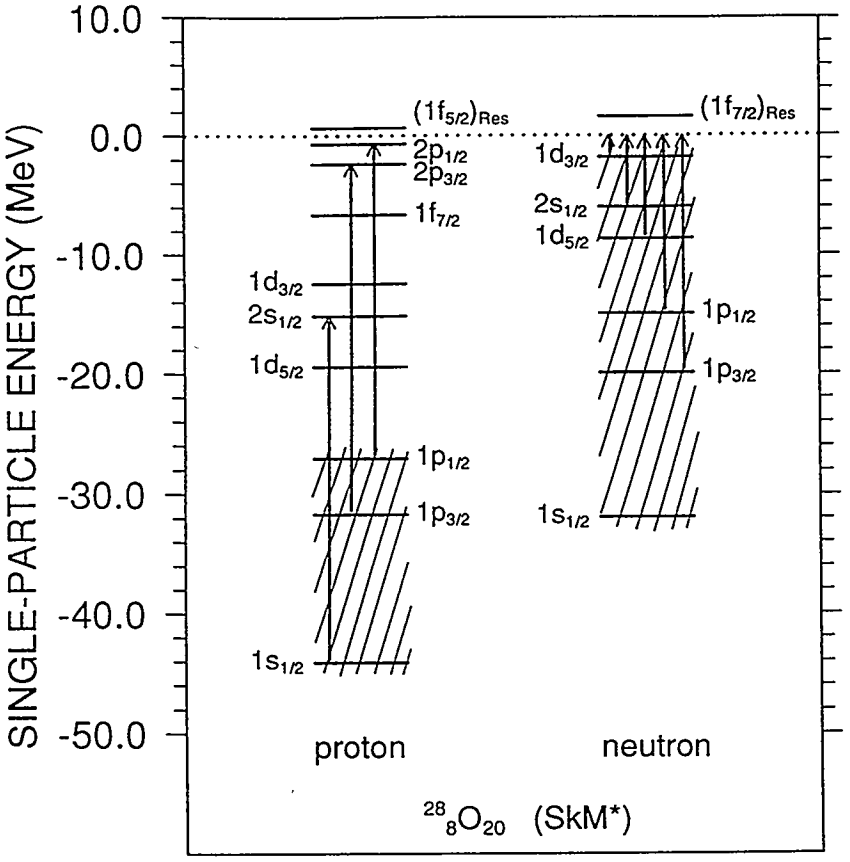


Fig.1. HF one-particle levels of the neutron drip line nucleus, ${}^{28}_{8}O_{20}$ , calculated by using the SkM* interaction. The notation $(n\ell_j)_{Res}$ expresses the calculated one-particle resonant levels in the HF potential. Occupied levels are indicated by shadows, while major one-particle excitations for the monopole operator are shown by upward arrows.

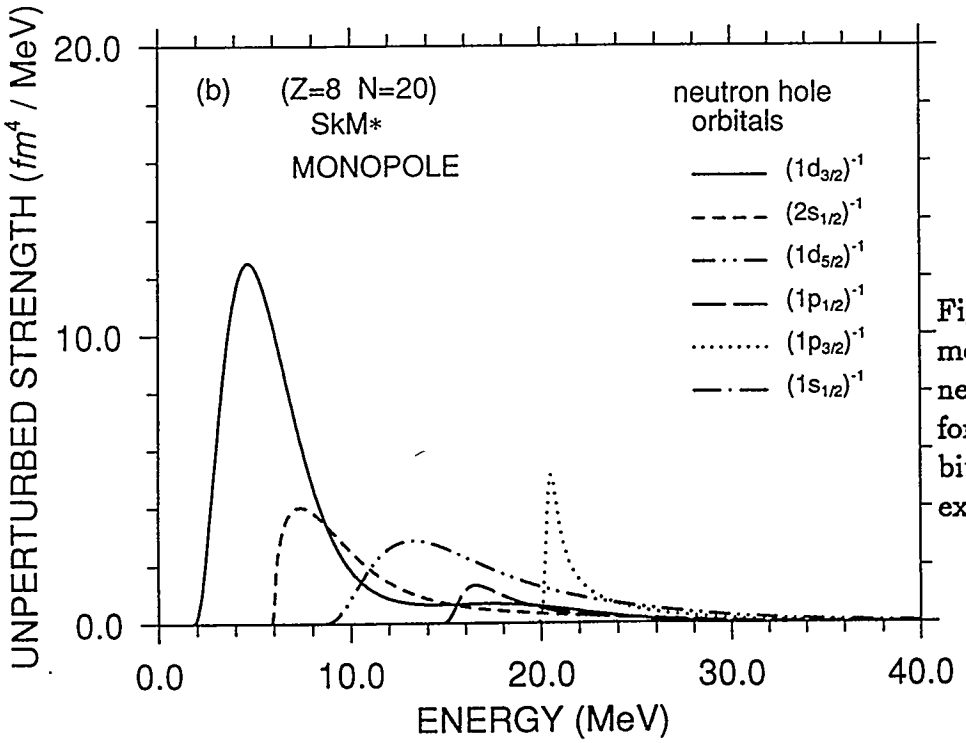


Fig.2. The unperturbed monopole strength for neutrons of ${}^{28}O$ is shown for respective hole orbitals as a function of excitation energy..

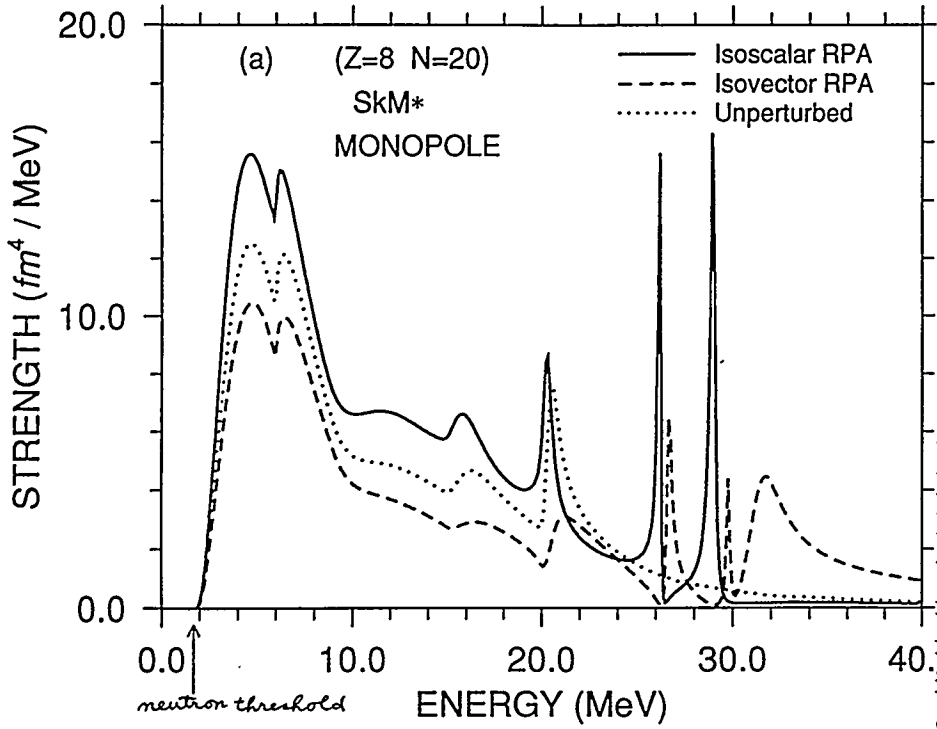


Fig.3. The unperturbed and RPA strength function for the monopole modes of $^{28}O$ as a function of excitation energy. We note that in the harmonic oscillator model the monopole unperturbed strength lies at $2\hbar\omega_0$(=27 MeV for A=28), which is in fact almost equal to the frequency of observed isoscalar monopole giant resonances of $\beta$-stable medium-heavy nuclei.

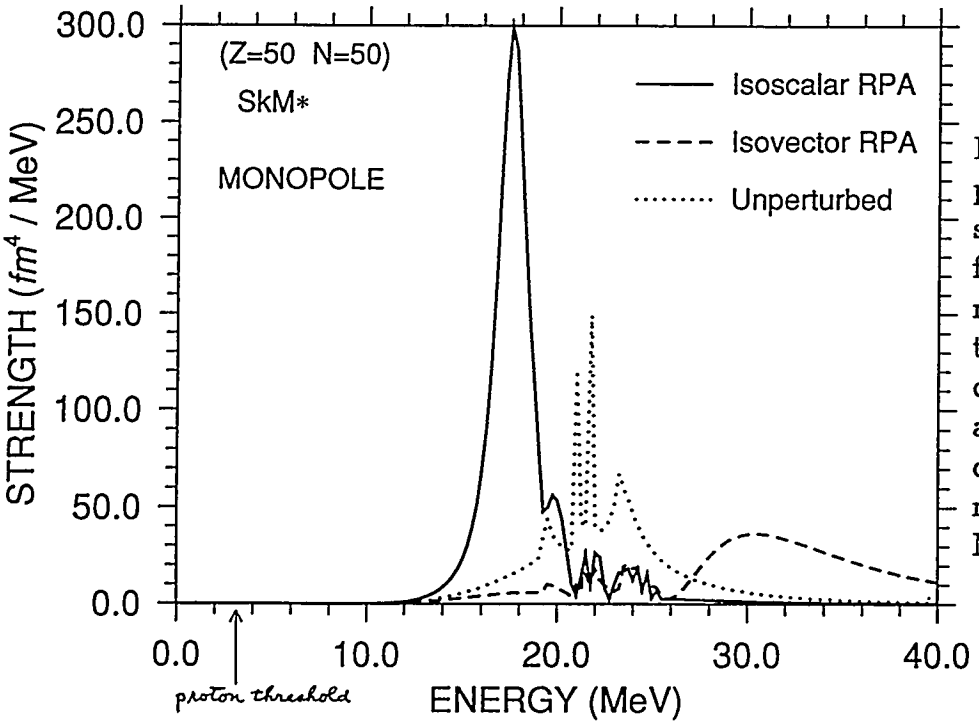


Fig.4. The unperturbed and RPA strength function for the monopole modes of the proton drip line nucleus, $^{100}_{50}Sn_{50}$, as a function of excitation energy. We note that $2\hbar\omega_0$=17.6 MeV for A=100.

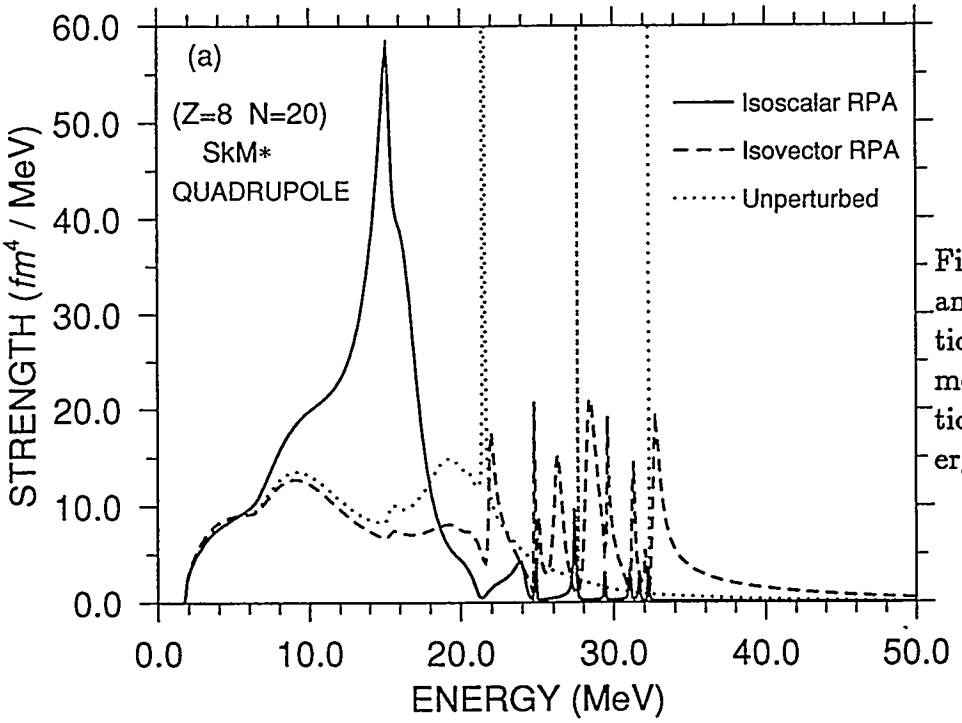


Fig.5. The unperturbed and RPA strength function for the quadrupole modes of $^{28}O$ as a function of excitation energy.

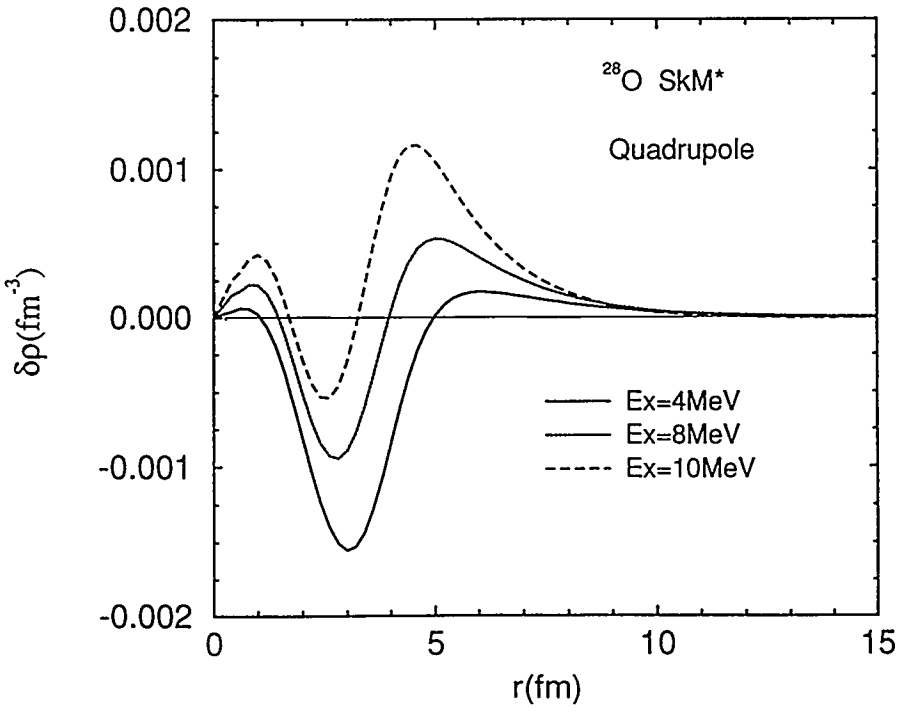


Fig.6. The radial transition densities of the low-lying RPA isoscalar quadrupole excitations of $^{28}O$ at various excitation energies, $E_x$ , as a function of radial coordinate.

# DISCOVERY OF ELEMENT 112

S. Hofmann
GSI, D-64220 Darmstadt, Germany

**Abstract**

The new elements 110, 111 and 112 were synthesized and unambiguously identified in experiments at SHIP. Due to strong shell effects the dominant decay mode is not fission, but emission of alpha particles. Theoretical investigations predict that maximum shell effects should exist in nuclei near proton number 114 and neutron number 184. Our measurements give hope that isotopes of element 114 close to the island of spherical Superheavy Elements could be produced by fusion reactions using $^{208}$Pb as target. Systematic studies of the reaction cross-sections indicate that transfer of nucleons is the important processs to initiate the fusion.

## 1 Introduction

The special stability of nuclei with magic numbers for protons or neutrons becomes evident in two fundamental properties: The nuclear binding energies, as deduced from nuclear masses, are exceptionally high, and the nuclei are spherical and stiff against deformation. The highest stability is observed for doubly magic nuclei.

Various theoretical calculations predicted the next double shell closures beyond $^{208}$Pb at proton numbers Z=114 or 126, and at neutron number N=184 [1, 2, 3]. Recent models based on the Nilsson-Strutinsky approach [4], predicted strong shell correction energies and spherical shapes for nuclei with Z=114 [5, 6, 7], whereas Hartree-Fock calculations predict the highest stability at proton number Z=126 [8]. Responsible for the different predictions are the energies of the three low spin subshells $2f_{5/2}$, $3p_{3/2}$ and $3p_{1/2}$, which are filled between proton number Z=114 and 126.

Experiments to search for superheavy nuclei near the predicted double magic $^{298}$114 were negative so far [9, 10]. In parallel, experimental methods were refined, in order to produce and identify lighter new elements [11, 12]. At SHIP these experiments were successful during the first ten years of UNILAC operation in identifying the elements Z=107-109 [13], for which the names nielsbohrium (Ns), hassium (Hs) and meitnerium (Mt) were proposed.

For further experimental investigation of new elements and small branching ratios, the set-up at SHIP at GSI in Darmstadt was upgraded to reach a level of detection sensitivity of at least 1 pb [14]. Experiments with the new set-up were carried out starting in 1994. As a result, the three elements 110, 111 and 112 were discovered [15, 16, 17, 18]. The reaction mechanism was investigated by measurement of excitation functions using small energy steps. A possible interpretation of the measured phenomena seems to be given by a fusion process initiated by transfer (FIT) [19]. New data on the binding energies of nuclei near the predicted magic number Z=114 were obtained by $\alpha$-decay chains.

## 2 Experimental Method

In parallel to the construction of SIS, the facilities at GSI for production of heavy elements at low beam energies were upgraded. At the UNILAC, a new high charge injector was built including an ECR ion-source. The separator SHIP was modified, and a new improved detection system was built (see Fig. 1). The aims of the SHIP modifications were: 1. To increase the solid angle and thus increase the transmission for fusion-reaction products; 2. To reduce the background in order to accept higher beam currents and to increase simultaneously the significance of detected correlated events, and 3. To increase the overall stability of all components of the set-up in order to achieve high total experimental efficiencies. The improvements resulted in a sensitivity for detection of one heavy element decay-chain within 10 days at a cross-section of 1 pb.

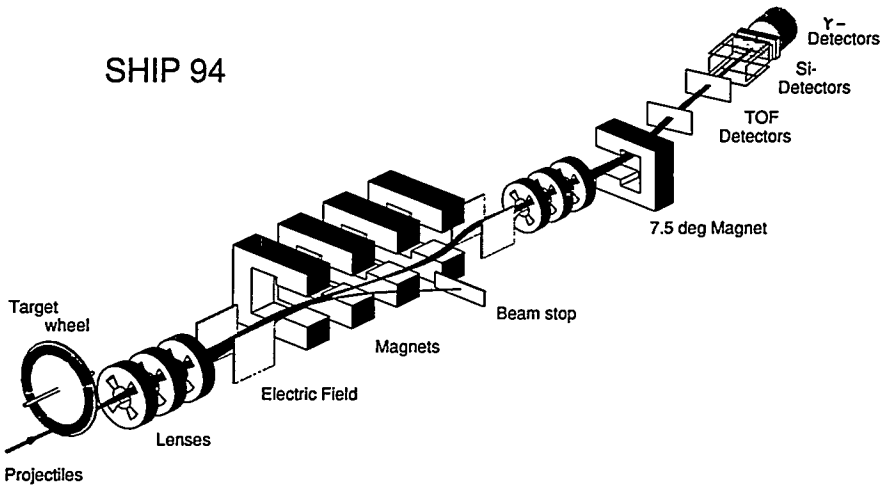


Figure 1: The modified velocity filter SHIP (Separator for Heavy Ion reaction Products) and the new detection system. The length of SHIP from the target to the detector is 11 m. The target wheel has a radius up to the center of the targets of 155 mm. It rotates with 1125 rpm synchronously to the beam macrostructure [20]. The detector system consists of two large area secondary-electron time-of-flight detectors [21] and a position-sensitive silicon-detector array [15]. The flight time of the reaction products through SHIP is 2 $\mu$s. The filter, consisting of two electric and 4 magnetic dipol fields plus two quadrupol triplets, was extended by a fifth deflection magnet in order to position the detectors out of the straight beam line for further reduction of the background.

# 3 Decay Properties of Heavy Elements

Recently, the stability of heavy and superheavy nuclei was investigated theoretically [5, 6, 7, 22] using refined models based on the Nilsson-Strutinsky approach. The ground-state microscopic shell-corrections show two minima: One of about 8 MeV centered at $^{272}_{162}108$ with maximum deformation $\beta_2$=0.22, the other of about 9 MeV at $^{292}_{178}114$ forming an island of spherical superheavy nuclei, see Fig. 3, top. The binding energies, $\beta$-, $\alpha$-, and fission half-lives were calculated. The measured data, including those of the decays of $^{267}110$ and $^{273}110$ obtained in experiments in Berkeley [23] and Dubna [24], respectively, could be reproduced with good accuracy. A rough sketch of the half-lives obtained is shown in Fig. 3, bottom. As a result, we can deduce that most nuclei, that can be produced with stable projectiles and the available targets are predicted to be $\alpha$ emitters with half-lives between 1 $\mu$s and 1 s.

The nucleus $^{278}_{164}114$ is predicted to be deformed in its ground state and to decay by $\alpha$

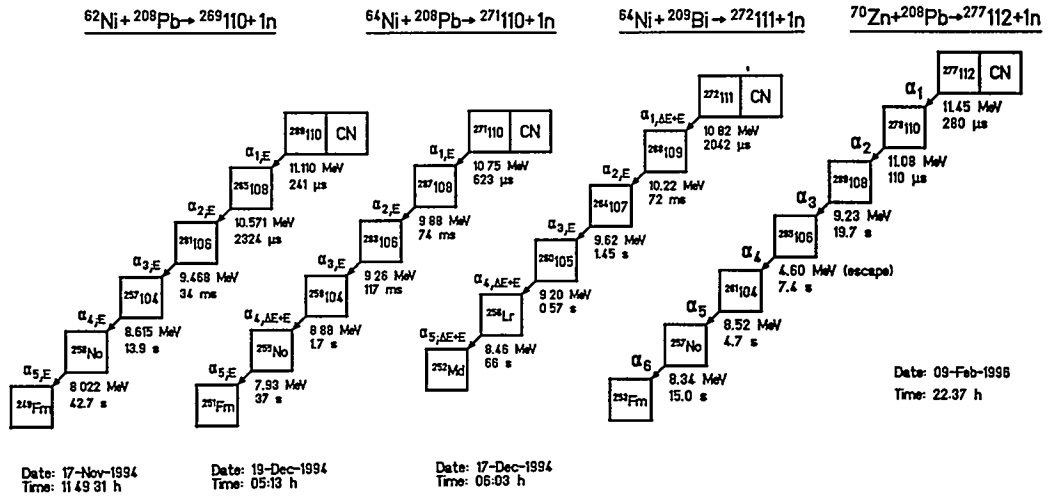


Figure 2: Four representative decay chains of the new elements 110, 111 and 112.

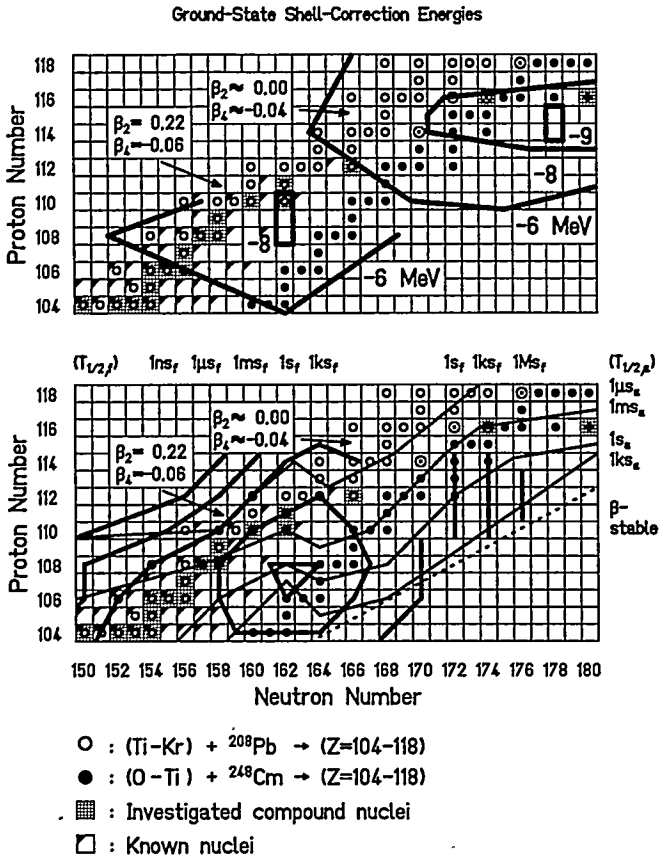


Figure 3: Rough sketch of calculated microscopic shell correction energies (top) and half-lives (bottom) of even-even nuclei; bold lines: partial fission half-lives; fine lines: partial $\alpha$ half-lives; broken line: $\beta$-stability line. The data are from Ref. [5, 6, 7, 22]. The fission half-lives of odd and odd-odd nuclei may be longer as a result of additional hindrance factors. The arrows point to the region of strongly deformed nuclei centered at $^{270}$108 and to the region of spherical superheavies at around $^{292}$114; increased stability of spherically shaped nuclei might be expected also near Z=114 and N=164, see text; open circles: compound nuclei of reactions (Ti to Kr) + $^{208}$Pb →(Z=104 to 118); dots: compound nuclei of reactions (O to Ti) + $^{248}$Cm →(Z=104 to 118); full triangles: known nuclei; shaded: compound systems investigated in experiments at SHIP.

emission with a half-life close to 1 $\mu$s (see Fig. 3). Increased stability may occur also for spherical shapes due to the shell closure of the major shells $\nu j_{15/2}$ and $\nu i_{11/2}$ at N=164, (see Fig. 4 in Ref. [25]) in combination with the spherical shell closure for the protons at Z=114. The interplay with the increased stability of deformed shapes at neutron number N=162 may lead to existence of shape isomerism. Experimentally, the nuclei near $^{278}$114 could be investigated by reactions of $^{70}$Ge or $^{72}$Ge beams with $^{208}$Pb targets.

Isomerism has been definitely observed for the nuclei $^{263}$106, $^{262}$107, $^{265}$108, $^{271}$110 and $^{273}$110. An assignment is not possible on the basis of the few data available, but theoretical investigations present candidates for spin isomerism of those odd-neutron nuclei [22]. Their appearance is closely connected with the bunching of levels of spin values from 1/2 to 13/2 at neutron number 162 for deformed nuclei.

The two measured decay chains of $^{277}$112 reveal two very different $\alpha$-decay properties of $^{273}$110: $E_\alpha$=9.73 MeV, $T_{1/2}$=120 ms for chain 1, and $E_\alpha$=11.08 MeV, $T_{1/2}$=76 $\mu$s for chain 2 [18]. Presently, it remains open, if the extraordinary big difference is due to spin isomerism or, if shape isomerism is responsible. Due to this uncertainty, a ground-state mass evaluation for nuclei beyond $^{269}$108 based on $Q_\alpha$ values is jeopardized until more data will become available.

The closest approach to the island of spherical superheavy nuclei can be achieved with stable projectiles and targets using $^{76}$Ge and $^{208}$Pb. The nuclei produced by one neutron emission or possibly by radiative capture could have almost spherical shapes, and they are predicted to decay by $\alpha$ emission with half-lives of $\approx$1 ms. Synthesis of $^{283}$114 or $^{284}$114 is certainly the most interesting aim of the next series of experiments, especially, in the shade of the present uncertainy concerning predictions of shell closures at Z=114 or 126.

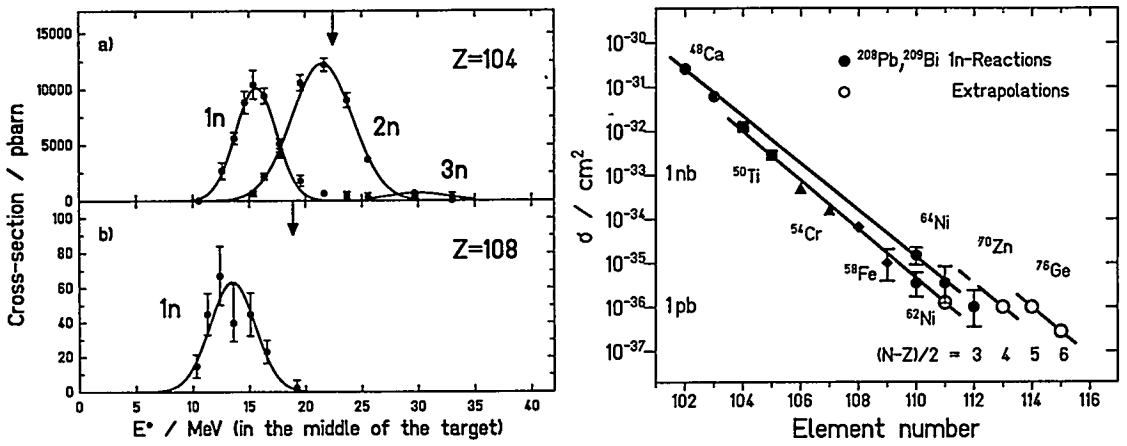


Figure 4: Measured excitation functions for production of element 104 and 108 by reactions of $^{50}$Ti and $^{58}$Fe projectiles with $^{208}$Pb targets. The cross-sections are plotted as function of the dissipated energy E*, calculated from the center-of-mass beam-energies in the middle of the target thicknesses and the Q-values using the mass tables of Ref. [26]. The arrows mark the interaction barriers of the reactions according to the fusion model by Bass [27].

Figure 5: Systematics of measured cross-sections and extrapolations.

# 4 Reaction Properties

## 4.1 Excitation Functions

The search for the new element 110 was complicated by the fact that no excitation function for production of lighter elements down to Z=103 was known accurately enough to fix a maximum of the cross-section. In addition, predictions of extrapush theories influenced the choice of the beam energies in the previous investigations of elements up to Z=109. Therefore, we started our experiments to aim at complete excitation functions of two known even elements at least.

The measured excitation functions for production of the elements 104 and 108 are shown in Fig. 4. The data points were narrow enough to allow for a safe determination of the positions for the cross-sections maxima. As a function of the excitation energy, the maxima decrease with increasing element number. The beam energy for the production of element 110 by the reaction $^{62}$Ni+$^{208}$Pb $\rightarrow$$^{269}$110+1n was obtained by linear extrapolation.

A systematics of measured cross-sections up to element 112 is shown in Fig. 5. An ordering in terms of the projectile isospin is obvious and allows for predictions by extrapolation. An estimate for production of $^{283}$114 results in $\sigma \approx$1pb.

The measured value of 1 pb for production of $^{277}$112 is smaller than the extrapolated value, but still in agreement within the error bars. A smaller value may also be the result of a beam energy chosen not accurately enough to cover the maximum production cross-section.

In case of element 112 isotopes, a cross-section "inversion" as function of isospin may occur, if the shell-correction energies of the fusion products influence the production probabilities. The isotope $^{275}$112, which may be produced using a $^{68}$Zn beam, is predicted to be stronger bound than $^{277}$112, produced with a $^{70}$Zn beam. A more complete excitation-function systematics for production of element 112 isotopes would be highly desirable.

## 4.2 Fusion Initiated by Transfer (FIT)

Fig. 4 shows that the largest cross-sections were measured "below the barrier". The energy relations determining the barrier are drawn in Fig. 6 in case of the reaction $^{64}$Ni+$^{208}$Pb and a barrier according to the fusion model by Bass [27].

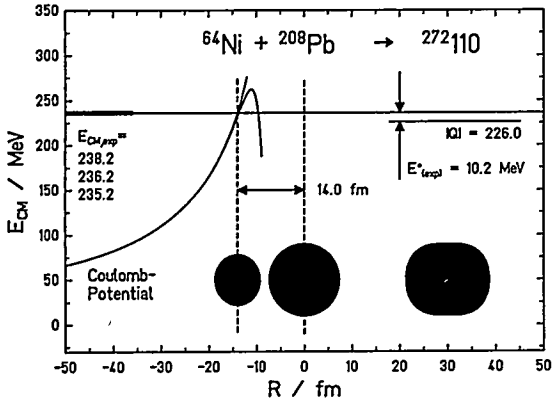


Figure 6: Energy and distance relations resulting in maximum cross-sections. The kinetic energy of the system is exhausted by the Coulomb potential at a distance of 14.0 fm in a central collision. Projectile and target nuclei come to rest before the fusion starts.

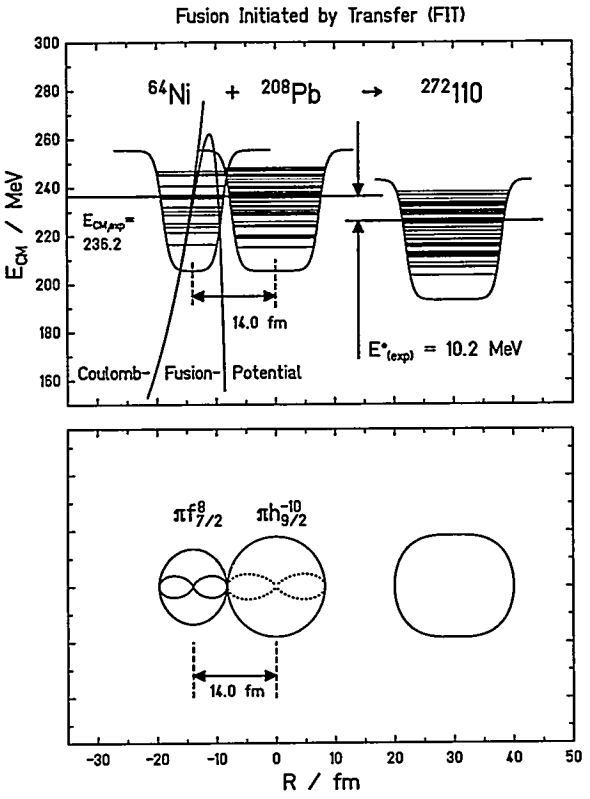


Figure 7: Energy-distance diagram for the reaction $^{64}$Ni+$^{208}$Pb. At the measured maximum cross-section the reaction partners were brought to rest before fusion starts. The occupied levels at the Fermi surface are just in contact so nucleons or pairs of nucleons leave the projectile and move into free orbits of the target nucleus. The lower panel shows the proton orbitals at the contact point. By transfer of protons the Coulomb repulsion and, thus, the probability for reseparation is reduced.

A tunneling process through this barrier cannot explain the measured cross-sections. A semiclassical WKB approximation results in a tunneling probability of $2 \times 10^{-21}$, which is much too low to contribute to the measured cross-section. The conclusion is that additional effects must allow for fusion.

Compared to more sophisticated investigations of fusion [28], we can make some simplifications in our case in order to explain the observations: 1. The reactions are limited to spherical target nuclei and nearly spherical projectiles. 2. The reactions are head-on collisions with angular momenta close to zero and, therefore, high rotational symmetry. 3. The reactions proceed at extremely low dissipative energies as a result of nearly compensating Q-value and center-of-mass energy.

Fig. 6 shows that the reaction partners came to rest before the fusion process starts. At a distance of 14.0 fm between the centers of the nuclei the initially existing kinetic energy of 236.2 MeV is exhausted by the Coulomb potential. At that distance only nucleons at the outer surface are just in contact. Nevertheless, at that energy this heavy system has highest probability to fuse and to survive.

We remember that the kinetic energy of orbiting nucleons is low at the surface. Therefore, at the touching point of two nuclei in a central collision the probability is highest that nucleons or pairs of nucleons leave the orbit of one nucleus and move into a free orbit of the reaction partner. The process is shown schematically in Fig. 7. An adequate theoretical description could be obtained by use of the two-center shell model [29].

The transfer of nucleons from the projectile to the target is especially attractive in case of lead as target. In $^{208}$Pb the $h_{11/2}$ proton subshell and the $h_{9/2}$ and $i_{13/2}$ neutron subshells are filled. The free orbits are for the protons $h_{9/2}$ and $i_{13/2}$. The proton transfer profits first from the attractive proton-proton and after filling of the $h_{9/2}$ subshell from the attractive proton-neutron interaction. Similarly, neutrons transfered into free $i_{11/2}$ orbits are attracted by the neutrons in the already filled $i_{13/2}$ subshell.

Because of pairing energies and high orbital angular momenta involved, the transfer of pairs is more likely than that of single nucleons. The described process is a frictionless pair transfer happening at the contact point in a central collision at longitudinal momenta close to zero in irradiations of $^{208}$Pb targets.

Already after transfer of 2 protons from $^{64}$Ni to $^{208}$Pb the Coulomb barrier is decreased by 14 MeV allowing to keep the reaction partners in close contact and to continue fusion initiated by transfer. Important factors, which determine the cross-section at the very beginning of the fusion process, are: 1. The probability for a head-on collision and 2. The probability of proton transfer in competition to reseparation. These first steps of the fusion process at low energies can be investigated experimentally by measurement of transfer products in forward direction.

The recent technical developments serve as a basis for new experiments with positive results in the region of superheavy elements. Important questions are open, that need to be answered by future experiments. A short list is given in the following: 1. Proof of the shell effect at Z=114. 2. Ground-state to ground-state $\alpha$ decay of even-even nuclei for more accurate evaluation of nuclear binding energies. 3. Search for $\alpha$ transitions of even-even nuclei into rotational levels for determination of the degree of deformation, especially in the region of nuclei near N=162. 4. Fission branchings of even-even nuclei to compare with theoretically predicted fission half-lives. 5. Extension of the cross-section systematics by measurement of complete excitation functions. 6. Search for radiative capture processes (0n channel).

## References


[1] W.D. Myers and W.J. Swiatecki, Nucl. Phys. 81 (1966) 1.
[2] H. Meldner, Ark. Fys. 36 (1966) 593.
[3] U. Mosel and W. Greiner, Z. Phys. A222 (1969) 261.
[4] V.M. Strutinsky, Nucl. Phys. A95 (1967) 420.
[5] A. Sobiczewski, Physics of Particles and Nuclei 25 (1994) 295.
[6] R. Smolanczuk et al., Phys. Rev. C52 (1995) 1871.
[7] P. Möller and J.R. Nix, J. Phys. G: Nucl. Part. Phys. 20 (1994) 1681.
[8] S. Cwiok, private communication (1996).
[9] Yu.Ts. Oganessian, et al., Nucl. Phys. A294 (1978) 213.
[10] P. Armbruster et al., Phys. Rev. Lett. 54 (1985) 406.
[11] G. Münzenberg et al., Nucl. Instr. and Meth. 161 (1979) 65.
[12] S. Hofmann et al., Nucl. Instr. and Meth. 223 (1984) 312.
[13] G. Münzenberg, Rep. Prog. Phys. 51 (1988) 57.
[14] S. Hofmann, Journal of Alloys and Compounds 213/214 (1994) 74.
[15] S. Hofmann et al., Z. Phys. A350 (1995) 277.
[16] S. Hofmann et al., Z. Phys. A350 (1995) 281.
[17] S. Hofmann et al., GSI Nachrichten 02-95 (1995) 4.
[18] S. Hofmann et al., Z. Phys. A354 (1996) 229.
[19] S. Hofmann, Proc. XV. Nucl. Phys. Conf., St. Petersburg (1995) 305.
[20] H. Folger et al., Nucl. Instr. and Meth. A362 (1995) 64.
[21] S. Sharo et al., Nucl. Instr. and Meth. (1995) to be published.
[22] S. Cwiok et al., Nucl. Phys. A573 (1994) 356.
[23] A. Ghiorso et al., Phys. Rev. C51 (1995) R2293.
[24] Yu.A. Lazarev et al., Phys. Rev. C (1996) to be published.
[25] J.R. Nix and P. Möller, Proc. Conf. ENAM-95, Arles (1995) 23.
[26] G. Audi and A.H. Wapstra, Nucl Phys. A565 (1993) 1.
[27] R. Bass, Nucl. Phys. A231 (1974) 45.
[28] W. Reisdorf, J. Phys. G: Nucl. Part. Phys. 20 (1994) 1297.
[29] D. Scharnweber et al., Nucl Phys. A164 (1971) 257.

# SYNTHESIS OF SUPERHEAVY ELEMENTS AND DINUCLEAR-SYSTEM CONCEPT OF COMPOUND-NUCLEUS FORMATION

N.V.ANTONENKO, G.G.ADAMIAN, E.A.CHEREPANOV, A.K.NASIROV, and V.V.VOLKOV
*Joint Institute for Nuclear Research, 141980 Dubna, Russia*

ABSTRACT

Dinuclear system concept is applied to the analysis of reactions used for the synthesis of elements with $Z$ =110, 112, 114, and 116. The inner fusion barriers obtained for these reactions are in good agreement with the experimental estimations resulted from the excitation energies of compound nuclei. A model is suggested for the calculation of the competition between complete fusion and quasifission in reactions with heavy nuclei. The fusion rate through the inner fusion barrier in mass asymmetry is found by using the multidimensional Kramers-type stationary solution of the Fokker–Planck equation. The influence of dissipative effects on the dynamics of nuclear fusion is considered.

## 1. Introduction

At present, great activity occurs in the investigations on the synthesis of superheavy elements (SHE). At GSI (Darmstadt), the nuclei with $Z$ =110, 111, 112 were produced and an attempt was done to obtain the element with $Z$ =116. At JINR (Dubna), the heaviest isotope of the element with $Z$ =110 was obtained. To prepare that kind of experiments, the expected properties (the life-time and modes of decay) of the new nuclei and the production cross section should be known, and the optimal bombarding energy should be chosen. In the present report, the optimal bombarding energies for the synthesis of SHE are estimated and the competition between the complete fusion and quasifission is considered by using the dinuclear system concept (DNS-concept).

The fusion process is considered in [1,2] as the evolution of a dinuclear system (DNS) caused by nucleon transfers from a light nucleus to a heavy one (DNS-concept) [1]. The DNS is formed at the initial stage of the reaction when the kinetic energy transforms into the excitation energy of the nuclei. After the formation, the initial DNS is at the minimum ($R = R_m$, $R$ is the relative distance between the interacting nuclei) of the pocket of the nucleus-nucleus potential $V(R)$ (Fig. 1). Then the DNS evolves (diffusion process) in the charge (mass) asymmetry degree of freedom $Z$ ($Z$ is the charge of one of the nuclei in the DNS) to a compound nucleus (fusion) (Fig. 1). The diffusion process in $R$ is responsible for the decay of the DNS (quasifission). Thus, in the process of quasifission, the DNS should overcome the potential barrier ($B_{qf}$) which coincides with the depth of the pocket in the potential $V(R)$. The important peculiarity of the DNS evolution to the compound nucleus is the appearance of inner fusion barrier $B^*_{fus}$ in $Z$ for the initial DNS. The top of this barrier (the Businaro-Gallone point) coincides with the maximum of the DNS potential energy as a function of $Z$ (Fig. 1). The value of $B^*_{fus}$ supplies the hindrance for the complete fusion in the DNS-concept. The energy required to overcome the fusion barrier $B^*_{fus}$ comes from the DNS excitation energy $E^* = E_{\rm c.m.} - V(R_m)$. If $E^* \geq B^*_{fus}$, then the fusion is possible.

Based on the DNS-concept, the cross section $\sigma_{CN}$ of complete fusion is defined in the following way [2]

$$\sigma_{CN}(E_{\rm c.m.}) = \sigma_c(E_{\rm c.m.})P_{CN}(E_{\rm c.m.}), \qquad (1)$$

where $\sigma_c(E_{\rm c.m.})$ is the capture cross section at the bombarding energy $E_{\rm c.m.}$ and the second multiplier (the probability of complete fusion after the capture stage of collision) takes into account the competition between the fusion and quasifission processes.

The macroscopic dynamical model [3] was the first one in which the fate of the nuclear system is considered after the capture stage. In this model, the result of collision depends on a relationship between the kinetic energy $E_{\rm c.m.}$ of the collision, the Coulomb barrier $B_C$, and

the extra-extra push energy $E_{xx}$. For $E_{c.m.} > B_C + E_{xx}$, $P_{CN} = 1$ and for $E_{c.m.} < B_C + E_{xx}$, $P_{CN} = 0$. However, large values of $E_{xx}$ predicted in [3] for producing the SHE were refuted in the experiments on the synthesis of the nucleus with $Z$ =110 in the $^{62,64}$Ni+$^{208}$Pb reaction [6]. The complete fusion occurred there at $E_{c.m.}$ slightly above the entrance barrier.

The competition between the complete fusion and quasifission processes has not been considered in the existing models [3,4,5] used to calculate $\sigma_{CN}$. However, in the reactions with heavy nuclei, the quasifission channel dominates and leads to a strong reduction (few orders of magnitude) of the fusion cross section $\sigma_{CN}$ [2].

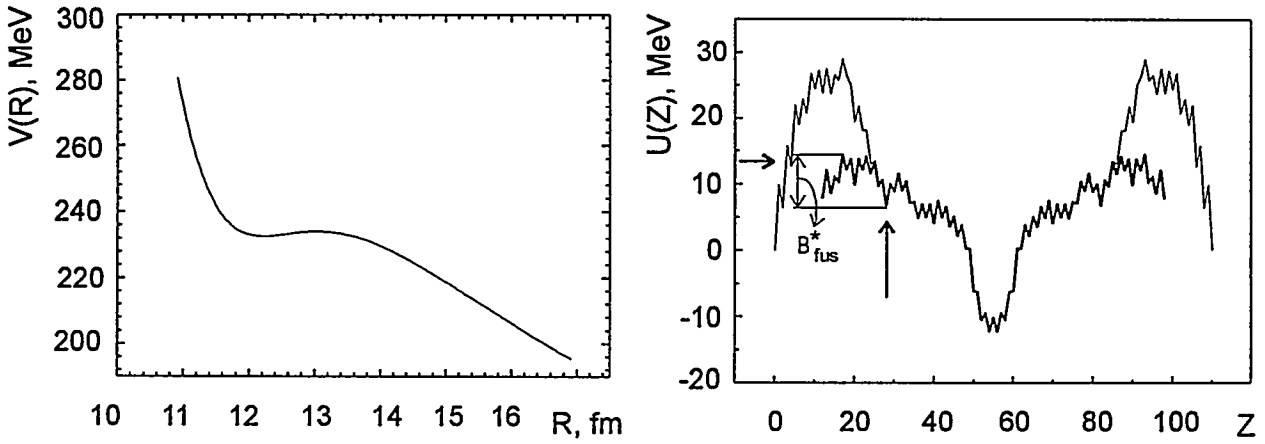


Fig. 1. Nucleus-nucleus potential as a function of $R$ for the $^{62}$Ni+$^{208}$Pb reaction (left). The DNS potential energy as a function of $Z$ calculated for the system $^{270}$110 without (thin line) and with (thick line) the deformation effect (right). The initial DNS is marked by a vertical arrow. The experimental excitation energy of the element $^{270}$110 is marked by a horizontal arrow.

## 2. Analysis of the SHE synthesis in the DNS-concept

### *2.1. Calculation of inner fusion barrier $B^*_{fus}$*

The DNS evolution is determined by the potential energy

$$U(R, Z, J) = B_1 + B_2 + V(R, J) - [B_{12} + V'_{rot}(J)]. \quad (2)$$

Here $B_1$, $B_2$, and $B_{12}$ are the binding energies of the DNS nuclei and compound nucleus. The nucleus-nucleus potential $V(R, J)$ consists of the nuclear $V_n$, Coulomb $V_{Coul}$, and centrifugal $V_{rot}$ parts. The liquid-drop masses for sufficiently large excitation energies and real masses [16] for small excitation energies were used to obtain $B_1$, $B_2$, and $B_{12}$. The isotopic composition of the nuclei forming the DNS is chosen by using the condition of the $N/Z$-equilibrium in the system. The value of $U(R, Z, J)$ in (2) is normalized to the energy of the rotating compound nucleus by $B_{12}+V'_{rot}$. The method for the calculation of the nucleus-nucleus potential $V(R, J)$ was described in [17]. Due to a large moment of inertia of the heavy DNS and a restricted set of angular momenta for the complete fusion, we neglect the dependence of $U(R, Z, J)$ on $J$. Thus, $U(R, Z, J) \approx U(R, Z)$ and $V(R, J) \approx V(R)$.

The calculated driving potentials $U(R_m, Z) = U(Z)$ as functions of $Z$ and nucleus–nucleus potentials $V(R)$ as functions of $R$ for the DNS formed in the reactions used in the synthesis of new elements are presented in Figs. 1–4. For these reactions, the deformation effect was taken into account. The spherical nuclei were taken in the initial DNS and deformed heavy nucleus (in its ground state) were taken near the top of the fusion barrier (the mutual orientation of the nuclei in the DNS corresponds to the minimum of potential energy). Due to the deformation effect, the value of $V(R_m)$ decreases as compared to that calculated with spherical nuclei. As a result, $B^*_{fus}$ decreases considerably. Since, in the $^{48}$Ca+$^{244}$Pu reaction,

the heavy nucleus is deformed even in the initial DNS, the consideration of the deformation of the nuclei leads to larger $B^*_{fus}$ as compared to the calculation with the spherical nuclei (Table 1) [8], while the deformation effect in other reactions promotes the decrease of $B^*_{fus}$. In the $^{62}$Ni+$^{208}$Pb and $^{70}$Zn+$^{208}$Pb reactions, the fusion barriers $B^*_{fus}$ are in good agreement with the experimental estimations resulted from the excitation energies of the compound nuclei. For the $^{82}$Se+$^{208}$Pb reaction, the bombarding energies in four cases (horizontal arrows in Fig.3) did not allow overcoming the inner fusion barrier.

The calculated values of $B^*_{fus}$ and $B_{qf}$ are presented in Table 2 for some symmetric and almost symmetric reactions. For these reactions, the liquid drop masses and spherical nuclei comprising the DNS were used in (2). As is seen from Tables 1 and 2, the energy threshold of the complete fusion related to the fusion barrier $B^*_{fus}$, can be much smaller than the extra-extra push energy (e.g., $E_{xx}$= 60 MeV in the $^{110}$Pd+$^{110}$Pd reaction). For the reactions used for the synthesis of the elements with $Z$ =110, 112, and 116, the predicted $E_{xx}$ vary from 30 to few hundred MeV and depend on the set of parameters used in [3]. Thus, in our model, there is no need in a very large excess of the kinetic energy above the entrance Coulomb barrier to produce the SHE.

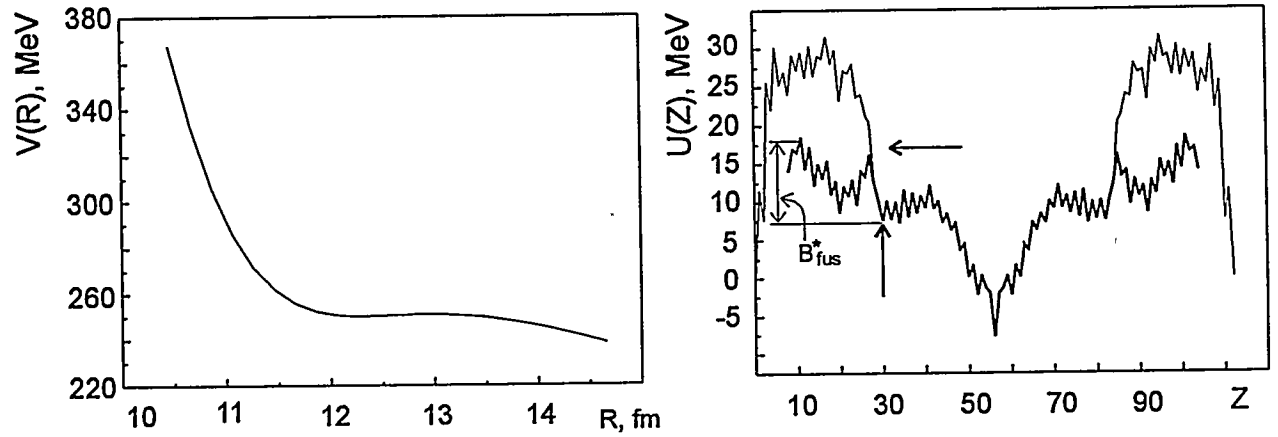


Fig. 2. The same as in Fig.1, but for the $^{70}$Zn+$^{208}$Pb$\rightarrow^{278}$112 reaction.

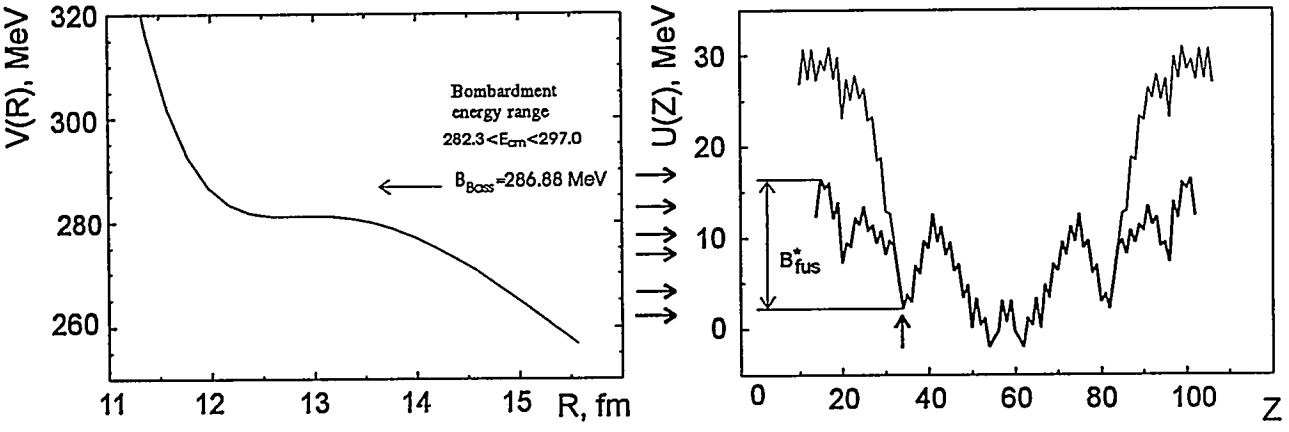


Fig. 3. The same as in Fig.1, but for the $^{82}$Se+$^{208}$Pb$\rightarrow^{290}$116 reaction.

*2.2. Calculation of probability of complete fusion*

The dynamical behavior of large-amplitude collective nuclear motion, such as the one taking place in the fission, quasifission, and complete fusion, depends on dissipative effects. Therefore, the nuclear dissipative systems are analyzed within the transport theory. It is known that the Kramers expression [9] yields an excellent approximation to the fission rate as defined by the solution of the Fokker-Planck equation [10,11]. One of the ways to calculate the

Table 1. The calculated fusion probability $P_{CN}$ for the asymmetric reactions used for producing the superheavy nuclei. The calculations were performed at $E^* = 15$ MeV except the $^{48}$Ca+$^{244}$Pu reaction (see the text) and different friction parameters $\Gamma$. The deformation effects are taken into consideration. For the $^{48}$Ca+$^{244}$Pu reaction, the calculated results without deformation effects (sph.) are presented for comparison.

| Reactions | $B^*_{fus}$ (MeV) | $B_{qf}$ (MeV) | $P_{CN}$ | | |
|---|---|---|---|---|---|
| | | | $\Gamma$=0 MeV | $\Gamma$=2 MeV | $\Gamma$=4 MeV |
| $^{62}$Ni+$^{208}$Pb $\rightarrow^{270}$ 110 | 8 | 1.5 | $1.0\times10^{-4}$ | $1.6\times10^{-4}$ | $2.3\times10^{-4}$ |
| $^{70}$Zn+$^{208}$Pb $\rightarrow^{278}$ 112 | 9.5 | 1 | $6.6\times10^{-6}$ | $1.1\times10^{-5}$ | $1.6\times10^{-5}$ |
| $^{82}$Se+$^{208}$Pb $\rightarrow^{290}$ 116 | 12.5 | 0.5 | $6.8\times10^{-8}$ | $1.1\times10^{-7}$ | $1.6\times10^{-7}$ |
| $^{48}$Ca+$^{244}$Pu $\rightarrow^{292}$ 114 | 12 | 4 | $2.7\times10^{-4}$ | $4.5\times10^{-4}$ | $6.6\times10^{-4}$ |
| (sph.) $^{48}$Ca+$^{244}$Pu $\rightarrow^{292}$ 114 | 7 | 3 | $1.7\times10^{-3}$ | $2.8\times10^{-3}$ | $4.1\times10^{-3}$ |

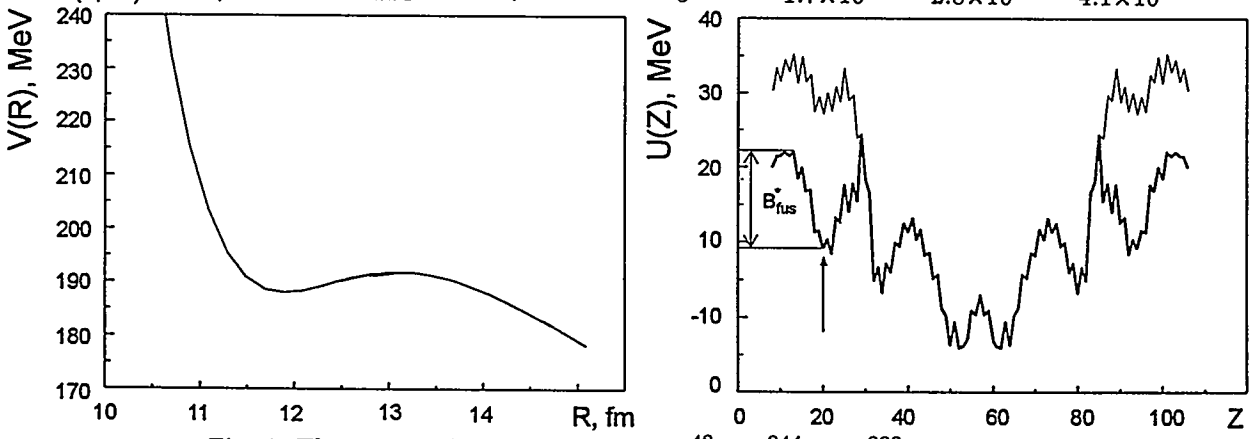


Fig. 4. The same as in Fig.1, but for the $^{48}$Ca+$^{244}$Pu$\rightarrow^{292}$114 reaction.

fusion probability $P_{CN}$ (1) is to use the Kramers-type expression for the fusion rate through the inner fusion barrier.

The variables $R$ and $Z$ are the relevant collective ones used in [2] to describe the DNS evolution. The neck degree of freedom [3] that is important in the macroscopic dynamical model is not considered at all in [2] and in the present paper. As follows from our analysis in [12], the extension of the relevant collective variable set by the neck variable may be questionable for the values of $R$ considered in the DNS. The simultaneous consideration of the transport processes in $Z$ and $R$ allows us to calculate the fusion and quasifission probabilities. The leakage of probability through the fusion barrier in $Z$ is defined by

$$P_{CN} = \frac{1}{\ln 2}\frac{\lambda_Z^{Kr}}{\lambda_R^{Kr}}. \tag{3}$$

Thus, the problem is reduced to obtain the asymptotic fusion and quasifission rates $\lambda_i^{Kr}$ $(i = R, Z)$. For this purpose, we use the formalism elaborated in the theory of nuclear fission [10,11] for the quasistationary diffusion over a multidimensional potential barrier. The approximate expression (a Kramers-type formula) for $\lambda_i^{Kr}$ [11] is

$$\lambda_i^{Kr} = \frac{1}{2\pi}\frac{\omega_i^2}{\sqrt{\omega_i^{B_R}\omega_i^{B_Z}}}\left(\sqrt{\left[\frac{(\Gamma/\hbar)^2}{\omega_i^{B_R}\omega_i^{B_Z}}\right]^2+4}-\frac{(\Gamma/\hbar)^2}{\omega_i^{B_R}\omega_i^{B_Z}}\right)^{1/2}\exp\left[-\frac{B_i}{T}\right], \tag{4}$$

where $B_i$ defines the height of the fusion ($B_Z = B^*_{fus}$) or quasifission ($B_R = B_{qf}$) barrier. The possibility to use the Kramers-type expression for relatively small barriers ($B_i/T > 0.5$) was demonstrated in [13]. The local thermodynamic temperature $T$ is calculated by the expression $T = \sqrt{E^*/a}$, where $a = A/12$ MeV$^{-1}$. In (4), $\omega_i^{B_j}$ is the frequency of the inverted harmonic

oscillator approximating the potential with respect to the variable $i$ on the top of the barrier $B_j$, and $\omega_i$ is the frequency of the harmonic oscillator approximating the potential with respect to the variable $i$ for the initial DNS. In our calculations, we use the simple approximate expression for the friction coefficients $\gamma_{ii'} = \frac{\Gamma}{\hbar}\mu_{ii'}$ ($i, i' = R, Z$ and $\Gamma$ is the friction parameter) obtained in the linear response theory [14]. The calculation of the mass parameters $\mu_{ii'}$ is given in [15]. The values of the frequencies in (4) are easily found by using the calculations of the DNS potential energy.

Table 2. The calculated fusion probability $P_{CN}$ in the symmetric and almost symmetric reactions for $E^* = 30$ MeV and different friction parameters $\Gamma$.

| Reactions | $B^*_{fus}$ (MeV) | $B_{qf}$ (MeV) | $P_{CN}$ | | |
|---|---|---|---|---|---|
| | | | $\Gamma$=0 MeV | $\Gamma$=2 MeV | $\Gamma$=4 MeV |
| $^{90}$Zr+$^{90}$Zr | 6 | 5 | $2.7\times10^{-1}$ | $4.8\times10^{-1}$ | $6.7\times10^{-1}$ |
| $^{100}$Mo+$^{100}$Mo | 10 | 4 | $6.0\times10^{-3}$ | $1.1\times10^{-2}$ | $1.5\times10^{-2}$ |
| $^{110}$Pd+$^{110}$Pd | 15 | 3 | $4.7\times10^{-5}$ | $8.3\times10^{-5}$ | $1.1\times10^{-4}$ |
| $^{136}$Xe+$^{136}$Xe | 22.5 | 0.5 | $2.6\times10^{-9}$ | $4.4\times10^{-9}$ | $6.3\times10^{-9}$ |
| $^{110}$Pd+$^{136}$Xe | 15.5 | 0.5 | $2.3\times10^{-6}$ | $4.0\times10^{-6}$ | $5.5\times10^{-6}$ |
| $^{86}$Kr+$^{136}$Xe | 8.5 | 4 | $1.7\times10^{-2}$ | $2.9\times10^{-2}$ | $4.1\times10^{-2}$ |

In the synthesis of the SHE, the minimum excitation energy of the compound nucleus is preferable to increase the surviving probability. For a low excitation energy of the initial DNS in the asymmetric $^{62}$Ni+$^{208}$Pb $\rightarrow^{270}$ 110, $^{70}$Zn+$^{208}$Pb $\rightarrow^{278}$ 112, $^{82}$Se+$^{208}$Pb $\rightarrow^{290}$ 116, and $^{48}$Ca+$^{244}$Pu $\rightarrow^{292}$ 114 reactions, the initial DNS is at the local minimum of $U(Z)$ due to shell effects (the real masses are taken in (2)) [8]. In this case, we can use the Kramers–type expression (4) to estimate the upper limit of $P_{CN}$ for asymmetric reactions (Table 1). For the $^{48}$Ca+$^{244}$Pu reaction, the choice of the initial excitation energies in the calculations of $P_{CN}$ with ($E^* = 33$ MeV) and without ($E^* = 15$ MeV) deformation effect supplies the same excitation energy of the compound nucleus ($\approx 40$ MeV).

Using the results presented in Table 1, one can explain a smaller yield of the element with $Z = 112$ as compared to the yield of the elements with $Z = 110$ [6]. It is seen that the formation probability of the superheavy nucleus with $Z = 116$ in the $^{82}$Se+$^{208}$Pb reaction is very small. Despite a larger value of $P_{CN}$ in the $^{48}$Ca+$^{244}$Pu reaction as compared with others in Table 2, the compound nucleus is more excited due to the $Q$–value. The de-excitation process is accompanied by a high fission probability for the compound nucleus that can strongly reduce the evaporation-residues cross section.

The values of $P_{CN}$ (Table 2) for some symmetric and almost symmetric reactions are in agreement with the ones extracted from the experimental data [7] and our previous calculations [2,8]. For example, for the $^{110}$Pd+$^{110}$Pd reaction, $P_{CN} \approx 10^{-4}$ allows us to obtain a good agreement with the experimental data on $\sigma_{CN}(E_{\rm c.m.})$, while $\sigma_{CN}(E_{\rm c.m.})$ [2] calculated in the macroscopic dynamical model is about three orders of magnitude as large as the experimental one. Thus, the competition between the complete fusion and quasifission processes is extremely important in the DNS evolution. Comparing $P_{CN}$ in the Tables with $P_{CN}$ given in experimental papers, we should bear in mind that these values are extracted from the evaporation-residues cross sections using the model assumptions about the surviving probability for the excited compound nucleus. One can see that $B^*_{fus}$ becomes very large for a heavy symmetric system. Therefore, the use of these reactions in producing the SHE may be questionable.

The fusion and quasifission rates decrease with increasing $\Gamma$. However, $P_{CN}$ increases rapidly and reaches the plateau at $\Gamma \approx 4$MeV. The reason for this interesting effect is that the quasifission rate decreases more rapidly than the fusion rate with increasing friction coefficients. The dissipative effects in $Z$ and $R$ compensate each other. Therefore, the influence of the dissipative effects on the calculation of $P_{CN}$ seems to be not crucial.

## 3. Summary

The DNS-concept of the fusion process was used to analyse the reactions producing nuclei with $Z$ =110, 112, 114, and 116. The inner fusion barriers in these reactions were estimated. The fusion barriers in the DNS-concept seem to be smaller than the extra-extra push energies predicted in the macroscopic dynamical model. For the reactions used to produce the elements with $Z$ =110 and 112, the $B^*_{fus}$ values are in good agreement with the experimental results. The new model suggested to calculate the probability of the fusion of heavy nuclei is efficient in describing the experimental data. A satisfactory description of $P_{CN}$ in this model can be considered as an evidence for the DNS–concept providing a realistic interpretation of the mechanism of fusion process.

We are grateful to Prof. Dr. W.Scheid for fruitful discussions. This work was supported in part by the RFBR under Grants N 96–02–17749, N 95–02–05975, and DFG under Grant 436 RUS 113/74/0. One of the authors (N.V.A.) is grateful to the Organizing Committee and RFBR for supporting the participation in the Conference.

1. V.V.Volkov, Proc. Intern. School-Seminar on Heavy Ion Physics (Dubna, 1986), D7-87-68 (JINR, Dubna, 1987) p.528; Izv. AN SSSR ser. fiz. 50 (1986) 1879.
2. N.V.Antonenko et al., Phys. Lett. B 319 (1993) 425; Phys. Rev. C 51 (1995) 2635; E.A.Cherepanov et al., Nucl. Phys. A 459 (1996) 145.
3. W.J. Swiatecki, Phys. Scripta 24 (1981) 113; S.Bjornholm and W.J.Swiatecki, Nucl. Phys. A 391 (1982) 471; J.P.Blocki, H.Feldmeier, and W.J.Swiatecki, Nucl. Phys. A 459 (1986) 145.
4. A.S. Iljinov, Yu.Ts. Oganessian, and E.A. Cherepanov, Sov. J. Nucl. Phys. 36 (1982) 118.
5. D.H.E. Gross, R.C. Nayak, and L. Satpathy, Z. Phys. A 299 (1981) 63; P. Fröbrich, Phys. Rep. 116 (1984) 337.
6. S. Hofmann et al., Z. Phys. A 350 (1995) 277; Z. Phys. A 350 (1995) 281; Z. Phys. A (1996) (in press).
7. W.Morawek et al., in: GSI Scientific Report (GSI, 1988) p.38; K.H.Schmidt, W.Morawek, Rep. Prog. Phys. 54 (1991) 949; W.Morawek et al., Z. Phys. A 341 (1991) 75.
8. V.V.Volkov et al., in: Proc. Int. Conf. on Low Energy Nuclear Dynamics, St.Petersburg, 1995, eds. Yu.Oganessian, R.Kalpakchieva, and W. von Oertzen (World Scientific, Singapore, 1995) p. 336.
9. H.A. Kramers, Physica. 7 (1940) 284.
10. V.M. Strutinsky, Phys. Lett. B 47 (1973) 121; H. Hofmann and J.R. Nix, Phys. Lett. B 122 (1983) 117; P. Grange, Jun-Qing Li, and H.A. Weidenmüller, Phys. Rev. C 27 (1983) 2063.
11. H.A. Weidenmüller and Jing-Shang Zhang, J. Stat. Phys. 34 (1984) 191.
12. G.G.Adamian et al., Phys. Rev. C (submitted).
13. I.I.Gonchar and G.I.Kosenko, Sov. J. Nucl. Phys. 53 (1991) 133.
14. H.Hofmann and P.J.Siemens, Nucl. Phys. A 257 (1976) 165.
15. G.G.Adamian, N.V.Antonenko, and R.V.Jolos, Nucl. Phys. A 584 (1995) 205.
16. A.M. Wapstra and G. Audi, Nucl. Phys. A 440 (1985) 327.
17. G.G.Adamian et al., Int. J. Mod. Phys. E 5 (1996) 191.

# Relativistic Hartree-Bogoliubov Description of the Halo Nuclei.*

J. Meng and P. Ring
*Physik-Department der Technischen UniversitätMünchen,*
*D-8046 Garching,FRG*
(September 10, 1996)

Here we report the development of the relativistic Hartree-Bogoliubov theory in coordinate space. Pairing correlations are taken into account by both density dependent force of zero range and finite range Gogny force. As a primary application the relativistic HB theory is used to describe the chain of Lithium isotopes reaching from $^{6}$Li to $^{11}$Li. In contrast to earlier investigations within a relativistic mean field theory and a density dependent Hartree Fock theory, where the halo in $^{11}$Li could only be reproduced by an artificial shift of the $1p_{1/2}$ level close to the continuum limit, the halo is now reproduced in a self-consistent way without further modifications using the scattering of Cooper pairs to the $2s_{1/2}$ level in the continuum. Excellent agreement with recent experimental data is observed.

PACS numbers : 27.70.+q, 21.10.Hw, 21.60.-n, 21.60.Ev, 21.60.Jz

In a recent work, using a density dependent force of zero range, taking care of pairing correlations, the relativistic Hartree-Bogoliubov theory in coordinate space has successfully descripe the halo nuclei in $^{11}$Li [1]. As it is well-known, that since the experimental discovery of neutron halo phenomena in $^{11}$Li [2], the study of exotic nuclei has become a very challenging topic in nuclear physics. Experimentally a sudden rise in the interaction cross-sections has been observed for light neutron-rich nuclei, specifically while going from $^{9}$Li to $^{11}$Li, $^{12}$Be to $^{14}$Be and $^{15}$B to $^{17}$B. This sudden increase in the interaction cross-sections has been attributed to a relatively large *rms* matter radius as compared to that expected from the conventional mass dependence $1.2A^{1/3}$. This large radius has been interpreted by the fact that filling in more and more neutrons in the nuclear well, the Fermi surface for the neutrons comes close to the continuum limit in the nucleus $^{11}$Li. Due to the small single-neutron separation energy, the tails of the two wavefunctions of the last filled orbital ($1p_{1/2}$) reach very far outside of the nuclear well and a neutron halo is formed [2]. Although this simple interpretation is based on the mean field picture, several microscopic theoretical investigations within self-consistent mean field models [3–6] have failed. In fact, it would be a strange accident if the last occupied neutron level in $^{11}$Li, the $1p_{1/2}$ orbit, would so close to the continuum limit that the tail of the last two uncorrelated neutron wave functions reaches so far out as would be necessary to reproduce the large experimental radius observed. Therefore, in the non-relativistic scheme Bertsch et al [3] and Sagawa [5] introduced an artificial modification to the potential in order to reproduce the small separation energy in their mean field calculations using Skyrme interactions. In this way the authors were able to reproduce qualitatively the observed trends, although some discrepancies still remained.

Koepf et al [4] were the first to investigate the neutron halo in relativistic mean field (RMF) theory for both spherical symmetrical and axially deformed cases. They found large deformations for the lighter Li isotopes, but a spherical shape for $^{11}$Li and as in the non-relativistic investigations the binding energy of the $1p_{1/2}$ was too large so as to reproduce a neutron halo. Zhu et al [6] improved the result of the RMF calculations by applying a similar modification to the potential as in Ref. [5] in order to adjust the proper size of the halo.

Bertsch and Esbensen [7] recognized that pairing correlations play an essential role. Performing a quasiparticle continuum RPA calculation using a core of $^{9}$Li and a density dependent interaction of zero range in the pairing channel, they found a large neutron halo $^{11}$Li and could reproduce the proper size of the experimental matter radius.

The present investigation is based on a similar idea. Pairing correlations and the scattering of Cooper pairs into the continuum are taken into account in a fully self-consistent way using a continuum Hartree-Bogoliubov formulism in the framework of relativistic mean field theory. A consistent treatment of pairing correlations within the framework of a generalized relativistic mean field approximation has been developed by Kucharek et al [8]. However, applications of this theory to nuclear matter clearly show that a quantitative description of pairing correlations in the nuclear many-body system cannot be achieved in this way with the presently used parameter sets of relativistic mean field theory. The behavior of the meson exchange forces entering this theory is simply not properly adjusted at large momentum transfer. In principle these forces have finite range and kinematical factors guarantee the convergence of the relativistic gap equation. The

large masses of the $\sigma$- and the $\omega$-mesons, however, do not yield a realistic cut off. Therefore the situation is similar to that of Skyrme forces with zero range: The short range of the relativistic forces produces no problem in the Hartree case, where only momenta up to the Fermi surface are involved, but it causes severe problems in the description of pairing, which allows scattering to very high momentum states.

The present work is based on a similar idea and combines the advantages of a relativistic description in the framework of RMF-theory in the Hartree channel with that of a phenomenological force in the pairing channel. In a recent investigation by Gonzalez-Llarena et al [9] a similar concept for the solution of the relativistic Hartree-Bolgoliubov equation in an oscillator basis with a finite range force of Gogny's type in the pairing channel has been used with great success . At present the application of finite range forces and density dependent zero range force in the pairing channel of continuum Hartree-Bogoliubov is developed. The density dependent $\delta$-force of the form [7] has been used:

$$V(r_1,r_2) = V_0\delta(r_1-r_2)\frac{1}{4}\left[1-\sigma_1\sigma_2\right]\left(1-\frac{\rho(r)}{\rho_0}\right) \tag{1}$$

The starting point is the RMF Lagrangian which describes the nucleons as Dirac spinors moving in meson fields:

$$\begin{aligned}\mathcal{L} = \bar{\psi}\left(\not{p} - g_\omega\not{\omega} - g_\rho\not{\vec{\rho}}\vec{\tau} - \frac{1}{2}e(1-\tau_3)\not{A} - g_\sigma\sigma - M_N\right)\psi \\ +\frac{1}{2}\partial_\mu\sigma\partial^\mu\sigma - U(\sigma) - \frac{1}{4}\Omega_{\mu\nu}\Omega^{\mu\nu} + \frac{1}{2}m_\omega^2\omega_\mu\omega^\mu \\ -\frac{1}{4}\vec{R}_{\mu\nu}\vec{R}^{\mu\nu} + \frac{1}{2}m_\rho^2\vec{\rho}_\mu\vec{\rho}^\mu - \frac{1}{4}F_{\mu\nu}F^{\mu\nu}\end{aligned} \tag{2}$$

where $M_N$ is the bare nucleon mass and $\psi$ is its Dirac spinor. We have in addition the scalar meson ($\sigma$), isoscalar vector mesons ($\omega$),isovector vector mesons ($\vec{\rho}$) and the photons $A^\mu$, with the masses $m_\sigma$, $m_\omega$ and $m_\rho$ and the coupling constants $g_\sigma$, $g_\omega$, $g_\rho$. The field tensors for the vector mesons are given as

$$\Omega_{\mu\nu} \;=\; \partial_\mu\omega_\nu - \partial_\nu\omega_\mu \tag{3}$$

and by similar expressions for the $\rho$-meson and the photon. For simplicity we neglect in the following equations these fields, however, they are fully taken into account in the calculations.

For a realistic description of nuclear properties a nonlinear self-coupling for the scalar mesons has turned out to be crucial [10]:

$$U(\sigma) \;=\; \frac{1}{2}m_\sigma^2\sigma^2 \;+\; \frac{g_2}{3}\sigma^3 \;+\; \frac{g_3}{4}\sigma^4 \tag{4}$$

Using Greens function techniques it has been shown in Ref. [8] how one can derive a relativistic Hartree-Fock-Bogoliubov theory from such a Lagrangian: After a full quantization of the system the mesonic degrees of freedom are eliminated and, in full analogy to the non-relativistic case, the higher order Greens functions are factorized in the sense of Gorkov [11]. Finally, neglecting retardation effects one ends up with relativistic Dirac-Hartree-Bogoliubov (RHB) equations

$$\begin{pmatrix} h & \Delta \\ -\Delta^* & -h^* \end{pmatrix}\begin{pmatrix} U \\ V \end{pmatrix}_k \;=\; E_k\begin{pmatrix} U \\ V \end{pmatrix}_k, \tag{5}$$

$E_k$ are quasiparticle energies and the coefficients $U_k$ and $V_k$ are four-dimensional Dirac spinors normalized in the following way

$$\int U_k^+U_{k'} \;+\; V_k^+V_{k'}\,d^3r \;=\; \delta_{kk'} \tag{6}$$

Neglecting the Fock term, as is it mostly done in relativistic mean field theory, we obtain for the average field

$$h \;=\; \boldsymbol{\alpha p} \;+\; g_\omega\omega \;+\; \beta(M+g_\sigma\sigma) \;-\; \lambda \tag{7}$$

where $\sigma$ and $\omega$ are the meson fields determined self-consistently from the Klein Gordon equations:

$$\{-\Delta + m_\sigma^2\}\,\sigma = -g_\sigma \rho_s \; - \; g_2\sigma^2 \; - \; g_3\sigma^3, \tag{8}$$

$$\{-\Delta + m_\omega^2\}\,\omega = g_\omega \rho_B \tag{9}$$

with the scalar density $\rho_s$ and the baryon density $\rho_B$

$$\rho_s \; = \; \sum_k \bar{V}_k V_k, \qquad \rho_B \; = \; \sum_k V_k^+ V_k, \; . \tag{10}$$

where the sum over $k$ runs only over all the particle states in the *no-sea approximation.*

The pairing potential $\Delta$ in Eq.(5) is given by

$$\Delta_{ab} \; = \; \frac{1}{2}\sum_{cd} V^{pp}_{abcd}\kappa_{cd} \tag{11}$$

It is obtained from the pairing tensor $\kappa = U^* V^T$ and the one-meson exchange interaction $V^{pp}_{abcd}$ in the $pp$-channel. More details are given in Ref. [8]. As mentioned above, these forces are not able to reproduce even in a semi-quantitative way proper pairing in the realistic nuclear many-body problem. We therefore replace $V^{pp}_{abcd}$ in Eq. (11) by the density dependent two-body force of zero range given in Eq. (1).

For a zero range force in the pairing channel, the RHB equations (5) are a set of four coupled differential equations for the HFB Dirac spinors $U(r)$ and $V(r)$. They are solved in a self-consistent way by the shooting method and the Runge-Kutta algorithm. The details will be published elsewhere. The calculation is done in a spherical box of radius $R = 20$ fm with a step size of 0.1 fm and proper boundary conditions. For each spin-parity channel 20 radial wavefunctions are taken into account, which corresponds roughly to a cut-off energy of 200 MeV.

We use here the non-linear Lagrangian parameter set NL2 which was designed in Ref: [12] for light nuclei: $M_N$=938, $m_\sigma$ = 504.89, $m_\omega$ = 780, $m_\rho$ = 760 MeV and $g_\sigma$ = 10.444, $g_\omega$ = 12.945, $g_\rho$ = 4.383, $g_2$=-6.6099 fm$^{-1}$, $g_3$=13.783. Pairing is neglected for the three protons and the strength $V_0$ of the pairing force (1) for the neutrons is determined by a calculation in the nucleus $^7$Li adjusting the corresponding pairing energy -$\frac{1}{2}Tr\Delta\kappa$ to that of a RHB-calculation in an oscillator basis using the finite range part of the Gogny force D1S of Ref. [13] in the pairing channel. For $\rho_0$ we use the nuclear matter density 0.152 fm$^{-3}$.

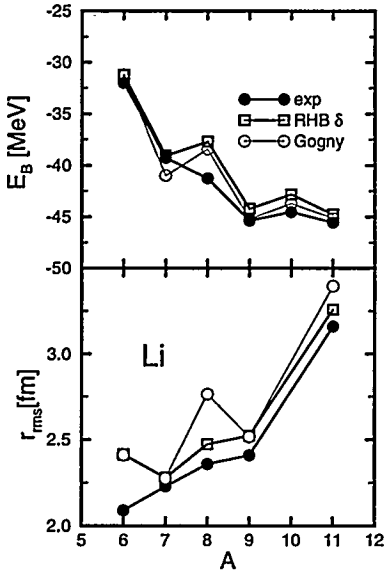


Fig. 1 Binding energies (upper part) and matter radii (lower part) for Li isotopes: RHB calculations with density dependent $\delta$-force ( empty squares ) and Gogny force ( empty circles ) are compared with experimental values (full dots).

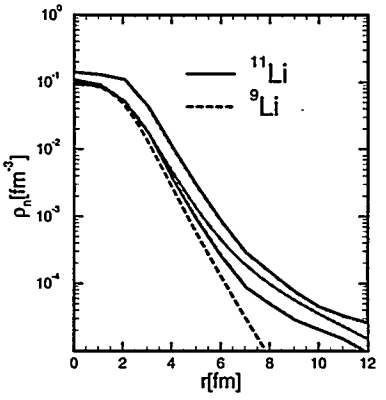


Fig. 2 Calculated and experimental density distribution in $^{11}$Li and $^9$Li. The solid line shows the result of $^{11}$Li while the dashed line corresponds to the calculation $^9$Li. The shaded area gives the experimental results with error bars.

In Fig. 1 we show the calculated binding energies $E_B$ and the *rms* matter radii for the Li isotopes with mass numbers $A = 6$ to $A = 11$ and compare them with experimental values. In order to correct for the center of mass motion a spurious energy of an harmonic oscillator $E_{cm} = 0.75\hbar\omega_0$ with $\hbar\omega_0 = 41A^{-1/3}$ is subtracted. The calculated values show a small under-binding and the odd-even staggering is somewhat exaggerated by our blocking calculations, but in general the agreement is very satisfactory and in full agreement with experiment. The matter radius shows a considerable increase when going from the nucleus $^9$Li to $^{11}$Li. In contrast to the earlier mean field calculations of Refs. [3,5,6] these results are obtained without any artificial modifications of the potential.

In Fig. 2 we show she corresponding density distribution for the neutrons in the isotopes $^9$Li and $^{11}$Li. It is clearly seen that the increase of the matter radius is caused by a large neutron halo in the nucleus $^{11}$Li. Its density distribution is in very good agreement with the experimental density of this isotope show with its error bars by the shaded area.

In order to understand the microscopic structure of this halo, we show is Fig. 3 the mean field $S(r)+V(r) = g_\sigma\sigma + g_\omega\omega \pm g_\rho\rho + eA$ for the protons and neutrons together with the energy levels $\epsilon_n = \langle n|h|n\rangle$ in the canonical basis [14]. The Fermi level for the neutrons is very close to the continuum limit in close vicinity to the $\nu 1p_{1/2}$ and to the $\nu 2s_{1/2}$ level. The length of these energy levels in Fig.2 is proportional to the corresponding occupation. We clearly see that pairing correlations cause a partial occupation of both the $\nu 1p_{1/2}$ and the $\nu 2s_{1/2}$ level, i.e. a scattering of Cooper pairs to the continuum.

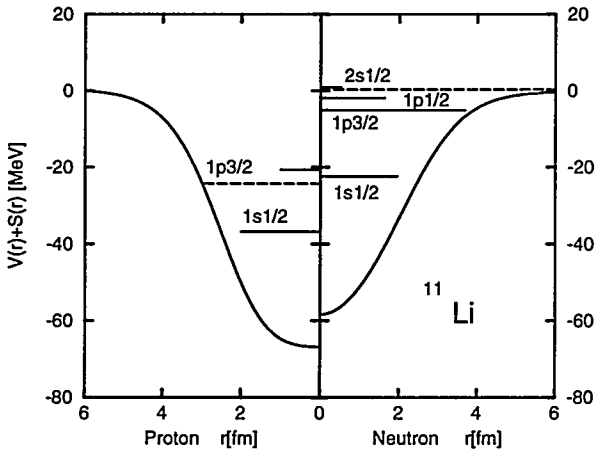


Fig. 3 The mean field potential $S + V$ for protons (l.h.s.) and neutrons (r.h.s.). The chemical potential is given by a dashed line. The energy levels in the canonical basis are indicated by horizontal lines with various lengths proportional to the occupation of the corresponding orbit.

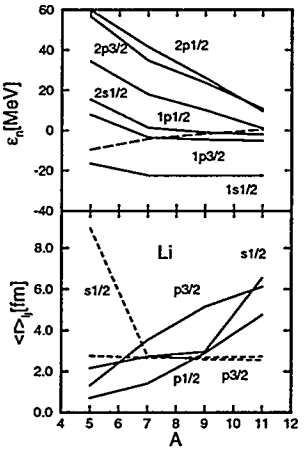


Fig. 4 Single particle energies for neutrons in the canonical basis (upper part) and contributions to the matter radius for various spin-parity channels as a function of the mass number. In the upper part the dashed line corresponds to the chemical potential and in the lower part the dashed lines correspond to proton contributions.

Fig. 4 shows the single particle levels in the canonical bases for the isotopes with even neutron number as a function of the mass number together with the contribution of the different spin-parity channels to the matter radius:

$$\langle r\rangle_{lj} = \left(\int r^2 \rho_{lj} d^3r\right)^{1/2} \tag{12}$$

The total *rms* matter radius is obtained from this quantities as

$$\langle r^2\rangle = \frac{1}{A}\sum_{lj}\langle r\rangle^2_{lj} \tag{13}$$

Going from $A = 9$ to $A = 11$ we observe a continuous increase of the contribution of the $p_{1/2}$ channel to the total *rms* matter radius and in addition a sudden increase of the contribution of the $s_{1/2}$ channel. This means that the halo in $^{11}$Li is formed by the sudden occupation of the $2s_{1/2}$ level in this nucleus, which approaches the Fermi surface for this mass number, as seen in the upper part of Fig. 4.

Summarizing we can say that we have solved for the first time the Hartree-Bogoliubov equations in the continuum [15] in the framework of relativistic mean field theory. A density dependent force of zero range has been used in the pairing channel, whose strength is adjusted for the isotope $^7$Li to a similar calculation with Gogny's force D1S in the pairing channel. Good agreement with experimental values is found for the total binding energies and the radii of the isotope chain $^6$Li to $^{11}$Li. In excellent agreement with the experiment we obtain a neutron halo for $^{11}$Li without any artificial adjustment of the potential, as it was necessary in earlier calculations. In contrast to these investigations the halo is not formed by two neutrons occupying the $1p_{1/2}$ level very close to the continuum limit, but is is formed by Cooper-pairs scattered mainly in the two levels $1p_{1/2}$ and $2s_{1/2}$. This is made possible by the fact that the $2s_{1/2}$ comes down close to the Fermi level in this nucleus and by the density dependent pairing interaction coupling the levels below the Fermi surface to the continuum. In contrast to the previous explaination which use the accidental coincidence that one single particle level is so close to continuum threshold so that the tail of its wave function forms a halo, this is a much more general mechanism, which could possibly be observed in other halo nuclei also. One needs only several single particle levels with small orbital angular momenta and correspondingly small centrifugal barrier close, but not directly at, the continuum limit.

---

* Supported by the Alexander von Humboldt Foundation and by the Bundesministerium für Forschung und Technologie under the project 06 TM 743.

[1] J. Meng, and P. Ring, to be published.
[2] I. Tanihata et al, Phys. Rev. Lett. **55**, 2676 (1985)
[3] G.F. Bertsch, B.A. Brown, and H. Sagawa, Phys. Rev. **C39**, 1154 (1989)
[4] W.Koepf, Y.K. Gambhir, P. Ring, and M.M. Sharma, Z. Phys. **A340**, 119 (1991)
[5] H. Sagawa, Phys. Lett. **286B** (1992) 7
[6] Z.Y. Zhu, W.Q. Shen, Y.H. Cai, and Y.G. Ma, Phys. Lett. **328B** (1994) 1
[7] G.F. Bertsch and H. Esbensen; Ann. Phys. (N.Y.) **209** (1991) 327
[8] H. Kucharek and P. Ring; Z. Phys. **A339** (1991) 23
[9] T. Gonzalez-Llarena, J.L.Egido, G.A. Lalazissis, and P. Ring; Phys.Lett. **B** in print
[10] J. Boguta and A.R. Bodmer; Nucl. Phys. **A292** (1977) 413
[11] L.P. Gorkov; Sov. Phys. JETP **7** (1958) 505
[12] S.J. Lee et al; Phys. Rev. Lett. **57** (1986) 2916
[13] J.F.Berger, M. Girod, and D. Gogny; Nucl. Phys. **A428** (1984) 32c
[14] P. Ring and P. Schuck; *The Nuclear Many-body Problem*, Springer Verlag, Heidelberg (1980)
[15] J.Dobaczewski, H. Flocard and J.Treiner, Nucl. Phys. **A422** (1984) 103.

# New High Spin States and Isomers in the $^{208}$Pb and $^{207}$Pb Nuclei

R.Broda, J.Wrzesinski, T.Pawlat, B.Fornal, Z.Grabowski[1)] - ***INP Cracow***, D.Bazzacco, S.Lunardi, C.Rossi Alvarez -***INFN and University Padova***, G.de Angelis, A.Gadea - ***INFN LNL Legnaro***, K.-H.Maier - ***HMI Berlin***

The two most prominent examples of the heavy doubly closed shell (DCS) nuclei, $^{208}$Pb and $^{132}$Sn, are not accessible by conventional heavy-ion fusion processes populating high-spin states. This experimental difficulty obscured for a long time the investigation of yrast high-spin states in both DCS and neighbouring nuclei and consequently restricted the study of the shell model in its most attractive regions. Recent technical development of multidetector gamma arrays opened new ways to exploit more complex nuclear processes which populate the nuclei of interest with suitable yields for gamma spectroscopy and involve population of moderately high spin states. This new possibility extended the range of accessible spin values and is a promising way to reach new yrast states. Some of these states are expected to be of high configurational purity and can be a source of important shell model parameters which possibly can be used later to check the validity of the spherical shell model description at yet higher spin and higher excitation energy.

The nuclei in the closest vicinity of $^{132}$Sn are produced in spontaneous fission and states with spin values up to I=14 can be reached in fission gamma spectroscopy studies with the presently achieved sensitivity of gamma arrays. New results on yrast states in the $^{134}$Te and $^{135}$I nuclei populated in fission of the $^{248}$Cm and presented at this conference [1] illustrate such application of the resolving power offered by modern gamma techniques.

Recently we have demonstrated that also in the region of spherical shell model nuclei around $^{208}$Pb the study of high spin states is possible using the thick target method of gamma spectroscopy in deep-inelastic heavy-ion reactions. In those early experiments new yrast states in $^{207}$Pb [2] and $^{208}$Pb [3] were populated in bombardment of the $^{208}$Pb target with $^{64}$Ni and $^{82}$Se ions at energies exceeding by 20-30 MeV the Coulomb barrier. Even the moderate quality gamma-gamma coincidences obtained then with the 12 detector OSIRIS gamma array at HMI Berlin allowed to extract useful information on high spin states [2,3]. Important aspects of the gamma spectroscopy analysis in deep-inelastic heavy-ion collisions were reported earlier [4] and such technique was already applied successfully in the study of neutron rich Ni isotopes [5], which included the N=40 closed subshell $^{68}$Ni nucleus [6].

The new results on high spin states in $^{208}$Pb and $^{207}$Pb discussed in the present work were obtained from an experiment originally planned as continuation of this Ni isotopes study and aimed specifically to search for the $^{70}$Ni structure. The 420 MeV $^{76}$Ge beam from the ALPI Linac accelerator at the INFN Legnaro bombarded a 20mg/cm$^2$ thick $^{208}$Pb target placed in the center of the GASP gamma array. The beam was pulsed with 400 ns repetition time and the collected gamma-gamma coincidence data included time parameters which allowed to separate in a clean way the prompt and delayed events as well as delayed coincidences involving up to 800 ns delay time between two gamma transitions. The observed production yields of neutron-rich Ni isotopes indicated that the $^{70}$Ni nucleus is populated, but the obtained statistics were not good enough to perform necessary identification. Whereas the $^{70}$Ni structure identification had to be postponed to future experiments, the data analysis revealed surprisingly strong population of high spin states in the heavy nuclei produced in binary reactions. For example, the high spin states in $^{206}$Pb were found to be strongly populated up to the highest spin state I=20, known from a recent spectroscopic study with a heavy ion fusion reaction [7]. Even higher spin state of I=30 could be observed in the well known $^{212}$Rn shell model nucleus [8], which in the present experiment was apparently produced by complex processes involving transfer of four protons to the $^{208}$Pb target nucleus. This

favorable high spin population prompted us to analyse the same data to extract potentially new information on yrast states in the $^{208}$Pb and $^{207}$Pb nuclei. In the following the results obtained from this analysis will be discussed separately for both nuclei.

### The $^{208}$Pb nucleus.

In the DCS $^{208}$Pb nucleus high spin states up to I=14 can be formed by simple particle-hole excitations. Promotion of the neutron from $i_{13/2}$ orbital to the one of the available high j orbitals - $g_{9/2}$, $i_{11/2}$ or $j_{15/2}$, gives rise to multiplets of states, of which the highest spin members are yrast states. Similar proton excitations occur at significantly higher energies and the I=12 highest spin can be reached from the $i_{13/2}\ h^{-1}_{11/2}$ coupling. In highly elaborated (e,e') experiments [e.g.9] several high spin states could be placed within 5 keV accuracy and few of them were assigned including the highest spin $14^-$ neutron $j_{15/2}i^{-1}_{13/2}$ excitation. In our early experiments [3] we were able to place four yrast states lying above the 4895 keV $10^+$ isomer; two of them are the $14^-$ and $12^+$ states known from (e,e') experiments [9] and were observed then for the first time by gamma spectroscopy. The two new levels populated in the gamma yrast decay were assigned as the $13^-$ and $11^+$ states. This status of the $^{208}$Pb high spin state study was the starting point in the present analysis of the $^{208}$Pb + $^{76}$Ge gamma coincidence data.

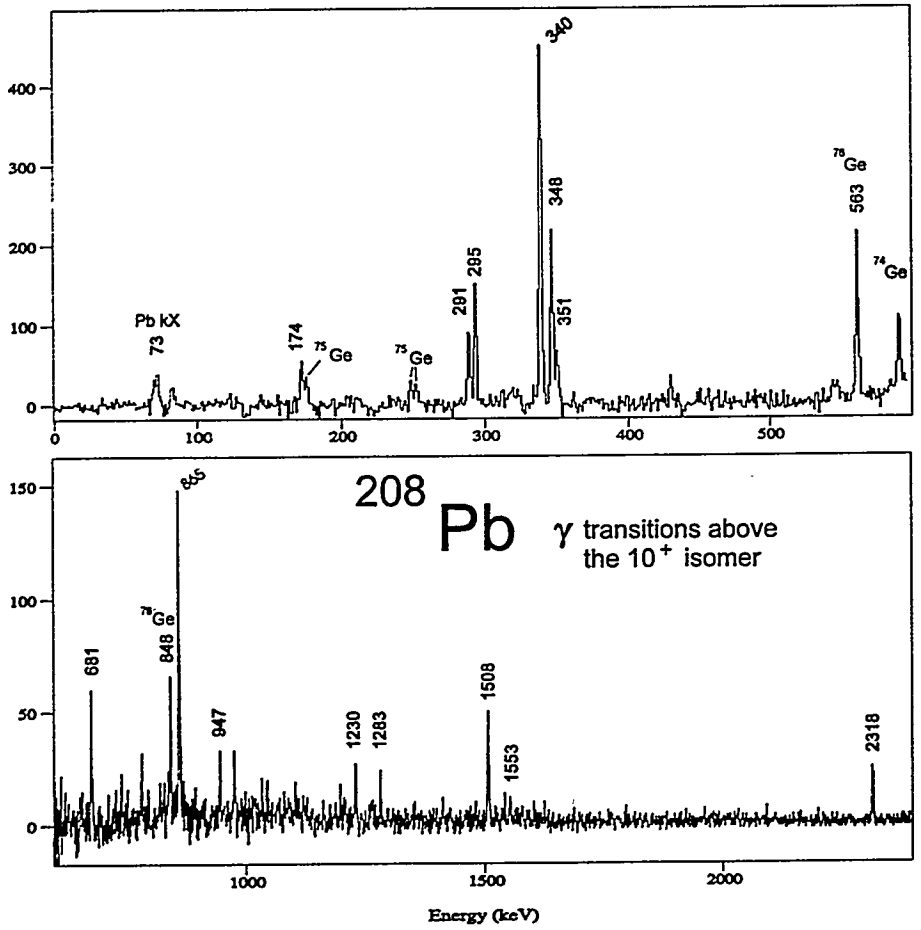


*Fig.1 Gamma spectrum of prompt transitions preceding in time the delayed gates set on four strongest transitions occurring in the decay of the 500 ns $10^+$ isomer in $^{208}$Pb. Lines with indicated energies correspond to $^{208}$Pb high spin transitions; those with isotope assignment arise from Ge isotopes occurring simultaneously with $^{208}$Pb in the $^{208}$Pb + 414 MeV $^{76}$Ge collision exit channel.*

The half-life, $T_{1/2}$ = 500 ns, of the $10^+$ isomer in $^{208}$Pb greatly simplified the identification of high spin gamma transitions located above it. Delayed coincidences with gates set on several gamma transitions below the isomer produced the gamma spectrum which is shown in Fig.1 and includes all gamma transitions preceding the isomeric decay. Only few of these transitions arise from the prompt gamma decay of excited Ge isotopes which appear simultaneously with the $^{208}$Pb

nucleus in the reaction exit channel. They are marked by the assigned isotope which often indicates substantial involvement of neutron evaporation in the processes populating the $^{208}$Pb high spin states. All other transitions with indicated energies seen in the spectrum of Fig.1 belong to the $^{208}$Pb nucleus. Whereas the four previously known [3] transitions appear as the most intense ones, the spectrum shows many new weaker gamma lines in a broad energy range up to the 2318 keV high energy transition. The analysis of prompt gamma coincidences established the level scheme of $^{208}$Pb shown in Fig.2. Few weak transitions could not be placed in the level scheme due to the complexity of the prompt coincidence data.

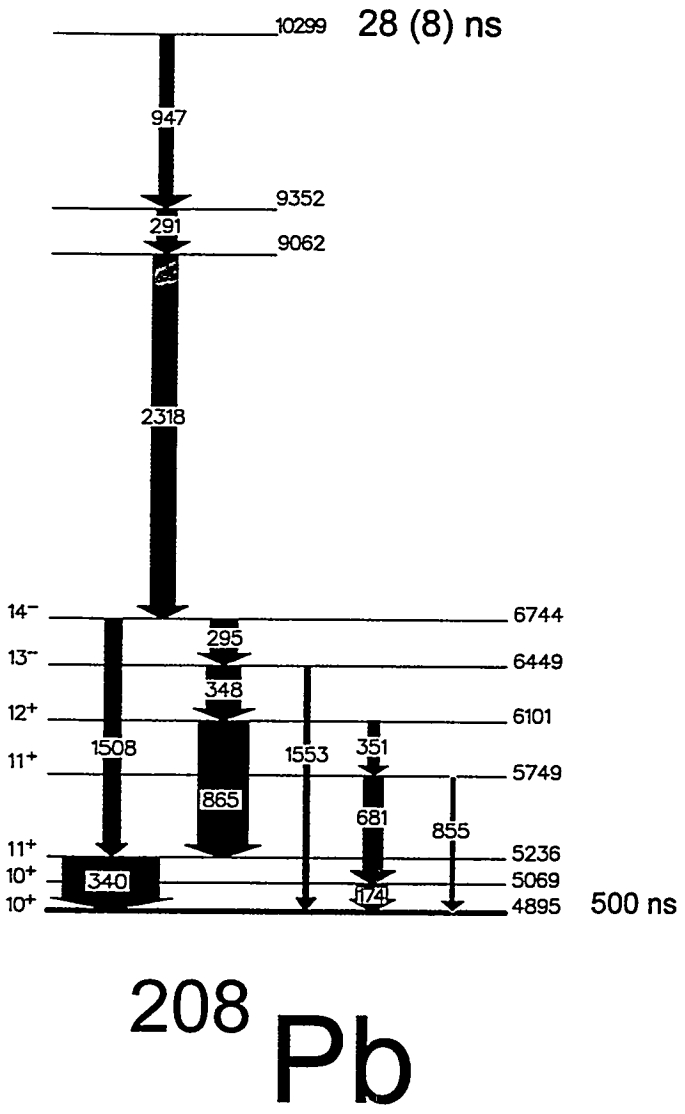


*Fig.2 High spin states in $^{208}$Pb above the 500 ns $10^+$ isomer.*

The cascade of three transitions of 2318,291 and 947 keV energy firmly located above the $14^-$ level did show a delayed component, thus indicating the existence of a new high spin isomer in the $^{208}$Pb nucleus. Detailed analysis of timing data sorted into $E_\gamma$ - $E_\gamma$ - t cubes allowed to extract the 28(8)ns half-life of the isomer but its location could not be established. In any case, the three new high spin states lying above the $14^-$ highest spin neutron particle-hole excitation must involve

additional core excitations and thus are the first two particle-two hole states of high spin observed in $^{208}$Pb. In the absence of experimental spin assignments and calculations of 2p-2h states it is too early to speculate in the present report on the nature of these states and especially on the structure of the isomer. A clear interpretation is possible for the new features established in the present work in the lower part of the level scheme. Here, below the $14^-$ state, a fairly complex gamma decay was observed, which established the new $11^+$ level at 5749 keV and involved population of previously known [10] second $10^+$ level at 5069 keV. In the following we shall discuss three points related to this gamma decay between states of well defined predominant structures which involve the coupling of the $i_{13/2}$ neutron hole with a neutron particle, namely: $j_{15/2}$ ($14^-$, $13^-$), $i_{11/2}$ ($12^+$, $11^+$ at 5749 keV) and $g_{9/2}$ ($11^+$ at 5236 keV, $10^+$ at 5069 and 4895 keV).

The first point concerns the surprising competition between the 1508 keV E3 and 295 keV M1 transitions observed in the decay of the $14^-$ state. The configurations of the involved states as indicated above define the $14^- \rightarrow 11^+$ 1508 keV E3 as the $j_{15/2} \rightarrow g_{9/2}$ transition with the $i_{13/2}$ neutron hole acting as spectator. Such an E3 is also observed in the lower part of the $^{208}$Pb level scheme i.e. the 1413 keV transition connecting the $8^+$ and $5^-$ states with correspondingly the $j_{15/2}$ and $g_{9/2}$ neutron coupled to the $p_{1/2}$ hole. In $^{209}$Pb this $j_{15/2} \rightarrow g_{9/2}$ E3 of 1423 keV is observed directly and its 1.5ns half-life defines it as the fast E3 transition. On the other hand the competing 295 keV M1 transition between the states of the $j_{15/2}i^{-1}_{13/2}$ multiplet must be very slow since the B(M1) is proportional to the squared g-factor difference of two high j components. The estimated B(M1) value gives 5ns for the 295 keV transition partial half-life which is fully compatible with the observed branching. It is worth noting that also the observed weak $13^- \rightarrow 10^+$ 1553 keV transition (Fig.2) is of the same E3 nature competing with the forbidden E1 transition.

Second point is the consideration of possible mixing between the two $11^+$ states of predominant $i_{11/2}i^{-1}_{13/2}$ (5749 keV) and $g_{9/2}i^{-1}_{13/2}$ (5236 keV) configurations. The M1 branching of $I_\gamma(865\text{keV})/I_\gamma(351\text{keV}) = 3$ observed in the decay of the pure $i_{11/2}i^{-1}_{13/2}$ $12^+$ state at 6101 keV is nicely reproduced by assuming pure wave functions for both $11^+$ states; the mixing allowed by this branching must be smaller than 0.2 in amplitude squared. This mixing is even further restricted by the absence of an M1 transition between both $11^+$ states, which leads to the conclusion that both states are exceptionally pure.

The third point concerns the M1 branching in the decay of the upper $11^+$ state at 5749 keV to the two lower lying $10^+$ states. Without going into details the conclusion is that this branching is well reproduced by the known [10] complex structure of both $10^+$ states. Quantitatively this branching settles the -0.05(8) $i_{11/2}i^{-1}_{13/2}$ amplitude in the wave function of the isomeric lower $10^+$ state.

In conclusion, new high spin two-particle two-hole excitations were established in the $^{208}$Pb nucleus including an isomeric state with spin close to I=20 and excitation energy higher than 10 MeV. The level structure and the gamma decay observed below the $14^-$ 6744 keV state are well understood within a simple shell model and give very relevant structure information.

**The $^{207}$Pb nucleus.**

The level scheme of the $^{207}$Pb high spin states established in the present work is shown in Fig.3. States below the tentatively assigned $29/2^+$ state at 6047 keV were known from the previous study [2], except for the two relatively strongly populated near yrast states at 5282 and 5966 keV. The main cascade of three intense transitions above the $29/2^-$ state located new high spin levels which were found to be populated in the decay of a high spin long-lived isomer. The isomeric half-life was determined as 360(80)ns, but the isomeric decay could not be fully resolved. Many new transitions seen in this decay could not be placed with confidence due to small intensity. Consequently, the placement of the isomer is uncertain. Nevertheless it must lie very close to the highest energy

observed state at 8475 keV, which is the expected position of the one-particle two-hole state of the $j_{15/2}i^{-2}_{13/2}$ configuration. Any other considerations of the observed high spin structures in $^{207}$Pb must be postponed until spin-parity assignments and full clarification of the level scheme are resolved by future experiments.

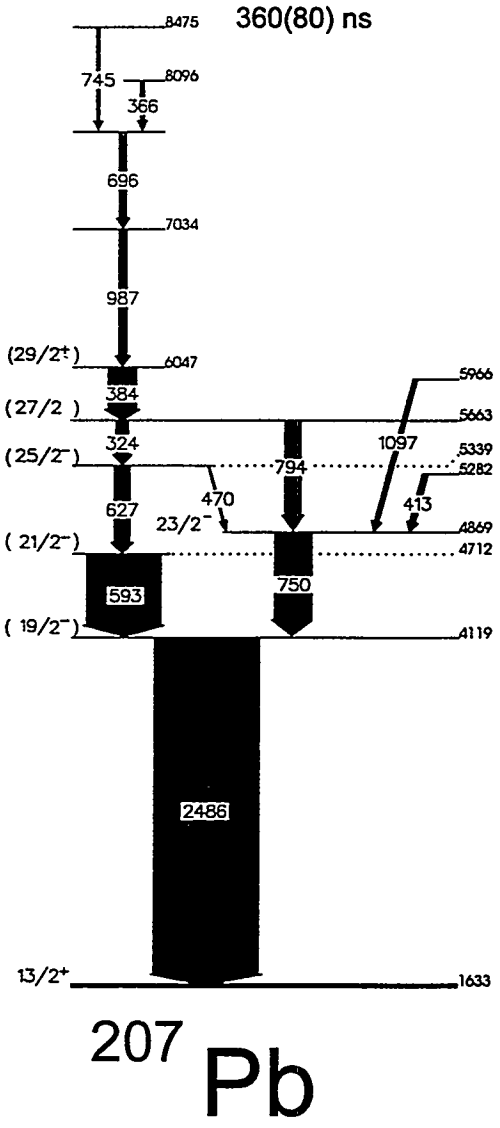


*Fig.3 High spin states in $^{207}$Pb above the $i_{13/2}$ isomer.*

In summary. using the gamma-gamma coincidence data obtained from the thick target $^{208}$Pb + 414 MeV $^{76}$Ge experiment we were able to extract new information on hitherto unknown high spin states in the $^{208}$Pb and $^{207}$Pb shell model nuclei. This results exemplify new prospects for the gamma spectroscopy in deep-inelastic heavy ion reactions opened by the impressive technical development achieved in gamma ray detection. Recently we performed at GSI Darmstadt new experiments with $^{136}$Xe and $^{208}$Pb beams on $^{208}$Pb targets using 5 new cluster detectors and the crystal ball. These experiments were dedicated to gamma spectroscopy studies in the $^{208}$Pb shell model region and the obtained data promise further interesting findings.

*This work was supported by the INFN -IFJ italian - polish collaboration and by the Polish Scientific Committee under grant no. 1044/P03-96-10*

[1)] *Permanent address: Dept. of Physics Purdue Univ. 47907 IN, USA*

[1] P.J.Daly *at al.*, lecture presented at this conference
[2] M. Schramm *et al.*, Z. Phys. **A344**, 121(1992)
[3] M. Schramm *et al.*, Z. Phys. **A344**, 363(1993)
[4] R. Broda *et al.*, Phys. Rev. **C49**, R575(1994)
[5] T. Pawlat *et al.*, Nucl.Phys. **A574**, 623(1994)
[6] R. Broda *et al.*, Phys.Rev.Lett. **74**, 868(1995)
[7] A.R. Poletti *et al.*, Nucl.Phys. **A580**, 43(1994)
[8] A.E. Stuchbery et al., Nucl.Phys. **A486**, 397(1988)
[9] J.P. Connelly *et al.*, Phys. Rev. **C45**, 2711(1992)
[10] M.Schramm - PHD Thesis, Report of the Hahn-Meitner-Institut. **HMI-B508** March 1993

# YRAST EXCITATIONS AROUND $^{132}$Sn: THE TWO AND THREE VALENCE-PROTON N=82 ISOTONES $^{134}$Te AND $^{135}$I

P.J. Daly, C.T. Zhang, P. Bhattacharyya, R. Broda[a)], Z.W. Grabowski, D. Nisius
Chemistry and Physics Depts., Purdue University, West Lafayette, IN 47907, USA

I. Ahmad, T. Ishii[b)], M.P. Carpenter, L.R. Morss
Physics Division, Argonne National Laboratory, Argonne, IL 60439, USA

W.R. Phillips, J.L. Durell, M. J. Leddy, A. G. Smith, W. Urban, B.J. Varley
Dept. of Physics and Astronomy, University of Manchester,
M13 9PL Manchester, United Kingdom

N. Schulz, E. Lubkiewicz, M. Bentaleb
Centre de Recherches Nucleaires, Universite Louis Pasteur,
F-67037 Strasbourg, France

J. Blomqvist
Dept. of Physics Frescati, Royal Institute of Technology, S-10405 Stockholm, Sweden

The Z=50, N=82 nucleus $^{132}$Sn is the most magic of all heavy nuclei, with pronounced shell closures for both protons and neutrons manifested by the absence of excited states below 4.0 MeV excitation energy [1]. What we know about $^{132}$Sn and nearby nuclei comes mainly from $\beta^-$ decay studies of short-lived fission products; consequently, our knowledge about simple excitation modes, single particle energies, effective nucleon-nucleon interactions and other basic properties in this region is far from complete. The spectroscopy of $^{132}$Sn and its neighbors should in many ways resemble that of the well studied region around Z=82, N=126 $^{208}$Pb, where a substantial body of empirical nuclear structure information has accrued. Several groups [2-5] have discussed the possibility of developing a "universal" theoretical description of shell model properties with some parameter variation in familiar and remote areas of the nuclidic chart, and they have stressed the desirability of detailed comparison between experimental data

from the $^{208}$Pb and $^{132}$Sn regions. Progress along these lines has been hampered by a scarcity of information about simple excitation modes in the $^{132}$Sn region. The development of large multidetector $\gamma$-ray arrays, which can separate the prompt $\gamma$-ray cascades within a single fission product nucleus (of moderate yield) from the bulk of prompt $\gamma$-rays, has now opened new prospects for detailed studies of yrast excitations in $^{132}$Sn and the few valence particle nuclei around it.

Measurements were performed at Eurogam II using a $^{248}$Cm source consisting of about 5 mg of curium oxide embedded in a pellet of potassium chloride. This source delivered $\sim 6.3 \times 10^4$ fissions/sec, with stopping of the fission fragments in $\sim 1$ ps and subsequent emission of almost all the de-excitation $\gamma$-rays from nuclei at rest [6]. Eurogam II at the time consisted of 52 escape-suppressed spectrometers incorporating 124 Ge detector elements, here augmented by four LEPS spectrometers. A total of $2 \times 10^9$ threefold or higher-fold coincidence events were recorded. A first inspection showed that these data included known $\gamma$-ray cascades in $^{132}$Sn and its neighbors, as well as many strong unidentified cascades, so we embarked on a detailed investigation of yrast excitations in the Z=50-54, N=80-84 range of nuclei. Cross coincidences observed between $\gamma$-rays from partner light and heavy fission fragments were often of critical importance in establishing isotopic assignments for previously unknown cascades; in other cases, some overlap with the $\gamma$-rays known from $\beta$-decay studies provided vital first clues. Although the analysis is far from complete, substantial advances have already been made in the spectroscopy of many of the nuclei in the targeted range. Here, we feature the results for the two and three valence proton N=82 isotones $^{134}$Te and $^{135}$I which exhibit simple clearcut excitation modes, thus resembling $^{210}$Po and $^{211}$At, their well studied N=126 counterparts in the $^{208}$Pb region.

In the two-proton nucleus $^{134}$Te, many members of the $\pi g_{7/2}^2$, $\pi g_{7/2} d_{5/2}$ and $\pi g_{7/2} h_{11/2}$ multiplets are known from $^{134}$Sb $\beta^-$ decay studies, especially the recent work of Omtvedt et al. [7]. The present fission product measurements identified two dominant high-energy $\gamma$-rays feeding the 1691 keV $\pi g_{7/2}^2$ $6^+$ state in $^{134}$Te, one the 2322 keV $9^- \rightarrow 6^+$ E3 transition known from $\beta$-decay [7], the other a 2866 keV $\gamma$-ray from a $^{134}$Te level at 4557 keV. Gating on this 2866 keV $\gamma$-ray revealed many new $^{134}$Te $\gamma$-rays, and the full $\gamma\gamma\gamma$ results established the level sequence above 4557 keV shown to the left in the $^{134}$Te scheme (Fig. 1). Since the only possible two-proton state with I>9 is $(\pi h_{11/2}^2)$ $10^+$, expected in $^{134}$Te above 7 MeV, the

obvious conclusion is that these new states must involve excitation of the $^{132}$Sn core. We interpret them as $\pi g_{7/2}{}^2 \nu f_{7/2} h_{11/2}{}^{-1}$ states, with strong support from shell model calculations.

Nothing was known up to now about high-spin states in the N=82 nucleus $^{135}$I, but a $^{135}$Te $\beta^-$-decay study [8] has located $11/2^+$ and $9/2^+$ levels at 1134 and 1184 keV respectively above the $^{135}$I $\pi g_{7/2}$ ground state. In the present work, we started a search for other $^{135}$I transitions by setting a single coincidence gate on 1134 keV $\gamma$-rays. Strong 288, 572, 690, 725, 1661, 1695 and 2247 keV coincident $\gamma$-rays were identified, and by generating a series of double gated $\gamma$-ray spectra including these transitions, they were all confirmed as $^{135}$I $\gamma$-rays. A compilation of many doubly gated $\gamma$-ray spectra then established the $^{135}$I level scheme presented in Fig. 1.

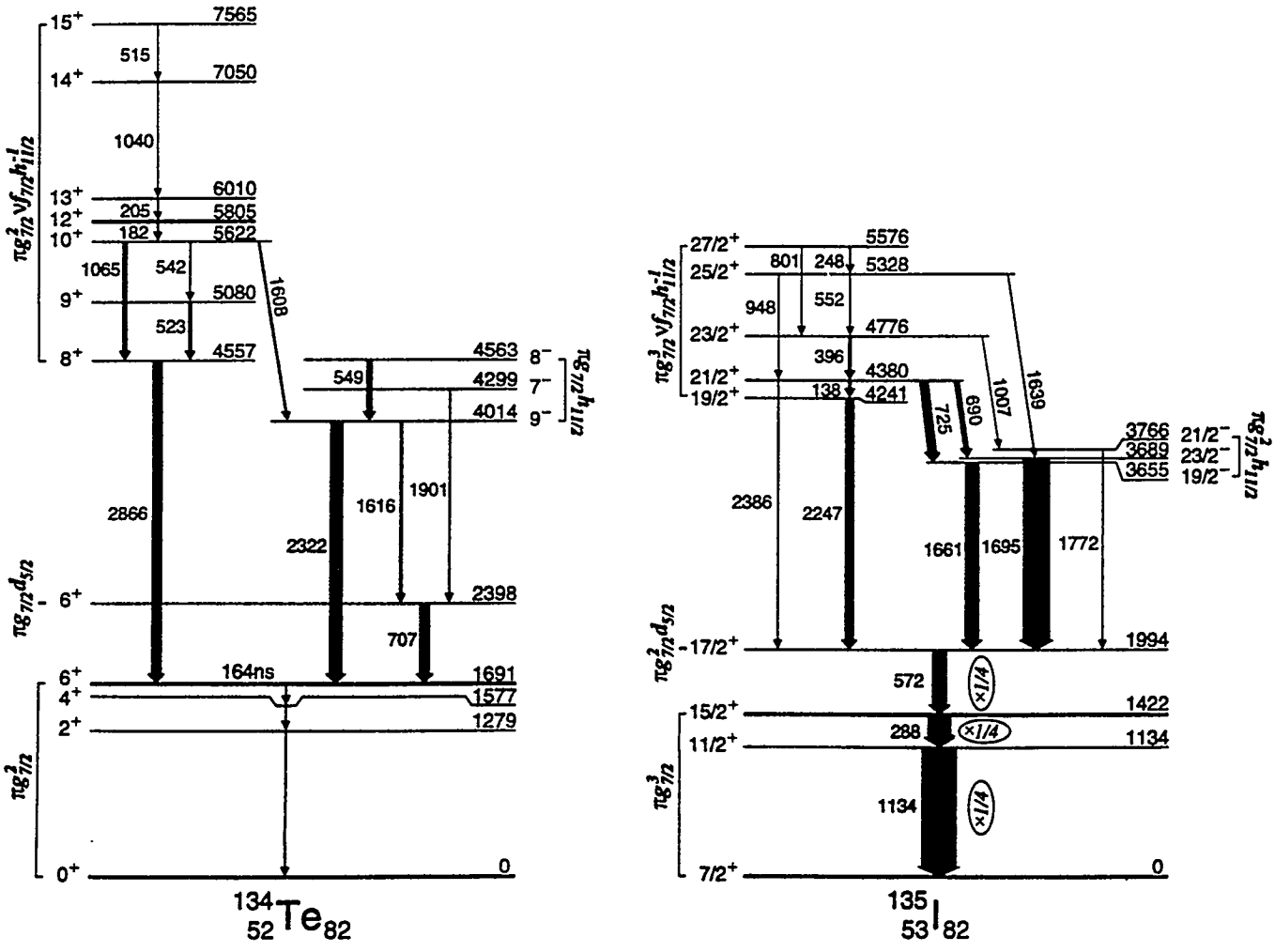


Fig. 1: Yrast level spectra established for $^{134}$Te and $^{135}$I, with assigned configurations.

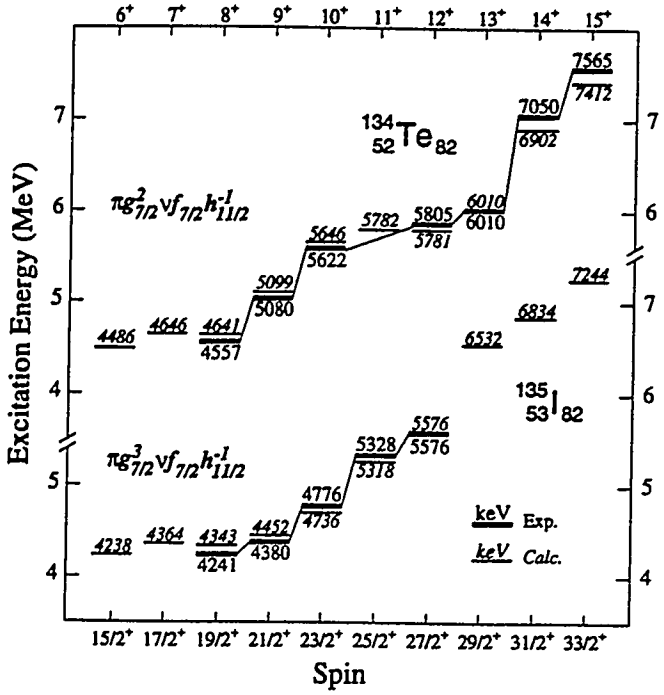


Fig. 2: A comparison of observed level energies in $^{134}$Te and $^{135}$I with those calculated for $\pi g_{7/2}{}^{n}\nu f_{7/2}h_{11/2}{}^{-1}$ yrast states and normalized to match the experimental $13^+$ 6010 keV level in $^{134}$Te and $27/2^+$ 5576 keV level in $^{135}$I.

The spin-parity assignments and the interpretation of the $^{135}$I levels below 4 MeV as $\pi g_{7/2}{}^3$, $\pi g_{7/2}{}^2 d_{5/2}$ and $\pi g_{7/2}{}^2 h_{11/2}$ states are based in part on the results of the shell model calculations. It is no surprise that the yrast excitations of $^{135}$I are found to resemble closely those of the other three-proton nucleus $^{211}$At, which has low-lying states of $\pi h_{9/2}{}^3$, $\pi h_{9/2}{}^2 f_{7/2}$, and $\pi h_{9/2}{}^2 i_{13/2}$ character. The energies of three-proton states in $^{135}$I were calculated with nucleon-nucleon interactions taken directly from the $^{134}$Te level spectrum (the few missing matrix elements could be estimated accurately). The results agree satisfactorily with experiment, although the agreement is not quite as good as similar calculations for $^{211}$At excitations based on two proton interactions from $^{210}$Po. However, we have found that in both $^{135}$I and $^{211}$At, the remaining discrepancies between calculated energies and experiment can be removed by allowing a moderate amount of configuration mixing. Since a high-lying ($\pi h_{11/2}{}^3$) $27/2^-$ state (close to 7 MeV) is the only expected three-proton excitation with $I>23/2$, the sequence of levels above 4241 keV in $^{135}$I must involve core excitations, and we naturally interpret them

as $\pi g_{7/2}^{3} \nu f_{7/2} h_{11/2}^{-1}$ states directly related to the core-excited states in $^{134}$Te above 4.5 MeV. Particle-hole states of $\nu f_{7/2} h_{11/2}^{-1}$ character having $I^{\pi}=2^{+}$ to $8^{+}$ are known [1] in $^{132}$Sn in the 4-5 MeV energy range; their energies (together with estimates for two missing multiplet members) provided some of the two-body interactions needed for calculating $\pi g_{7/2}^{n} \nu f_{7/2} h_{11/2}^{-1}$ states. In addition, $\pi g_{7/2} \nu h_{11/2}^{-1}$ and $\pi g_{7/2} \nu f_{7/2}$ interactions were also needed, but since $^{132}$Sb and $^{134}$Sb excitations are still poorly known, these matrix elements had to be estimated from the $\pi h_{9/2} \nu i_{13/2}^{-1}$ and $\pi h_{9/2} \nu g_{9/2}$ multiplets in $^{208}$Bi and $^{210}$Bi, respectively, with scaling as $A^{-1/3}$ to take account of nuclear size variation [2]. Calculations of $\pi g_{7/2}^{n} \nu f_{7/2} h_{11/2}^{-1}$ energies were performed using the OXBASH shell model code, with no adjustment of input parameters to fit the data. The results are displayed in Fig. 2 with the calculated energies normalized to 6010 keV for the $^{134}$Te $13^{+}$ level, and to 5576 keV for the $^{135}$I $27/2^{+}$ level. The excellent overall agreement with experiment in both cases provides persuasive support for the proposed interpretations. It is apparent that, while lower spin $\pi g_{7/2}^{n} \nu f_{7/2} h_{11/2}^{-1}$ levels are available in the two N=82 nuclei, they receive negligible population because the yrast $8^{+}$ and $19/2^{+}$ states both de-excite preferentially by favorable >2 MeV transitions.

The shell model calculations described above yielded relative excitation energies only, because the appropriate ground state nuclear masses were not included in the supplied input, for reasons that will become obvious. Mezilev et al. [4] recently revised the Audi-Wapstra 1993 masses [9] for nuclei around $^{132}$Sn by precision $\beta$-decay endpoint determinations; updated mass excesses for the N=82 isotones $^{132}$Sn, $^{133}$Sb, $^{134}$Te, and $^{135}$I are -76.620(29), -78.984(32), -82.399(34), and -83.787(23) MeV [4,9]. The present results enabled us to check the consistency of these N=82 mass values by shell model reduction techniques [10]. The aligned $\pi g_{7/2}^{3}$ $15/2^{+}$ state in $^{135}$I may be decomposed into simpler configurations with fewer valence particles, which correspond to known levels in $^{134}$Te ($4^{+}$, $6^{+}$), $^{133}$Sb ($7/2^{+}$) and $^{132}$Sn ($0^{+}$). As previously shown for similar decompositions [10,11], a mass "window" W, comprising a specific combination of N=82 ground state masses, can thus be related to experimental energies by the equation:

$$W = M(^{132}Sn) - 3M(^{133}Sb) + 3M(^{134}Te) - M(^{135}I) = E(15/2^{+}) - 3\ (c.f.p.)^{2}\ E(4^{+}, 6^{+}).$$

Here, the excitation energy $E(15/2^{+})$ in $^{135}$I is 1422 keV, and $E(4^{+}, 6^{+})$ are energies of $\pi g_{7/2}^{2}$ states in $^{134}$Te, weighted by appropriate coefficients of fractional parentage (c.f.p.). The result from spectroscopy is W = -3570 keV. This differs by almost 500 keV from the value

W = -3080(150) keV obtained directly from the N=82 masses given above. [In contrast, for the analogous mass window in the N=126 isotones, the W value from decomposition of the $^{211}$At $\pi h_{9/2}^3$ $21/2^-$ state agrees within 5 keV with the one computed from Audi-Wapstra masses]. We are forced to the conclusion that one or more of the accepted N=82 masses is inaccurate by considerably more than the estimated errors. The $^{134}$Te and/or $^{133}$Sb masses appear the most likely suspects since they are weighted heavily in the W expression: possibly the $\beta$-decay schemes adopted for these nuclei may not be entirely correct.

In summary, neutron-rich fission product nuclei around doubly magic $^{132}$Sn have now become accessible for detailed study by prompt $\gamma$-ray measurements using multidetector arrays. Yrast excitations to above 5.5 MeV excitation energy in the two- and three-proton nuclei $^{134}$Te and $^{135}$I have been established and interpreted with the help of precise shell model calculations using empirical nucleon-nucleon interactions. These results open possibilities for exploring simple excitation modes in the $^{132}$Sn region under conditions that are comparable with but not identical to those in the well-studied $^{208}$Pb region.

This work was supported by the U.S. Department of Energy under contract nos. DE-FG02-87ER40346 and W-31-109-ENG-38, by the Science and Engineering Council of the UK under grant no. GRH 71161, and by Polish Scientific Committee grant no. 1044-PO3-96-10. The authors are indebted for the use of $^{248}$Cm to the Office of Basic Energy Sciences, US Dept. of Energy through the transplutonium element production facilities at the Oak Ridge National Laboratory.

References

a) On leave from Institute of Nuclear Physics, PL-31342, Cracow, Poland
b) On leave from JAERI, Tokai, Ibaraki, 319-11 Japan

[1] B. Fogelberg et al., Physica Scripta T56, 79 (1995).
[2] J. Blomqvist, in Proc. 4th Int. Conf. on Nuclei Far From Stability, Helsingor, 1981 p. 536.
[3] G. A. Leander et al., Phys. Rev. C30, 416 (1984).
[4] K. A. Mezilev et al., Physica Scripta T56, 272 (1995).
[5] K. I. Erokhina and V. I. Isakov, Yad. Fiz. 59, 621 (1996).
[6] A. G. Smith et al., Phys. Rev. Lett. 73, 2540 (1994).
[7] J. P. Omtvedt et al., Phys. Rev. Lett. 75, 3090 (1995).
[8] M. Samri et al., Phys. A321, 255 (1985), and references therein.
[9] G. Audi and A. H. Wapstra, Nucl. Phys. A565, 1 (1993).
[10] e.g. J. Blomqvist, P. Kleinheinz and P. J. Daly, Z. Phys. A312, 27 (1983).
[11] R. H. Mayer et al., Phys. Lett. B336, 308 (1994).

# ROLE OF NUCLEAR COUPLINGS IN THE INELASTIC EXCITATION OF WEAKLY-BOUND NEUTRON-RICH NUCLEI

C.H. Dasso [a], S.M. Lenzi [b] and A. Vitturi [b]

The Niels Bohr Institute, Blegdamsvej 17, Copenhagen Ø, Denmark [a]
Dipartimento di Fisica and INFN, Università di Padova, Padova, Italy [b]

Much effort is presently devoted to the study of nuclear systems far from the stability line. Particular emphasis has been placed in light systems such as $^{11}$Li, $^{8}$B and others, where the very small binding energy of the last particles causes their density distribution to extend considerably outside of the remaining nuclear core. Some of the properties associated with this feature are expected to characterize also heavier systems in the vicinity of the proton or neutron drip lines.

Special relevance has been given to the – somewhat unexpected – appearance of a strong component in the multipole response of these systems for low-energy transitions into the continuum. This component seems to be comparable in magnitude to contributions arising from high-lying collective states. Evidence for the presence of this additional strength in the response function has been experimentally found [1] for example in the inelastic break-up of $^{11}$Li and $^{8}$B, and its occurrence has been afterwards confirmed by a number of theoretical calculations. The extent to which such a concentration of low-lying strength can be thought of as associated with a "state" of resonant or collective character has been a matter of long debate. Different prescriptions have been used to describe the reaction mechanism leading to the excitation of these low-lying, strongly-coupled states in the continuum and the consequences of their presence in other reactions regimes – such as fusion – have also been investigated. Still, the relative importance of nuclear and Coulomb contributions as well as the precise connection between inelastic transitions into the continuum and the break-up process remain to be fully clarified.

It is by now well established that low-lying concentrations of multipole strength arise from pure configurations in which a peculiar matching between the wavelength of the continuum wavefunction of the particles and the range of the weakly-bound hole states occurs [2–3]. An important element in arriving to this explanation is provided by the choice of a radial dependence of the multipole operator of the form $r^{\lambda}$, which favours large values of $r$. One should stress that the shapes of the multipole strength distributions will not be directly reflected in the energy dependence of inelastic cross sections observed in a heavy-ion induced reaction. And this is not only because of kinematical conditions governing the transitions (optimum $Q$-value effects) but also because the external fields

generated by the reaction partner may be characterized by different radial dependences. Thus, for example, it is not a priori clear whether the matching conditions that favour certain energies in the continuum in the case of the electromagnetic transition operator will also apply to the short-range nuclear interaction [4].

We have addressed these issues within the framework of a simple schematic model. To this end we consider the break-up of a weakly-bound system in a heavy-ion collision and focus our attention in the inelastic excitation of the low-lying part of the continuum. We make use of the fact that previous investigations [3] have shown that the multipole response in this region is not of a collective nature and describe our excited states as pure particle-hole configurations. Since the relevant parameter determining the strength distributions is the binding energy of the last bound orbital we find it most convenient to use single-particle wavefunctions generated by a spherical square-well potential with characteristic nuclear dimensions and whose depth has been adjusted to give rise to a situation in which the last occupied neutron orbital is loosely-bound. Spin-orbit couplings are, for our present purpose, ignored. These choices have the clear advantage of allowing the treatment of both bound single-particle wavefunctions and scattering states in terms of analytic functions.

We have modelled our system to be representative of the case of the excitation of a very neutron rich nucleus close to the drip-line. By choosing a square potential with a radius of 4 fm and a depth of 53 MeV forty neutrons fill all the states up to the last $2p$ orbital, which remains bound by only about one MeV. Thus, under this proposition, $^{60}$Ca turns out to be a system at the edge of the neutron separation zone. In the sequence of bound levels and resonances for the aforementioned potential, which can be found in ref. [2], one notes that the next-to-last filled level, $1f$, has a binding energy of about 8 MeV. Consequently, the continuum excitation spectrum up to this energy involves only particle-hole transitions from the weakly-bound $2p$ state. Furthermore, the first resonant state in the continuum is the sharp $1g$ state, which also lies at $E \approx 8$ MeV. Since the lowest possible resonant transition is the octupole $[2p^{-1}1g]$ configuration of about 9 MeV of excitation energy one can conclude that in our case all inelastic transitions to the low-energy part of the spectrum involve only continuum states of non-resonant character.

We can then proceed on to construct microscopically the formfactors associated with transitions into the continuum for all possible multipolarities. This is done by folding the corresponding transition densities with the nucleon-nucleus interaction generated by the target, which incorporates the Coulomb term and a Woods-Saxon-type nuclear component. In our model case microscopic formfactors have been constructed for the collision between a $^{60}$Ca projectile and a $^{40}$Ca target. As a first example we consider in fig. 1 the formfactor associated with the dipole transition from the weakly-bound state $2p$ to states of angular momentum two in the continuum ($2p$-$d_c$) [†]. The radial dependence of the matrix elements has been calculated for a fine mesh of the continuum energy $E$ covering the interval [0,10]

[†] Note that in the dipole case the inelastic formfactor incorporates a "Coulomb" component that

MeV, and is shown as a function of $r$ and $E$. The frames a) and b) show the formfactors obtained by including only either the Coulomb or the nuclear interaction, while in c) both contributions have been allowed to interfere. The presence of very large couplings at low values of the excitation energy becomes apparent in the three landscapes displayed in the figure. It is interesting to note, in addition, the rich structure of nodes that characterizes the nuclear component.

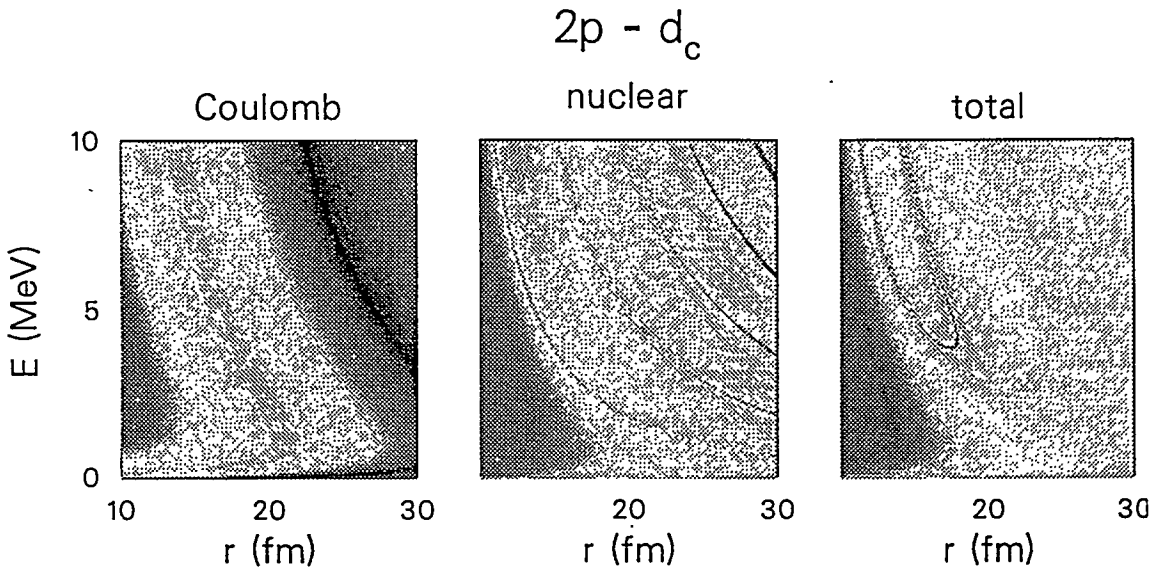


**Fig. 1** *Contour plot of the formfactor for the dipole transition from the 2p bound state to the continuum $d_c$ state, as a function of the ion-ion separation $r$ and of the continuum energy $E$. The frames a) and b) show the formfactors obtained by including only either the Coulomb or the nuclear interaction, while in c) both contributions have been allowed to interfere.*

The microscopic construction of the nuclear and Coulomb formfactors revealed a very unusual radial extension of the former. This feature may come as a surprise, given the fact that conventional wisdom localizes the nuclear interactions at the contact radii of the colliding ions. The explanation of this lies in the fact that we concern ourselves with nuclear formfactors for the excitation of particle-hole configurations which involve the last, loosely bound orbital. The corresponding transition densities (basically a product between the slowly decaying wavefunction of the bound orbital and unlocalized continuum wavefunctions) feel the presence of a reaction partner far before the bulk of the nuclear

---

reflects the neutron effective charge $e_{eff}=-eZ/A$ that accounts for recoil of the nuclear bulk. Such an effective charge is zero in leading order for $\lambda \geq 2$. Let us here note that we shall also neglect in leading order spurious center-of-mass motion corrections affecting nuclear couplings.

densities begin to overlap. As an example, Fig. 2a shows the radial dependence of the Coulomb and nuclear couplings for a fixed value of the energy in the continuum, $E$= 1.0 MeV. This corresponds roughly to the value of energy for which the relative maxima of the functions for the $2p$-$d_c$ case displayed in fig. 1 were found. The Coulomb formfactor assumes for large distances the expected long-range $1/r^2$ dependence. Note, however, that the nuclear formfactor extends also considerably beyond the potential radius. The unusual character of this feature becomes evident if one compares with the results obtained for a "standard" dipole transition, such as the excitation from the deeply-bound $1f$ state to the resonant $1g$ state, displayed in fig. 2b. In this case the nuclear formfactor exhibits the rapid fall-off characteristic of ordinary nuclear couplings.

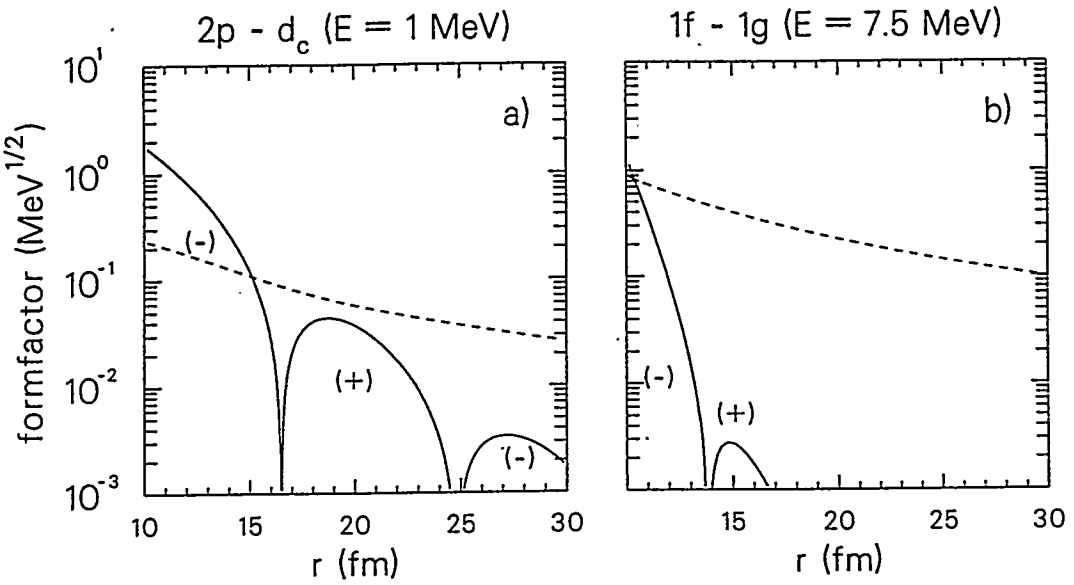


**Fig. 2** *Radial dependence of the formfactors at a fixed value of the energy E in the continuum. The frames refer to dipole transitions, with both nuclear (solid line) and Coulomb formfactor (dashed line) displayed. More precisely, fig. a) refers to a $2p$-$d_c$ transition (at a continuum energy E=1 MeV) and fig. b) to a $1f$-$1g$ transition (E=7.5 MeV).*

Reaction calculations employing the microscopic nuclear and Coulomb formfactors were performed within a semiclassical coupled-channel framework. Numerical results revealed the importance of the dynamical matching conditions that control the inelastic excitation processes. These limit the population of the continuum to the lowest energy range and yield Q-value distributions of cross sections that may differ in shape significantly from the original multipole distributions that identify the location and strength of the different reaction channels. If projectile break-up is triggered by the promotion of

the valence neutrons into the continuum one finds that the processes almost exclusively involve concentrations of strength at the positive-energy spectrum that are not of resonant character.

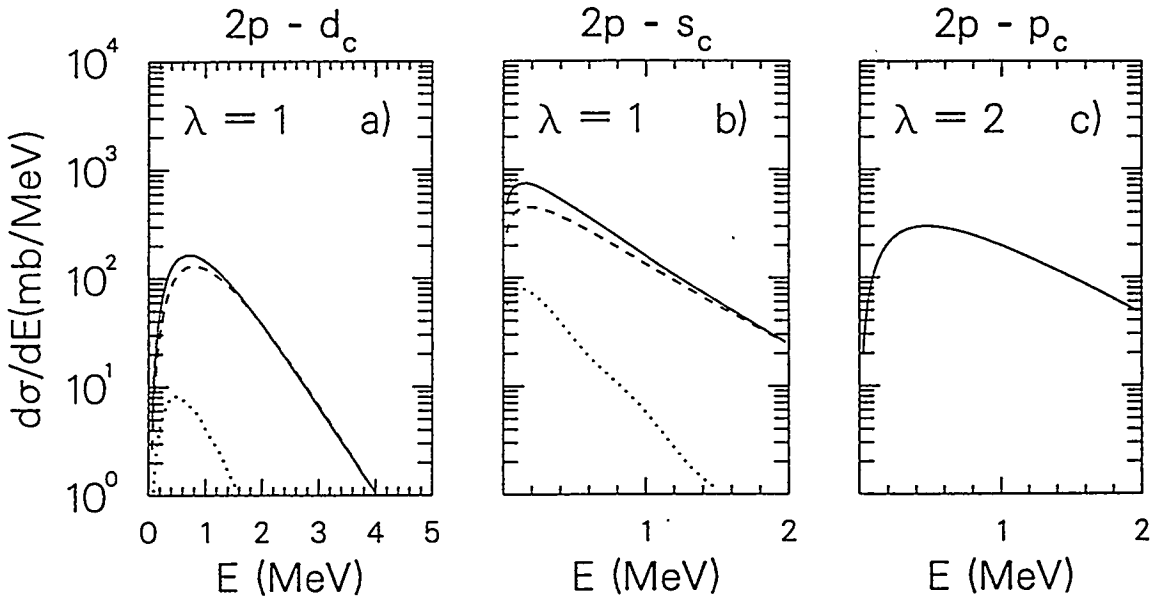


**Fig. 3** *Q-value distributions $d\sigma/dE$ for the reaction $^{60}Ca + ^{40}Ca$ as a function of the energy in the continuum. The three cases correspond to the dipole transitions $2p$-$d_c$ and $2p$-$s_c$ and to the quadrupole transition $2p$-$p_c$. The calculations correspond to a bombarding energy $E_{cm}$= 51 MeV, and separately gives the results obtained by only including the nuclear coupling (dashed lines) or the Coulomb coupling (dotted lines), together with the full results (solid lines).*

As a typical example, total (i.e. angle integrated) inelastic cross sections are displayed in fig. 3 for selected transitions to the continuum. All those shown in the figure involve a particle excitation from the weakly-bound $2p$ orbital. More precisely, the cases correspond to the dipole transitions $2p$-$d_c$ and $2p$-$s_c$ and to the quadrupole transition $2p$-$p_c$. The bombarding energy was set equal to $E_{cm}$= 51 MeV (approximately around the Coulomb barrier) and the figures show, separately, what is obtained by including only the nuclear or Coulomb couplings together with their combined results. One can immediately notice that the excitation functions are rather large and strongly peaked close to the continuum threshold, as expected from the energy dependence of the corresponding formfactors. Most of the inelastic excitation (and consequent break-up) will therefore be concentrated at low excitation energies. The kinematic $Q$-value conditions – that favour low excitation energies – have shifted the maxima of the distributions to even lower values than the corresponding ones in the formfactors. One can also see that for the dipole transitions, where both nuclear and Coulomb couplings are present, the nuclear one is predominant. This dominance of the nuclear inelastic excitation was found to survive even at energies

well below the barrier, where the excitation due to the long-ranged Coulomb interaction is normally by far dominating. Again this is a simple consequence of the unusual extension of the nuclear formfactors which characterizes this case.

To summarize, the results of our investigation clearly indicate that nuclear couplings have the predominant role in causing projectile dissociation in many circumstances, even at bombarding energies remarkably below the Coulomb barrier. It should be noted that nuclear couplings exploit rather evenly the different $\lambda$-transfer channels that are compatible with angular-momentum selection rules and thus one should avoid concentrating attention only on the dipole excitations. The results reported here also suggest that previous studies of break-up processes of weakly-bound nuclei based only on the action of the electric field should be critically reviewed.

## References


1. K. Ieki *et al*, Phys. Rev. Lett. **70** (1993) 730;
   D. Sackett *et al*, Phys. Rev. **C48** (1993) 118;
   F. Humbert *et al*, Phys. Lett. **B347** (1995) 198;
   T. Motobayashi *et al*, Phys. Rev. Lett. **73** (1994) 2680
2. F. Catara, C.H. Dasso and A. Vitturi, Nucl. Phys. **A602** (1996) 181
3. H. Sagawa, N. Van Giai, N. Takigawa, M. Ishihara and K. Yazaki, in Proc. Riken Int. Workshop 1993; H. Sagawa, N. Van Giai, N. Takigawa, M. Ishihara and K. Yazaki, Z. Phys. **A351** (1995) 385
   M. Yokoyama, T. Otsuka and N. Fukunishi, Phys. Rev. **C52** (1995) 1122; T. Otsuka, A. Muta, M. Yokoyama, N. Fukunishi and T. Suzuki, Nucl. Phys. **A588** (1995) 113c.
   I. Hamamoto, H. Sagawa and X.Z. Zhang, Phys. Rev. **C53** (1996) 765; I. Hamamoto and H. Sagawa, Phys. Rev. **C53** (1996) R1492; I. Hamamoto and H. Sagawa, Preprint Lund MPh 96/05 (April 1996).
   F. Ghielmetti, G. Colò, E. Vigezzi, P.F. Bortignon and R.A. Broglia, private communication, and to be published
4. R. Shyam, I.J. Thompson and A.K. Dutt-Mazumder, Phys. Lett. **B371** (1996) 1;
   F. Barranco, E. Vigezzi and R.A. Broglia, Phys. Lett. **B319** (1993) 387

# The Nuclear Structure of Neutron-Rich Isotopes with Z from 38-42

J.L.Durell, M.A.Jones, W.R.Phillips, A.G.Smith, W.Urban and B.J.Varley
Department of Physics and Astronomy, University of Manchester, M13 9PL, U.K
I.Ahmad, C.J.Lister, L.R.Morss, K.L.Nash and C.W.Williams
Argonne National Laboratory, Argonne, IL 60439, U.S.A
N.Schulz, A.Guessous, E.Lubkiewicz and M.Bentaleb
Centre de Recherches Nucléaires, IN2P3-CNRS, Université Louis Pasteur, 67037 Strasbourg, France

## Introduction

With the advent of $\gamma$-ray arrays containing many Ge detectors detailed studies of the spectroscopy of neutron-rich nuclei have been made possible [1-3]) through the observation of discrete, prompt $\gamma$ rays emitted following fission. Spontaneous fission has proved to be particularly productive and has enabled a wide range of isotopes far from stability to be observed. These prompt $\gamma$-ray investigations have complemented the experiments studying neutron-rich nuclei through the $\beta$ decay of fission products. A large body of data is now available in the Z=40-44 and 52-58 region of neutron-rich nuclides (corresponding to the peak yields of fragments) and a coherent picture of the variation of nuclear properties with Z and N is emerging in these parts of the chart of the nuclides.

In this report results from a study of the nuclei produced in the spontaneous fission of $^{248}$Cm will be presented. The present paper will concentrate on recent results on neutron-rich Sr, Zr and Mo nuclei with N=58-64. These isotopes are of particular interest because of the way their shapes change as a function of both proton and neutron number. The basic characteristics of these shape changes have been established for some time by $\beta$ decay studies of low-spin states. The new data on prompt $\gamma$ rays extend our knowledge of the behaviour of these nuclei quite considerably. The great sensitivity of Ge arrays has lead to the observation [4,5]) of non-yrast bands, providing more detailed information on nuclear structure; the large number of detectors and the geometry of the CLOVER detectors incorporated into EUROGAM II have allowed the measurement of angular correlations [6]) and linear polarisations, putting spin and parity assignments on to a firm footing; a further advance in the study of fission fragment spectroscopy is the determination [7,8]) of the lifetimes of yrast states by a new Doppler attenuation technique. These lifetime measurements give new information on the way nuclear shapes change as a function of rotational frequency.

## Experimental Details

The data discussed in this report were obtained using the EUROGAM II array in Strasbourg. The array consisted of 52 large Ge detectors in anti-Compton shields, including 24 four-crystal CLOVER detectors. In addition four LEPS detectors were incorporated into the

array, in order to observe X rays and low energy $\gamma$ rays with high resolution. The $^{248}$Cm spontaneous fission source comprised 5 mg of curium oxide mixed uniformly with KCl. The powder was then compressed into a pellet 0.5 mm thick and 5 mm in diameter. The KCl was used in order to reduce absorption of low energy photons, and to give a characteristic slowing down time for fission fragments of 1-2 ps. This slowing down time enabled Doppler attenuation effects to be observed and measured for $\gamma$ rays emitted from intermediate spin states. The geometry of the CLOVER detectors allowed them to be used as Compton polarimeters.

In total about 2.5 billion coincidence events were recorded of fold equal to or greater than three. In order to analyse the data various high dispersion (up to 3000 channels on each axis) 3-dimensional histograms were created, which could be gated interactively in any direction. The primary tool used to create level schemes was a $\gamma\gamma\gamma$ cube containing $2\text{x}10^{10}$ triple-$\gamma$ events. This was assisted by the use of a triples cube in which events from the LEPS detectors formed one of the axes. Having determined partial decay schemes it is important to establish, where possible, the spins and parities of the states involved. To this end special cubes were constructed to enable triple gamma correlations in the form of DCO ratios to be measured. Also double correlations were used, where, in addition to conventional double correlations, a third, uncorrelated $\gamma$ ray was included to allow for isotope selection. Finally, the particular properties of the CLOVER detectors were used to extract linear polarisations from direction-polarisation correlations. Details of the analysis techniques used to extract spins and parities are given in ref. [6]).

As mentioned above, the source was constructed in such a way as to allow the determination of nuclear lifetimes. In the fission process yrast states are fed either by fast, statistical $\gamma$ rays from the entry point populated after the emission of neutrons, or by the yrast state above. This means that $\gamma$-ray lines from yrast states with lifetimes of around 1 ps will exhibit Doppler broadening. In the circumstances of the present experiment, states which are members of a rotational band with spins in the range J=8 to 12 have lifetimes which can be measured. Because the fission fragments are emitted with equal probability in all directions, the $\gamma$-ray lineshapes are symmetrical. These lineshapes are fitted using a development [7]) of the standard DSAM method. An example is shown in Fig 1. This spectrum was obtained using quadruples data, using the 2-0 and 4-2 transitions to select the nucleus, and by then gating above the levels of interest.

### The Axially Symmetric Rotors: Sr and Zr Isotopes

A well-established feature of neutron-rich nuclei in the A=100 region is the sudden onset of deformation in strontium and zirconium isotopes at the neutron number N=60. While the low-lying states of $^{96}$Sr and $^{98}$Zr with N=58 show features of spherical nuclei, the isotopes having only two more neutrons are strongly-deformed, axially-symmetric rotors with deformations of $0.35 \leq \beta_2 \leq 0.40$, as determined from the lifetimes of low-lying states. The extension of the ground-state bands in Sr and Zr isotopes by Hotchkis et al. [1]) provided further evidence for the "good" rotational character of these neutron-rich nuclei. We have now measured [8]) the lifetimes of higher-lying members of the ground-state bands of $^{98}$Sr and $^{100,102,104}$Zr, in order to investigate the stability of the deformation with rotation. The

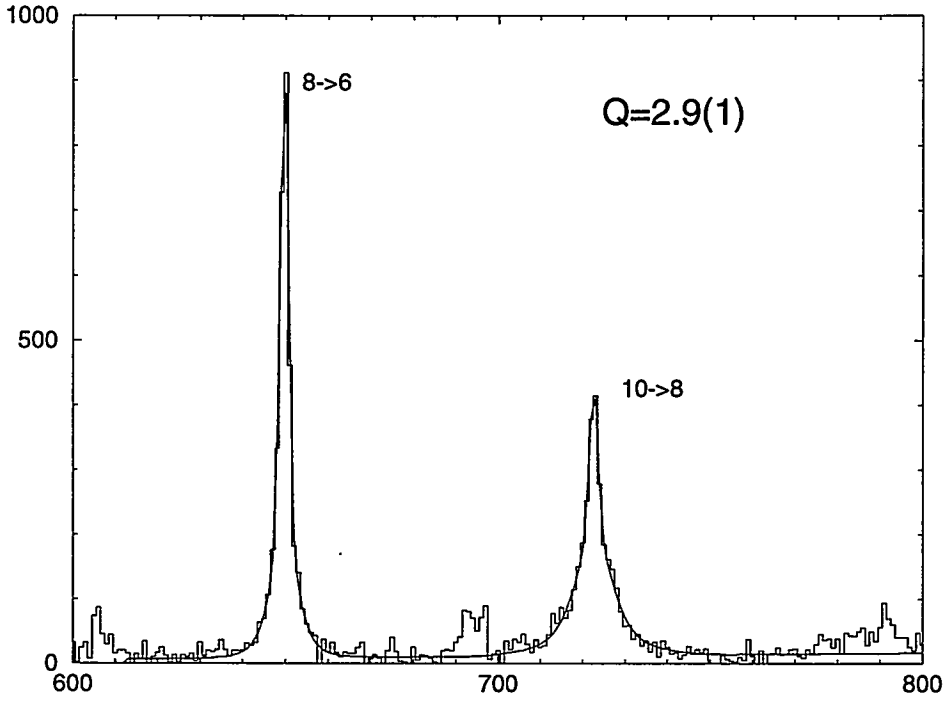


Figure 1: Example of $\gamma$ ray lineshapes. The spectrum is of yrast transitions in $^{112}$Ru, 8 neutrons from the heaviest stable isotope. The solid line shows the fit to the data using a quadrupole moment of 2.9 eb.

measured lifetimes have been transformed into quadrupole moments within a rotational model description. The present results, which correspond to a fit to the lineshapes of $\gamma$ rays from the decay of the J=8,10 and 12 members of the ground-state bands, are given in the final column of the table below. The column Raman [9]) shows the values of the quadrupole moment derived from the lifetimes of $2^+$ states; that labelled Moller [10]) shows theoretical predictions of ground-state moments. The units are eb.

| Nucleus | Raman | Moller | Present |
|---|---|---|---|
| $^{98}$Sr | 3.12(18) | 3.14 | 3.17(20) |
| $^{100}$Zr | 3.01(19) | 3.36 | 3.19(10) |
| $^{102}$Zr | 4.01(40) | 3.51 | 3.52(17) |
| $^{104}$Zr | | 3.68 | 3.72(16) |

It can be seen that the new data strongly suggest that the shape of these well-deformed nuclei does not change with angular momentum, at least up to spin $12\hbar$. This is consistent with theoretical expectations from calculations of Total Routhian Surfaces (TRS) [8]).

The sharp transition in the ground-state shape from N=58 to 60 is now recognised as being due to the crossing in energy of the "spherical" configuration that lies lower in the isotopes

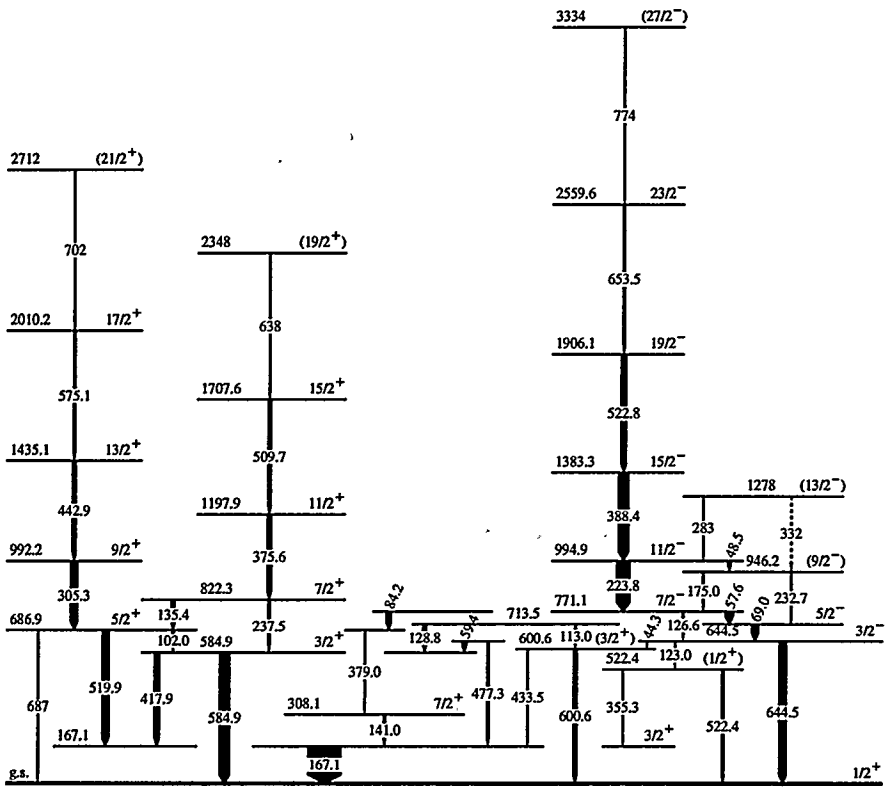


$^{97}$Sr

Figure 2: Partial level scheme of $^{97}$Sr.

near the stability line and the "deformed" configuration that becomes the ground state at N=60. One should therefore expect that in the transition region both configurations will coexist. It is clearly of interest to see whether it is possible to follow the behaviour of the two separate configurations as a function of neutron number. We have used our present data to search for and identify rotational structures in the N=58 nuclei $^{96}$Sr, $^{98}$Zr and the N=59 nuclei $^{97}$Sr, $^{99}$Zr, and to measure the lifetimes within these bands in order to determine their deformation. One example of a level scheme determined in the present work is shown in Fig 2, where that for $^{97}$Sr is shown. It can be seen that rotational-like bands appear at around 700 - 800 keV in excitation. The quadrupole moments of the bands based upon the $\frac{5}{2}^+$ level at 686.9 keV and the $\frac{7}{2}^-$ level at 771.1 keV have been extracted from measurements of the lifetimes of the high-lying members of these two bands. The moments have been determined to be 3.05(15) eb and 2.80(15) eb for the positive and negative bands respectively. Similar measurements have been made on the other N=58,59 isotopes of interest. By combining our measurements with previously published data [11–14]) we arrive

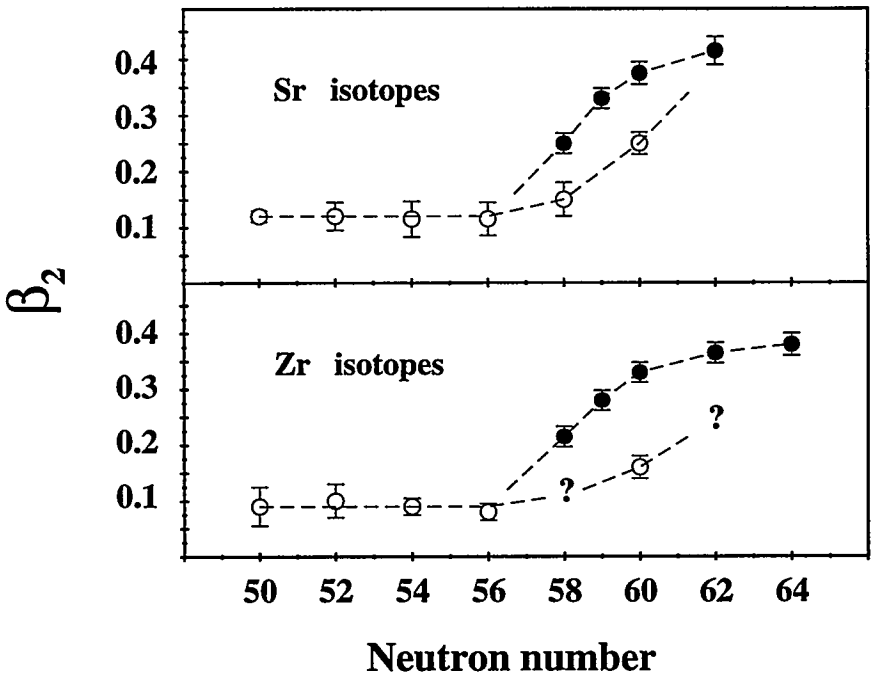


Figure 3: The deformation parameters in Sr and Zr isotopes (see text).

at the deformation parameters for the "spherical" and "deformed" configurations shown in Fig 3. The filled circles correspond to $\beta_2$ values derived from present lifetime measurements for deformed states; open circles represent $\beta_2$ values for the coexisting "spherical" structures [11–14]); and question marks indicate unknown values of $\beta_2$. Fig 3 shows clearly the evolution of the deformation of the two coexisting configurations. Further analysis is required to investigate the possible mixing between the two structures in the transition region.

### The $\gamma$ Soft Isotopes of Mo

We have observed [4]) in $^{106}$Mo perhaps the best example of a harmonic two-phonon $\gamma$-vibrational band. The band-head level lies 500 keV below the pairing gap, avoiding problems with two quasi-particle bands; and the observed branching ratios are in excellent agreement with model predictions. The existence of such a configuration is consistent with TRS calculations [8]) which show a minimum in the potential energy surface of Mo isotopes that is soft in the $\gamma$ degree of freedom. These same TRS calculations predict that, as the nuclei rotate, the yrast states take on a triaxial shape, due to the alignment of $h_{\frac{11}{2}}$ neutrons.

The role of the $\gamma$ degree of freedom in the Mo isotopes is of interest, because the Ru isotopes exhibit [15]) characteristics of rigid triaxiality. Thus the transition from axial symmetry in the Sr and Zr isotopes to rigid triaxiality in Ru, via the $\gamma$ soft Mo isotopes needs further investigation. One consequence of the predicted shape change with rotation in the yrast states of the Mo isotopes would be a change in the quadrupole moment as one moves up the band. This should be in sharp contrast to the constancy of the quadrupole moment in the ground-state bands of Sr and Zr nuclei discussed above.

We have measured [8]) the lifetimes of the J=8 to 12 yrast states in $^{102-108}$Mo and extracted quadrupole moments within a rotational model prescription to compare them to the moments determined for the J=2 states. The results are summarised below:

| Nucleus | Raman | Moller | Present |
|---|---|---|---|
| $^{102}$Mo | 3.26(19) | 3.29 | 2.44(17) |
| $^{104}$Mo | 3.29(13) | 3.54 | 2.84(14) |
| $^{106}$Mo | 3.62(10) | 3.70 | 2.85(13) |
| $^{108}$Mo | 3.68(42) | 3.46 | 2.79(20) |

It can be seen from these results, in contrast to the previous table, that a consistent reduction of 20% in the quadrupole moments of the intermediate spin states in the Mo isotopes is observed. This reduction is entirely in agreement with the theoretical predictions and indicates that there is a change in shape towards a positive non-zero value of $\gamma$ as the nuclei rotate.

## Summary

A brief summary has been presented of some of our results from the study of prompt $\gamma$ rays from the spontaneous fission of $^{248}$Cm. The report has attempted to illustrate the advances that are being made in our understanding of the nuclear structure of neutron-rich isotopes, using the power of modern $\gamma$-ray arrays. The most significant advance has been in the measurement of lifetimes, since, to achieve this, high statistics triple and quadruple coincidence data are required. It will be interesting to see what further advances can be made with the next generation of arrays.

## References


[1]) M A C Hotchkis et al., Nucl Phys A530 (1991) 111
[2]) I Ahmad and W R Phillips, Rep Prog in Phys 58 (1995) 1415
[3]) J H Hamilton et al., Prog Nucl Part Phys 35 (1995) 635
[4]) A Guessous et al., Phys Rev Lett 75 (1995) 2280
[5]) J L Durell et al., Phys Rev C52 (1995) R2306
[6]) W Urban et al., Nucl Instr Meth A365 (1995) 596
[7]) A G Smith et al., Phys Rev Lett 73 (1994) 2540
[8]) A G Smith et al., Phys Rev Lett, to be published
[9]) S Raman et al., At Dat Nucl Data Tables 36 (1987) 1
[10]) P Moller et al., At Dat Nucl Data Tables 59 (1995) 1
[11]) F K Wohn et al., Nucl Phys A507 (1990) 141c
[12]) H Mach et al., Nucl Phys A523 (1991) 197
[13]) F Schussler et al., Nucl Phys A339 (1980) 415
[14]) H Mach et al., Phys Lett B230 (1989) 21
[15]) J A Shannon et al., Phys Lett B336 (1994) 136

# Spectroscopy Of Reflection-Asymmetric Nuclei Using Multinucleon Transfer Reactions

J.F.C.Cocks[1], P.A.Butler[1], K.J.Cann[1], P.T.Greenlees[1], G.D.Jones[1], R.Broda[3], B.Fornal[3], P.M.Jones[2], R.Julin[2], S.Juutinen[2], D.Müller[2], M.Piiparinen[2], A.Savelius[2], J.F.Smith[6], I.Ahmad[4], S. Asztalos[5], P.Bhattacharyya[7], D.J.Blumenthal[4], M.P.Carpenter[4], R.M.Clark[5], B.Crowell[4], M.A.Delaplanque[5], R.M.Diamond[5], P.Fallon[5], R.V.F.Janssens[4], T.L.Khoo[4], T.Lauritsen[4], I.Y.Lee[5], A.O.Macchiavelli[5], R.W.MacLeod[5], D.Nisius[4], F.S.Stephens[5], C.T.Zhang[7]

*(1) Oliver Lodge Laboratory, University of Liverpool, Liverpool. L69 3BX U.K.*

*(2) Accelerator Laboratory, University of Jyväskylä, FIN-40351, Jyväskylä, Finland*

*(3) Institute of Nuclear Physics, Radzikowskiego 152, PL-31-342, Kraków, Poland*

*(4) Physics Division, Argonne National Laboratory, Argonne, IL 60439, USA*

*(5) Lawrence Berkeley Laboratory, 1 Cyclotron Road, Berkeley, California 94720, USA*

*(6) State University of New York, Stony Brook, New York, NY11794-3800, USA*

*(7) Chemistry Department, Purdue University, West Lafayette, Indiana 47907, USA*

**Abstract**

The heavy-ion collisions of $^{56}$Fe + $^{232}$Th, $^{86}$Kr + $^{232}$Th and $^{136}$Xe + $^{232}$Th with beam energies 15-20% above the Coulomb barrier were used to populate nuclei in the light-actinide region. Yield distributions of the binary reaction products stopped in thick targets were obtained by measuring $\gamma$-$\gamma$ coincidence intensities. The $^{136}$Xe + $^{232}$Th reaction was repeated at Lawrence Berkeley National Laboratory using a recent implementation of the GAMMASPHERE array. Many interesting discoveries concerning the high-spin structure of octupole-deformed light-actinide nuclei have been made.

Nuclei with Z$\simeq$88 and N$\simeq$134 have their neutron and proton Fermi levels in close proximity to the octupole-driving $\nu(j_{15/2}$ and $g_{9/2})$ and $\pi(i_{13/2}$ and $f_{7/2})$ orbitals. Thus these light-actinide nuclei are susceptible to octupole deformation [1], [2]. Nuclei in this region can be studied using fusion-evaporation reactions but low production cross-sections ($\leq$millibarns) and large fission cross-sections [3] make these nuclei difficult to study by these means. This

| Reaction | Target ($mg/cm^2$) | Beam | | | Germanium Detector Array | Facility |
|---|---|---|---|---|---|---|
| | | Species | Energy (MeV) | %above CB | | |
| I | $^{232}$Th (30) | $^{56}$Fe | 362 | 20 | 12 TESSA-type (23% efficiency) detectors | K-130 cyclotron, JYFL, Jyväskylä |
| II | $^{232}$Th (30) | $^{86}$Kr | 511 | 16 | TESSA3 frame: 12 detectors + 50-element multiplicity filter | K-130 cyclotron, JYFL, Jyväskylä |
| III | $^{232}$Th (40) | $^{136}$Xe | 830 | 15 | Argonne–Notre Dame: 12 25%-efficiency detectors + 50-element BGO ball | ATLAS, Argonne National Laboratory |

Table 1: Summary of experimental details. The Coulomb barrier energy is defined as $E_{CB} = \frac{1.44(\frac{A_p}{A_t}+1)Z_pZ_t}{1.16(A_p^{1/3}+A_t^{1/3}+2)}$ where $A_p$, $Z_p$, $A_t$ and $Z_t$ are the mass and proton numbers of the projectile and target respectively.

population mechanism is limited further by a lack of suitable projectiles and stable targets above $^{209}$Bi. Virtually no information exists concerning the excited states in $^{222}$Ra and the octupole-deformed Rn isotopes with A $\geq$ 218. We have used multinucleon transfer reactions to populate this region of nuclei. Three experiments were carried out in which thick $^{232}$Th targets were bombarded by different heavy ions at energies between 15% and 20 % above the Coulomb barrier. The details of these experiments are summarised in Table 1.

For each system, measurements of the yield of the populated nuclei were produced using quantitative in-beam and out-of-beam $\gamma$-$\gamma$ coincidence analyses, where the intensities were corrected for efficiency and internal conversion [4]. Figure 1 shows the target-like product yields for the reactions $^{56}$Fe + $^{232}$Th, $^{86}$Kr + $^{232}$Th and $^{136}$Xe + $^{232}$Th. The yields were normalised by matching the yield of the Coulomb-excited $2^+$ state in $^{232}$Th. The least neutron-rich of the projectiles, $^{56}$Fe, picks up most neutrons from the target and shifts the distribution of heavy products into the region which is already accessible by compound-nucleus reactions. The $^{86}$Kr and $^{136}$Xe projectiles populate the region which cannot be accessed by presently-

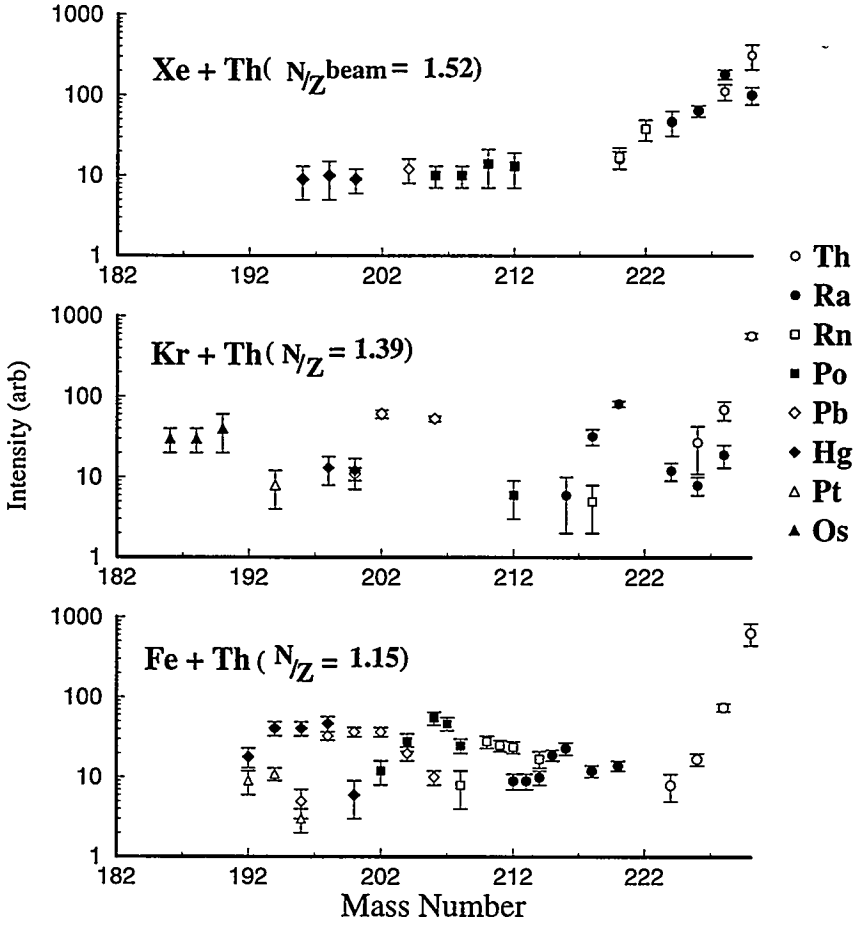


Figure 1: A comparison of the yields of target-like nuclei produced in the $^{56}$Fe + $^{232}$Th, $^{86}$Kr + $^{232}$Th and $^{136}$Xe + $^{232}$Th reactions.

available fusion-evaporation reactions. The $^{136}$Xe projectile, with the largest neutron-to-proton ratio, populates octupole-deformed Rn and Ra isotopes in the light-actinide region with the greatest intensity.

The $^{136}$Xe + $^{232}$Th reaction was repeated at Lawrence Berkeley National Laboratory using the high-efficiency GAMMASPHERE array. The array consisted of 73 large-volume (~75% relative efficiency) Compton-suppressed germanium detectors [5], [6], 27 of which were segmented [7]. After 54 hours of collecting gamma-ray events of fold 3 or higher, subsequent unpacking of events revealed a total of 1.1 $\times$ $10^{10}$ triple and 6.7 $\times$ $10^{9}$ fourfold Compton-suppressed gamma-ray coincidences. The typical spectra shown in figure 2 serve to illustrate the quality of these data. Figure 2(a) is a threefold gamma-ray spectrum which shows transitions in $^{218}$Rn. The spectrum was produced by double-gating on transitions in the ground state rotational band in $^{218}$Rn in a $\gamma$-$\gamma$-$\gamma$-correlation matrix. Figure 2(b) is a fourfold spectrum showing transitions in $^{224}$Ra. This spectrum was produced by double-gating on transitions in the ground state rotational band in $^{224}$Ra in a gated $\gamma$-$\gamma$-$\gamma$-correlation matrix. The initial

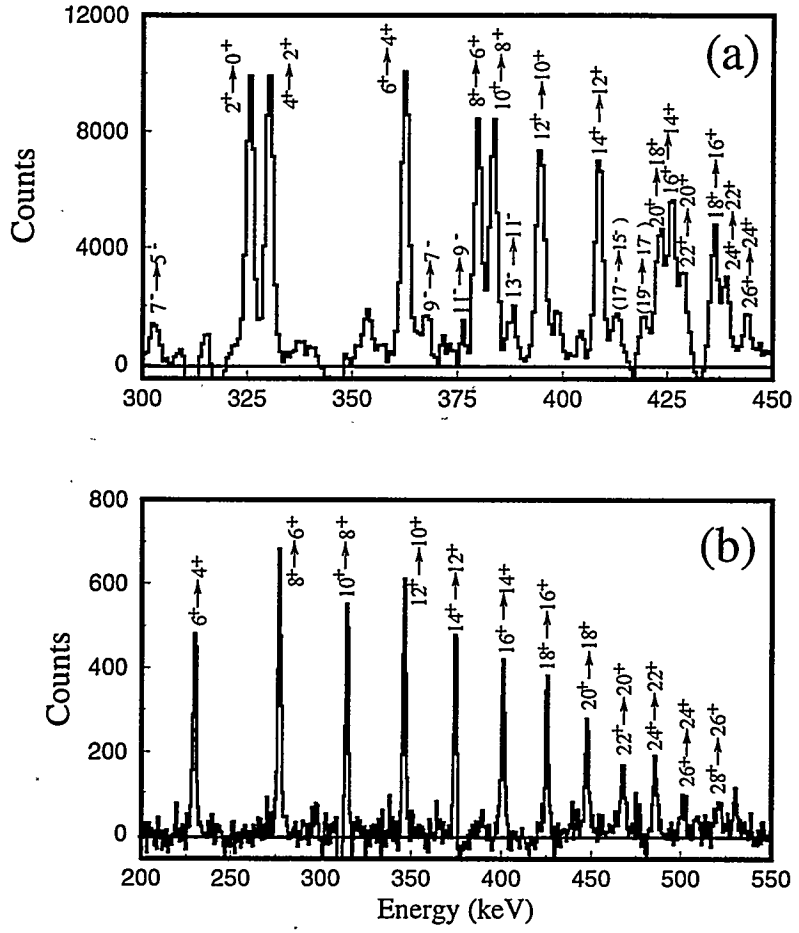


Figure 2: (a) Threefold gamma-ray spectrum showing transitions in $^{218}$Rn. (b) Gamma-ray spectrum showing transitions above and including the $6^+$ to $4^+$ transition in $^{224}$Ra. This spectrum is from unpacked fourfold coincidence events where one of the gamma rays has the same energy as the $4^+$ to $2^+$ transition in $^{224}$Ra.

gate was set on the $4^+$ to $2^+$ transition in $^{224}$Ra.

High-spin states in many light-actinide nuclei have been observed. The level schemes of $^{218}$Rn, $^{220}$Rn and $^{222}$Rn are shown in figure 3. Previous to the present work, only the 5 lowest-lying states in each nucleus were known [8], [9]. In the present work, alignment effects for the positive parity states in $^{218}$Rn and $^{220}$Rn have been observed at $\hbar\omega \approx 0.22$ MeV. Cranked shell model calculations predict a strong alignment of a pair $i_{13/2}$ protons close to this rotational frequency in these two nuclei.

The level schemes of $^{222}$Ra, $^{224}$Ra and $^{226}$Ra are shown in figure 4. Previous knowledge of these nuclei can be found in references [10], [11], [12] and [13]. The level schemes of $^{222}$Ra, $^{224}$Ra and $^{226}$Ra have been considerably extended in the present work and interleaving positive- and negative-parity states have been observed for the first time in $^{222}$Ra.

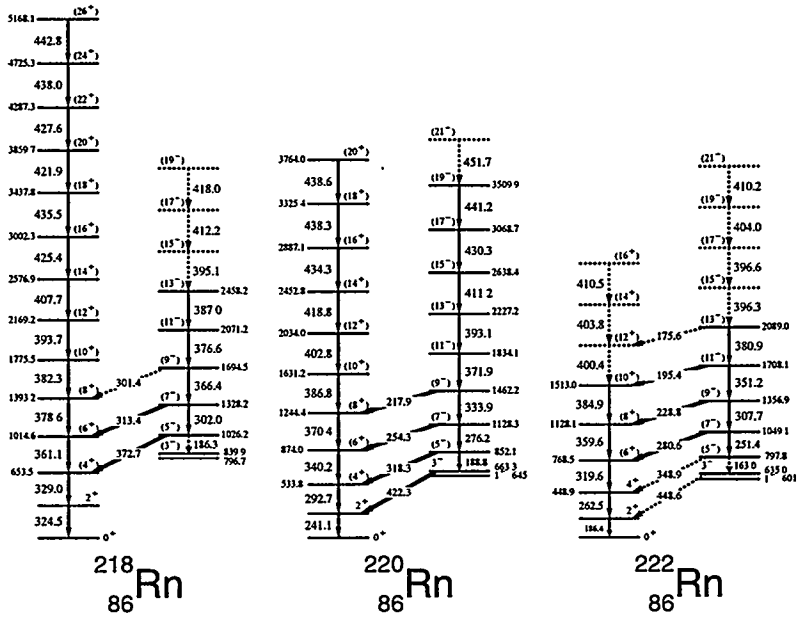


Figure 3: Level scheme of $^{218}$Rn, $^{220}$Rn and $^{222}$Rn, produced using energy sums and intensity balance arguments. The transition energies have errors which range from 0.2 keV for low-lying transitions in the positive parity bands to 0.5 keV for $5^-$ to $3^-$ and $7^-$ to $5^-$ transitions and transitions between the highest spin states observed.

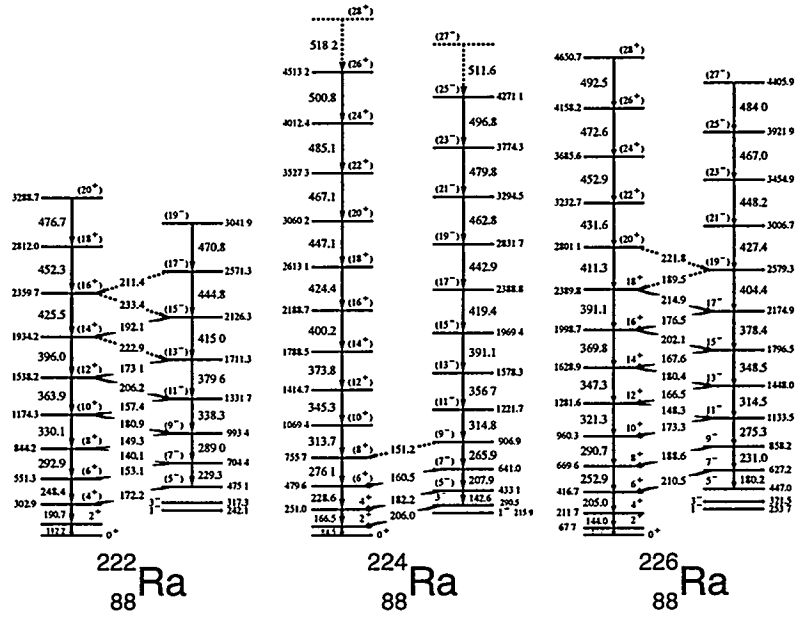


Figure 4: Level scheme of $^{222}$Ra, $^{224}$Ra and $^{226}$Ra, produced using energy sums and intensity balance arguments. The transition energies have errors which range from 0.2 keV for low-lying transitions in the positive parity bands to 0.5 keV for $5^-$ to $3^-$ and $7^-$ to $5^-$ transitions and transitions between the highest spin states observed.

For each state that is depopulated by both E1 and E2 transitions in the six nuclei, intrinsic electric dipole-to-quadrupole ($\frac{D_0}{Q_0}$) ratios were extracted from $\frac{B(E1)}{B(E2)}$ branching ratios. Upper limits were obtained for high-spin states in $^{224}$Ra. The $\frac{D_0}{Q_0}$ values were constant within each nucleus. Using weighted mean values of $\frac{D_0}{Q_0}$ and published values of $Q_0$ [14], a measure of the intrinsic electric dipole moment, $D_0$, was determined for the Rn and Ra isotopes. The intrinsic electric dipole moment measured for $^{224}$Ra, 0.030(1) e.fm, is much lower than those for $^{222}$Ra, 0.27(4) e.fm, and $^{226}$Ra, 0.18(2) e.fm. The anomalously low dipole moment in $^{224}$Ra persists to high spins (<0.09 in the spin range I=12-23$\hbar$). At low spin, the calculations of Butler and Nazarewicz [15] reproduced an anomalously low $D_0$ for $^{224}$Ra by treating the intrinsic electric dipole moment as the sum of a macroscopic (liquid drop) component and a microscopic (shell correction) term. These two components cancel for $^{224}$Ra but the addition of the two contributions results in large intrinsic electric dipole moments for $^{222}$Ra and $^{226}$Ra. Good agreement between the experimental and theoretical $D_0$ values for the Rn isotopes was observed.

## References


[1] P. A. Butler and W. Nazarewicz, Rev. Mod. Phys. **68** (1996).

[2] I. Ahmad and P. A. Butler, Ann. Rev. Nucl. Part. Sci **43**, 71 (1993).

[3] J. F. Smith *et al*, Phys. Rev. Lett. **75**, 1050 (1995).

[4] J. F. C. Cocks *et al*, submitted to Phys. Rev C.

[5] A. M. Baxter *et al*, NIM **A317**, 101 (1992).

[6] M. P. Carpenter *et al*, NIM **A353**, 243 (1994).

[7] A. O. Macchiavelli *et al*, Proceedings of Conference on Physics From Large $\gamma$-ray Detector Arrays, Lawrence Berkeley National Laboratory, August 2-6 1994, Volume 2 p.149

[8] R. J. Poynter *et al*, J. Phys. G. **15**, 449 (1989).

[9] W. Kurcewicz *et al*, Nucl. Phys. **A270**, 175 (1976).

[10] E. Ruchowska *et al*, J. Phys. G. **18**, 131 (1992).

[11] R. J. Poynter *et al*, Phys. Lett. **232B**, 447 (1989).

[12] M. Marten-Tölle *et al*, Z. Phys. **A336**, 27 (1990).

[13] H. J. Wollersheim *et al*, Nucl. Phys. **A556**, 261 (1993).

[14] S. Raman *et al*, At. Data Nucl. Data Tables **36**, 1 (1987).

[15] P. A. Butler and W. Nazarewicz, Nucl. Phys. **A533**, 249 (1991)

# Deformation in the neutron rich sulfur isotopes $^{40}$S and $^{42}$S

T. Glasmacher[1], H. Scheit[1], B.A. Brown[1], P.D. Cottle[3], M. Hellström[4], R. Ibbotson[1], J.K. Jewell[3], K.W. Kemper[3], D.J. Morrissey[2], M. Steiner[1], P. Thirolf[1]*, and M. Thoennessen[1]

[1]National Superconducting Cyclotron Laboratory and Department of Physics and Astronomy, Michigan State University, East Lansing, Michigan 48824
[2]National Superconducting Cyclotron Laboratory and Department of Chemistry, Michigan State University, East Lansing, Michigan 48824
[3]Department of Physics, Florida State University, Tallahassee, Florida 32306
[4]Gesellschaft für Schwerionenforschung, D-64291 Darmstadt, Germany

For many years Coulomb excitation has been used to study low lying states in stable nuclei. In these experiments the incident beam energy was chosen to be below the Coulomb barrier to avoid excitations of the nuclei by the strong interaction. Stable enriched targets were bombarded with a heavy beam which excites low lying states in the target through exchange of a virtual photon. A real photon is emitted when the nucleus deexcites and can be detected in a high resolution photon detector. Alternatively, a particle beam of interest can impinge on and be stopped in a heavy target. In this case the emitted photon will be Doppler shifted and Doppler broadened; however due to the generally slow beam velocity these effects are small. In the case of exotic nuclei far from the valley of $\beta$-stability and with short lifetimes, the fabrication of targets is not possible. Instead, one can produce radioactive beams of high isotopic purity with energies of several tens of MeV/A and bombard a heavy target. The projectile is excited in the Coulomb and strong fields of the target and deexcites from a bound state by emission of a discrete photon, thus establishing the existence and energy of this state. In the energy region of several tens of MeV/A the Coulomb excitation cross section can be much larger than the nuclear excitation cross section for small scattering angles. In cases where the nuclear excitation cross section is negligible (at forward angles) it is not only possible to measure the excitation energy of a state, but also absolute cross section measurements of photon yields allow the determination of transition matrix elements. For example, the $2^+$ state of the neutron-rich nucleus $^{32}$Mg has recently been studied using a beam of $^{32}$Mg at 50 MeV/A and a $^{208}$Pb target at RIKEN [1]. The only other published intermediate energy Coulomb excitation experiment was a study of helium and beryllium isotopes at GANIL [2].

The A1200 fragment separator at the NSCL [3] provides many different beams of exotic nuclei, at energies of several tens of MeV/nucleon. We have constructed and tested a high efficiency photon spectrometer which is matched to these beam energies. With our detector we can identify and measure the excitation energies of bound states in even-even nuclei far from the valley of $\beta$-stability with secondary beam rates of as low as 10 particles/second.

*Current address: Ludwig Maximilians Universität München, D-85748 Garching, Germany.

The typical secondary beam rates in this experiment were 1000-20000 particles/second, well above the minimum sensitivity.

The array consists of 42 position sensitive cylindrical NaI(Tl) detectors, each of which is read out by two phototubes, one at each end. The energies and interaction points of the incident photons can be reconstructed from the two photomultiplier tube signals. The measured scattering angle of the photon is used to correct for its Doppler shift, and thus to reduce the considerable Doppler broadening of the photopeak. (Typical beam velocities are $\beta = 0.3$). The NaI(Tl) crystals are 18 cm long and 5.75 cm in diameter and are arranged in three concentric rings around a 6 inch diameter beamline. The crystals were previously used in a PET imaging machine at Washington University in St. Louis. To shield the array from room background photons and to provide an environment with stable temperature, the detector array is shielded on each side by a 16.5 cm thick wall of low background lead. Figure 1 shows front and side views of the detector array, the support table, and the lead shielding.

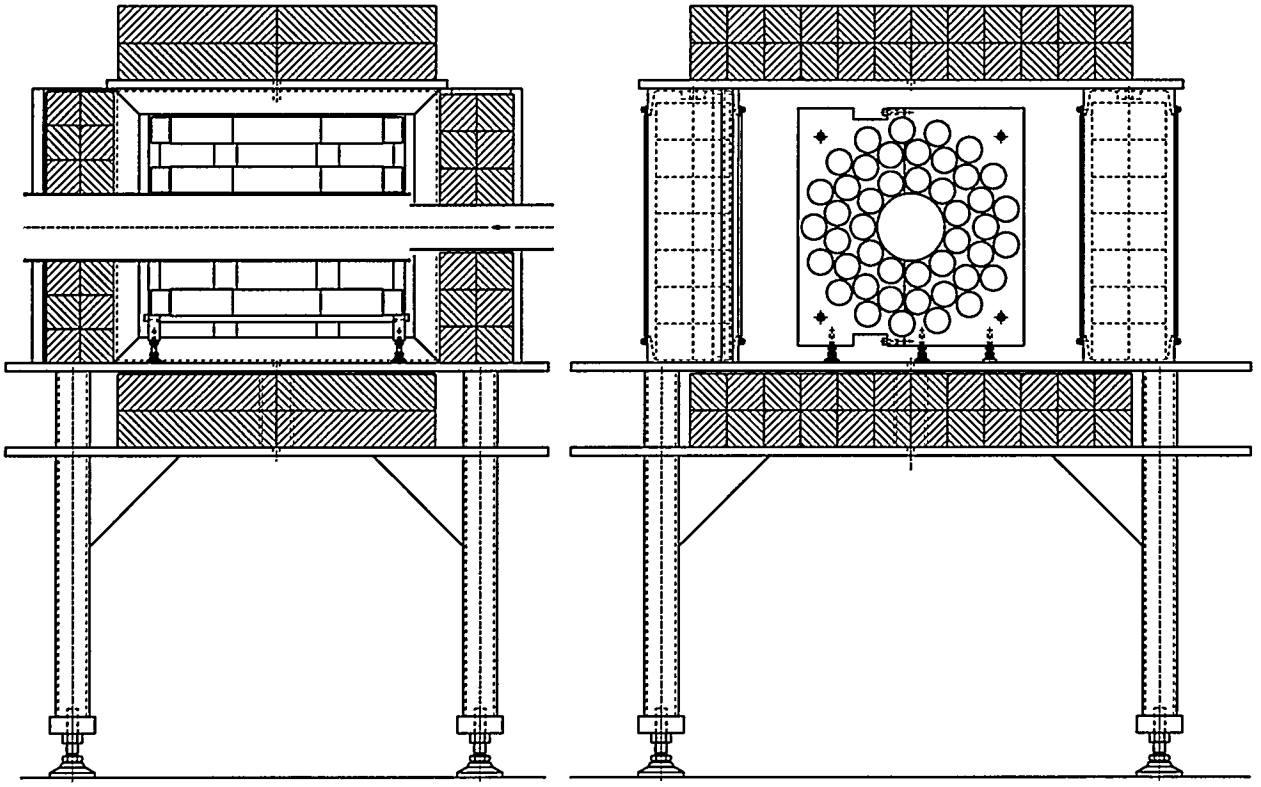

Figure 1: Mechanical setup of the NaI(Tl) detector array, the support structure and the lead shielding (hatched). In the left figure the beam moves from the right to the left, while the figure on the right is looking in direction of the beam.

In the experiment described here radioactive beams of $^{40,42}$S and $^{44,46}$Ar ($E \approx 40$ MeV/nucl.) were produced in the A1200 fragment separator at the National Superconducting Cyclotron Laboratory at Michigan State University by fragmenting an 80 MeV/nucleon $^{48}Ca^{13+}$ beam in a 379 mg/cm$^2$ $^9$Be target. The exotic ions were positively identified by a time of flight measurement before interacting with the secondary gold target (93.5 mg/cm$^2$ or 184.1 mg/cm$^2$).

After interacting with the virtual photon field in the gold target, fragments scattered into a lab angle of less than 4.1° were detected in a fast/slow plastic phoswich detector located downstream from the secondary target. The energy loss – total energy measurement allowed the rejection of events which led to the breakup of the projectile in the target. Photons from the deexcitation of the projectile were measured in coincidence with beam particles. The photons emitted from the excited projectile can be clearly distinguished from photons coming from the target by their Doppler shift and Doppler broadening. In figure 2 we show the energy of the detected photons in the laboratory frame (upper panels) and in the projectile frame (lower panels). In the laboratory frame the line corresponding to the $(7/2^+ \rightarrow g.s.)$ transition in $^{197}$Au is clearly visible, while the photons corresponding to the transition in the neutron rich sulfur and argon isotopes are Doppler shifted and do not form a peak. Only after transforming the energies into the projectile frame does the photopeak become visible. The energies of the peaks corresponding to the first excited states in $^{40,42}$S and $^{44,46}$Ar as measured in this experiment are $891 \pm 13$ keV, $890 \pm 15$ keV, $1144 \pm 17$ keV, and $1554 \pm 26$ keV, respectively.

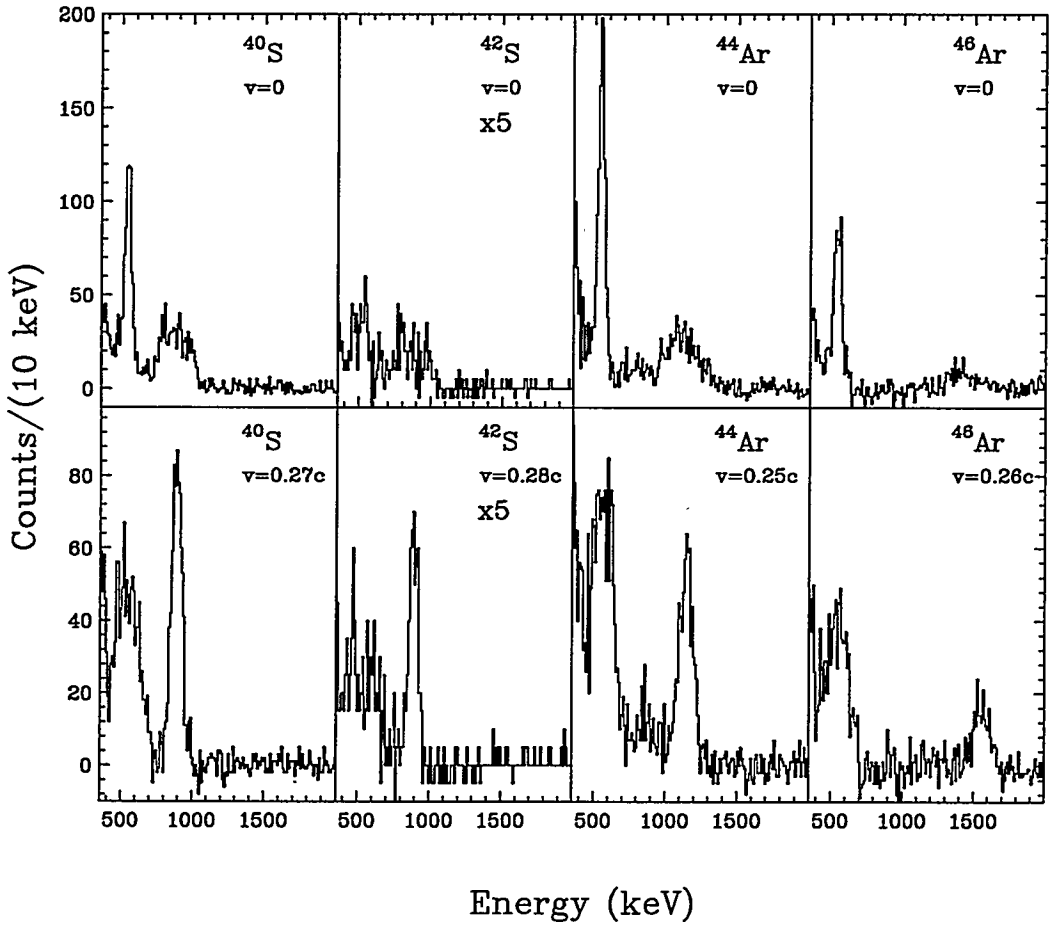


Figure 2: Observed photon energies without Doppler correction (top panel). The 547 keV $(7/2^+ \rightarrow g.s.)$ transition in the gold target is visible and the $(2^+ \rightarrow 0^+)$ transitions in the sulfur and argon isotopes are very broad. After shifting the data into the projectile frame (bottom panel) the photopeak of the transitions in the beam particles become visible and the gold peak broadens.

Shell model calculations in a model space in which the protons occupy the $0d_{5/2}$, $0d_{3/2}$ and $1s_{1/2}$ ($sd$) orbitals and the neutrons occupy the $0f_{7/2}$ and $1p_{3/2}$ orbitals with the Wildenthal $sd$-shell interaction [4], the recent FPD6 $pf$-shell interaction [5] and the WBMB $sd-pf$ cross-shell interactions [6] can well reproduce the experimentally observed energy levels. As shown in Figure 3, the shell model calculations successfully reproduce the behavior of $E(2^+)$ in all even-even $N \geq 20$ isotopes of sulfur, argon and calcium. In addition the calculations predict that the $2_1^+$ state of the $N = 28$ isotope $^{44}$S is located at 1.7 MeV, which, if measured experimentally, would indicate a spherical structure and the persistence of the $N = 28$ major shell gap. The energies of the first excited states in $^{40,42}$S are almost as low as the first excited states in the isotones $^{48,50}$Cr (752 keV and 783 keV, respectively). The chromium isotopes are strongly deformed ($\beta_2 = 0.34$ and $\beta_2 = 0.29$, respectively) [7]. A preliminary analysis of the Coulomb excitation cross section measured in this experiment indicates similarly large deformations for the sulfur isotopes $^{40,42}$S.

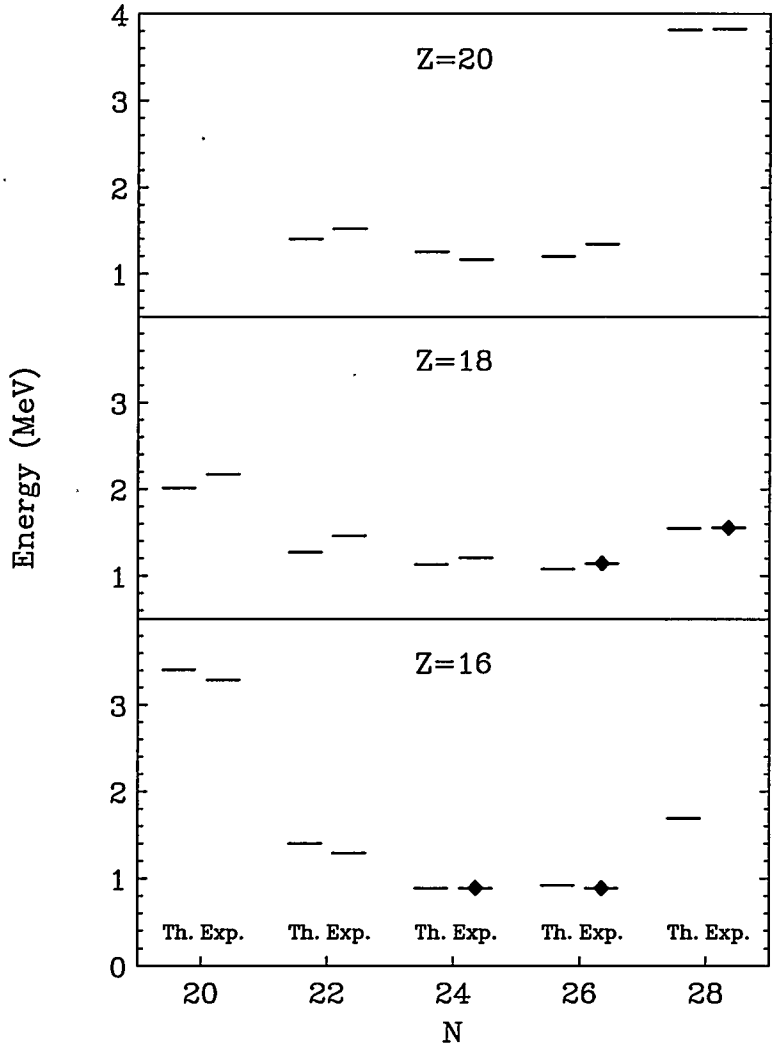


Figure 3: Comparison between measured excitation energies (right) and shell model calculations described in the text (left) for different calcium ($Z = 20$), argon ($Z = 18$) and sulfur ($Z = 16$) isotopes. The excitation energies measured in the experiment described here are indicated by diamonds.

We thank Professor Lee Sobotka, who salvaged the NaI(Tl) detectors and made them available to us. M. H. acknowledges the support of the Alexander von-Humboldt Foundation. This work was supported by the National Science Foundation under Grant Nos. PHY-9528844, PHY-9523974 and PHY-9403666.

# References

[1] T. Motobayashi *et al.*, Phys. Lett. B **346**, 9 (1995).

[2] R. Anne *et al.*, Z. Phys. A **352**, 397 (1995).

[3] B.M. Sherrill *et al.*, Nucl. Instr. Methods **B56**, 1106 (1991).

[4] B.A. Brown and B.H. Wildenthal, Ann. Rev. Nucl. Sci. **38**, 29 (1988).

[5] W.A. Richter *et al.*, Nucl. Phys. **A523**, 325 (1991).

[6] E.K. Warburton, J.A. Becker and B.A. Brown, Phys. Rev. C**41**, 1147 (1990).

[7] S. Raman *et al.*, At. Data Nucl. Data Tables **36**, 1 (1987).

# Identical Gamma-Vibrational Bands in $^{165}$Ho.

D.C. Radford[a], A. Galindo-Uribarri[a], V.P. Janzen[a], D. Ward[a], S. Flibotte[b], S.M. Mullins[b†], J.C. Waddington[b], M. Cromaz[c], J. DeGraaf[c] and T.E. Drake[c]

[a]AECL, Chalk River Laboratories, Chalk River, ON K0J 1J0, Canada
[b]Department of Physics and Astronomy, McMaster University, Hamilton, ON L8S 4M1, Canada
[c]Department of Physics, University of Toronto, Toronto, ON M5S 1A7, Canada
[†]Present address: Department of Nuclear Physics, ANU, RSPhysSE, Canberra, ACT 0200, Australia

## Abstract

The structure of $^{165}$Ho at moderate spins has been investigated by means of Coulomb excitation. Two $\gamma$-vibrational bands ($K^\pi = \frac{11}{2}^-$ and $K^\pi = \frac{3}{2}^-$) are observed, with very nearly identical in-band $\gamma$-ray energies. Gamma-ray branching ratios are analysed to extract information on Coriolis mixing, and the role of the K quantum number in identical bands is discussed.

## 1. Introduction

The recent discovery of "identical" (isospectral) superdeformed bands between neighbouring isotopes and isotones [1,2] has lead to a great deal of interest in isospectral bands, both superdeformed and normally deformed. Models have been proposed to explain how these pairs of bands can arise, based on such concepts as pseudospin symmetry [2,3]; complete understanding of the origins of such bands has however proved elusive.

If simpler cases of isospectral bands, such as identical bands in the same nucleus, can be found and understood, this may perhaps assist in obtaining theoretical understanding of the more complex case of identical bands in neighbouring nuclei. One candidate for such a pair of bands is the case of collective $\gamma$-vibrational bands built on the rotational ground state band of odd nuclei.

## 2. Experiment and analysis

The structure of $^{165}$Ho at moderate spins has been investigated by means of Coulomb excitation with 5.4 MeV/u $^{209}$Bi ions from the TASCC facility at Chalk River. Gamma-gamma coincidences were detected in the $8\pi$ spectrometer, composed of 20 Compton-suppressed HPGe detectors around a 71-element BGO ball. Two separate experiments were performed. In the first one, a thick Ho target was used, and 1.6 million $\gamma$-$\gamma$ events were collected with at least 2 HPGe detectors and 3 elements of the BGO ball in coincidence. The target for the second experiment consisted of 2 mg/cm$^2$ of Ho on a thick gold backing in order to stop the recoiling Ho ions more rapidly. Over 2 million $\gamma$-$\gamma$ events were collected in this

experiment, with the same required conditions. No Doppler-shift corrections were applied to the data from either experiment. The reduced stopping time in the gold-backed target allowed observation of typically one to two more transitions at the top of each band.

It should be noted that the beam energy used here is above what would normally be considered "safe" for Coulomb excitation experiments, *i.e.* nuclear excitations and transfer may not be excluded. No attempt has been made to extract absolute transition quadrupole moments, *etc.*; rather, Coulomb excitation has been used simply as a means of populating the states to be studied.

The data were replayed into two-dimensional matrices, and analysed using the code escl8r [4]. Excellent sensitivity was obtained from the use of $\gamma$-$\gamma$ coincidences; cascades of intensity less than 0.1% of the total intensity are easily observable.

## 3. Results and discussion

The level scheme deduced from the present work is shown in figure 1. In addition to the $\frac{7}{2}^-[523]$ ground band, two $\gamma$-vibrational bands are populated. These bands have $K^\pi = \frac{11}{2}^-$ and $K^\pi = \frac{3}{2}^-$, arising from the parallel and anti-parallel alignment of the $K = 2$ $\gamma$ vibration with the ground band. They are observed to spins of $(\frac{37}{2})$ and $(\frac{33}{2})$, respectively; in previous experiments [5] they were identified to spins of $(\frac{15}{2})$ and $(\frac{13}{2})$. Figure 2 shows gated spectra for these two bands, together with the total projection. Also observed to higher spins than in previous experiments are the $\frac{3}{2}^+[411]$ and $\frac{1}{2}^+[411]$ bands. Two new structures are shown in figure 1, and appear to form a coupled band with large signature splitting; no structural assignment has yet been made for these bands. The ground state band and $K = \frac{11}{2}$ band have also been studied recently by the Rochester group [6].

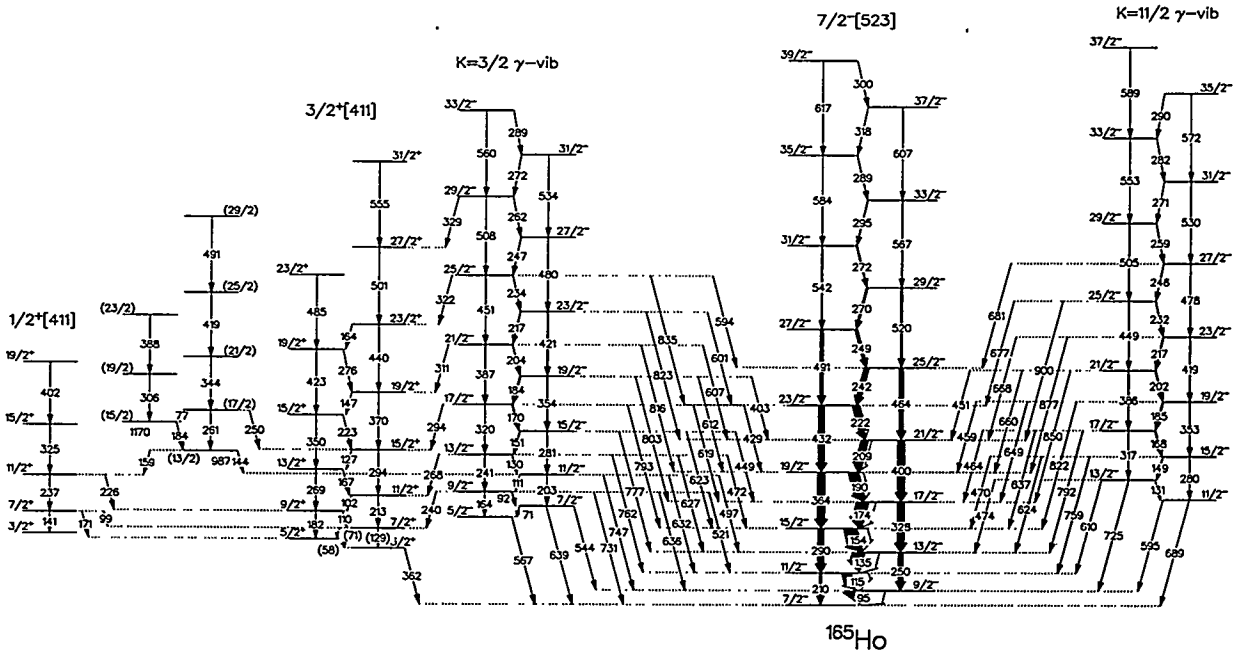


Figure 1: Partial level scheme of $^{165}$Ho, as observed in the present work.

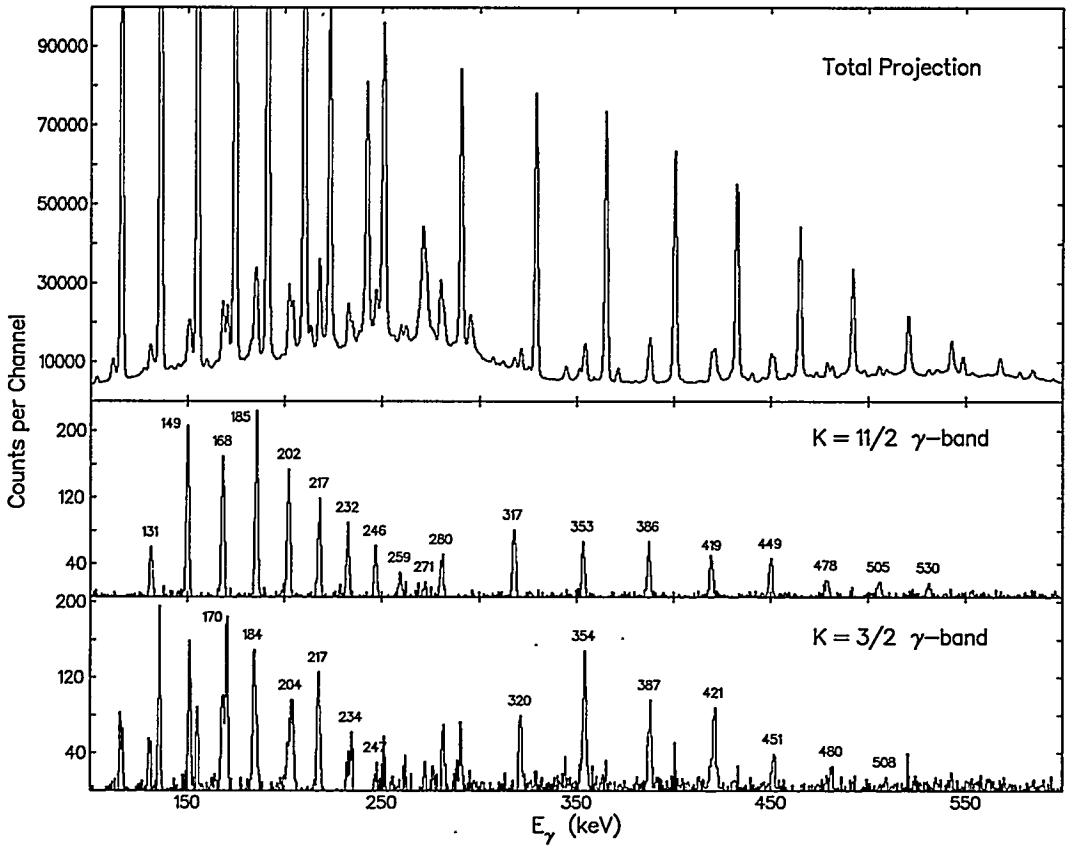


Figure 2: Spectra gated on transitions from the $K = \frac{3}{2}$ and $K = \frac{11}{2}$ $\gamma$-vibrational bands, together with the total projection spectrum, from the experiment with the gold-backed target.

Many transitions are observed from the decay of the $\gamma$ bands to the ground band; for $K = \frac{3}{2} \rightarrow K = \frac{7}{2}$ we observe transitions with $J \rightarrow J+1, J \rightarrow J$ and $J \rightarrow J-1$, while for $K = \frac{11}{2} \rightarrow K = \frac{7}{2}$ we observe $J \rightarrow J, J \rightarrow J-1$ and $J \rightarrow J-2$.

If these transitions were between pure-$K$ states, any M1 admixture would be forbidden by the $\Delta K \leq \lambda$ selection rule. If we assume that the transitions are indeed pure E2, then we can use the observed branching ratios to calculate B(E2;$K \rightarrow K \pm 2$)/B(E2; $K \rightarrow K$) ratios. The results of such a calculation, using preliminary values of the branching ratios, show a range of ratios that cover three orders of magnitude. If we extract ratios of transition quadrupole moments from these B(E2) ratios, we can also make a (modified) Mikhailov plot of

$$\frac{Q_T(K \rightarrow K \pm 2)}{Q_T(K \rightarrow K)} = \sqrt{\frac{B(E2; K \rightarrow K \pm 2)}{B(E2; K \rightarrow K)}} \frac{< J_i \;\; K \;\; 2 \;\; 0 \mid (J_i - 2) \;\; K >}{< J_i \;\; K \;\; 2 \;\; \pm 2 \mid J_f \;\; K \pm 2 >}$$

*versus* $J_f(J_f+1) - J_i(J_i+1)$, as shown in figure 3.

In a Mikhailov plot [7], the value of the slope provides a measure of the strength of the Coriolis mixing. M. Matsuzaki, Y. Shimizu and T. Nakatsukasa have recently performed calculations [8,9] using the cranked shell model with RPA and adding a particle-vibration coupling. They extract matrix elements for the E2 strengths from the $\gamma$ bands to the ground

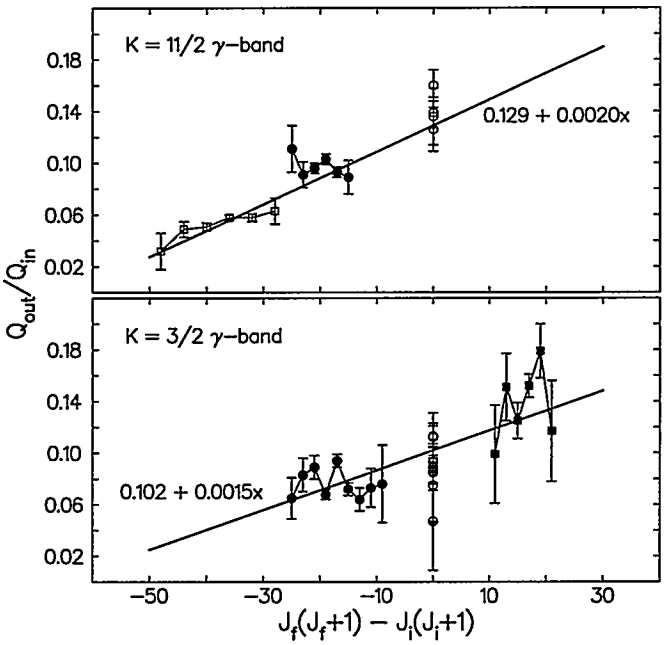


Figure 3: Mikhailov plot of observed ratios of transition quadrupole moments for the two $\gamma$ bands. The solid lines are least-squares fits to the experimental data, where $x = J_f(J_f+1) - J_i(J_i+1)$.

band. The results are listed together with the experimental numbers in table 1, where the nomenclature

$$Q_T(K \to K) = Q_0$$

and

$$Q_T(K \to K \pm 2) = Q_a + Q_b[J_f(J_f+1) - J_i(J_i+1)]$$

is used. The agreement between the calculated and observed ratios is excellent.

**Table 1**

Ratios of spin-independent and spin-dependent components of the transition quadrupole moments in $^{165}$Ho.

| | Experiment | Theory [8,9] |
|---|---|---|
| $Q_a/Q_0; K = \frac{11}{2}$ | 0.13 | 0.17 |
| $Q_b/Q_0; K = \frac{11}{2}$ | 0.0020 | 0.0021 |
| $Q_a/Q_0; K = \frac{3}{2}$ | 0.10 | 0.17 |
| $Q_b/Q_0; K = \frac{3}{2}$ | 0.0015 | 0.0025 |

One striking aspect of the data is that these two $\gamma$-vibrational bands are isospectral, *i.e.*, have very nearly identical $\gamma$-ray energies for the in-band transitions originating from states of the same spin. A plot of the incremental alignment [3] between the two bands is shown

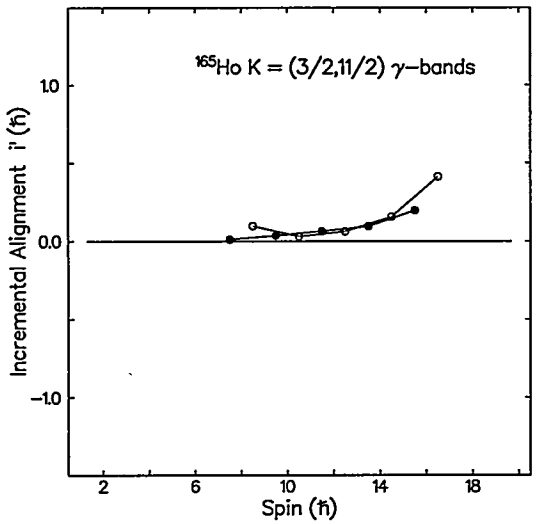


Figure 4: Incremental alignment between the two $\gamma$-vibration bands in $^{165}$Ho.

in figure 4; values are less than 0.1 $\hbar$ below spin 29/2, at which point the bands appear to enter a backbending region.

These isospectral bands arise through a simple recoupling of the collective and single-particle degrees of freedom, rather than through the addition or removal of nucleons. The recoupling changes the direction of the total angular momentum vector, and thus the value of $K$. In a one-dimensional cranking model [10], the different $K$-values result in very different rotational frequencies, and thus alignments, for the two bands; see for example figure 5. The recoupling of the vibration, however, should not change its alignment, and thus in such a model it is very difficult to understand how the two bands could be isospectral.

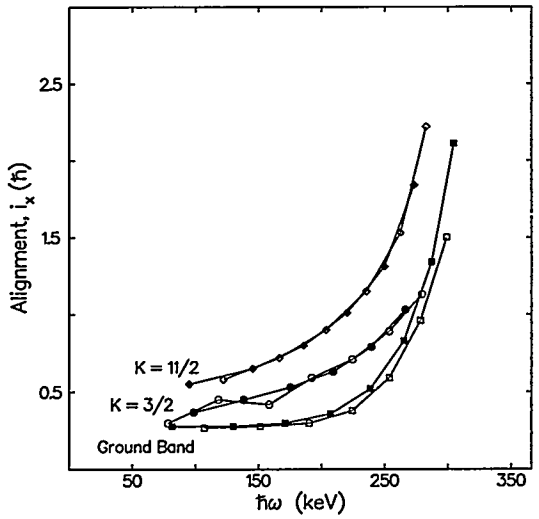


Figure 5: Alignments of the two $\gamma$ bands, extracted from the data using the normal cranked shell model methodology, and subtracting a reference with Harris parameters $J_0 = 44.5$ MeV$^{-1}\hbar^2$ and $J_1 = 110$ MeV$^{-3}\hbar^4$.

In a tilted-axis or three-dimensional cranking model [11], the rotational frequency is simply defined as one-half of the the in-band E2 transition energy, and is thus identical for isospectral bands. This clearly allows a better explanation of the observed results. Nevertheless, an intuitive semiclassical picture would have the deformed nucleus exhibiting different moments of inertia as it rotates about different axes. Thus it appears that these bands show a striking example of strong coupling, where the moment of inertia is unaffected by the vibrational coupling, *i.e.*, is independent of the value of the $K$ quantum number.

## References


1. Th. Byrski *et al.*, Phys. Rev. Lett **64** (1990) 1650
2. W. Nazarewicz, P.J. Twin, P. Fallon and J.D. Garrett, Phys. Rev. Lett **64** (1990) 1654
3. F.S. Stephens *et al.*, Phys. Rev. Lett **65** (1990) 301
4. D.C. Radford, Nucl. Instr. and Meth. **A361** (1995) 297
5. R.M. Diamond, B. Elbek and F.S. Stephens, Nucl. Phys. **43** (1963) 560;
   G.G. Seaman, E.M. Bernstein and J.M. Palms, Phys. Rev. **161** (1967) 1223
6. M.W. Simon, D. Cline, M. Devlin, R Ibbotson and C.Y. Wu, Proc. of Conf. on Physics from Large Gamma-ray Det. Arrays, Berkeley CA, 1994, Vol. 1, p. 114
7. V.M. Mikhailov, Izv. Akad. Nauk. USSR, Ser. Fiz. **30** (1966) 1334;
   B.R. Mottelson, Proc. Int. Conf. on Nucl. Str., Tokyo, 1967, p. 87
8. M. Matsuzaki and Y.R. Shimizu, private communication
9. Y.R Shimizu and T. Nakatsukasa, Nucl. Phys. **A**, in press
10. R. Bengtsson and S. Frauendorf, Nucl. Phys. **A314** (1979) 27
11. S. Frauendorf, Nucl. Phys. **A557** (1993) 259c

# Fragmentation of two-phonon $\gamma$-vibrational strength in deformed nuclei

C.Y. Wu and D. Cline

*Nuclear Structure Research Laboratory, University of Rochester, Rochester, NY 14627*

Rotational and vibrational modes of collective motion are very useful in classifying the low-lying excited states in deformed nuclei. The rotational mode of collective motion is characterized by rotational bands having correlated level energies and strongly-enhanced E2 matrix elements. The lowest intrinsic excitation with $I,K^\pi = 2,2^+$ in even-even deformed nuclei, typically occurring at $\approx$1 MeV, is classified as a one-phonon $\gamma$-vibration state[1]. In a pure harmonic vibration limit, the expected two-phonon $\gamma$-vibration states with $I,K^\pi = 0,0^+$ and $4,4^+$ should have excitation energies at twice that of the $I,K^\pi = 2,2^+$ excitation, i.e. $\approx$2 MeV, which usually is above the pairing gap leading to possible mixing with two-quasiparticle configurations. Therefore, the question of the localization of two-phonon $\gamma$-vibration strength has been raised[2] because mixing may lead to fragmentation of the two-phonon strength over a range of excitation energy.

For several well-deformed nuclei, an assignment of $I,K^\pi = 4,4^+$ states as being two-phonon vibrational excitations has been suggested based on the excitation energies and the predominant $\gamma$-ray decay to the $I,K^\pi = 2,2^+$ state[3]. However, absolute B(E2) values connecting the presumed two- and one-phonon states are the only unambiguous measure of double phonon excitation. Such B(E2) data are available for $^{156}$Gd[4], $^{160}$Dy[5], $^{168}$Er[6,19], $^{232}$Th[7,8,20], and $^{186,188,190,192}$Os [9,10,11]. Except for $^{160}$Dy, the measured B(E2) values range from 2 - 3 Weisskopf units in $^{156}$Gd to 10 - 20 Weisskopf units in osmium nuclei; enhancement that is consistent with collective modes of motion.

Statements regarding the phonon character that are based on a comparison of the measured E2 matrix elements, are ambiguous because the interband E2 matrix elements depend on the mixing of the $\Delta K = 2$ bands, due to coupling of the rotational and intrinsic motion, as well as the intrinsic E2 matrix element between the bands. The intrinsic E2 matrix elements are required for an unambiguous measure of the multiphonon structure. In this paper, these intrinsic E2 matrix elements are extracted from the measured E2 matrix elements by assuming a first order angular momentum dependence of the coupling between the rotation and intrinsic motion [12]. The interband E2 matrix elements are assumed to be correlated by the following equation (Eq. (4-210) in Ref. [1])

$$\sqrt{B(E2, I_{K'} \rightarrow I_K)} = \langle I_{K'} K' 2 - 2 | I_K K \rangle \cdot [M_1 - M_2(I_K(I_K+1) - I_{K'}(I_{K'}+1))] \xi \quad (1)$$

where $M_1$ and $M_2$ are the fitting parameters, $K' = K + 2$ and $\xi$ is equal to $\sqrt{2}$ if $K = 0$ and equal to 1 otherwise. This relation underlies use of the Mikhailov plot[12]. The

applicability of Eq. (1) is based on the assumption that both bands are rotational bands having the same intrinsic deformation. The intrinsic matrix elements between bands are related to the $M_1$ and $M_2$ matrix elements by the Eq. (2) (Eq. (4-211) in

$$\langle K'|E2|K\rangle = M_1 + 4(K+1)M_2 \qquad (2)$$

Ref. [1]). The matrix elements coupling the $\Delta K = 2$ bands can be deduced from the the level-energy spacing and the wavefunction mixing amplitude derived from $M_2$ (p161 in ref. 1).

The above method has been used to extract intrinsic E2 matrix elements for $^{156}$Gd, $^{160}$Dy, $^{168}$Er, $^{186,188,190,192}$Os and $^{232}$Th. These are nuclei for which the absolute E2 data are available from either lifetime measurements, or Coulomb excitation measurements that are sufficiently complete to give unambiguous matrix elements. The justification for the use of Eq. (2) to correlate the interband E2 matrix elements between $K = 0$ and 2 bands and between $K = 2$ and 4 bands is demonstrated by analyses using the rotational-invariant technique[10,15] applied to cases such as $^{168}$Er[18] and $^{186,188,190,192}$Os[9,10,11]. These studies show almost constant centroids of both the magnitude and asymmetry for the quadrupole deformation of the $K = 0$ and 2 bands in these nuclei, as well as an additional $K = 4$ band in the osmium nuclei. This is consistent with the interpretation that, in each nucleus, these bands are rotational bands with similar intrinsic deformation.

For the osmium nuclei, the excitation energy for the I,quasi-$K^\pi = 2,2^+$ state ranges from 489 keV in $^{192}$Os to 767 keV in $^{186}$Os. Possible two-phonon $\gamma$-vibrational I,quasi-$K^\pi = 4,4^+$ states exist at about twice the one-phonon energies and these states decay predominantly to members of the one-phonon quasi-$K = 2$ band[13,14]. Coulomb excitation work on $^{186,188,190,192}$Os has determined nearly complete sets of E2 matrix elements and these can be described approximately by a $\gamma$-soft type of collective model[9,10,11].

The interband E2 matrix elements between $K = 2$ and 0 bands are correlated well using Eq. (1) for $^{186,188}$Os and moderately well for $^{190}$Os, as shown in Fig. 1. The matrix elements, $M_1$ and $M_2$, determined from a least-square fit of Eq. (1) to the data, are given in Fig. 1. From these matrix elements, the intrinsic E2 matrix element between $K = 2$ and 0 bands can be deduced from Eq. (2) and are listed in Table 1. The same analysis has been applied for the decay of I,$K^\pi = 4,4^+$ state to members of $K = 2$ band. The data are well correlated by Eq. (1) for $^{186,188,190}$Os as shown in Fig. 2. The extracted matrix elements, $M_1$ and $M_2$, and deduced intrinsic E2 matrix element between $K = 4$ and 2 bands were listed in Fig. 2 and Table 1, respectively.

The matrix elements coupling the intrinsic $K = 2$ and 0 bands range from $-2$ keV for $^{186}$Os to $-4$ keV for $^{190}$Os. The coupling matrix elements between $K = 4$ and 2 bands cannot be estimated reliably via the method outlined in p161 of ref.

1 due to the larger coupling and have been estimated to be −3 keV from a three-band-mixing (K = 0, 2, and 4 bands) calculation. The estimated intrinsic E2 matrix elements between the K = 2 and 0 bands and between the K = 4 and 2 bands, from the three-band-mixing calculation, are consistent with those obtained from Mikhailov plot analyses.

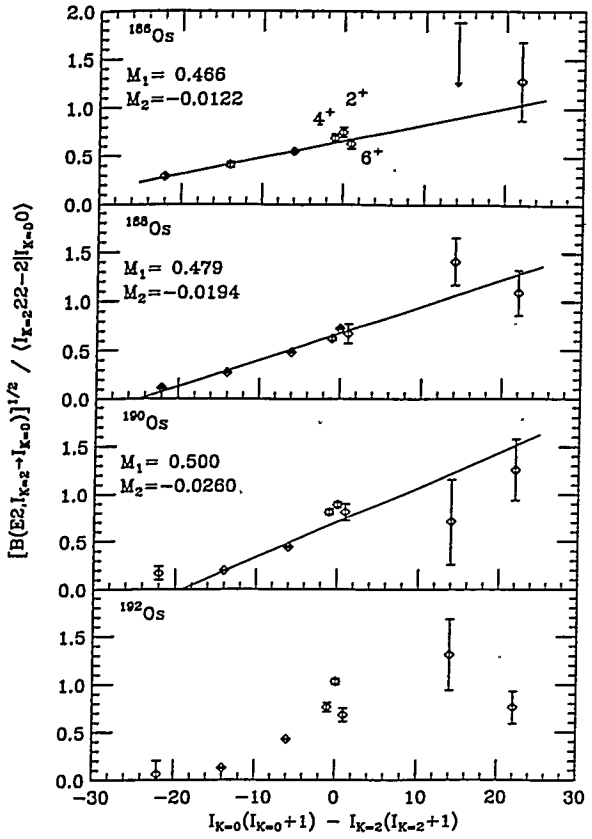


Fig. 1 Mikhailov plot for the interband E2 transitions between K = 2 and 0 bands in osmium nuclei together with the best fit (solid line) using Eq. (1) and parameters shown. Spin is labelled for transitions with ΔI = 0.

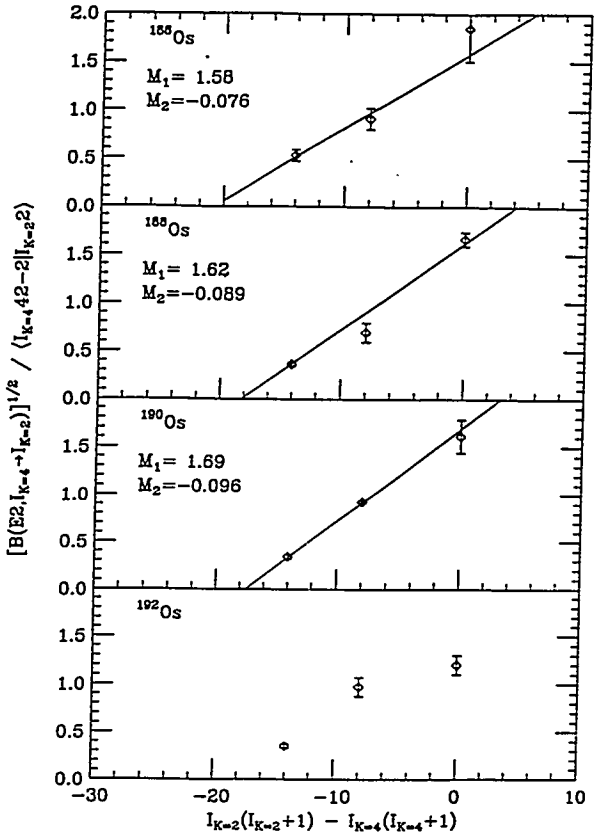


Fig. 2 Mikhailov plot for the interband E2 transitions between $I,K^\pi = 4,4^+$ state and band members of K = 2 in osmium nuclei together with the best fit (solid line) using Eq. (1) and parameters shown.

For the case of $^{192}$Os, a three-band-mixing (K = 0, 2, and 4 bands) calculation was performed to estimate the intrinsic E2 matrix elements and coupling matrix elements. Good agreement can be achieved with the band-mixing calculation. The estimated intrinsic E2 matrix elements and coupling matrix elements have the same magnitude as those in other osmium nuclei.

A possible two-phonon vibrational $I,K^\pi = 0,0^+$ state exists in all the osmium nuclei studied here, in that the energy and decay properties are consistent with the characteristic of two-phonon excitations. However, the intrinsic E2 matrix element, derived from the matrix element, $\langle 0, K = 0' \parallel E2 \parallel 2, K = 2\rangle$, accounts only for about 70% of the harmonic vibration limit implying significant mixing with other low-lying

K = 0 states, such as the one-phonon $\beta$-vibration excitation. Although there is some information regarding branching ratios, no absolute B(E2) values are known for possible two-phonon $0^+$ states in other deformed nuclei. Thus the following discussion is limited to two-phonon $4^+$ states.

To illustrate the extent to which the multiphonon $\gamma$-vibration scheme can be applied to I,K$^\pi$ = 2,2$^+$ and 4,4$^+$ states in osmium and other deformed nuclei, the ratio of the intrinsic E2 matrix element between K = 4 and 2 bands to that between the K = 2 and 0 bands versus the ratio of experimental excitation energies is plotted in Fig 3. Note that a pure harmonic vibrator has an intrinsic E2 matrix element ratio equal to $\sqrt{2}$. Both the excitation energy and intrinsic moment ratios are consistent with the interpretation of I,K$^\pi$ = 4,4$^+$ states in osmium and $^{232}$Th nuclei being predominantly harmonic two-phonon $\gamma$-vibration states. The slightly lower ratio of intrinsic E2 matrix elements and increased excitation-energy ratio for $^{192}$Os probably is a reflection of anharmonic vibrational motion[16,17]. A common factor for these two-phonon states, is that their excitation energies are below the pairing gap. In contrast to the uniform one-phonon vibrational strengths in $^{156}$Gd, $^{160}$Dy,

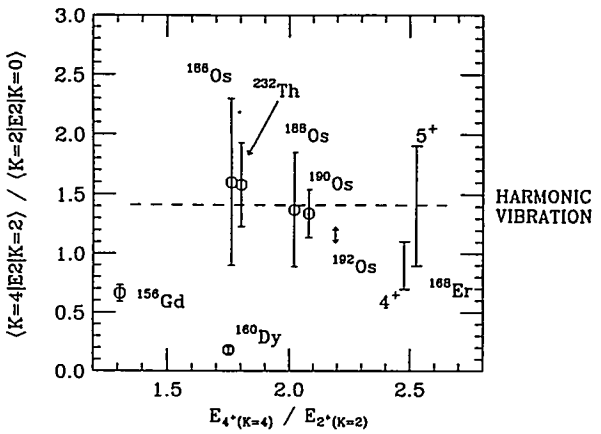


Fig. 3 The ratio of intrinsic E2 moments vs. the ratio of experimental excitation energies between two- and one-phonon vibration for all cases studied here.

Table 1. Extracted intrinsic E2 moments(eb) between bands with $\Delta$K = 2.

| Nucleus | ⟨ K=2 \| E2 \| K=0 ⟩ | ⟨ K=4 \| E2 \| K=2 ⟩ | Ratio* |
|---|---|---|---|
| $^{156}$Gd | 0.238±0.004 | 0.157±0.017 | 0.66±0.07 |
| $^{160}$Dy | 0.253±0.006 | 0.045±0.007 | 0.18±0.03 |
| $^{168}$Er | 0.243±0.008 | 0.16 < < 0.28[a] | 0.7< < 1.1 |
| | | 0.21 < < 0.47[b] | 0.9< < 1.9 |
| $^{186}$Os | 0.417±0.011 | 0.67±0.29 | 1.60±0.70 |
| $^{188}$Os | 0.401±0.017 | 0.55±0.19 | 1.37±0.48 |
| $^{190}$Os | 0.396±0.037 | 0.53±0.06 | 1.34±0.20 |
| $^{192}$Os | 0.45[c] | 0.50 − 0.55[c] | 1.11 − 1.22 |
| $^{232}$Th | 0.31[d] | 0.49±0.11 | 1.58±0.35 |

*a*. From the decay of the $4^+$ state.
*b*. From the decay of the $5^+$ state.
*c*. From three-band-mixing (K = 0, 2, and 4) calculation.
*d*. From three-band-mixing (K = 0, 2, and 0′) calculation.
* The ratio of ⟨ K=4 | E2 | K=2 ⟩ to ⟨ K=2 | E2 | K=0 ⟩.

and $^{168}$Er (listed in Table 1), substantial strength fragmentation for the two-phonon vibration in $^{156}$Gd and $^{160}$Dy is suggested by the intrinsic E2 matrix element ratios, as shown in Fig. 3. However, the appreciable two-phonon strength for the observed transitions in $^{156}$Gd at 1.511 MeV and $^{168}$Er at 2.055 MeV, suggests that the centroid of the two-phonon strength may not be as high as 3 - 4 MeV proposed in Ref. [2]. The anharmonicity exhibited by the excitation energy ratio for $^{168}$Er is consistent with a reduced ratio of intrinsic E2 matrix elements relative to the harmonic vibration limit[16,17].

Many of the I,K$^{\pi} = 4,4^{+}$ states, suggested as candidates for two-phonon excitation in well-deformed nuclei[3], may contain significant two-quasiparticle components, as has been addressed by Burke[21] based on nucleon-transfer and $\beta$-decay data. This appears true for $^{156}$Gd and $^{160}$Dy discussed in the present study. For $^{190,192}$Os, the two-phonon strength is shown to approach the harmonic vibration limit despite the proposed[21] existence of a significant hexadecapole phonon component. The magnitude of this hexadecapole component is still an open question due to the uncertainty involved in the $(t,\alpha)$ reaction mechanism[22]. The static E2 matrix element, as well as the three $\Delta$K = 2 E2 transition matrix elements, measured for the I,quasi-K$^{\pi} = 4,4^{+}$ states, in each osmium nucleus, all are consistent with coupled rotation-vibrational models[9,10,11]. The enhancement of these four E2 matrix elements, is strong evidence that the two-phonon components dominate over two-quasiparticle components in the structure of these states. Contrary to statements made in Ref. 21, including the $g$-boson[23] in the interacting boson model[24], which is equivalent to the hexadecapole phonon, actually underestimates the measured B(E2) values[9] by up to a factor of 4 for the osmium nuclei.

In summary, the intrinsic $\Delta$K = 2 E2 matrix elements between the presumed double, single and zero phonon $\gamma$-vibrational intrinsic states have been deduced from measured interband E2 matrix elements for $^{156}$Gd, $^{160}$Dy, $^{168}$Er, $^{232}$Th, and $^{186,188,190,192}$Os. These intrinsic E2 matrix elements, which are a sensitive measure of multiphonon structure, plus the excitation energies, show unambiguously the existence of rather pure harmonic double-phonon $\gamma$-vibrational I,K$^{\pi} = 4,4^{+}$ intrinsic states in $^{232}$Th and the osmium nuclei. Even though there is evidence for anharmonicity, the double-phonon $\gamma$-vibrational strength still is largely focussed in a single state in $^{168}$Er, whereas significant fragmentation of the two-phonon strength is manifest in $^{156}$Gd and $^{160}$Dy. The localization of double-phonon intrinsic states, demonstrated here, opens the possibility of identifying other multiphonon structures in nuclei.

[1] A. Bohr and B.R. Mottleson, Nuclear Structure Vol. II, Benjamin, Reading, MA (1975).
[2] V.G. Soloviev and N.Yu. Shirihova, Z. Phys. **A 301** (1981) 263.
[3] X. Wu *et al.*, Phys. Rev. **C 49** (1994) 1837.
[4] A. Bäcklin *et al.*, Nucl. Phys. **A 380** (1982) 189.
[5] C.W. Reich, Nucl. Data Sheets **68** (1993) 405; reference therein.
[6] H.G. Börner *et al.*, Phys. Rev. Lett. **66** (1991) 691.
[7] W. Korten *et al.*, Phys. Lett. **B 317** (1993) 19.
[8] W. Korten *et al.*, Z. Phys. **A 351** (1995) 143.
[9] C.Y. Wu *et al.*, Nucl. Phys. A (1996), in press and references therein.
[10] D. Cline, Ann. Rev. Nucl. Part. Sci. **36** (1986) 683.
[11] D. Cline, Nucl. Phys. **A 557** (1993) 615c.
[12] V.M. Mikhailov, Izv. Akad. Nauk. SSSR, Ser. Fiz. **30** (1966) 1334.
[13] S.W. Yates *et al.*, Nucl. Phys. **A 222** (1974) 276; *ibid.* (1974) 301.
[14] R.F. Casten and J.A. Cizewski, Nucl. Phys. **A 309** (1978) 477.
[15] D. Cline and C. Flaum, Proc. of the Inter. Conf. on Nuclear Structure Studies Using Electron Scattering and Photoreaction, Sendai 1972, ED., K. Shoda and H. Ui, Tohoku University, Vol. 5, p.61 (1972).
[16] A. Bohr and B.R. Mottelson, Physica Scripta **25** (1982) 28.
[17] T.S. Dumitrescu and I. Hamamoto, Nucl. Phys. **A 383** (1982) 205.
[18] B. Kotlinski *et al.*, Nucl. Phys. **A 517** (1990) 365.
[19] W.F. Davidson *et al.*, J. Phys. **G 7** (1981) 455.
[20] F.K. McGowan and W.T. Milner, Nucl. Phys. **A 562** (1993) 241.
[21] D.G. Burke, Phys. Rev. Lett. **73** (1994) 1899.
[22] R.D. Bagnell *et. al.*, Phys. Rev. **C 20** (1979) 42.
[23] F. Iachello and A. Arima, The interacting-boson model, Cambridge Univ. Press, Cambridge (1987).
[24] V.S. Lac and S. Kuyucak, Nucl. Phys. **A 539** (1992) 418.

# ONSET OF DEFORMATION IN POLONIUM NUCLEI

W. Younes and J.A. Cizewski
*Department of Physics & Astronomy, Rutgers University*
*New Brunswick, New Jersey 08903 USA*

**Abstract:** We have been able to reproduce the systematics of the positive–parity states in $^{192-208}$Po within the framework of the Particle–Core Model. The wavefunctions of the $2_1^+$ states have been extracted using the Quasiparticle Random Phase Approximation. The increase in the collective motion of the lighter isotopes comes from the increased proton–neutron interaction when the neutrons and protons both occupy high–$j$ orbitals.

It has long been recognized that nuclei with a single–closed shell do not become deformed in their ground states. The classic example is the Sn region, where the excitation energies of the $2_1^+$ states in the Sn isotopes remain fairly high and constant over a wide range of neutron numbers. In contrast the $2_1^+$ states in the Te and Cd isotopes, with two valence protons, drop in energy when the neutron shell is opened and have properties characteristic of collective motion. It has been suggested that the proton–neutron interaction for particles in relatively high–$j$ orbitals with similar quantum numbers drives the collective motion.[1]

Recently,[2–6] the excitations in neutron–deficient polonium isotopes have been studied experimentally. The systematical behavior of the positive–parity excitations in these nuclei is displayed in Fig. 1, which includes the recent measurements[3,6] of $^{194}$Po and $^{192}$Po. The semi-magic $^{210}$Po is a textbook example of two protons in the $1h_{9/2}$ orbital with a residual surface–delta interaction.[1] When the neutron shell is opened, the $2_1^+$ state drops in energy to about 600 keV and remains constant until A=198 when these energies begin a gradual downtrend. The positive–parity levels in $^{196}$Po have the spacings characteristic of a harmonic vibrator, with degenerate members of the 2– and 3–phonon multiplets.[2] The collectivity increases in $^{192-194}$Po, but the level spacings continue the trends of an anharmonic vibrator.[3]

In the present work we study the change in structure of the positive–parity states in the polonium isotopes as a function of neutron number as well as spin. We have chosen two models to facilitate this analysis: the Particle–Core Model (PCM),[7,8] in which 2 particles (protons) are coupled to a phenomenological phonon (neutron) core, and the Quasiparticle Random Phase Approximation (QRPA),[7,9] which we will use to obtain a semi–microscopic description of the wavefunctions of the $2_1^+$ states.

In the PCM calculations[7] we have assumed that two protons, in the $1h_{9/2}$ orbital and interacting via a surface–delta interaction, are coupled adiabatically to a vibrational core, with a maximum of four phenomenological phonons. The parameters in this model are the strength of the proton–proton interaction (which is assumed to follow a 1/A dependence), the phonon energy (which we assume to be constant), and the strength of the particle–core interaction. We have assumed that the particle–core interaction strength is a single value for A$\geq$198, and allowed to vary freely for each A$\leq$200 isotope. We used 50 level energies of positive–parity states in $^{192-208}$Po to determine 7 free parameters. The results from this calculation are quite robust; we have also allowed both the particle–core interaction and the phonon energy to vary freely for each isotope, and essentially the same results are obtained.[7]

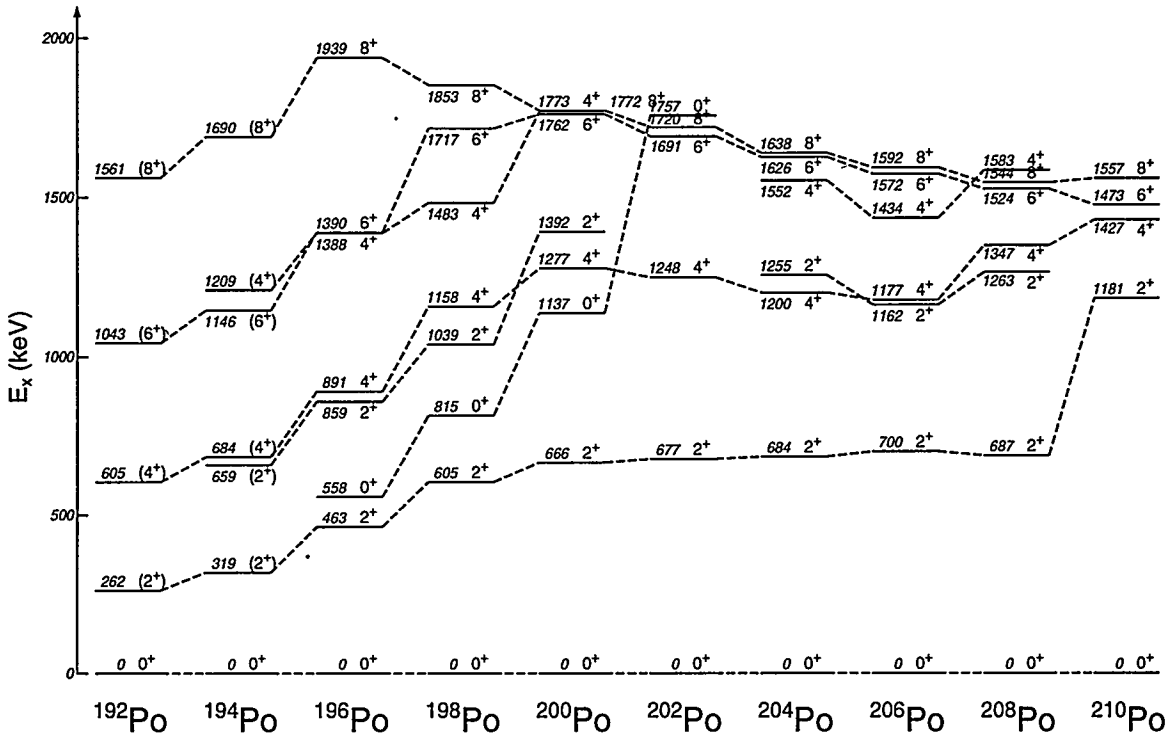


Figure 1: Positive–parity levels in $^{192-210}$Po.

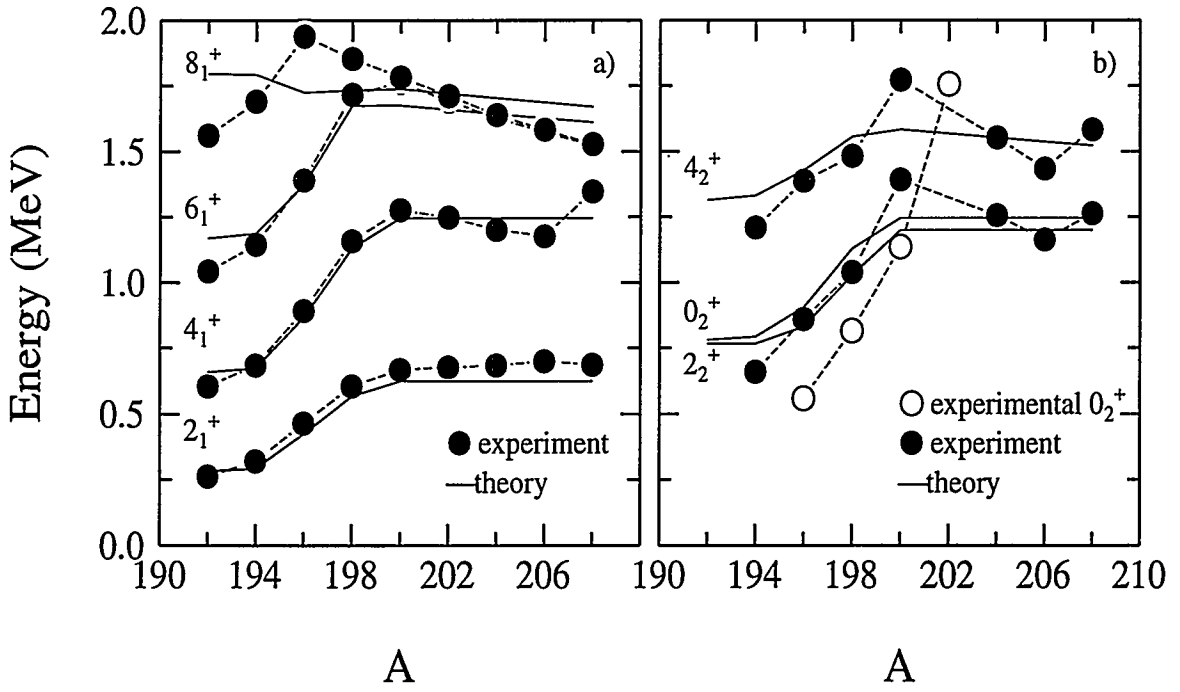


Figure 2: Comparison between experiment and PCM fits for (a) yrast and (b) non–yrast levels in $^{192-208}$Po. The experimental $0_2^+$ energies were not used to determine the fit parameters.

In Fig. 2 we display the fits to (a) the yrast and (b) non–yrast positive–parity states in the Po isotopes; we are able to reproduce the data quite well. In particular, we are able to reproduce the energies of the $2_2^+$ and $4_2^+$ non–yrast states, although we are unsuccessful with the trend in the $0_2^+$ energies.[5] The data suggest that these levels are more collective than the PCM calculations indicate, and therefore, there may be a need to include 4p–2h configurations in the $0_2^+$ states,[5] although there is no compelling evidence for such components in the other non–yrast excitations.[2] Our calculations have some difficulty in reproducing the energies of the $8^+$ states in A<200 isotopes; this may be due to the truncation of the phonon and/or two–particle spaces to a maximum spin of 8.

In Fig. 3 we display the PCM wavefunctions for selected states. The $2_1^+$ and $4_1^+$ states are predominantly 1– and 2–phonon excitations, respectively, with significant admixtures of higher configurations, a signature of enhanced collectivity, for A<198. The $2_2^+$ state also is predominantly a 2–phonon excitation. In contrast, the $6^+$ state is predominantly a 0–phonon, i.e., two–proton, excitation until A=198, when sizable 3–phonon components contribute to the wavefunction. The change in the purity of the wavefunctions for these states when A<200 corresponds to the increase in the strength of the particle–core interaction in the PCM calculations. However, within this model it is not possible to determine if the increase in collectivity is caused by the increase in the proton–neutron interaction, or a change in the structure of the phenomenological phonons.

To obtain a more microscopic understanding of the structure of the $2_1^+$ states in the Po isotopes, and hence the structure of the phonons in the PCM, we have carried out QRPA calculations[7] of the $2_1^+$ state wavefunctions. We used empirical proton and neutron single–particle and binding energies to extract proton and neutron pairing strengths.[10,11] For the long–range interaction, we have assumed a quadrupole proton–neutron interaction. We determined[7] that the strength of the quadrupole p–n interaction, our only free parameter, was essentially constant for $^{192-208}$Po. In Fig. 4 we display the results for the QRPA wavefunctions of the $2_1^+$ states in the Po nuclei. As expected, the proton wave function is concentrated in two protons in the $1h_{9/2}$ orbital, which was the assumption in our PCM calculations. However, the neutron wavefunction is more complicated. For A>200 the neutrons are predominantly in low–spin, $2f_{5/2}$, $3p_{3/2}$, $3p_{1/2}$, orbitals. However, for A<200 the $1i_{13/2}$ orbital increasingly becomes the dominant contribution to the neutron wavefunction.

One expects the proton–neutron interaction to be especially strong when the protons and neutrons are in orbitals with large overlap, which occurs when $j$ is large and the orbitals have the same principal quantum number and similar orbital angular momenta.[1] The collective motion will extend to higher spins when both protons and neutrons can contribute to these excitations, which requires both of these particles to be in orbitals with higher $j$. The results of our PCM and QRPA calculations then allow us to understand the evolution of the collective motion in the Po isotopes. The yrast positive–parity level structure in $^{210}$Po is predominantly two protons in the $1h_{9/2}$ orbital, as confirmed by our QRPA calculations. When the neutron shell is opened, with holes in the low–spin $3p_{1/2}$, $3p_{3/2}$ and $3f_{5/2}$ orbitals, the $2_1^+$ and $4_1^+$ states become collective, vibrational excitations. The $6^+$ and $8^+$ states remain high in energy and predominantly two–proton in character. Below $^{200}$Po, when the $\nu 1i_{13/2}$ orbital begins to be a dominant component in the $2_1^+$ phonon wavefunction, the collectivity increases and persists to higher angular momentum, because of the increase in the interac-

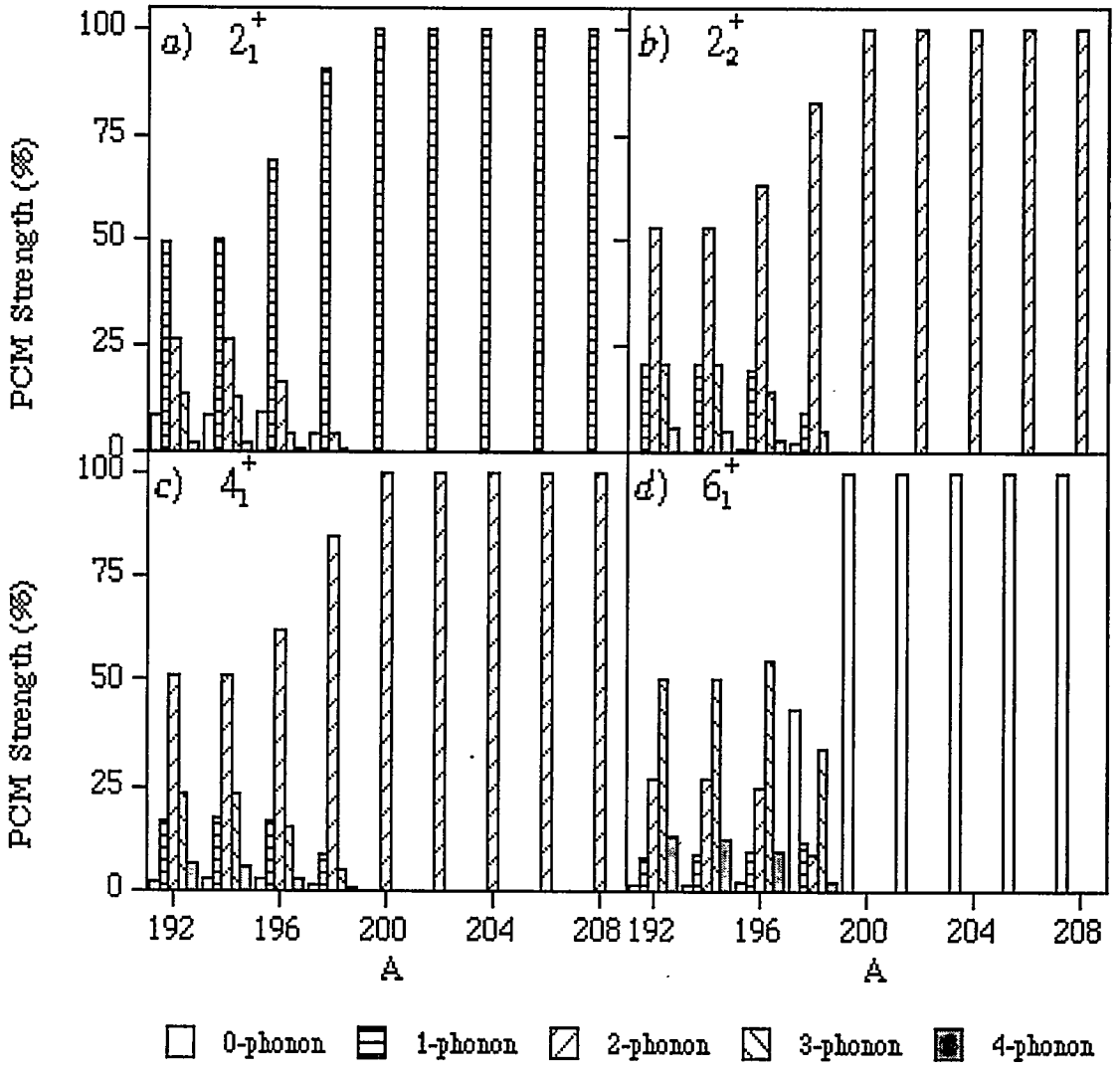


Figure 3: PCM wavefunctions for (a) $2_1^+$, (b) $2_2^+$, (c) $4_1^+$, and (d) $6_1^+$ levels in $^{192-208}$Po.

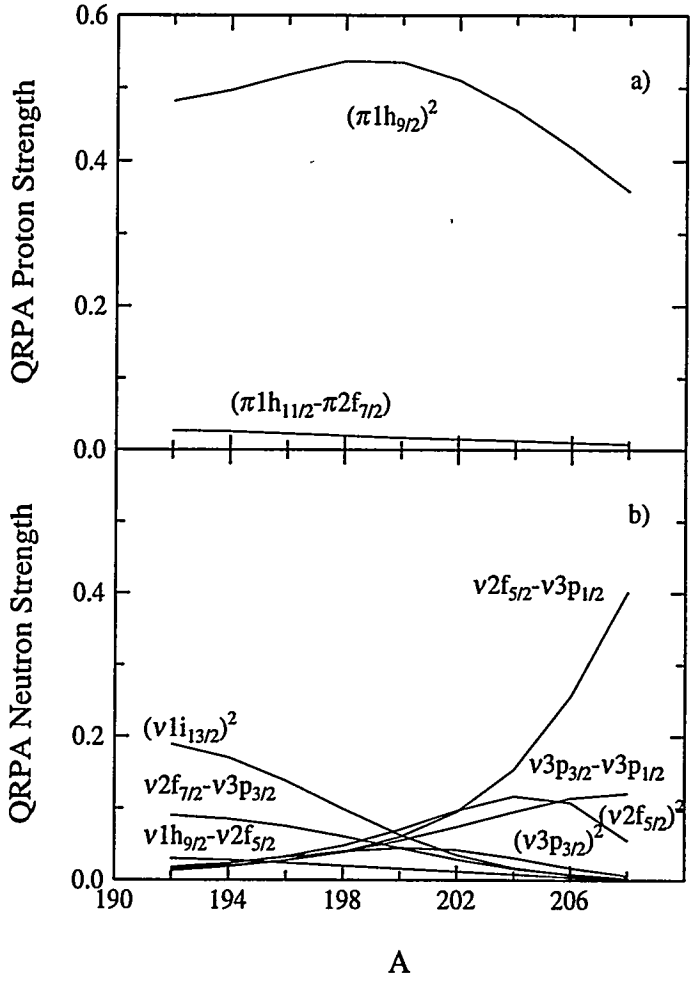


Figure 4: QRPA wavefunctions for $2_1^+$ states in $^{192-208}$Po.

tion between neutrons in the $1i_{13/2}$ and protons in the $1h_{9/2}$ orbitals.

## Acknowledgments

We would like to thank R. Julin for providing results on $^{192}$Po prior to publication. This work was supported in part by the U.S. National Science Foundation.

## References

1. R.F. Casten, *Nuclear Structure from a Simple Perspective*, Oxford Univ. Press (1990).
2. L.A. Bernstein *et al.*, Phys. Rev. **C52**, 621 (1995).
3. W. Younes *et al.*, Phys. Rev. **C52**, R1723 (1995).
4. Evaluated Nuclear Structure Data Files, Brookhaven National Laboratory, NY.
5. N. Bijnens *et al.*, Phys. Rev. Lett. **75**, 4571 (1995).
6. R. Julin, private communication (1996) and proceedings of this conference.
7. W. Younes and J. A. Cizewski, to be published (1996) and references therein.
8. K. Heyde and P.J. Brussaard, Nucl. Phys. **A104**, 81 (1967).
9. L.S. Kisslinger and R.A. Sorensen, Rev. of Mod. Phys. **35**, 853 (1963).
10. T.T.S. Kuo and G.H. Herling, U.S. Naval Research Laboratory Report 2258 (1971).
11. G. Audi and A.H. Wapstra, Nucl. Phys. **A565**, 1 (1993).

# Recent studies of heavy nuclei far from stability at JYFL

R. Julin, T. Enqvist, K. Helariutta, P. Jones, S. Juutinen, P. Jämsen, H. Kankaanpää, P. Kuusiniemi, M. Leino, M. Muikku, M. Piiparinen, A. Savelius, W.H. Trzaska, S. Törmänen, J. Uusitalo

Department of Physics, University of Jyväskylä, P.O.Box 35, 40351 Jyväskylä, Finland

R.G Allatt, P.A. Butler, K.J. Cann, J.F.C. Cocks, P.T.J. Greenlees, R.D. Page

Oliver Lodge Laboratory, Department of Physics, University of Liverpool, Liverpool, L69 3BX, UK

The new K=130 Cyclotron + ECR facility of the Physics Department of the University of Jyväskylä (JYFL) provides stable beams from protons up to krypton ions for nuclear structure studies. Two instruments designed especially for in-beam spectroscopic studies of heavy nuclei at JYFL are introduced in this contribution. Some results from recent measurements with them are reported.

## Recoil decay tagging measurements with RITU

The JYFL gas-filled (1 mbar of He) separator RITU (Recoil Ion Transport Unit) is a charge and velocity focusing device especially designed for separating recoiling heavy fusion evaporation products with high transmission [1]. Recoils are implanted into a 80 x 35 mm Si strip detector covering typically 70% of the recoil distribution at the focal plane. It is divided into 10 mm wide strips each of them having a position resolution of about 0.4 mm, resulting in a granularity needed in correlating the recoils with their subsequent alpha decays. During the last three years RITU has been used for discoveries of new neutron deficient At, Rn, Fr, Ra, Ac and Th isotopes and in studies of their $\alpha$- decay properties.

The power of RITU in in-beam $\gamma$ ray experiments utilizing the recoil decay tagging method [2][3] has been demonstrated in the studies of very neutron deficient $^{194}$Po and $^{192}$Po nuclei. These nuclei were produced in $^{170}$Yb($^{28}$Si,4n) and $^{160}$Dy($^{36}$Ar,4n) reactions with cross - sections of only about 500 $\mu$b and 10 $\mu$b, respectively. Prompt $\gamma$- rays from the target were detected by the DORIS array consisting of 9 TESSA type Compton suppressed Ge detectors in a truncated dodecahedron frame (eff. about 0.6% at 1.3MeV).

Signals from the Si strip detector for the energy, position as well as the detection time of the recoils and $\alpha$- particles were recorded. Singles $\gamma$- ray as well as $\gamma\gamma$ coincidence events from the DORIS array were recorded in coincidence with the detected recoils. In the analysis of the data, the events corresponding to the observation of a recoil and the subsequent $\alpha$- decay at the same position within a proper maximum time interval were selected.

For $^{194}$Po, high statistics $\alpha$- tagged $\gamma\gamma$ coincidence data were collected. The resulting level scheme is in agreement with the one proposed by Younes et al. [4] except for a 2620 keV level which we identify with $12^+$ instead of $11^-$ on the basis of our angular distribution information.

From the $^{192}$Po experiment, a projected $\alpha$- spectrum with the time interval of 200 ms and with a recoil-$\gamma$ coincidence condition is shown in the insert of Fig. 1. The $\alpha$ peaks in this spectrum are identified on the basis of known $\alpha$-decay energies. The half-life extracted from the projected time spectrum for the events in the $^{192}$Po $\alpha$ peak falls into the error bars of the earlier value [5].

A gate on the $^{192}$Po $\alpha$ peak yields a recoil gated $\gamma$- ray spectrum of Fig. 1 with new lines at 262, 343, 438 and 518 keV. Based on their intensities and the available level-energy systematics we tentatively identify those lines with an E2 cascade of the ground state band in $^{192}$Po. This interpretation is also supported by the recoil gated $\alpha$-tagged $\gamma\gamma$ coincidence spectra.

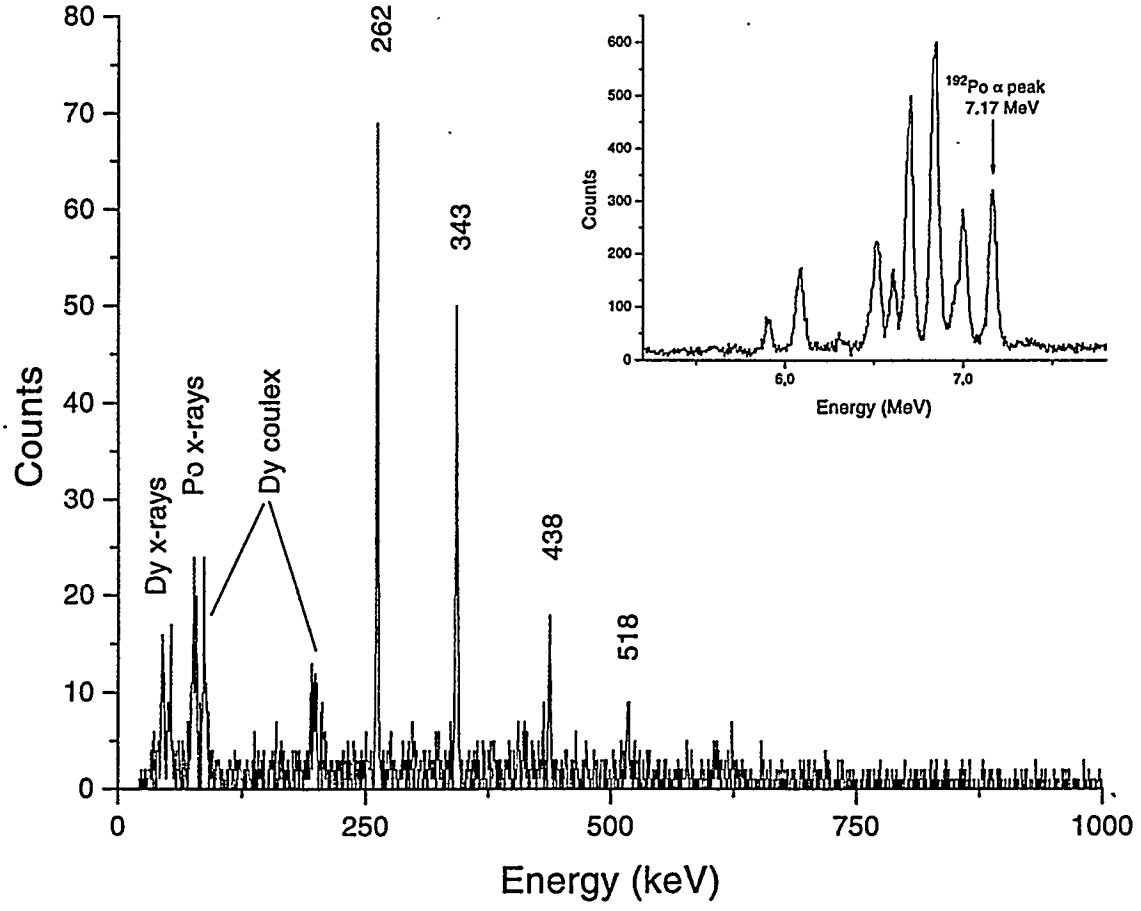


*Fig. 1. A singles $\gamma$-ray spectrum gated with fusion-evaporation residues and tagged with $\alpha$-particle events in the $^{192}$Po $\alpha$ peak of the spectrum shown in the insert . In the insert, a spectrum of $\alpha$ particles is shown, observed within a 200 ms time interva (6 half-lives of $^{192}$Po) after the detection of a recoil (in coincidence with prompt $\gamma$ rays) at the same position in the Si strip detector.*

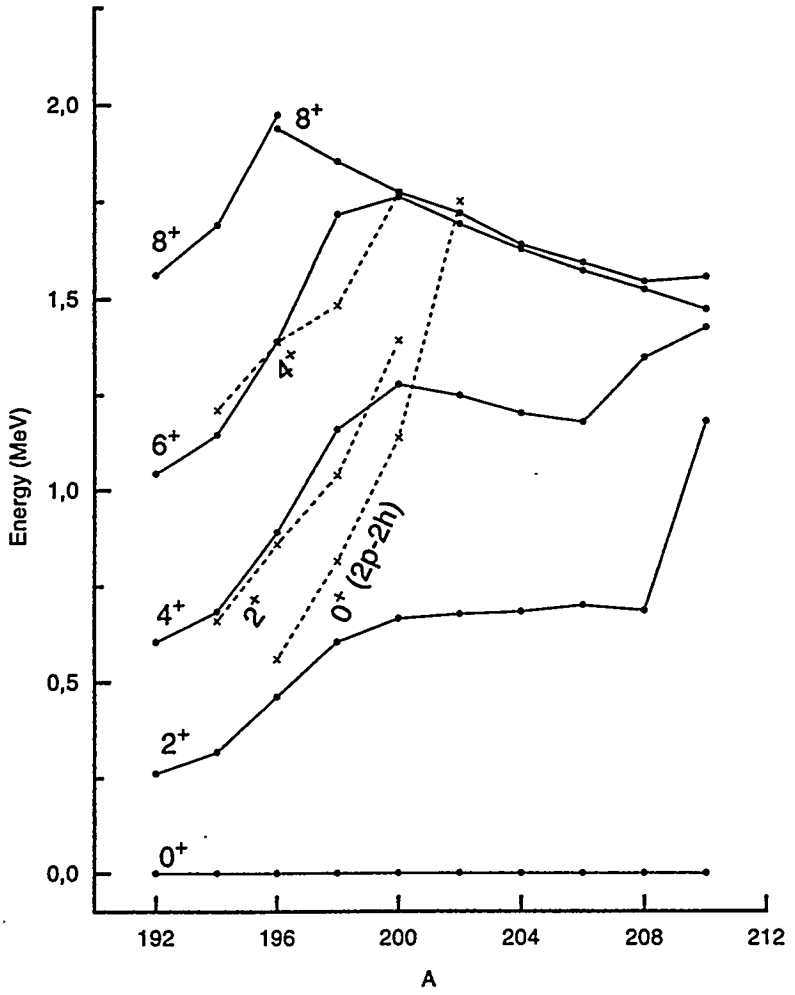


*Fig. 2. Level systematics for the even-mass $^{192-210}Po$.*

A level-energy systematics for the even-mass $^{192-210}$Po isotopes including our new data is shown in Fig. 2. A sudden drop of level energies when going from the heavier isotopes to $^{196}$Po is observed. The new $^{192}$Po results reveal signs of the smoothening of the systematics when going towards the neutron midshell. A similar behaviour has been observed in even-mass Pt nuclei where it has been interpreted as evidence for a ground state intruder configuration [6]. That the observed band structure in $^{192}$Po is indeed based on an intruding ground-state structure different from those for heavier Po isotopes is also indicated by simple mixing calculations [7]. It should be noted that based on the Nilsson-Strutinsky type of calculations, May et al. predicted that in $^{192}$Po an oblate deformed minimum becomes the ground state [8].

Similarly as in the Pt nuclei [6], the relatively high rotational parameter associated with the $2_1^+$ - $0_1^+$ energy spacing in $^{192}$Po can be explained by mixing of the $0_1^+$ and $0_2^+$ states with a consequent depression of the $0_1^+$ ground state. This is also in agreement with the above mentioned mixing calculation results and the $\alpha$- decay properties of $^{192}$Po [9].

Especially on the basis of recent $\alpha$- and $\beta$-decay studies by the Leuven group [7] the intruding structures in light Po isotopes are usually associated with proton 4p-2h

excitations across the main shell gap. In spite of the remarkable agreement with this proton intruder picture the role of deformation driving neutron orbitals in the behaviour of yrast states of light Po nuclei cannot be ruled out. Younes et al. [10] have shown that the $^{192}$Po level energies can be quite well reproduced without any proton-intruder configurations.

## In-beam conversion electron spectroscopy using the SACRED array

A conversion-electron spectrometer consisting of an superconducting solenoid magnet and a Silicon Array for ConveRsion Electron Detection (SACRED) has been constructed [11] and installed at the dedicated beam-line of the JYFL accelerator laboratory.

SACRED consists of a Si PIN detector divided to 25 pixels of 5x5mm. Presently, the pixels are connected to operate as 17 separate detectors with separate preamplifiers. The SACRED array has been designed for detecting high-multiplicity electron events from highly converted electromagnetic transition cascades in heavy nuclei, especially for searching for superdeformed structures. As shown in the sketch of Fig. 3 the electrons emitted from the target are collected through the solenoid field and spread over the SACRED array

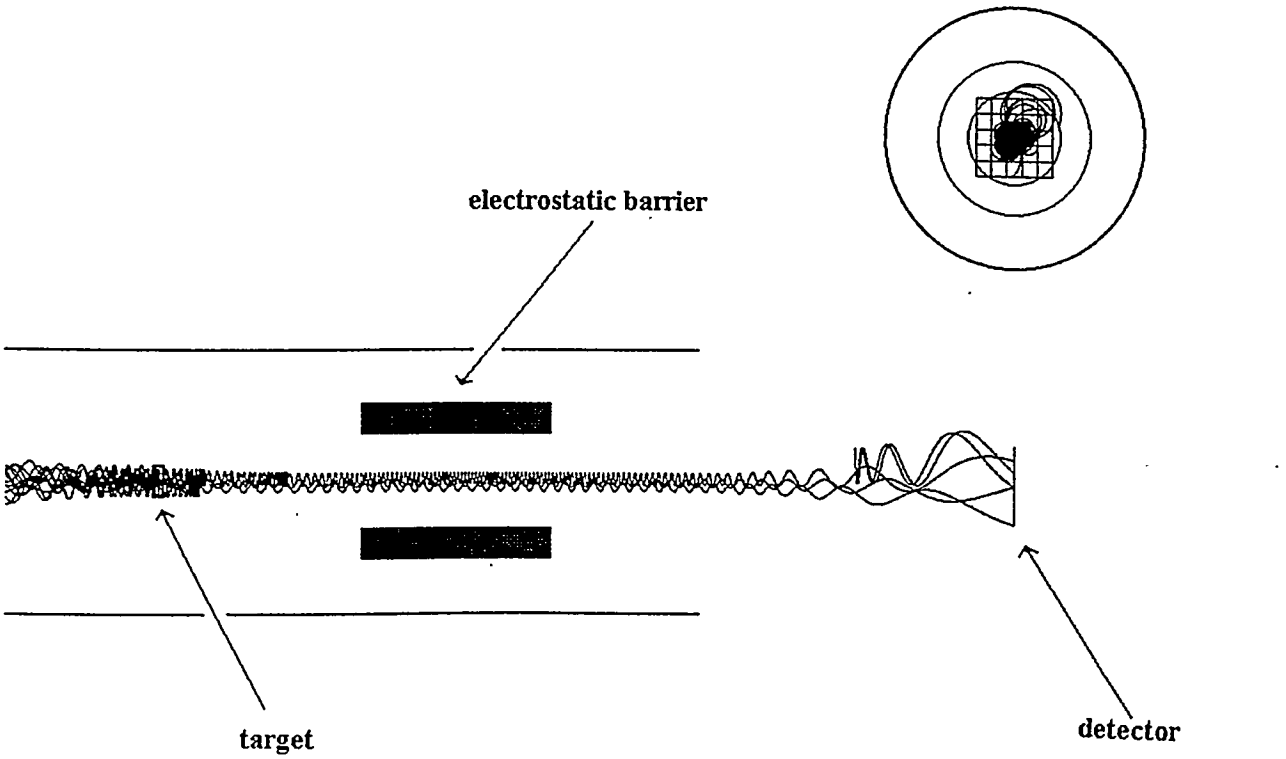


*Fig. 3. A scheme of the solenoid and SACRED showing trajectories of electrons in the magnetic field of the solenoid and the electric field of the barrier.*

sitting outside the magnetic field. Electron cascades are separated by requiring coincidences between the individual pixels. In first measurements performance of the spectrometer in $e^-$-$e^-$ coincidence measurements was demonstrated in the recoil-shadow mode of operation.

A HV deflector (Fig. 3) acting as an electrostatic barrier up to 40 kV against low-energy electrons has been designed for the spectrometer. In this way, the most intense part of the disturbing low-energy delta electrons can be suppressed, rendering it possible, for the first time, to perform prompt in-beam broad range $e^-$-$e^-$ coincidence measurements.

Figure 4 shows a background-corrected electron spectrum in coincidence with the L conversion electrons of the ground-state 183 keV transition in $^{222}$Th following the $^{208}$Pb($^{18}$O,4n) reaction at a bombarding energy of 95 MeV. The fraction of the total cross section for this channel is approximately 1%. A partial decay scheme is shown, which identifies those transitions which can clearly be observed in the spectrum.

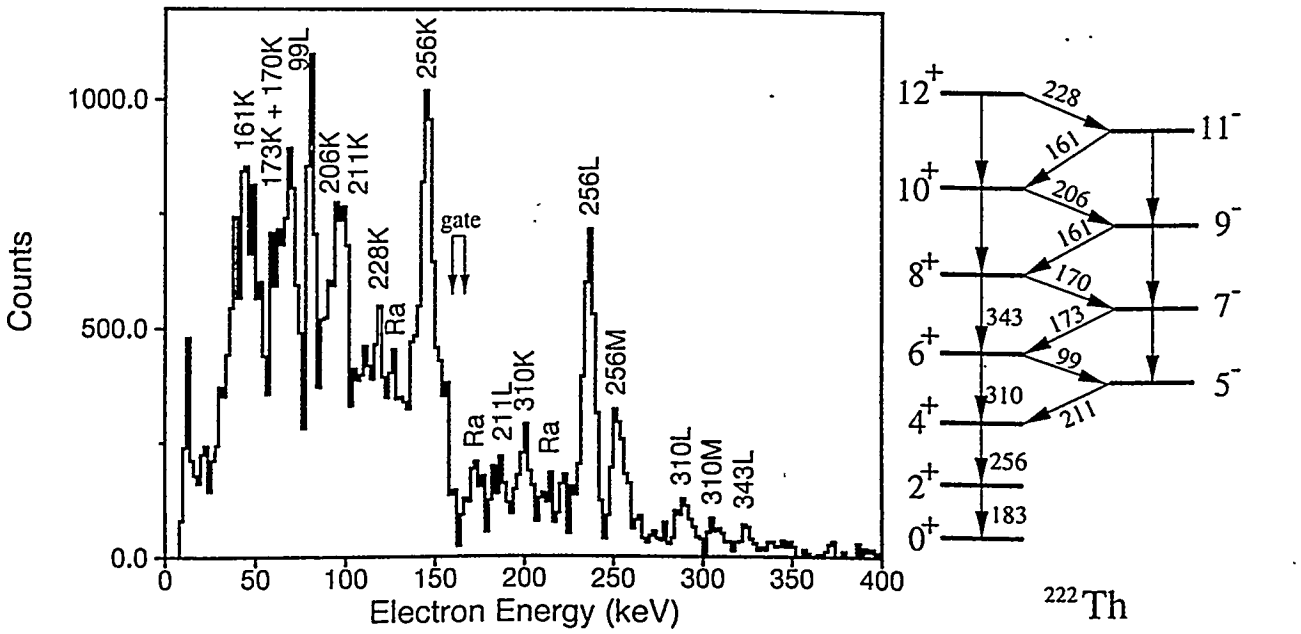


*Fig. 4. Prompt electron spectrum in coincidence with the L conversion electrons of the ground-state 183 keV transition in $^{222}$Th following the $^{208}$Pb($^{18}$O,4n) reaction.*

A double-gated $e^-$-$e^-$-$e^-$ coincidence spectrum extracted from this coincidence data for $^{222}$Th reveals a structure which we tentatively interpret as arising from a rotational-like E2 cascade with energies between 90 and 180 keV. While further measurements are necessary to confirm this identification, these measurements indicate that the SACRED

spectrometer system is sensitive to the detection of weakly populated highly converted transitions, in this case approximately $10^{-4}$ of the total nuclear cross section.

# References


[1] M. Leino et al., Nucl. Instr. Meth. B 99, 656 (1995)

[2] R.S. Simon et al., Z. Phys. A 325, 197 (1986)

[3] E.S. Paul et al., Phys. Rev. C 51, 78 (1995)

[4] W. Younes et al., Phys. Rev. C 52, R1723 (1995)

[5] M.E. Leino, S. Yashita and A. Ghiorso, Phys. Rev. C 24, 2370 (1981)

[6] J.L. Wood, K. Heyde, W. Nazarewicz, M. Huyse and P. Van Duppen, Phys. Rep. 215, 101 (1992)

[7] N. Bijnens et al., Phys. Rev. Lett. 75, 4571 (1995)

[8] F.R. May, V.V. Pashkevich and S. Frauendorf, Phys. Lett. 68B, 113 (1977)

[9] N. Bijnens et al., to be published

[10] W. Younes et al., this proceedings

[11] P.A. Butler et al., Nucl. Instr. and Meth. in press

# A multitude of rotational bands in $^{163}$Er and their mutual interaction

*P. Bosetti[1], A. Brockstedt[2], G.B. Hagemann[3],H. Ryde[2], H. Carlsson[2], L.P. Ekström[2], A. Nordlund[2], R.A. Bark[3],B. Herskind[3], S. Leoni[1], A. Bracco[1], F. Camera[1], S. Frattini[1], M. Mattiuzzi[1], B. Million[1], C. Rossi-Alvarez[4],G. de Angelis[4], D. Bazzacco[4], S. Lunardi[5] and M. de Poli[4]*

1 Dipartimento di Fisica, University of Milan, Italy

2 Department of Physics, University of Lund, Sweden

3 Niels Bohr Institute, University of Copenhagen, Roskilde, Denmark

4 Laboratori Nazionali de Legnaro, Italy

5 Dipartimento di Fisica, University of Padova, Italy

**Abstract:** Using the ($^{18}$O,5n)$^{163}$Er reaction a multitude of rotational bands have been established with firm spin and parity assignments in $^{163}$Er. In 16 out of $\sim$ 23 band crossings E2 cross-band transitions have been observed. The interaction strength varies between $\sim$ 1 and $\sim$ 50 keV. These interactions sample a variety of the lowest (multi)-quasiparticle configurations. Some of the band configurations, in particular those with high K-values, can be rather well established. Quite complicated changes in the wavefunctions must occur at these crossings, and, to explain the observed interaction strengths, one may have to invoke coupling to various vibrational degrees of freedom, in addition to possible residual neutron-proton interactions.

## Introduction.

With the new multi-detector Compton-suppressed $\gamma$-ray spectrometers it has become possible to measure simultaneously the correlation between a manifold of $\gamma$-rays from heavy ion reactions with high resolution, high efficiency and low background. Strongly populated rotational bands may be observed up to states with very high spins, but also many weakly-excited bands can be studied. An interesting aspect of such an observation of a multitude of rotational bands is the possibility of studying the interactions between the many bands and thus uncovering the nature of the intrinsic quasi-particle excitations. The interaction strength, being a result of the rotational perturbation, is expected to be dependent on the nuclear shape and the magnitude of the Coriolis coupling and pair correlation for each quasi-particle. However, the interaction may very well also be dependent on the alignment and/or other nuclear properties. The multitude of observed rotational bands and their many crossings in $^{163}$Er may serve as a testing ground for a study of these interactions.

## Construction of the level scheme

An experiment with high statistical accuracy was performed at the tandem accelerator and the GA.SP multi-detector array at L.N. di Legnaro using the reaction $^{150}$Nd($^{18}$O,5n)$^{163}$Er at a beam energy of 87 MeV. The data consisting of $\sim$ 2x10$^9$ triple events were sorted into a cube as well as into DCO matrices. Fold and sum-energy gating was used for selection of the 5n reaction channel. The data analysis has been carried out by means of the Radware program package [1].

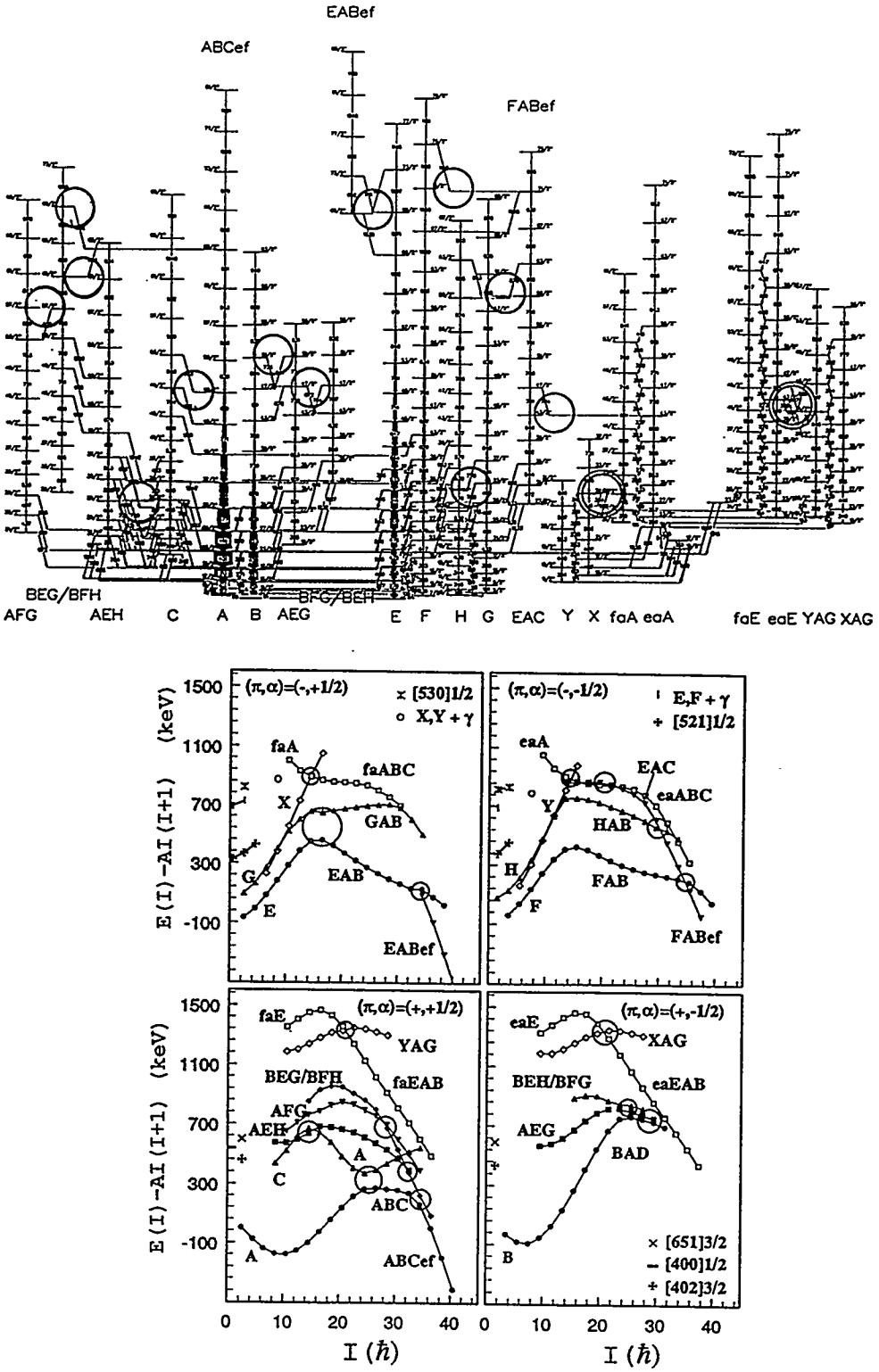


*Fig. 1. Level scheme of $^{163}Er$ from the present experiment (top, not intended for details) and excitation energy versus spin for the rotational bands in $^{163}Er$, separated into 4 symmetry groups, $(\pi, \alpha)$. Open(closed) symbols correspond to high(low) K-value (bottom). The bands are labelled according to the notation given in fig. 2. Large(small) letters refer to neutron(proton) configurations.*

The starting point for constructing the extended level scheme from the present data comprise the 10 bands of ref. [2] in which spin and parities for the high-K bands were determined tentatively only. In addition to extending the known band structures we have established several new rotational bands, some of them with high values of K. Most of these bands are populated up to $I_{max} \sim 77/2\hbar$. Spin and parity are deduced from observed DCO ratios, and from the mutual decay pattern between bands, which in many cases impose severe restrictions in a basically model-independent way.

The level scheme from the present experiment consists of 25 rotational bands, most of them well developed in large spin ranges, see fig. 1. Basis for the construction is coincidence relationships. For the ordering of levels of decoupled band structures the guideline has been relative intensity. However, one should be aware of the fact that in many cases there are fairly strong decays out of the bands. If such decays are not found this commonly used guideline may be misleading.

Some of the band configurations, in particular those with high K-values, can be rather firmly established mainly from their I→ I–1 M1 decay properties and relative alignments. The Nilsson orbits relevant for the expected spectrum of (multi)-quasiparticle excitations for $^{163}$Er are emphasized in the diagrams shown in fig. 2, which also shows the short notations used.

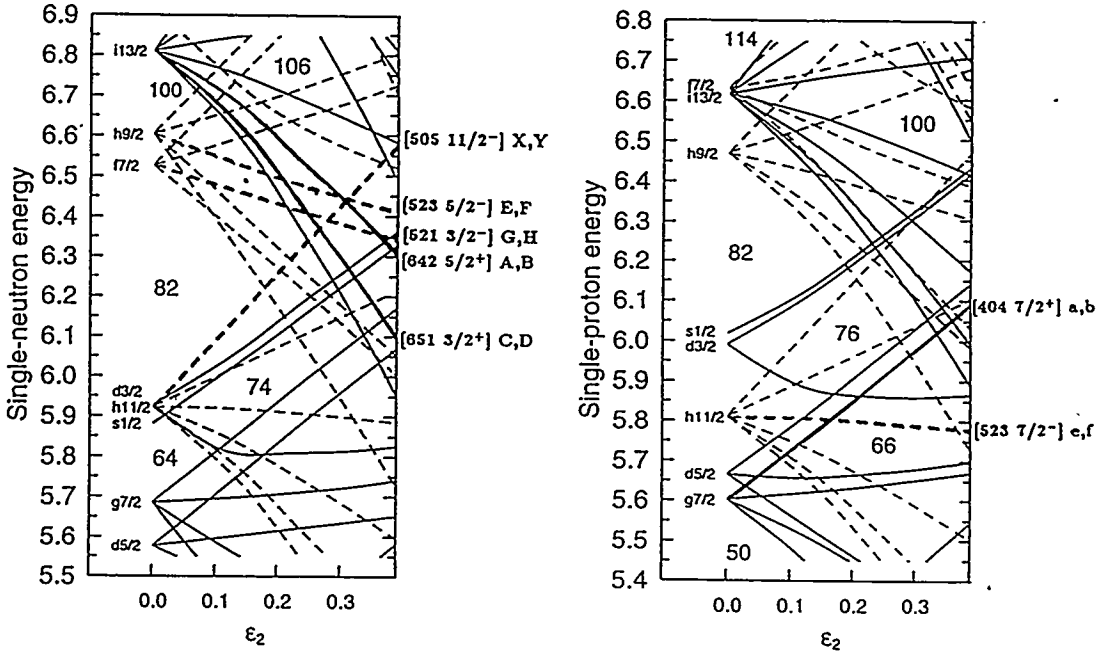


*Fig. 2. Nilsson diagrams with labels of orbits relevant for the present discussion on interactions.*

## Band interaction

Each time two rotational bands of the same parity and signature cross each other there is a potential possibility that an interaction takes place at the spin(s) where the levels come closest. The regular rotational pattern may thus be disturbed if the interaction is strong enough to shift the level energies, and $\gamma$-transitions may occur between the bands.

From the presentation of the band structures measured in $^{163}$Er in the bottom part of fig. 1 one can realize the possibility of ~23 potential crossings. Of these, E2 cross band transitions have been observed in 16 cases. These crossings are marked with circles in fig. 1.

The technique of analysing interactions between up to three bands follows the procedure given in ref. [3] and references therein. Most of the cases presented here are rather sharp crossings isolated from other near-lying bands. Therefore, the extracted interaction strength depends only weakly on the parameters used for describing the unperturbed band energies, as long as the fit to the perturbed energies is good for the few states with mixed wave functions. As a general rule, the value of the interaction strength is close to half the distance between the closest levels for sharp crossings, if out of band transitions are observed. The dependence on the difference between the values of quadrupole moments is largest if the interpolated crossing occurs halfway between two adjacent spin values, which causes cancellation effects from the relative phases of the mixed wavefunctions.

The band crossings observed in the present study of $^{163}$Er sample a variety of (multi)-quasiparticle configurations, and the extracted strengths are listed in table 1 organized according to type of crossing and relevant parameters such as number of quasi-particles, the values of K and the reliability of the assignments.

The crossing between two different one-quasiparticle bands occurs occasionally if the bands built on the basic Nilsson states have different alignment and/or moments of inertia. Examples of one quasi-particle crossings in $^{163}$Er are [X,Y] = [$\nu h_{11/2}$] crossing with [G,H] = [$\nu f_{7/2}$] with very small interactions. These orbits are in the Nilsson diagram of fig. 2 seen to have rather different slopes. They are reminiscent of the proton orbits $h_{9/2}[541\ 1/2^-]$ and $h_{11/2}[523\ 7/2^-]$, which are also high-j orbits of different slopes. The interaction is caused by the Coriolis force, and is small [4] as expected [5]. Another case in $^{163}$Er is a crossing between the similar orbits [G] = [$\nu f_{7/2}$] and [E] = [$\nu h_{9/2}$], which in the presence of the aligned [AB] neutrons has a considerably larger interaction.

Well known examples of crossings between one- and three quasiparticle bands are those corresponding to the g-S band crossing in even-even nuclei with the S-band composed of a pair of aligned quasiparticles in a high-j orbit. In the rare earths region the aligned pair [AB] of $i_{13/2}$ quasineutrons comprizes the S-band. This crossing is pairing induced, and the strength of the interaction is an oscillatory function of the position of the neutron Fermi level relative to the $i_{13/2}$ subshell. [6] A very well developed second $i_{13/2}$ [BC]-crossing with [C], [CAB] and [A] followed throughout the crossing region is observed in $^{163}$Er. The interaction at the proton $h^2_{11/2}$ (ef) alignment is determined in various configurations in $^{163}$Er varying between 15 and 30 keV.

Crossings with interaction between one- and three quasiparticle bands may also occur in cases where all the quasiparticle constituents are different. Likewise, bands built on various multi-quasiparticle structures may cross, where the number of quasiparticle constituents in the two bands differs by two, and several of the quasiparticle constituents are different. Several examples are given in table 1.

A whole family of crossings of multi-quasiparticle configurations occurring at rather high spin in $^{163}$Er show interaction strength of the order of 6-15 keV. The assignments here are not entirely certain with respect to the combination of signatures from the different orbits. There are, in most of these cases, changes in quasiparticle configuration as well as in constituent aligned pairs.

Table 1. Interactions between rotational bands in $^{163}$Er.
Orbits differing between the interacting configurations are underlined.

| $K_1$ | Interacting bands Label$_1$⟺Label$_2$ | $K_2$ | Strength V keV | $\sim \Delta K$ $\hbar$ | ~Spin $\hbar$ | $\sim \Delta i$ $\hbar$ |
|---|---|---|---|---|---|---|
| 1-qp band crossing 1-qp band: | | | | | | |
| 11/2 | X ⟺ G | 3/2 | < 2 | 4 | 11 | 0 |
| 11/2 | Y ⟺ H | 3/2 | < 2 | 4 | 11 | 0 |
| 5/2 | ABE ⟺ ABG | 3/2 | 50-80 | 1 | 16 | 0 |
| 1,3-qp band crossing 3,5-qp band with aligning pair: | | | | | | |
| 5/2 | A ⟺ ABC | 5/2 | 49 | 0 | 24 | 4 |
| 5/2 | ABC ⟺ ABCef | 5/2 | 25-30 | 0 | 35 | 5.5 |
| 5/2 | EAB ⟺ EABef | 5/2 | ~15 | 0 | 34 | 5 |
| 5/2 | FAB ⟺ FABef | 5/2 | ~15 | 0 | 34 | 4.5 |
| Multi-qp bands, low-K*, some assignments uncertain: | | | | | | |
| 5/2 | ABD ⟺ ABCEG | 9/2 | (~13) | 2 | 29 | 0 |
| 9/2 | ABEDH ⟺ ABECG | 9/2 | (~14) | 0 | 23 | 0 |
| 9/2 | ABCEH ⟺ ABCef | 5/2 | ~6 | 2 | 32 | 5 |
| 9/2 | ABCFG ⟺ ABCef | 5/2 | ~11 | 2 | 28 | 4 |
| 3/2 | ABH ⟺ ABFef | 5/2 | ~10 | 1 | 29 | 4 |
| Multi-qp bands, medium-K uncertain, high-K firm assignment: | | | | | | |
| 13/2 | ACE ⟺ Aea | 19/2 | 1-2 | 3 | 21 | 0 |
| Multi-qp bands, High-K, firm assignments : | | | | | | |
| 11/2 | X ⟺ Afa | 19/2 | 1.4 | 3 | 15 | 3.5 |
| 11/2 | Y ⟺ Aea | 19/2 | 1.3 | 3 | 15 | 3.5 |
| 19/2 | AXG ⟺ ABEea | 19/2 | 16 | 0 | 21 | 3.5 |
| 19/2 | AYG ⟺ ABEfa | 19/2 | 14 | 0 | 21 | 3.5 |

* Estimated K-value

In the cases of bands with high K-values and firm assignments listed in the bottom part of table 1, the bands [X,Y] = $[\nu h_{11/2}]$ crossing with [faA,eaA] = $[\pi h_{11/2} \otimes \pi g_{7/2} \otimes \nu i_{13/2}]$ have a difference in K of 3 units and the interaction is small, ~ 1.3 keV. (The two-quasiproton state, $[\pi h_{11/2} \otimes \pi g_{7/2}]_{K=7}$ is known in neighbouring even-even nuclei [7]). Here there is a change in parity between the quasineutron constituents and also between the two quasiprotons and one may have to invoke the octupole vibrational degrees of freedom, in addition to possible residual neutron-proton interactions. The additional high-K band crossings in $^{163}$Er, have more quasiparticles involved. The two bands, [faEAB,eaEAB] = $[\pi h_{11/2} \otimes \pi g_{7/2} \otimes \nu h_{9/2} \otimes \nu i^2_{13/2}]$ and [YAG,XAG] = $[\nu h_{11/2} \otimes \nu f_{7/2} \otimes \nu i_{13/2}]$ have the same K=19/2, and a much larger interaction of ~ 15 keV. Yet, quite complicated changes in the wavefunctions must occur at the crossing. There are changes in the relative signatures compared to the case involving the pure X and Y orbitals, and, probably also coupling to quadrupole degrees of freedom are important, in addition to the octupole degrees of freedom. Some of the ingoing configurations

are indeed known to have related enhanced E1 transition strength between them which have been interpreted [8] in terms of coupling to octupole vibrational degrees of freedom.

## Summary

The present paper has focussed on nuclear structure information that can be extracted from careful analyses of $\gamma$-transitions between the rotational band structures. Non-negligible interactions occur between bands of quite different structure. Specific cases of bands with firmly established configuration contain unique structural information. Furthermore, the average size of band interactions are of crucial importance for understanding phenomena at higher excitation such as rotational damping.

With improved arrays of considerably higher sensitivity such information will become available in much broader ranges of spin and excitation energy in the future. We may look forward to a possible mapping of band interactions with enough combinations to separate the effects of vibrational couplings from the residual two-body interactions of various kinds.

# References

[1] D.C. Radford, Nucl. Inst. and Meth. in Phys. Res. **A361** (1995) 297.

[2] A. Brockstedt, J. Lyttkens-Lindén, M. Bergström, L.P. Ekström, H. Ryde, J.C. Bacelar, J.D. Garrett, G.B. Hagemann, B. Herskind, F.R. May, P.O. Tjøm and S. Frauendorf, Nucl. Phys. **A571** (1994) 337

[3] R.A. Bark, G.B. Hagemann, B. Herskind, H.J. Jensen, W. Korten, J. Wrezesinski, H. Carlsson, M. Bergström, A. Brockstedt, A. Nordlund, H. Ryde, P. Bosetti, S. Leoni, F. Ingebretsen and P.O. Tjøm, Nucl. Phys. **A591** (1995) 265.

[4] H.J. Jensen, G.B Hagemann, P.O. Tjøm, S. Frauendorf, A. Ataç, M. Bergström, A. Bracco, A. Brockstedt, H. Carlsson, P. Ekström, J.M. Espino, B. Herskind, F. Ingebretsen, J. Jongman, S. Leoni, R.M. Lieder, T. Lönnroth, A. Maj, B. Million, A. Nordlund, J. Nyberg, M. Piiparinen, H. Ryde, M. Sugawara and A.Virtanen, Z.Phys. **A340** (1991) 351.

[5] S. Misotori and I. Hamamoto, Contr. 8th Nordic Meeting on Nuclear Physics, Ronneby Brunn, Sweden 1995, p. 74.

[6] R. Bengtsson, I. Hamamoto and B. Mottelson, Phys. Lett. **73B** (1978) 259.

[7] C.A. Fields, K.H. Hicks, R.A. Ristinen, F.W.N. de Boer, L.K. Peker, R.J. Peterson and P.M. Walker, Nucl. Phys. **A422** (1984) 215.

[8] G.B. Hagemann, I. Hamamoto and W. Satula, Phys. Rev. **C47** (1993) 2008.

# Shell Model for Warm Rotating Nuclei

M. Matsuo, K. Yoshida[a], T. Døssing[b], E. Vigezzi[c], and R.A. Broglia[b,c]

*Yukawa Institute for Theoretical Physics, Kyoto University, Kyoto 606-01, Japan*
[a] *Department of Physics, Kyoto University, Kyoto 606-01, Japan*
[b] *Niels Bohr Institute, University of Copenhagen, Copenhagen Ø, Denmark*
[c] *INFN sez. Milano, and Dept. of Physics, University of Milan, Italy*

**Abstract**

Utilizing a shell model which combines the cranked Nilsson mean-field and the residual surface and volume delta two-body forces, we discuss the onset of rotational damping in normal- and super-deformed nuclei. Calculation for a typical normal deformed nucleus $^{168}$Yb indicates that the rotational damping sets in at around 0.8 MeV above the yrast line, and about 30 rotational bands of various length exists at a given rotational frequency, in overall agreement with experimental findings. It is predicted that the onset of rotational damping changes significantly in different superdeformed nuclei due to the variety of the shell gaps and single-particle orbits associated with the superdeformed mean-field.

## 1 Introduction

In deformed nuclei, the collective rotational motion is a fundamental mode of excitation and the levels near the yrast line all form discrete rotational band structure characterized by sequence of strong intra-band E2 transitions. In some of normally deformed rare-earth nuclei, up to around 20 different rotational bands have been observed by recent discrete gamma ray spectroscopy studies. Far above the yrast line, on the other hand, the levels do not form anymore the rotational bands, implying damping of the collective rotational motion [1]. This is evidenced experimentally in the fluctuation analysis of the quasicontinuum $E_\gamma \times E_\gamma$ spectra [2, 3], which measures an effective number of rotational bands $\sim 30$ at a given rotational frequency.

In order to describe the transition from the discrete rotational band structures to the damped rotational motion, we formulate a shell model which combines the cranked Nilsson mean-filed and a residual effective two-body force [4]. In this model, unperturbed rotational bands are constructed for all many-particle many-hole configurations defined for the cranked Nilsson single-particle orbits. The residual effective two-body force acting among these unperturbed states is then taken into account by shell model diagonalization. When the level density is high, the unperturbed states with different alignment are admixed with complex amplitudes. This results in a dispersion of rotational frequency within each eigenstate, implying the damping of rotational motion.

We apply the same model to superdeformed nuclei [5]. The large shell gap characteristic to the superdeformed mean field is expected to cause significant weakening of the rotational damping effect [6]. It should be noticed that the shell gap varies with $N$ and $Z$ even within the $A \sim 150$ region. This causes significant variation of the onset of rotational damping in different superdeformed nuclei. In addition, we find that a specific single-particle property associated with the high-$K$ orbits located near the Fermi surface causes additional weakening of the rotational damping. As a consequence, the number of superdeformed rotational bands in a Hg isotope is predicted to be significantly increased, reaching about 150.

## 2 The model

We start with the cranked Nilsson single-particle Hamiltonian. The static pairing field is not included at this stage since we are interested mainly in levels at very high spins $I \gtrsim 30$, where the pairing gap is expected either

to be small or to vanish, due to the Coriolis anti-pairing effect. We construct *diabatic* single-particle basis of this Hamiltonian in a way similar to Ref.[7]. Since the interactions at the sharp crossings often present in the adiabatic orbits are removed, the diabatic orbits changes smoothly as a function of the rotational frequency. This enables us to define unperturbed rotational bands each of which has a specific $n$p-$n$h configuration. The energy of a $n$p-$n$h configuration $|\mu\rangle$ in the intrinsic frame is given by

$$E'_\mu(\omega) = \sum_{\text{occupied } i \text{ in } \mu} e'_i(\omega) \tag{1}$$

where the summation of the single-particle routhian $e'_i$ runs over the orbits which are occupied in the configuration. The energy $E_\mu(I)$ of a configuration $\mu$ in the laboratory frame is approximated by [6, 8]

$$E_\mu(I) = E'_\mu(\omega_I) + \omega_I I + \frac{(I - J_{x,\mu}(\omega_I))^2}{2J^{(2)}_\mu}, \tag{2}$$

where $J_{x,\mu}(\omega_I)$ is the projection of the angular momentum along the rotational axis and $J^{(2)}_\mu = dJ_{x,\mu}/d\omega$. This second order approximation is justified by the use of the diabatic basis which has smooth $\omega$ dependence. The rotational frequency $\omega_I$ is chosen so that the angular momentum condition $\langle J_x\rangle = I$ is satisfied for a given angular momentum $I$, where $\langle J_x\rangle$ represents the angular momentum projected along the rotational axis, averaged over configurations. The energy $E_\mu(I)$ is renormalized by the Strutinsky method in order to correct absolute rotational energy. The energies $\{E_\mu(I)\}$ and the many-body wave functions $\{|\mu(I)\rangle\}$ define the shell model basis at a given spin $I$.

As the effective two-body force, we adopt the surface delta interaction (SDI)[9]

$$v(1,2) = -4\pi V_0 \sum_{LM} Y^*_{LM}(\Omega_1) Y_{LM}(\Omega_2). \tag{3}$$

The strength $V_0$ is taken to be the standard value $V_0 = 27.5/A$ MeV [10]. In order to demonstrate that the result does not depend very much on the specific choice of the interaction, we also make calculation using the volume delta force $v(1,2) = v_\tau \delta(\vec{x}_1 - \vec{x}_2)$, whose strength is chosen as $v_{nn} = v_{pp} = 340$ fm$^3$MeV and $v_{pn} = 500$ fm$^3$MeV taken from Ref.[11], which are evaluated from comparison with more realistic residual interactions, independently of the SDI. Since the mean-field potential is represented by the Nilsson deformed potential, it is the residual part of the two-body nuclear effective force that is to be taken into account as the shell model two-body interaction. Thus the shell model Hamiltonian for the basis states $\{|\mu(I)\rangle\}$ at spin $I$ is constructed as

$$H(I)_{\mu\mu'} = E_\mu(I)\delta_{\mu\mu'} + V(I)_{\mu\mu'} \tag{4}$$

where $V(I)_{\mu\mu'} = \langle\mu(I)|V_{res}|\mu'(I)\rangle$ are the matrix elements of the residual two-body interaction. The energy eigenstates $|\alpha(I)\rangle = \sum_\mu X^\alpha_\mu(I)\,|\mu(I)\rangle$ and their level energies $E_\alpha(I)$ of the shell model Hamiltonian are obtained by numerical diagonalization. We consider all $n$p-$n$h excitations, but truncate them according to the energy; i.e., the lowest 1000 basis states $|\mu(I)\rangle$ are adopted for the diagonalization at given spin and parity. We found that the lowest 300 eigensolutions are rather stable against the truncation. This covers approximately up to 2.3 MeV and 4 MeV above the yrast line for the normal and super-deformed nuclei considered, respectively.

Assuming that a state at spin $I$ is connected to a state at $I-2$ with the same intrinsic configuration $|\mu\rangle$ by a constant E2 matrix elements, the E2 transition probability between the mixed eigenstates is given by $B(E2, \alpha I \to \alpha' I-2) = \frac{15}{128\pi} Q_o^2 p_{\alpha I,\alpha' I-2}$ with normalized strength $p_{\alpha I,\alpha' I-2} = \{\sum_\mu X^\alpha_\mu(I) X^{\alpha'}_\mu(I-2)\}^2$.

# 3 Normal deformed nucleus $^{168}$Yb

As a typical case of normal deformed nuclei, we show in Fig.1 the calculated energy levels and E2 transitions for $(+,0)$ states (positive parity and even spin) in $^{168}$Yb . In this picture, a reference rotational energy is subtracted from the calculated energy so that the vertical axis represents roughly the internal excitation energy of the nucleus. The solid lines connecting the energy levels represents strong E2 transitions. We use the convention that the E2 decay is "strong" if the associated normalized strength satisfies $p > 1/\sqrt{2} = 0.707$.

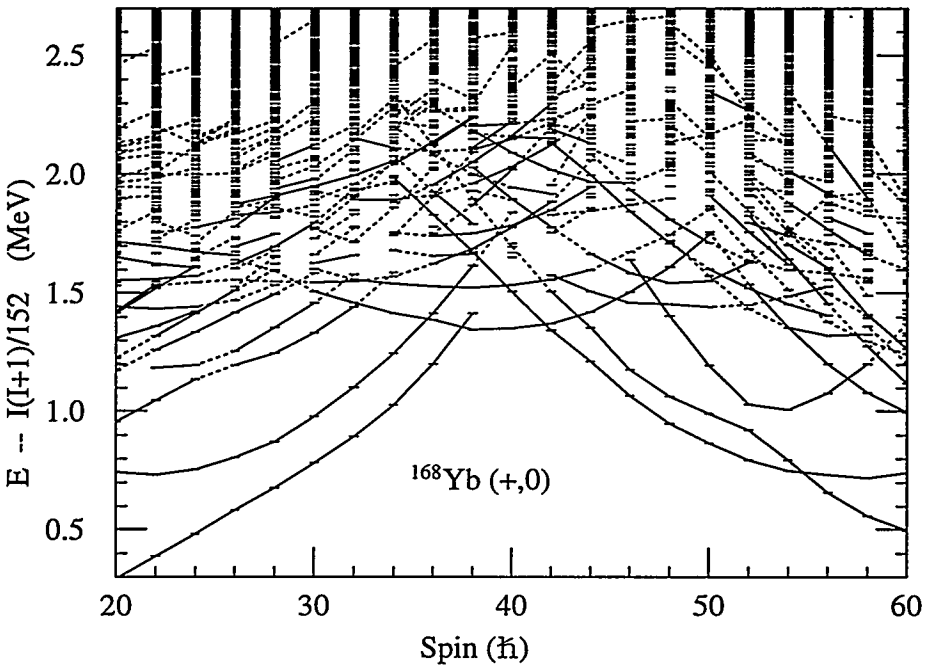


Figure 1: The levels in $^{168}$Yb with $(+,0)$ calculated with use of the SDI are shown with small horizontal bars. A reference energy $I(I+1)/2J$ with $J = 76$ MeV$^{-1}$ is subtracted. The stretched E2 transitions which have the normalized strength $p_{\alpha I,\alpha' I-2}$ larger than 0.707 are plotted with solid lines connecting initial and final levels of the transitions. Transitions with normalized strength between 0.5 and 0.707 are plotted with dashed lines.

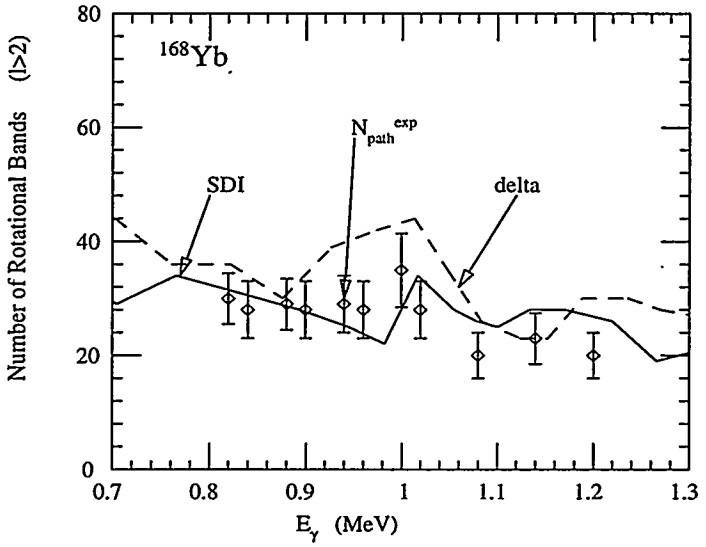


Figure 2: The calculated number of bands is compared with the experimental effective number of paths [3] extracted from the first ridge of $(E_{\gamma 1}, E_{\gamma 2})$ spectra in $^{168}$Yb . The horizontal axis denotes the average gamma-ray energy $E_\gamma = (E_{\gamma 1} + E_{\gamma 2})/2$.

Weaker transitions with $0.5 < p < 0.707$ are displayed with dashed lines. It is seen that the strong E2 transitions (solid lines) form sequences of levels which are aligned regularly along a parabola like curve. Such sequences of levels represent rotational band structures. Most of the rotational bands lie in the region near the yrast, while the levels at higher excitation energy as a rule do not form band structures. An convenient measure to quantify the rotational damping is the branching number [12, 13]

$$n_{\rm branch}(\alpha) \equiv \left( \sum_{\beta} p^2_{\alpha I, \beta I-2} \right)^{-1} \tag{5}$$

which counts effectively the number of the E2 branches for decays from a level $\alpha$ at $I$ to levels at $I-2$. One may define the onset of rotational damping by $n_{\rm branch} > 2$, implying that the stretched E2 decay from the level $\alpha$ has more than two branches. By the same token, the rotational bands are characterized by $n_{\rm branch} < 2$, which in fact does not differ very much from the criterion $p > 0.7$ used to plot Fig.1. As a function of the intrinsic excitation energy $U$ measured from the yrast line, the branching number increases exponentially. Its value exceeds 2 at around 0.8 MeV above yrast, implying the onset of damping at this energy. At higher excitation energy, the E2 strength are fragmented over many decay branches, e.g., $n_{branch} \sim 10$ and 40 at $U = 1.5$ and 2.0 MeV, respectively.

The calculated results can be compared with the experiments. The quasi-continuum fluctuation analysis extracts an effective number of gamma decay paths from the double-coincident $E_\gamma \times E_\gamma$ spectrum [2, 3]. When this method is applied to the first ridge in the spectrum, the effective number of paths essentially corresponds to the number of discrete rotational bands probed by two consecutive intra-band E2 transitions. A corresponding quantity can be defined in the present theory by counting the number of states which satisfy the criterion $n_{\rm branch} < 2$ for at least two consecutive steps $I+2 \to I \to I-2$.

The calculated number of rotational bands agrees quite well with the experimental effective number of path. Both the SDI and the volume delta force produce similar results. It should be remarked, however, that such interactions as the paring plus quadrupole-quadrupole force cannot bring about the rotational damping at this excitation energy region. We found [4, 12, 13] that the high-multipole components with $L \gtrsim 4$ contained in the SDI are essential for the rotational damping. The high multipoles are present also in the volume delta force, but not in the pairing plus quadrupole-quadrupole force.

More accurate comparison between the theory and the experiments requires evaluation of the feeding probabilities. This is possible by making a simulation of the whole gamma decay cascades combining microscopically calculated levels and E2 transitions with statistical description of E1 decays since the present model can describe levels up to about 2 MeV above yrast line at high spins, where most of the gamma decay cascades of a warm rotating compound nucleus proceed. Such a microscopic simulation has been developed recently[14]. From the $E_\gamma \times E_\gamma$ spectrum produced from the simulation, the effective number of paths is extracted in the same way as the experimental analysis. In this manner, we can make comparison which does not depend on the particular choice of the threshold for $n_{branch}$ used for the definition of the number of bands. It is found that the effective numbers of paths both in the simulation and in the experiments for $^{168}$Yb agree quite well [14].

# 4 Superdeformed nuclei

Because of the shell gap characteristic to the superdeformed mean-field, the level density of the SD states becomes much lower than in the normal deformed case. This implies that the onset of rotational damping takes place at higher intrinsic excitation energy $U$ than in normal deformed nuclei [6] since the configuration mixing effect is governed by the balance between the size of the residual interaction matrix elements (which is rather independent on deformation) and the level density [1]. However, the shell effects changes with $N$ and $Z$ even within the $A \sim 150$ region as the deformation and the Fermi surface move.

The calculation is done in a similar way to the normal deformation, but the deformation parameter $(\epsilon, \epsilon_4)$ is determined by minimizing the potential energy surface. We consider only the superdeformed states and neglect presence of the weakly deformed states by assuming the barrier between the SD and ND minima is high enough. Competition with the fission is also neglected.

Table 1 shows the calculated onset energy $U_{onset}$ defined by the condition $n_{branch} = 2$ and the number of superdeformed bands, which is calculated in the same way as in Fig.2, but averaged over spin range

| | $U_{\rm onset}$[MeV] | $N_{\rm band}$ | $A/a$[MeV] | $E_{\rm shell}$[MeV] |
|---|---|---|---|---|
| $^{143}$Eu | 2.1 | 47 | 18.5 | 3.56 |
| $^{146}$Gd | 2.4 | 56 | 17.6 | 3.94 |
| $^{147}$Gd | 2.3 | 53 | 17.5 | 4.02 |
| $^{148}$Gd | 2.5 | 58 | 19.1 | 4.31 |
| $^{149}$Gd | 2.8 | 68 | 19.4 | 4.59 |
| $^{150}$Gd | 3.0 | 88 | 23.9 | 5.14 |
| $^{150}$Tb | 2.5 | 66 | 19.0 | 4.43 |
| $^{151}$Tb | 2.8 | 72 | 22.6 | 5.08 |
| $^{152}$Tb | 2.4 | 87 | 18.2 | 4.53 |
| $^{151}$Dy | 1.7 | 68 | 13.8 | 3.09 |
| $^{152}$Dy | 2.4 | 74 | 18.9 | 4.55 |
| $^{153}$Dy | 1.9 | 74 | 15.9 | 4.19 |

Table 1: The onset energy $U_{onset}$ and the number of superdeformed bands $N_{band}$ calculated with the volume delta interaction. The level density parameters $a$,which are obtained by a fit to the calculated level density at $U = 2.5$ MeV and $I = 50$. Since the level density parameter is often expressed as $a = A/a_0$, the table lists the value of $a_0$ in unit of MeV instead of $a$. The fifth column lists the shell correction energy.

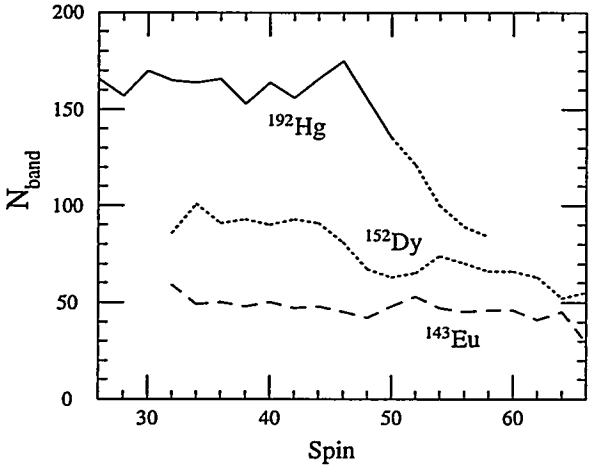


Figure 3: The calculated number of superdeformed bands for $^{143}$Eu , $^{152}$Dy , and $^{192}$Hg as a function of spin.

I=40-60, for several superdeformed nuclei in the $A \sim 150$ region. The onset energy $U_{onset} = 1.7 \sim 3.0$ MeV is much higher than in normal deformed $^{168}$Yb as expected from the above discussion. The number of bands $N_{band} = 50 - 90$ is also larger than $N_{band} \sim 30$ in $^{168}$Yb . The most striking feature is that the onset energy as well as the number of bands has strong variation of nearly factor 2, depending on nucleus. This variation is clearly connected to the property of the level density of superdeformed states and the shell effect of the mean-field. In the same table, we list the shell correction energy and the level density parameter $a$, which is extracted from a fit of the Fermi gas expression [8] $\rho(E) = \frac{\sqrt{\pi}}{48} a^{-\frac{1}{4}} E^{-\frac{5}{4}} \exp 2\sqrt{aE}$ to the microscopically calculated level density obtained from explicit counting of unperturbed superdeformed rotational bands. All these quantities show similar dependence on $N$ and $Z$ numbers. The onset energy and the number of bands become maximum in $^{150}$Gd, which has the largest superdeformed shell effect in the present calculation.

The same calculation is performed for superdeformed Hg isotopes in the $A = 190$ region. In these nuclei, the neutron single-particle orbits near the $N \sim 112$ Fermi surface have a specific feature which are not present in $A = 150$ region. Namely, there exist such orbitals as $\nu$[505]11/2, $\nu$[512]5/2, and $\nu$[514]7/2 which have high $K$ values and show very little alignment against rotational perturbation (the single-particle routhian energy of these orbits are almost constant as a function of rotational frequency). These orbits can contribute to creating particle-hole excitations, but have little contribution to the dispersion of rotational

frequency. In other words, these orbits do not affect rotational behavior no matter whether they are occupied or not. As a consequence, the rotational damping is effectively weakened by these orbits and the number of superdeformed bands is significantly increased, reaching about 150, as shown in Fig.3.

The predicted variation of the rotational damping effect has not been experimentally tested yet while there is one fluctuation analysis data for $^{143}$Eu , for which effective number of paths is about 10-40, depending on the gamma-ray energy [15]. Although the gamma-ray energy dependence could suggest possible barrier penetration between the SD and normal states and the fission competition, the maximum number $\sim 40$ is consistent with the present result. It should be interesting to search experimentally the significant variation of the rotational damping in superdeformed nuclei.

# References


[1] B.Lauritzen, T.Døssing and R.A.Broglia, Nucl. Phys. **A457**(1986) 61

[2] B.Herskind, A.Bracco, R.A.Broglia, T.Døssing, A.Ikeda, S.Leoni, J.Lisle, M.Matsuo, and E.Vigezzi, Phys. Rev. Lett. **68**(1992) 3008.

[3] T. Døssing, B. Herskind, S. Leoni, M. Matsuo, A. Bracco, R.A. Broglia, and Vigezzi, Phys. Rep. **268** (1996) 1.

[4] M. Matsuo, T. Døssing, E. Vigezzi, R.A. Broglia, and K. Yoshida, preprint.

[5] K. Yoshida and M. Matsuo, preprint nucl-th/9604015.

[6] S.Åberg, Phys. Rev. Lett. **64**(1990) 3119;
S.Åberg, Prog. Part. Nucl. Phys. vol.28 (Pergamon 1992) p.11.

[7] T.Bengtsson, Nucl. Phys. **A496** (1989) 56.

[8] S.Åberg, Nucl. Phys. **477** (1988) 18.

[9] I. M. Green and S. A. Moszkowski, Phys. Rev. **139** (1965)B790;
R.Arview and S.A.Moszkowski, Phys. Rev. **145** (1966)830.

[10] A. Faessler, Fortschr. Phys. **16** (1968) 309.

[11] B.W. Bush, G.F. Bertsch and B.A. Brown, Phys. Rev. **C45** (1992) 1709.

[12] M. Matsuo, T. Døssing, E. Vigezzi and R.A. Broglia, Phys. Rev. Lett. **70** (1993) 2694.

[13] M. Matsuo, T. Døssing, B. Herskind, S. Frauendorf, E. Vigezzi and R.A. Broglia, Nucl. Phys. **A557** (1993) 211c.

[14] A. Bracco, P. Bosetti, S. Frattini, E. Vigezzi, S. Leoni, T. Døssing, Herskind, and M. Matsuo, Phys. Rev. Lett. **76** (1996) 4484

[15] S. Leoni, B. Herskind, T. Døssing, K. Yoshida, M. Matsuo, A. Ataç, G.B. Hagemann, F. Ingebresten, H.J. Jensen, R.M. Lieder, G.V. Marti, N. Nica, J. Nyberg, M. Piparinen, H. Schnare, G. Sletten, K. Stähle, M. Sugawara, P.O. Tjøm, and A. Virtanen, Phys. Lett. **B353**(1995)179.

# Possible Conservation of the K-Quantum Number in Excited Rotating Nuclei

A.Bracco[1], P. Bosetti[1], S. Leoni[1], S. Frattini[1], T. Døssing[2], B. Herskind[2], G. B. Hagemann[2], M. Matsuo[3], and E. Vigezzi[1].

1. *Universitá di Milano and INFN sez. Milano, Milano(Italy)*

2. *The Niels Bohr Institute, Copenhagen*

3. *The Yukawa Institute, Kyoto, Japan*

## Abstract

The $\gamma$-cascades feeding into low-K and high-K bands in the nucleus $^{163}$Er are investigated by analyzing variances and covariances of the spectrum fluctuations. The study of the covariance between pairs of gated spectra reveals that the cascades feeding into the low-K bands are completely different from those feeding the high-K bands. In addition, the number of decay paths obtained analysing the ridge and the valley in spectra gated by high-K transitions is different than that deduced from the total spectrum. This result is well reproduced with microscopic calculations of strongly interacting bands. It is concluded that the K-selection rules are effective for the excited rotational bands within the angular momentum region probed by the experiment, $30\hbar \leq I \leq 40\hbar$.

## 1. Introduction

The $\gamma$-decay among the cold discrete rotational bands is governed by selection rules associated with the quantum numbers of the intrinsic structure. At excitation energies high above the yrast line, such selection rules may be lost. Here, the very large level density implies a strong fragmentation of the rotational decay [1] and the fragmented rotational states might have intrinsic structures that are a random combination of the available configurations [2].

The first attempt to investigate the validity of selection rules for unresolved rotational bands was made recently, focussing on the K-quantum number. The purity of the K-quantum number for neutron resonance states at low spin has attracted renewed interest [3,4]. With the present work we address a complementary problem, namely the validity of K-quantum number for nuclear states at higher rotational frequency but lower thermal energy than that of the neutron resonance states.

The method employed for this study is based on the analysis of the rotational quasi continuum using the Fluctuation Analysis Method (FAM) [5,6]. The nucleus chosen, $^{163}$Er, is an attractive case to study the interaction between low-K and high-K bands. It has rotational bands with K= 19/2 lying at rather high excitation energy above yrast (from 0.8 to 1.4 MeV) [7,8], a region that is expected to be dominated by the mixing

of rotational bands due to residual interaction. The problem of the conservation of K-quantum number can therefore be addressed by studying the configuration dependence of the mixing of the rotational bands.

In the following section we discuss the study of the experimental data by the fluctuation analysis method. In particular, a covariance analysis was made for the first time [9]. The comparison with theory, based on simulated spectra calculated with rotational bands mixed by residual interaction, is discussed in section 3.

It will be concluded from both the ridge and the valley analysis that K-selection rules are still effective for the excited rotational bands within the angular momentum region, $30\hbar \leq I \leq 40\hbar$, probed by the experiment.

## 2. The Experiment and the Fluctuation Analysis of the data

Three and higher folds of $\gamma$-ray coincidences were collected using the GA.SP multi-detector array at the Tandem Accelerator Laboratory of Legnaro (Italy). The reaction employed was $^{18}O+^{150}Nd$ with a bombarding energy , $E_{beam} = 87$ MeV, leading to the population of $^{162,163}Er$ as the main evaporation residua. A number of two-dimensional $E_{\gamma 1} \times E_{\gamma 2}$ spectra gated by low lying transitions in bands of both low-K and high-K quantum number were obtained (cf. Fig.1 in [9]).

The fluctuations of counts in each channel of these 2-D spectra is expressed as variance $\mu_2$ [5]. The correlations in fluctuations between two spectra are expressed by the covariance of counts [9], defined as,

$$\mu_{2,cov}(A,B) \equiv \frac{1}{N_{ch}} \sum_j (M_j(A) - \tilde{M}_j(A))((M_j(B) - \tilde{M}_j(B))$$

where $M(A)$ and $M(B)$ refer to measured gated spectra and $\tilde{M}$ denotes an average spectrum. The sum is over a two-dimensional 60 keV $\times$ 60 keV window, consisting of $N_{ch}$ channels. The first moment $\mu_1$, that is the average of counts over $N_{ch}$, and the second moment $\mu_2 = \mu_{2,cov}(A,A)$ spectra were also obtained. The program STATFIT [5,9,10] was used.

Typical $\mu_1$, $\mu_2$, and $\mu_{2,cov}$ spectra from matrices gated by low-K, high-K and yrast transitions are shown in figure 1. It should be noted that the ridge-valley structure is strongly enhanced in the $\mu_2$ spectra relative to the original intensity $\mu_1$ spectra. There is also a remarkable difference between the low K - low K covariance, which displays pronounced ridges, and that for low K - high K, which varies in a more random way.

To normalize the covariance and thereby to find the degree of correlation between the two spectra, the correlation coefficient $r(A,B)$ was extracted from the data:

$$r(A,B) \equiv \frac{\mu_{2,cov}(A,B)}{\sqrt{(\mu_2(A) - \mu_1(A))(\mu_2(B) - \mu_1(B))}}.$$

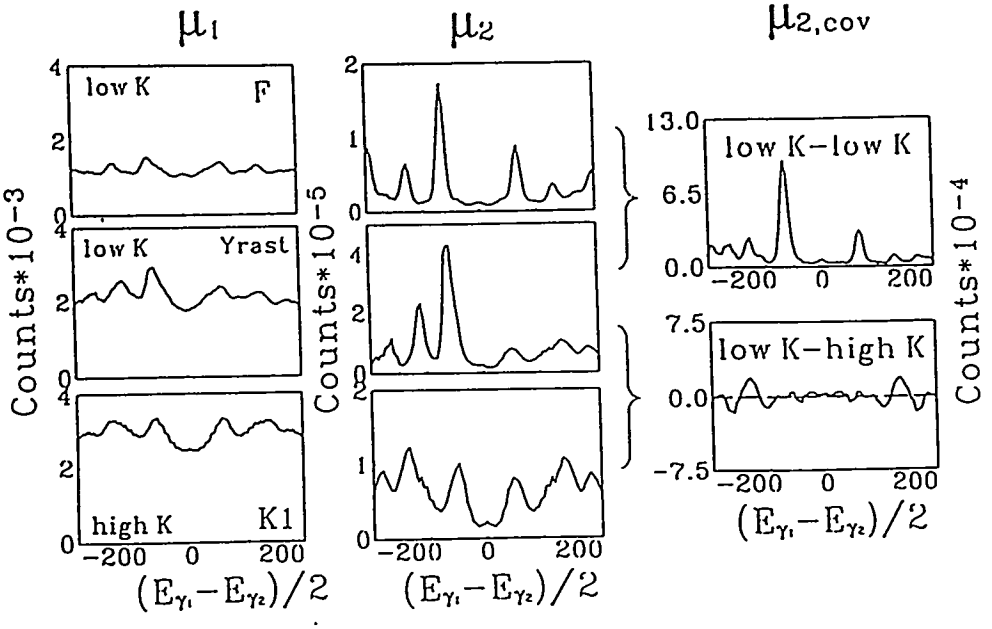


**Fig. 1.** *Spectra of $\mu_1$ (left hand side) and $\mu_2$ (middle) obtained from $\gamma$-$\gamma$ coincidences gated by three different bands (named in each panel). They were obtained projecting the $E_{\gamma 1} \times E_{\gamma 2}$ spectra along the $(E_{\gamma 1} + E_{\gamma 2})/2$ direction onto an $E_{\gamma 1} - E_{\gamma 2}$ axis, with a width of 60 keV. The average transiton energy is 940 keV. The right hand side shows the covariance between pairs of the gated spectra, and they are also evaluated in two dimensions, and then projected. The spectra are not symmetric about 0 because on the right hand side all known discrete transitions were removed before the fluctuation analysis was applied.*

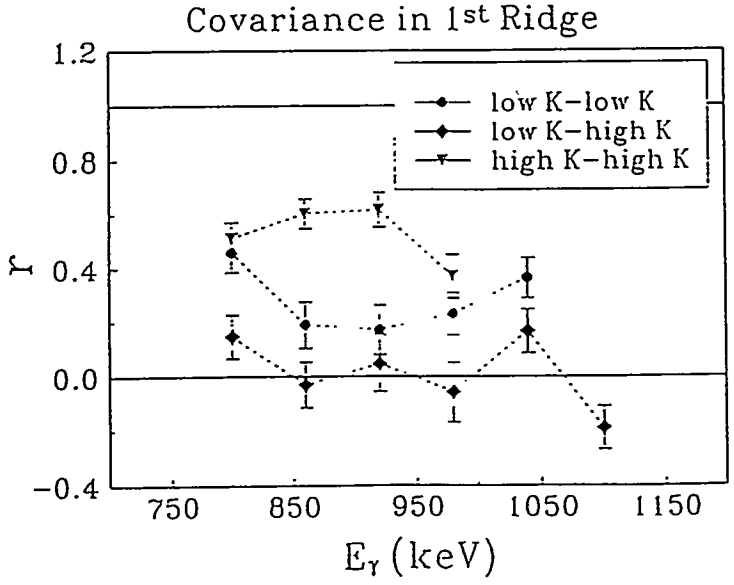


**Fig. 2.** *The correlation coefficients extracted from the first ridge are plotted as a function of $E_\gamma = (E_{\gamma_1} + E_{\gamma_2})/2$.*

The results for the ridge analysis are shown in Fig. 2. The fact that the low(high)-K with low(high)-K conbinations give positive values while low-K with high-K is approximately zero indicates that there are basically no cross-transitions between bands feeding high and low-K bands, suggesting the persistance of K-selection rules for the bands forming the ridges.

From the fluctuation spectra we have also extracted the effective number of decay paths, using the expression $N^{(2)}_{path} = N_{eve} \times (\mu_2/\mu_1 - 1)^{-1}$. Some results for the first ridge are shown in Figs. 3 and 4. About 15 to 20 unresolved bands feeding the high-K bands K2 and K1 are found to exist. In contrast, the analysis of the total spectrum yields 35 rotational bands, in agreement with the results for the $^{168}$Yb nucleus [6]. The number of paths obtained from the analyis of the valley is in the case of high-K bands a factor of 5 smaller than that of the ungated spectrum, as one can see in Fig. 4. It may be emphasised that the results for the total spectrum is very similar to that of the low-K bands (cf. [9]) and therefore a significantly different behaviour is found for the low and high-K bands also in the valley region.

## 3. Comparison with model predictions

In order to obtain a connection between theoretical prediction and the measured quasi continuum, a simulation model of the decay cascades of a rotational nucleus has been developed [11]. This model uses energy levels and transition probabilities calculated with the cranked shell model with residual interaction included.

Spectra of $\gamma$-ray transitions are calculated by assuming a statistical decay process of competing E1 ($\Delta I = 0,\pm 1$) and E2 ($\Delta I = 2$) transitions from the entry states of the residual nucleus to the yrast line via a decay-flow of $\gamma$ rays through microscopically calculated levels. The calculated E2 strengths are characterized by distributions which get more and more fragmented when the energy above yrast, denoted by U, increasees.

The first 400 levels of each spin, parity and signature $(I, \pi, \alpha)$, which are shown to be almost free of truncation problems, are used as input to the simulation and they cover the region up to U $\approx$ 2.5 MeV. Above this energy a continuous distribution of states with level density described by the Fermi gas model is assumed, with level density parameter obtained from the calculated levels. This calculated level density is also used to evaluate the E1 transition probability. The E2 distribution at U$>$ 2.5 MeV was assumed to have a gaussian shape with FWHM denoted by $\Gamma_{rot}$. The $\Gamma_{rot}$ values, extrapolated from the calculated E2 strengths, are of the order of 200 keV.

Because the levels populated by the decay paths are explicitly introduced, it is possible to perform the fluctuation analysis of the simulated spectra. In the case of $^{168}$Yb [11] it has been found that only when residual interaction is included, it is possible to reproduce the experimental $N_{path}$ values. In contrast, using calculations without residual interaction included, large discrepancies with the data are found.

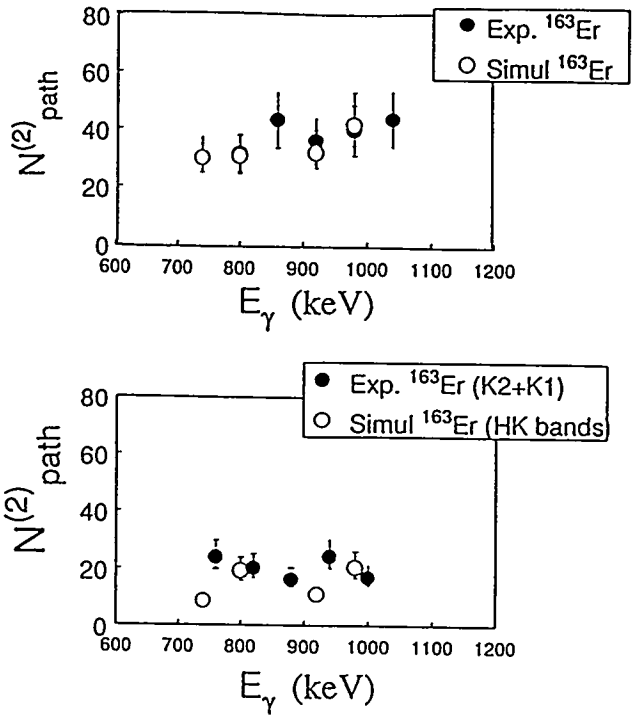


**Fig. 3** *The quantity $N^{(2)}_{path}$ extracted from the first ridge in the total spectrum (top part) and from that gated by high-K transitions. The same quantity is shown for the simulated spectra with open points.*

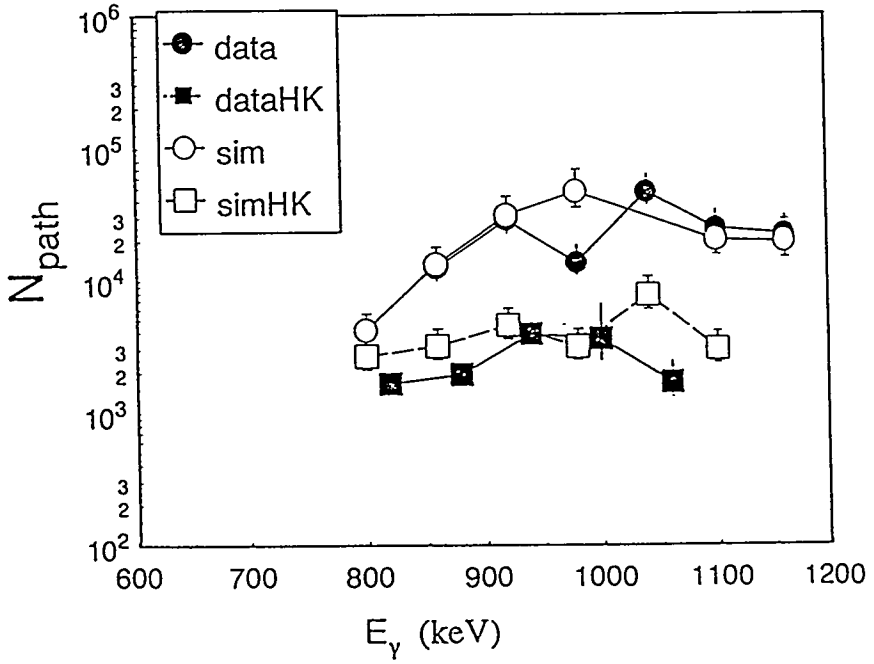


**Fig. 4** *The quantity $N^{(2)}_{path}$ extracted from the valley in the total spectrum and from the spectrum gated by high-K transitions. The same quantity is shown for the simulated spectra with open points.*

The same type of simulations, using microscopic calculations with residual interaction was made for $^{163}$Er to interprete the results of the total spectrum. As one can see in Figs. 3 and 4 the predictions for both the first ridge and for the valley agree with the data.

We have also made an attempt to interprete the results associated to high-K bands. This was done selecting only the $\gamma$-cascades that include at least one transition from high-K states (K$\geq$9.5). For transitions from high-K states we have also eliminated the E1 competition. In addition, since the E2 strength distribution for the calculated high-K states is very narrow, a $\Gamma_{rot} = 20$ KeV has been assumed for U$>$ 2 MeV.

The preliminary results, shown in Figs. 3 and 4, are in good agreement with the data. We can therefore conclude from this comparison that there is basically no mixing of low-K and high-K states also in the region in which low-K bands are strongly mixed.

## 4. Conclusion

The persistance of K-selection rules at high rotational frequency in the continuum region has been investigated in $^{163}$Er making use of the fluctuation analysis method. This technique has been applied to experimental and simulated spectra such that a direct comparison is possible. The results obtained indicate that the states in the quasi continuum from where the feeding of the high-K bands originates are different from those of the low-K bands. In addition, while in the region U$>$ 0.8 MeV low-K bands are found to become progressively strongly mixed by the residual interaction, this does not seem to be true for high-K bands. This can be interpreted as a signature of conservation of K selection rules.

## References


1) M. Matsuo et al.,Phys. Rev. Lett. **70**, (1993),2694.
2) B. R. Mottelson, Nucl. Phys. **A557** (1993)717c.
3) J. Rekstad et al., Phys. Rev. Lett. 65 (1990) 2122.
4) V. G. Soloviev, Phys. Lett. B317 (1993)501.
5) T. Døssing et al., Phys. Rep. 268(1996)1.
6) B. Herskind et al., Phys. Rev. Lett. **68**, (1992), 3008
7) A. Brockstedt et al., Nucl. Phys., **A 557**,(1993)469.
8) P. Bosetti et al. to be published.
9) P. Bosetti et al. Phys. Rev. Lett. **76**,(1996),1204.
10) S. Leoni, Ph. D. Thesis (1992), University of Milano.
11) A. Bracco et al. Phys. Rev. Lett. **76**,(1996),4484.

# Nuclear Structure at the Limits of Resolution: Looking through Individual Wave Functions

Vladimir G. ZELEVINSKY

*Department of Physics and Astronomy and National Superconducting Cyclotron Laboratory, Michigan State University, East Lansing, MI 48824*

60 years ago Niels Bohr [1] suggested the idea of the compound nucleus. Bohr's picture strongly resembles that of quantum chaos [2]. Here we come to the limits of resolution studying particular stationary states at high level density. Our knowledge comes from the experiment and from theoretical constructions, confirmed by the experiment at lower energies and extrapolated into the region where fine resolution measurements are not feasible. Such an analysis was carried out recently for heavy atoms [3] and shell model nuclei [4]. Among complicated states with the same values of integrals of motion, either (i) adjacent states have different structure or (ii) they "look the same" [5] on the microscopic scale. Only (ii) corresponds to strong mixing assumed in the compound nucleus theory. Many-body chaos in nuclei [6,7] is caused by residual interactions rather than by specific shape of the "container" as in quantum billiards. The shell model [8], including all degrees of freedom (in truncated space) along with the symmetry requirements, guarantees the correct level density up to some excitation energy [9]. Therefore one can extrapolate the calculations into *terra incognita* of high lying states.

With exact eigenvalues and many-body eigenfunctions we look first at standard signatures of quantum chaos [2,4,6] as nearest level spacing distribution, spectral rigidity and level dynamics. The limiting predictions based on the Gaussian Orthogonal Ensemble (GOE) of random matrices [2,10] are reached [4,11] already at the residual interaction strength $\approx 0.2$ of the realistic value. As seen with the microscope resolving individual states, the evolution of complexity is not over when the spectral characteristics acquire the GOE properties. Fig. 1 shows information entropy $S^\alpha = -\sum_k (C_k^\alpha)^2 \ln (C_k^\alpha)^2$ which quantifies the delocalization of an eigenstate $|\alpha\rangle = \sum_k C_k^\alpha |k\rangle$ presented in terms of the basis states $|k\rangle$. Roughly, $S^\alpha \sim \ln N^\alpha$ where $N^\alpha$ is a number of essential components $|k\rangle$ in a wave function $|\alpha\rangle$; the amplitudes are scaled as $|C_k^\alpha| \sim (N^\alpha)^{-1/2}$. The degree

of complexity is a smooth function of excitation energy, and the states in a given energy window "look the same" [5]. The states of the same intrinsic structure superimposed onto the center-of-mass excitation (Fig. 2) have the same entropy - the microscope is tuned to genuine complexity. The properties of wave functions cannot be expressed in an invariant manner. Theoretical arguments [12] and numerical evidence [4] strongly favor the mean field (MF) basis which separates global dynamics from local fluctuations in an optimal way.

The inverse problem of fragmentation of a simple configuration $|k\rangle$ over eigenstates $|\alpha\rangle$ is solved by the same matrix $C_k^\alpha$. The strength distributions $F_k(E) = \sum_\alpha (C_k^\alpha)^2 \delta(E - E_\alpha)$ of bare states $|k\rangle$ vary in fluctuations but the averaging reveals generic shape $F(E)$ [4,13]. As excitation energy increases, the width $\Gamma$ of $F(E)$ is saturated at a level determined by the magnitude of the residual interaction. As a function of this magnitude, the shape evolves from the Breit-Wigner (BW) at weak interaction to the Gaussian in the strong interaction limit, and $\Gamma$ changes from the quadratic dependence to the linear dependence, Fig. 3. The full theory of the strength function is not available yet but the qualitative predictions [7,14-16] follow from the scaling of the amplitudes $\sim N^{-1/2}$ in the chaotic limit [17]. The saturation of $\Gamma$ is known for isobaric analog states (IAS) and maybe for giant resonances (GR) built on the excited states. The deviations from the BW shape are amplified for the multiple GR. In accordance with data, one predicts [15] a more Gaussian-like strength distribution for double GR and the $n$-phonon width $\Gamma_n \propto \sqrt{n}$.

The structure of eigenfunctions can be related to the decoherence due to chaotic dynamics in the closed system, with no surrounding involved, and statistical equilibrium [4,18]. In many-body theory, a system is modeled by the gas of interacting quasiparticles. At high excitation energy, their lifetime shortens but the whole concept is valid just because of the chaotic dynamics. The occupation numbers $n_\lambda^\alpha$ of single-particle orbitals $\lambda$ for all eigenstates $|\alpha\rangle$ are smooth functions of excitation energy, nearly identical for different classes of states, Fig. 4, which can be fit by the Fermi-Dirac distribution. This gives the quasiparticle (Fermi-liquid) temperature $T_F^\alpha$ for individual wave functions, a quite unusual concept. At realistic interaction consistent with the MF, $T_F$ is identical to the thermodynamic scale determined by the level density [4]. Moreover, an alternative scale based on information entropy for individual eigenstates, $\partial S^\alpha / \partial E = 1/T^\alpha$, coincides with the

previous two.

Pairing gives an example of collectivity coexisting with chaotic dynamics and incorporated into the structure of each eigenstate. The correlations can be measured by the expectation values $\Delta^2 = \langle P^\dagger P \rangle$ where $P(P^\dagger)$ is the pair annihilation (creation) operator. For the isospin-invariant pairing ($T = 1$ pairs), Fig. 5, $\Delta^2$ decreases due to the second-order phase transition $\Delta \propto (1 - T/T_c)^{1/2}$, has a long exponential tail beyond $T_c$, and the background similar to that in a normal Fermi gas.

Dynamic enhancement of small perturbations; mixing of the $K$ quantum number, compound rotational bands, width of giant resonances, continuum effects are the interesting subjects accessible with the analysis of individual many-body states at high excitation energy. There exist deep links between intriguing aspects of complex quantum systems: mesoscopic physics, compound states, quantum chaos, complexity, information, decoherence, thermalization, mean field, effects of weak perturbations and phase transitions. Nuclear physics provides the best field for studying those phenomena in their integrity.

The work was supported by the NSF grants 94-03666 and 95-12831.

## References

[1] N.Bohr, Nature **137**, 344 (1936). [2] T.A.Brody *et al.*, Rev. Mod. Phys. **53**, 385 (1981). [3] V.V.Flambaum, A.A.Gribakina, G.F.Gribakin and M.G.Kozlov, Phys. Rev. **A50**, 267 (1994). [4] V.Zelevinsky, M.Horoi and B.A.Brown, Phys. Lett. **B350**, 141 (1995); M.Horoi, V.Zelevinsky and B.A.Brown, Phys. Rev. Lett. **74**, 5194 (1995); V.Zelevinsky, B.A.Brown, N.Frazier and M.Horoi, Phys. Rep., *in print*. [5] I.C.Percival, J. Phys. **B6**, L229 (1973). [6] O.Bohigas and H.A.Weidenmüller, Ann. Rev. Nucl. Part. Sci. **38**, 421 (1988). [7] V.G.Zelevinsky, Nucl. Phys. **A553**, 125c (1993); **A570**, 411c (1994). [8] B.A.Brown and B.H.Wildenthal, Ann. Rev. Nucl. Part. Sci. **38**, 29 (1988); B.A.Brown *et al.*, *OXBASH code*, MSUNSCL Report **524** (1988). [9] J.Brenneisen *et al.*, Z. Phys. **A352**, 149, 279, 403 (1995). [10] F. von Oppen, Phys. Rev. Lett. **73**, 798 (1994). [11] D.Kusnezov, B.A.Brown and V.Zelevinsky, Phys. Lett., *in print*. [12] V.G.Zelevinsky, Nucl. Phys. **A555**, 109 (1993). [13] N.Frazier, B.A.Brown and V.Zelevinsky,

Phys. Rev. C, *in print.* [14] C.A.Bertulani and V.G.Zelevinsky, Nucl. Phys. **A568**, 931 (1994). [15] C.H.Lewenkopf and V.G.Zelevinsky, Nucl. Phys. **A569**, 183 (1994). [16] B.Lauritzen *et al.*, Phys. Rev. Lett. **74**, 5190 (1995). [17] O.P.Sushkov and V.V.Flambaum, Sov. Phys. Usp. **25**, 1 (1982). [18] M.Srednicki, Phys. Rev. **E50**, 888 (1994).

**Figure captions.**

*Figure 1.* Localization length $\exp(S^{\alpha})$ for 3276 $2^+0$ states of 12 valence particles in the *sd* shell model as a function of excitation energy (a) and in the natural scale ($b$) where $\alpha$ corresponds to the state ordering in increasing energy. The horizontal line corresponds to the GOE limit of complete mixing.

*Figure 2.* Localization length for 1183 $0^+0$ states in $^{12}C$ calculated in the model space of 4 major shells with the cross-shell interaction of *E.K.Warburton and B.A.Brown*, Phys. Rev. **C46** (1992) 923, taking into account $(0+2)\hbar\omega$ excitations. The horizontal line corresponds to the GOE limit. The second arch contain the states with the excited center-of-mass motion.

*Figure 3.* Average spreading width of 400 $0^+0$ states in the middle of the spectrum (dimension $N = 839$) of 12 valence particles in the *sd* shell model as a function of the overall strength of residual interaction; $\lambda = 0$ corrresponds to the independent particle model while $\lambda = 1$ corresponds to the realistic strength.

*Figure 4.* Occupation numbers of individual $0^+0$ ($N = 839$, panel a), $2^+0$ ($N = 3276$, panel $b$) and $9^+0$ ($N = 657$, panel $c$) states of 12 valence particles in the *sd* shell model as a function of the natural ordering. In the left part the sets of points correspond to $0d_{5/2}$ (upper), $0d_{3/2}$ (middle) and $1s_{1/2}$ (lower) orbitals, respectively; neutron and proton occupancies coincide. At the center of the spectrum all orbitals are half-filled (infinite temperature).

*Figure 5.* Pairing correlator of individual $0^+0$ states for 8 ($N = 325$, panel a) and 12 ($N = 839$, panel $b$) valence particles in the *sd* shell model. The line corresponds to the fit described in the text.

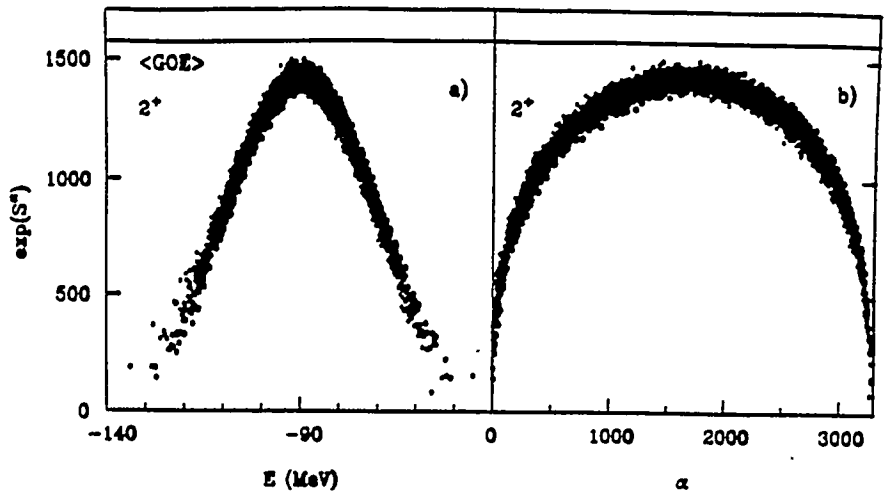


Figure 1

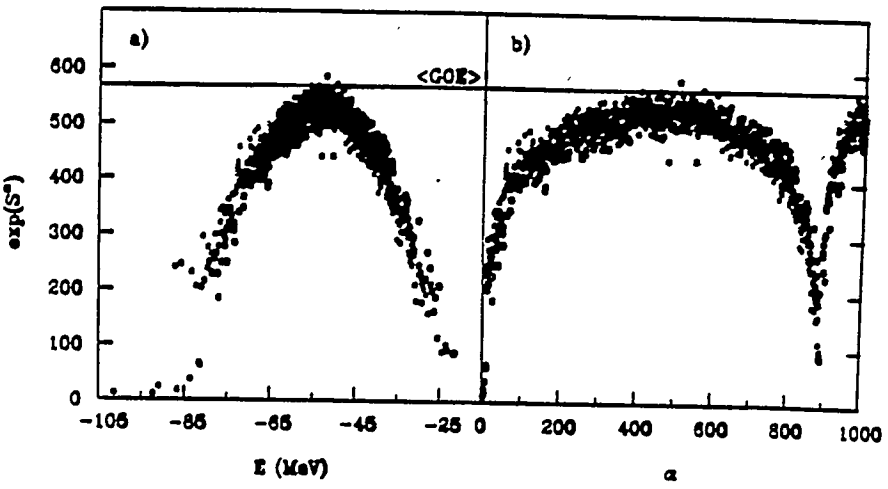


Figure 2

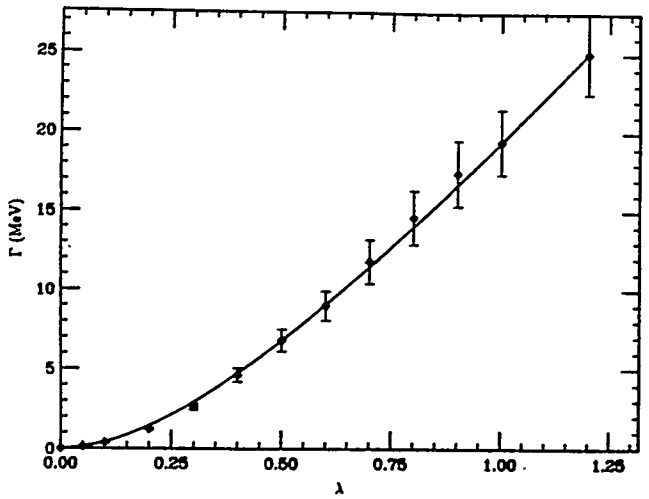


Figure 3

Figure 4

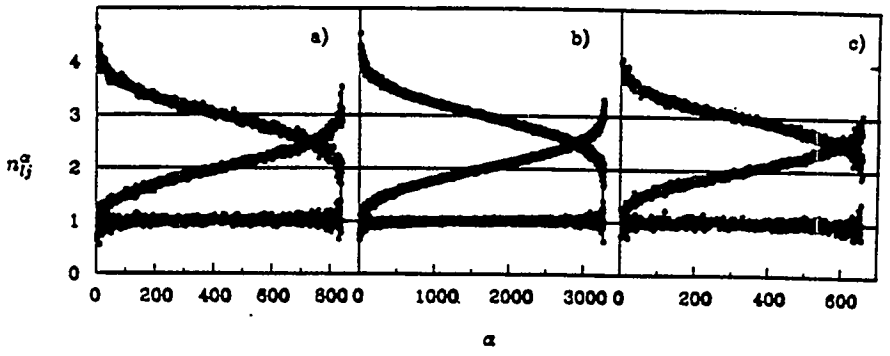


Figure 5

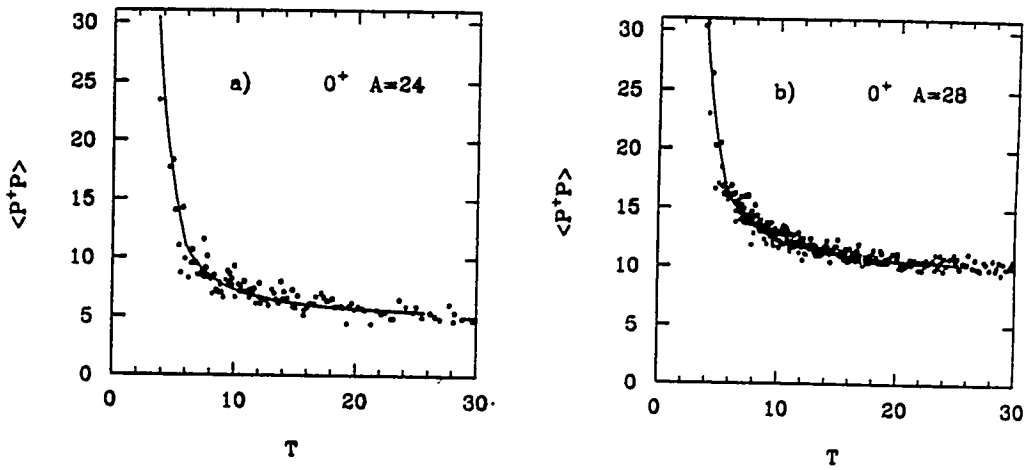

**CONFERENCE ON NUCLEAR STRUCTURE AT THE LIMITS**
**July 22-26, 1996**
**Argonne National Laboratory**
**Building 402 Auditorium**

**LIST OF PARTICIPANTS**


Dieter A. Ackermann
Physics Division
Argonne National Laboratory
Building 203
9700 South Cass Avenue
Argonne, IL 60439-4843
Phone: (630) 252-1514
Fax: (630) 252-2864
E-mail: ackermann@anlphy.phy.anl.gov

Yogeshwer K. Agarwal
Nuclear Reactions Group
Tata Institute
Homi Bhabha Road, Colaba
400005 Bombay
INDIA
Phone: 91-22-2152971 ext. 2238
Fax: 91-22-2152110
E-mail: agarwal@tifrvax.tifr.res.in

Irshad Ahmad
Physics Division
Argonne National Laboratory
Building 203
9700 South Cass Avenue
Argonne, IL 60439-4843
Phone: (630) 252-3612
Fax: (630) 252-6210
E-mail: ahmad@anlphy.phy.anl.gov

Yurdanur A. Akovali
Physics Division
Oak Ridge National Laboratory
P.O. Box 2008
Building 6000, MS 6371
Oak Ridge, TN 37830
Phone: (423) 574-4695
Fax: (423) 574-1268
E-mail: akovali@orph01.phy.ornl.gov

Jessica L. Allen
Department of Physics
Florida State University
REU Summer Program
Tallahassee, FL 33406

Hanan Amro
Physics Division
Argonne National Laboratory
Building 203
9700 South Cass Avenue
Argonne, IL 60439-4843
Phone: (630) 252-4730
Fax: (630) 252-6210
E-mail: amro@anlphy.phy.anl.gov

Nikolai V. Antonenko
Bogoluibov Theoretical Laboratory
Joint Institute for Nuclear Research
141980 Dubna, Moscow Region
RUSSIA
Phone: 7-09621-63143
Fax: 7-09621-65084
E-mail: jolos@thsun1.jinr.dubna.su

Ani Aprahamian
Department of Physics
University of Notre Dame
Notre Dame, IN 46556
Phone: (219) 631-8120
Fax: (219) 631-5952
E-mail: aprahamian.1@nd.edu

Stephen J. Asztalos
Nuclear Science Division
Lawrence Berkeley National Laboratory
Building 88
1 Cyclotron Road
Berkeley, CA 94720
Phone: (510) 486-6423
Fax: (510) 486-7983
E-mail: istvan@csg.lbl.gov

Faïsal Azaiez
Institute de Physique Nucleair
IPN Orsay
91406 Orsay
FRANCE
Phone: 33-1-6941-7105
Fax: 33-1-6941-7196
E-mail: azaiez@ipno.in2p3.fr

Cyrus Baktash
Physics Division
Oak Ridge National Laboratory
Building 6000, MS 6371
Oak Ridge, TN 37831-6371
Phone: (423) 576-7949
Fax: (423) 574-1268
E-mail: baktash@orph01.phy.ornl.gov

Robert A. Bark
University of Copenhagen
Niels Bohr Institute
DK-4000 Riso
DENMARK
Phone: 45-4677-5600
Fax: 45-4237-3516
E-mail: rob@nbital.nbi.dk

Allan M. Baxter
Physics Department, Faculty of Science
The Australian National University
0200 Canberra, ACT
AUSTRALIA
Phone: 61-6-2492806
Fax: 61-6-2490741
E-mail: amb103@nuc.anu.edu.au

Dino Bazzacco
Dipartimento di Fisca
Padova/INFN
Universita di Padova
Via Marzolo 8
35131 Padova
ITALY
Phone: 39-49-8277184
Fax: 39-49-8977102
E-mail: bazzacco@padova.infn.it

Cornelius W. Beausang
Department of Physics
University of Liverpool
Oxford Street
Liverpool L69 3BX
UNITED KINGDOM
Phone: 44-151-794-3382
Fax: 44-151-794-3348
E-mail: cwb@ns.ph.liv.ac.uk

Francis A. Beck
CRN, Strasbourg
BP 28
23 rue du Loess
67037 Strasbourg Cedex 02
FRANCE
Phone: 33-88-10-6588
Fax: 33-88-10-6893
E-mail: beck@frcpn11.in2p3.fr

John A. Becker
Department of Physics
Lawrence Livermore National Laboratory
MS L-280
Livermore, CA 94550
Phone: (510) 422-9676
Fax: (510) 422-8086
E-mail: becker@lll-winken.llnl.gov

Michael A. Bentley
Department of Physics
Staffordshire University
School of Sciences, College Road
Stoke-on-Trent, ST4 2DE
UNITED KINGDOM
Phone: 44-1782-294612
Fax: 44-1782-745506
E-mail: mab@nphsun.staffs.ac.uk

Pallab K. Bhattacharyya
Department of Chemistry
Purdue University
West Lafayette, IN 47907
Phone: (317) 496-1775
Fax: (317) 494-0239
E-mail: pall@physics.purdue.edu

Carrol R. Bingham
Department of Physics
University of Tennessee
401 Nielsen Physics Building
Knoxville, TN 37996-1200
Phone: (423) 974-7802
Fax: (423) 974-7843
E-mail: cbingham@utk.edu

Arnold R. Bodmer
Physics Division
Argonne National Laboratory
Building 203
9700 South Cass Avenue
Argonne, IL 60439-4843
Phone: (630) 252-4093
Fax: (630) 252-3903

Sandra Bouneau
Institut de Physique Nucleair
IPN Orsay
91406 Orsay
FRANCE
Phone: 33-1-6941-7105
Fax: 33-1-6941-7196
E-mail: bouneau@ipno.in2p3.fr

Angela Bracco
Department of Physics
Via Celoria, 16
20133 Milano
ITALY
Phone: 39-2-2392252
Fax: 39-2-2392487
E-mail: bracco@vaxmi.mi.infn.it

Matthew J. Brinkman
Physics Division
Oak Ridge National Laboratory
Building 6000, MS 6371
Oak Ridge, TN 37831-6341
Phone: (423) 241-5332
Fax: (423) 574-1268
E-mail: brinkman@orph01.phy.ornl.gov

Rafal J. Broda
Department of Nuclear Spectroscopy
Niewodniczanski Institute of Nuclear Physics
Radzikowskiego 152
31-342 Krakow
POLAND
Phone: 48-12-370222
Fax: 48-12-371881
E-mail: broda@bron.ifj.edu.pl

Timothy B. Brown
Department of Nuclear Research
Florida State University
Tallahassee, FL 32306
Phone: (904) 644-4182
Fax: (904) 644-9848
E-mail: brown@nucmar.physics.fsu.edu

Todd Brown
Physics Division
Argonne National Laboratory
Building 203
9700 South Cass Avenue
Argonne, IL 60439-4843
Phone: (630) 252-4051
Fax: (630) 252-2864
E-mail: brown@anlphy.phy.anl.gov

Jacob Burde
Racah Institute of Physics
The Hebrew University of Jerusalem
Givat Ram
91904 Jerusalem
ISRAEL
Phone: 972-2-6584433
Fax: 972-2-6586347
E-mail: burde@vms.huji.ac.il

Brian C. Busse
Physics Department
Oregon State University
Weniger Hall 301
Corvallis, OR 97331
Phone: (510) 486-4187
Fax: (510) 486-7983
E-mail: busse@nsa.lbl.gov

Michael P. Carpenter
Physics Division
Argonne National Laboratory
Building 203
9700 South Cass Avenue
Argonne, IL 60439-4843
Phone: (630) 252-5365
Fax: (630) 252-2864
E-mail: carpenter@anlphy.phy.anl.gov

Francesco Catara
Department of Physics
University of Catania
Corso Italia, 57
95129 Catania
ITALY
Phone: 39-95-7195440
Fax: 39-95-383023
E-mail: catara@ct.infn.it

Richard Chasman
Physics Division
Argonne National Laboratory
Building 203
9700 South Cass Avenue
Argonne, IL 60439-4843
Phone: (630) 252-3614
Fax: (630) 252-6008
E-mail: chasman@anlphy.phy.anl.gov

Partha Chowdhury
Department of Physics
University of Massachusetts at Lowell
One University Avenue
Lowell, MA 01854
Phone: (508) 934-3730
Fax: (508) 934-3068
E-mail: chowdhurp@woods.uml.edu

Marcus J. Chromik
NSCL
Michigan State University
East Lansing, MI 48824-1321
Phone: (517) 333-6420
Fax: (517) 353-5967
E-mail: chromik@nscl.msu.edu

S. Y. Frank Chu
Nuclear Science Division
Lawrence Berkeley National Laboratory
MS 50A-148
1 Cyclotron Road
Berkeley, CA 94720
Phone: (510) 486-7648
Fax: (510) 486-5757
E-mail: syfchu@lbl.gov

Marco Cinausero
Legnaro National Laboratory
Legnaro/INFN
Via Romea, 4
35020 Legnaro, Padova
ITALY
Phone: 39-49-8292411
Fax: 39-49-641925
E-mail: cinausero@lnl.infn.it

Jolie A. Cizewski
Department of Physics
Rutgers University
P.O. Box 849
Piscataway, NJ 08855-0849
Phone: (908) 445-3884
Fax: (908) 445-4343
E-mail: cizewski@physics.rutgers.edu

Roderick M. Clark
Nuclear Science Division
Lawrence Berkeley National Laboratory
Building 88
1 Cyclotron Road
Berkeley, CA 94720
Phone: (510) 486-4243
Fax: (510) 486-7983
E-mail: clark@csg.lbl.gov

Douglas Cline
Nuclear Structure Research Laboratory
University of Rochester
Rochester, NY 14627
Phone: (716) 275-4934
E-mail: cline@nsrl.rochester.edu

James F. C. Cocks
Department of Physics
University of Liverpool
Oliver Lodge Laboratory
Oxford Street
Liverpool L69 3BX
UNITED KINGDOM
Phone: 44-151-7943338
Fax: 44-151-7943348
E-mail: jfcc@ns.ph.liv.ac.uk

David M. Cullen
Department of Physics
University of Liverpool
Oliver Lodge Laboratory
Oxford Street
Liverpool L69 3BX
UNITED KINGDOM
Phone: 44-151-794-3713
Fax: 44-151-794-3444
E-mail: dmc@ns.ph.liv.ac.uk

Patrick J. Daly
Department of Chemistry
Purdue University
West Lafayette, IN 47907
Phone: (317) 494-5328
Fax: (317) 494-0239
E-mail: glshively@chem.purdue.edu

Cary N. Davids
Physics Division
Argonne National Laboratory
Building 203
9700 S. Cass Avenue
Argonne, IL 60439-4843
Phone: (630) 252-4062
Fax: (630) 252-2864
E-mail: davids@anlphy.phy.anl.gov

David J. Dean
Physics Division
Oak Ridge National Laboratory
P.O. Box 2008
Building 6003, MS 6373
Oak Ridge, TN 37831-6373
Phone: (423) 576-5229
Fax: (423) 574-4745
E-mail: dean@orph01.phy.ornl.gov

James H. DeGraaf
Department of Physics
University of Toronto
60 St. George Street
Toronto, ON M5S 1A7
CANADA
Phone: (416) 978-7114
Fax: (416) 978-2537
E-mail: degraaf@physics.utoronto.ca

Marie-Agnès Deleplanque-Stephens
Nuclear Science Division
Lawrence Berkeley National Laboratory
Building 88
1 Cyclotron Road
Berkeley, CA 94720
Phone: (510) 486-5384
Fax: (510) 486-7983
E-mail: mads@lbl.gov

Matt Devlin
Department of Chemistry
Washington University
Campus Box 1134
1 Brookings Drive
St. Louis, MO 63130
Phone: (314) 935-6570
Fax: (314) 935-6184
E-mail: devlin@wuchem.wustl.edu

Richard M. Diamond
Nuclear Science Division
Lawrence Berkeley National Laboratory
Building 88
1 Cyclotron Road
Berkeley, CA 94720
Phone: (510) 486-5720
Fax: (510) 486-7983
E-mail: rmdiamond@lbl.gov

Kwan Ying W. Ding
Department of Physics & Astronomy
Rutgers University
Piscataway, NJ 08855
Phone: (908) 445-2405
Fax: (908) 445-4343
E-mail: dingding@physics.rutgers.edu

Hans J. Döring
Department of Physics
Florida State University
Tallahassee, FL 32306
Phone: (904) 644-2436
Fax: (904) 644-8630
E-mail: doering@fslcd2.physics.fsu.ed

George D. Dracoulis
Department of Nuclear Physics
The Australian National University
0200 Canberra A.C.T.
AUSTRALIA
Phone: 61-6-249-2090
Fax: 61-6-249-0748
E-mail: gdd103@phys.anu.edu.au

Tom Drake
Department of Physics
University of Toronto
60 St. George Street
Toronto, ON M5S 1A7
CANADA
Phone: (416) 978-7267
Fax: (416) 978-2537
E-mail: drake@physics.utoronto.ca

Chrystian H. Droste
Department of Physics
Warsaw University
Hoza 69
00-681 Warszawa
POLAND
E-mail: droste@zfjavs.fuw.edu.pl

Jerzy Dudek
Universite Louis Pasteur
CRN, Strasbourg
67037 Strasbourg Cedex 2
FRANCE
Phone: 33-88-10-64-98
Fax: 33-88-10-62-64
E-mail: jerzy@crnhp1.in2p3.fr

John L. Durell
Department of Physics & Astronomy
The University of Manchester
The Schuster Laboratory
Manchester M13 9PL
UNITED KINGDOM
Phone: 44-161-275-4152
Fax: 44-161-275-5509
E-mail: nsd@mags.ph.man.ac.uk

J. Luis Egido
Departamento de Fisica Teórica
Universidad Autonoma de Madrid
28049 Madrid
SPAIN
Phone: 34-1-3974892
Fax: 34-1-3973936
E-mail: egido@alpha1.ft.uam.es

Henning Esbensen
Physics Division
Argonne National Laboratory
Building 203
9700 South Cass Avenue
Argonne, IL 60439-4843
Phone: (630) 252-4098
Fax: (630) 252-3903
E-mail: esbensen@anlphy.phy.anl.gov

Paul Fallon
Nuclear Science Division
Lawrence Berkeley National Laboratory
MS 88-253
1 Cyclotron Road
Berkeley, CA 94720
Phone: (510) 486-7018
Fax: (510) 486-7983
E-mail: pfallon@lbl.gov

Susan Fischer
Physics Division
Argonne National Laboratory
Building 203
9700 S. Cass Avenue
Argonne, IL 60439-4843
Phone: (630) 252-4048
Fax: (630) 252-2864
E-mail: fischer@sun0.phy.anl.gov

Stéphane Flibotte
Department of Physics & Astronomy
McMaster University
1280 Main Street West
Hamilton, ON L8S 4M1
CANADA
Phone: (905) 525-9140 ext. 23632
Fax: (905) 546-1252
E-mail: flibotte@zinnia.physics.mcmaster.ca

David B. Fossan
Physics Department
SUNY at Stony Brook
Stony Brook, NY 11794-3800
Phone: (516) 632-8113
Fax: (516) 632-8573
E-mail: fossan@nuclear.physics.sunysb.edu

Sean J. Freeman
Department of Physics & Astronomy
The University of Manchester
Brunswick Street
Manchester M13 9PL
UNITED KINGDOM
Phone: 44-161-275-4161
Fax: 44-161-275-4149
E-mail: sjf@mags.ph.man.ac.uk

Alfredo Galindo-Uribarri
AECL, Chalk River Laboratories
Chalk River, ON KOJ 1JO
CANADA
Phone: (613) 584-8811 ext. 4106
Fax: (613) 584-1800
E-mail: uribarria@crl.aecl.ca

Benoit Gall
CRN, Strasbourg
23 rue du Loess
67037 Strasbourg Cedex 2
FRANCE
Phone: 33-1-88-10-64-61
Fax: 33-1-88-10-64-79
E-mail: gall@crn.in2p3.fr

Umesh Garg
Physics Department
University of Notre Dame
Notre Dame, IN 46556
Phone: (219) 631-7352
Fax: (219) 631-5952
E-mail: garg@nd.edu

Jerry D. Garrett
Physics Division
Oak Ridge National Laboratory
MS 6368
Oak Ridge, TN 37831-6368
Phone: (423) 576-5489
Fax: (423) 574-1268
E-mail: garrettjd@ornl.gov

William Gelletly
Department of Physics
University of Surrey
Guildford
Surrey GU2 5XH
ENGLAND
Phone: 44-483-259400
Fax: 44-483-259501
E-mail: w.gelletly@ph.surrey.ac.uk

Guillaume Gervais
Department of Physics & Astronomy
McMaster University
ABB 241
1280 Main Street West
Hamilton, ON L8S 4M1
CANADA
Phone: (905) 525-5140 ext. 22457
E-mail: gervais@poppy.mcmaster.ca

Sandeep S. Ghugre
Physics Department
University of Notre Dame
Notre Dame, IN 46556
Phone: (219) 631-7716
Fax: (219) 631-5952
E-mail: sghugre@altair.phys.nd.edu

Thomas Glasmacher
NSCL
Michigan State University
East Lansing, MI 48824
Phone: (517) 333-6418
Fax: (517) 353-5967
E-mail: glasmacher@nscl.msu.edu

B. Gvirol Goldring
Department of Particle Physics
Weizmann Institute
Rehovot 76100
ISRAEL
Phone: 972-8-9343836
Fax: 972-8-344106
E-mail: Goldring@weizmann.weizmann.ac.il

Indra M. Govil
Department of Physics
University of Notre Dame
Notre Dame, IN 46556
Phone: (219) 631-7716
Fax: (219) 631-5952
E-mail: govil@gamma.phys.nd.edu

Zbigniew W. Grabowski
Department of Physics
Purdue University
West Lafayette, IN 47907-1396
Phone: (317) 494-6321
Fax: (317) 494-0706
E-mail: grabz@physics.purdue.edu

Bernard Haas
CRN, Strasbourg
B.P. 28
23 rue du Loess
67037 Strasbourg Cedex 2
FRANCE
Phone: 33-88-10-6214
Fax: 33-88-10-6292
E-mail: haasb@crn.in2p3.fr

Gregory S. Hackman
Physics Division
Argonne National Laboratory
Building 203
9700 S. Cass Avenue
Argonne, IL 60439-4843
Phone: (630) 252-1925
Fax: (630) 252-2864
E-mail: hackman@sun0.phy.anl.gov

Gudrun B. Hagemann
University of Copenhagen
Niels Bohr Institute
DK 4000 Riso, Roskilde
DENMARK
Phone: 45-46-77-5607
Fax: 45-42-37-3516
E-mail: gh@nbital.nbi.dk

Ikuko Hamamoto
Department of Mathematical Physics
Lund University
P.O. Box 118
S-22100 Lund
SWEDEN
Phone: 46-46-2229085
Fax: 46-46-2224416
E-mail: ikuko.hamamoto@matfys.lth.se

Esko J. Hammarén
Department of Physics
University of Jyväskylä
P.O. Box 35
FIN-40351 Jyväskylä
FINLAND
Phone: 358-41-602350
Fax: 358-41-602351
E-mail: hammaren@jyfl.jyu.fi

Fazia Hannachi
IN2P3 - CNRS
CSNSM Orsay
bat. 104, Campus d'Orsay
91405 Orsay
FRANCE
Phone: 33-16941-5081
Fax: 33-16941-5008
E-mail: hannachi@csnsm.in2p3.fr

P. Gregers Hansen
NSCL
Michigan State University
East Lansing, MI 48824-1322
Phone: (517) 333-6433
Fax: (517) 353-5967
E-mail: hansen@nscl.msu.edu

Daryl J. Hartley
Physics Department
Florida State University
Tallahassee, FL 32306
Phone: (904) 644-2878
Fax: (904) 644-9848
E-mail: hartley@nucmar.physics.fsu.edu

Michael Hass
Department of Particle Physics
Weizmann Institute
Rehovot 76100
ISRAEL
Phone: 972-8-9343997
Fax: 972-8-9344166
E-mail: fnhass@wis.weizmann.ac.il

Karl Hauschild
Lawrence Livermore National Laboratory
P.O. Box 808
MS L-280
7000 East Avenue
Livermore, CA 94550
Phone: (510) 423-5848
Fax: (510) 422-0883
E-mail: boz@dmark.llnl.gov

Walter F. Henning
Physics Division
Argonne National Laboratory
Building 203
9700 South Cass Avenue
Argonne, IL 60439-4843
Phone: (630) 252-4004
Fax: (630) 252-3903
E-mail: henning@anlphy.phy.anl.gov

Bent Herskind
Niels Bohr Institute
University of Copenhagen
DK 4000 Riso, Roskilde
DENMARK
Phone: 45-46775630
Fax: 45-42-373516
E-mail: bh@nbital.nbi.dk

Sigurd Hofmann
GSI
Planck-Str. 1
D-64291 Darmstadt
GERMANY
Phone: 49-6159-712734
Fax: 49-6159-712902
E-mail: s.hofmann@gsi.de

Takatoshi Horibata
Cyclotron Laboratory
RIKEN
Hirosawa 2-1
Wako-City, Saitama 351-01
JAPAN
Phone: 81-48-467-9462
Fax: 81-48-461-5301
E-mail: horibata@aomori.riken.go.jp

Eiji Ideguchi
Radiation Laboratory
RIKEN
Hirosawa 2-1, Wako-shi
Saitama 351-01
JAPAN
Phone: 81-48-462-1111
Fax: 81-48-462-4641
E-mail: ideguchi@rikaxp.riken.go.jp

Akitsu Ikeda
Division of General Education
Shizuoka Institute of Science & Technology
2200-2 Toyosawa
Fukuroi, Shizuoka 437
JAPAN
Phone: 81-0538-45-0186
Fax: 81-0538-45-0110
E-mail: ikeda@ns.sist.ac.jp

Robert V. F. Janssens
Physics Division
Argonne National Laboratory
Building 203
9700 South Cass Avenue
Argonne, IL 60439-4843
Phone: (630) 252-8426
Fax: (630) 252-6210
E-mail: janssens@anlphy.phy.anl.gov

Victor P. Janzen
TASCC
AECL, Chalk River Laboratories
Chalk River, ON KOJ 1JO
CANADA
Phone: (613) 584-3311, ext. 4096
Fax: (613) 584-1800
E-mail: janzenv@crl.aecl.ca

Cheng-lie Jiang
Physics Division
Argonne National Laboratory
Building 203
9700 South Cass Avenue
Argonne, IL 60439-4843
Phone: (630) 252-4786
Fax: (630) 252-6210
E-mail: jiang@anlphy.phy.anl.gov

Noah R. Johnson
Physics Division
Oak Ridge National Laboratory
P.O. Box 2008
Oak Ridge, TN 37831-6371
Phone: (423) 574-4739
Fax: (423) 574-1268
E-mail: johnson@orph01.phy.ornl.gov

Rauno J. Julin
Department of Physics
University of Jyväskylä
P.O. Box 35
FIN-40351 Jyväskylä
FINLAND
Phone: 358-41-602426
Fax: 358-41-602351
E-mail: julin@jyfl.jyu.fi

Roscislaw Kaczarowski
Department of Nuclear Spectroscopy
Soltan Institute for Nuclear Studies
05-400 Otwock-Swierk
POLAND
Phone: 48-22-779-8686
Fax: 48-22-779-3481
E-mail: slawek@india.cyf.gov.pl

Robert A. Kaye
Department of Physics
Florida State University
Tallahassee, FL 32306
Phone: (904) 644-4182
Fax: (904) 644-9848
E-mail: kaye@nucmar.physics.fsu.edu

Bachir Kharraja
Department of Physics
University of Notre Dame
Notre Dame, IN 46556
Phone: (219) 631-7716
Fax: (219) 631-5952
E-mail: bkharraj@altair.phys.nd.edu

Teng Lek Khoo
Physics Division
Argonne National Laboratory
Building 203
9700 South Cass Avenue
Argonne, IL 60439-4843
Phone: (630) 252-4034
Fax: (630) 252-6210
E-mail: khoo@anlphy.phy.anl.gov

Takashi Kishida
Radiation Laboratory
RIKEN
2-1 Hirosawa
Wako, Saitama 351-01
JAPAN
Phone: 81-48-467-9444
Fax: 81-48-462-4641
E-mail: kishida@rikaxp.riken.go.jp

Noémie Koller
Department of Physics & Astronomy
Rutgers University
New Brunswick, NJ 08903
Phone: (908) 445-2525
Fax: (908) 445-4343
E-mail: nkoller@physics.rutgers.edu

Reiner Krücken
Nuclear Science Division
Lawrence Berkeley National Laboratory
MS 88-249
1 Cyclotron Road
Berkeley, CA 94720
Phone: (510) 486-5708
Fax: (510) 486-7983
E-mail: kruecken@csg.lbl.gov

Theodore M. Lach
433 Roe Ct.
Downers Grove, IL 60516
Phone: (630) 979-0246
Fax: (630) 979-1389
E-mail: tedlach@ihgp7.att.com

Dennis R. LaFosse
Chemistry Department
Washington University
1 Brookings Drive
St. Louis, MO 63130
Phone: (314) 935-6570
Fax: (314) 935-6184
E-mail: lafosse@wuchem.wustl.edu

Gregory J. Lane
Department of Physics
Nuclear Structure Laboratory
SUNY at Stony Brook
Stony Brook, NY 11794-3800
Phone: (516) 632-7023
Fax: (516) 632-8573
E-mail: lane@nuclear.physics.sunysb.edu

Torben Lauritsen
Physics Division
Argonne National Laboratory
Building 203
9700 South Cass Avenue
Argonne, IL 60439-4843
Phone: (630) 252-4026
Fax: (630) 252-6210
E-mail: torben@anl.gov

Chun S. Lee
Department of Physics
Chung-Ang University
Huksuk-Dong 221, Dongjak-ku
Seoul 156-756
SOUTH KOREA
Phone: 82-2-820-5195
Fax: 82-2-825-4988
E-mail: cslee@aladdin.phys.cau.ac.kr

I-Yang Lee
Nuclear Science Division
Lawrence Berkeley National Laboratory
Building 88
1 Cyclotron Road
Berkeley, CA 94720
Phone: (510) 486-5727
Fax: (510) 486-7983
E-mail: iylee@lbl.gov

T.-S. Harry Lee
Physics Division
Argonne National Laboratory
Building 203
9700 South Cass Avenue
Argonne, IL 60439-4843
Phone: (630) 252-4094
Fax: (630) 252-3903
E-mail: lee@anlphy.phy.anl.gov

Silvia M. Lenzi
Dipartimento di Fisica "Galileo Galilei"
University of Padova
Via F. Marzolo 8
I-35131 Padova
ITALY
Phone: 39-49-8277180
Fax: 39-49-8277102
E-mail: lenzi@padova.infn.it

Fritz A. Lerma
Chemistry Department
Washington University
1 Brookings Drive
University City, MO 63130
Phone: (314) 935-6570
Fax: (314) 935-6184
E-mail: lerma@wuchem.wustl.edu

Matej Lipoglavsek
The Svedberg Laboratory
Uppsala University
Thunbergsvägen 5A
75121 Uppsala
SWEDEN
Phone: 46-38661-1773325
Fax: 46-38661-219385
E-mail: matej.lipoglavsek@ijs.si

John C. Lisle
Department of Physics & Astronomy
The University of Manchester
Schuster Laboratory
Manchester M13 9PL
ENGLAND
Phone: 44-161-275-4107
Fax: 44-161-275-5509
E-mail: lisle@mags.ph.man.ac.uk

Kim Lister
Physics Division
Argonne National Laboratory
Building 203
9700 South Cass Avenue
Argonne, IL 60439-4843
Phone: (630) 252-4040
Fax: (630) 252-2864
E-mail: lister@anlphy.phy.anl.gov

Giovanni Lo Bianco
Dip. di Matematica e Fisica
University of Camerino
Via Madonna Delle Carceri
I-62032 Camerino (MC)
ITALY
Phone: 39-737-40097
E-mail: lobianco@camars.unicam.it

Araceli P. Lopez-Martens
CSNSM Orsay
bat. 104, Campus d'Orsay
91405 Orsay
FRANCE
Phone: 33-16941-5081
Fax: 33-16941-5008
E-mail: lopez@csnsm.in2p3.fr

Jun Lu
Department of Physics
University of Tsukuba
Tandem Accelerator Center
Tsukuba, Ibaraki 305
JAPAN
Phone: 81-0298-53-2497
Fax: 81-0298-53-2565
E-mail: lu@tac.tsukuba.ac.jp

Renée L. Lucas
DAPNIA/SPhN
CEA Saclay
91191 Gif sur Yvette
FRANCE
Phone: 33-1-6908-3663
Fax: 33-1-6908-7584
E-mail: lucas@jhnx7.saclay.cea.fr

Santo Lunardi
Department of Physics
University of Padova
Via Marzolo 8
35131 Padova
ITALY
Phone: 39-49-827-7177
Fax: 39-49-827-7102
E-mail: lunardi@padova.infn.it

Wenchao Ma
Department of Physics & Astronomy
Mississippi State University
P.O. Drawer 5167
Mississippi State, MS 39762
Phone: (601) 325-0627
Fax: (601) 325-8898
E-mail: mawc@ra.msstate.edu

Augusto O. Macchiavelli
Nuclear Science Division
Lawrence Berkeley National Laboratory
1 Cyclotron Road
Berkeley, CA 94720
Phone: (510) 486-4428
Fax: (510) 486-7983
E-mail: aom@lbl.gov

Randy W. Macleod
Nuclear Science Division
Lawrence Berkeley National Laboratory
Building 88
1 Cyclotron Road
Berkeley, CA 94720
Phone: (510) 486-7756
Fax: (510) 486-7983
E-mail: rwmacleod@lbl.gov

Michael R. Maier
Department of Engineering
Lawrence Berkeley National Laboratory
Building 29
1 Cyclotron Road
Berkeley, CA 94720
Phone: (510) 486-5599
Fax: (510) 486-7557
E-mail: mecl@lbl.gov

Amnon Y. Marinov
Racah Institute of Physics
The Hebrew University of Jerusalem
Givat Ram
91904 Jerusalem
ISRAEL
Phone: 972-2-6584339
Fax: 972-2-6586347
E-mail: marinov@vms.huji.ac.il

Masayuki Matsuo
Yukawa Institute for Theoretical Physics
Kyoto University
Kitashirakawa Sakyo-ku
Kyoto 606-01
JAPAN
Phone: 81-75-753-7008
Fax: 81-75-753-7010
E-mail: matsuo@yukawa.kyoto-u.ac.jp

Ralf H. Mayer
Department of Physics & Astronomy
Rutgers University
P.O. Box 849
Piscataway, NJ 08855
Phone: (908) 445-3569
Fax: (908) 445-4343
E-mail: rmayer@physics.rutgers.edu

J. B. McGrory
Department of Nuclear Physics
U.S. Department of Energy, ER-23
G42 OGTN
19901 Germantown Avenue
Germantown, MD 20879
Phone: (301) 903-3613
Fax: (301) 903-3833
E-mail: joe.mcgrory@oer.doe.gov

Dennis P. McNabb
Department of Physics & Astronomy
Rutgers University
P.O. Box 849
Piscataway, NJ 08855-0849
Phone: (908) 445-2405
Fax: (908) 445-4343
E-mail: mcnabb@physics.rutgers.edu

Jie Meng
Physics Department, T30
Technical University of Munich
James-Franck Str. 1
D-85747 Garching
GERMANY
Phone: 89-2891-2724
Fax: 89-2891-2296
E-mail: meng@physik.tu-muenchen.de

Shoujirou Mizutori
Joint Institute for Heavy Ion Research
Oak Ridge National Laboratory
P.O. Box 2008
Building 6008, MS 6374
Oak Ridge, TN 37831
Phone: (423) 576-6076
Fax: (423) 576-5780
E-mail: mizutori@orph01.phy.ornl.gov

Frank Moore
Department of Physics
North Carolina State University
P.O. Box 8202
Raleigh, NC 27695-8202
Phone: (919) 515-6138
Fax: (919) 515-6538
E-mail: frank_moore@ncsu.edu

Tomasz Morek
Department of Physics
Warsaw University
Hoza 69
00681 Warszawa
POLAND
E-Mail: morek@zfjavs.fuw.edu.pl

Wilhelm F. Mueller
Department of Physics
University of Tennessee
401 Nielsen Physics Building
Knoxville, TN 37996-1200
Phone: (423) 974-7807
E-mail: wmueller@utk.edu

Simon M. Mullins
Department of Nuclear Physics
The Australian National University
RS Phys SE
0200 Canberra, ACT
AUSTRALIA
Phone: 61-6-249-0375
Fax: 61-6-249-0748
E-mail: smmi03@nuc.anu.edu.au

Mangalam A. Nagarajan
Legnaro National Laboratory
Legnaro/INFN
Via Romea 4
35020 Legnaro, Padova
ITALY
Phone: 39-49-8292502
Fax: 39-49-641925
E-mail: nagarajan@lnl.infn.it

Takashi Nakatsukasa
TASCC
AECL, Chalk River Laboratories
Chalk River, ON KOJ 1JO
CANADA
Phone: (613) 584-3311 ext. 6483
Fax: (613) 584-1849
E-mail: nakatsukasat@crl.aecl.ca

François Naulin
IPN Orsay
F-91406 Orsay-Cedex
FRANCE
Phone: 33-1-69-41-50-92
Fax: 33-1-69-41-64-70
E-mail: naulin@ipno.in2p3.fr

Witold Nazarewicz
Department of Physics & Astronomy
University of Tennessee
A. Nielsen Physics Building
Knoxville, TN 37996
Phone: 423) 574-4580
Fax: (423) 574-4745
E-mail: witek-nazarewicz@utk.edu

David T. Nisius
Physics Division
Argonne National Laboratory
Building 203
9700 South Cass Avenue
Argonne, IL 60439-4843
Phone: (630) 252-4730
Fax: (630) 252-6210
E-mail: nisius@sun0.phy.anl.gov

Jerry Nolen
Physics Division
Argonne National Laboratory
Building 203
9700 South Cass Avenue
Argonne, IL 60439-4843
Phone: (630) 252-6418
Fax: (630) 252-9647
E-mail: nolen@anl.gov

Makito Oi
Department of Physics
University of Tokyo
3-8-1 Komaba Meguro
Tokyo 153
JAPAN
Phone: 81-03-5454-6544
E-mail: mon@phys20.c.u-tokyo.ac.jp

Naoki Onishi
Institute of Physics
University of Tokyo
Graduate School of Arts & Sciences
3-8 Komaba
Meguro-ku, Tokyo
JAPAN
Phone: 81-3-5454-6512
E-mail: onishi@nt1.c.u-tokyo.ac.jp

Shashikumar D. Paul
Nuclear Reaction Group
Tata Institute
Homi Bhabha Road, Coloba
Bombay, Maharashtra 400005
INDIA
Phone: 91-22-2152971
Fax: 91-22-2152110
E-mail: sdpaul@tifrvax.tifr.res.in

Costel M. Petrache
Department of Physics
University of Padova
Via Marzolo 8
35131 Padova
ITALY
Phone: 39-49-8277176
Fax: 39-49-8277102
E-mail: petrache@padova.infn.it

Jeff Pfohl
Department of Physics
Florida State University
Nuclear Research Building
Tallahassee, FL 32306
Phone: (904) 644-1598
Fax: (904) 644-9848
E-mail: pfohl@nucalf.physics.fsu.edu

Marie-Geneviève Porquet
Centre de spectrométrie Nucléaire
CSNSM Orsay
bat. 104-108
91405 Orsay
FRANCE
Phone: 33-169415243
Fax: 33-169415008
E-mail: porquet@frcpn11.in2p3.fr

David C. Radford
TASCC
AECL, Chalk River Laboratories
Chalk River, ON KOJ 1J0
CANADA
Phone: (613) 584-3311
Fax: (613) 584-1800
E-mail: radford@crl.aecl.ca

Ingemar Ragnarsson
Department of Mathematical Physics
Lund University
P.O. Box 118
S-22100 Lund
SWEDEN
Phone: 46-46-2229083
Fax: 46-46-2224416
E-mail: ingemar@matfys.lth.se

Nadine Redon
Institut de Physique Nucleaire de Lyon
Universite Claude Bernard Lyon
43 Boulevard du 11 Novemdre 1918
69622 Villeurbanne
FRANCE
Phone: 33-72-43-10-64
Fax: 33-32-44-80-04
E-mail: nadine@lyosu4.in2p3.fr

Walter Reviol
Physics Department
University of Tennessee
Knoxville, TN 37996
Phone: (423) 974-7803
Fax: (423) 974-7843
E-mail: wreviol@utk.edu

Josette V. Ricker
Department of Physics
Florida State University
Tallahassee, FL 32306
Phone: (904) 644-4161
Fax: (904) 644-9848
E-mail: ricker@nucmar.physics.fsu.edu

Lee L. Riedinger
Department of Physics
University of Tennessee
401 Nielsen Building
Knoxville, TN 37996-1200
Phone: (423) 974-7805
Fax: (423) 974-7843
E-mail: lrieding@utk.edu

Catherine Rigollet
CRN, Strasbourg
B.P. 28
23 rue du Loess
67037 Strasbourg Cedex 2
FRANCE
Phone: 33-8810-6607
Fax: 33-8810-6292
E-mail: rigollet@crn.in2p3.fr

Mark A. Riley
Department of Physics
Florida State University
Tallahassee, FL 32306
Phone: (904) 644-2066
Fax: (904) 644-8630
E-mail: riley@fsulcd.physics.fsu.edu

Luis M. Robledo
Departamento Fisica Teorica C-X1
Universidad Autonoma de Madrid
28049 Madrid
SPAIN
Phone: 34-1-3975566
Fax: 34-1-3973936
E-mail: robledo@alpha1.ft.uam.es

Pat Sangsingkeow
Detector Manufacturing & Development
EG&G ORTEC
100 Midlan Road
Oak Ridge, TN 37830
Phone: (423) 481-2416
Fax: (423) 483-2133
E-mail: pat_sangsingkeow@eeginc.com

Demetrios G. Sarantites
Chemistry Department
Washington University
1 Bookings Drive
University City, MO 63130
Phone: (314) 935-6504
Fax: (314) 935-6184
E-mail: dgs@proton.wustl.edu

Wojciech Satula
Joint Institute for Heavy Ion Research
Oak Ridge National Laboratory
P.O. Box 2008
Building 6008, MS 6374
Oak Ridge, TN 37831
Phone: (423) 576-8763
Fax: (423) 576-5780
E-mail: satula@orph39.ornl.phy.gov

John P. Schiffer
Physics Division
Argonne National Laboratory
Building 203
9700 South Cass Avenue
Argonne, IL 60439-4843
Phone: (630) 252-4066
Fax: (630) 252-2864
E-mail: schiffer@anl.gov

Gregory J. Schmid
Nuclear Science Division
Lawrence Berkeley National Laboratory
Building 88
1 Cyclotron Road
Berkeley, CA 94720
Phone: (510) 486-5702
Fax: (510) 486-7983
E-mail: gjschmid@lbl.gov

Claire A. Schück
CSNSM Orsay
91405 Orsay
FRANCE
Phone: 33-1-69-41-52-39
Fax: 33-1-69-41-50-08
E-mail: schuck@csnsm.in2p3.fr

Dirk Schwalm
MPI Heidelberg
Postfach 103980
D69029 Heidelberg
GERMANY
Phone: 6221-516360
Fax: 6221-516606
E-mail: schwalm@zooey.mpi-hd.mpg.de

Jazmin Schwartz
Physics Division
Argonne National Laboratory
Building 203
9700 South Cass Avenue
Argonne, IL 60439-4843
Phone: (630) 252-3642
Fax: (630) 252-2864
E-mail: schwartz@anlphy.phy.anl.gov

Jeffrey M. Sears
Physics Department
SUNY at Stony Brook
Stony Brook, NY 11794-3800
Phone: (516) 632-8115
Fax: (516) 632-8573
E-mail: sears@nuclear.physics.sunysb.edu

Paul B. Semmes
Physics Department
Tennessee Technological University
P.O. Box 5051
Cookeville, TN 38505
Phone: (615) 372-3145
Fax: (615) 372-6351
E-mail: pbs1492@tntech.edu

Dariusz Seweryniak
Physics Division
Argonne National Laboratory
Building 203
9700 South Cass Avenue
Argonne, IL 60439-4843
Phone: (630) 252-1514
Fax: (630) 252-2864
E-mail: seweryn@anlphy.phy.anl.gov

Yoshifumi R. Shimizu
Department of Physics
Kyushu University
6-10-1 Hakozaki
Fukuoka 812
JAPAN
Phone: 81-92-642-2558
Fax: 81-92-642-2553
E-mail: shimizu@jpnyitp.yukawa.kyoto.u.acjp

John F. Smith
Physics Department
SUNY at Stony Brook
Stony Brook, NY 11794-3800
Phone: (516) 632-7023
Fax: (516) 632-8573
E-mail: jfsmith@nuclear.physics.sunysb.edu

Krzysztof Starosta
Department of Physics
Warsaw University
Hoza 69
00-681 Warsaw
POLAND
E-mail: chris@zfjavs.fuw.edu.pl

Frank S. Stephens
Department of Nuclear Science
Lawrence Berkeley National Laboratory
Building 88
1 Cyclotron Road
Berkeley, CA 94720
Phone: (510) 486-5724
Fax: (510) 486-7983
E-mail: fss@lbl.gov

Huibin Sun
Department of Physics
Florida State University
Tallahassee, FL 32306-3016
Phone: (904) 644-1429
Fax: (904) 644-8630
E-mail: huibin@fsulcd.physics.fsu.edu

Yang Sun
Joint Institute for Heavy Ion Research
Oak Ridge National Laboratory
Oak Ridge, TN 37831-6374
Phone: (423) 576-8763
Fax: (423) 576-5780
E-mail: yangsun@utknp3.phys.utk.edu

Carl E. Svensson
Department of Physics & Astronomy
McMaster University
ABB-241
Hamilton, ON L8S 4M1
CANADA
Phone: (905) 525-9140 ext. 27457
E-mail: sven@poppy.physics.mcmaster.ca

Geoffrey N. Sylvan
Department of Physics
Florida State University
Tallahassee, FL 32306
Phone: (904) 644-4182
Fax: (904) 6344-9848
E-mail: sylvan@nucmar.physics.fsu.edu

Samuel L. Tabor
Department of Physics
Florida State University
Tallahassee, FL 32306
Phone: (904) 644-5528
Fax: (904) 644-9848
E-mail: tabor@fsulcd.physics.fsu.edu

Gurgen M. Ter-Akopian
Flerov Laboratory of Nuclear Reactions
Joint Institute for Nuclear Research
141980 Dubna, Moscow Region
RUSSIA
Phone: 7-09621-65941
Fax: 7-09621-65083
E-mail: gurgen@ljar15.jinr.dubna.su

Jun Terasaki
Service de Physique Theorique
CEA Saclay
91191 Gif-sur-Yvette
FRANCE
Phone: 33-1-6908-7373
Fax: 33-1-6908-8120
E-mail: terasaki@amoco.saclay.cea.fr

Michael Thoennessen
NSCL
Michigan State University
East Lansing, MI 48824-1321
Phone: (517) 333-6323
E-mail: thoennessen@nscl.msu.edu

Peter J. Twin
Department of Physics
University of Liverpool
Oliver Lodge Laboratory
Oxford Street
Liverpool L69 3BX
UNITED KINGDOM
Phone: 44-151-794-3378
Fax: 44-151-794-3348
E-mail: pjt@ns.liv.ac.uk

Kai M. Vetter
Nuclear Science Division
Lawrence Berkeley National Laboratory
MS 88-232
1 Cyclotron Road
Berkeley, CA 94720
Phone: (510) 486-6423
Fax: (510) 486-7983
E-mail: kvetter@lbl.gov

Giuseppe Viesti
Department of Physics
University of Padova
Via Marzolo 8
35100 Padova
ITALY
Phone: 39-49-8277124
Fax: 39-49-8762641
E-mail: viesti@lnl.infn.it

Enrico Vigezzi
Milano/INFN
Via Celoria 16
20133 Milano
ITALY
Phone: 39-2-2392251
Fax: 39-2-2392487
E-mail: vigezzi@mi.infn.it

Andrea Vitturi
Department of Physics
University of Padova
Via Marzolo 8
I-35131 Padova
ITALY
Phone: 39-49-8277235
Fax: 39-49-8277102
E-mail: vitturi@padova.infn.it

Jim C. Waddington
Department of Physics & Astronomy
McMaster University
ABB 241
Main Street West
Hamilton, ON L8S 4G5
CANADA
Phone: (905) 525-9140 ext. 23635
Fax: (905) 546-1252
E-mail: jcw@talvax.mcmaster.ca

Robert Wadsworth
Department of Physics
University of York
Heslington
York YO1 5DD
UNITED KINGDOM
Phone: 44-1904-432242
Fax: 44-1904-432214
E-mail: oew@yksc.york.ac.uk

Philip M. Walker
Department of Physics
University of Surrey
Guildford
Surrey GU2 5XH
ENGLAND
Phone: 44-1483-300800
Fax: 44-1483-259501
E-mail: p.walker@surrey.ac.uk

William B. Walters
Department of Chemistry
University of Maryland
College Park, MD 20742
Phone: (301) 405-1801
Fax: (301) 314-9121
E-mail: ww3@umail.umd.edu

David Ward
Department of Nuclear Physics
AECL, Chalk River Laboratories
Chalk River, ON KOJ 1JO
CANADA
Phone: (613) 584-3311
Fax: (613) 584-1800
E-mail: schroedh@crl2.crl.aecl.ca

Jody A. White
Department of Physics
California Institute of Technology
Caltech Mail Code 106-38
Pasadena, CA 91106
Phone: (818) 395-4666
Fax: (818) 564-8708
E-mail: jody@krl.caltech.edu

Jonathan N. Wilson
Department of Physics
McMaster University
1280 Main Street West
Hamilton, ON L8S 4M1
CANADA
Phone: (905) 525-9160 ext. 27458
Fax: (905) 546-1252
E-mail: wilsonj@minerva.physics.mcmaster.ca

Ching-Yen Wu
Nuclear Structure Research Laboratory
University of Rochester
271 East River Road
Rochester, NY 14627
Phone: (716) 275-8960
Fax: (716) 473-5384
E-mail: wu@nsrl.rochester.edu

Walid Younes
Department of Physics
Rutgers University
P.O. Box 849
Piscataway, NJ 08855-0849
Phone: (908) 445-2405
Fax: (908) 445-4343
E-mail: younes@physics.rutgers.edu

Chang-Hong Yu
Physics Division
Oak Ridge National Laboratory
P.O. Box 2008
Building 6000
MS 6371
Oak Ridge, TN 37831-6371
Phone: (423) 574-4493
Fax: (423) 574-1268
E-mail: chy@orph01.phy.ornl.gov

Vladimir G. Zelevinsky
Department of Physics & Astronomy
Michigan State University
NSCL
East Lansing, MI 48824-1321
Phone: (517) 333-6331
Fax: (517) 353-5967
E-mail: zelevinsky@nscl.msu.edu

Chengteng Zhang
Chemistry Department
Purdue University
West Lafayette, IN 47906
Phone: (317) 496-1775
E-mail: ctzhang@physics.purdue.edu

Jing-Ye Zhang
Physics Department
University of Tennessee
Knoxville, TN 37996-1200
Phone: (423) 974-7814
Fax: (423) 974-7843
E-mail: jingye@utk.edu

Lihua Zhu
Legnaro National Laboratory
Legnaro/INFN
Via Romea 4
35020 Legnaro, Padova
ITALY
Phone: 39-49-8292366
Fax: 39-49-641925
E-mail: zhu@lnl.infn.it

Andreas H. Zilges
Physics Department
Yale University
272 Whitney Avenue
New Haven, CT 06520
Phone: (203) 432-5193
Fax: (203) 432-3522
E-mail: zilges@oasis.physics.yale.edu

# AUTHOR INDEX